Exploring the Regulatory Landscape of Signaling Pathways: From Protein Domain Functionality to RAS-MAPK Signaling in Health and Disease

Dissertation

This dissertation is submitted for the degree of Doctor of Philosophy

to the Faculty of Mathematics and Natural Sciences at the

Heinrich Heine University Düsseldorf

Presented by

Mehrnaz Mehrabipour

From

Kerman, Iran

Düsseldorf, August 2024

From the Institute of Biochemistry and Molecular Biology II

At the Heinrich Heine University Düsseldorf

Published by permission of the

Faculty of Mathematics and Natural Sciences

At the Heinrich Heine University Düsseldorf

1st Supervisor: Prof. Dr. Reza Ahmadian

2nd Supervisor: Prof. Dr. Lutz Schmitt

Date of the oral examination: February 17, 2025

Zusammenfassung

Zelluläre Reaktionen auf verschiedene äußere und innere Konditionen werden durch komplexe und hochdynamische Signalnetzwerke gesteuert. Mehrere Lücken in unserem Verständnis der Proteininteraktionen beeinträchtigen unser Wissen darüber, wie Proteine mit anderen Molekülen kommunizieren, um funktionale Signalosomen zu bilden. Protein-Protein- (PPI) und Protein-Lipid-Interaktionen sind von grundlegender Bedeutung für die Regulierung von zellulären Signalwegen und physiologischen Prozessen. Proteine bestehen aus verschiedenen funktionellen Modulen, einschließlich Domänen und Motiven, die diese Interaktionen koordinieren. In dieser Arbeit wird insbesondere die selektive Natur von PPIs untersucht, indem SH3 (Src Homology 3)-Domänen-PRM (Prolin-reiche Motive)-Interaktionen als Modell zur Erforschung zellulärer Signalnetzwerke verwendet werden. Durch die Untersuchung von SH3-Domänen bietet diese Forschung einen verfeinerten Klassifizierungs- und Selektivitätsrahmen für das Verständnis, wie diese Domänen mit PRM in ihren Bindungspartnern interagieren, und verdeutlicht so die Komplexität von Proteininteraktionen. Neben PPIs sind Protein-Lipid-Interaktionen für Prozesse wie Signaltransduktion, Membranumbau und -dynamik sowie inter- und intrazelluläre Kommunikation von wesentlicher Bedeutung. Daher wird in dieser Studie untersucht, wie verschiedene Proteinmodule unterschiedliche Struktur- und Erkennungsmechanismen nutzen, um mit Lipiden zu interagieren, was ihre Bedeutung bei Krankheitsprozessen und ihr Potenzial als therapeutische Ziele hervorhebt. Darüber hinaus konzentriert sich eine weitere Studie auf das Verständnis der Interaktionsmodalitäten innerhalb des RAS-MAPK-Signalwegs und verwandter Signalkaskaden. Der RAS-MAPK-Signalweg ist entscheidend um wichtige zelluläre Prozesse wie Proliferation, Überleben, Wachstum, Zellpolarität und Mobilität steuert. Aufbauend auf dem grundlegenden Verständnis von PPIs und Protein-Lipid-Interaktionen in Signalwegen wird in dieser Forschungsarbeit die negative Regulierung von CRAF, einer onkogenen Proteinkinase im RAS-MAPK-Signalweg, durch das Tumorsuppressorprotein SIRT4 über spezifische PPIs weiter untersucht. Außerdem untersuchen wir die Regulierung von SIRT4 unter pseudohypoxischem Stress, indem wir die Mechanismen seines proteasomalen Abbaus aufdecken. Darüber hinaus wird in der Studie die Rolle dieser Interaktionen bei humanen Krankheiten untersucht, was auf ihr Potenzial als Angriffspunkte für die therapeutische Entwicklung hinweist. Der RAS-MAPK-Signalweg ist bei pathologischen Zuständen von zentraler Bedeutung, wobei seine Dysregulation bei kardiovaskulären Störungen wie arteriovenösen Malformationen (AVMs) beobachtet wird. RIT1, ein Mitglied der RAS-Superfamilie der kleinen GTPasen, und SOS1, ein positiver Regulator dieser Kaskade, werden speziell im Zusammenhang mit AVMs untersucht. Unsere Ergebnisse zeigen, dass neuartige Missense-Mutationen in RIT1 und SOS1 zu einer Hyperaktivierung des RAS-MAPK-Signalwegs führen und damit zur Pathogenese der AVM beitragen. Desweiteren untersuchen wir einen weiteren wichtigen nachgeschalteten Signalweg von RAS, den PI3K-AKT-Signalweg, im Zusammenhang mit vaskulären Anomalien. Darüber hinaus wird die Wirksamkeit verschiedener pharmakologischer Maßnahmen zur Verringerung des Fortschreitens von AVM untersucht und ihr Potenzial als therapeutische Strategien bewertet. Insgesamt erweitert diese Forschung unser Verständnis darüber, wie PPIs und Protein-Lipid-Wechselwirkungen Signalwege, insbesondere den MAPK-Signalweg, beeinflussen, und verdeutlicht die Auswirkungen von krankheitsassoziierten Mutationen. Die Ergebnisse erweitern nicht nur unser Wissen über zelluläre Signalwege, sondern zeigen auch potenzielle therapeutische Ziele für Krankheiten auf, die mit dysregulierten Signalwegen zusammenhängen.

Summary

Cellular responses to various external and internal conditions are orchestrated by complex and highly dynamic signaling networks. Several gaps in our understanding of protein interactions affect our knowledge of how proteins communicate with other molecules to form functional signalosomes. Protein-protein (PPI) and protein-lipid interactions are fundamental to the regulation of cellular pathways and physiological processes. Proteins consist of various functional modules, including domains and motifs, which coordinate these interactions. Specifically, this study examines the selective nature of PPIs by using SH3 (Src Homology 3) domain-PRM (Proline-Rich Motif) interactions as a model to explore cellular signaling networks. By examining SH3 domains, this research offers a refined classification and selectivity framework for understanding how these domains interact with PRM in their binding partners, thereby clarifying the complexities of protein interactions. Besides PPIs, protein-lipid interactions are essential for processes such as signal transduction, membrane remodeling and dynamics, and inter- and intra-cellular communication. Therefore, this study investigates how different protein modules use diverse structural and recognition mechanisms to interact with lipids, highlighting their significance in disease processes and their potential as therapeutic targets. Furthermore, this study focuses on understanding the modes of interaction within the RAS-MAPK signaling and related pathways. The RAS-MAPK pathway is a crucial cascade that controls key cellular processes, including proliferation, survival, growth, cell polarity, and mobility. Building on the foundational understanding of PPIs and protein-lipid interactions in signaling pathways, this research further explores the negative regulation of CRAF, an oncogenic protein kinase in the RAS-MAPK pathway, through the tumor suppressor protein SIRT4 via specific PPIs. Additionally, we address the regulation of SIRT4 under pseudohypoxic stress which uncovers mechanisms of its proteasomal degradation. This study further explores the role of these interactions in human diseases, pointing to their potential as drug targets for therapeutic development. The RAS-MAPK pathway is essential in pathological conditions, with its dysregulation observed in cardiovascular disorders such as arteriovenous malformations (AVMs). RIT1, a member of the RAS superfamily of small GTPases, and SOS1, a positive regulator of this cascade, are specifically investigated in relation to AVMs. Our finding reveals novel missense mutations in RIT1 and SOS1 lead to hyperactivation of the RAS-MAPK signaling pathway, contributing to AVM pathogenesis. Additionally, we examine another major downstream pathway of RAS, the PI3K-AKT pathway, in the context of vascular anomalies. The research further explores the efficacy of various pharmacological interventions in reducing AVM progression and evaluates their potential as therapeutic strategies. Overall, this research broadens our understanding of how PPIs and protein-lipid interactions influence signaling pathways, particularly the MAPK pathway, and highlights the implications of disease-associated mutations. The findings not only advance our knowledge of cellular signaling but also pinpoint potential therapeutic targets for diseases related to dysregulated signaling.

List of Abbreviations

Abbreviation	Protein Name
3′-UTR	3′ Untranslated Regions
ACVRL1/ALK 1	Activin A Receptor type II-Like 1/Activin receptor-Like Kinase 1
AKT/PKB	AKT serine/threonine kinase/Protein Kinase B
AML	Acute Myeloid Leukemia
AMPK	AMP-Activated Protein Kinase
ANT2	ADP/ATP Translocase 2
AP-2α	Activating enhancer binding Protein 2 alpha
ARF	ADP Ribosylation Factor
ARHGAP12	Rho GTPase Activating Protein 12
ASK1	Apoptosis Signal-regulating Kinase 1
ATP	Adenosine Triphosphate
AVM	Arteriovenous Malformation
BAD	Bcl-2 associated Agonist of cell Death
BCL2	B-Cell Leukemia/Lymphoma 2
BIM	Bcl-2 Interacting Mediator of cell death
BLCA	Urothelial Bladder Cancer
BMP9/10	Bone Morphogenetic Protein 9/10
BR	Basic Rich
CAP-Gly	Cytoskeleton-Associated Protein-Glycine-rich
CDC25H	Homologous to Cell Division Cycle 25
CDC37	Cell Division Cycle 37
CDC42	Cell Division Control protein 42 homolog
CHK2	Checkpoint Kinase 2
CM-AVM	Capillary Malformation AVM
CMML	Chronic Myelomonocytic Leukemia
CNK1	Connector enhancer of Kinase suppressor of RAS 1
CRD	Cysteine-Rich Domain
CRs	Conserved Regions
CS	Costello Syndrome
CTLH	C-Terminal to Lissencephaly-1 Homology motif
DH	Dbl Homology
DLC1	Deleted In Liver Cancer 1 protein
DMPK	Myotonic Dystrophy Protein Kinase
DRP1	Dynamin-Related Protein 1
DRR	DNA Damage Response
E3B1	Eps8 SH3 domain-Binding protein 1
eEF1A ½	elongation Factor 1A 1/2
EGFR	Epidermal Growth Factor Receptor
eIF4E	eukaryotic translation Initiation Factor 4E
ELK-1	ETS Like-1 protein
EMT	Epithelial-Mesenchymal Transition
ENG	Endoglin
EPHB4	Ephrin type-B receptor 4
EPS8	Epidermal growth factor receptor Pathway Substrate 8
ERK1/2	Extracellular Signal-Regulated Kinase 1 and 2
ETS	Erythroblast Transformation-Specific
EVH1	Ena/VASP Homology domain 1
FAK	Focal Adhesion Kinase
FOS	Fos proto-oncogene
FOXO	Forkhead Box O
G domain	Guanine nucleotide-binding domain
GAB1	GRB2-Associated-Binding protein 1
GAP	GTPase-Activating Proteins
GDH	Glutamate Dehydrogenase
GDI	Guanine nucleotide Dissociation Inhibitors
GDP	Guanosine Diphosphate
GEF	Guanine Nucleotide Exchange Factor
GPCRs	G-Protein-Coupled Receptors
GRB2	Growth Factor Receptor-Bound protein 2
GRF	Growth-Regulating Factor

GRP	Gastrin-Releasing Peptide
GSK3	Glycogen Synthase Kinase 3
GTP	Guanosine Triphosphate
GuaKin/GK	Guanylate Kinase
GYF	Glycine-Tyrosine-Phenylalanine
Gαq	G protein alpha q subunit
HD	Histone fold Domain
HDACs	Histone Deacetylases
HGF-1	Hereditary Gingival Fibromatosis-1
HHT	Hereditary Hemorrhagic Telangiectasia
HRAS	Harvey Rat Sarcoma virus
HSP90	Heat Shock Protein 90
HVR	Hypervariable Region
I2H	*In silico* 2 Hybrid
IDE	Insulin-Degrading Enzyme
IKK	IκB Kinase
JUN	Jun proto-oncogene
KRAS	Kirsten Rat Sarcoma virus
KSR 1/2	Kinase Suppressor of RAS ½
LATS1	Large Tumor Suppressor kinase 1
LGG	Lower Grade Glioma
LIHC	Liver Hepatocellular Carcinoma
LIM 4	Lin-11/Isl-1/Mec-3 4
L-OPA1	Large GTPases OPA1 (Optic Atrophy 1)
LPRD	Leopard Syndrome
LUAD	Lung Adenocarcinoma
LUSC	Lung Squamous Cell Carcinoma
LZTR1	Leucine-Zipper-like Transcriptional Regulator 1
MAP1/2/4	Microtubule-Associated Protein 1/2/4
MAPK	Mitogen-Activated Protein Kinase
MCD	Malonyl-CoA Decarboxylase
MDM2	Mouse Double Minute 2 homolog
MEK	Mitogen-Activated Protein Kinase Kinase
miRNA	Micro Ribonucleic Acid
MNK1/2	MAP kinase-interacting serine/threonine-protein kinase 1/2
MnSOD	Manganese Superoxide Dismutase
MRAS	Muscle RAS oncogene homolog
mRNA	messenger Ribonucleic Acid
MSK1/2	Mitogen- and Stress-activated Kinase 1/2
MST2/STK3	Mammalian STE20-like kinase 2/Serine Threonine-protein Kinase 3
mTORC1	mammalian Target of Rapamycin Complex 1
mTORC2	rapamycin-insensitive mTOR-rich kinase Complex 2
MTS	Mitochondrial Targeting Sequences
MYC	Myelocytomatosis oncogene
NAD	Nicotinamide Adenine Dinucleotide
NCK1	Non-Catalytic region of tyrosine Kinase adaptor protein 1
NF-κB	Nuclear Factor kappa-light-chain-enhancer of activated B cells
NLS	Nuclear Localization Signals
NRAS	Neuroblastoma RAS viral oncogene homolog
NS	Noonan Syndrome
NSCLC	Non-Small Cell Lung Cancer
NTA	Acidic N-Terminus
p27Kip1	Cyclin-dependent kinase inhibitor 1B
PA	Phosphatidic Acid
PAK	P21-Activating Kinase
Par6	Partitioning defective 6
PDCD6	Programmed Cell Death Protein 6
PDH	Pyruvate Dehydrogenase
PDK1	Phosphoinositide-Dependent Kinase 1
PH	Pleckstrin Homology
PHB1	Prohibitin 1

PHLPP 1/2	PH domain and Leucine-rich repeat Protein Phosphatases ½
PI3K	Phosphatidylinositol 3-Kinase
PIP2	Phosphatidylinositol-4,5-bisphosphate
PIP3	phosphatidylinositol-3,4,5-trisphosphate
PKA	Protein Kinase A
PKCα	Protein Kinase C alpha type
PLC	Phospholipase C
PLCβ	Phospholipase C beta
PLK1	Polo-Like Kinase 1
PP	Protein Phosphatase
PPARα	Peroxisome Proliferator-Activated Receptor α
PPIs	Protein-Protein Interactions
PRM	Proline-Rich Motifs
PRMT5/6	Protein Arginine Methyltransferase 5/6
PRPs	Proline-Rich Peptides
PRR	Proline-Rich-Region
PtdIns	Phosphatidylinositols
PTEN	Phosphatase and Tensin Homolog
PWS	Parkes-Weber Syndrome
PX	Phox homology
RAB	RAS-Associated Binding
RAC1	RAS-related C3 botulinum toxin substrate 1
RAD	RAS Associated with Diabetes
RAF	Rapidly Accelerated Fibrosarcoma
RAL	RAS-Like
RAN	RAS-related Nuclear
RanBPM	Ran Binding Protein M
RAP	RAS Proximate RAS-Related Protein
RAS	Rat Sarcoma virus
RASA1	RAS GTPase-Activating protein 1
Rb	Retinoblastoma protein
RBD	RAS-Binding Domain
REM	RAS Exchange Motif
RGL3	Ral Guanine nucleotide dissociation stimulator-Like 3/Ral GEF-like 3
RHEB	RAS Homolog Enriched in Brain
RHO	Rhodopsin
RHOA	RAS Homolog family member A
RIC	RAS-related protein which Interacted with Calmodulin
RIN	RAS-like protein in Neurons
RIT	RIC-related gene expressed Throughout the organism or RAS-like protein in many Tissues
RKIP	RAF Kinase Inhibitory Protein
RKTG	RAF Kinase Trapping to Golgi
ROK-α/ROCK-II	RHO-associated protein Kinase 2
ROS	Reactive Oxygen Species
RSK	Ribosomal S6 Kinase
RTKs	Receptor Tyrosine Kinases
RUVBL1	RuvB-Like 1
SAP	Signaling lymphocyte Activation molecule-associated Protein
SCFD1	Sec1 Family Domain containing 1
SCLC	Small Cell Lung Cancer
SH2	Src Homology 2
SH3	Src Homology 3
SHP2	SRC Homology-2 Protein tyrosine phosphatase
SIRT	SIRTUIN
SKMC	Skin Cutaneous Melanoma
SMAD	Mothers Against Decapapentaplegic
SNARE	Soluble N-ethylmaleimide-sensitive factor Activating protein Receptor
SOS	Son of Sevenless
SPFH	Stomatin/Prohibitin/Flotillin/Hflkc
SPRY2	Sprouty 2
TAP-MS	Tandem Affinity Purification-Mass Spectroscopy
TAU	Tubulin Associated Unit
TCA	Tricarboxylic Acid
TCR	T-Cell Receptor

TSC2	Tuberous Sclerosis Complex 2
UCEC	Uterine Corpus Endometrial Carcinoma
UEV	Ubiquitin E2 Variant
USP13	Ubiquitin-Specific Protease 13
VEGF	Vascular Endothelial Growth Factor
WRCH1/RHOU	Wnt-1 Responsive CDC42 Homolog 1/RAS Homolog family member U
WW	two highly conserved tryptophan amino acids
Y2H	encompass Yeast 2 Hybrid
YAP	Yes-Associated Protein 1
γ-H2AX	gamma H2A histone family member X

List of Amino Acids

Amino acid	**3-Letter code**	**1-Letter code**
Alanine	Ala	A
Arginine	Arg	R
Asparagine	Asn	N
Aspartic Acid	Asp	D
Cysteine	Cys	C
Glutamic acid	Glu	E
Glutamine	Gln	Q
Glycine	Gly	G
Histidine	His	H
Isoleucine	Ile	I
Leucine	Leu	L
Lysine	Lys	K
Methionine	Met	M
Phenylalanine	Phe	F
Proline	Pro	P
Serine	Ser	S
Threonine	Thr	T
Tryptophan	Trp	W
Tyrosine	Tyr	Y
Valine	Val	V

Table of Contents

1 General Introduction

1.1 Cell Signaling

Effective communication and information transfer are vital for the proper functioning of cells, tissues, and organisms. Throughout evolution, diverse mechanisms have evolved to accomplish these crucial tasks, resulting in a highly complex signaling network. Biological signaling processes are primarily driven by interactions between proteins and other biomolecules, including protein-protein, protein-lipid, protein-DNA/RNA, protein-chemical molecules (such as metabolites and drugs), and protein-carbohydrate interactions [1, 2]. These interactions enable proteins to function not in isolation but as part of complex networks and scaffolds, facilitating the flow of cell signaling in biological processes [2, 3]. Disruptions in these networks can lead to pathological conditions. In cancer, aberrant signaling pathways due to mutations or dysregulation of growth and survival proteins lead to uncontrolled protein interactions [2, 4]. Similarly, improper protein interactions can contribute to neurodegenerative diseases like Alzheimer's [5]. As such, understanding these interactions and their biological relevance is crucial for elucidating disease mechanisms and developing targeted therapies.

In the following sections, we will particularly focus on protein-protein interactions (PPIs) and protein-lipid interactions. We will also explore how processes such as growth, proliferation, differentiation, survival, and cytoskeletal organization are governed by molecular interactions within the RAS (Rat Sarcoma virus)-MAPK (Mitogen-Activated Protein Kinase) and the PI3K (Phosphatidylinositol 3-Kinase)-AKT (AKT serine/threonine kinase)-mTOR pathways, and discuss the diseases associated with the dysregulation of these cascades.

1.1.1 Protein-Protein Interaction

Proteins, as central macromolecules in biological systems, are indispensable for executing nearly all cellular functions and dynamics. However, their actions seldom occur in isolation. Instead, most molecular processes rely on molecular machines, intricate assemblies of proteins interconnected through direct physical PPIs. These interactions, facilitated by specialized regions known as protein modules, enable the communication and coordination between individual proteins. Biochemical events, including non-covalent electrostatic forces, hydrogen bonding, and the hydrophobic effect, drive PPIs [6]. The protein modules allow the formation of PPIs and are necessary for cellular functions, including mediating functions such as detecting environmental stimuli, assisting in signal transmission, regulating the metabolic and signaling enzymes, transforming energy into mechanical movement, and preserving cellular structure [7]. Various methodologies have been developed for analyzing PPIs due to their pivotal role in mediating signaling pathways. In PPI studies, both *in vitro* and *in vivo* techniques are utilized. *In vitro* methods include TAP-MS (Tandem Affinity Purification-Mass Spectroscopy), Affinity Chromatography, Co-immunoprecipitation, Protein Microarrays, Protein-Fragment Complementation, Phage Display, X-ray Crystallography, and NMR Spectroscopy, enabling precise detection and analysis of interactions at the molecular level. *In vivo* approaches encompass Y2H (Yeast 2 Hybrid) screening and Synthetic Lethality studies, focusing on functional interactions within living systems [8]. Additionally, *in silico* methodologies such as Ortholog-Based and Domain-Pairs-Based Sequence approaches, Structure-Based Predictions, Gene Neighborhood, Gene Fusion, I2H (*In silico* 2 Hybrid), Phylogenetic Tree, Phylogenetic Profile, and Gene Expression Analysis are employed to infer PPI based on computational models and evolutionary relationships, offering insights into

potential interactions before experimental validation [8]. These diverse techniques collectively contribute to a comprehensive understanding of protein interactions in biological systems.

Almost all cellular processes demand proteins to precisely recognize a multitude of diverse interaction partners. This diversity in protein interactions is categorized into different types based on various factors. A fundamental classification depends on the composition of protein complexes: homo-oligomers comprise identical proteins, while hetero-oligomers consist of different proteins. Additionally, interactions can be classified as obligate or non-obligate based on their duration/stability, and as permanent or transient based on binding affinity [9]. Moreover, the specificity of protein interfaces determines whether interactions are simultaneous or mutually exclusive [10]. Different interaction types are implicated in various cellular processes, highlighting the importance of understanding and characterizing PPIs and their impact on biological functions. Protein domains play a crucial role in mediating these interactions, as they often contain binding sites that facilitate specific recognition and association with their interaction partners, thus contributing to the specificity and dynamics of protein complexes in cellular processes. Understanding the roles and interactions of these protein domains is essential for unraveling the complexities of cellular functions and regulatory mechanisms. Thus, examining PPIs at the domain level provides invaluable insights into the mechanisms governing cellular signaling and function and increases our knowledge regarding the evolution of organisms and function. It also offers potential avenues for therapeutic intervention in diseases where these interactions are dysregulated.

1.1.1.1 SH3 Domains: Building Blocks of Protein-Protein Interactions

Within the complex network of PPIs, motifs and domains are structural protein elements that facilitate specific binding and functional interactions. Domains are distinct conserved, stable, and often independently folding regions within a protein that are responsible for specific functions, such as binding or enzymatic activity. Motifs are shorter, non/conserved sequences within proteins that play a role in mediating interactions, often contributing to the overall function of the protein [11]. A key domain in these interactions is the SH3 (Src Homology 3) domain, which directs the assembly and disassembly of macromolecular complexes involved in cellular processes. SH3 domains were discovered in the late 1980s based on homology between the PLC (phospholipase C) and SRC oncogenes [12]. They are compact protein modules typically spanning about 60 amino acids and adopt a structural motif characterized by a five/six-stranded β-barrel-like tertiary structure connected by various loops, including the RT loop (named for the conserved arginine and threonine residues), n-Src loop, distal loop, and a 3_{10}-helix (Figure 1) [13, 14]. Despite their modest size, SH3 harbors a distinct binding pocket that selectively recognizes and engages PRM (Proline-Rich Motifs), also known as proline-dependent interactions, present in target proteins. PRMs generally consist of proline (P) and hydrophobic (X) amino acids, characterized by a core motif of XPxXP, where 'x' can be any amino acid. The SH3 domain can bind to its binding partners in two opposite orientations, determined by the relative positioning of non-proline residues, predominantly consisting of positively charged residues. This is denoted as +x/x+, which influences the orientation of peptide binding relative to the conserved proline residues at either the N-terminal (+xXPxXP, class I) (Figure1A) [13] or the C-terminal (XPxXPx+, class II) positions of the PxXP core (Figure 1B) [14]. Some SH3 domains display alternative specificity towards both class I and II PRM ligands (referred to as class I/II). For instance, the FYN SH3 domain demonstrates interaction with both class I and II PRMs found in the TAU (Tubulin Associated Unit)

protein [15]. In certain instances, the specificity of other SH3 domains towards ligands containing a combination of proline and non-proline residues is observed (referred to as Class III). An example is seen in the interaction between the second SH3 domain of NCK2 and the PxxDY motif in the cytoplasmic tail of CD3ε of the TCR (T-Cell Receptor) [16]. Furthermore, many SH3 domains demonstrate an expanded range of binding sequences, referred to as proline-independent binding. This capability allows SH3 domains to facilitate a wider spectrum of interactions, encompassing engagements with various domains such as GAP (GTPase-Activating Proteins), kinase-catalytic, BR (basic rich), GuaKin/GK (Guanylate Kinase), SH3, DH (Dbl Homology), SH2 (Src Homology 2), PX (Phox homology), and LIM4 (Lin-11/Isl-1/Mec-3 4), as well as other targets such as RNA, helices, arginine-lysine residues, spectrin repeat, lipid, and extracellular matrix molecules [17].

SH3 domains play a crucial role in linking cellular proteins and influencing cellular pathways, including almost all essential cellular functions, such as cell survival, proliferation, differentiation, migration, and polarity, through proline-dependent or independent PPIs [17, 18]. This underscores their significance in malfunction, as observed in various diseases such as neurological defects, cancer, and infectious diseases [17]. Therefore, understanding the fundamentals of selectivity and specificity in regulating their PPIs across complex cellular pathways could aid in the drug development that precisely targets and inhibits SH3 domains.

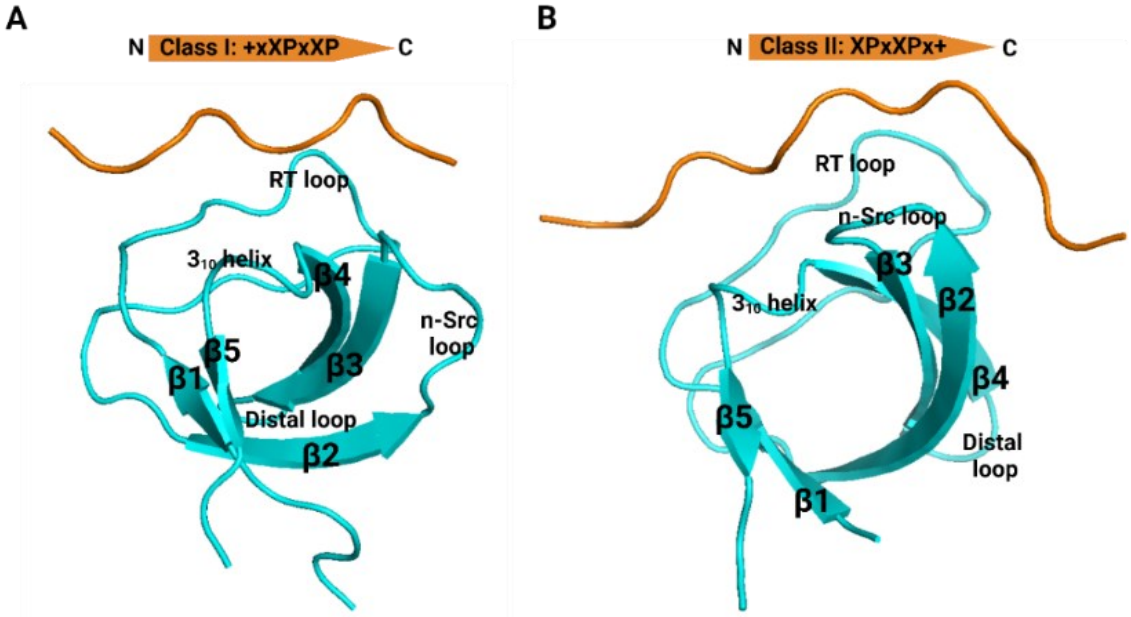

Figure 1. Structural representation of SH3 Domains. (A) The cartoon depiction of the SH3 structure of the CTTN SH3 domain (PDB code: 2D1X) in complex with class I peptide is presented. (B) The cartoon depiction of the SH3 structure of the CD2AP SH3-2 domain (PDB code: 3U23) in complex with class II peptide is presented. The figure illustrates the five β strands along with the RT, n-Src, distal loops, and 3_{10}-helix that connect local structural elements.

1.1.2 Protein-Lipid Interaction

Cellular membranes serve as dynamic barriers that enclose and compartmentalize the cell, facilitating vital processes such as signaling, transport, and cell-cell communication. Mammalian cells generate a wide array of unique lipid species, and the composition of lipids can significantly differ based on various factors such as cell type [19], metabolic state [20], disease condition [21], and external influences (such as dietary intake) [22]. Central to their functionality are the intricate interactions between proteins and lipids within the membrane matrix. Proteins have evolved an array of motifs and domains to detect and respond to specific lipids, as well as broader membrane properties such as curvature, thickness, or specialized microdomains [23].

Membrane proteins can be classified as integral (including transmembrane and anchored membrane proteins) and peripheral proteins [24]. Essentially, lipids possess the inherent capability to function as solvents, substrates, and regulatory co-factors concurrently, thereby influencing the activity of membrane proteins [25]. Integral membrane proteins display alpha helices that interact with specific hydrophobic membrane lipids. These proteins can be classified into three main categories: monotopic, bitopic, and polytopic [26]. Monotopic proteins have a single hydrophilic domain exposed on one side of the membrane, while a hydrophobic domain anchors the polypeptide chain to the hydrophobic core of the bilayer [27]. Bitopic proteins traverse the membrane once, with interspersed hydrophobic domains and a hydrophilic domain on each side of the membrane [28], and polytopic passing the membrane multiple times [29]. In addition to these classifications, integral proteins can also be structured as beta barrels, extending through the membrane, with the outer beta sheets containing hydrophobic residues that interact with lipids [30]. Integral membrane proteins perform various functions, such as molecular transportation, receptor activity, linking different cellular components, enzymatic catalysis, signal transduction, cell adhesion, and anchoring within and outside the cell in tissue [31]. Moreover, peripheral membrane proteins are soluble proteins recruited to the cell periphery of biological membranes, where they recognize specific lipid head groups or membrane features, functioning as second messengers to control the spatiotemporal recruitment and activation of specific protein effectors [23]. Peripheral proteins are transiently and loosely associated with the membrane [32], without penetrating the hydrophobic core of the phospholipid bilayer.

According to the Human Protein Atlas, 11 percent (2286 proteins) of all human proteins are detected experimentally in the plasma membrane. Exploring the diverse mechanisms through which membrane proteins integrate into and interact with membranes, including lipid-binding domains, transmembrane domains, and lipid modifications, provides insight into the fundamental principles governing cellular membrane dynamics. This comprehensive examination provides the opportunity to uncover the roles of protein-lipid interactions in shaping membrane organization, protein localization, and cellular signaling pathways, thus advancing the understanding of cellular physiology and pathology at the molecular level.

1.1.3 The RAS-MAPK Pathway

The RAS-MAPK pathway is a crucial signaling cascade involved in transducing extracellular signals into various cellular responses, such as proliferation, cell survival and growth, and cytoskeletal remodeling [33]. The pathway begins with the activation of RTKs (Receptor Tyrosine Kinases) or GPCRs (G-Protein-Coupled Receptors) (Figure 2) [34]. Activation of RTK leads to the recruitment and activation of adapter proteins like GRB2 (Growth Factor Receptor-Bound protein 2). GRB2, in turn, binds to the SOS (Son of Sevenless), facilitating its activation [35]. SOS acts as a GEF (Guanine Nucleotide Exchange Factor) that catalyzes the exchange of GDP (Guanosine Diphosphate) for GTP (Guanosine Triphosphate) on RAS proteins, thereby activating RAS [36]. Active RAS subsequently recruits and activates RAF (Rapidly Accelerated Fibrosarcoma) kinases, including ARaf, BRaf, and CRaf (also known as RAF1) [37]. RAF then phosphorylates and activates MEK (Mitogen-Activated Protein Kinase Kinase), which in turn phosphorylates and activates the terminal kinases ERK1/2 (Extracellular Signal-Regulated Kinase 1/2). Activated ERK1/2 regulates both cytosolic and nuclear targets, where it phosphorylates various transcription factors and regulatory proteins, ultimately regulating gene expression and mediating the biological responses associated with the MAPK pathway [33, 38, 39]. Additionally, GPCR-mediated activation of MAPKs is regulated by the production of intracellular messengers. GPCR activity stimulates the $G\alpha_q$ (G protein alpha q subunit)/PLCβ (Phospholipase C beta)/PKC (Protein Kinase C) as a second messenger, which can enhance the RAS-CRAF-ERK1/2 pathway [34] (Figure 2).

Some of the main downstream targets of the RAS-MAPK pathway include: **(a) Transcription factors:** ERK regulates nuclear transcription factors, including ELK-1 (ETS Like-1 protein), FOS (Fos proto-oncogene), MYC (Myelocytomatosis oncogene), JUN (Jun proto-oncogene), members of the ETS (Erythroblast Transformation-Specific) family, and others [40]. **(b) Protein kinases:** one example is RSK (Ribosomal S6 Kinase), which is activated by ERK1/2 and then phosphorylates various substrates, including transcription factors and other proteins [41]. Moreover, MNK1/2 (MAP kinase-interacting serine/threonine-protein kinase 1/2) is phosphorylated by ERK1/2, involved in the regulation of protein synthesis through phosphorylation of eIF4E (eukaryotic translation Initiation Factor 4E) and cell cycle progression [42]. Besides, MSK1/2 (Mitogen- and Stress-activated Kinase 1/2) is activated by ERK and is primarily involved in the regulation of nuclear responses and transcription [43]. Furthermore, GSK3 (Glycogen Synthase Kinase 3) is inhibited by ERK1/2 [44, 45], which might affect glycogen metabolism and cell cycle. **(c) Cell cycle regulators:** Cyclin D1 expression is up-regulated by ERK signaling, promoting progression through the G1 phase of the cell cycle [46]. **(d) Proteins involved in apoptosis:** BAD (Bcl-2 associated Agonist of cell Death) phosphorylation mediated by ERK1/2 can lead to its degradation, promoting cell survival. Moreover, BIM (Bcl-2 Interacting Mediator of cell death) protein ERK1/2-mediated phosphorylation can lead to its degradation, thus preventing apoptosis [47]. **(e) Cytoskeletal remodeling:** ERK also affects PAXILLIN and FAK (Focal Adhesion Kinase) by catalyzing the phosphorylation of PAXILLIN, which enhances its association with FAK, thereby playing a role in cell migration, adhesion, and spreading [33]. Moreover, activated ERK1/2 phosphorylates cytoskeletal components like MAP1, MAP2, and MAP4 (Microtubule-Associated Proteins) to regulate cell morphology and cytoskeletal redistribution [48]. All the above-mentioned targets illustrate the diverse roles of the RAS-MAPK pathways in cellular function. Through these downstream effectors, the pathway influences a wide range of biological processes essential for normal cellular operation and response to external stimuli.

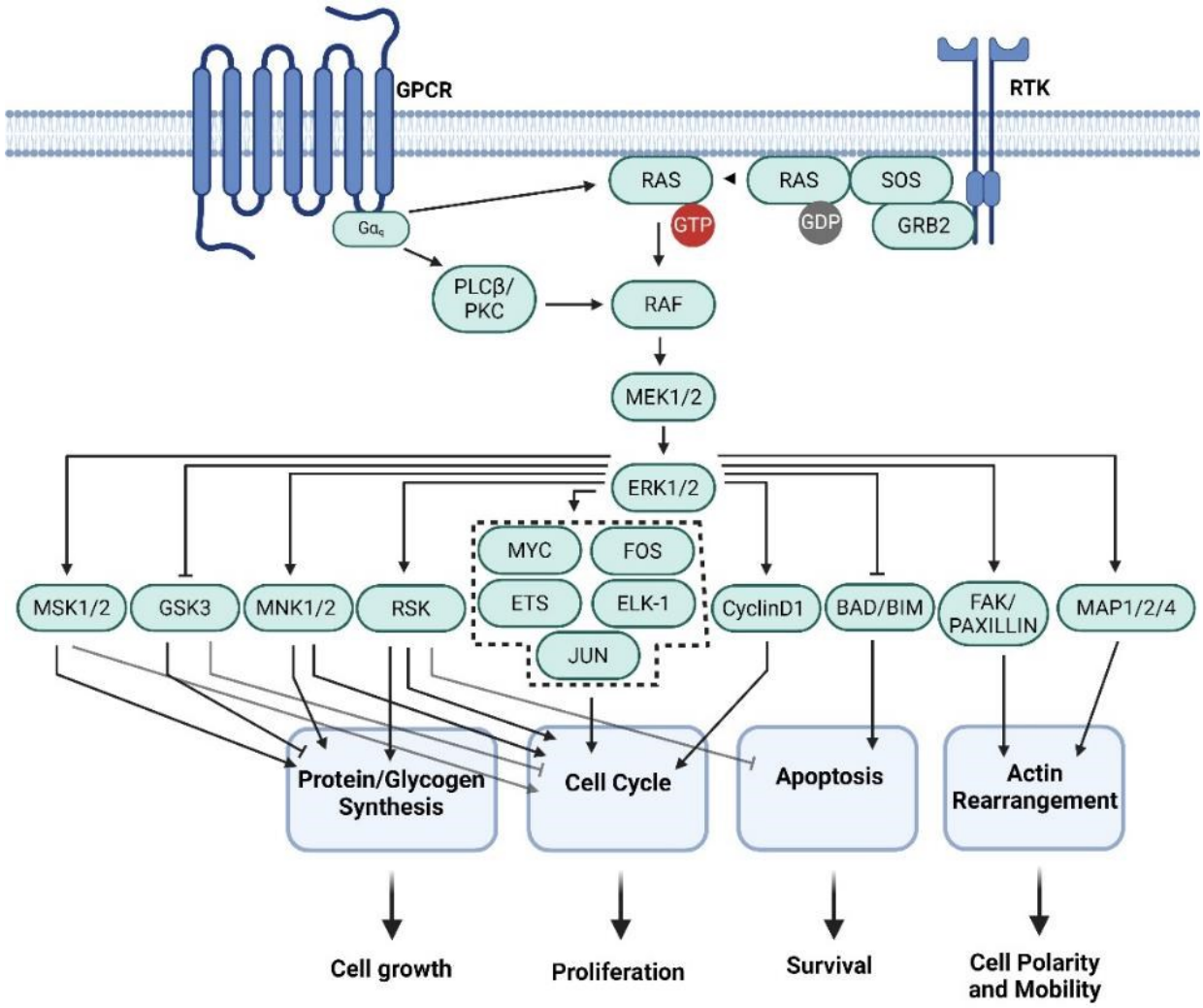

Figure 2. The RAS-MAPK pathway and its main downstream targets. The MAPK pathway is initiated by activation of receptor tyrosine kinases (RTKs) or G-protein-coupled receptors (GPCRs). Activated RTKs recruit and activate adapter proteins like GRB2, which then activates SOS, leading to the activation of RAS proteins. Active RAS recruits RAF kinases, which phosphorylate and activate MEK. MEK then activates ERK1/2, which regulates various downstream targets. Additionally, GPCR-mediated activation enhances the RAS-CRAF-ERK1/2 pathways through second messengers like $G\alpha_q$/PLCβ/PKC. Key downstream targets of the RAS-MAPK pathway include (a) Transcription factors (ELK-1, FOS, MYC, JUN, ETS family members), (b) Protein kinases (RSK, MNK1/2, MSK1/2, and GSK3), (c) Cell cycle regulators (Cyclin D1), (d) Apoptosis-related proteins (BAD, BIM), (e) Cytoskeletal remodeling (PAXILIN/FAK, MAP1/2/4). These targets illustrate the pathway's role in regulating diverse biological processes essential for cell growth, proliferation, survival, and cytoskeletal remodeling. This image was made with BioRender (https://biorender.com/).

1.1.4 The PI3K-AKT-mTOR Pathway

The PI3K-AKT pathway controls various cellular functions such as metabolism, growth, proliferation, survival, and cell migration (Figure 3) [49]. PI3Ks are categorized into three classes (I–III) based on their substrate preference and sequence homology (reviewed in REF. [49]). Each class of PI3K has unique roles in cellular signal transduction, with different isoforms within each class contributing to these roles. Particularly, Class I PI3Ks are activated by RTKs and GPCRs (Figure 3). PI3K catalyzes the phosphorylation of inositol-containing lipids, specifically PtdIns (Phosphatidylinositols). Its main substrate *in vivo* is PIP2 (phosphatidylinositol-4,5-bisphosphate), which is converted into PIP3 (phosphatidylinositol-3,4,5-trisphosphate), a crucial second messenger. PIP3 acts as a docking site for proteins with PH (Pleckstrin Homology) domains, facilitating their recruitment to the plasma membrane and subsequent activation. PIP3 binding leads to the translocation of AKT, also known as PKB (Protein kinase B), through its PH domain to the membrane which positions it near upstream regulatory kinases like PDK1 (Phosphoinositide-Dependent Kinase 1), which is also recruited by its PH domain to PIP3 and phosphorylates AKT at T308, a critical step for AKT activation. However, full activation of AKT also necessitates phosphorylation at S473 by the mTORC2 (rapamycin-insensitive mTOR-rich kinase Complex 2). Subsequently, the full activation of AKT leads to the phosphorylation of numerous target proteins, thereby regulating a wide array of cellular functions [49].

The main downstream targets of AKT include: **(a) GSK3**: phosphorylation by AKT inhibits GSK3, promoting glycogen synthesis and cell cycle [50]. **(b) mTORC1 (mammalian Target of Rapamycin Complex 1)**: AKT activates mTORC1, which regulates protein synthesis and cell growth [51]. **(c) FOXO (Forkhead Box O) transcription factors**: AKT phosphorylates FOXO, causing its exclusion from the nucleus and inhibiting its transcriptional activity, which is involved in apoptosis, cell cycle inhibition, and gluconeogenesis [52, 53]. **(d) BAD**: AKT phosphorylation inactivates BAD, promoting cell survival by preventing apoptosis [54]. **(e) p27Kip1 (Cyclin-dependent kinase inhibitor 1B)**: AKT phosphorylates p27, which leads to its cytoplasmic retention and degradation, promoting cell cycle progression [55]. **(f) TSC2 (Tuberous Sclerosis Complex 2)**: phosphorylation by AKT inhibits TSC2, leading to the activation of mTORC1 and stimulation of protein synthesis and cell growth [56]. **(g) IKK (IκB Kinase)**: AKT activates IKK, which leads to the activation of NF-Kb (Nuclear Factor kappa-light-chain-enhancer of activated B cells), a transcription factor involved in inflammatory responses and cell survival [57]. **(h) MDM2 (Mouse Double Minute 2 homolog)**: AKT phosphorylates MDM2, enhancing its activity to degrade p53, thereby reducing p53-mediated apoptosis [54]. **(i) Small GTPase**: AKT influences the activity of RHO-GTPases (RHOA (Ras Homolog family member A), RAC1 (Ras-related C3 botulinum toxin substrate 1), CDC42 (Cell Division Control protein 42 homolog)), which are crucial regulators of the cytoskeleton [58-60].

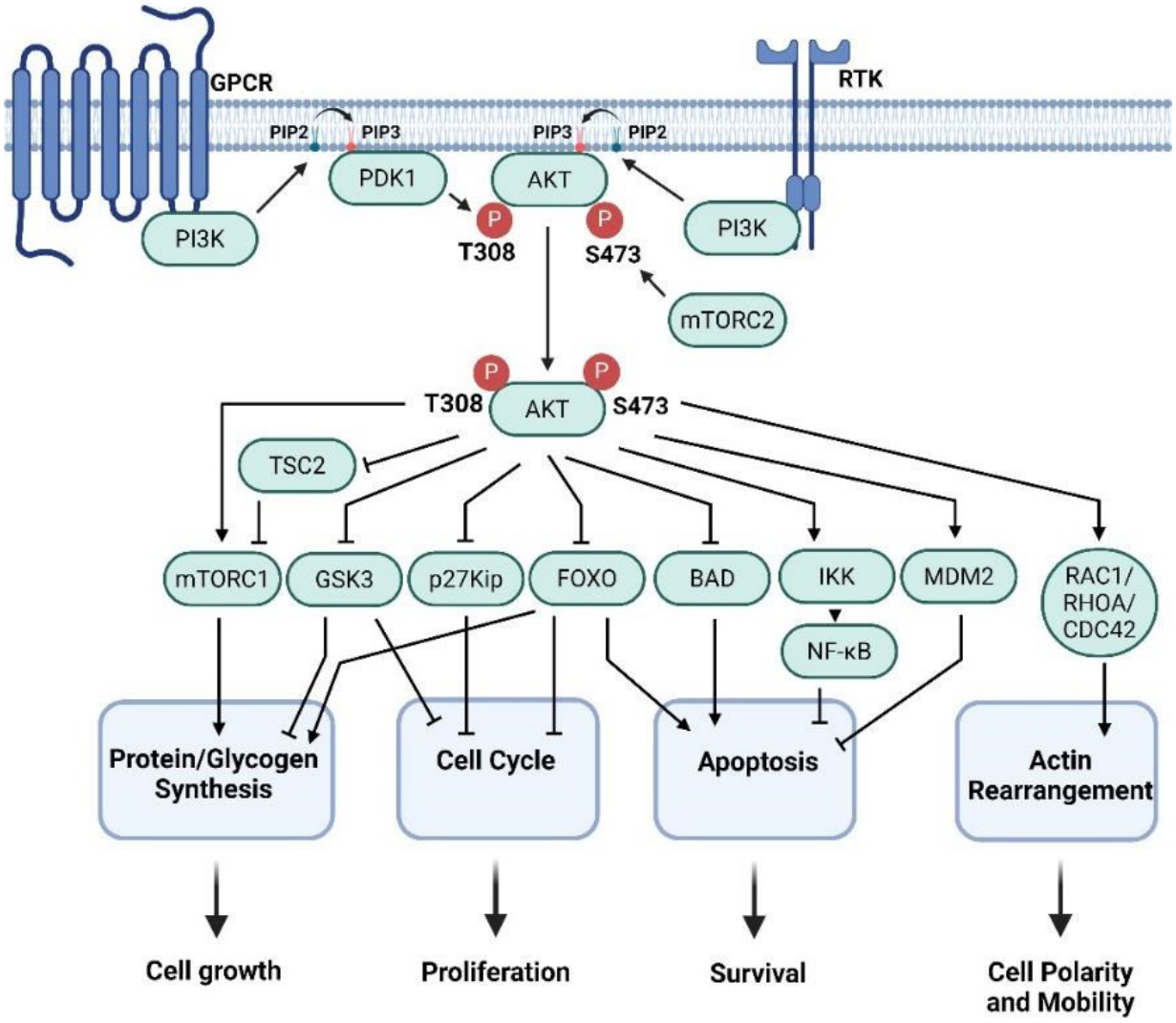

Figure 3. The PI3K-AKT pathway. This pathway regulates various cellular functions, including growth, proliferation, and survival, and cell polarity and mobility. The PI3Ks are activated by receptor tyrosine kinases (RTKs) and G-protein-coupled receptors (GPCRs), leading to the phosphorylation of phosphatidylinositol-4,5-bisphosphate (PIP2) to form phosphatidylinositol-3,4,5-trisphosphate (PIP3). PIP3 serves as a docking site for proteins with PH (Pleckstrin homology) domains, including AKT and PDK1 (phosphoinositide-dependent kinase 1). AKT is fully activated through phosphorylation at T308 by PDK1 and at S473 by mTORC2. Activated AKT phosphorylates multiple downstream targets to regulate protein and glycogen synthesis, transcriptional activity, cell survival and apoptosis, cell cycle progression and actin rearrangement. Figure created using Biorender (https://biorender.com/).

1.1.5 Crosstalk Between the RAS-MAPK and PI3K-AKT Pathways

The interaction at multiple levels between the RAS-MAPK and PI3K-AKT pathways is crucial for fine-tuning cellular responses (Figure 4). A key point of intersection between these pathways occurs at the level of RAS activation. RAS, a small GTPase, is a critical upstream activator of the MAPK pathway. Upon activation, RAS not only initiates the MAPK cascade but also directly binds to and activates PI3K [61]. This dual activation by RAS ensures a coordinated and robust response to growth signals. Additionally, the interaction between RAF and AKT constitutes a complex network of regulatory events that vary based on cell type and physiological conditions. During muscle cell differentiation, AKT inhibits RAF [62], and persistent RAF-MEK1 signaling triggers negative feedback to inhibit RAS and AKT during cell cycle arrest [63]. Additionally, RAF can stimulate RAS and AKT activation in epithelial cells [64], further pointing out the intricate regulation between these pathways. Another layer of crosstalk involves the modulation of TSC2 activity. TSC2 is a critical inhibitor of mTORC1, and AKT phosphorylates TSC2, leading to its inhibition and subsequent activation of mTORC1. Similarly, ERK can phosphorylate TSC2, contributing to the regulation of mTORC1 activity [65]. Feedback mechanisms also play a significant role in the crosstalk between these pathways. For example, mTORC1 activation can lead to a negative feedback loop that inhibits the PI3K and RAS pathway signaling [66]. Moreover, it is known that activated ERK phosphorylates GAB1 (GRB2-Associated-Binding protein 1), thereby inhibiting GAB1-mediated recruitment of PI3K to EGFR (Epidermal Growth Factor Receptor) for activation [67]. Additionally, MEK1 inhibits PI3K-AKT signaling by promoting the membrane localization of PTEN (Phosphatase and Tensin homolog), which dephosphorylates PIP3, counteracting PI3K activity and limiting AKT activation [68]. These feedback loops are crucial for maintaining signaling homeostasis and preventing overactivation that could lead to uncontrolled cell proliferation and cancer. Understanding these interactions provides valuable insights into potential therapeutic strategies for diseases characterized by dysregulated signaling.

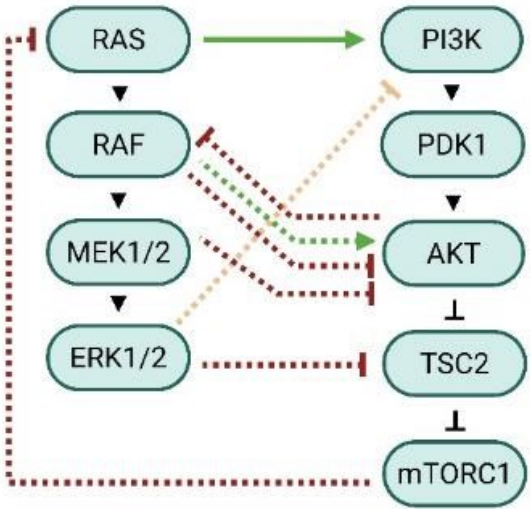

Figure 4. Interplay between RAS-MAPK and PI3K-AKT pathways. A green arrow signifies stimulation, while a red line indicates inhibition. This image was created with BioRender (https://biorender.com/).

1.1.6 Components of the RAS-MAPK Signaling Pathway

The following sections provide a comprehensive overview of the molecular interactions and regulatory mechanisms of key components of the RAS-MAPK signaling pathway. This will underscore their significance in cell signaling and emphasize the importance of studying these components to enhance our understanding and develop potential treatments for diseases associated with these pathway components.

1.1.6.1 Structure and Function of SOS Proteins

SOS proteins are members of the main mammalian RAS-GEF families (SOS, GRF (Growth-Regulating Factor), and GRP (Gastrin-Releasing Peptide)) that stimulate GTP/GDP exchange. These proteins facilitate the dissociation of GDP from RAS, promoting the transition of RAS from its inactive GDP-bound form to its active GTP-bound state [69]. In humans, there are two paralogs, SOS1 and SOS2, which are the most widely expressed and functionally relevant GEFs for RAS and RAC activation in response to upstream cellular signals [70]. The SOS proteins possess a complex domain organization, including an N-terminal HD (Histone fold Domain), DH and PH domains, a REM (RAS Exchange Motif) domain, a CDC25H (Homologous to Cell Division Cycle 25; a RAS-GEF in yeast) domain, and a C-terminal PRR (Proline-Rich-Region) motif (Figure 5A). These domains collectively contribute to the regulation of their cellular functions, mediating interactions with lipids, proteins, and other regulatory molecules, ensuring precise control over RAS and RAC signaling pathways.

In the cytosolic state, the N-terminal domains (HD, DH, and PH) maintain SOS auto-inhibition through interactions that stabilize an inactive conformation [71, 72] (Figure 5B). PRR can also have an inhibitory effect, independently of the N-terminal, by obstructing allosteric RAS binding [73]. Upon stimulation, the SOS1/2 proteins are activated by membrane recruitment, which relieves their native auto-inhibition. This proceeds with SH3-mediated complexes with SH3-containing proteins like GRB2. The C-terminal PRR, when bound to GRB2 [35], aids in membrane recruitment, where the PH domain binds to membrane phospholipids (PIP3 and lesser extent PIP2) [74], and the HD domain interacts with negatively charged membranes [72], both contributing to the release of inhibition. The central region of the CDC25H catalytic domain facilitates GDP/GTP exchange on RAS, while the interaction of the REM domain with RAS-GTP enhances SOS activation, creating a positive feedback loop [75] (Figure 5B). Phosphorylation of the C-terminal region and competitive binding of proteins like p27kip1 can inhibit SOS, constituting a negative regulatory feedback mechanism [70]. In addition, SOS1/2 plays a crucial role in RAC activation through distinct interactions. The C-terminal PRR recruits SOS to activated receptors via binding to particularly E3B1 (Eps8 SH3 domain-Binding protein 1)-SH3 domains, forming the SOS-E3B1-EPS8 (Epidermal growth factor receptor Pathway Substrate 8) complex at actin filaments, where RAC is localized. This interaction enables SOS to promote the exchange of GDP for GTP on RAC [76]. Thus, SOS1/2 integrates signals to simultaneously activate both RAS and RAC pathways, coordinating cellular responses like proliferation, cytoskeletal remodeling and migration [70].

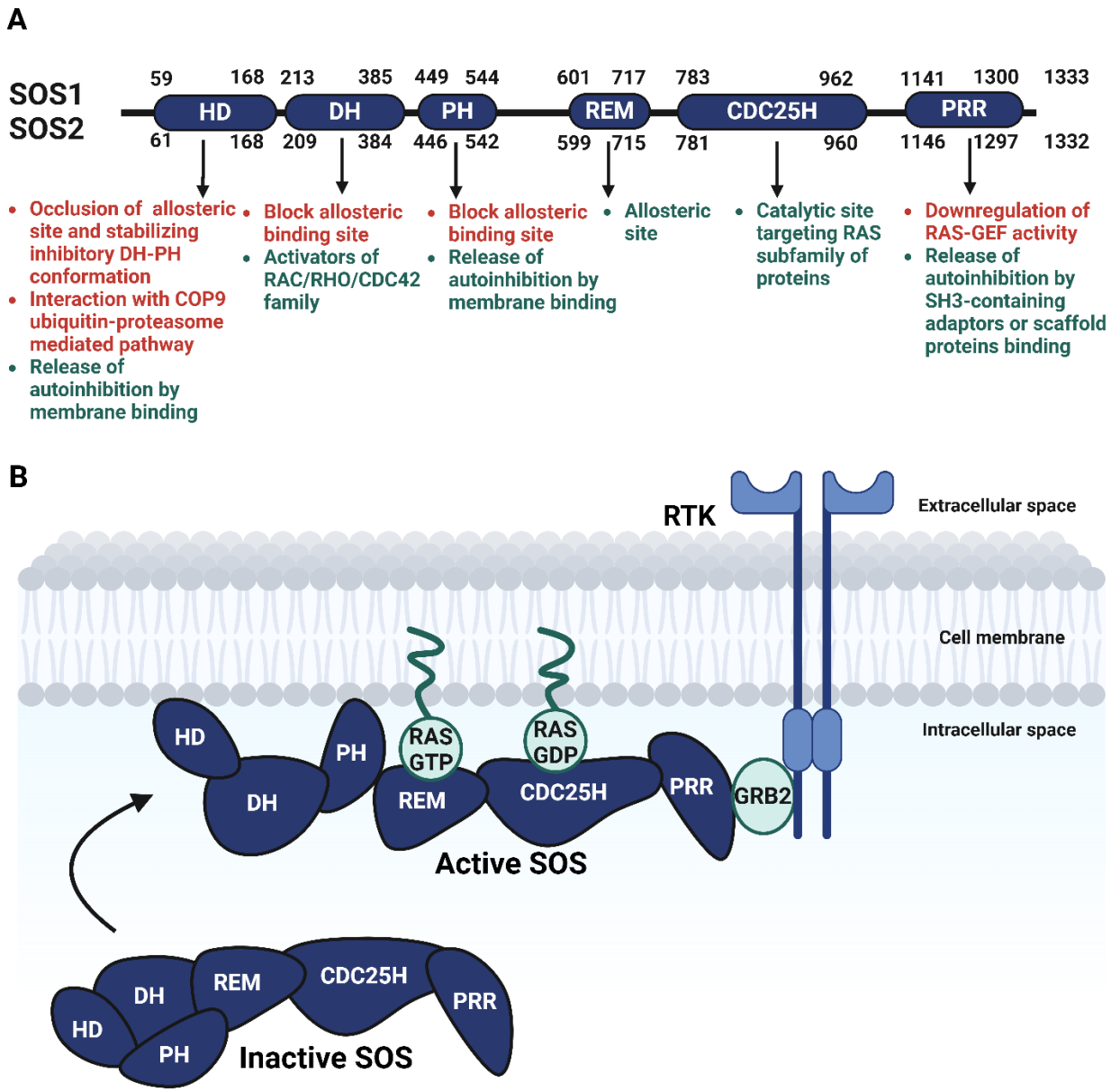

Figure 5. Domain organization and activation/deactivation mechanisms of SOS1/2 proteins. (A) The primary structure of SOS1/2 proteins displays a linear, modular organization with distinct functional domains that each contribute to its regulatory roles. The N-terminal region contains the Histone-like (HD), Dbl Homology (DH), and Pleckstrin Homology (PH) domains, which maintain auto-inhibition and facilitate membrane attachment. The central region includes the REM (RAS Exchange Motif) and CDC25H (homologous to Cell Division Cycle 25) domains, responsible for allosteric and catalytic activation of RAS, respectively. The C-terminal region features multiple PRR (Proline-Rich-Region) motifs that mediate interactions with adaptor proteins like GRB2 and regulate the allosteric site. The regulatory role of each domain in protein function is highlighted, with positive regulatory roles indicated in green text and negative regulatory roles indicated in red text. (B) In its native cytosolic state, SOS is auto-inhibited through interactions within its N-terminal domains and independent contribution or PRR motif in inhibition. Activation occurs upon recruitment to the plasma membrane, where interactions with membrane phospholipids and adaptor proteins release auto-inhibition. The N-terminal HD and PH domain interacts with membrane phospholipids, leading to a conformational change that activates the catalytic module, and the C-terminal PRR interacts with GRB2 to facilitate RAS activation. Catalytic activation involves the coordinated action of the REM allosteric site (activated by RAS-GTP) and the CDC25H catalytic site, which reorients its helical hairpin (region between PH and REM domains) to facilitate GDP/GTP exchange, creating a positive feedback loop. Visual representation designed with BioRender (https://biorender.com/).

Recent studies increasingly highlight the role of SOS-GEFs, especially SOS1, in human tumors and other pathologies. Numerous gain-of-function mutations in various SOS1 domains (and rarely in SOS2) have been identified in inherited RASopathies like NS (Noonan Syndrome) [77-79] and HGF-1 (Hereditary Gingival Fibromatosis-1) [80], CS (Costello Syndrome) [81], and LPRD (Leopard Syndrome) [70] as well as pure mucosal neuroma syndrome [82]. Additionally, SOS-associated mutations are identified in sporadic cancers such as AML (Acute Myeloid Leukemia), BLCA (Urothelial Bladder Cancer), LGG (Lower Grade Glioma), LIHC (Liver Hepatocellular Carcinoma), LUAD (Lung Adenocarcinoma), LUSC (Lung Squamous Cell Carcinoma), SKMC (Skin Cutaneous Melanoma) and UCEC (Uterine Corpus Endometrial Carcinoma) (Reviewed in Reference [70]). Efforts from academic and industry researchers are focused on developing drugs that modulate SOS up/down-regulation and GEF activity, as well as those that disrupt functional interactions with RAS targets (RAS complexes) and signaling regulators (such as GRB2 or ABI1 interactions) [70].

Using single-cell transcriptome data from the Tabula Muris database, as well as data from specific mouse and human lung cell types, endothelial cells have been identified as the cell type with the highest expression levels of human SOS1 mRNA [70]. This is supported by data showing the significant role of SOS-GEFs in endothelial cells and angiogenesis [83, 84]. In this regard, there are examples of novel AVM (Arteriovenous Malformation)-associated mutations in the SOS gene in endothelial cells that need biochemical characterization and drug screening to identify potential therapeutic targets and effective treatments.

1.1.6.2 RAS Superfamily of Small GTPases: Insights into the RIT Subfamily

The RAS small GTPase superfamily consists of low molecular weight (20–30 kDa) proteins that function as molecular switches, regulating various cellular processes by cycling between active (GTP-bound) and inactive (GDP-bound) states. This superfamily encompasses over 150 members divided into five major families: RAB (RAS-Associated Binding), RAS, ARF (ADP Ribosylation Factor), RHO (Rhodopsin) and RAN (RAS-related Nuclear), each with distinct roles in cellular signaling (Figure 6A) [85, 86].

These proteins share a conserved core G domain (Guanine nucleotide-binding domain) crucial for their function and interaction with regulatory and effector proteins [85]. The G domain of the RHO family is uniquely characterized by a "RHO insert" sequence of up to 13 amino acids, which is critical for their activation [87]. The G domain activity relies on the binding and hydrolysis of guanine nucleotides. In the GTP-bound state, they activate downstream signaling pathways and the conversion from GTP to GDP leads to a conformational change that reduces signaling activity (Figure 6B). This nucleotide cycling is regulated by GEFs, which promote GTP binding, and GAPs, which enhance GTP hydrolysis [88, 89]. Additionally, RHO GTPases are regulated by GDIs (Guanine nucleotide Dissociation Inhibitors) [90], which manage their subcellular localization by transporting them from the membrane to the cytosol (Figure 6C). Notably, GEFs and GAPs are not universally identified for all family members, and in certain cases, the presence of these regulators may not be crucial for the functionality of the proteins [86]. Additionally, the C-terminal HVR (Hypervariable Region) of the RAS, RHO, and RAB families is essential for membrane localization (Figure 6B). In contrast, ARF family members rely on N-terminal regions for membrane binding. With some exceptions, the membrane-binding regions of these families depend on modifications such as prenylation, myristoylation, and palmitoylation to ensure proper subcellular targeting and function, significantly influencing their signaling outcomes. Moreover, the RAN family

does not interact with membranes and is not modified by lipidation. Instead, its C-terminal extension undergoes conformational changes during GDP–GTP cycling, which is crucial for its role in nuclear transport [86].

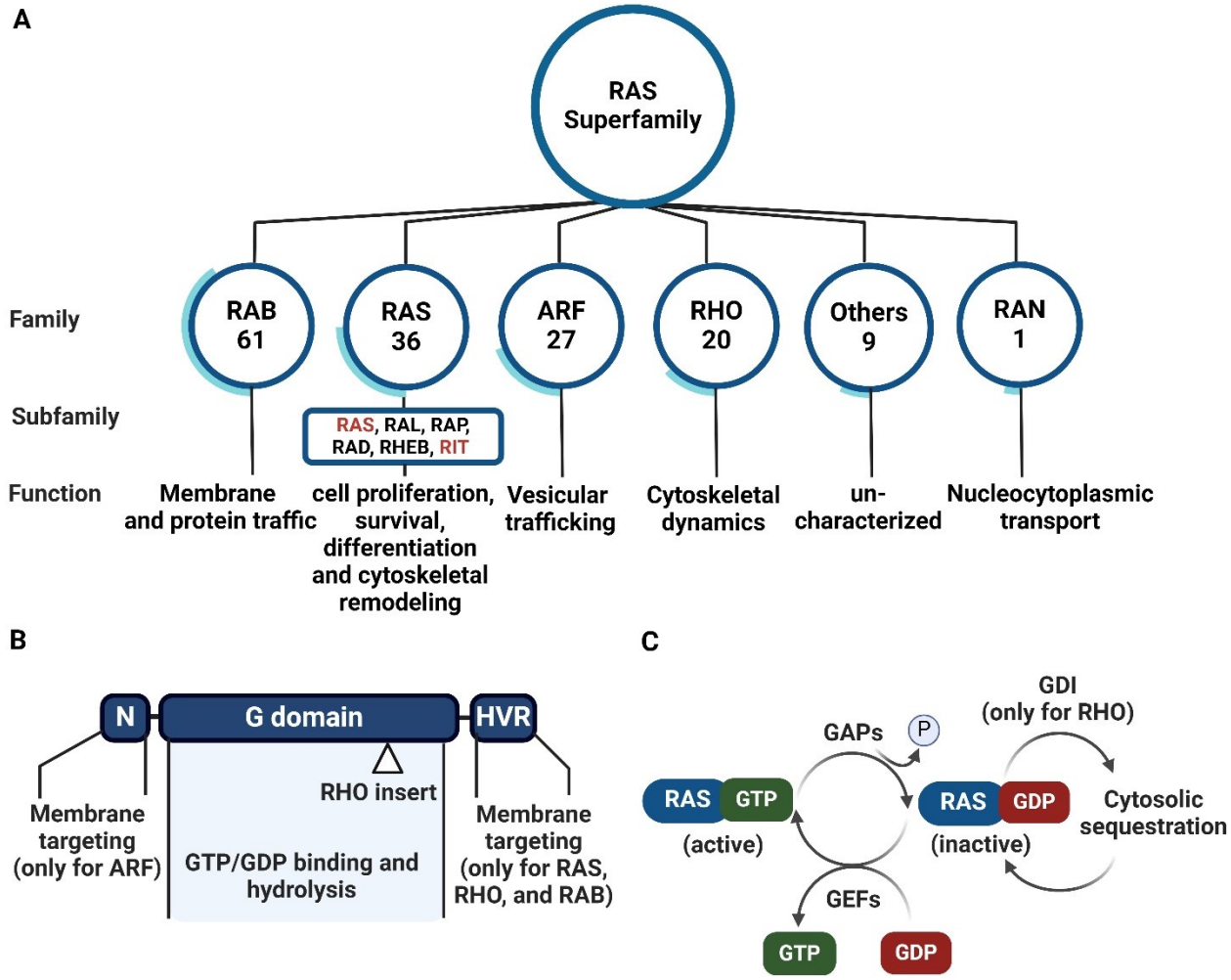

Figure 6. Structural and functional aspects of RAS superfamily proteins. (A) The pie charts depict the distribution of the 154 members across different subfamilies within the RAS superfamily, including RAB, RAS, ARF, RHO, RAN, and others. (B) The schematic representation of domain organization highlights the N-terminal region, G domain, and C-terminal HVR (Hypervariable Region). The N-terminal region is crucial for ARF family membrane binding, while the HVR is essential for the membrane localization of RAS, RHO, and RAB families, relying mostly on modifications like prenylation, myristoylation, and palmitoylation. The G domain is responsible for GTP/GDP binding and hydrolysis. The G domain features a unique "Rho insert" sequence in RHO proteins. (C) The nucleotide exchange activity involves the roles of GAP (GTPase-Activating Proteins) and GEF (Guanine nucleotide Exchange Factors) in regulating the active and inactive states of these GTPases. Additionally, GDIs (Guanine nucleotide Dissociation Inhibitors) specifically regulate RHO GTPases by rendering proteins in inactive state and controlling their subcellular localization. Image developed with BioRender (https://biorender.com/).

RAS family consists of six subfamilies: RAS, RAL (RAS-Like), RAP (RAS-Proximate or RAS-Related Protein), RAD (RAS Associated with Diabetes), RHEB (RAS Homolog Enriched in Brain), and RIT (RIC-related gene expressed Throughout the organism or RAS-like protein in many Tissues) [39] (Figure 6A). Within the RIT subfamily, there are 4 members of RIT1, RIT2, RIN (RAS-like protein in Neurons), and RIC (RAS-related protein which Interacted with Calmodulin) specifically involved in neuronal differentiation and survival [85]. Among these, RIT1 (RAS-like without CAAX 1) was identified over two decades ago [91].

RIT1 has three isoforms, each with a distinct N-terminal domain (Figure 7A). The function and biochemical properties of the N-terminal extensions of RIT1 have not yet been assessed, but they could potentially lead to different interacting partners [92]. The G-domain of RIT1 shares approximately 51% sequence identity with members of the RAS subfamily (particularly HRAS (Harvey Rat Sarcoma virus), NRAS (Neuroblastoma RAS viral oncogene homolog), and KRAS (Kirsten Rat Sarcoma virus)) composed of α1-α5 helices, β1-β6 sheets as well as, switch I and switch II, effector binding sites, and a set of highly conserved G box guanine nucleotide-binding elements (G1–G5) (Figure 7B) [89]. Yet, it harbors key structural differences that likely influence its mode of interaction with effector and regulatory proteins. The RIT1 G-domain, similar to other RAS superfamily members, is involved in intrinsic GTP binding and activates RIT1 by inducing a conformational change in the flexible effector binding interface consisting of switch I and switch II. However, the slow intrinsic GTP/GDP exchange rate ($7.8 \pm 0.7 \times 10^{-2}$ min^{-1}), which is about four times faster than HRAS [93], suggests that RIT1 exchange may be controlled by GEFs *in vivo*, even though they have not yet been discovered. Additionally, the intrinsic GTPase activity of RIT1 mediates the hydrolysis of GTP and the release of γ-phosphate returns switch I and switch II to their inactive ground-state conformation. Similarly, the slow intrinsic hydrolysis rate ($8.8 \pm 1.3 \times 10^{-3}$ min^{-1}) [93] indicates potential regulation by GAPs. However, the specific GEFs and GAPs that regulate RIT1's activity remain to be elucidated. It is worth mentioning that pathogenic mutations in the RIT1 gene mainly occur in the G-domain, particularly around the switch II region modulating their nucleotide/effector binding [92, 94]. Another distinctive feature of RIT1 is its HVR, which lacks lipidation. This contrasts with other RAS proteins, where lipidation typically aids in membrane anchorage. Instead, RIT1's HVR contains clusters of positively charged amino acids and hydrophobic residues (Figure 7B) that promote plasma membrane association through electrostatic interactions with negatively charged phospholipids [95].

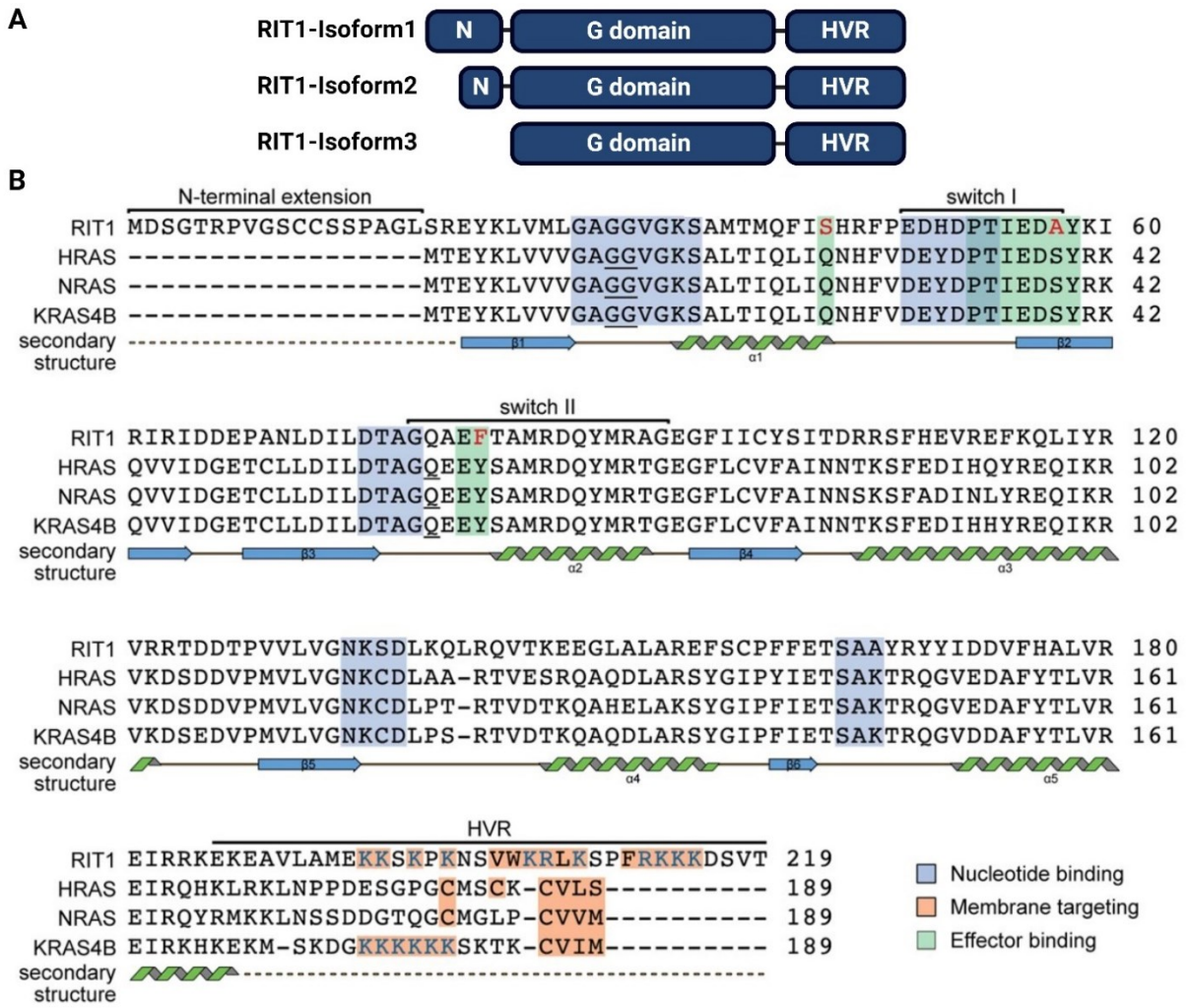

Figure 7. Overview of RIT1 isoforms and structure. (A) Schematic representation of the three isoforms of RIT, each featuring distinct N-terminal domains. This figure was generated using BioRender (https://biorender.com/). (B) Alignment of the amino acid sequences of RIT1 (isoform 2), NRAS, HRAS, and KRAS (isoform 4B) is presented, with different amino acids highlighted for their roles in nucleotide binding (blue), effector binding (green), and membrane targeting (orange). This figure is adapted from Castel, P., & McCormick, F. et al. (2020) [92].

To date, the key signaling outcomes of activated RIT1 remain poorly defined due to insufficient consensus on its principal signaling pathways and downstream effects. This might be because of the cell-context behavior of RIT1 or the lack of a multidimensional proteomic approach to fully explore the signaling networks activated by RIT1. The functional impact of wild-type RIT1 is often underexplored, with most studies focusing on pathogenic mutations that may lead to neomorphic activities. Studies have suggested that RIT1 involvement in p38 MAPK, AKT, and RAF/MEK/ERK signaling (Figure 8A) [92, 96-98]. Further study on role of RIT1 in activating AKT in response to ROS (Reactive Oxygen Species) through the p38 pathway revealed that this activation is mediated through mTORC2, rather than mTORC1 [99]. Moreover, previous studies have demonstrated that RIT1 preferentially interacts with both BRAF and CRAF and can activate ERK in a BRAF-dependent manner. This highlights its crucial role in modulating the MAPK signaling pathway [100]. Additionally, RIT1 interaction with RGL3 (Ral Guanine nucleotide dissociation stimulator-Like 3/Ral GEF-like 3), a regulator of the RAL GTP-binding proteins, has been observed and

suggested to act as its downstream effector [101]. In terms of cytoskeletal dynamics, RIT1 interacts with Par6 (Partitioning defective 6), PAK (P21-Activating Kinases), RAC, and CDC42, linking it to actin remodeling processes [102, 103]. RIT1's signaling is further modulated by LZTR1 (Leucine-Zipper-like Transcriptional Regulator 1), which negatively regulates RIT1 through ubiquitination and proteasomal degradation (Figure 8A) [104]. Overall, RIT1 is a multifunctional protein that integrates diverse signaling pathways, profoundly impacting cellular behavior and responses in various physiological and pathological contexts.

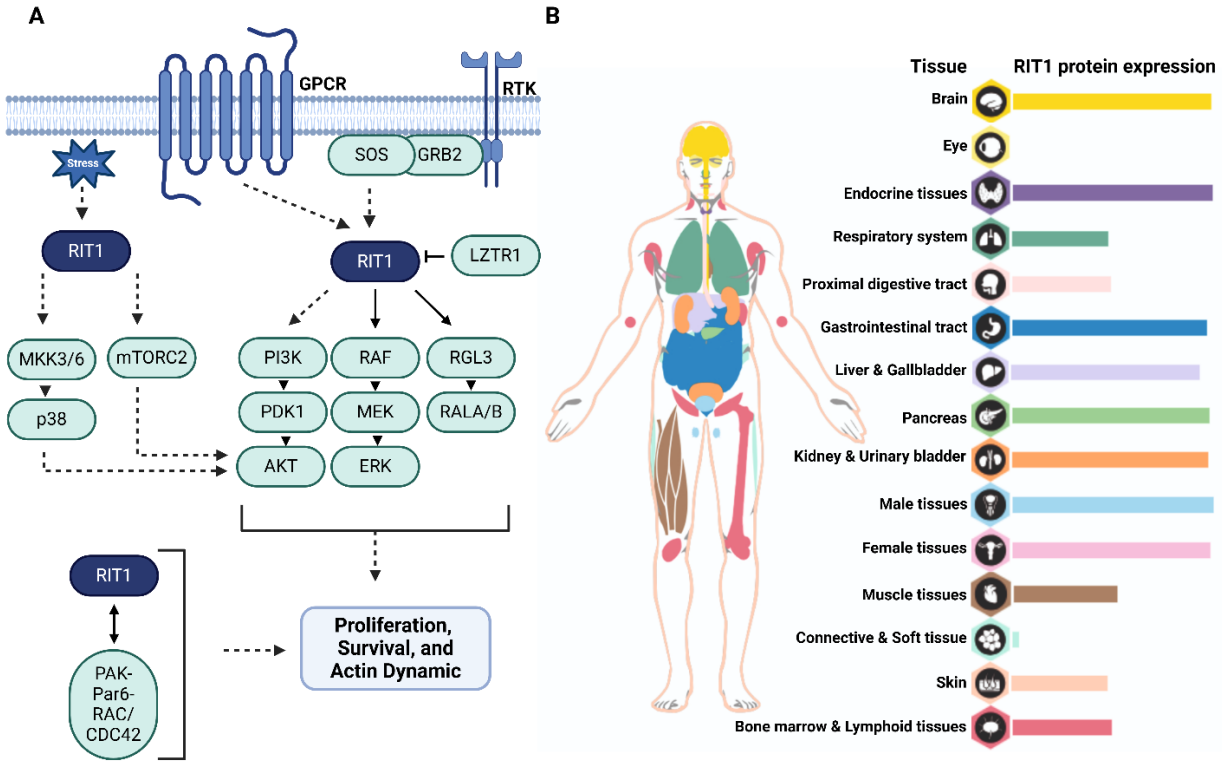

Figure 8. Multifaceted signaling pathways and tissue expression of RIT1. (A) The diagram depicts the complex signaling pathways and molecular interactions of activated RIT1. RIT1 participates in p38 MAPK, AKT, and RAF/MEK/ERK signaling pathways, demonstrating its role in various cellular processes. Additionally, RIT1 interacts with RGL3, as well as with Par6, PAK, RAC, and CDC42, implicating it in actin remodeling. LZTR1 modulates RIT1 activity by promoting its ubiquitination and subsequent degradation. Illustration produced using BioRender (https://biorender.com/). This figure is adapted from Castel, P., & McCormick, F. et al. (2020) [92]. (B) Anatomogram showcasing the expression levels of RIT1 protein across different human tissues, illustrating its varied presence and potential functional diversity in the body (expression level data and figure obtained from the Human Protein Atlas database).

RIT1 is mostly described in neural tissue regulating proliferation, differentiation, and survival [96]. As indicated in Figure 8B, RIT1 protein is widely expressed across various tissues, with particularly high levels in the brain, endocrine system, gastrointestinal tract, liver, gallbladder, pancreas, kidneys, urinary bladder, and both male/female reproductive tissues. Furthermore, there are moderate levels of RIT1 expression in the respiratory system, digestive tract, muscle, skin, bone marrow, and lymphatic tissue (data obtained from the Human Protein Atlas database). In this direction, recent clinical findings suggest a significant role of RIT1 in various tissues, with implications in conditions such as NS and cancer [92, 94]. For instance, the high birth weight, lymphatic abnormalities, and cardiovascular defects in the NS are all representations of the impact

of RIT1 mutations on the development and function of related tissues [92, 105, 106]. Moreover, RIT1 abnormalities, such as activating mutations and gene amplifications, are present in myeloid neoplasms and are notably common in CMML (Chronic Myelomonocytic Leukemia) [107]. Thus, understanding the distinct biological and biochemical roles of RIT1 mutants in various tissues could provide valuable insights into the potential roles of wild-type RIT1 and its broader implications for therapeutic targeting.

1.1.6.3 RAF Family Kinases: Spotlight on CRAF Activity

The RAF family of kinases, comprising ARAF, BRAF, and CRAF/RAF1, is crucial for connecting upstream signals to downstream responses within the MAPK signaling pathway. The first member of the RAF family was identified in 1983 with the discovery of the viral oncogene v-RAF from the transforming murine retrovirus 3611-MSV [108]. Soon after, the cellular homolog CRAF was discovered [109], followed by the identification of its paralogues ARAF and BRAF [110, 111]. They function downstream of RAS proteins. When activated by upstream signals, active and membrane-localized RAS binds to RAF kinases, promoting their homo-/hetro-dimerization and activating them through conformational changes, leading to their recruitment to the membrane. This interaction greatly enhances the kinase activity of RAFs, allowing them to phosphorylate and activate MEK proteins, which subsequently propagate the signaling cascade and ultimately activate ERK [112] (Figure 9A).

The RAF family kinases share three conserved regions (CRs) that play critical roles in their function (Figure 9B). CR1 contains the RAS-binding domain (RBD) and a cysteine-rich domain (CRD). The RBD is essential for interacting with active RAS proteins, featuring five β-sheets and several α-helices that allow it to bind the switch I region (also known as the effector loop) of RAS, thereby promoting RAF activation. Additionally, the RBD can participate in membrane association. The second domain in CR1, CRD, interacts with membrane lipids and enhances RAS/RBD affinity at the membrane, leading to stabilizing the RAS-RAF complex and facilitating RAF activation. CR2 serves as a serine/threonine-rich phosphorylation site, acting mainly to negatively regulate RAF activity through multi-phosphorylation events and 14-3-3 binding that regulates RAF kinase activation [37]. CR3, located at the C-terminus, contains a kinase domain adjacent to an acidic N-terminus (NTA) and a regulatory C-terminus. The NTA motif in RAF proteins undergoes phosphorylation and plays a crucial role in regulating RAF activation and dimerization-driven transactivation [113]. The catalytic kinase domain is characterized by two lobes that open and close to bind ATP (Adenosine Triphosphate) and substrates. In its open state, the small lobe, characterized by an antiparallel β-sheet structure, binds and positions ATP. In its closed state, the α-helical large lobe interacts with protein substrates, such as the ubiquitously expressed MEK1/2 [37]. Moreover, the regulatory C-terminus contains a secondary 14-3-3 binding site which promotes dimerization [113].

Despite high conservation among RAF paralogues, their kinase activities differ, with BRAF exhibiting the highest activity for MEK activation, followed by CRAF and ARAF. One reason is the different regulatory mechanisms in each paralog. For example, the NTA motif directly influences the degree of autoinhibition relief, dimerization efficiency, and overall kinase activity, leading to the differential activities observed among the RAF family members. In BRAF, the NTA motif's SSDD sequence includes aspartic acids that provide an initial negative charge, facilitating neighboring serine phosphorylation and resulting in constitutive phosphorylation. This persistent negative charge more effectively relieves autoinhibition, leading to a higher basal kinase activity

for BRAF compared to the other RAF isoforms. Moreover, the phosphorylation status of the NTA motif directly impacts transactivation, making BRAF the most potent activator within RAF dimers, significantly boosting its activity. CRAF, on the other hand, has an NTA motif with an SSYY sequence, requiring phosphorylation of both serine and tyrosine residues, a process regulated by SRC family kinases. This dual phosphorylation is more complex and tightly regulated, contributing to a lower intrinsic kinase activity compared to BRAF. ARAF, which is quite similar to CRAF (SSGY), is also targeted by SRC family kinases for phosphorylation at specific tyrosine residues, contributing to its unique regulatory properties [113].

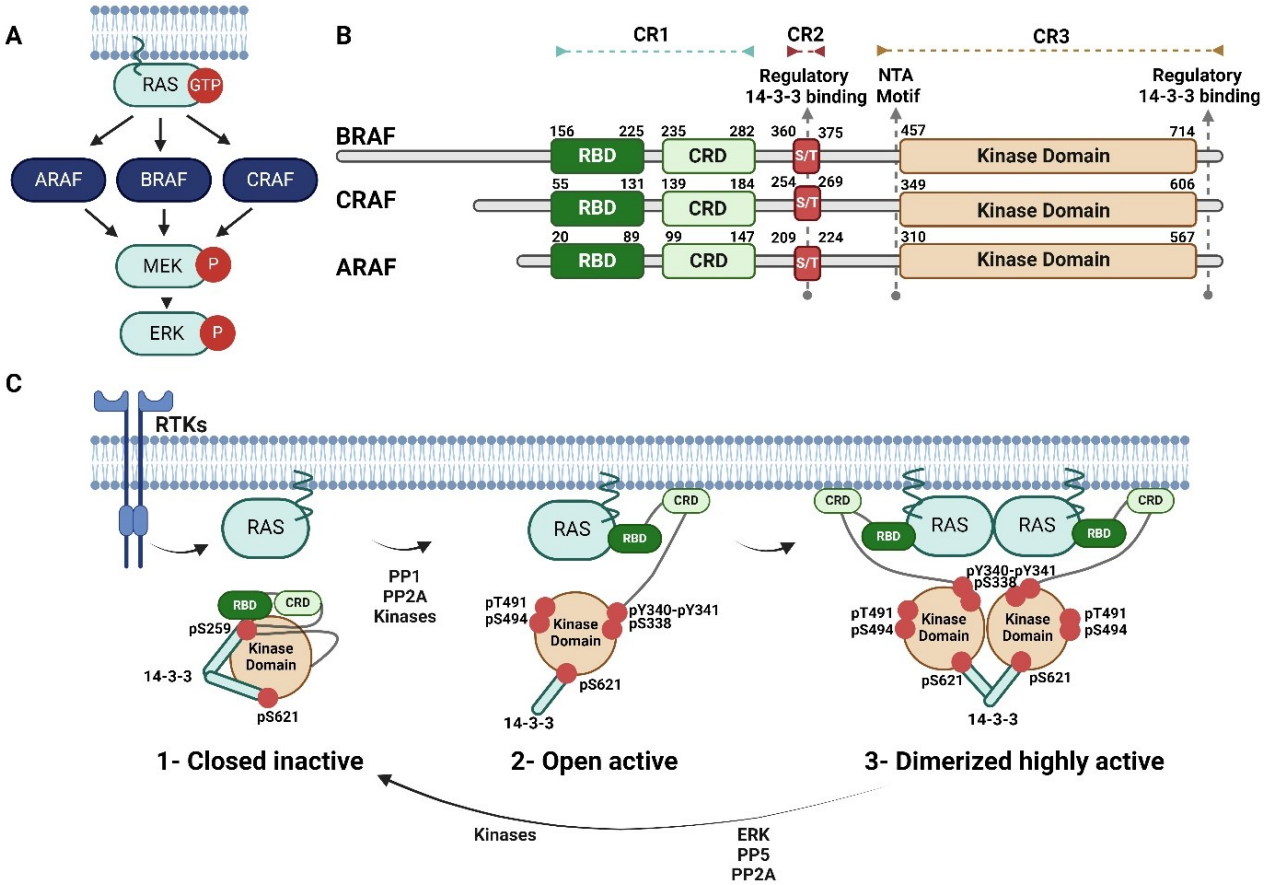

Figure 9. Overview of RAF family kinase. (A) The role of RAF kinases (ARAF, BRAF, CRAF/RAF1) in the MAPK signaling pathway, highlighting their activation by RAS and subsequent effects on MEK/ERK activation. (B) RAF kinases domain organization, including the conserved regions (CR1-3). (C) Activation and deactivation processes of CRAF kinase. This figure was generated using BioRender (https://biorender.com/).

RAF family kinases are activated and inactivated through a multistep process that involves de/phosphorylation events, protein-protein interactions, and conformational reorganization. While there are common themes in these processes, they involve distinct regulatory proteins and phosphorylation sites that specifically regulate RAF kinase activity. In particular, the diagram in Figure 9C illustrates the key steps involved in the activation and deactivation of CRAF. Initially, in unstimulated quiescent cells, CRAF is kept in an inactive state through the binding of 14-3-3 proteins and phosphorylation at sites such as S259 (within CR2) and S621 (within the C-terminus of CR3). Upon signal arrival and RAS activation, RAS binding to the CRAF-RBD domain mediates membrane recruitment, and subsequent dephosphorylation of S259 by PP1/PP2A (Protein

Phosphatases1 and 2A) allows for 14-3-3 release and further membrane recruitment via the CRD domain. Subsequent phosphorylation of key residues in the NTA motif of CR3, S338 and Y340-Y341 (^{338}SSYY^{341}), leads to activation and promotes dimerization and allosteric transactivation [114]. Moreover, other phosphorylations within the activation loop of the kinase domain (T491 and S494) further assist CRAF kinase activity toward downstream MEK [113, 115]. Inactivation is mediated through negative feedback regulation involving ERK phosphorylation and dephosphorylation of activating sites by phosphatases PP5 and PP2A. This process is further complemented by the rephosphorylation of S259, which facilitates the transition back to a closed, inactive state [114].

Besides the canonical RAF-MEK-ERK pathway for RAF family kinases, CRAF can also contribute to another downstream signaling, as illustrated in Figure 10A. CRAF has been identified to target various other proteins, including cell cycle regulators (e.g., Rb (Retinoblastoma protein) [116], CDC25 [117], AuroraA-PLK1 (Polo-Like Kinase 1) [118], CHK2 (Checkpoint Kinase 2) [119]), apoptosis modulators (e.g., BCL2 (B-Cell Leukemia/Lymphoma 2) [120], ASK1 (Apoptosis Signal-regulating Kinase 1) [121], MST2/STK3 (Mammalian STE20-like kinase 2/Serine Threonine-protein Kinase 3) [122], BAD [123], eEF1A1/2 (elongation Factor 1A 1/2)[124]), and cytoskeletal components (e.g., ROK-α/ROCK-II (RHO-associated protein Kinase 2) [125], NF-κB [126], and DMPK (Myotonic Dystrophy Protein Kinase) [127]). Importantly, dysregulation or mutations in CRAF can disrupt these pathways, contributing to the pathogenesis of various diseases. For instance, genomic alterations in CRAF contribute to various cancers, including colorectal carcinoma (intron 9 mutations), acute myeloid Leukemia (exon 12 mutations), SCLC (Small Cell Lung Cancer; chromosomal rearrangements), and squamous cell carcinoma (4bp deletion in exon 17). Additional involvement in Noonan and Leopard's syndromes caused by CRAF missense mutation has been observed [128]. It is also affected by gene amplification and elevated expression in NSCLC (Non-Small Cell Lung Cancer), glioblastoma, osteosarcoma, breast cancer, ependymoma, hepatocellular carcinoma, and mantle cell lymphoma. Additionally, increased activation of CRAF is observed in cancers like pancreatic carcinoma (reviewed in [129]).

Based on the involvement of CRAF in diverse signaling networks and its pivotal role in health and disease, understanding its regulatory pathways is crucial for developing effective treatments that manipulate cellular signaling pathways. CRAF can be regulated at various levels (Figure 10B), including epigenetic modifications. miRNAs, such as miR-15a/b, miR-16, and miR-195, modulate CRAF gene expression by interacting with the 3′-UTR (3′ Untranslated Regions), leading to mRNA degradation or inhibition of translation, and have been shown to regulate CRAF [130]. Additionally, transcriptional regulation by transcription factors and activators, such as AP-2α (Activating enhancer binding Protein 2 alpha), plays pivotal roles in regulating the CRAF gene by modulating its transcription. [131]. Another level of regulation beyond transcription involves post-translational modifications (de/phosphorylation, de/ubiquitination, methylation, O-GlcNAcylation) and/or in/direct PPIs that control its stability, structural conformation, and activity [132]. For example, RanBPM (Ran Binding Protein M), a component of the CTLH (C-Terminal to Lissencephaly-1 Homology motif) complex, interacts directly with CRAF through its C-terminal domain, facilitating CRAF ubiquitination and subsequent degradation [133]. Moreover, CRAF methylation mediated by PRMT5 (Protein Arginine Methyltransferase) leads to the degradation of activated CRAF [134]. PRMT6 also inhibits the binding of CRAF to RAS by binding and methylating CRAF at residue R100 [135] On the other hand, USP13 (Ubiquitin-Specific Protease 13) deubiquitinates and

maintains CRAF stability [136]. Similarly, O-GlcNAcylation of CRAF stabilizes CRAF by suppressing its ubiquitination in EMT (Epithelial-Mesenchymal Transition) promotion [137]. In addition, CRAF activity is modulated by various proteins such as KSR1/2 (Kinase Suppressor of RAS 1/2), arrestins-2, MRAS (Muscle RAS oncogene homolog)-SHOC2-PP1c, PHB1 (Prohibitin 1), 14-3-3, HSP90-CDC37 (Heat Shock Protein 90-Cell Division Cycle 37), PP5, CNK1 (Connector enhancer of Kinase suppressor of RAS 1)-SRC, PAK1, AKT, PLK1, PDCD6 (Programmed Cell Death Protein 6), RUVBL1 (RuvB-Like 1), PP2A, RKIP (RAF Kinase Inhibitory Protein), BRAF, PKA (Protein Kinase A), PKCα (Protein Kinase C alpha type), SPRY2 (Sprouty 2), PHLPP1/2 (PH domain and Leucine-rich repeat Protein Phosphatases 1/2), RKTG (RAF Kinase Trapping to Golgi), and RAP1 (Figure 10B).

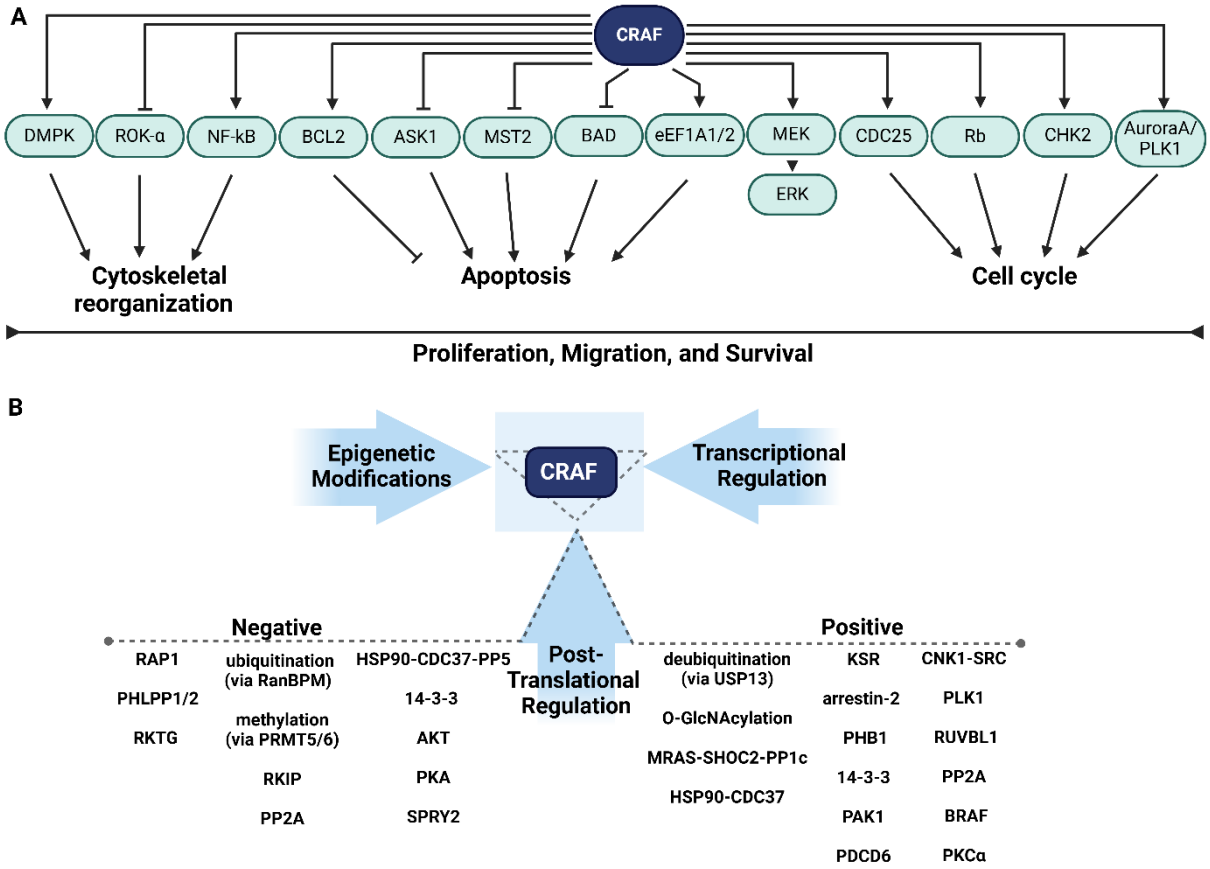

Figure 10. CRAF downstream signaling and regulation. (A) Diverse roles beyond the canonical RAF-MEK-ERK pathway include targeting cell cycle regulators (e.g., Rb, CDC25, AuroraA-PLK1, CHK2), apoptosis modulators (e.g., BCL2, ASK1, MST2, BAD, eEF1A1/2), and cytoskeletal components (e.g., ROK-α, NF-Kb, and DMPK). (B) CRAF regulation involves epigenetic modification (mediated by miRNA interaction), transcriptional modulation, post-translational modifications (e.g., phosphorylation, de/ubiquitination, methylation) and/or protein-protein interactions, which can positively or negatively affect its stability, conformation, and activity. Figure illustration created with BioRender's resources (https://biorender.com/).

Research has shown that KSR dimerizes with CRAF and enhances the catalytic activity of CRAF within the ERK pathway under metabolic stress conditions [138]. Furthermore, the interaction between CRAF-RBD and arrestin-2, which scaffolds ERK2, MEK1, and CRAF, has been identified and proposed to aid in releasing the kinase domain, thereby facilitating the phosphorylation of MEK1 [139]. In another example, the MRAS-SHOC2-PP1c complex stimulates CRAF kinase

activity by dephosphorylating the inhibitory S259 site of CRAF [140]. Moreover, PHB1, a key member of the SPFH (Stomatin/Prohibitin/Flotillin/Hflkc) domain family; a pleiotropic membrane protein), directly interacts with CRAF and is essential for displacing 14-3-3 from its binding site at S259. This displacement is crucial for the interaction between RAS and CRAF at the plasma membrane. Loss of PHB1 results in CRAF not localizing to membranes, leading to increased S259 phosphorylation and 14-3-3 binding in the cytosol, thereby inactivating CRAF kinase [141]. Another activator complex involves CNK1, which mediates SRC-dependent tyrosine phosphorylation and activation of CRAF by forming a trimeric complex with preactivated CRAF and activated SRC, facilitating cross-talk between SRC and CRAF and being essential for its full activation and subsequent ERK activation [142]. Moreover, PAK1 is a key physiological mediator of CRAF activation by directly binding and phosphorylating CARF at S338, a pivotal step in the activation process [143]. Another potent activator of CRAF is PLK1 which associates with CRAF and activates it by directly phosphorylating CRAF at S338 and S339, but not at S621 [144]. Another study proposes that PDCD6 interacts with CRAF upon binding Ca^{2+}, forming a stable complex that activates the RAF/MEK/ERK pathway and promotes colorectal cancer growth [145]. The other novel CRAF binding protein, RUVBL1, a member of the AAA+ superfamily of ATPases, activates the RAF/MEK/ERK pathway by preventing phosphorylation of CRAF at S259, thereby promoting lung tumor progression [146]. Interestingly, BRAF can act as an allosteric activator of CRAF in its dimeric state. With the NTA motif of BRAF being constitutively phosphorylated, BRAF initially functions to activate CRAF [147]. Additionally, PKCα directly phosphorylates and activates CRAF at several sites, including S499. This phosphorylation is crucial for CRAF activation by PKCα and the transformation of NIH3T3 cells [148].

The findings reveal that AKT interacts with both the C-terminal and N-terminal regions of CRAF, thereby inhibiting CRAF activity via direct phosphorylation of CRAF-S259, thereby highlighting significant crosstalk between the RAF-MEK-ERK and PI3K–AKT signaling pathways as well [149]. Moreover, upon PKA activation, it phosphorylates CRAF and promotes the recruitment of 14-3-3 proteins, which prevents CRAF from being recruited to the plasma membrane and blocks its activation [150]. The RKIP is also shown to inhibit CRAF phosphorylation at residues S338 and Y340-Y341 and its ability to phosphorylate its substrate MEK. This inhibition occurs through the attachment of RKIP to the N-terminal region of CRAF, stabilized by its strong interaction with high-affinity binding sites at the terminal ends of CRAF [151-154]. Additionally, data indicate that SPRY2 functions as a negative regulator downstream of BCR stimulation, playing a crucial role in the attenuation of RAS-MAPK signaling by interacting with CRAF [155]. PHLPP1 and 2 were found to dephosphorylate CRAF at S338, inhibiting its kinase activity and thereby regulating tumor progression and invasive and migratory activities of colorectal cancer [156]. Furthermore, RKTG is proposed to control the spatial distribution of CRAF by sequestering it to the Golgi, which modifies the interaction of CRAF with RAS and MEK1 and subsequently inhibits ERK signaling [157]. In addition, RAP1 is found to inhibit MAPK signaling by interacting with the CRD domain of CRAF, reducing the number of oncogenic RAS clusters, and thereby suppressing CRAF activation. Within these nanoclusters, RAP1 competes with RAS for binding to CRAF, resulting in decreased CRAF activation [158].

The 14-3-3 chaperon protein can have a dual role in binding to specific phosphorylation sites of CRAF and enhancing its dimerization in an active state (Figure 9C) [159] or inducing the formation of the autoinhibitory closed conformation in an inactive state [160]. Mitra et al. showed the role of

HSP90 in interacting with CRAF and aiding in the phosphorylation of S621 on CRAF and protecting the kinase from degradation, before RAS interaction, with co-chaperone CDC37 supporting this phosphorylation process [161]. However, other data indicate the involvement of HSP90 and CDC37 in the CARF inactivation process as part of an HSP90-CDC37-CRAF complex. The data reveals how HSP90 both activates and scaffolds PP5's association with the bound CRAF, leading to the dephosphorylation of phosphorylation sites (pS338 and pS621) adjacent to the kinase domain [162]. As observed in Figure 9C, PP2A holoenzymes establish stable interactions with CRAF and directly dephosphorylate it at S259, leading to its activation [163]. In addition, PP2A dephosphorylates attenuated CRAF on p(S/T)P consensus motifs, making it essential for both CRAF activation and recycling [164].

1.1.7 Pathological Impact of RAS-MAPK and PI3K-AKT Pathways: Implications for Arteriovenous Malformation (AVM)

Arteriovenous malformation (AVM) is a disorder characterized by an abnormal tangle of blood vessels connecting arteries and veins, bypassing the capillary system. This condition can occur in various parts of the body, but is most commonly found in the brain and spinal cord [165]. AVMs can lead to serious health issues due to the high-pressure blood flow through these abnormal vessels, which may cause them to rupture. Symptoms of AVM vary depending on their location and size but can include headaches, seizures, neurological deficits, and, in severe cases, hemorrhagic stroke due to vessel rupture [166]. AVMs can be asymptomatic and discovered incidentally for other reasons [167]. While most AVMs are sporadic and occur without a family history [168], some can be inherited, particularly in syndromes like HHT (Hereditary Hemorrhagic Telangiectasia), CM-AVM (Capillary Malformation AVM), and PWS (Parkes-Weber Syndrome) [169].

Genetic abnormalities associated with AVM are often linked to disruptions in key signaling pathways. Notably, mutations in the VEGF (Vascular Endothelial Growth Factor) signaling pathway plays a significant role in the development of AVMs. VEGF receptors belong to the RTK and are a critical regulator of blood vessel formation by activation of MAPK and PI3K-AKT-mTOR leading to proliferation and differentiation. The overexpression or activating mutations of VEGF pathway components can lead to abnormal angiogenesis features and is a hallmark of AVM [170, 171]. For instance, studies have identified somatic mutations in the KRAS and BRAF genes activating the MAPK-ERK signaling in brain and spinal cord AVMs (Figure 11) [172, 173]. Moreover, functionally significant somatic mutations in the MEK1 gene found in extracranial AVM samples underscore the crucial role of the overactive RAS-MAPK signaling pathway in the development of these vascular malformations (Figure 11) [174]. Similarly, another paper identified a somatic HRAS mutation causing extracranial AVM in a patient with a facial AVM, resulting in higher levels of phosphorylated ERK (pERK) [175].

In addition, increased PI3K activity contributes to accelerating AVM development by intensifying angiogenesis in HHT. This is supported by findings showing that loss-of-function mutations in the ACVRL1/ALK1 (Activin A Receptor type II-Like 1/Activin receptor-Like Kinase 1) and ENG (Endoglin) genes, which is involved BMP9/10 (Bone Morphogenetic Protein 9/10)-ENG-ALK1-SMAD1/5/8-SMAD4 (Mothers Against Decapapentaplegic) pathway in regulating blood vessel development and homeostasis, hinder its ability to activate PTEN. By disrupting the negative regulatory function of PTEN, these mutations result in increased PI3K activity (Figure 11) [176,

177]. Moreover, RASA1 (RAS GTPase-Activating protein 1) encodes the p120 RAS-GAP protein, a GTPase-activating protein that negatively regulates RAS GTPases and the downstream MAPK pathway. There are many reports of inactivating RASA1 mutations detected in CM-AVM [178], with data showing that loss of RASA1 is probably due to the impaired ability of GAP to effectively regulate the RAS-MAPK signal transduction pathway [179, 180]. Interestingly, disease development requires somatic "second hit" inactivating mutations of RASA1 [181]. Moreover, the presence of somatic RASA1 mutations in patients with CM-AVM, even without germline RASA1 variants [182], suggests that RASA1 plays a role in both sporadic and hereditary cases. Notably, RASA1 can also be dysregulated by mutations in other genes. Researchers have identified EPHB4 (Ephrin type-B receptor 4) as a second gene that is mutated in patients with CM-AVM. They propose a mechanism whereby these mutations disrupt the EPHB4-RASA1 interaction, leading to dysregulation and constitutive activation of downstream RAS-MAPK signaling [183]. Moreover, experimental data strongly support a functional link between EPHB4, RASA1 and mTORC1 [184].

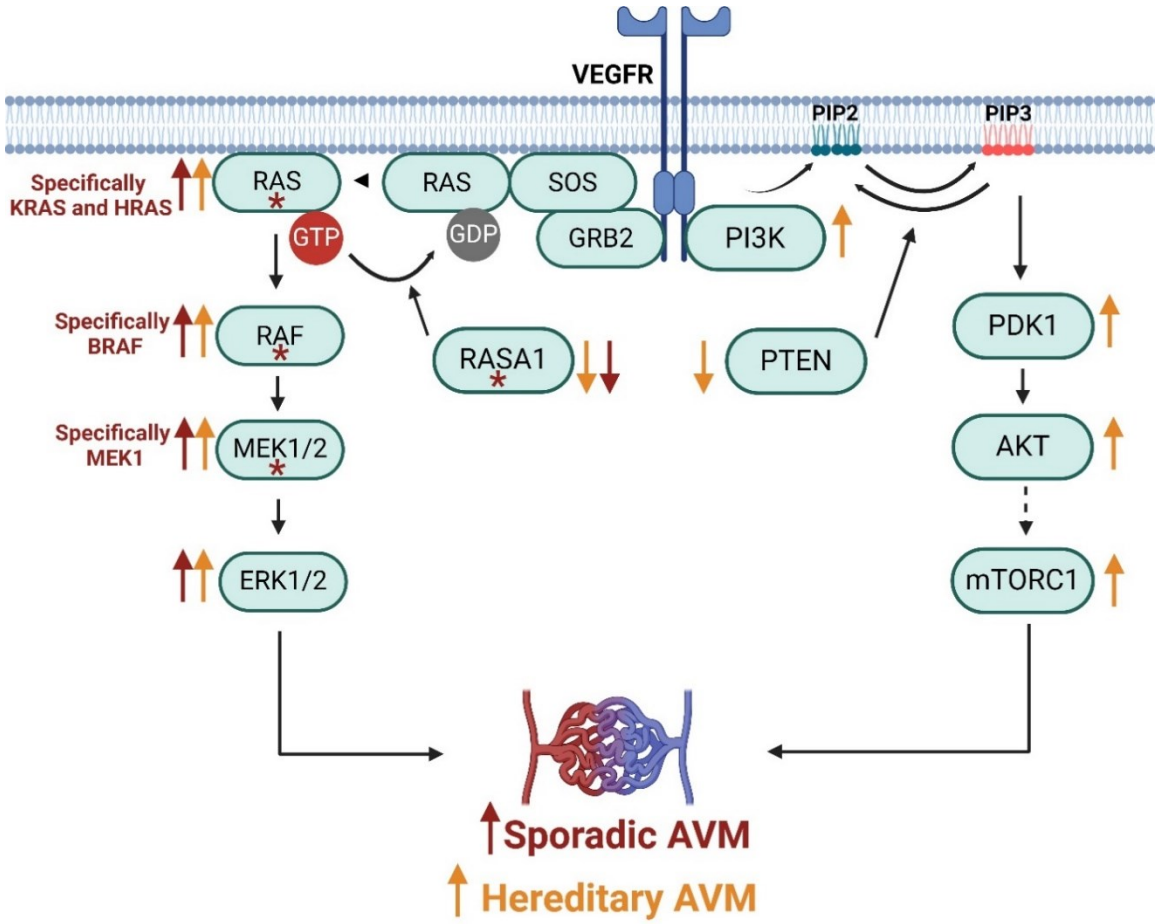

Figure 11. RAS-MAPK and PI3K-AKT pathways are involved in AVM development. Mechanisms involved in hereditary-related AVMs (indicated by orange arrows). Typically, ALK1 and ENG stimulate PTEN activity, leading to a reduction in PI3K signaling. However, HHT mutations in ALK1 or ENG reduce PTEN activity, leading to increased PI3K activity and, consequently, enhanced angiogenesis. In sporadic cases (indicated by red arrows), somatic activating mutations in genes such as KRAS, HRAS, BRAF, and MEK1 elevate the levels of pMEK and pERK, promoting the development of AVMs. Moreover, both somatic and hereditary RASA1 mutations can contribute to further dysregulation of the RAS-MAPK and PI3K-AKT pathways. Visualization prepared with BioRender software (https://biorender.com/).

In addition to the VEGF pathway, other signaling pathways have been implicated in the formation and maintenance of AVMs, including TGF-β/BMP and Notch signaling pathways. The TGF-β/BMP pathway is crucial for maintaining vascular homeostasis and structural integrity [185]. Mutations in genes associated with TGF-β signaling, such as ENG, ACVRL1/ALK1, and SMAD4, are linked to HHT, which is characterized by AVMs [170]. Moreover, Notch signaling is crucial for governing arteriovenous specification, which distinguishes arteries from veins. Dysregulation of Notch signaling has been associated with the abnormal development of blood vessels seen in AVMs [186]. The increasing identification of AVM-associated mutations underscores the critical need to study the underlying molecular pathways involved in AVMs, which is essential for developing targeted therapies that could improve management and outcomes for patients with this complex vascular disorder.

1.1.8 SIRTUIN Family: Exploring the Critical Roles of SIRT4 in Cell Signaling

The SIRTUIN (SIRT) family of NAD^+ (Nicotinamide Adenine Dinucleotide$^+$)-dependent enzymes comprises conserved proteins essential for regulating cellular metabolism, gene expression, stress responses, energy homeostasis, aging, DNA repair, and immune function [187]. They belong to class III of HDACs (Histone Deacetylases) and include seven homologous sirtuins in mammals (SIRT1 to SIRT7) [188], each with unique subcellular localizations and functions (Figure 12).

Central to all sirtuins is the conserved catalytic core domain, which is responsible for enzymatic activity, with deacetylation being their primary and most prevalent activity. Nevertheless, other paralogs possess other enzymatic activities. This core domain is composed of a large rossmann fold domain that binds NAD^+, and a smaller zinc-binding domain that helps stabilize the protein structure [189]. The highly homologous region in the middle of sirtuins is centered around a highly conserved histidine, which acts as a proton acceptor and is essential for enzymatic activity [190]. In addition to their core domain, sirtuins possess variable N- and C-terminal extensions that influence their susceptibility to post-translational modifications (such as phosphorylation) as well as contributing to substrate specificity and regulatory mechanisms by mediating protein interactions and directing sirtuins to various subcellular locations [187]. The retention signals of NLS (Nuclear Localization Signals) and MTS (Mitochondrial Targeting Sequences) within these terminal regions direct sirtuins to their specific cellular compartments [191]. SIRT1 is mainly found in the nucleus and cytoplasm; however, SIRT2 shuttles between these locations and is primarily situated in the cytoplasm. Furthermore, SIRT3 and SIRT5 are predominantly mitochondrial, although they can be found outside the mitochondria in the cytoplasm and nucleus. Similarly, SIRT4 is primarily located in the mitochondria, yet recent data indicate it also has a cytoplasmic presence. In contrast, SIRT6 and SIRT7 reside mainly in the nucleus [192, 193].

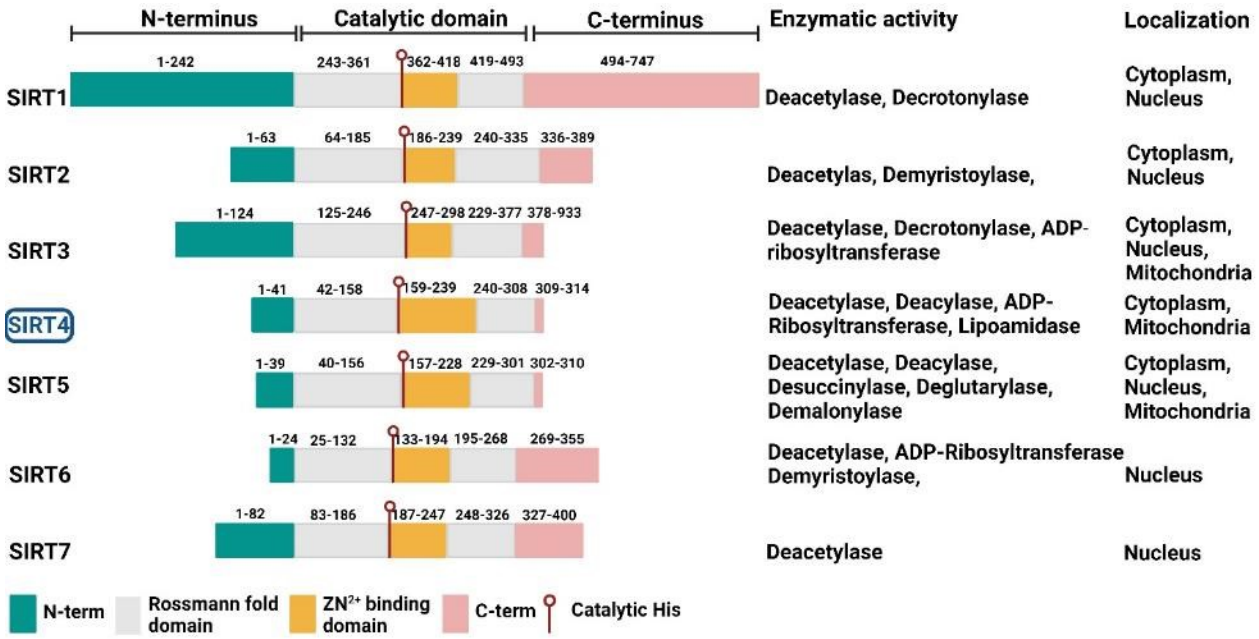

Figure 12. Domain structure, function, and subcellular localization of SIRT1-7. All sirtuins feature a conserved catalytic core, which includes a rossmann fold domain (gray), a Zn^{2+}-binding domain (orange), and a catalytic histidine (red arrow). Sirtuins also possess distinct N-terminal (green) and C-terminal (pink) regions that differ in length and sequence. The main enzymatic functions and subcellular localizations of each SIRT protein are depicted. The figure was designed with the help of BioRender's tools (https://biorender.com/).

SIRT4, one of the least studied members of the sirtuin family, is gaining attention as recent research has begun to elucidate its important biochemical roles. SIRT4 consists of 314 amino acids and possesses the MTS in its N-terminal region facilitating its translocation to the mitochondria [191]. The enzymatic functions of SIRT4 are activated by the cleavage of the protein at amino acid 28, which occurs during its import into mitochondria [192, 194]. Within mitochondria, SIRT4 plays a critical role in maintaining mitochondrial integrity and functions by regulating fusion-fission dynamics and mitophagy. SIRT4 inhibits mitophagy by promoting mitochondrial fusion and inhibiting fission. It stabilizes and enhances L-OPA1 (Large GTPases OPA1 (Optic Atrophy 1)) levels, increases fusion, and suppresses DRP1 (Dynamin-Related Protein 1) by inhibiting its ERK-mediated phosphorylation, reducing fission. Collectively, these effects inhibit mitophagy by decreasing the number of mitochondria-targeted for degradation [195, 196] (Figure 13).

Another mitochondrial role of SIRT4 is in cellular energy metabolism, which affects proliferation, insulin secretion, and fatty acid oxidation. SIRT4 ADP-ribosylates and inhibits GDH (Glutamate Dehydrogenase), an enzyme that converts glutamate to α-ketoglutarate, leading to ATP production and increased insulin secretion. Ultimately, SIRT4-mediated regulation of GDH limits amino acid metabolism and the TCA (Tricarboxylic Acid) cycle, which leads to the down-regulation of insulin secretion [197]. Similarly, IDE (Insulin-Degrading Enzyme) and ADP/ATP carrier protein ANT2 (ADP/ATP Translocase 2) are other substrate of SIRT4 and play a role in negatively regulating insulin secretion in response to glucose [198]. Additionally, by inhibiting PDH (Pyruvate Dehydrogenase), which converts pyruvate into acetyl-CoA, SIRT4 can affect the flux of metabolites into the TCA cycle [199]. In general, by inhibiting TCA cycle enzymes, SIRT4 can reduce energy metabolism, which in turn may lead to decreased cell proliferation. Interestingly, this anti-proliferative role of SIRT4 in inhibiting tumor growth explains why its expression is often

reduced in many cancer cells [200]. Moreover, SIRT4 regulates fatty acid metabolism in muscle and adipose tissue. When the body is in a fed state, SIRT4 reduces the activity of mitochondrial MCD (Malonyl-CoA Decarboxylase), leading to elevated levels of malonyl-CoA and consequently promoting fat synthesis and repressing fatty acid oxidation [201]. In addition, it is suggested that SIRT4 influences fatty acid metabolism by affecting the AMPK (AMP-Activated Protein Kinase)-SIRT1 pathway to decrease fatty acid oxidation capacity [202] and suppressing PPARα (Peroxisome Proliferator-Activated Receptor α) activity, which in turn lowers the expression of genes involved in fatty acid catabolism [203] (Figure 13).

SIRT4 can regulate stress conditions by controlling oxidative stress caused by ROS and maintaining genomic stability. ROS are by-products of oxidative metabolism, primarily from oxidative phosphorylation and various enzymatic reactions within the mitochondria. Moderate ROS levels are crucial for physiological processes like signaling and stress responses, but excessively high or low levels can be pathogenic and lead to dysfunction from drastic oxidative environment changes [198]. SIRT4 regulates mitochondrial ROS production by inhibiting the MnSOD (Manganese Superoxide Dismutase) binding to SIRT3. This inhibition increases MnSOD acetylation, reducing its activity, leading to higher ROS levels, increased oxidative stress, and promoting cardiac hypertrophy [204]. In addition, fatty acid oxidation is linked to mitochondrial ROS production, and although SIRT4 is expected to reduce ROS by decreasing fatty acid oxidation, in patients with nonalcoholic fatty liver disease, SIRT4 modulation reduces free fatty acids but paradoxically increases ROS production [205]. Moreover, decreased mitophagy leads to the accumulation of dysfunctional mitochondria and increased ROS production, as previously explained, associated with the stabilization and interaction of SIRT4 with L-OPA1 [206]. Conversely, a different study demonstrated that overexpressing SIRT4 could prevent apoptosis of podocytes induced by glucose through a mitochondrial mechanism. This protective effect was associated with an increase in mitochondrial membrane potential and a decrease in ROS production [207]. These findings indicate that the impact of SIRT4 on mitochondrial ROS levels is context-dependent. Additionally, DNA damage induces a DNA damage response (DDR) that assists in maintaining genomic integrity. DDR includes promoting cell cycle arrest through the phosphorylation of proteins such as CHK1, CHK2, and γ-H2AX (gamma H2A histone family member X) [208]. Another aspect of DDR involves metabolic responses, including the up-regulation of nucleotide synthesis pathways for DNA repair [209]. Furthermore, SIRT4 has been reported to play a role in DDR by assisting in metabolic responses through the inhibition of glutamine metabolism. This metabolic response plays a crucial role in managing cell cycle progression and sustaining genomic stability in response to DNA damage [210] (Figure 13).

SIRT4, traditionally known for its mitochondrial functions, also localizes to the cytosol where it dynamically associates with centrosomes, interacting with microtubule components and influencing cell cycle progression and likely microtubule dynamics [193]. Moreover, cytoplasmic SIRT4 regulates the Wnt/β-catenin pathway by deacetylating AXIN1 at K147, which activates the Wnt signaling pathway. This process decreases β-catenin degradation, allowing β-catenin to accumulate and enhance Wnt signaling [211]. In addition, SIRT4 acts as a tumor suppressor by deacetylating LATS1, thereby reinstating Hippo pathway activity and countering YAP-driven oncogenesis [212]. Other findings reveal that SIRT4 is involved in SNARE (Soluble N-ethylmaleimide-sensitive factor Activating protein Receptor) complex formation by deacetylating SCFD1 (Sec1 Family Domain containing 1) at K126 and K515. This deacetylation enhances

SNARE complex assembly, which facilitates the fusion of autophagosomes with lysosomes [213] (Figure 13). Nevertheless, the full spectrum of cytosolic SIRT4 functions remains largely unknown.

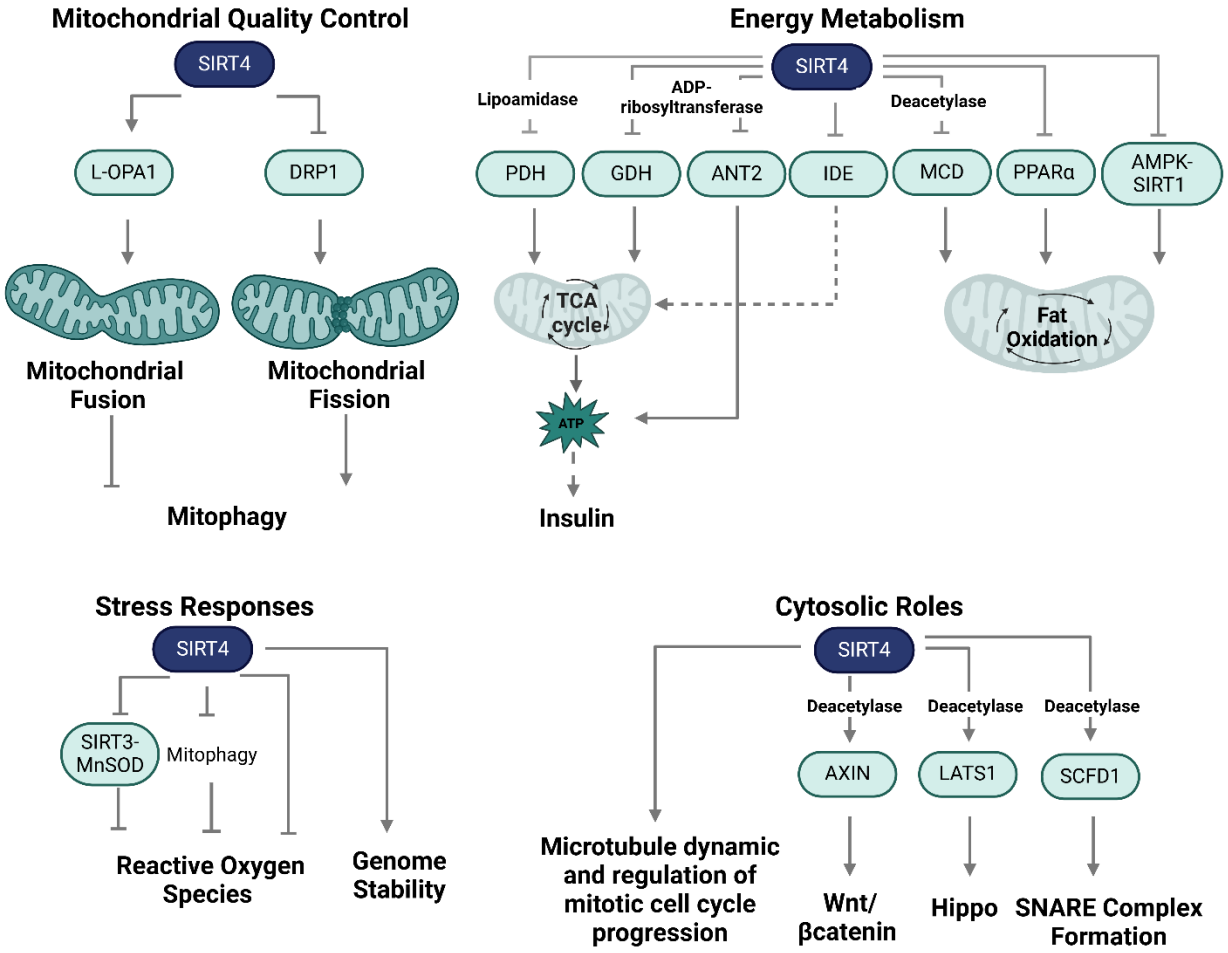

Figure 13. Functional roles of SIRT4. Within the mitochondria, it plays a critical role in regulating mitochondrial integrity and function (impact on mitochondria fusion-fission and mitophagy), energy metabolism (affects proliferation, insulin secretion, and fatty acid oxidation), and stress responses (controlling oxidative stress and genome stability) through its activity. SIRT4, traditionally known for its mitochondrial functions, also localizes to the cytosol where it regulates microtubule dynamics and mitotic cell cycle progression, Wnt/β-catenin and Hippo signaling pathways, and the formation of the SNARE complex crucial for autophagosome-lysosome fusion. The figure was created using BioRender software (https://biorender.com/).

2 Aims and Objectives

This thesis explores the intricate mechanisms of protein interactions and cellular signaling, emphasizing their implications for human diseases and potential therapeutic strategies. It is organized into eight chapters, each addressing distinct but interconnected aspects of protein function and disease pathology.

Proteins are composed of various functional modules, such as domains and motifs, that facilitate complex and dynamic protein-protein and protein-lipid interactions, forming intricate signaling pathways. This study focuses on the selective nature of PPIs, specifically through the SH3 domain. It investigates contribution of SH3 domains to the formation of protein complexes by interacting with PRMs and other non-canonical binding sites on partner proteins, analyzing their significance across human SH3-containing proteins and their involvement in human diseases like cancer and Alzheimer's (Chapter I). By conducting a phylogenetic analysis of human SH3 domain-containing proteins, the research classifies these domains functionally and examines their binding specificities towards PRMs. Experimental evaluations of SH3-PRM interactions identify potential new interactions and establish a framework that enhances the understanding of SH3-mediated protein networks and offers predictive insights for broader PPIs (Chapter II). In addition, chapter III explores the essential role of protein-lipid interactions in regulating intracellular signaling, membrane dynamics, and protein localization. This chapter examines how these proteins with membrane-binding modules employ various strategies and mechanisms, including post-translational modifications to engage with lipids. It also underscores the importance of these interactions in disease processes and explores their potential as therapeutic targets.

In addition, building on the foundational understanding of PPIs and protein-lipid interactions in signaling pathways, this study focuses on understanding the modes of interaction within the RAS-MAPK signaling pathway and related pathways. The RAS-MAPK pathway is a crucial cascade that controls key cellular processes, including proliferation, survival, growth, cell polarity, and mobility. Activation of CRAF, an oncogenic protein kinase in the RAS-MAPK pathway, is linked to tumor growth and developmental disorders. Chapter IV identifies and characterizes a specific protein interaction between CRAF and SIRT4, investigates the functional implications of this interaction, and proposes a novel role for SIRT4 as a cytosolic tumor suppressor that regulates RAS-MAPK signaling. Furthermore, the regulation of SIRT4 protein stability and degradation under pseudohypoxic stress is explored. This study identifies the mechanisms involved in its degradation and determines how stability of SIRT4 is affected by mitochondrial autophagy/mitophagy and proteasomal pathways (Chapter V).

Moreover, this study investigates the role of dysregulation in these interactions in human diseases, specifically focusing on proteins in the RAS-MAPK pathway involved in cardiovascular disorders such as arteriovenous malformations (AVMs). Findings suggest that missense mutations in RIT1, a member of the RAS superfamily of small GTPases, and SOS1, a positive regulator of this cascade, are particularly relevant to AVMs. Chapters VI and VII aim to identify and characterize novel mutations in SOS1 and RIT1 associated with AVMs, explore their impact on the RAS-MAPK signaling pathway and another key downstream pathway of RAS, the PI3K-AKT pathway, and evaluate the potential of targeted inhibitors to reduce hyperactive signaling and alleviate AVM symptoms and progression.

Lastly, chapter VIII aims to develop and apply a non-invasive, targeted imaging technique using fluorine-loaded nanotracers to map and monitor neutrophil dynamics throughout the body in real-time, particularly in response to cardiovascular injury, to improve the understanding of neutrophil behavior in inflammation and identify critical disease states in cardiovascular conditions.

Overall, this dissertation aims to advance the understanding of protein interactions and signaling pathways, identify novel mutations, propose therapeutic targets, and develop innovative diagnostic tools, ultimately contributing to improved research and treatment strategies for various diseases.

Chapter I. A Systematic Compilation of Human SH3 Domains: A Versatile Superfamily in Cellular Signaling

Authors: ***Mehrnaz Mehrabipour***, *Neda S. Kazemein Jasemi, Radovan Dvorsky, Mohammad R. Ahmadian*

DOI: *10.3390/cells12162054*

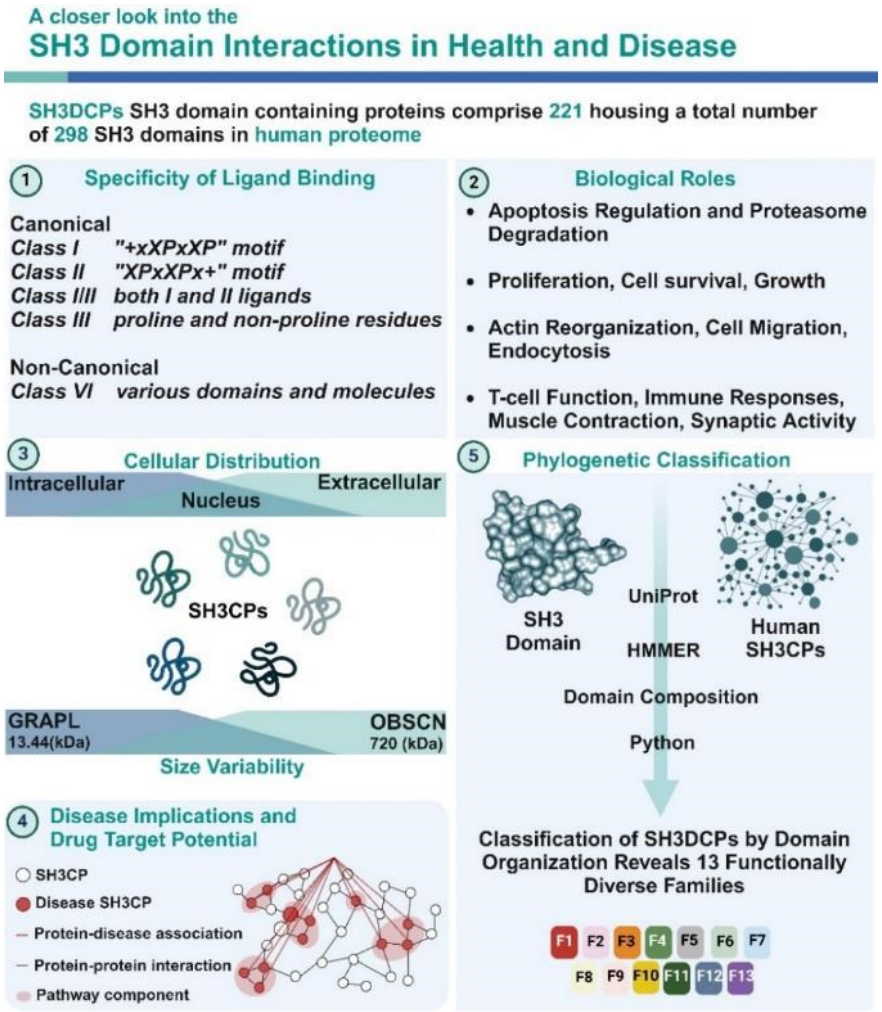

Status: Published in August 2023

Journal: Cells

JIF: 5.1

Contribution: 70%

Responsible for drafting, writing, and finalizing the manuscript, as well as collecting data for specificity and disease-associated tables. Conducted the collection of SH3CP protein families, performed sequence alignment and phylogenetic analysis, carried out gene ontology analysis, and generated the figures.

cells

MDPI

Review

A Systematic Compilation of Human SH3 Domains: A Versatile Superfamily in Cellular Signaling

Mehrnaz Mehrabipour [1], Neda S. Kazemein Jasemi [1], Radovan Dvorsky [1,2,*] and Mohammad R. Ahmadian [1,*]

[1] Institute of Biochemistry and Molecular Biology II, Medical Faculty and University Hospital Düsseldorf, Heinrich Heine University Düsseldorf, 40225 Düsseldorf, Germany; mehrnaz.mehrabipour@hhu.de (M.M.); neda.jasemi@hhu.de (N.S.K.J.)

[2] Center for Interdisciplinary Biosciences, P. J. Šafárik University, 040 01 Košice, Slovakia

* Correspondence: radovan.dvorsky@gmail.com (R.D.); reza.ahmadian@hhu.de (M.R.A.); Tel.: +49-2118112384 (M.R.A.)

Abstract: SRC homology 3 (SH3) domains are fundamental modules that enable the assembly of protein complexes through physical interactions with a pool of proline-rich/noncanonical motifs from partner proteins. They are widely studied modular building blocks across all five kingdoms of life and viruses, mediating various biological processes. The SH3 domains are also implicated in the development of human diseases, such as cancer, leukemia, osteoporosis, Alzheimer's disease, and various infections. A database search of the human proteome reveals the existence of 298 SH3 domains in 221 SH3 domain-containing proteins (SH3DCPs), ranging from 13 to 720 kilodaltons. A phylogenetic analysis of human SH3DCPs based on their multi-domain architecture seems to be the most practical way to classify them functionally, with regard to various physiological pathways. This review further summarizes the achievements made in the classification of SH3 domain functions, their binding specificity, and their significance for various diseases when exploiting SH3 protein modular interactions as drug targets.

Keywords: proline-rich motifs (PRM); protein interaction; SH3 domain; SH3 domain-containing proteins; signal transduction; SRC homology 3

Citation: Mehrabipour, M.; Jasemi, N.S.K.; Dvorsky, R.; Ahmadian, M.R. A Systematic Compilation of Human SH3 Domains: A Versatile Superfamily in Cellular Signaling. *Cells* **2023**, *12*, 2054. https://doi.org/10.3390/cells12162054

Academic Editor: Roger Schneiter

Received: 1 July 2023
Revised: 2 August 2023
Accepted: 2 August 2023
Published: 12 August 2023

1. General Introduction

The SRC homology 3 (SH3) domain was first described in 1988 as a region of approximately 60 amino acids found in different intracellular signaling proteins, such as SRC and PLC [1,2]. SH3 domains are arranged as small protein modules in a compact β-barrel fold made of five β-strands connected by RT, n-SRC, distal loops, and a 3_{10}-helix (Figure 1) [3]. Thousands of SH3 domains present in eukaryotes, prokaryotes, and viruses have been investigated and characterized as modules mediating the protein–protein interaction/association [4,5]. SH3 domain-mediated protein–protein interactions have significant diversification as the binding partners regulate almost all essential cellular functions, including cell survival, proliferation, differentiation, migration, and polarity. Moreover, findings underscore the significance of SH3 domains in shaping protein–protein interaction, their potential influence on protein folding and positioning, their impact on cellular phenotypes, and the essential role they play in protein function [6]. Mutations and malfunctions of the SH3 domain can lead to significant neurological defects, cancer, and infectious diseases [7–9].

SH3 domain-containing proteins (SH3DCPs) have a complex array of potential physiological partners due to their ability to recognize diverse structural scaffolds that are both dependent on, and independent of, the consensus proline-rich motif (PRM). This allows them to favor typical and atypical specific recognition sites. Biochemical and structural studies have been published on peptide libraries recognized by SH3 domains. These studies have been used to predict potential binding partners containing this sequence to

gain a better understanding of SH3-mediated biological responses [10]. Human SH3DCPs represent a populous and well-characterized family with almost 300 domains embedded in 221 large multidomains and small monodomain proteins. A novel multidomain phylogenetic analysis of SH3DCPs shows their co-occurrence across a large set of protein domains, and it provides insight into their functional prerequisites in different signaling pathways. In this review, we focus on the specificity landscape underlying protein–protein interactions that are mediated by SH3 modules and the functional diversification of SH3 domains in human signaling pathways based on their phylogenies and relations to different diseases.

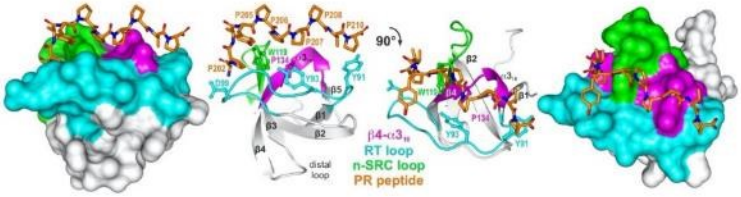

Figure 1. A representative structure of an SH3 domain PRM complex. A detailed view into the structure (PDB code: 1FYN) of the SH3 domain of FYN tyrosine kinase (left: surface representation; right: ribbon representation; UniProt ID: P06241) in complex with 3BP-2 PR peptide (PAYPPPPVP; orange; UniProt ID: P78314) which shows the characteristic arrangement of beta strands and the PRM-interacting variable loops, referred to as β4-$\alpha3_{10}$ (magenta), RT (cyan), and hydrophobic patch (W1190) flanked by n-SRC loop (green). Conserved residues that are crucial for the interaction are Y91, Y93, D99, W119, and P134. FYN SH3 shows the typical topology of two perpendicular three-stranded β-sheets and a single turn of $\alpha3_{10}$.

2. Specificity of Binding

SH3 domains, among other peptide-binding modules, provide multivalent binding by increasing the avidity of interactions and promoting phase transition during physical interactions with a pool of ligands called proline-rich motifs (PRMs) [11–13]. As certain interactions between the SH3 domain and PRMs are fundamental to the assembly of multiprotein complexes, it is reasonable to assume that the SH3DCPs are involved in a wide variety of cellular processes [14–16]. A set of five types of PRM-binding modules, including SH3, WW, EVH1, GYF, and UEV, have been reported to date [15,17–20]. PRMs are typically composed of proline (P) and hydrophobic (X) amino acids, with a core canonical motif XPxXP (where x can be any amino acid). The distinctive cyclic structure of proline's side chain gives proline an exceptional conformational rigidity compared with other amino acids. This unique structural property of proline may interfere with the regular formation of secondary structures, making it more abundant in unstructured regions. Consequently, proline residues are frequently exposed on the surface of proteins, making them accessible for interaction with other proteins or molecules [21]. The outstanding feature of PRMs is the actual degree of combinatorial diversity, which is determined by the presence of one or more proline residues [22–24]. The PRMs can be classified into three different types, including short linear sequence motifs with prolines that are involved in protein–protein interactions, like canonical PxXP [25,26], tandem repeats containing multiple copies of the same motifs in a row, like the two adjacent PPII helical PxXP motifs involved in the interaction with IRTKS-SH3 [26], and clustered motifs, which are multiple copies of the same motif that are found near each other. An example of proline clustering is an assembly of synaptic vesicle proteins that are bound with *SH3DCPs* in nerve terminals [27].

A canonical SH3 domain interaction with proline-rich peptides (PRPs) is characterized by specific hydrophobic contact recognition and the interaction of positively charged PRP residues with negatively charged residues of the SH3 domain [24,28]. Additionally, there are also water-mediated hydrogen bonds contributing to binding that is crucial for the stabilization of complexes [29,30]. The spatial arrangement of conserved amino acids located close to each other on the surface of the SH3 domain presents the PRM

binding surface. PRM binding occurs at three major sites, involving the hydrophobic patch (Tryptophan), which is flanked by the n-SRC loop, as well as the RT loop and β4-$\alpha 3_{10}$ of the SH3 domain (Figure 1) [31,32]. The SH3 domain can bind to their binding partners in two opposite orientations, defined by the relative positioning of non-proline residues, which are mostly positively charged residues [32,33]. The location of this basic residue, designated as +x/x+, determines the orientation of peptide binding in relation to the conserved proline residues at the N-terminal (+xXPxXP, class I) or the C-terminal (XPxXPx+, class II) positions of PxXP core [26,34,35]. For all SH3 domains, Arg is the basic residue defining the orientation, aside from some exceptions wherein Lys is the flanking residue for the second SH3 domain of TSPOAP1, the first SH3 domain of CRK, and SH3 domain of CTTN [10,36]. In both classes I and II, the structural and mutational analysis and studies suggest that the SH3–PRM interaction can, after initial major binding recognition, engage flanked areas outside the proline-rich core which regulates and increases binding specificity [37]. A structural comparison of SH3 domain binding sites shows that the higher variability and flexibility of loop regions account for the specificity and affinity in PRP binding [38,39]. The selectivity of the SH3 domain in particular PRPs is generally modest, with affinities usually in the low micromolar range [23,31–33,40]. An example of class I is a complex between the SH3 domain of MYO1E through the N-terminal Arginine 358, and Prolines 371 and 374 in FAK [41]. The crystalline structure of the second SH3 domain of CD2AP in complex with Pro-457, Pro-459, and Arg-462 in RIN3, shows the preference for class II orientation [42]. Some SH3 domains can bind to either class I or class II categories; FYN-SH3 is one such example [34,43–45]. A comprehensive study on binding specificities for 115 SH3 domains has shown that numerous SH3 domains exhibit extended alternative selectivity to non-proline residues in a peptide motif [10]. A crystallography and isothermal titration calorimetry (ITC) study of GRAP2-SH3C (MONA) and GRB2-SH3N clearly shows an unexpected binding combination concerning the essential RXXK motif of HPK1, which complements the PxXP motif [46]. A micromolar range affinity has also been found between the SH3 domain of STAM2 and GRB2-SH3C with the PX(V/I)(D/N)RXXKP motif of UBPY and SLP-7, respectively [47,48]. Another consensus PXXDY sequence was identified in ABI1 (E3B1) and RN-tre, in which DY was found to be crucial for binding, and the proline residue provided considerable specificity for EPS8-SH3 [49]. Furthermore, NCK2-SH3.1 forms a connection with the unique PxxDY motif found in the cytoplasmic tail of CD3ε. This motif includes Tyr166 within the ITAM subdomain of CD3ε. By associating with this motif, NCK2-SH3.1 hinders the phosphorylation of Tyr166, subsequently regulating the activity of the T-cell receptor [50]. The N-terminal SH3 domain of NCK1, together with EPS8, is also verified to show specificity for the PxxDY motif [51].

SH3 domains in several studies recently discovered that SH3DCPs also exhibit an extended repertoire of binding sequences, known as proline-independent binding, allowing SH3DCPs to mediate a broader array of interactions [19]. An example of atypical binding is the SH3 domain of RASA1, the RAS-specific GAP (p120RASGAP), which interacts with the catalytic GAP and kinase domains of DLC1 and Aurora kinases, respectively, thereby inhibiting their activities [52,53]. Other findings demonstrate a specific Intramolecular interaction between the SH3 and Guanylate Kinase (GuaKin/GK) domain of DLG4 (PSD-95) that predominates over intermolecular associations. Unlike the typical binding of SH3 domains to poly-proline motifs, SH3/GK binding occurs through a bi-domain interaction that necessitates intact motifs [54]. As a non-traditional binding mode, the SH3 domain can also play a role in facilitating the formation of intricate scaffold structures. The binding of the SH3-SH3 domains in ITSN1 and SH3GL2 (endophilin1) leads to their association, and this complex is recruited to locations wherein the clathrin-mediated recycling of synaptic vesicles takes place. This association facilitates the uncoating of vesicles at neural synapses [55]. In another study, the five SH3 domains of ITSN1 are associated with the autoinhibition of the DH domain, indicating that the PxXP-binding groove on the SH3 domain does not play a role in this interaction [56]. Interestingly, SH3 domains can also be involved in RNA binding. According to a study from Pankivskyi et al. in 2021, the

interaction between ITSN1-SH3D and mRNA promotes the solubilization of RNA-binding protein, SAM68. This occurs via interactions with ITSN1-SH3A and the mRNA-binding protein, SAM68-PRM; this triple complex may lead to the recruitment of specific mRNA for splicing regulation [57]. Other atypical interactions involve helix structures as interacting partners for *SH3 domains*. The C-terminal SH3 domain of NCF2 (p67phox) binds to the non-PxXP peptide segment of NCF1(p47phox) in helix–turn–helix arrangements [58]. Further research has indicated that non-PxXP alpha-helical motifs are essential and adequate for the binding of Pex5p to the PEX13-SH3 domain [58,59]. A notable feature of PEX13 is that it can simultaneously bind to both the canonical type II PRM sequence on Pex14p and the non-canonical binding site on Pex5p with a different binding surface on the SH3 domain [60,61]. In another study on *C. elegans* muscle, the interaction between UNC-89's SH3 (homologs of human OBSCN-SH3) and coiled α-helical structures of paramyosin, which shares a strong homology with skip2 residues on human cardiac Myosin (MYH7), leads to the mislocalization of paramyosin [62]. In a separate investigation, it was discovered that the interaction between FYN-SH3 and the N-terminal "RKxxYxxY" motif of SKAP55 necessitates the presence of arginine and lysine residues [28]. This study found that the RKxxYxxY motif was also recognized by SH3 domains that can bind to canonical class I motifs, whereas class II SH3 domains, like GRB-2, were unable to do so [28]. However, it was also shown that GRB2-SH3$_{c\text{-term}}$ and Gads can recognize and bind to an R-X-X-K motif of SLP-76 [63]. Moreover, the 40-fold difference in binding affinity for GRB2 suggests that GRB2-SLP-76 formation does not occur in vivo, in comparison with Gads, to facilitate receptor T cell signaling, suggesting that other factors are involved in mediating complex formation [48,63]. In another example, the interaction between BIN1-SH3 and its internal domain, referred to as Exon10, contains the basic sequence RKKSKLFSRLRRKKN, which hinders the SH3 domain from interacting with its typical PxXP ligand in dynamin [64]. Similarly, CdGAP activity is inhibited by the SH3 domain of ITSN1 by direct binding to its central basic-rich (BR) region comprising Lys and Arg residues (xKx(K/R)K motif) [65,66]. Another non-canonical binding of SH3 domains is found in the trinary SLAM–SAP–FYN-SH3 complex, in which the SAP-SH2 domain binds to FYN-SH3, thus linking FYN to SLAM immune receptors [67,68]. NCF1 (p47phox) also contains Arg70-Ile-Ile-Pro-His-Leu-Pro76, a canonical class I SH3 binding residue within the PX domain that can be recognized by its C-terminal SH3 domain; however, the surrounding PX structure also contributes to the production of a higher affinity [69]. The MACF1 protein belongs to the plectin family, which contains spectrin repeats (SR) and an SH3 domain in the middle, suggesting an SR4–SH3 interaction that stabilizes intermolecular contacts [70]. In addition, other domains, such as the LIM4 domain of PINCH-1, can also trigger rapid focal adhesion by transiently interacting with NCK2-SH3.3 [71]. In another interesting example of non-canonical binding, the single SH3 domain of CASKIN1 lacks key aromatic residues from the canonical binding groove, causing the protein to behave differently. There is a recent report suggesting that it might bind to membrane surfaces with high levels of LPA [72]. As with PRAM1-SH3, charged residues in the RT loop mediate a relatively high affinity for PI(4)P, and to a lesser extent, PIP_2 [73]. Protein–protein interactions in extracellular environments can also be mediated by *SH3 domains*. As an example, the MIA protein interacts directly with extracellular matrix molecules via its SH3 domain, which comprises a new binding pocket opposite the canonical binding site, resulting in cell separation and metastasis [74].

Although it is not an exhaustive compilation, the list above comprises several extensively researched binding partners of SH3 domains. The typical proline-containing sequences recognized by these domains are part of a broader group of protein–protein interaction sites, which are well-known for their capacity to selectively bind to modular domains. The specific recognition patterns can vary depending on the specific SH3 domain and its interacting partner in canonical proline-dependent interactions. In general, the binding site of the SH3 domain is highly conserved across different SH3 domains, allowing it to bind to a variety of proline-rich sequences with high specificity. For proline-rich independent interactions on the structure of SH3 domains, binding can vary depending

on the specific features of binding moieties. The binding site for proline-rich independent interactions on SH3 domains is not uniform or absolute. It is intricate and varies based on numerous factors, including the amino acid sequence, the conformation of the SH3 domain, and the target protein.

It is worth mentioning that different SH3 domains may have distinct binding specificities, and a single target protein can be recognized by several SH3 domains with different binding sites. Furthermore, the provided findings suggest that SH3 domains do not solely dictate their interaction partners. Instead, they have a complex impact on protein–protein interactions that cannot be accurately predicted based solely on their intrinsic specificity [6,75]. The specificity of SH3-dependent interactions in living cells can be determined by various factors including SH3 domain features, surrounding amino acids, a combination of multiple SH3 domains and peptide motifs, the co-expression and co-localization of SH3 domain proteins and partners, allosteric intramolecular interactions, and protein context, which includes their position within the host protein and potential intramolecular interactions [75]. This highlights the existence of intricate interactions between SH3 domains and their respective targets [6]. The interplay between the SH3 domain and the target protein is crucial for establishing specificity in protein–protein interaction networks, shedding light on how these networks evolve, and their relevance to diseases like cancer. Multi-domain analysis and the classification of human SH3CPs is essential for comprehending the patterns and characteristics of SH3 domains within a protein context, enabling a deeper comprehension of potential specificity and intramolecular interactions.

3. DCPs Belong to a Versatile Superfamily

Proteins containing SH3 domains are frequently identified by the similarity of their sequences [31]. From a total number of 394,887 SH3DCPs, which are present in all organisms, 1132 are reviewed; in humans, a set of 237 out of 770 proteins have been analyzed and characterized [76]. A combination of advanced searching methods with a detailed sequence comparison, using multiple sequence alignments of inputs generated by the ClustalW algorithm, was used to review the SH3DCPs and identify the accuracy of the regions annotated as SH3 domains [77]; this yielded 298 SH3 domains embedded in 221 human SH3DCPs (Table S1). Though the basic classification of the SH3DCP superfamily is based on their ability to interact with a specific target (Table 1), they can also be classified functionally. They encompass a wide range of protein families that are highly divergent in terms of function and size, however, they are only somewhat well-characterized. Cell processes involving SH3DCPs are regulated in many types of tissues and cells. Gene Ontology describes SH3DCPs in terms of three independent categories: biological process, molecular function, and protein class (Figure S1). These categories are distributed across three compartments: cytosol, extracellular, and nucleus.

Table 1. Binding Specificity of SH3 domains.

Binding	Class	Ligand	SH3DP Example	Ref.
Canonical	Class I	+xXPxXP	MYO1E interaction with FAK-PRM1	[41]
	Class II	XPxXPx+	CD2AP-2nd-SH3 in interaction with RIN3	[42]
	Class I/II	Specificity of both ligands of I/II	FYN interaction with different PRMs Tau	[43]
	Class III	Combination of proline with non-proline residues	GRAP2-SH3C (MONA) and GRB2-SH3N interaction with HPK1 STAM2 interaction with UBPY; GRB2-SH3C interaction with SLP-7; EPS8 interaction with ABI1 (E3B1) and RN-tre; NCK1/2 N-Terminal-SH3 interaction with cytoplasmic tail of CD3ε	[46–51]

Table 1. *Cont.*

Binding	Class	Ligand	SH3DP Example	Ref.
Non-canonical	Class VI	GAP domain	RASA1 interaction with DLC1-GAP domain	[52]
		Kinase–Catalytic domain	RASA1 interaction with Aurora kinases-catalytic domain	[53]
		Guanylate–Kinase domain (GuaKin/GK)	DLG4 (PSD-95) inter-domain interaction	[54]
		SH3 domain	ITSN1 and SH3GL2 SH3-SH3 domain complex	[55]
		DH domain	ITSN1 interaction with internal domain	[56]
		RNA	ITSN1 SH3D interaction with mRNA	[57]
		Helix	NCF2 (p67phox) SH3D interaction with NCF1(p47phox) N-term helical region; PEX13 interaction with helical segment of Pex5p; UNC-89 SH3 (homologs of human OBSCN-SH3) interaction with Paramyosin (homologs of human MYH7-skip2) coiled α-helical structures	[58,59,62,65]
		Arginine–Lysine residues	FYN-SH3 interaction with SKAP55; Gads-SH3 and GRB2-SH3$_{C\text{-term}}$ interaction with SLP-76; BIN1-SH3 interaction with internal domain; ITSN1 interaction with CdGAP-Basic rich domain (xKx(K/R)K motif)	[28,48,63–66]
		SH2 domain	FYN-SH3 interaction with SAP-SH2	[67,68]
		PX domain	NCF1(p47phox) inter-domain interaction	[69]
		Spectrin repeat	MACF1 inter-domain interaction	[70]
		LIM4 domain	NCK-2 SH3.3 interaction with PINCH-1	[71]
		Lipid	CASKIN1 interaction with lysophosphatidic acid (LPA) PRAM1-SH3 interaction with PI(4)P and PIP2	[72,73]
		Extracellular matrix molecules	MIA-SH3	[74]

These proteins are typically located at the interface between cytosol and membranes, especially plasma membranes, and they act as molecular components for the formation and stabilization of junctional complexes and synaptic connections [78,79]. SH3DCPs are also observed in a variety of scaffolding proteins, including cytoskeletal components, such as Myosin and spectrin, to maintain and regulate stability and motility [80,81]. Moreover, SH3 domains employ liquid–liquid phase separation as a mechanism for cellular compartmentalization through interactions with PRMs to arrange the constituent components of distinct pathways for the forthcoming signal transduction [82–85]. Furthermore, the MIA protein family consists of secreted extracellular proteins that contain a single SH3 domain, with a conserved SH3 domain-like fold, supplemented by a beta paralleled beta-sheet and two disulfide bonds. These proteins serve as extracellular matrix constituents that are essential for tissue reorganization and cellular attachment [86,87].

SH3DCPs also control the molecular functions of enzymes, receptor activities, and transport processes [88,89]. SH3 domains are protein binding modules in enzymes like phospholipase Cγ [90]. Adaptor and docking SH3DCPs are involved with influencing signaling pathways, including non-receptor tyrosine kinases of the SRC family, for the regulation of its catalytic activity and/or mediating interactions [91]. It is important to mention that SH3DCP can enter the nucleus under certain circumstances. One such example is when CASK acts as a molecular regulatory coactivator of Tbr-1 to induce transcription of T-element-containing genes, such as reelin, which is required for cerebrocortical development [92]. However, the CASK-GK domain is enough for this interaction, and further research is needed to fully understand the involvement of indirect effects or interactions between other proteins with the SH3 domain in the co-activation of Tbr-1 by CASK. In another example, through the SH3 domain, SPTAN1 (αII-spectrin) could potentially contribute to the repair of DNA interstrand cross-links in the nucleus [93]. Hence, this implies

that the SH3 domain serves as a mediator of complex formation, linking signaling proteins at the right time and in the right place with the corresponding signaling pathways [31]. Figure 2 depicts the formation of various protein complexes through SH3 domain-mediated protein–protein interactions, which bind to partner proteins and play a general role in different signaling pathways. Biologically, the roles of proteins from SH3DCPs are vastly diverse, ranging from signaling pathways related to proliferation, cell survival, cell growth, actin reorganization, cell migration, endocytosis, apoptosis regulation, and proteasome degradation (Figure 2A). SH3 domains mediate the involvement of numerous proteins both upstream and downstream of the EGFR-receptor tyrosine kinase (RTK). For instance, GRB2, NCK, BTK, and SRC SH3 domains interact with EGFR, resulting in the activation of downstream pathways involved in cell proliferation and actin reorganization. In addition, a huge number of SH3CPs regulate actin dynamics and cell migration via the direct mediation of SH3 domains. The role of complex formations, mediated by SH3 domains, is also clear in Vesicular trafficking. Moreover, several complexes that are mediated by SH3 also contribute to T-cell function, immune responses, muscle contraction, and synaptic activity (Figure 2B).

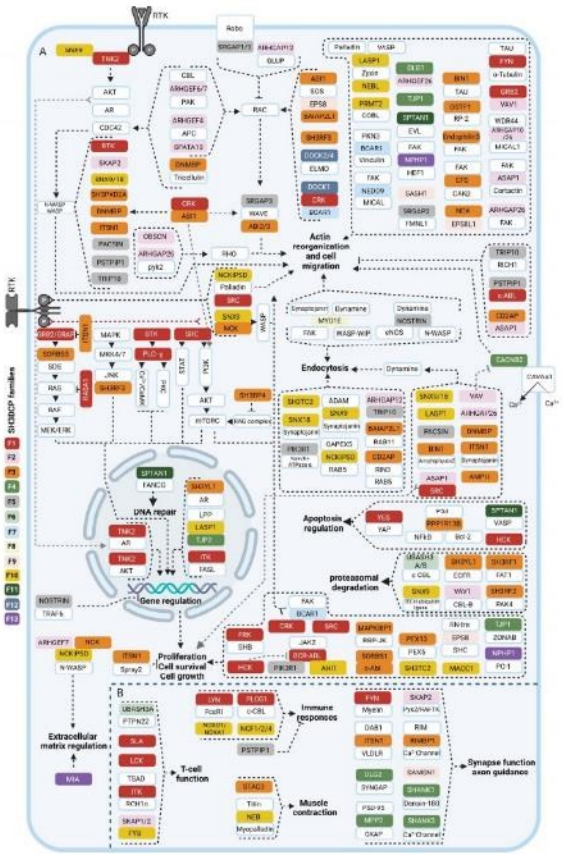

Figure 2. Schematic diagram of SH3DCPs in diverse signaling pathways. SH3DCPs are crucial signaling proteins, and they include adaptor proteins, kinases, RAS GEFs, RAS GAPs, scaffold proteins, and effectors. They are involved in various signaling processes in the cell. The dashed separation in the figure distinguishes general cellular functions (**A**) from specific functions in various cell types (**B**). All information presented in this figure is cited as references in Table S1.

The number and nature of domains in many SH3DCPs are striking, especially the abundance of lipid membrane binding domains, along with protein interaction domains, such as SH2, WW, and Ig-like domains, and a large number of catalytic and regulatory domains, such as kinase, REM, GAP and GEF domains (Table S2, Figure S2). In particular, ITSN1/2 (also known as EHSH1 or SH3P17, and SH3P18; Table S1) and DNMBP (also known as ARHGEF36 or TUBA) are CDC42GEFs, and they contain five and six SH3 domains, respectively (Figure S2) [94]. They play crucial roles in linking Exo-/endocytosis, actin dynamics, and signal transduction through the small GTPase of the RHO family [95–99]. The association of the C-terminal SH3 domain of DNMBP (TUBA) with the N-terminal cytoplasmic PRM of tricellulin (PLPPPPLPLQPP; aa 46–57) results in TUBA-mediated CDC42 activation, which is required for the regulation of junctional tension in epithelial cells [100]. In addition, ITSN1 recruits Endophilin 1 (SH3GL2) at sites of clathrin-mediated synaptic vesicle recycling via an SH3-SH3 domain-mediated complex formation. The second SH3 domain of ITSN1 appears to be essential for endophilin1-SH3 interactions in this process [55].

The SH3DCPs are available in a wide range of molecular weights. The largest SH3DCP is OBSCN (obscurin or ARHGEF30; approximately 720 kDa), a giant sarcomeric protein of the RHOGEF family that interacts with calmodulin and titin [101]. OBSCN contains mainly I-set (Ig domains) which provide segmental flexible binding sites for proteins like titin during the assembly of the sarcomere, as well as the SH3 domain near the tandem DBL homology (DH)/RHOGEF and pleckstrin homology (PH) domains. Interestingly, a polyproline stretch within the DH domain has been proposed as a potential regulatory component as it acts like an intramolecular ligand in the SH3 domain [101]. The observation that CaMKII selectively phosphorylates the isolated SH3 domain, but not the SH3-DH fragment, suggests the presence of functional interplay between the SH3 and DH domains and their potential influence on phosphorylation events in obscurin. However, the role of the DH and SH3 domains with regard to the functioning of obscurin appears to be intricate and dependent on various factors [102]. Additionally, investigations into UNC-89, a *C. elegans* counterpart of human OBSCN, have disclosed its location at the sarcomeric M-line of the muscle. It interacts with paramyosin via the SH3 domain, and when the SH3 domain is overexpressed, it results in paramyosin mislocalization [62]. Another giant filamentous SH3DCP is NEB (Nebulin; isoform size varies from 600 to 800 kDa), which has an SH3 domain preceded by a Serine-rich region, both of which are essentially involved in the interactions between several key signaling molecules (e.g., titin, N-WASP, α-actinin, myopalladin, and zyxin). These interactions allow for the association of NEB with the sarcomeric Z-line in skeletal and cardiac muscles, and the regulation of thin filament lengths and contractility [103]. Two other giant proteins belonging to the plakin family are MACF1 (ACF7; 620 kDa) and DST (dystonin or BPAG1; 629.78 kDa), which are responsible for interacting with a variety of signaling proteins, and they provide the versatility to create links between different components of the cytoskeleton, including actin microfilaments, microtubules, and intermediate filaments [104]. An SH3 domain is positioned within the central region of the plectin domain in these proteins, and it has been proposed to interact with the SR4 domain intermolecularly to stabilize the structure and aid with ligand-binding affinities, particularly in plectin or other plectin family members such as MACF1 and DST [70]. This indicates that the SH3 domain plays a crucial role in facilitating interactions and functional interplay within these large proteins, likely contributing to their stability, ligand-binding affinity, and overall functionality. On the other hand, GRAPL, OTOR, and MIA are the smallest SH3DCPs, with molecular weights of 13.44, 14.33, and 14.5 kDa, respectively. GRAPL is similar to GRAP1/2 and GRB2 proteins, but it contains only one SH3 and one SH2 domain (Figure S2). It is likely involved with linking intracellular tyrosine kinase signals to RAS GTPases. OTOR (otoraplin or MIAL1) and MIA belong to several extracellular SH3DCPs of the melanoma-inhibiting activity (MIA) family [86], and they contain only one SH3 domain. A crucial question concerns the role of such 'mini-proteins' and what they are, as well as how they are involved in extracellular processes. MIA has been designated as a cartilage-derived retinoic acid-sensitive protein that is mainly

secreted as an 11-kDa protein in cartilage tissue during embryogenesis and adulthood [105]. In this respect, MIA appears to influence the action of bone morphogenetic protein 2 and transforming growth factor beta 3 during mesenchymal stem cell differentiation by promoting the chondrogenic phenotype and inhibiting osteogenic differentiation [105]. MIA interacts with fibronectin during this process, and it competes with integrin binding, detaching cells from the extracellular matrix [106].

4. Phylogenetic Classification of SH3DCPs

The next question we addressed concerned how to classify or categorize SH3DCPs, taking into account their heterogeneous domain composition. As the phylogenetic tree based on similarities of isolated SH3 domains was not of practical use, we have used an approach based on the similarities of domain compositions between SH3DCPs. For this purpose, primary sequences of an entire collection of 221 human SH3DCPs were first retrieved from the UniProt database, and they were analyzed for occurrences of protein domains. Next, mutual similarities in terms of domain composition between all protein pairs in the collection were evaluated. The resultant matrix was then subjected to phylogenetic analysis using MEGA software (version 7.0). The final phylogenic tree shed light on the evolutionary relationships between the human SH3DCP superfamily, and it allowed the superfamily to be classified into thirteen different SH3DCP families (Figure 3). An inspection of individual families, based on the respective domain organizations (Figure S2), revealed the following findings. (i) They differ in terms of the number of SH3DCPs per family, ranging from 2 (family 6) to 54 (family 3). (ii) The classification of SH3DCPs into individual families is often based on the combination of the SH3 domain with at least one or two similar domains, for example, SH2 and/or KinYST domains (Family 1); membrane-binding BAR and PH domains, RHOGAP, or RHOGEF domains (Family 2); single or several SH3 domains combined with other shared domains (Family 3); PDZ and/or the GuaKin domain (Family 4); FCH and/or RHOGAP domains (Family 5); UBA and HPhos domains (Family 6), S-rich and CAS-C domains (Family 7); Myosin and/or MyTH4 (Family 8); SAM* along with PTB and SLY in some SH3CPs (Family 9); spectrin domain and EF-hand (Family 11); DOCK and DHR domains (Family 12); and some were also classified with only a single SH3 domain (Family 13), except Family 10, which comprises diverse combinations of the SH3 domain. (iii) Exploiting combinations of SH3, with specific domains in each family of the SH3CPs' domain–organization, indicates that the parallel domain–combination is evolving. This also explains the functional differentiation of the SH3 domain in different pathways. (iv) *SH3 domains* can function as adaptors, scaffolds, modulators, and regulatory domains.

4.1. Family 1

Proteins belonging to Family 1 share a mostly conserved domain called the tyrosine kinase domain, which is responsible for their catalytic activity and phosphorylation of target proteins. They can be classified into four groups of non-receptor Tyrosine Kinases (SRC, FYN, YES, HCK, LCK, BLK, FGR, FRK, SRMS, BTK, ITK, TEC, TXK, ABL1, ABL2, MATK, CSK, LYN, PTK6, TNK2, TNK1 [107,108]), adaptor Proteins (GRB2, GRAP, GRAP2, GRAPL, CRK, CRKL, SLA, SLA2 [109–112]), tyrosine Kinase-associated Signaling Proteins (RASA1, MAP3K21, MAP3K10, MAP3K11 [113,114], and Phospholipase C, including PLCG1 and PLCG2 [115,116]). The main feature of these proteins is that they are all involved in signal transduction pathways. More specifically, when transmitting signals from the cell surface to the cytoplasm and nucleus, they can affect gene expression and various cellular processes. The SH3 domain plays a crucial mediating interaction-based and regulatory role in this family. For example, SH3 domains of adaptor proteins, such as GRB2 and CRK, bind to proline-rich motifs in other signaling proteins, allowing them to link receptor tyrosine kinases to downstream signaling pathways [40,117]. In some cases, the SH3 domain affects the catalytic activity of the kinase domain. For instance, the SH3 domain of the non-receptor tyrosine kinase, SRC, can interact with its own SH2 domain and N-terminal fragment of the kinase domain, leading to the inactivation of its kinase activity [118].

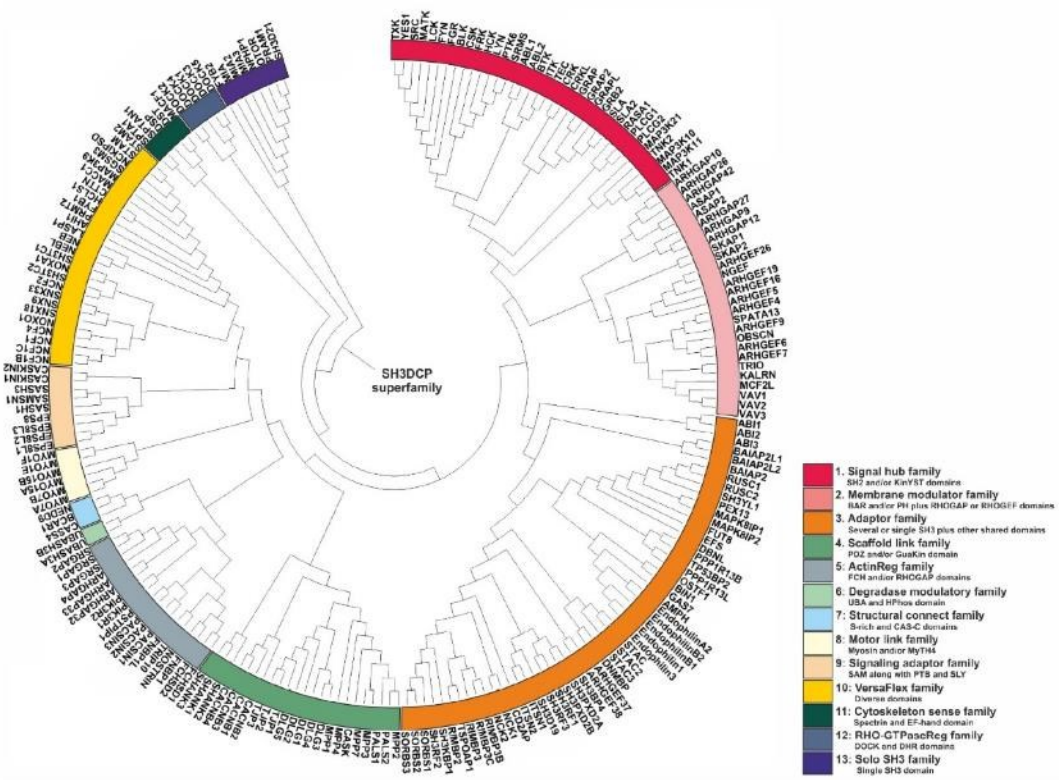

Figure 3. Phylogenetic tree of the SH3DCP superfamily. The tree was generated on the basis of the similarities between domain compositions. The SH3DCP superfamily can be divided into thirteen families, which are marked by different colors of classes at the outer ring.

4.2. Family 2

The proteins listed in Family 2 are primarily involved in the regulation of Rho family GTPases, and in some cases, those of the ARF family, which are critical for regulating the actin cytoskeleton and an array of essential cellular processes; these encompass cell migration, cell division, cell adhesion, and membrane trafficking. They can be classified further into two subcategories: GTPase-activating proteins (GAPs) and guanine nucleotide exchange factors (GEFs). GAPs are negative regulators of Rho or ARF family GTPases, and they stimulate the intrinsic GTPase activity of GTPases, which leads to their inactivation. The proteins of this family are GAPs, as follows: ARHGAP10, ARHGAP26, ARHGAP42, ARHGAP12, ARHGAP27, ARHGAP9 as RHOGAPs, and ASAP1, ASAP2 are ARF GAPs [119–122]. GEFs, on the other hand, activate GTPases by promoting the exchange of GDP for GTP. The proteins in the list are Rho-GEFs, as follows: SPATA13, ARHGEF4, ARHGEF26, NGEF, ARHGEF19, ARHGEF16, ARHGEF5, ARHGEF9, ARHGEF6, ARHGEF7 [120,123–126]. TRIO, KALRN, MCF2L, VAV1, VAV2, and VAV3 are multi-domain GEFs that regulate Rho family GTPases and other signaling pathways [120,127,128]. TRIO and KALRN activate RHO GTPases, RAC1 and RHOA, and they are involved in cell migration and differentiation [129]. VAV proteins and MCF2L activate RAC1, RHOA, and CDC42, and they are involved in cell growth, differentiation, and immune responses [127,130]. SKAP1 and SKAP2 do not have a canonical guanine nucleotide exchange factor (GEF) domain. Instead, they have been shown to act as RAP1 GTPase activators through a non-canonical mechanism that involves interactions with other

proteins. More specifically, SKAP1 has been shown to bind to RIAM (RAP1-interacting adapter molecule), which, in turn, recruits activated GTP-bound RAP1 by promoting the membrane translocation of RAP1 for T-cell adhesion [131,132]. SKAP2 might also interact with RIAM, and it can similarly activate RAP1. Therefore, although SKAP1 and SKAP2 do not have a canonical GEF domain, they function as GEFs for RAP1 through protein–protein interactions with RIAM. There is a possibility that SH3 domains, similarly to other enzymes, control the activity of the GEF and GAP domains through inter/intra-molecular interactions. For example, unique characteristics were observed in this KALRN (kalirin) SH3 domain, including the presence of novel binding sites for the intramolecular PxxP ligand, as well as for binding to the adaptor protein, CRK, to inhibit the GEF activity of KALRN [133].

4.3. Family 3

The presence of multiple SH3 domains, in most members of Family 3, may confer several advantages, including increased specificity. First, having multiple SH3 domains with different binding specificities allows proteins to interact with a larger number of partner proteins and potentially simultaneously modulate multiple signaling pathways. Second, it might lead to cooperative binding, which means that the presence of multiple SH3 domains can allow a protein to bind to multiple sites on a single partner protein, which can enhance the affinity of the interaction and potentially stabilize protein complexes. A study conducted on a SH3RF3 protein from this family used a detailed functional scaffolding analysis that revealed that its fourth SH3 domain interacts with MKK7. Additionally, it was found that the first and second SH3 domains of SH3RF3 interact with JIP3 and JNK1. These findings suggest that SH3RF3 plays an important part in aiding the assembly of the MKK–JNK complex via JIP, which leads to the activation of JNK-JUN [134]. Thirdly, the regulation of protein–protein interactions occurs when the SH3 domains in a protein can interact with each other, or with other domains within the same protein, to regulate protein–protein interactions. For example, autoinhibitory interactions of SH3 domains can block binding sites and prevent interactions until a regulatory signal is received. For example, ITSN1-L, which is a RHO-GEF, plays a crucial role in regulating both endocytosis and actin cytoskeletal rearrangements, and its SH3 domains are important for controlling its exchange activity. The SH3 domains block the binding of CDC42 to the RHO-GEF domain (or DH domain) via inter-domain interactions, which inhibits exchange activity [98]. Lastly, localization concerns the presence of multiple SH3 domains with different binding specificities, which can also allow proteins to target different subcellular compartments and interact with different sets of proteins in those locations. Interestingly, the specific order and arrangement of the SH3 domains were found to be important for maintaining the integrity of protein–protein networks in SH3CPs with multiple SH3 domains [6].

Members of this family can also function as adaptor proteins that typically contain multiple domains, and they can couple together different signaling molecules or components of cellular pathways. Many proteins of Family 3 (SH3CPs) fall into this category. For example, CD2AP (CD2-associated protein) is an adaptor protein that interacts with CD2, a transmembrane receptor protein on T cells [135], and other cytosolic proteins such as nephrin, a protein important for maintaining the integrity of the glomerular filtration barrier in the kidney [136]. The SH3 domains in CD2AP are thought to mediate protein–protein interactions with other signaling molecules and cytoskeletal components [137]. NCK1 and NCK2 (non-catalytic region of tyrosine kinase) proteins are adaptor proteins that link signaling molecules with downstream effector proteins involved in cytoskeletal regulation, membrane trafficking, and gene expression [137,138]. They contain several protein-binding domains, including SH3 domains, that enable them to simultaneously interact with multiple partners. In addition, all RIMBP proteins (RIMBP2, RIMBP3, RIMBP3B, RIMBP3C) are part of the synaptic vesicle release machinery and are involved in regulating neurotransmitter release [139]. They contain several domains that allow them to interact with other proteins involved in the synaptic vesicle cycle. Another category that some mem-

bers of this family fall into is signaling proteins that act as intermediates or effectors in various signaling pathways. Some examples of MAPK8IP1 and MAPK8IP2 are as follows. MAPK8IP proteins (mitogen-activated protein kinase 8 interacting protein) are involved in the regulation of the JNK (c-Jun N-terminal kinase) signaling pathway, which is important for stress responses and apoptosis [140]. The SH3 domain in these proteins mediates protein–protein interactions with upstream and downstream components of the pathway. STAC, STAC2, and STAC3 are types of STAC protein that are involved in the regulation of calcium channels, and they play a role in skeletal muscle function. They contain several domains, including the SH3 domain, that interact with different components of the calcium channel complex [141]. OSTF1 (Osteoclast-stimulating factor 1) is another example of the protein involved in the regulation of bone resorption by osteoclasts [142]. The SH3 domain in OSTF1 is thought to mediate interactions using signaling molecules involved in the regulation of osteoclast activity. SH3 domain-containing cytoskeletal proteins, categorized as cytoskeletal proteins, such as Endophilins (Endophilin A2, Endophilin B1, Endophilin B2, Endophilin 1, Endophilin 3), are involved with controlling the organization and dynamics of the cell cytoskeleton. They are involved in the formation and recycling of clathrin-coated vesicles and the regulation of the actin cytoskeleton. Endophilins contain, among others, a BAR domain which further contributes to their membrane curvature recognition [143]. They also interact with proteins such as dynamin and synaptojanin via the SH3 domain which regulates the formation of clathrin-coated vesicles during endocytosis [144,145]. DNMBP or TUBA (Dynamin-binding protein) is also involved in actin cytoskeleton organization, and it is thought to play a role in endocytosis. The SH3 domains in DNMBP are involved in protein–protein interactions with other cytoskeletal and signaling proteins [95].

4.4. Family 4

Proteins listed in this family share SH3 domains and/or PDZ and/or Guanylate Kinase (GuaKin/GK) domains, and they often have similar functions associated with the regulation of protein complexes and the structure and function of the synapse, a junction between two neurons that allows for the transmission of information. SHANK1, SHANK2, and SHANK3 are scaffolding proteins that play a crucial role in the organization and function of the postsynaptic density (PSD), a protein-rich area of the synapse [146]. SHANK proteins interact with other proteins to anchor neurotransmitter receptors and signaling molecules in the PSD, thereby regulating the strength of synaptic transmission [147]. MPP1, MPP2, MPP3, MPP4, MPP7, PALS1, and PALS2 are members of the membrane-associated guanylate kinase (MAGUK) family in synapse organization and function. MAGUK proteins interact with other proteins to form a complex network of signaling molecules at the synapse, thereby regulating synaptic transmission and plasticity [148,149]. CASK is a protein in the same subfamily that interacts with other synaptic proteins, including β-neurexins, and Rabphilin3a via the PDZ domain; it plays a role in the regulation of neurotransmitter release [148]. DLG1, DLG2, DLG3, DLG4, and DLG5 are members of the Discs Large (DLG) subfamily of proteins belonging to the MAGUK family; they are involved in the formation and control of neurotransmitter release [150,151]. CACNB1, CACNB2, CACNB3, and CACNB4 are subunits of voltage-gated calcium channels (VGCCs) belonging to the MAGUK family; they regulate the entry of calcium ions into neurons. Calcium influx through VGCCs is important for synaptic plasticity and neurotransmitter release [152]. In contrast, TJP1, TJP2, and TJP3, which belong to the ZO subfamily, are also members of the MAGUK family. They are not expressed in neurons, but in the brain, and they play a crucial role in maintaining the blood–brain barrier [153].

Overall, although the SH3 domain's interaction with its targets is less understood compared with PDZ domains, studies on MAGUK proteins, such as DLG, provide insights into the complex regulation of SH3 domain interactions and their potential roles in cellular processes. The N-terminal region of the human DLG undergoes alternative proline-rich region insertion splicing that can bind in vitro to multiple SH3 domains and control the formation of protein clusters [154]. For example, the N-terminal portion of DLG1 (SAP-97)

can bind to the SH3 segment of DLG4 (PSD-95), indicating a potential heteromeric interaction between these two proteins. This interaction may play a role in dendritic clustering and the trafficking of GluR-A AMPA receptors [155]. Other studies suggest that the SH3 domain of DLG1 (SAP-97) and DLG4 (PSD-95) forms a specific interaction with its GK domain, and this intramolecular interaction prevents intermolecular associations; this sheds light on the role of the SH3 domain with regard to MAGUK function and oligomerization [156–158]. Recent findings suggest that the SH3 domain modulates the GK domain through an allosteric mechanism rather than by blocking the GK binding surface [159]. The SH3-HOOK-GK domain configuration is present in most MAGUK proteins, suggesting that this interaction is a shared characteristic among MAGUK proteins [157,160]. Overall, these proteins play important roles in regulating the organization and function of the synapse, and the dysregulation of their activity has been linked to various neurological and psychiatric disorders.

4.5. Family 5

Proteins classified into this family share a similar domain architecture. They all contain at least one SH3 domain, either a FCH or RHOGAP domain, or both. This combination of domains is unique to this protein family and sets them apart from other proteins. The combination of the SH3 domain with the FCH and/or RHOGAP domains in this group of proteins suggests that they may play a role in regulating actin cytoskeleton dynamics and membrane trafficking. Proteins containing the FCH domain may participate in protein–protein interactions, and they may potentially contribute to the organization of RHO proteins and the actin cytoskeleton [161]. Conversely, the RHOGAP domain regulates RHO family GTPases, which are important regulators of actin cytoskeleton dynamics.

4.6. Family 6

UBASH3A and UBASH3B are two proteins that belong to the same protein family, called the Ubiquitin-associated and SH3 domain-containing protein (UBASH3) family. These proteins are involved in the regulation of signal transduction pathways, including T-cell receptor signaling and cytokine production [162–164]. Functionally, both UBASH3A and UBASH3B contain an Ubiquitin-associated (UBA) domain and a SRC homology 3 (SH3) domain. The UBA domain enables the interaction between these proteins and ubiquitin, a protein that plays a critical role in the regulation of protein degradation, DNA repair, and immune response [165]. The SH3 domain allows UBASH3A and UBASH3B to bind to proline-rich motifs in other proteins, including signaling proteins, receptors, and enzymes, thereby regulating their activity [163,166,167]. Structurally, UBASH3A and UBASH3B are similar in size, each consisting of 504 amino acid residues. Both proteins share a high degree of sequence identity, with 80% sequence similarity. The overall structure of these proteins is similar, with an N-terminal UBA domain followed by a central SH3 domain and a C-terminal HPhos region. However, there are some differences in the sequence and structure of the UBA and SH3 domains between UBASH3A and UBASH3B, which may contribute to their distinct functions.

4.7. Family 7

BCAR1, NEDD9, and CASS4 also share other domains in addition to the SH3 domain, namely, the S-RICH and CAS-C domains. The S-RICH domain, which is a stretch of amino acids enriched with serine residues, is located in the N-terminal region of all three proteins. It has been shown to be crucial for the localization and activity of these proteins at focal adhesions, which are sites of cell adhesion and signaling, by binding to 14-3-3 proteins [168]. The CAS-C domain is a domain that is found in the C-terminal region of all three proteins, and it assists with binding to other signaling molecules, such as the adapter protein, SRC, which mediates downstream signaling events [169,170]. Therefore, the common structural feature of the SH3 domain, coupled with the S-RICH and CAS-C domains, contributes to the functional similarities between BCAR1, NEDD9, and CASS4; this is because it allows

them to interact with the other proteins involved in cell adhesion and signaling pathways, leading to similar functional roles in terms of regulating cell adhesion, migration, and proliferation [169].

4.8. Family 8

These proteins share common structural features in that they all contain SH3 with myosin domains belonging to the myosin superfamily. Myosins are a family of motor proteins that use the energy from ATP hydrolysis to generate force and move along actin filaments, resulting in the generation of force and motion [171]. Functionally, myosins are involved in a wide range of cellular processes, including muscle contraction, cell migration, membrane trafficking, and organelle transport [172]. The specific functions of listed myosins may vary depending on their expression patterns, subcellular localization, and interactions with other proteins. For example, MYO7A is involved in hearing and balance [173], whereas MYO5A is involved in melanosome transport and pigmentation [174]. Other myosins, such as MYO1E, are involved in cell migration and the regulation of the actin cytoskeleton [175]. Myosins can be divided into two broad categories, as follows: conventional and unconventional myosins. Conventional myosins are typically found in muscle tissue and are responsible for generating the force and movement required for muscle contraction [176]. Unconventional myosins, on the other hand, have a more diverse range of functions, and they are found in a variety of cell types and tissues throughout the body [177]. Some examples of these unconventional roles include acting as tension sensors and dynamic tethers, organizing F-actin during endo- and exocytosis, and maintaining the mitotic spindle structure [178]. Unconventional myosins often have a more complex domain structure than conventional myosins, and the SH3 domain is one of the additional domains that is commonly found in these proteins [177]. The SH3 domain in some myosins, given their interaction with other proteins, may carry out these functions [80]. All listed myosins contain a single SH3 domain, which is involved in mediating protein–protein interactions, and this is consistent with the idea that these myosins play roles in diverse unconventional processes. For example, MYO1E, which is an unconventional myosin involved in the cell migration and regulation of the actin cytoskeleton, contains a SH3 domain that has been shown to interact with a protein called ZO-1 [175]. This interaction is thought to play a role in regulating junctional integrity in kidney podocytes by contributing to the slit diaphragm complex [179]. Similarly, MYO7A, which is involved in hearing and balance, contains an SH3 domain that contributes to the interaction with the protein harmonin. This interaction is important for the localization of MYO7A to the stereocilia in the inner ear, where it is involved in generating mechanical force and movement [180].

4.9. Family 9

The concurrent presence of SH3 domains and SAM*, PTB, and SLY domains in some of the proteins listed in Family 9 suggests that they play roles in various aspects of signal transduction and protein–protein interactions. The SAM* (sterile alpha motif) domain is a conserved protein domain of around 70 amino acids that is present in many proteins involved in signal transduction and transcriptional regulation [181]. SAM* domains are known to mediate protein–protein interactions and are believed to function as regulatory domains that can influence the activity or localization of their associated proteins [182]. The PTB (phosphotyrosine binding) domain is another protein domain that is commonly found in signaling proteins. PTB domains bind to specific phosphorylated tyrosine residues in other proteins, and they are involved in mediating protein–protein interactions that are essential for the proper functioning of signaling pathways [183]. The SLY domain, a conserved family of lymphocyte signaling adapter proteins domain, is present in eukaryotes and is associated with SH3 and SAM domains. It is identified in various proteins, including SLY1/SASH1, SASH3, and SAMSN1 [184]. The combined presence of these domains in listed proteins suggests that they likely function as adaptors or scaffold proteins that help to assemble and organize signaling complexes, and that they mediate the protein–protein

interactions that are critical for signaling and regulation. Adaptor proteins contain protein–protein interaction domains that link receptors to downstream signaling components, whereas scaffold proteins provide a physical platform for multiple signaling components to interact with and regulate each other's activity. Based on their known functions and structural features, EPS8, EPS8L1-3 [185], SASH1 [186], SASH3, and SAMSN1 [187] are believed to function as adaptor proteins, whereas CASKIN1 and CASKIN2 are scaffold proteins. CASKIN1 and CASKIN2 contain multiple domains which enable them to function as scaffold proteins that can organize multi-protein complexes [188]. The structural investigation of CASKIN2's SH3 domain using NMR revealed that its peptide-binding cleft differed from the typical binding sites for polyproline ligands due to the presence of non-canonical basic amino acids. Mutations in the cleft suggested that the SH3 domain in CASKIN2 may have lost its functional ability to promote protein–protein interactions beyond the conventional roles typically associated with SH3 domains [189].

4.10. Family 10

Although SH3 domains may be a shared feature among these proteins, their overall domain architectures and functions are diverse. Therefore, it is important to note that some of these proteins may have multiple functions, or they may interact with multiple signaling pathways; their precise classification can depend on context and experimental findings. However, they can be primarily classified into the following functional categories: signal transduction (STAM, STAM2 [190], NCKIPSD [191], MAP3K9 [192], MACC1 [193], PRMT2 [194], AHI1 [195], LASP1 [196], SGSM3 [197]), cytoskeletal remodeling (HCLS1 [198], CTTN [199], NEBL, NEB [103], LASP1 [196], FYB [200]), endocytosis (SH3TC1, SH3TC2 [201], SNX9, SNX33, SNX18 [202]), and immune system function (NCF1, NCF1B, NCF1C, NCF2, NCF4 [203], NOXO1, NOXA1 [204]). Furthermore, many of these proteins have multiple SH3 domains, and some may have other protein–protein interaction domains or motifs that contribute to their functions.

4.11. Family 11

The shared structural and functional features of these proteins are primarily related to their roles in cytoskeletal organization and cell adhesion. The spectrin domain is a key structural component that provides mechanical stability to the cytoskeleton. It forms a long, flexible rod-like structure that can interact with other proteins, cytoskeletal elements, and lipids to provide support and resistance against deformation [205–207]. The SH3 domain, on the other hand, plays a key role in cytoskeletal organization and cell adhesion by regulating protein–protein interactions and localization. The EF-hands have a high affinity for Ca2+, they undergo a conformational change when bound to it, and they are essential for maintaining the structural integrity of the skeleton [206]. Together, the SH3, spectrin, and EF-hand domains found in these proteins can work together to regulate critical protein–protein interactions that maintain the structural integrity of the cytoskeleton and regulate cellular adhesion and signaling. Although each of these proteins have unique features and functions, they all share common structural and functional elements that reflect their common ancestry and evolutionary history.

4.12. Family 12

These proteins share both structural and functional similarities as they all belong to the same family of guanine nucleotide exchange factors (GEFs), known as the DOCK family. Structurally, they all contain a conserved DHR-2-C (DOCK homology region 2) domain which is responsible for the GEF activity of these proteins, as well as other domains such as DHR-2-A (lipid-binding DOCK homology region) and the SH3 domain. Functionally, they play important roles in the regulation of cytoskeletal dynamics, cell migration, and immune and neural cell function [208,209]. In the DOCK family, the SH3 domain plays a regulatory role by mediating interactions with proline-rich motifs in other proteins, allowing DOCK proteins to bind to, and regulate the activity of, a variety of cytoskeletal and signaling

proteins. There are some examples of how the SH3 domain in DOCK proteins can play a role in regulating protein–protein interactions. The SH3 domain of DOCK2 interacts with the PRM of ELMO1, which may relieve their autoinhibition to promote the activation of RAC in lymphocyte chemotaxis [210,211]. Moreover, the DOCK1–ELMO1 interaction was identified for the localization and regulation of RAC1 in cytoskeletal organization and cell migration [211,212]. The C-terminal PRM region of DOCK1 can also interact with the SH3 domain of several proteins, including the adaptor protein, NCKβ, and CRK, which helps to control cell migration [213–215]. Thus, the SH3 domain is an important structural component that facilitates these interactions to influence the subcellular activity of DOCK proteins, as well as their ability to activate downstream signaling pathways.

4.13. Family 13

All of these proteins contain only one SH3 domain. The specific function of each protein may be different, but they all share the ability to interact with other proteins via their SH3 domain. For example, FYB2 (FYN binding protein 2) regulates T-cell receptor signaling and is involved in the formation of the immunological synapse [216]. Another study found that MIA, a protein secreted from malignant melanoma cells, enhances melanoma cell migration and invasion by interacting with extracellular matrix proteins and integrin [87,217]. In addition, cadherin-7 was identified as a new MIA-binding protein that negatively regulates the expression and activity of MIA, and it plays a role in the migration of melanoma cells during tumor development [218]. Another review integrates research on *Drosophila Tango1* and human MIA/cTAGE proteins to provide an evolutionary perspective on ER-Golgi transport, which highlights the role of the MIA protein involved in the regulation of the ER-Golgi transport of proteins [219]. OTOR (melanoma inhibitory activity-like (alias MIAL)) may play a role in the development and maintenance of the inner ear [220]. NPHP1 (Nephrocystin-1) plays a role in the macromolecular complex formation and function of cilia, and disruptions to these complexes can cause renal cystogenesis [221]. PRAM (PML-RAR alpha-regulated adapter molecule) is involved in the regulation of the differentiation of hematopoietic cells [222]. SH3D21′s (SH3 domain-containing protein 21) function is currently unknown, and further research is needed to fully understand the specific role and mechanisms of SH3D21 with regard to signaling processes. The cellular localization of these proteins may vary depending on their specific function and the cell type in which they are expressed. Although some proteins may have a predominant localization to a particular subcellular compartment, others may be distributed more broadly throughout the cell.

5. SH3 Domain-Specific Disorders, Diseases, and Potential as Drug Targets

The mutational disruption of SH3-target interactions is associated with a variety of human diseases (Table 2). SH3 domain mutations have been linked to the development of various diseases such as Joubert syndrome, leukemia, lymphomas, Usher Syndrome or nonsyndromic deafness, centronuclear myopathy, schizophrenia, and other neurodevelopmental disorders (Table 2). Cancer cells can invade by inducing epithelial-to-mesenchymal transition via SH3DCPs such as SRC family kinases [91]. Elevated levels of other SH3DCPs, such as GBR2, CRK, and SAMSN1 adaptor proteins are also detectable in a large percentage of breast cancers and human colon and lung cancer samples, respectively [223,224]. In multiple in vitro experiments, SH3 domains have also been shown to be prone to amyloid fiber formation under acidic conditions, and they underwent conformational changes during the aggregation process [225–227]. Various identified mutations in the SH3-binding motifs can affect the function and interactions of the protein; this shows the importance of SH3 mediating interactions. For example, a novel homozygous mutation (p.Ser236Phe) in the SH3 binding motif of the STAMBP gene was found in a two-year-old boy with microcephaly-capillary malformation syndrome, leading to protein instability and the prevention of STAM binding [228]. Moreover, viral and bacterial pathogens adapt SH3 protein modules or PRMs from the host to mimic and modulate host cell signaling for their

own purposes [229,230]. Interesting results have also been obtained regarding the presence of PRM located at the N-terminus of the Nef protein in HIV, which is essential for the induction and progression of AIDS-like diseases [231–233]. Several approaches screened host–viral relationships by identifying the potential interactions between SH3DCPs, including GRB2, FYN, NCK1, HCK, and ARHGEF7, and viral proline-rich sequences [234]. The prevalence and critical regulatory roles of SH3-PRP interactions in human diseases, coupled with the impact of SH3 domain mutational dysfunction on signaling pathways and human disease and pathogenicity, allows the exploitation of their protein–protein interaction to be a potential candidate for a new drug design [80,223,230,235–237]. SH3 domains can be found in oncoproteins as well as in proteins that are excessively expressed in irregular signaling pathways in cancerous cells. There may be potential for pharmacological intervention in signaling cascades to inhibit proliferation; this could occur by targeting SH3 domains, with small peptides and molecules mimicking binding, and a high degree of specificity and affinity to specific SH3 domains. These molecules may represent new cytostatic agents for proliferative diseases, but they may have difficulty distinguishing between normal and cancerous cells, and they may need to be carefully dosed to avoid completely inhibiting normal cellular growth responses [8]. In addition, although SH3 domains can recognize ligands due to their modest affinity, they exhibit limited selectivity within the SH3 family, and thus, using non-specific SH3 inhibitors may lead to the de/activation of alternative pathways and resistance. The structure of SH3 domains provides important clues for designing effective antagonists. The SH3 domain can obtain selectivity through the involvement of other regions that are not accessible for ligand interactions, thereby expanding the binding site, and in some cases, via unique SH3-ligand interactions, both of which seem strategic for future drug designs [238]. On the other hand, research indicated that the presence of SH3 domains plays a crucial role in enabling the SLAP's ability to oppose the oncogenic activity of SRC in fibroblasts [239,240]. Achieving anti-oncogenic activity through a mechanism involving SH3 indicates a potential anti-tumor function for SH3 when counteracting oncogenic activity, in addition to its role in oncogene tumor-driven SH3CPs.

Table 2. Diseases associated with the SH3 family.

SH3DCP	Mutation	Disease	Refs.
AHI1	FsX1103	Joubert syndrome	[241]
	Deletion of the SH3 domain	Leukemia and lymphomas	[242]
MYO7A	Missense mutation (A1628S) and truncation/deletion mutations (c.4838delA, c.5146-5148delGAG)	Usher Syndrome or nonsyndromic deafness (DFNB2)	[243,244]
FRK	R64Q	Cervix and vulva cancer	[245]
YES1	K113Q	Breast and colon cancer	[245]
ACK1	M393T, M409I	Colon, Gastric adenocarcinoma	[245–248]
AMPH	Q434X, K436X, Q573X, K575X	Centronuclear Myopathy	[249,250]
ARHGAP10	Lacking the RHOGAP and SH3 domains	Schizophrenia	[251]
ARHGEF9	G55A	Hzperekplexia, seizures or epilepsy, developmental Delay, or intellectual disability	[252]
ARHGEF23	Missense and nonsense mutations	Neurodevelopmental disorders	[253]
ARHGEF30	V5668A	Breast cancer	[101]
	A5660V	Cardiomyopathies	[254]

Table 2. *Cont.*

SH3DCP	Mutation	Disease	Refs.
CD2AP	K301M	Sporadic nephrotic syndrome and focal segmental glomerulosclerosis (FSGS)	[255]
BIN1	Q434X, K436X, Q573X, K575X, P593HfsX54, X594DfsX53	Centronuclear myopathy (CNM)	[249,256]
	rs138047593 (K358 R (KR))	Alzheimer's disease	[257,258]
BLK	A71T	Autoimmune diseases, (e.g., systemic lupus erythematosus (SLE))	[259]
BTK	Deletion of C-terminal 14 aa residues of SH3 domain	X-linked agammaglobulinemia (XLA)	[260,261]
LYN	SH3 mutations (transformative and non-transformative)	Cancer (uterine, sarcoma, thyroid, liver, head and neck, melanoma, lung, glioma, kidney, breast, hematologic)	[39]
MIA	High expression	Melanoma development, progression and metastasis	[74]
MYO15A	G2909S, G2941Vfs*94, W2931Gfs*103, R2923*, P2880Rfs*19, R2903*, R2924H, G2938R, V2940fs*3034	Human Deafness	[262,263]
NPHP1	2q13	Autosomal recessive cystic kidney disease	[264]
	L180P	Familial Juvenile Nephronophthisis	[265]
PEX13	Missense mutation at SH3, nonsense mutation of W234ter, temperature sensitive mutation of I326T, W313G	Peroxisome-biogenesis disorders (PBDs) including Zellweger syndrome (ZS), neonatal adrenoleukodystrophy (NALD), and infantile Refsum disease	[266–269]
PLC-γ1	Substitution mutations	Adult T cell leukemia/lymphoma, angioimmunoblastic T-cell lymphomas, T-cell prolymphocytic leukemia, Sézary Syndrome, PLAID, autoinflammation, immune deficiency	[270–273]
PSTPIP1	D384G, G403E, G403R, R405C	Autoinflammatory diseases (most notably in the PAPA syndrome; pyogenic sterile arthritis, pyoderma gangrenosum, and acne) and CVID (common variable immunodeficiency)	[274,275]
PTK6	L16F	Cancer	[276]
RASA1	Missense, nonsense, frame shift, and splice site mutation	Cancer, capillary malformation (CM)	[277,278]
RIMBP1	G1808S	Autosomal recessive dystonia	[279]
SASH1	S587R, M595T, E617K, I586M, S587R, M595T	DUH (dyschromatosis universalis hereditaria) and lentiginous phenotype	[280,281]
SH3PXD2B	Non-synonymous coding sequence variations (G245R, E396K, G481R)	Axenfeld–Rieger syndrome	[282]
	BDCS3 deletion (deletion of two C-terminus SH3 domains)	Borrone dermato-cardio-skeletal syndrome	[283]
SHANK1	R874H	Autism spectrum disorder	[284]
SHANK2	S557N, R569H	Autism spectrum disorder	[285]
SHANK3	Lacking parts of the SH3 domain in case of G1527A	Autism spectrum disorder and intellectual disability (ID)	[286]
SPTAN1	D2303_L2305dup	Epileptic encephalopathy	[287]
VAV1	L801P	Cancer	[288]
STAC3	W > S substitution	Native American myopathy	[289]
	P269R, N281S, W284S, F295L, H311R, K329N	Native American myopathy, dystrophin-deficient muscles	[289–292]
OBSCN	V5668A	Breast cancer	[293]
CASK	G659D	Severe intellectual disability (ID), microcephaly and pontine, and cerebellar hypoplasia in girls (MICPCH)	[294]

One study focused on the design of spirolactam-based peptidomimetics aimed at the SH3 domain of a LYN that produced ligands with extended conformations; this resulted in comparable binding affinities to reference peptides (XPpX motif) [295]. Moreover, scientists developed the mirror-image phage display method to identify D-peptide ligands that are enzyme-resistant. This method involved creating a mirror image version of the protein and selecting peptide molecules from a peptide library that could bind to it in a solvent (water) that does not require chiral cofactors. This method can be used to identify molecules that can bind to specific target proteins, including cyclic D-peptides, that partially obstruct the binding site of the c-SRC protein. [296]. In another study, highly selective and efficient peptides that bind to the SH3 domains of CRK and CRKL proteins were developed and tested for their ability to interfere with SH3 binding in living cells [297].

Furthermore, various laboratories have conducted sophisticated experiments using combinatorial chemistry to discover novel non-peptide ligands for SH3 domains [298]. By designing ligands that complement the topography of the binding pocket, researchers were able to discover ligands with greater selectivity and affinity for the SRC-SH3, and they also discovered specific ligands for HCK-SH3 [299,300]. By adopting a similar approach, a ligand that was designed to be an SH3 inhibitor, with a high affinity for the GRB2 SH3 domain, was obtained by replacing key prolines with non-natural N-substituted residues during ligand screening [301]. Extracellular SH3CP MIAs interact with other proteins in the extracellular matrix, particularly fibronectin (FN), to facilitate the detachment of cancer cells and promote their migration and invasion into surrounding tissues [74]. A small molecule that was discovered using a binding site prediction approach and in vitro fragment screening can disrupt the MIA–FN interaction by binding to a specific pocket on the MIA protein; it can serve as a potential target during future drug development against melanoma [74]. Moreover, 2-aminoquinolines and related compounds have been identified as potential high-affinity small molecule ligands for the SRC Homology 3 (SH3) domains; this could be useful for developing novel therapeutics that treat human diseases caused by abnormal cell signaling pathways [302]. In conclusion, the collective findings from the above studies provide insights into the application of combinatorial libraries and structural biology when elucidating the intricacies of protein–ligand interactions and the potential use of small molecule ligands as drugs.

Currently, there are no approved drugs that directly target SH3 domains. However, there is ongoing research to develop small molecule ligands that can selectively bind to SH3 domains and potentially be used as therapeutics for diseases caused by abnormal signaling pathways. The identification of compounds as potential high-affinity ligands for particular SH3 domains is a basic step toward developing such drugs. However, further testing may find their efficacy and safety in vivo unsatisfactory. To address this issue, it may be beneficial to develop new strategies that can specifically target certain interactions within one or several SH3 domains of particular SH3DCPs while avoiding cross-interactions with other SH3DCPs. This could help to minimize any unintended effects on other targets. Furthermore, the aforementioned unconventional SH3 targets present exciting opportunities for potential drug development.

Moreover, understanding the intricate details of protein–protein interactions, as exemplified by the multifaceted behavior of SH3 domains, unveils novel opportunities for therapeutic interventions. Recent research has shed light on the role of SH3 domains in mediating and regulating protein–protein interactions through their proline-rich binding grooves, as well as their opposite binding sites, characteristics that might be common among many SH3 domains. For instance, the analysis of ITSN1's structure reveals that its SH3(E) domain exhibits two distinct binding surfaces, as follows: one interacts with the catalytic DH domain to modulate GEF activity [98], and the other specifically binds proteins containing polyproline residues to facilitate the cellular specific targeting of dynamin to endocytic complexes [56,303]. Notably, the proline binding pocket of the SH3 domain does not interfere with the inhibitory function of the SH3 domains with regard to nucleotide exchange [98]. In another example, the proline-rich region of the N-WASP has

been identified as an activator of ITSN1 via its interaction with the ITSN1 SH3 domain [304]. However, this activation is not observed with recombinant ITSN1 fragments alone, suggesting the involvement of an unidentified additional protein interaction on the ITSN1 SH3 domain [98], potentially occurring on the other binding surface. These findings emphasize the potential value of both the front and back sides of SH3 domains, and both surfaces can be used as promising targets for future drug development. Additionally, the complex interplay and lack of sole dependency on intrinsic binding specificities make it difficult to design drugs that effectively target and inhibit SH3 domains. Multiple factors, including the identity of the host protein and the position of the SH3 domains, play crucial roles in determining the specificity of these interactions [6,75]. Therefore, achieving the selective inhibition of SH3 domains requires a comprehensive understanding of these factors and their intricate relationships.

6. Concluding Remarks

The fact that SH3 domains regulate a wide range of cellular functions raises the question regarding the specificity of SH3 domain interaction networks (Figure 2). Multiple studies noted that the interaction between SH3 domains, with canonical and non-canonical target sequences in binding partners, leads to specificity among the pool of ligands (Table 1). Remarkably, in canonical binding, proline is the only N-substituted amino acid found in nature that can form the polyproline type II (PPII) helix conformation, which exposes a binding pocket for SH3 domain residues, mainly from the RT and n-SRC loops [19,61,301]. Previous studies also revealed that the poly-proline amino acid stretch is involved in SH3 domain ligand recognition [305]. Despite intensive research, the specificity of the interaction of SH3 domains for proline-rich motifs remains unknown. Understanding the molecular basis for the specific and diverse binding of SH3 domains to PRMs will provide insights into the regulation of signaling pathways. Multiple studies have been conducted to investigate and classify the interactions between SH3 domains and various ligands, resulting in diverse categorizations based on different criteria. Cesareni and coworkers have investigated the interaction landscape of the human SH3 protein family using a combination of information extraction strategy and experimental approaches, including a type of new peptide chip technology; this occurred in order to characterize the specificity and promiscuity of proline-rich binding domains and to map their interaction network. Two main groups of SH3 domains were identified based on their interaction with similar peptide ligands, as follows: SH3 domains that bind to "classical" PxXP core motifs along with positively charged amino acids, and atypical SH3 domains that lack the core motif [23]. Sidhu also performed versatile canonical and non-canonical specificity profiling of SH3 domains using peptide-phage displays with deep sequencing in 2017 [10]. Moreover, a comprehensive analysis of SH3 domain interactions concerning the evolution of four yeast species, *Saccharomyces cerevisiae*, *Ashbya gossypii*, *Candida albicans*, and *Schizosaccharomyces*, revealed that nearly 75 percent of SH3 families generated within the phylogenetic tree have a conserved SH3 specificity profile over 400 million years of evolution [306]. Moreover, numerous SH3 domains exhibit an extended repertoire of binding sequences, known as proline-independent binding. This enables SH3DCPs to mediate a broader array of interactions, including interactions with other domains, like GAP, kinase–catalytic, basic rich (BR), Guanylate Kinase (GuaKin/GK), SH3, DH, SH2, PX, and LIM4, or other targets like RNA, helixes, arginine–lysine residues, spectrin repeat, lipid, and extracellular matrix molecules. It is important to highlight that these non-traditional targets may hold substantial promise as viable candidates regarding future drug development. In recent years, to better understand the mechanisms underlying SH3-mediated cellular responses, numerous attempts to develop different methodologies for studying and mapping SH3-PRM dependent and independent binding have been conducted. Nevertheless, it can still be argued that the function of most proteins is intimately dependent upon their native tertiary structures [307]. The systematic analysis of the sequence–structure–function relationships of SH3-PRM

interactions, coupled with biochemical annotations, is needed to explore correct functional sites and categories from a structure-based perspective.

Our work illustrates the evolutionary relationship of the 221 human SH3DCP superfamily, and it allows for the functional classification of these proteins into thirteen families. Such classifications provide insights into their diverse roles and interactions within cellular processes. Furthermore, it allows us to identify patterns of SH3 domains and their co-occurrence with other domains in multidomain proteins, and it allows us to uncover potential functional modules or regulatory units within proteins. This classification approach aids in the understanding of SH3 domain-mediated interactions and their contributions to intramolecular activation and deactivation, intermolecular inhibition or networking, as well as their role as scaffolding and adaptor elements in cellular function and disease mechanisms. Moreover, the potential of targeting SH3 domains, for future drug designs, as presented in this review, will help to develop novel therapeutic approaches. Several in vitro strategies for designing peptide and non-peptide targets, such as peptidomimetics, mirror image phage display, and combinatorial chemistry, have been explored in order to design ligands with enhanced affinity and selectivity for specific SH3 domains regarding the inhibition of their protein–protein interaction. Challenges such as selectivity and specificity need to be addressed when designing inhibitors, as non-specific inhibition may lead to the deactivation of alternative pathways and resistance. Moreover, uncovering the full potential of non-canonical SH3 domain binding targets may provide new possibilities for therapeutic interventions. Furthermore, the intricate interplay between, and absence of an exclusive reliance upon intrinsic binding specificities pose challenges for the development of drugs that can precisely target and inhibit SH3 domains. Continued research and exploration into SH3 domain interactions hold great promise for the future of treating diseases caused by abnormal signaling pathways.

Supplementary Materials: The following supporting information can be downloaded at: https://www.mdpi.com/article/10.3390/cells12162054/s1, Table S1: Phylogenetic classification of the human SH3DCP superfamily into thirteen families; Table S2: List of SH3DCP domains (alphabetical order); Figure S1: Gene Ontology analysis of the superfamily of human SH3 domain-containing; Figure S2. Domain organization of the SH3DCP superfamily.

Author Contributions: M.R.A. conceived and coordinated the study. M.M., N.S.K.J. and R.D. analyzed the sequence-structure-function relationships and generated the figures. All authors have read and agreed to the published version of the manuscript.

Funding: This study was supported by the German Research Foundation (Deutsche Forschungsgemeinschaft or DFG; AH 92/8-3) and the European Network on Noonan Syndrome and Related Disorders (NSEuroNet, 01GM1602B).

Informed Consent Statement: Not applicable.

Acknowledgments: We are grateful to our colleagues from the Institute of Biochemistry and Molecular Biology II of the Medical Faculty of the Heinrich-Heine University, Düsseldorf, for their support, helpful advice, and stimulating discussions. Additionally, we extend our thanks and acknowledgment to Pymol for providing Figure 1, "BioRender.com" (accessed on 11 October 2022), which was used for the design and creation of Figure 2, MEGA software (version 7.0), to construct the phylogenetic tree of the SH3DCP superfamily, as illustrated in Figure 3, the PANTHER 17.0 database for gene ontology functionality and the design and development of Figure S1, and the Python programming language, HMMER, Pfam, OpenCV, and Pillow for assistance crafting Figure S2, which showcases the domain organization of SH3DCPs with clarity and precision.

Conflicts of Interest: The authors declare no conflict of interest.

References

1. Mayer, B.J.; Hamaguchi, M.; Hanafusa, H. A novel viral oncogene with structural similarity to phospholipase C. *Nature* **1988**, *332*, 272. [CrossRef] [PubMed]
2. Stahl, M.L.; Ferenz, C.R.; Kelleher, K.L.; Kriz, R.W.; Knopf, J.L. Sequence similarity of phospholipase C with the non-catalytic region of src. *Nature* **1988**, *332*, 269–272. [CrossRef] [PubMed]

3. Musacchio, A.; Noble, M.; Pauptit, R.; Wierenga, R.; Saraste, M. Crystal structure of a Src-homology 3 (SH3) domain. *Nature* **1992**, *359*, 851–855. [CrossRef] [PubMed]
4. Gmeiner, W.H.; Horita, D.A. Implications of SH3 domain structure and dynamics for protein regulation and drug design. *Cell Biochem. Biophys.* **2001**, *35*, 127–140. [CrossRef] [PubMed]
5. Whisstock, J.C.; Lesk, A.M. SH3 domains in prokaryotes. *Trends Biochem. Sci.* **1999**, *24*, 132–133. [CrossRef] [PubMed]
6. Dionne, U.; Bourgault, É.; Dubé, A.K.; Bradley, D.; Chartier, F.J.M.; Dandage, R.; Dibyachintan, S.; Després, P.C.; Gish, G.D.; Pham, N.T.H.; et al. Protein context shapes the specificity of SH3 domain-mediated interactions in vivo. *Nat. Commun.* **2021**, *12*, 1597. [CrossRef] [PubMed]
7. Morel, B.; Varela, L.; Azuaga, A.I.; Conejero-Lara, F. Environmental conditions affect the kinetics of nucleation of amyloid fibrils and determine their morphology. *Biophys. J.* **2010**, *99*, 3801–3810. [CrossRef]
8. Smithgall, T.E. SH2 and SH3 domains: Potential targets for anti-cancer drug design. *J. Pharmacol. Toxicol. Methods* **1995**, *34*, 125–132. [CrossRef]
9. Kadaveru, K.; Vyas, J.; Schiller, M.R. Viral infection and human disease--insights from minimotifs. *Front. Biosci.* **2008**, *13*, 6455–6471. [CrossRef]
10. Teyra, J.; Huang, H.; Jain, S.; Guan, X.; Dong, A.; Liu, Y.; Tempel, W.; Min, J.; Tong, Y.; Kim, P.M.; et al. Comprehensive Analysis of the Human SH3 Domain Family Reveals a Wide Variety of Non-canonical Specificities. *Structure* **2017**, *25*, 1598–1610.e1593. [CrossRef] [PubMed]
11. Mayer, B.J. The discovery of modular binding domains: Building blocks of cell signalling. *Nat. Rev. Mol. Cell Biol.* **2015**, *16*, 691–698. [CrossRef]
12. Case, L.B.; Zhang, X.; Ditlev, J.A.; Rosen, M.K. Stoichiometry controls activity of phase-separated clusters of actin signaling proteins. *Science* **2019**, *363*, 1093–1097. [CrossRef]
13. Huang, W.Y.; Alvarez, S.; Kondo, Y.; Lee, Y.K.; Chung, J.K.; Lam, H.Y.M.; Biswas, K.H.; Kuriyan, J.; Groves, J.T. A molecular assembly phase transition and kinetic proofreading modulate Ras activation by SOS. *Science* **2019**, *363*, 1098–1103. [CrossRef] [PubMed]
14. Mayer, B.J. SH3 domains: Complexity in moderation. *J. Cell Sci.* **2001**, *114*, 1253–1263. [CrossRef] [PubMed]
15. Kaneko, T.; Li, L.; Li, S. The SH3 domain–a family of versatile peptide-and protein-recognition module. *Front. Biosci.* **2008**, *13*, 4938–4952. [CrossRef] [PubMed]
16. Kay, B.K. SH3 domains come of age. *FEBS Lett.* **2012**, *586*, 2606–2608. [CrossRef] [PubMed]
17. Holt, M.R.; Koffer, A. Cell motility: Proline-rich proteins promote protrusions. *Trends Cell Biol.* **2001**, *11*, 38–46. [CrossRef]
18. Zarrinpar, A.; Bhattacharyya, R.P.; Lim, W.A. The structure and function of proline recognition domains. *Sci. STKE* **2003**, *2003*, re8. [CrossRef]
19. Li, S.S.-C. Specificity and versatility of SH3 and other proline-recognition domains: Structural basis and implications for cellular signal transduction. *Biochem. J.* **2005**, *390*, 641–653. [CrossRef]
20. Zafra-Ruano, A.; Luque, I. Interfacial water molecules in SH3 interactions: Getting the full picture on polyproline recognition by protein–protein interaction domains. *FEBS Lett.* **2012**, *586*, 2619–2630. [CrossRef]
21. Ladbury, J.E.; Arold, S.T. Energetics of Src homology domain interactions in receptor tyrosine kinase-mediated signaling. In *Methods in Enzymology*; Elsevier: Houston, TX, USA, 2011; Volume 488, pp. 147–183.
22. Cesareni, G.; Panni, S.; Nardelli, G.; Castagnoli, L. Can we infer peptide recognition specificity mediated by SH3 domains? *FEBS Lett.* **2002**, *513*, 38–44. [CrossRef] [PubMed]
23. Carducci, M.; Perfetto, L.; Briganti, L.; Paoluzi, S.; Costa, S.; Zerweck, J.; Schutkowski, M.; Castagnoli, L.; Cesareni, G. The protein interaction network mediated by human SH3 domains. *Biotechnol. Adv.* **2012**, *30*, 4–15. [CrossRef] [PubMed]
24. Ball, L.J.; Kühne, R.; Schneider-Mergener, J.; Oschkinat, H. Recognition of proline-rich motifs by protein–protein-interaction domains. *Angew. Chem. Int. Ed.* **2005**, *44*, 2852–2869. [CrossRef]
25. Sparks, A.B.; Rider, J.E.; Hoffman, N.G.; Fowlkes, D.M.; Quillam, L.A.; Kay, B.K. Distinct ligand preferences of Src homology 3 domains from Src, Yes, Abl, Cortactin, p53bp2, PLCgamma, Crk, and Grb2. *Proc. Natl. Acad. Sci. USA* **1996**, *93*, 1540–1544. [CrossRef]
26. Aitio, O.; Hellman, M.; Kazlauskas, A.; Vingadassalom, D.F.; Leong, J.M.; Saksela, K.; Permi, P. Recognition of tandem PxxP motifs as a unique Src homology 3-binding mode triggers pathogen-driven actin assembly. *Proc. Natl. Acad. Sci. USA* **2010**, *107*, 21743–21748. [CrossRef]
27. Linial, M. Proline clustering in proteins from synaptic vesicles. *NeuroReport* **1994**, *5*, 2009–2015. [CrossRef]
28. Kang, H.; Freund, C.; Duke-Cohan, J.S.; Musacchio, A.; Wagner, G.; Rudd, C.E. SH3 domain recognition of a proline-independent tyrosine-based RkxxYxxY motif in immune cell adaptor SKAP55. *EMBO J.* **2000**, *19*, 2889–2899. [CrossRef] [PubMed]
29. Palencia, A.; Camara-Artigas, A.; Pisabarro, M.T.; Martinez, J.C.; Luque, I. Role of interfacial water molecules in proline-rich ligand recognition by the Src homology 3 domain of Abl. *J. Biol. Chem.* **2010**, *285*, 2823–2833. [CrossRef]
30. Martin-Garcia, J.M.; Ruiz-Sanz, J.; Luque, I. Interfacial water molecules in SH3 interactions: A revised paradigm for polyproline recognition. *Biochem. J.* **2012**, *442*, 443–451. [CrossRef]
31. Mayer, B.J.; Eck, M.J. SH3 domains: Minding your p's and q's. *Curr. Biol.* **1995**, *5*, 364–367. [CrossRef]
32. Saksela, K.; Permi, P. SH3 domain ligand binding: What's the consensus and where's the specificity? *FEBS Lett.* **2012**, *586*, 2609–2614. [CrossRef]

33. Panni, S.; Dente, L.; Cesareni, G. In vitro evolution of recognition specificity mediated by SH3 domains reveals target recognition rules. *J. Biol. Chem.* **2002**, *277*, 21666–21674. [CrossRef] [PubMed]
34. Feng, S.; Chen, J.K.; Yu, H.; Simon, J.A.; Schreiber, S.L. Two binding orientations for peptides to the Src SH3 domain: Development of a general model for SH3-ligand interactions. *Science* **1994**, *266*, 1241–1247. [CrossRef] [PubMed]
35. Lim, W.A.; Richards, F.M.; Fox, R.O. Structural determinants of peptide-binding orientation and of sequence specificity in SH3 domains. *Nature* **1994**, *372*, 375–379. [CrossRef] [PubMed]
36. Wu, X.; Knudsen, B.; Feller, S.M.; Zheng, J.; Sali, A.; Cowburn, D.; Hanafusa, H.; Kuriyan, J. Structural basis for the specific interaction of lysine-containing proline-rich peptides with the N-terminal SH3 domain of c-Crk. *Structure* **1995**, *3*, 215–226. [CrossRef] [PubMed]
37. Feng, S.; Kasahara, C.; Rickles, R.J.; Schreiber, S.L. Specific interactions outside the proline-rich core of two classes of Src homology 3 ligands. *Proc. Natl. Acad. Sci. USA* **1995**, *92*, 12408–12415. [CrossRef]
38. Cámara-Artigas, A.; Martínez-Rodríguez, S.; Ortiz-Salmerón, E.; Martín-García, J.M. 3D domain swapping in a chimeric c-Src SH3 domain takes place through two hinge loops. *J. Struct. Biol.* **2014**, *186*, 195–203. [CrossRef]
39. Berndt, S.; Gurevich, V.V.; Iverson, T. Crystal structure of the SH3 domain of human Lyn non-receptor tyrosine kinase. *PLoS ONE* **2019**, *14*, e0215140. [CrossRef]
40. Kazemein Jasemi, N.S.; Herrmann, C.; Magdalena Estirado, E.; Gremer, L.; Willbold, D.; Brunsveld, L.; Dvorsky, R.; Ahmadian, M.R. The intramolecular allostery of GRB2 governing its interaction with SOS1 is modulated by phosphotyrosine ligands. *Biochem. J.* **2021**, *478*, 2793–2809. [CrossRef]
41. Heim, J.B.; Squirewell, E.J.; Neu, A.; Zocher, G.; Sominidi-Damodaran, S.; Wyles, S.P.; Nikolova, E.; Behrendt, N.; Saunte, D.M.; Lock-Andersen, J.; et al. Myosin-1E interacts with FAK proline-rich region 1 to induce fibronectin-type matrix. *Proc. Natl. Acad. Sci. USA* **2017**, *114*, 3933–3938. [CrossRef]
42. Rouka, E.; Simister, P.C.; Janning, M.; Kumbrink, J.; Konstantinou, T.; Muniz, J.R.; Joshi, D.; O'Reilly, N.; Volkmer, R.; Ritter, B.; et al. Differential Recognition Preferences of the Three Src Homology 3 (SH3) Domains from the Adaptor CD2-associated Protein (CD2AP) and Direct Association with Ras and Rab Interactor 3 (RIN3). *J. Biol. Chem.* **2015**, *290*, 25275–25292. [CrossRef]
43. Lau, D.H.W.; Hogseth, M.; Phillips, E.C.; O'Neill, M.J.; Pooler, A.M.; Noble, W.; Hanger, D.P. Critical residues involved in tau binding to fyn: Implications for tau phosphorylation in Alzheimer's disease. *Acta Neuropathol. Commun.* **2016**, *4*, 49. [CrossRef] [PubMed]
44. Alexandropoulos, K.; Cheng, G.; Baltimore, D. Proline-rich sequences that bind to Src homology 3 domains with individual specificities. *Proc. Natl. Acad. Sci. USA* **1995**, *92*, 3110–3114. [CrossRef] [PubMed]
45. Camara-Artigas, A.; Ortiz-Salmeron, E.; Andujar-Sánchez, M.; Bacarizo, J.; Martin-Garcia, J.M. The role of water molecules in the binding of class I and II peptides to the SH3 domain of the Fyn tyrosine kinase. *Acta Crystallogr. F Struct. Biol. Commun.* **2016**, *72*, 707–712. [CrossRef]
46. Lewitzky, M.; Harkiolaki, M.; Domart, M.-C.; Jones, E.Y.; Feller, S.M. Mona/Gads SH3C Binding to Hematopoietic Progenitor Kinase 1 (HPK1) Combines an Atypical SH3 Binding Motif, R/KXXK, with a Classical PXXP Motif Embedded in a Polyproline Type II (PPII) Helix*. *J. Biol. Chem.* **2004**, *279*, 28724–28732. [CrossRef]
47. Kaneko, T.; Kumasaka, T.; Ganbe, T.; Sato, T.; Miyazawa, K.; Kitamura, N.; Tanaka, N. Structural insight into modest binding of a non-PXXP ligand to the signal transducing adaptor molecule-2 Src homology 3 domain. *J. Biol. Chem.* **2003**, *278*, 48162–48168. [CrossRef] [PubMed]
48. Liu, Q.; Berry, D.; Nash, P.; Pawson, T.; McGlade, C.J.; Li, S.S.-C. Structural Basis for Specific Binding of the Gads SH3 Domain to an RxxK Motif-Containing SLP-76 Peptide: A Novel Mode of Peptide Recognition. *Mol. Cell* **2003**, *11*, 471–481. [CrossRef]
49. Mongioví, A.M.; Romano, P.R.; Panni, S.; Mendoza, M.; Wong, W.T.; Musacchio, A.; Cesareni, G.; Paolo Di Fiore, P. A novel peptide–SH3 interaction. *EMBO J.* **1999**, *18*, 5300–5309. [CrossRef] [PubMed]
50. Takeuchi, K.; Yang, H.; Ng, E.; Park, S.Y.; Sun, Z.Y.; Reinherz, E.L.; Wagner, G. Structural and functional evidence that Nck interaction with CD3epsilon regulates T-cell receptor activity. *J. Mol. Biol.* **2008**, *380*, 704–716. [CrossRef]
51. Santiveri, C.M.; Borroto, A.; Simón, L.; Rico, M.; Alarcón, B.; Jiménez, M.A. Interaction between the N-terminal SH3 domain of Nckα and CD3ε-derived peptides: Non-canonical and canonical recognition motifs. *Biochim. Et Biophys. Acta (BBA)—Proteins Proteom.* **2009**, *1794*, 110–117. [CrossRef]
52. Jaiswal, M.; Dvorsky, R.; Amin, E.; Risse, S.L.; Fansa, E.K.; Zhang, S.-C.; Taha, M.S.; Gauhar, A.R.; Nakhaei-Rad, S.; Kordes, C. Functional cross-talk between ras and rho pathways: A Ras-specific GTPase-activating protein (p120RasGAP) competitively inhibits the RhoGAP activity of deleted in liver cancer (DLC) tumor suppressor by masking the catalytic arginine finger. *J. Biol. Chem.* **2014**, *289*, 6839–6849. [CrossRef] [PubMed]
53. Gigoux, V.; L'Hoste, S.b.; Raynaud, F.; Camonis, J.; Garbay, C. Identification of Aurora kinases as RasGAP Src homology 3 domain-binding proteins. *J. Biol. Chem.* **2002**, *277*, 23742–23746. [CrossRef] [PubMed]
54. Shin, H.; Hsueh, Y.P.; Yang, F.C.; Kim, E.; Sheng, M. An intramolecular interaction between Src homology 3 domain and guanylate kinase-like domain required for channel clustering by postsynaptic density-95/SAP90. *J. Neurosci.* **2000**, *20*, 3580–3587. [CrossRef] [PubMed]
55. Pechstein, A.; Gerth, F.; Milosevic, I.; Jäpel, M.; Eichhorn-Grünig, M.; Vorontsova, O.; Bacetic, J.; Maritzen, T.; Shupliakov, O.; Freund, C.; et al. Vesicle uncoating regulated by SH3-SH3 domain-mediated complex formation between endophilin and intersectin at synapses. *EMBO Rep.* **2015**, *16*, 232–239. [CrossRef]

56. Ahmad, K.F.; Lim, W.A. The minimal autoinhibited unit of the guanine nucleotide exchange factor intersectin. *PLoS ONE* **2010**, *5*, e11291. [CrossRef] [PubMed]
57. Pankivskyi, S.; Pastré, D.; Steiner, E.; Joshi, V.; Rynditch, A.; Hamon, L. ITSN1 regulates SAM68 solubility through SH3 domain interactions with SAM68 proline-rich motifs. *Cell Mol. Life Sci.* **2021**, *78*, 1745–1763. [CrossRef] [PubMed]
58. Kami, K.; Takeya, R.; Sumimoto, H.; Kohda, D. Diverse recognition of non-PxxP peptide ligands by the SH3 domains from p67(phox), Grb2 and Pex13p. *Embo J.* **2002**, *21*, 4268–4276. [CrossRef]
59. Barnett, P.; Bottger, G.; Klein, A.T.; Tabak, H.F.; Distel, B. The peroxisomal membrane protein Pex13p shows a novel mode of SH3 interaction. *Embo J.* **2000**, *19*, 6382–6391. [CrossRef]
60. Pires, J.R.; Hong, X.; Brockmann, C.; Volkmer-Engert, R.; Schneider-Mergener, J.; Oschkinat, H.; Erdmann, R. The ScPex13p SH3 Domain Exposes Two Distinct Binding Sites for Pex5p and Pex14p. *J. Mol. Biol.* **2003**, *326*, 1427–1435. [CrossRef]
61. Douangamath, A.; Filipp, F.V.; Klein, A.T.; Barnett, P.; Zou, P.; Voorn-Brouwer, T.; Vega, M.C.; Mayans, O.M.; Sattler, M.; Distel, B. Topography for independent binding of α-helical and PPII-helical ligands to a peroxisomal SH3 domain. *Mol. Cell* **2002**, *10*, 1007–1017. [CrossRef]
62. Qadota, H.; Mayans, O.; Matsunaga, Y.; McMurry, J.L.; Wilson, K.J.; Kwon, G.E.; Stanford, R.; Deehan, K.; Tinley, T.L.; Ngwa, V.M.; et al. The SH3 domain of UNC-89 (obscurin) interacts with paramyosin, a coiled-coil protein, in Caenorhabditis elegans muscle. *Mol. Biol. Cell* **2016**, *27*, 1606–1620. [CrossRef] [PubMed]
63. Berry, D.M.; Nash, P.; Liu, S.K.-W.; Pawson, T.; McGlade, C.J. A high-affinity Arg-XX-Lys SH3 binding motif confers specificity for the interaction between Gads and SLP-76 in T cell signaling. *Curr. Biol.* **2002**, *12*, 1336–1341. [CrossRef] [PubMed]
64. Kojima, C.; Hashimoto, A.; Yabuta, I.; Hirose, M.; Hashimoto, S.; Kanaho, Y.; Sumimoto, H.; Ikegami, T.; Sabe, H. Regulation of Bin1 SH3 domain binding by phosphoinositides. *Embo J.* **2004**, *23*, 4413–4422. [CrossRef]
65. Jenna, S.; Hussain, N.K.; Danek, E.I.; Triki, I.; Wasiak, S.; McPherson, P.S.; Lamarche-Vane, N. The activity of the GTPase-activating protein CdGAP is regulated by the endocytic protein intersectin. *J. Biol. Chem.* **2002**, *277*, 6366–6373. [CrossRef]
66. Primeau, M.; Ben Djoudi Ouadda, A.; Lamarche-Vane, N. Cdc42 GTPase-activating protein (CdGAP) interacts with the SH3D domain of Intersectin through a novel basic-rich motif. *FEBS Lett.* **2011**, *585*, 847–853. [CrossRef]
67. Li, C.; Iosef, C.; Jia, C.Y.; Gkourasas, T.; Han, V.K.; Shun-Cheng Li, S. Disease-causing SAP mutants are defective in ligand binding and protein folding. *Biochemistry* **2003**, *42*, 14885–14892. [CrossRef] [PubMed]
68. Chan, B.; Lanyi, A.; Song, H.K.; Griesbach, J.; Simarro-Grande, M.; Poy, F.; Howie, D.; Sumegi, J.; Terhorst, C.; Eck, M.J. SAP couples Fyn to SLAM immune receptors. *Nat. Cell Biol.* **2003**, *5*, 155–160. [CrossRef] [PubMed]
69. Hiroaki, H.; Ago, T.; Ito, T.; Sumimoto, H.; Kohda, D. Solution structure of the PX domain, a target of the SH3 domain. *Nat. Struct. Biol.* **2001**, *8*, 526–530. [CrossRef]
70. Ortega, E.; Buey, R.M.; Sonnenberg, A.; de Pereda, J.M. The structure of the plakin domain of plectin reveals a non-canonical SH3 domain interacting with its fourth spectrin repeat. *J. Biol. Chem.* **2011**, *286*, 12429–12438. [CrossRef]
71. Vaynberg, J.; Fukuda, T.; Chen, K.; Vinogradova, O.; Velyvis, A.; Tu, Y.; Ng, L.; Wu, C.; Qin, J. Structure of an ultraweak protein-protein complex and its crucial role in regulation of cell morphology and motility. *Mol. Cell* **2005**, *17*, 513–523. [CrossRef]
72. Tőke, O.; Koprivanacz, K.; Radnai, L.; Merő, B.; Juhász, T.; Liliom, K.; Buday, L. Solution NMR Structure of the SH3 Domain of Human Caskin1 Validates the Lack of a Typical Peptide Binding Groove and Supports a Role in Lipid Mediator Binding. *Cells* **2021**, *10*, 173. [CrossRef]
73. Heuer, K.; Sylvester, M.; Kliche, S.; Pusch, R.; Thiemke, K.; Schraven, B.; Freund, C. Lipid-binding hSH3 domains in immune cell adapter proteins. *J. Mol. Biol.* **2006**, *361*, 94–104. [CrossRef]
74. Yip, K.T.; Zhong, X.Y.; Seibel, N.; Pütz, S.; Autzen, J.; Gasper, R.; Hofmann, E.; Scherkenbeck, J.; Stoll, R. Small molecules antagonise the MIA-Fibronectin interaction in malignant melanoma. *Sci. Rep.* **2016**, *6*, 1–12. [CrossRef] [PubMed]
75. Dionne, U.; Percival, L.J.; Chartier, F.J.; Landry, C.R.; Bisson, N. SRC homology 3 domains: Multifaceted binding modules. *Trends Biochem. Sci.* **2022**, *47*, 772–784. [CrossRef]
76. The UniProt, C. UniProt: The Universal Protein Knowledgebase in 2023. *Nucleic Acids Res.* **2023**, *51*, D523–D531. [CrossRef]
77. Thompson, J.D.; Higgins, D.G.; Gibson, T.J. CLUSTAL W: Improving the sensitivity of progressive multiple sequence alignment through sequence weighting, position-specific gap penalties and weight matrix choice. *Nucleic Acids Res.* **1994**, *22*, 4673–4680. [CrossRef]
78. Dimitratos, S.D.; Woods, D.F.; Stathakis, D.G.; Bryant, P.J. Signaling pathways are focused at specialized regions of the plasma membrane by scaffolding proteins of the MAGUK family. *Bioessays* **1999**, *21*, 912–921. [CrossRef]
79. McPherson, P.S. Regulatory role of SH3 domain-mediated protein-protein interactions in synaptic vesicle endocytosis. *Cell Signal* **1999**, *11*, 229–238. [CrossRef]
80. Kurochkina, N.; Guha, U. SH3 domains: Modules of protein–protein interactions. *Biophys. Rev.* **2013**, *5*, 29–39. [CrossRef] [PubMed]
81. Bialkowska, K.; Saido, T.C.; Fox, J.E.B. SH3 domain of spectrin participates in the activation of Rac in specialized calpain-induced integrin signaling complexes. *J. Cell Sci.* **2005**, *118*, 381–395. [CrossRef]
82. Pechstein, A.; Tomilin, N.; Fredrich, K.; Vorontsova, O.; Sopova, E.; Evergren, E.; Haucke, V.; Brodin, L.; Shupliakov, O. Vesicle Clustering in a Living Synapse Depends on a Synapsin Region that Mediates Phase Separation. *Cell Rep.* **2020**, *30*, 2594–2602.e2593. [CrossRef] [PubMed]

83. Ghosh, A.; Mazarakos, K.; Zhou, H.-X. Three archetypical classes of macromolecular regulators of protein liquid–liquid phase separation. *Proc. Natl. Acad. Sci.* **2019**, *116*, 19474–19483. [CrossRef] [PubMed]
84. Pak, C.W.; Kosno, M.; Holehouse, A.S.; Padrick, S.B.; Mittal, A.; Ali, R.; Yunus, A.A.; Liu, D.R.; Pappu, R.V.; Rosen, M.K. Sequence determinants of intracellular phase separation by complex coacervation of a disordered protein. *Mol. Cell* **2016**, *63*, 72–85. [CrossRef] [PubMed]
85. Li, P.; Banjade, S.; Cheng, H.-C.; Kim, S.; Chen, B.; Guo, L.; Llaguno, M.; Hollingsworth, J.V.; King, D.S.; Banani, S.F.; et al. Phase transitions in the assembly of multivalent signalling proteins. *Nature* **2012**, *483*, 336–340. [CrossRef]
86. Stoll, R.; Bosserhoff, A. Extracellular SH3 domain containing proteins-features of a new protein family. *Curr. Protein Pept. Sci.* **2008**, *9*, 221–226. [CrossRef] [PubMed]
87. Bauer, R.; Humphries, M.; Fässler, R.; Winklmeier, A.; Craig, S.E.; Bosserhoff, A.-K. Regulation of integrin activity by MIA. *J. Biol. Chem.* **2006**, *281*, 11669–11677. [CrossRef]
88. Chew, C.S.; Parente, J.A.; Chen, X.; Chaponnier, C.; Cameron, R.S. The LIM and SH3 domain-containing protein, lasp-1, may link the cAMP signaling pathway with dynamic membrane restructuring activities in ion transporting epithelia. *J. Cell Sci.* **2000**, *113*, 2035–2045. [CrossRef]
89. Skolnik, E.; Lee, C.; Batzer, A.; Vicentini, L.; Zhou, M.; Daly, R.; Myers, M., Jr.; Backer, J.; Ullrich, A.; White, M. The SH2/SH3 domain-containing protein GRB2 interacts with tyrosine-phosphorylated IRS1 and Shc: Implications for insulin control of ras signalling. *EMBO J.* **1993**, *12*, 1929–1936. [CrossRef]
90. Kohda, D.; Hatanaka, H.; Odaka, M.; Mandiyan, V.; Ullrich, A.; Schlessinger, J.; Inagaki, F. Solution structure of the SH3 domain of phospholipase C-gamma. *Cell* **1993**, *72*, 953–960. [CrossRef]
91. Ortiz, M.A.; Mikhailova, T.; Li, X.; Porter, B.A.; Bah, A.; Kotula, L. Src family kinases, adaptor proteins and the actin cytoskeleton in epithelial-to-mesenchymal transition. *Cell Commun. Signal.* **2021**, *19*, 67. [CrossRef]
92. Hsueh, Y.-P.; Wang, T.-F.; Yang, F.-C.; Sheng, M. Nuclear translocation and transcription regulation by the membrane-associated guanylate kinase CASK/LIN-2. *Nature* **2000**, *404*, 298–302. [CrossRef] [PubMed]
93. Lefferts, J.A.; Wang, C.; Sridharan, D.; Baralt, M.; Lambert, M.W. The SH3 domain of alphaII spectrin is a target for the Fanconi anemia protein, FANCG. *Biochemistry* **2009**, *48*, 254–263. [CrossRef]
94. Jaiswal, M.; Dvorsky, R.; Ahmadian, M.R. Deciphering the molecular and functional basis of Dbl family proteins: A novel systematic approach toward classification of selective activation of the Rho family proteins. *J. Biol. Chem.* **2013**, *288*, 4486–4500. [CrossRef] [PubMed]
95. Salazar, M.A.; Kwiatkowski, A.V.; Pellegrini, L.; Cestra, G.; Butler, M.H.; Rossman, K.L.; Serna, D.M.; Sondek, J.; Gertler, F.B.; De Camilli, P. Tuba, a novel protein containing bin/amphiphysin/Rvs and Dbl homology domains, links dynamin to regulation of the actin cytoskeleton. *J. Biol. Chem.* **2003**, *278*, 49031–49043. [CrossRef] [PubMed]
96. Sato, M.; Kitaguchi, T.; Numano, R.; Ikematsu, K.; Kakeyama, M.; Murata, M.; Sato, K.; Tsuboi, T. The small GTPase Cdc42 modulates the number of exocytosis-competent dense-core vesicles in PC12 cells. *Biochem. Biophys. Res. Commun.* **2012**, *420*, 417–421. [CrossRef] [PubMed]
97. Momboisse, F.; Ory, S.; Ceridono, M.; Calco, V.; Vitale, N.; Bader, M.F.; Gasman, S. The Rho guanine nucleotide exchange factors Intersectin 1L and β-Pix control calcium-regulated exocytosis in neuroendocrine PC12 cells. *Cell Mol. Neurobiol.* **2010**, *30*, 1327–1333. [CrossRef]
98. Zamanian, J.L.; Kelly, R.B. Intersectin 1L guanine nucleotide exchange activity is regulated by adjacent src homology 3 domains that are also involved in endocytosis. *Mol. Biol. Cell* **2003**, *14*, 1624–1637. [CrossRef]
99. Malacombe, M.; Ceridono, M.; Calco, V.; Chasserot-Golaz, S.; McPherson, P.S.; Bader, M.F.; Gasman, S. Intersectin-1L nucleotide exchange factor regulates secretory granule exocytosis by activating Cdc42. *Embo J.* **2006**, *25*, 3494–3503. [CrossRef]
100. Oda, Y.; Otani, T.; Ikenouchi, J.; Furuse, M. Tricellulin regulates junctional tension of epithelial cells at tricellular contacts through Cdc42. *J. Cell Sci.* **2014**, *127*, 4201–4212.
101. Young, P.; Ehler, E.; Gautel, M. Obscurin, a giant sarcomeric Rho guanine nucleotide exchange factor protein involved in sarcomere assembly. *J. Cell Biol.* **2001**, *154*, 123–136. [CrossRef]
102. Koch, D.; Kho, A.L.; Fukuzawa, A.; Alexandrovich, A.; Vanaanen, K.J.; Beavil, A.; Pfuhl, M.; Rees, M.; Gautel, M. Obscurin Rho GEF domains are phosphorylated by MST-family kinases but do not exhibit nucleotide exchange factor activity towards Rho GTPases in vitro. *PLoS ONE* **2023**, *18*, e0284453.
103. Yuen, M.; Ottenheijm, C.A.C. Nebulin: Big protein with big responsibilities. *J. Muscle Res. Cell Motil.* **2020**, *41*, 103–124. [CrossRef] [PubMed]
104. Cusseddu, R.; Robert, A.; Côté, J.F. Strength Through Unity: The Power of the Mega-Scaffold MACF1. *Front. Cell Dev. Biol.* **2021**, *9*, 641727. [CrossRef]
105. Tscheudschilsuren, G.; Bosserhoff, A.K.; Schlegel, J.; Vollmer, D.; Anton, A.; Alt, V.; Schnettler, R.; Brandt, J.; Proetzel, G. Regulation of mesenchymal stem cell and chondrocyte differentiation by MIA. *Exp. Cell Res.* **2006**, *312*, 63–72. [CrossRef]
106. Stoll, R.; Renner, C.; Zweckstetter, M.; Brüggert, M.; Ambrosius, D.; Palme, S.; Engh, R.A.; Golob, M.; Breibach, I.; Buettner, R.; et al. The extracellular human melanoma inhibitory activity (MIA) protein adopts an SH3 domain-like fold. *Embo J.* **2001**, *20*, 340–349. [CrossRef] [PubMed]

107. Siveen, K.S.; Prabhu, K.S.; Achkar, I.W.; Kuttikrishnan, S.; Shyam, S.; Khan, A.Q.; Merhi, M.; Dermime, S.; Uddin, S. Role of Non Receptor Tyrosine Kinases in Hematological Malignances and its Targeting by Natural Products. *Mol. Cancer* **2018**, *17*, 31. [CrossRef]
108. Mahajan, K.; Mahajan, N.P. PI3K-independent AKT activation in cancers: A treasure trove for novel therapeutics. *J. Cell. Physiol.* **2012**, *227*, 3178–3184. [CrossRef]
109. Pawson, T. Specificity in Signal Transduction: From Phosphotyrosine-SH2 Domain Interactions to Complex Cellular Systems. *Cell* **2004**, *116*, 191–203. [CrossRef]
110. Lundby, A.; Franciosa, G.; Emdal, K.B.; Refsgaard, J.C.; Gnosa, S.P.; Bekker-Jensen, D.B.; Secher, A.; Maurya, S.R.; Paul, I.; Mendez, B.L.; et al. Oncogenic Mutations Rewire Signaling Pathways by Switching Protein Recruitment to Phosphotyrosine Sites. *Cell* **2019**, *179*, 543–560.e526. [CrossRef]
111. Birge, R.B.; Kalodimos, C.; Inagaki, F.; Tanaka, S. Crk and CrkL adaptor proteins: Networks for physiological and pathological signaling. *Cell Commun. Signal.* **2009**, *7*, 13. [CrossRef]
112. Moharram, S.A.; Rönnstrand, L.; Kazi, J.U. Src-Like Adapter Protein (SLAP). In *Encyclopedia of Signaling Molecules*; Choi, S., Ed.; Springer International Publishing: Cham, Switzerland, 2018; pp. 5145–5149. [CrossRef]
113. Pamonsinlapatham, P.; Hadj-Slimane, R.; Lepelletier, Y.; Allain, B.; Toccafondi, M.; Garbay, C.; Raynaud, F. P120-Ras GTPase activating protein (RasGAP): A multi-interacting protein in downstream signaling. *Biochimie* **2009**, *91*, 320–328. [CrossRef] [PubMed]
114. Chadee, D.N. Involvement of mixed lineage kinase 3 in cancer. *Can. J. Physiol. Pharmacol.* **2013**, *91*, 268–274. [CrossRef] [PubMed]
115. Kim, H.Y.; Suh, P.-G.; Kim, J.-I. The Role of Phospholipase C in GABAergic Inhibition and Its Relevance to Epilepsy. *Int. J. Mol. Sci.* **2021**, *22*, 3149. [CrossRef] [PubMed]
116. Emmanouilidi, A.; Lattanzio, R.; Sala, G.; Piantelli, M.; Falasca, M. The role of phospholipase Cγ1 in breast cancer and its clinical significance. *Future Oncol.* **2017**, *13*, 1991–1997. [CrossRef]
117. Schumacher, C.; Knudsen, B.S.; Ohuchi, T.; Fiore, P.P.D.; Glassman, R.H.; Hanafusa, H. The SH3 Domain of Crk Binds Specifically to a Conserved Proline-rich Motif in Eps15 and Eps15R (∗). *J. Biol. Chem.* **1995**, *270*, 15341–15347. [CrossRef]
118. Tatosyan, A.; Mizenina, O. Kinases of the Src family: Structure and functions. *BIOCHEMISTRY C/C OF BIOKHIMIIA* **2000**, *65*, 49–58.
119. Santy, L.C.; Casanova, J.E. GTPase Signaling: Bridging the GAP between ARF and Rho. *Curr. Biol.* **2002**, *12*, R360–R362. [CrossRef]
120. Vigil, D.; Cherfils, J.; Rossman, K.L.; Der, C.J. Ras superfamily GEFs and GAPs: Validated and tractable targets for cancer therapy? *Nat. Rev. Cancer* **2010**, *10*, 842–857. [CrossRef]
121. Furukawa, Y.; Kawasoe, T.; Daigo, Y.; Nishiwaki, T.; Ishiguro, H.; Takahashi, M.; Kitayama, J.; Nakamura, Y. Isolation of a novel human gene, ARHGAP9, encoding a rho-GTPase activating protein. *Biochem. Biophys. Res. Commun.* **2001**, *284*, 643–649. [CrossRef]
122. Sakakibara, T.; Nemoto, Y.; Nukiwa, T.; Takeshima, H. Identification and characterization of a novel Rho GTPase activating protein implicated in receptor-mediated endocytosis. *FEBS Lett.* **2004**, *566*, 294–300. [CrossRef]
123. Bourgeois, J.S.; Wang, L.; Rabino, A.F.; Everitt, J.; Alvarez, M.I.; Awadia, S.; Wittchen, E.S.; Garcia-Mata, R.; Ko, D.C. ARHGEF26 enhances Salmonella invasion and inflammation in cells and mice. *PLoS Pathog.* **2021**, *17*, e1009713. [CrossRef] [PubMed]
124. Zhang, M.; Lin, L.; Wang, C.; Zhu, J. Double inhibition and activation mechanisms of Ephexin family RhoGEFs. *Proc. Natl. Acad. Sci.* **2021**, *118*, e2024465118. [CrossRef] [PubMed]
125. Zamboni, V.; Jones, R.; Umbach, A.; Ammoni, A.; Passafaro, M.; Hirsch, E.; Merlo, G.R. Rho GTPases in intellectual disability: From genetics to therapeutic opportunities. *Int. J. Mol. Sci.* **2018**, *19*, 1821. [CrossRef] [PubMed]
126. López Tobón, A.; Suresh, M.; Jin, J.; Vitriolo, A.; Pietralla, T.; Tedford, K.; Bossenz, M.; Mahnken, K.; Kiefer, F.; Testa, G.; et al. The guanine nucleotide exchange factor Arhgef7/βPix promotes axon formation upstream of TC10. *Sci. Rep.* **2018**, *8*, 8811. [CrossRef]
127. Maiwald, S.; Motazacker, M.M.; van Capelleveen, J.C.; Sivapalaratnam, S.; van der Wal, A.C.; van der Loos, C.; Kastelein, J.J.; Ouwehand, W.H.; Hovingh, G.K.; Trip, M.D.; et al. A rare variant in MCF2L identified using exclusion linkage in a pedigree with premature atherosclerosis. *Eur. J. Hum. Genet.* **2016**, *24*, 86–91. [CrossRef]
128. Paskus, J.D.; Herring, B.E.; Roche, K.W. Kalirin and Trio: RhoGEFs in synaptic transmission, plasticity, and complex brain disorders. *Trends Neurosci.* **2020**, *43*, 505–518. [CrossRef]
129. Grubisha, M.J.; DeGiosio, R.A.; Wills, Z.P.; Sweet, R.A. Trio and Kalirin as unique enactors of Rho/Rac spatiotemporal precision. *Cell Signal* **2022**, *98*, 110416. [CrossRef]
130. Abe, K.; Rossman, K.L.; Liu, B.; Ritola, K.D.; Chiang, D.; Campbell, S.L.; Burridge, K.; Der, C.J. Vav2 is an activator of Cdc42, Rac1, and RhoA. *J. Biol. Chem.* **2000**, *275*, 10141–10149. [CrossRef]
131. Kliche, S.; Breitling, D.; Togni, M.; Pusch, R.; Heuer, K.; Wang, X.; Freund, C.; Kasirer-Friede, A.; Menasche, G.; Koretzky, G.A.; et al. The ADAP/SKAP55 signaling module regulates T-cell receptor-mediated integrin activation through plasma membrane targeting of Rap1. *Mol. Cell Biol.* **2006**, *26*, 7130–7144. [CrossRef]
132. Ménasché, G.; Kliche, S.; Chen, E.J.; Stradal, T.E.; Schraven, B.; Koretzky, G. RIAM links the ADAP/SKAP-55 signaling module to Rap1, facilitating T-cell-receptor-mediated integrin activation. *Mol. Cell Biol.* **2007**, *27*, 4070–4081. [CrossRef]
133. Schiller, M.R.; Chakrabarti, K.; King, G.F.; Schiller, N.I.; Eipper, B.A.; Maciejewski, M.W. Regulation of RhoGEF activity by intramolecular and intermolecular SH3 domain interactions. *J. Biol. Chem.* **2006**, *281*, 18774–18786. [CrossRef]

134. Zhang, P.; Liu, Y.; Lian, C.; Cao, X.; Wang, Y.; Li, X.; Cong, M.; Tian, P.; Zhang, X.; Wei, G. SH3RF3 promotes breast cancer stem-like properties via JNK activation and PTX3 upregulation. *Nat. Commun.* **2020**, *11*, 1–13. [CrossRef]
135. Binder, C.; Cvetkovski, F.; Sellberg, F.; Berg, S.; Paternina Visbal, H.; Sachs, D.H.; Berglund, E.; Berglund, D. CD2 immunobiology. *Front. Immunol.* **2020**, *11*, 1090. [CrossRef]
136. Martin, C.E.; Jones, N. Nephrin signaling in the podocyte: An updated view of signal regulation at the slit diaphragm and beyond. *Front. Endocrinol.* **2018**, *9*, 302. [CrossRef]
137. Machuca, E.; Benoit, G.; Antignac, C. Genetics of nephrotic syndrome: Connecting molecular genetics to podocyte physiology. *Hum. Mol. Genet.* **2009**, *18*, R185–R194. [CrossRef] [PubMed]
138. Li, W.; Fan, J.; Woodley, D.T. Nck/Dock: An adapter between cell surface receptors and the actin cytoskeleton. *Oncogene* **2001**, *20*, 6403–6417. [CrossRef] [PubMed]
139. Brockmann, M.M.; Zarebidaki, F.; Camacho, M.; Grauel, M.K.; Trimbuch, T.; Südhof, T.C.; Rosenmund, C. A Trio of Active Zone Proteins Comprised of RIM-BPs, RIMs, and Munc13s Governs Neurotransmitter Release. *Cell Rep.* **2020**, *32*, 107960. [CrossRef]
140. Hammouda, M.B.; Ford, A.E.; Liu, Y.; Zhang, J.Y. The JNK signaling pathway in inflammatory skin disorders and cancer. *Cells* **2020**, *9*, 857. [CrossRef]
141. Flucher, B.E.; Campiglio, M. STAC proteins: The missing link in skeletal muscle EC coupling and new regulators of calcium channel function. *Biochim. Et Biophys. Acta (BBA)—Mol. Cell Res.* **2019**, *1866*, 1101–1110. [CrossRef] [PubMed]
142. Vermeren, M.; Lyraki, R.; Wani, S.; Airik, R.; Albagha, O.; Mort, R.; Hildebrandt, F.; Hurd, T. Osteoclast stimulation factor 1 (Ostf1) KNOCKOUT increases trabecular bone mass in mice. *Mamm. Genome* **2017**, *28*, 498–514. [CrossRef] [PubMed]
143. Milosevic, I.; Giovedi, S.; Lou, X.; Raimondi, A.; Collesi, C.; Shen, H.; Paradise, S.; O'Toole, E.; Ferguson, S.; Cremona, O.; et al. Recruitment of endophilin to clathrin-coated pit necks is required for efficient vesicle uncoating after fission. *Neuron* **2011**, *72*, 587–601. [CrossRef] [PubMed]
144. Ringstad, N.; Nemoto, Y.; De Camilli, P. Differential Expression of Endophilin 1 and 2 Dimers at Central Nervous System Synapses*. *J. Biol. Chem.* **2001**, *276*, 40424–40430. [CrossRef]
145. Cestra, G.; Castagnoli, L.; Dente, L.; Minenkova, O.; Petrelli, A.; Migone, N.; Hoffmüller, U.; Schneider-Mergener, J.; Cesareni, G. The SH3 Domains of Endophilin and Amphiphysin Bind to the Proline-rich Region of Synaptojanin 1 at Distinct Sites That Display an Unconventional Binding Specificity*. *J. Biol. Chem.* **1999**, *274*, 32001–32007. [CrossRef]
146. Kreienkamp, H.-J. Scaffolding proteins at the postsynaptic density: Shank as the architectural framework. In *Protein-Protein Interactions as New Drug Targets*; Springer: Berlin/Heidelberg, Germany, 2008; pp. 365–380.
147. Shi, R.; Redman, P.; Ghose, D.; Hwang, H.; Liu, Y.; Ren, X.; Ding, L.J.; Liu, M.; Jones, K.J.; Xu, W. Shank Proteins Differentially Regulate Synaptic Transmission. *Eneuro* **2017**, *4*. [CrossRef]
148. Oliva, C.; Escobedo, P.; Astorga, C.; Molina, C.; Sierralta, J. Role of the MAGUK protein family in synapse formation and function. *Dev. Neurobiol.* **2012**, *72*, 57–72. [CrossRef]
149. De Mendoza, A.; Suga, H.; Ruiz-Trillo, I. Evolution of the MAGUK protein gene family in premetazoan lineages. *BMC Evol. Biol.* **2010**, *10*, 93. [CrossRef]
150. Budnik, V.; Koh, Y.-H.; Guan, B.; Hartmann, B.; Hough, C.; Woods, D.; Gorczyca, M. Regulation of Synapse Structure and Function by the Drosophila Tumor Suppressor Gene dlg. *Neuron* **1996**, *17*, 627–640. [CrossRef]
151. Wilkinson, B.; Coba, M.P. Molecular architecture of postsynaptic Interactomes. *Cell Signal* **2020**, *76*, 109782. [CrossRef] [PubMed]
152. Rima, M.; Daghsni, M.; Fajloun, Z.; M'rad, R.; Brusés, J.L.; Ronjat, M.; De Waard, M. Protein partners of the calcium channel β subunit highlight new cellular functions. *Biochem. J.* **2016**, *473*, 1831–1844. [CrossRef]
153. Wolburg, H.; Lippoldt, A. Tight junctions of the blood–brain barrier: Development, composition and regulation. *Vasc. Pharmacol.* **2002**, *38*, 323–337. [CrossRef]
154. McLaughlin, M.; Hale, R.; Ellston, D.; Gaudet, S.; Lue, R.A.; Viel, A. The Distribution and Function of Alternatively Spliced Insertions in hDlg*. *J. Biol. Chem.* **2002**, *277*, 6406–6412. [CrossRef]
155. Cai, C.; Li, H.; Rivera, C.; Keinänen, K. Interaction between SAP97 and PSD-95, Two Maguk Proteins Involved in Synaptic Trafficking of AMPA Receptors*. *J. Biol. Chem.* **2006**, *281*, 4267–4273. [CrossRef]
156. McGee, A.W.; Bredt, D.S. Identification of an Intramolecular Interaction between the SH3 and Guanylate Kinase Domains of PSD-95*. *J. Biol. Chem.* **1999**, *274*, 17431–17436. [CrossRef]
157. McGee, A.W.; Dakoji, S.R.; Olsen, O.; Bredt, D.S.; Lim, W.A.; Prehoda, K.E. Structure of the SH3-Guanylate Kinase Module from PSD-95 Suggests a Mechanism for Regulated Assembly of MAGUK Scaffolding Proteins. *Mol. Cell* **2001**, *8*, 1291–1301. [CrossRef]
158. Wu, H.; Reissner, C.; Kuhlendahl, S.; Coblentz, B.; Reuver, S.; Kindler, S.; Gundelfinger, E.D.; Garner, C.C. Intramolecular interactions regulate SAP97 binding to GKAP. *Embo J.* **2000**, *19*, 5740–5751. [CrossRef]
159. Marcette, J.; Hood, I.V.; Johnston, C.A.; Doe, C.Q.; Prehoda, K.E. Allosteric control of regulated scaffolding in membrane-associated guanylate kinases. *Biochemistry* **2009**, *48*, 10014–10019. [CrossRef]
160. Tavares, G.A.; Panepucci, E.H.; Brunger, A.T. Structural Characterization of the Intramolecular Interaction between the SH3 and Guanylate Kinase Domains of PSD-95. *Mol. Cell* **2001**, *8*, 1313–1325. [CrossRef]
161. Aspenström, P. A Cdc42 target protein with homology to the non-kinase domain of FER has a potential role in regulating the actin cytoskeleton. *Curr. Biol.* **1997**, *7*, 479–487. [CrossRef]
162. Wang, Z.; Wang, Y.; Peng, M.; Yi, L. UBASH3B is a novel prognostic biomarker and correlated with immune infiltrates in prostate cancer. *Front. Oncol.* **2020**, *9*, 1517. [CrossRef]

163. Ge, Y.; Paisie, T.; Chen, S.; Concannon, P. UBASH3A regulates the synthesis and dynamics of T-cell receptor-CD3 complexes. *J. Immunol.* **2019**, *203*, 2827–2836. [CrossRef]
164. Yamagata, K.; Nakayamada, S.; Zhang, T.; Nguyen, A.P.; Ohkubo, N.; Iwata, S.; Kato, S.; Tanaka, Y. IL-6 production through repression of UBASH3A gene via epigenetic dysregulation of super-enhancer in CD4+ T cells in rheumatoid arthritis. *Inflamm. Regen.* **2022**, *42*, 46. [CrossRef] [PubMed]
165. Hoeller, D.; Crosetto, N.; Blagoev, B.; Raiborg, C.; Tikkanen, R.; Wagner, S.; Kowanetz, K.; Breitling, R.; Mann, M.; Stenmark, H.; et al. Regulation of ubiquitin-binding proteins by monoubiquitination. *Nat. Cell Biol.* **2006**, *8*, 163–169. [CrossRef]
166. Feshchenko, E.A.; Smirnova, E.V.; Swaminathan, G.; Teckchandani, A.M.; Agrawal, R.; Band, H.; Zhang, X.; Annan, R.S.; Carr, S.A.; Tsygankov, A.Y. TULA: An SH3- and UBA-containing protein that binds to c-Cbl and ubiquitin. *Oncogene* **2004**, *23*, 4690–4706. [CrossRef]
167. Ge, Y.; Paisie, T.K.; Newman, J.R.B.; McIntyre, L.M.; Concannon, P. UBASH3A Mediates Risk for Type 1 Diabetes Through Inhibition of T-Cell Receptor-Induced NF-κB Signaling. *Diabetes* **2017**, *66*, 2033–2043. [CrossRef] [PubMed]
168. Briknarová, K.; Nasertorabi, F.; Havert, M.L.; Eggleston, E.; Hoyt, D.W.; Li, C.; Olson, A.J.; Vuori, K.; Ely, K.R. The Serine-rich Domain from Crk-associated Substrate (p130^{cas}) Is a Four-helix Bundle *. *J. Biol. Chem.* **2005**, *280*, 21908–21914. [CrossRef] [PubMed]
169. Guerrero, M.S.; Parsons, J.T.; Bouton, A.H. Cas and NEDD9 Contribute to Tumor Progression through Dynamic Regulation of the Cytoskeleton. *Genes. Cancer* **2012**, *3*, 371–381. [CrossRef]
170. Tornillo, G.; Defilippi, P.; Cabodi, S. Cas proteins: Dodgy scaffolding in breast cancer. *Breast Cancer Res.* **2014**, *16*, 1–9. [CrossRef]
171. Heissler, S.M.; Sellers, J.R. Myosins. In *Encyclopedia of Cell Biology*; Bradshaw, R.A., Stahl, P.D., Eds.; Academic Press: Waltham, MA, USA, 2016; pp. 597–607. [CrossRef]
172. Rogers, S.L.; Gelfand, V.I. Membrane trafficking, organelle transport, and the cytoskeleton. *Curr. Opin. Cell Biol.* **2000**, *12*, 57–62. [CrossRef]
173. Li, S.; Mecca, A.; Kim, J.; Caprara, G.A.; Wagner, E.L.; Du, T.-T.; Petrov, L.; Xu, W.; Cui, R.; Rebustini, I.T.; et al. Myosin-VIIa is expressed in multiple isoforms and essential for tensioning the hair cell mechanotransduction complex. *Nat. Commun.* **2020**, *11*, 2066. [CrossRef]
174. Ehl, S.; de Saint Basile, G. Chapter 20—Genetic Diseases Predisposing to HLH. In *Stiehm's Immune Deficiencies*; Sullivan, K.E., Stiehm, E.R., Eds.; Academic Press: Amsterdam, The Netherlands, 2014; pp. 437–460. [CrossRef]
175. Navinés-Ferrer, A.; Martín, M. Long-Tailed Unconventional Class I Myosins in Health and Disease. *Int. J. Mol. Sci.* **2020**, *21*, 2555. [CrossRef] [PubMed]
176. Berg, J.S.; Powell, B.C.; Cheney, R.E. A millennial myosin census. *Mol. Biol. Cell* **2001**, *12*, 780–794. [CrossRef] [PubMed]
177. Fili, N.; Toseland, C.P. Unconventional Myosins: How Regulation Meets Function. *Int. J. Mol. Sci.* **2020**, *21*, 67. [CrossRef] [PubMed]
178. Woolner, S.; Bement, W.M. Unconventional myosins acting unconventionally. *Trends Cell Biol.* **2009**, *19*, 245–252. [CrossRef]
179. Bi, J.; Chase, S.E.; Pellenz, C.D.; Kurihara, H.; Fanning, A.S.; Krendel, M. Myosin 1e is a component of the glomerular slit diaphragm complex that regulates actin reorganization during cell-cell contact formation in podocytes. *Am. J. Physiol. -Ren. Physiol.* **2013**, *305*, F532–F544. [CrossRef] [PubMed]
180. Yu, I.-M.; Planelles-Herrero, V.J.; Sourigues, Y.; Moussaoui, D.; Sirkia, H.; Kikuti, C.; Stroebel, D.; Titus, M.A.; Houdusse, A. Myosin 7 and its adaptors link cadherins to actin. *Nat. Commun.* **2017**, *8*, 15864. [CrossRef]
181. Grimshaw, S.J.; Mott, H.R.; Stott, K.M.; Nielsen, P.R.; Evetts, K.A.; Hopkins, L.J.; Nietlispach, D.; Owen, D. Structure of the Sterile α Motif (SAM) Domain of the Saccharomyces cerevisiae Mitogen-activated Protein Kinase Pathway-modulating Protein STE50 and Analysis of Its Interaction with the STE11 SAM*. *J. Biol. Chem.* **2004**, *279*, 2192–2201. [CrossRef]
182. Qiao, F.; Bowie, J.U. The Many Faces of SAM. *Sci. STKE* **2005**, *2005*, re7. [CrossRef]
183. Grossmann, A.; Benlasfer, N.; Birth, P.; Hegele, A.; Wachsmuth, F.; Apelt, L.; Stelzl, U. Phospho-tyrosine dependent protein–protein interaction network. *Mol. Syst. Biol.* **2015**, *11*, 794. [CrossRef]
184. Toonen, R.F.G.; Verhage, M. Vesicle trafficking: Pleasure and pain from SM genes. *Trends Cell Biol.* **2003**, *13*, 177–186. [CrossRef]
185. Offenhäuser, N.; Borgonovo, A.; Disanza, A.; Romano, P.; Ponzanelli, I.; Iannolo, G.; Di Fiore, P.P.; Scita, G. The eps8 family of proteins links growth factor stimulation to actin reorganization generating functional redundancy in the Ras/Rac pathway. *Mol. Biol. Cell* **2004**, *15*, 91–98. [CrossRef]
186. Jaufmann, J.; Franke, F.C.; Sperlich, A.; Blumendeller, C.; Kloos, I.; Schneider, B.; Sasaki, D.; Janssen, K.P.; Beer-Hammer, S. The emerging and diverse roles of the SLy/SASH1-protein family in health and disease-Overview of three multifunctional proteins. *Faseb J.* **2021**, *35*, e21470. [CrossRef] [PubMed]
187. Kwan, J.J.; Slavkovic, S.; Piazza, M.; Wang, D.; Dieckmann, T.; Johnson, P.E.; Wen, X.-Y.; Donaldson, L.W. HACS1 signaling adaptor protein recognizes a motif in the paired immunoglobulin receptor B cytoplasmic domain. *Commun. Biol.* **2020**, *3*, 672. [CrossRef]
188. Bencsik, N.; Pusztai, S.; Borbély, S.; Fekete, A.; Dülk, M.; Kis, V.; Pesti, S.; Vas, V.; Szűcs, A.; Buday, L.; et al. Dendritic spine morphology and memory formation depend on postsynaptic Caskin proteins. *Sci. Rep.* **2019**, *9*, 16843. [CrossRef] [PubMed]
189. Kwan, J.J.; Donaldson, L.W. A lack of peptide binding and decreased thermostability suggests that the CASKIN2 scaffolding protein SH3 domain may be vestigial. *BMC Struct. Biol.* **2016**, *16*, 14. [CrossRef] [PubMed]

190. Yamada, M.; Ishii, N.; Asao, H.; Murata, K.; Kanazawa, C.; Sasaki, H.; Sugamura, K. Signal-transducing adaptor molecules STAM1 and STAM2 are required for T-cell development and survival. *Mol. Cell Biol.* **2002**, *22*, 8648–8658. [CrossRef] [PubMed]
191. Kim, H.; Oh, H.; Oh, Y.S.; Bae, J.; Hong, N.H.; Park, S.J.; Ahn, S.; Lee, M.; Rhee, S.; Lee, S.H.; et al. SPIN90, an adaptor protein, alters the proximity between Rab5 and Gapex5 and facilitates Rab5 activation during EGF endocytosis. *Exp. Mol. Med.* **2019**, *51*, 1–14. [CrossRef]
192. Davis, R.J. Signal transduction by the JNK group of MAP kinases. *Cell* **2000**, *103*, 239–252. [CrossRef]
193. Radhakrishnan, H.; Walther, W.; Zincke, F.; Kobelt, D.; Imbastari, F.; Erdem, M.; Kortüm, B.; Dahlmann, M.; Stein, U. MACC1-the first decade of a key metastasis molecule from gene discovery to clinical translation. *Cancer Metastasis Rev.* **2018**, *37*, 805–820. [CrossRef]
194. Bedford, M.T.; Clarke, S.G. Protein arginine methylation in mammals: Who, what, and why. *Mol. Cell* **2009**, *33*, 1–13. [CrossRef] [PubMed]
195. Esmailzadeh, S.; Jiang, X. AHI-1: A novel signaling protein and potential therapeutic target in human leukemia and brain disorders. *Oncotarget* **2011**, *2*, 918–934. [CrossRef]
196. Butt, E.; Howard, C.M.; Raman, D. LASP1 in Cellular Signaling and Gene Expression: More than Just a Cytoskeletal Regulator. *Cells* **2022**, *11*, 3817. [CrossRef] [PubMed]
197. Jung, S.E.; Choi, J.W.; Moon, H.; Oh, S.; Lim, S.; Lee, S.; Kim, S.W.; Hwang, K.C. Small G protein signaling modulator 3 (SGSM3) knockdown attenuates apoptosis and cardiogenic differentiation in rat mesenchymal stem cells exposed to hypoxia. *PLoS ONE* **2020**, *15*, e0231272. [CrossRef]
198. Carrizosa, E. Role and Regulation of the Actin-Regulatory Protein HS1 in TCR Signaling. Ph.D. Thesis, University of Pennsylvania, Philadelphia, PA, USA, 2009.
199. Cosen-Binker, L.I.; Kapus, A. Cortactin: The gray eminence of the cytoskeleton. *Physiology* **2006**, *21*, 352–361. [CrossRef] [PubMed]
200. Krause, M.; Sechi, A.S.; Konradt, M.; Monner, D.A.; Gertler, F.B.; Wehland, J. Fyn-Binding Protein (Fyb)/Slp-76–Associated Protein (Slap), Ena/Vasodilator-Stimulated Phosphoprotein (Vasp) Proteins and the Arp2/3 Complex Link T Cell Receptor (Tcr) Signaling to the Actin Cytoskeleton. *J. Cell Biol.* **2000**, *149*, 181–194. [CrossRef] [PubMed]
201. Arnaud, E.; Zenker, J.; de Preux Charles, A.S.; Stendel, C.; Roos, A.; Médard, J.J.; Tricaud, N.; Kleine, H.; Luscher, B.; Weis, J.; et al. SH3TC2/KIAA1985 protein is required for proper myelination and the integrity of the node of Ranvier in the peripheral nervous system. *Proc. Natl. Acad. Sci. USA* **2009**, *106*, 17528–17533. [CrossRef]
202. Zelazny, E.; Ivanov, R.; Gaude, T. The Plant SNX Family and Its Role in Endocytosis. In *Endocytosis in Plants*; Šamaj, J., Ed.; Springer: Berlin/Heidelberg, Germany, 2012; pp. 233–247. [CrossRef]
203. Chen, Y.; He, F.; Wang, R.; Yao, M.; Li, Y.; Guo, D.; He, S. NCF1/2/4 Are Prognostic Biomarkers Related to the Immune Infiltration of Kidney Renal Clear Cell Carcinoma. *Biomed. Res. Int.* **2021**, *2021*, 5954036. [CrossRef]
204. Taylor, J.P.; Tse, H.M. The role of NADPH oxidases in infectious and inflammatory diseases. *Redox Biol.* **2021**, *48*, 102159. [CrossRef]
205. Scott, K.A.; Batey, S.; Hooton, K.A.; Clarke, J. The folding of spectrin domains I: Wild-type domains have the same stability but very different kinetic properties. *J. Mol. Biol.* **2004**, *344*, 195–205. [CrossRef]
206. Machnicka, B.; Czogalla, A.; Hryniewicz-Jankowska, A.; Bogusławska, D.M.; Grochowalska, R.; Heger, E.; Sikorski, A.F. Spectrins: A structural platform for stabilization and activation of membrane channels, receptors and transporters. *Biochim. Et Biophys. Acta (BBA)—Biomembr.* **2014**, *1838*, 620–634. [CrossRef]
207. Hale, J.; An, X.; Guo, X.; Gao, E.; Papoin, J.; Blanc, L.; Hillyer, C.D.; Gratzer, W.; Baines, A.; Mohandas, N. αI-spectrin represents evolutionary optimization of spectrin for red blood cell deformability. *Biophys. J.* **2021**, *120*, 3588–3599. [CrossRef]
208. Mosaddeghzadeh, N.; Ahmadian, M.R. The RHO Family GTPases: Mechanisms of Regulation and Signaling. *Cells* **2021**, *10*, 1831. [CrossRef] [PubMed]
209. Kunimura, K.; Uruno, T.; Fukui, Y. DOCK family proteins: Key players in immune surveillance mechanisms. *Int. Immunol.* **2020**, *32*, 5–15. [CrossRef] [PubMed]
210. Hanawa-Suetsugu, K.; Kukimoto-Niino, M.; Mishima-Tsumagari, C.; Akasaka, R.; Ohsawa, N.; Sekine, S.-i.; Ito, T.; Tochio, N.; Koshiba, S.; Kigawa, T.; et al. Structural basis for mutual relief of the Rac guanine nucleotide exchange factor DOCK2 and its partner ELMO1 from their autoinhibited forms. *Proc. Natl. Acad. Sci. USA* **2012**, *109*, 3305–3310. [CrossRef] [PubMed]
211. Laurin, M.; Côté, J.F. Insights into the biological functions of Dock family guanine nucleotide exchange factors. *Genes. Dev.* **2014**, *28*, 533–547. [CrossRef]
212. Gumienny, T.L.; Brugnera, E.; Tosello-Trampont, A.-C.; Kinchen, J.M.; Haney, L.B.; Nishiwaki, K.; Walk, S.F.; Nemergut, M.E.; Macara, I.G.; Francis, R.; et al. CED-12/ELMO, a Novel Member of the CrkII/Dock180/Rac Pathway, Is Required for Phagocytosis and Cell Migration. *Cell* **2001**, *107*, 27–41. [CrossRef]
213. Tu, Y.; Kucik, D.F.; Wu, C. Identification and kinetic analysis of the interaction between Nck-2 and DOCK180. *FEBS Lett.* **2001**, *491*, 193–199. [CrossRef]
214. Côté, J.-F.o.; Vuori, K. Identification of an evolutionarily conserved superfamily of DOCK180-related proteins with guanine nucleotide exchange activity. *J. Cell Sci.* **2002**, *115*, 4901–4913. [CrossRef]
215. Akakura, S.; Kar, B.; Singh, S.; Cho, L.; Tibrewal, N.; Sanokawa-Akakura, R.; Reichman, C.; Ravichandran, K.S.; Birge, R.B. C-terminal SH3 domain of CrkII regulates the assembly and function of the DOCK180/ELMO Rac-GEF. *J. Cell. Physiol.* **2005**, *204*, 344–351. [CrossRef]

216. Griffiths, E.K.; Krawczyk, C.; Kong, Y.-Y.; Raab, M.; Hyduk, S.J.; Bouchard, D.; Chan, V.S.; Kozieradzki, I.; Oliveira-dos-Santos, A.J.; Wakeham, A.; et al. Positive Regulation of T Cell Activation and Integrin Adhesion by the Adapter Fyb/Slap. *Science* **2001**, *293*, 2260–2263. [CrossRef]
217. Sasahira, T.; Kirita, T.; Nishiguchi, Y.; Kurihara, M.; Nakashima, C.; Bosserhoff, A.K.; Kuniyasu, H. A comprehensive expression analysis of the MIA gene family in malignancies: MIA gene family members are novel, useful markers of esophageal, lung, and cervical squamous cell carcinoma. *Oncotarget* **2016**, *7*, 31137–31152. [CrossRef]
218. Winklmeier, A.; Contreras-Shannon, V.; Arndt, S.; Melle, C.; Bosserhoff, A.K. Cadherin-7 interacts with melanoma inhibitory activity protein and negatively modulates melanoma cell migration. *Cancer Sci.* **2009**, *100*, 261–268. [CrossRef] [PubMed]
219. Feng, Z.; Yang, K.; Pastor-Pareja, J.C. Tales of the ER-Golgi Frontier: Drosophila-Centric Considerations on Tango1 Function. *Front. Cell Dev. Biol.* **2020**, *8*, 619022. [CrossRef] [PubMed]
220. Rendtorff, N.D.; Frödin, M.; Attié-Bitach, T.; Vekemans, M.; Tommerup, N. Identification and Characterization of an Inner Ear-Expressed Human Melanoma Inhibitory Activity (MIA)-like Gene (MIAL) with a Frequent Polymorphism That Abolishes Translation. *Genomics* **2001**, *71*, 40–52. [CrossRef] [PubMed]
221. McConnachie, D.J.; Stow, J.L.; Mallett, A.J. Ciliopathies and the Kidney: A Review. *Am. J. Kidney Dis.* **2021**, *77*, 410–419. [CrossRef] [PubMed]
222. Moog-Lutz, C.; Peterson, E.J.; Lutz, P.G.; Eliason, S.; Cavé-Riant, F.; Singer, A.; Di Gioia, Y.; Dmowski, S.; Kamens, J.; Cayre, Y.E. PRAM-1 is a novel adaptor protein regulated by retinoic acid (RA) and promyelocytic leukemia (PML)-RA receptor α in acute promyelocytic leukemia cells. *J. Biol. Chem.* **2001**, *276*, 22375–22381. [CrossRef] [PubMed]
223. Feller, S.M.; Lewitzky, M. Potential disease targets for drugs that disrupt protein-protein interactions of Grb2 and Crk family adaptors. *Curr. Pharm. Des.* **2006**, *12*, 529–548. [CrossRef]
224. Yan, Y.; Zhang, L.; Xu, T.; Zhou, J.; Qin, R.; Chen, C.; Zou, Y.; Fu, D.; Hu, G.; Chen, J. SAMSN1 is highly expressed and associated with a poor survival in glioblastoma multiforme. *PLoS ONE* **2013**, *8*, e81905. [CrossRef]
225. De Laureto, P.P.; Taddei, N.; Frare, E.; Capanni, C.; Costantini, S.; Zurdo, J.; Chiti, F.; Dobson, C.M.; Fontana, A. Protein aggregation and amyloid fibril formation by an SH3 domain probed by limited proteolysis. *J. Mol. Biol.* **2003**, *334*, 129–141. [CrossRef]
226. Guijarro, J.I.; Sunde, M.; Jones, J.A.; Campbell, I.D.; Dobson, C.M. Amyloid fibril formation by an SH3 domain. *Proc. Natl. Acad. Sci. USA* **1998**, *95*, 4224–4228. [CrossRef]
227. Zurdo, J.; Guijarro, J.; Jiménez, J.L.; Saibil, H.R.; Dobson, C.M. Dependence on solution conditions of aggregation and amyloid formation by an SH3 domain. *J. Mol. Biol.* **2001**, *311*, 325–340. [CrossRef]
228. Hori, I.; Miya, F.; Negishi, Y.; Hattori, A.; Ando, N.; Boroevich, K.A.; Okamoto, N.; Kato, M.; Tsunoda, T.; Yamasaki, M. A novel homozygous missense mutation in the SH3-binding motif of STAMBP causing microcephaly-capillary malformation syndrome. *J. Hum. Genet.* **2018**, *63*, 957–963. [CrossRef]
229. Bliska, J. How pathogens expolit interactions mediated by SH3 domains. *Chem. Biol.* **1996**, *3*, 7–11. [CrossRef]
230. Ravi Chandra, B.; Gowthaman, R.; Raj Akhouri, R.; Gupta, D.; Sharma, A. Distribution of proline-rich (PxxP) motifs in distinct proteomes: Functional and therapeutic implications for malaria and tuberculosis. *Protein Eng. Des. Sel.* **2004**, *17*, 175–182. [CrossRef] [PubMed]
231. Hanna, Z.; Weng, X.; Kay, D.G.; Poudrier, J.; Lowell, C.; Jolicoeur, P. The pathogenicity of human immunodeficiency virus (HIV) type 1 Nef in CD4C/HIV transgenic mice is abolished by mutation of its SH3-binding domain, and disease development is delayed in the absence of Hck. *J. Virol.* **2001**, *75*, 9378–9392. [CrossRef]
232. Saksela, K. Interactions of the HIV/SIV pathogenicity factor Nef with SH3 domain-containing host cell proteins. *Curr. HIV Res.* **2011**, *9*, 531–542. [CrossRef] [PubMed]
233. Moroco, J.A.; Alvarado, J.J.; Staudt, R.P.; Shi, H.; Wales, T.E.; Smithgall, T.E.; Engen, J.R. Remodeling of HIV-1 nef structure by Src-Family kinase binding. *J. Mol. Biol.* **2018**, *430*, 310–321. [CrossRef] [PubMed]
234. Carducci, M.; Licata, L.; Peluso, D.; Castagnoli, L.; Cesareni, G. Enriching the viral–host interactomes with interactions mediated by SH3 domains. *Amino Acids* **2010**, *38*, 1541–1547. [CrossRef]
235. Vidal, M.; Gigoux, V.; Garbay, C. SH2 and SH3 domains as targets for anti-proliferative agents. *Crit. Rev. Oncol. /Hematol.* **2001**, *40*, 175–186. [CrossRef]
236. Weisman, G.A.; Wang, M.; Kong, Q.; Chorna, N.; Neary, J.; Sun, G.Y.; González, F.A.; Seye, C.; Erb, L. Molecular determinants of P2Y 2 nucleotide receptor function. *Mol. Neurobiol.* **2005**, *31*, 169–183. [CrossRef]
237. Bustelo, X.R. Vav family exchange factors: An integrated regulatory and functional view. *Small GTPases* **2014**, *5*, e973757. [CrossRef]
238. Dalgarno, D.C.; Botfield, M.C.; Rickles, R.J. SH3 domains and drug design: Ligands, structure, and biological function. *Pept. Sci.* **1997**, *43*, 383–400. [CrossRef]
239. Sirvent, A.; Leroy, C.; Boureux, A.; Simon, V.; Roche, S. The Src-like adaptor protein regulates PDGF-induced actin dorsal ruffles in a c-Cbl-dependent manner. *Oncogene* **2008**, *27*, 3494–3500. [CrossRef] [PubMed]
240. Naudin, C.; Chevalier, C.; Roche, S. The role of small adaptor proteins in the control of oncogenic signaling driven by tyrosine kinases in human cancer. *Oncotarget* **2016**, *7*, 11033. [CrossRef] [PubMed]
241. Parisi, M.A.; Doherty, D.; Chance, P.F.; Glass, I.A. Joubert syndrome (and related disorders)(OMIM 213300). *Eur. J. Hum. Genet.* **2007**, *15*, 511–521. [CrossRef] [PubMed]

242. Jiang, X.; Hanna, Z.; Kaouass, M.; Girard, L.; Jolicoeur, P. Ahi-1, a novel gene encoding a modular protein with WD40-repeat and SH3 domains, is targeted by the Ahi-1 and Mis-2 provirus integrations. *J. Virol.* **2002**, *76*, 9046–9059. [CrossRef]
243. Wu, L.; Pan, L.; Wei, Z.; Zhang, M. Structure of MyTH4-FERM domains in myosin VIIa tail bound to cargo. *Science* **2011**, *331*, 757–760. [CrossRef]
244. Riazuddin, S.; Nazli, S.; Ahmed, Z.M.; Yang, Y.; Zulfiqar, F.; Shaikh, R.S.; Zafar, A.U.; Khan, S.N.; Sabar, F.; Javid, F.T. Mutation spectrum of MYO7A and evaluation of a novel nonsyndromic deafness DFNB2 allele with residual function. *Hum. Mutat.* **2008**, *29*, 502–511. [CrossRef] [PubMed]
245. Ruhe, J.E.; Streit, S.; Hart, S.; Wong, C.-H.; Specht, K.; Knyazev, P.; Knyazeva, T.; Tay, L.S.; Loo, H.L.; Foo, P.; et al. Genetic Alterations in the Tyrosine Kinase Transcriptome of Human Cancer Cell Lines. *Cancer Res.* **2007**, *67*, 11368–11376. [CrossRef]
246. Prieto-Echagüe, V.; Gucwa, A.; Craddock, B.P.; Brown, D.A.; Miller, W.T. Cancer-associated mutations activate the nonreceptor tyrosine kinase Ack1. *J. Biol. Chem.* **2010**, *285*, 10605–10615. [CrossRef]
247. Chua, B.T.; Lim, S.J.; Tham, S.C.; Poh, W.J.; Ullrich, A. Somatic mutation in the ACK1 ubiquitin association domain enhances oncogenic signaling through EGFR regulation in renal cancer derived cells. *Mol. Oncol.* **2010**, *4*, 323–334. [CrossRef]
248. Mahajan, K.; Mahajan, N.P. ACK1/TNK2 tyrosine kinase: Molecular signaling and evolving role in cancers. *Oncogene* **2015**, *34*, 4162–4167. [CrossRef] [PubMed]
249. Wu, T.; Shi, Z.; Baumgart, T. Mutations in BIN1 associated with centronuclear myopathy disrupt membrane remodeling by affecting protein density and oligomerization. *PLoS ONE* **2014**, *9*, e93060. [CrossRef] [PubMed]
250. Prokic, I. Pathological mechanisms of autosomal recessive centronuclear myopathy. Ph.D. Thesis, Université de Strasbourg, Strasbourg, France, 2013.
251. Sekiguchi, M.; Sobue, A.; Kushima, I.; Wang, C.; Arioka, Y.; Kato, H.; Kodama, A.; Kubo, H.; Ito, N.; Sawahata, M. ARHGAP10, which encodes Rho GTPase-activating protein 10, is a novel gene for schizophrenia risk. *Transl. Psychiatry* **2020**, *10*, 1–15. [CrossRef] [PubMed]
252. Hines, D.J.; Contreras, A.; Garcia, B.; Barker, J.S.; Boren, A.J.; Moufawad El Achkar, C.; Moss, S.J.; Hines, R.M. Human ARHGEF9 intellectual disability syndrome is phenocopied by a mutation that disrupts collybistin binding to the GABAA receptor α2 subunit. *Mol. Psychiatry* **2022**, *27*, 1729–1741. [CrossRef]
253. Bircher, J.E.; Koleske, A.J. Trio family proteins as regulators of cell migration and morphogenesis in development and disease–mechanisms and cellular contexts. *J. Cell Sci.* **2021**, *134*, jcs248393. [CrossRef]
254. Forleo, C.; D'Erchia, A.M.; Sorrentino, S.; Manzari, C.; Chiara, M.; Iacoviello, M.; Guaricci, A.I.; De Santis, D.; Musci, R.L.; La Spada, A. Targeted next-generation sequencing detects novel gene–phenotype associations and expands the mutational spectrum in cardiomyopathies. *PLoS ONE* **2017**, *12*, e0181842. [CrossRef]
255. Gigante, M.; Pontrelli, P.; Montemurno, E.; Roca, L.; Aucella, F.; Penza, R.; Caridi, G.; Ranieri, E.; Ghiggeri, G.M.; Gesualdo, L. CD2AP mutations are associated with sporadic nephrotic syndrome and focal segmental glomerulosclerosis (FSGS). *Nephrol. Dial. Transplant.* **2009**, *24*, 1858–1864. [CrossRef]
256. Hohendahl, A.; Roux, A.; Galli, V. Structural insights into the centronuclear myopathy-associated functions of BIN1 and dynamin 2. *J. Struct. Biol.* **2016**, *196*, 37–47. [CrossRef]
257. Perdigão, C.; Barata, M.A.; Burrinha, T.; Almeida, C.G. Alzheimer's disease BIN1 coding variants increase intracellular Aβ levels by interfering with BACE1 recycling. *J. Biol. Chem.* **2021**, *297*, 101056. [CrossRef]
258. Lasorsa, A.; Malki, I.; Cantrelle, F.-X.; Merzougui, H.; Boll, E.; Lambert, J.-C.; Landrieu, I. Structural basis of tau interaction with BIN1 and regulation by tau phosphorylation. *Front. Mol. Neurosci.* **2018**, *11*, 421. [CrossRef]
259. Diaz-Barreiro, A.; Bernal-Quiros, M.; Georg, I.; Marañón, C.; Alarcon-Riquelme, M.; Castillejo-López, C. The SLE variant Ala71Thr of BLK severely decreases protein abundance and binding to BANK1 through impairment of the SH3 domain function. *Genes. Immun.* **2016**, *17*, 128–138. [CrossRef] [PubMed]
260. Patel, H.V.; Tzeng, S.R.; Liao, C.Y.; Chen, S.H.; Cheng, J.W. SH3 domain of Bruton's tyrosine kinase can bind to proline-rich peptides of TH domain of the kinase and p120cbl. *Proteins: Struct. Funct. Bioinform.* **1997**, *29*, 545–552. [CrossRef]
261. Hansson, H.; Mattsson, P.T.; Allard, P.; Haapaniemi, P.; Vihinen, M.; Smith, C.E.; Härd, T. Solution structure of the SH3 domain from Bruton's tyrosine kinase. *Biochemistry* **1998**, *37*, 2912–2924. [CrossRef]
262. Rehman, A.U.; Bird, J.E.; Faridi, R.; Shahzad, M.; Shah, S.; Lee, K.; Khan, S.N.; Imtiaz, A.; Ahmed, Z.M.; Riazuddin, S. Mutational spectrum of MYO15A and the molecular mechanisms of DFNB3 human deafness. *Hum. Mutat.* **2016**, *37*, 991–1003. [CrossRef]
263. Zhang, J.; Guan, J.; Wang, H.; Yin, L.; Wang, D.; Zhao, L.; Zhou, H.; Wang, Q. Genotype-phenotype correlation analysis of MYO15A variants in autosomal recessive non-syndromic hearing loss. *BMC Med. Genet.* **2019**, *20*, 60. [CrossRef] [PubMed]
264. Hildebrandt, F.; Otto, E.; Rensing, C.; Nothwang, H.G.; Vollmer, M.; Adolphs, J.; Hanusch, H.; Brandis, M. A novel gene encoding an SH3 domain protein is mutated in nephronophthisis type 1. *Nat. Genet.* **1997**, *17*, 149–153. [CrossRef]
265. Saunier, S.; Calado, J.; Benessy, F.; Silbermann, F.; Heilig, R.; Weissenbach, J.; Antignac, C. Characterization of the NPHP1 locus: Mutational mechanism involved in deletions in familial juvenile nephronophthisis. *Am. J. Hum. Genet.* **2000**, *66*, 778–789. [CrossRef]
266. Liu, Y.; Björkman, J.; Urquhart, A.; Wanders, R.J.; Crane, D.I.; Gould, S.J. PEX13 is mutated in complementation group 13 of the peroxisome-biogenesis disorders. *Am. J. Hum. Genet.* **1999**, *65*, 621–634. [CrossRef]

267. Shimozawa, N.; Suzuki, Y.; Zhang, Z.; Imamura, A.; Toyama, R.; Mukai, S.; Fujiki, Y.; Tsukamoto, T.; Osumi, T.; Orii, T. Nonsense and temperature-sensitive mutations in PEX13 are the cause of complementation group H of peroxisome biogenesis disorders. *Hum. Mol. Genet.* **1999**, *8*, 1077–1083. [CrossRef]
268. Krause, C.; Rosewich, H.; Woehler, A.; Gärtner, J. Functional analysis of PEX13 mutation in a Zellweger syndrome spectrum patient reveals novel homooligomerization of PEX13 and its role in human peroxisome biogenesis. *Hum. Mol. Genet.* **2013**, *22*, 3844–3857. [CrossRef]
269. Hashimoto, K.; Kato, Z.; Nagase, T.; Shimozawa, N.; Kuwata, K.; Omoya, K.; Li, A.; Matsukuma, E.; Yamamoto, Y.; Ohnishi, H. Molecular mechanism of a temperature-sensitive phenotype in peroxisomal biogenesis disorder. *Pediatr. Res.* **2005**, *58*, 263–269. [CrossRef] [PubMed]
270. Hajicek, N.; Keith, N.C.; Siraliev-Perez, E.; Temple, B.R.; Huang, W.; Zhang, Q.; Harden, T.K.; Sondek, J. Structural basis for the activation of PLC-γ isozymes by phosphorylation and cancer-associated mutations. *Elife* **2019**, *8*, e51700. [CrossRef] [PubMed]
271. Patel, V.M.; Flanagan, C.E.; Martins, M.; Jones, C.L.; Butler, R.M.; Woollard, W.J.; Bakr, F.S.; Yoxall, A.; Begum, N.; Katan, M. Frequent and persistent PLCG1 mutations in Sezary cells directly enhance PLCγ1 activity and stimulate NFκB, AP-1, and NFAT signaling. *J. Investig. Dermatol.* **2020**, *140*, 380–389.e384. [CrossRef] [PubMed]
272. Koss, H.; Bunney, T.D.; Behjati, S.; Katan, M. Dysfunction of phospholipase Cγ in immune disorders and cancer. *Trends Biochem. Sci.* **2014**, *39*, 603–611. [CrossRef] [PubMed]
273. Vallois, D.; Dobay, M.P.D.; Morin, R.D.; Lemonnier, F.; Missiaglia, E.; Juilland, M.; Iwaszkiewicz, J.; Fataccioli, V.; Bisig, B.; Roberti, A. Activating mutations in genes related to TCR signaling in angioimmunoblastic and other follicular helper T-cell–derived lymphomas. *Blood J. Am. Soc. Hematol.* **2016**, *128*, 1490–1502. [CrossRef]
274. Manso, J.A.; Marcos, T.; Ruiz-Martín, V.; Casas, J.; Alcón, P.; Sánchez Crespo, M.; Bayón, Y.; de Pereda, J.M.; Alonso, A. PSTPIP1-LYP phosphatase interaction: Structural basis and implications for autoinflammatory disorders. *Cell. Mol. Life Sci.* **2022**, *79*, 1–17. [CrossRef]
275. Starnes, T.W.; Bennin, D.A.; Bing, X.; Eickhoff, J.C.; Grahf, D.C.; Bellak, J.M.; Seroogy, C.M.; Ferguson, P.J.; Huttenlocher, A. The F-BAR protein PSTPIP1 controls extracellular matrix degradation and filopodia formation in macrophages. *Blood J. Am. Soc. Hematol.* **2014**, *123*, 2703–2714. [CrossRef]
276. Tsui, T.; Miller, W.T. Cancer-associated mutations in breast tumor kinase/PTK6 differentially affect enzyme activity and substrate recognition. *Biochemistry* **2015**, *54*, 3173–3182. [CrossRef]
277. Sung, H.; Kanchi, K.L.; Wang, X.; Hill, K.S.; Messina, J.L.; Lee, J.-H.; Kim, Y.; Dees, N.D.; Ding, L.; Teer, J.K. Inactivation of RASA1 promotes melanoma tumorigenesis via R-Ras activation. *Oncotarget* **2016**, *7*, 23885. [CrossRef]
278. Eerola, I.; Boon, L.M.; Mulliken, J.B.; Burrows, P.E.; Dompmartin, A.; Watanabe, S.; Vanwijck, R.; Vikkula, M. Capillary malformation–arteriovenous malformation, a new clinical and genetic disorder caused by RASA1 mutations. *Am. J. Hum. Genet.* **2003**, *73*, 1240–1249. [CrossRef]
279. Mencacci, N.E.; Brockmann, M.M.; Dai, J.; Pajusalu, S.; Atasu, B.; Campos, J.; Pino, G.; Gonzalez-Latapi, P.; Patzke, C.; Schwake, M.; et al. Biallelic variants in TSPOAP1, encoding the active-zone protein RIMBP1, cause autosomal recessive dystonia. *J. Clin. Investig.* **2021**, *131*, e140625. [CrossRef] [PubMed]
280. Wu, N.; Tang, L.; Li, X.; Dai, Y.; Zheng, X.; Gao, M.; Wang, P. Identification of a novel mutation in SASH1 gene in a Chinese family with dyschromatosis universalis hereditaria and genotype-phenotype correlation analysis. *Front. Genet.* **2020**, *11*, 841. [CrossRef]
281. Cao, L.; Zhang, R.; Yong, L.; Chen, S.; Zhang, H.; Chen, W.; Xu, Q.; Ge, H.; Mao, Y.; Zhen, Q.; et al. Novel missense mutation of SASH1 in a Chinese family with dyschromatosis universalis hereditaria. *BMC Med. Genom.* **2021**, *14*, 168. [CrossRef]
282. Mao, M.; Solivan-Timpe, F.; Roos, B.R.; Mullins, R.F.; Oetting, T.A.; Kwon, Y.H.; Brzeskiewicz, P.M.; Stone, E.M.; Alward, W.L.; Anderson, M.G.; et al. Localization of SH3PXD2B in human eyes and detection of rare variants in patients with anterior segment diseases and glaucoma. *Mol. Vis.* **2012**, *18*, 705–713.
283. Wilson, G.R.; Sunley, J.; Smith, K.R.; Pope, K.; Bromhead, C.J.; Fitzpatrick, E.; Di Rocco, M.; van Steensel, M.; Coman, D.J.; Leventer, R.J.; et al. Mutations in SH3PXD2B cause Borrone dermato-cardio-skeletal syndrome. *Eur. J. Hum. Genet.* **2014**, *22*, 741–747. [CrossRef] [PubMed]
284. Qin, Y.; Du, Y.; Chen, L.; Liu, Y.; Xu, W.; Liu, Y.; Li, Y.; Leng, J.; Wang, Y.; Zhang, X.-Y.; et al. A recurrent SHANK1 mutation implicated in autism spectrum disorder causes autistic-like core behaviors in mice via downregulation of mGluR1-IP3R1-calcium signaling. *Mol. Psychiatry* **2022**, *27*, 2985–2998. [CrossRef] [PubMed]
285. Leblond, C.S.; Heinrich, J.; Delorme, R.; Proepper, C.; Betancur, C.; Huguet, G.; Konyukh, M.; Chaste, P.; Ey, E.; Rastam, M. Genetic and functional analyses of SHANK2 mutations suggest a multiple hit model of autism spectrum disorders. *PLoS Genet.* **2012**, *8*, e1002521. [CrossRef]
286. Cochoy, D.M.; Kolevzon, A.; Kajiwara, Y.; Schoen, M.; Pascual-Lucas, M.; Lurie, S.; Buxbaum, J.D.; Boeckers, T.M.; Schmeisser, M.J. Phenotypic and functional analysis of SHANK3 stop mutations identified in individuals with ASD and/or ID. *Mol. Autism* **2015**, *6*, 23. [CrossRef]
287. Syrbe, S.; Harms, F.L.; Parrini, E.; Montomoli, M.; Mütze, U.; Helbig, K.L.; Polster, T.; Albrecht, B.; Bernbeck, U.; Van Binsbergen, E. Delineating SPTAN1 associated phenotypes: From isolated epilepsy to encephalopathy with progressive brain atrophy. *Brain* **2017**, *140*, 2322–2336. [CrossRef]
288. Shalom, B.; Farago, M.; Pikarsky, E.; Katzav, S. Vav1 mutations identified in human cancers give rise to different oncogenic phenotypes. *Oncogenesis* **2018**, *7*, 80. [CrossRef]

289. Horstick, E.J.; Linsley, J.W.; Dowling, J.J.; Hauser, M.A.; McDonald, K.K.; Ashley-Koch, A.; Saint-Amant, L.; Satish, A.; Cui, W.W.; Zhou, W. Stac3 is a component of the excitation–contraction coupling machinery and mutated in Native American myopathy. *Nat. Commun.* **2013**, *4*, 1–11. [CrossRef] [PubMed]
290. Rufenach, B.; Christy, D.; Flucher, B.E.; Bui, J.M.; Gsponer, J.; Campiglio, M.; Van Petegem, F. Multiple Sequence Variants in STAC3 Affect Interactions with CaV1.1 and Excitation-Contraction Coupling. *Structure* **2020**, *28*, 922–932.e925. [CrossRef] [PubMed]
291. Polster, A.; Nelson, B.R.; Olson, E.N.; Beam, K.G. Stac3 has a direct role in skeletal muscle-type excitation-contraction coupling that is disrupted by a myopathy-causing mutation. *Proc. Natl. Acad. Sci. USA* **2016**, *113*, 10986–10991. [CrossRef]
292. Ashida, Y.; Himori, K.; Tokuda, N.; Naito, A.; Yamauchi, N.; Takenaka-Ninagawa, N.; Aoki, Y.; Sakurai, H.; Yamada, T. Dissociation of SH3 and cysteine-rich domain 3 and junctophilin 1 from dihydropyridine receptor in dystrophin-deficient muscles. *Am. J. Physiol. -Cell Physiol.* **2022**, *323*, C885–C895. [CrossRef] [PubMed]
293. Rajendran, B.K.; Deng, C.-X. A comprehensive genomic meta-analysis identifies confirmatory role of OBSCN gene in breast tumorigenesis. *Oncotarget* **2017**, *8*, 102263. [CrossRef]
294. LaConte, L.E.W.; Chavan, V.; Elias, A.F.; Hudson, C.; Schwanke, C.; Styren, K.; Shoof, J.; Kok, F.; Srivastava, S.; Mukherjee, K. Two microcephaly-associated novel missense mutations in CASK specifically disrupt the CASK-neurexin interaction. *Hum. Genet.* **2018**, *137*, 231–246. [CrossRef]
295. Witter, D.J.; Famiglietti, S.J.; Cambier, J.C.; Castelhano, A.L. Design and synthesis of SH3 domain binding ligands: Modifications of the consensus sequence XPpXP. *Bioorganic Med. Chem. Lett.* **1998**, *8*, 3137–3142. [CrossRef]
296. Schumacher, T.N.; Mayr, L.M.; Minor, D.L., Jr.; Milhollen, M.A.; Burgess, M.W.; Kim, P.S. Identification of D-peptide ligands through mirror-image phage display. *Science* **1996**, *271*, 1854–1857. [CrossRef]
297. Kardinal, C.; Posern, G.; Zheng, J.; Knudsen, B.S.; Moarefi, I.; Feller, S.M. Rational development of cell-penetrating high affinity SH3 domain binding peptides that selectively disrupt the signal transduction of Crk family adapters. Amgen Peptide Technology Group. *Ann. N. Y. Acad. Sci.* **1999**, *886*, 289–292. [CrossRef]
298. Morken, J.P.; Kapoor, T.M.; Feng, S.; Shirai, F.; Schreiber, S.L. Exploring the leucine-proline binding pocket of the Src SH3 domain using structure-based, split-pool synthesis and affinity-based selection. *J. Am. Chem. Soc.* **1998**, *120*, 30–36. [CrossRef]
299. Kapoor, T.M.; Andreotti, A.H.; Schreiber, S.L. Exploring the specificity pockets of two homologous SH3 domains using structure-based, split-pool synthesis and affinity-based selection. *J. Am. Chem. Soc.* **1998**, *120*, 23–29. [CrossRef]
300. Combs, A.P.; Kapoor, T.M.; Feng, S.; Chen, J.K.; Daudé-Snow, L.F.; Schreiber, S.L. Protein structure-based combinatorial chemistry: Discovery of non-peptide binding elements to Src SH3 domain. *J. Am. Chem. Soc.* **1996**, *118*, 287–288. [CrossRef]
301. Nguyen, J.T.; Turck, C.W.; Cohen, F.E.; Zuckermann, R.N.; Lim, W.A. Exploiting the basis of proline recognition by SH3 and WW domains: Design of N-substituted inhibitors. *Science* **1998**, *282*, 2088–2092. [CrossRef] [PubMed]
302. Inglis, S.R.; Stojkoski, C.; Branson, K.M.; Cawthray, J.F.; Fritz, D.; Wiadrowski, E.; Pyke, S.M.; Booker, G.W. Identification and Specificity Studies of Small-Molecule Ligands for SH3 Protein Domains. *J. Med. Chem.* **2004**, *47*, 5405–5417. [CrossRef]
303. Okamoto, M.; Schoch, S.; Südhof, T.C. EHSH1/Intersectin, a Protein That Contains EH and SH3 Domains and Binds to Dynamin and SNAP-25: A protein connection between exocytosis and endocytosis? *J. Biol. Chem.* **1999**, *274*, 18446–18454. [CrossRef]
304. Hussain, N.K.; Jenna, S.; Glogauer, M.; Quinn, C.C.; Wasiak, S.; Guipponi, M.; Antonarakis, S.E.; Kay, B.K.; Stossel, T.P.; Lamarche-Vane, N.; et al. Endocytic protein intersectin-l regulates actin assembly via Cdc42 and N-WASP. *Nat. Cell Biol.* **2001**, *3*, 927–932. [CrossRef]
305. Ren, R.; Mayer, B.J.; Cicchetti, P.; Baltimore, D. Identification of a ten-amino acid proline-rich SH3 binding site. *Science* **1993**, *259*, 1157–1161. [CrossRef]
306. Verschueren, E.; Spiess, M.; Gkourtsa, A.; Avula, T.; Landgraf, C.; Mancilla, V.T.; Huber, A.; Volkmer, R.; Winsor, B.; Serrano, L. Evolution of the SH3 domain specificity Landscape in Yeasts. *PLoS ONE* **2015**, *10*, e0129229. [CrossRef]
307. Sadowski, M.; Jones, D. The sequence–structure relationship and protein function prediction. *Curr. Opin. Struct. Biol.* **2009**, *19*, 357–362. [CrossRef]

Supplementary Information

A Systematic Compilation of Human SH3 Domains: A Versatile Superfamily in Cellular Signaling

Mehrnaz Mehrabipour, Neda S. Kazemein Jasemi, Radovan Dvorsky and Mohammad R. Ahmadian
Institute of Biochemistry and Molecular Biology II, Medical Faculty and University Hospital Düsseldorf, Heinrich Heine University Düsseldorf, 40225 Düsseldorf, Germany

Phylogenetic analysis

To identify proteins containing SH3 domains, we employed an advanced search technique with a combination of sequence similarity identification. The initial step involved identifying SH3 domain-containing proteins (SH3DCPs) which was accomplished by conducting a comprehensive search using available UniProt protein database. From the total pool of 394,887 SH3DCPs identified across various organisms, we focused on a subset of 1,132 proteins that had undergone review. In the case of human SH3DCPs, 237 out of 770 proteins were subjected to further analysis and characterization. In the next step, we employed a sequence comparison approach using the ClustalW algorithm to align and compare the input sequences to accurately identify the regions annotated as SH3 domains within the SH3DCPs. This analysis led to the discovery of 298 SH3 domains embedded in 221 human SH3DCPs.
To address the classification and categorization of SH3 domain-containing proteins (SH3DCPs) considering their diverse domain compositions, we employed an approach based on similarities in domain compositions between these proteins. For this purpose, we focused on the collected 221 human SH3DCPs retrieved in the previous steps. To retrieve the primary sequences of these proteins, we accessed the UniProt database and extracted the necessary data for analysis. The primary sequences were then analyzed to identify the occurrence of protein domains within each SH3DCP. This analysis aimed to capture the domain composition diversity across the entire collection. To evaluate the mutual similarities in domain composition between all protein pairs in the collection, a matrix was generated. This matrix represented the similarities and dissimilarities in domain compositions among the SH3DCPs. Next, the resulting matrix was subjected to phylogenetic analysis using the MEGA software (version 7.0). The phylogenetic analysis aimed to uncover the evolutionary relationship within the human SH3DCP superfamily based on their domain compositions. By analyzing the generated phylogenetic tree, we were able to classify the human SH3DCP superfamily into thirteen distinct SH3DCP families (Figure 3). This classification provided insights into the evolutionary relationships and allowed for a more comprehensive understanding of the diversification and organization of SH3DCPs. This approach, utilizing sequence analysis, domain composition comparison, and phylogenetic analysis, facilitated a meaningful classification of SH3DCPs based on their heterogeneous domain compositions. To support this analysis, we created a supplementary Table (Table S1) to document the specific SH3 domains found within each human SH3DCP, providing further insights into the functionality and distribution of SH3 domains in the human proteome.

Domain organization

In order to analyze the domain composition of SH3DCPs, we first collected sequences of all human proteins from UniProt that contain at least one SH3 domain. All collected proteins were then scanned for protein domains using the utility hmmscan from the HMMER package against the protein domains profile database obtained from Pfam. Outputs from hmmscan were parsed with Python programming language utilizing the Biopython library and domain composition for each protein in the collection was retrieved. Similarities and/or differences in domain composition for each pair of proteins were then calculated with Python script in the form distance matrix which was then used in MEGA software to generate a phylogenetic tree by UPGMA method. The phylogenetic tree from the previous step was finally used for clustering/grouping of SH3DCp while a graphical representation of domain composition for each protein, generated using Python image libraries OpenCV and Pillow, was added to it for better visualization.

Table S1. Phylogenetic classification of the human SH3DCP superfamily into thirteen families.

Fam	Entry name (no. of SH3 dom)	Aliases, interactions & functions[a]	Uniprot ID[b]	References
1: SH2 and/or KinYST domains	TXK (1)	PTK4; BTKL; RKL; regulates the development and differentiation of conventional T-cells	P42681	-
	YES (1)	HST441; regulates cell growth, adhesion, cytoskeleton remodeling, and differentiation	P07947	-
	SRC (1)	THC6; ASV; participates in transcription, immunity, adhesion, apoptosis, migration	P12931	1-6
	MATK (1)	CHK; CTK, HYL; LSK; has an inhibitory role in the control of T-cell proliferation	P42679	-
	LCK (1)	LSK; YT16; targets RUNX3, PYK2, MAPT, RHOH and TYROBP in T-cell regulation	P06239	7
	FYN (1)	SLK; SYN; regulates cell growth and survival, adhesion, motility, & axon guidance	P06241	8-11
	FGR (1)	SRC2; regulates immune responses via AKT1, ABL1, CBL, CTTN, FAK1, PYK2 & VAV2	P09769	-
	BLK (1)	MODY11; p55; B-cell receptor signaling & development	P51451	-
	CSK (1)	CYL; regulates cell growth, migration & immune response	P41240	-
	FRK (1)	PTK5; RAK; GTL; stabilizes PTEN & negatively regulates cell proliferation	P42685	12
	HCK (1)	p59; targets ADAM15, BCR, ELMO1, GAB1*, RAPGEF1, STAT5B, TP73, VAV1 & WAS	P08631	13,14
	LYN (1)	JTK8; regulates growth factor/cytokine/integrin-mediated innate immune responses	P07948	15
	PTK6 (1)	BRK; controls the differentiation and maintenance of normal epithelia & tumor growth	Q13882	16
	SRMS (1)	PTK70; phosphorylates DOK1, KHDRBS1/SAM68 and VIM	Q9H3Y6	-
	ABL1 (1)	Proto-oncogene tyrosine-protein kinase; regulates adhesion, motility & differentiation	P00519	-
	ABL2 (1)	Proto-oncogene tyrosine-Protein kinase; regulates adhesion, motility & differentiation	P42684	-
	BTK (1)	ATK; BPK; XLA; B-cell development & differentiation & signaling	Q06187	17-22
	ITK (1)	LYK; EMT; binds GATA3; regulates T-cell development, function & differentiation	Q08881	23,24
	TEC (1)	PSCTK4; regulates the development, function and differentiation of diverse cell types	P42680	-
	CRK (2)	CRKII; regulates cell adhesion, spreading & migration	P46108	1,3,25,26
	CRKL (2)	CRK-like adaptor protein that activate the RAS & JUN kinase signaling pathways	P46109	-
	GRAP1 (2)	DFN114; a BCR-ABL binding enzyme involved in RAS signaling pathway	Q13588	27
	GRAP2 (2)	GRID; MONA; binds SHC, GAB1, LCP2, SLP76; involved in NF-AT activation	O75791	-
	GRAPL (1)	Involved in receptor tyrosine kinase binding	Q8TC17	-
	GRB2 (2)	ASH; NCKAP2; binds SHC, GAB1, FRS2, CBL; links surface receptors to RAS signaling	P62993	28-31
	SLA (1)	SLAP1; SLA1; links ZAP70 with CBL & negatively regulates T-cell receptor signaling	Q13239	32,33
	SLA2 (1)	SLAP2; MARS; links ZAP70 with CBL & negatively regulates T-cell receptor signaling	Q9H6Q3	-
	RASA1 (1)	p120RASGAP; CMAVM1; acts as a GAP of RAS	P20936	34
	PLCG1 (1)	PLC1; PLC148; NCKAP3; catalyzes DAG & IP3 production	P19174	35-38
	PLCG2 (1)	PLCIV; APLAID; FCAS3; catalyzes DAG & IP3 production	P16885	-
	MAP3K21 (1)	MLK4, negative regulator of TLR4 signaling	Q5TCX8	-
	TNK2 (1)	ACK1; phosphorylates AKT1, AR, WASP; mediates CDC42-dependent cell migration	Q07912	39,40
	MAP3K10 (1)	MLK2, MST; MEKK10; activates JNK & SEK1 pathways	Q02779	-
	MAP3K11 (1)	MLK3; PTK1; MEKK11; SPRK; activates BRAF, ERK, p38 and JNK1 pathways	Q16584	-
	TNK1 (1)	Negative regulates the RAS-MAPK pathway; utilized broadly during fetal development	Q13470	-
2: BAR and/or PH plus RHOGAP or RHOGEF domains	ARHGAP10 (1)	GRAF2; PSGAP; acts as a GAP on CDC42 & RHOA; involved in actin organization	A1A4S6	41
	ARHGAP26 (1)	GRAF1; acts as a GAP on RHO family proteins in pathways related focal adhesion	Q9UNA1	41-43
	ARHGAP42 (1)	GRAF3; acts as a GAP on RHO family proteins in vascular smooth muscle	A6NI28	-
	ASAP1 (1)	AMAP1; Centaurinβ4; ARF1/ARF5GAP; coordinate membrane trafficking; ciliogenesis	Q9ULH1	44-47
	ASAP2 (1)	AMAP2; Centaurinβ3; ARFGAP; PYK2 & SRC substrate; regulates vesicular transport	O43150	-
	ARHGAP27 (1)	CAMGAP1; SH3D20; acts as a GAP on RHO family proteins in endocytosis	Q6ZUM4	-
	ARHGAP9 (1)	RGL1; acts as a CDC42/RAC1 GAP; regulates matrix adhesion of hematopoietic cells	Q9BRR9	-
	ARHGAP12 (1)	Acts as a GAP on RHO family proteins, maybe downstream of the GPCR Signaling	Q8IWW6	48
	SKAP1 (1)	SCAP1; SKAP55; positively regulates T-cell receptor and promotes the MAPK pathway	Q86WV1	49
	SKAP2 (1)	SCAP2; PRAP; SAPS; involved in B-cell and macrophage adhesion processes	O75563	50-53
	ARHGEF26 (1)	SGEF; RHOGGEF; macropinocytosis; trans-endothelial migration of leukocytes	Q96DR7	-
	NGEF (1)	ARHGEF27; EPHEXIN1; involved in ephrin-induced axon & spine morphogenesis	Q8N5V2	-
	ARHGEF19 (1)	Ephexin2; WGEF; RHOAGEF; interacts with BRAF & activates MAPK pathway	Q8IW93	-
	ARHGEF16 (1)	Ephexin4; RHOG/CDC42GEF; cell migration	Q5VV41	-
	ARHGEF5 (1)	Ephexin-3; p60TIM; RHOAGEF; involved in SRC-induced podosome formation	Q12774	-
	ARHGEF4 (1)	ASEF1; STM6; a CDC42 GEF, involved in cell-cell adhesion & migration	Q9NR80	54-56
	SPATA13 (1)	ASEF2; ARHGEF29; acts as a CDC42GEF in cell migration & adhesion	Q96N96	54-56
	ARHGEF9 (1)	HPEM1; Collybistin; RAC/CDC42GEF; formation of GABAergic & glycinergic synapses	O43307	-
	OBSCN (1)	ARHGEF30; Obscurin; a giant sarcomeric protein; calmodulin and titin binding	Q5VST9	57
	ARHGEF6 (1)	αPIX; COOL2; associated with X-linked intellectual disability	Q15052	58-60
	ARHGEF7 (1)	βPIX, CCOL1; cell adhesion, spreading & migration	Q14155	61-63
	TRIO (2)	ARHGEF23; MRD44; acts as a dual RAC1/RHOAGEF in hippocampal neurons	O75962	-
	KALRN (2)	Kalirin; ARHGEF24; DUO; TRAD; regulates as a RHOGEF neuronal growth & plasticity	O60229	-
	MCF2L (1)	ARHGEF14; RHOA/CDC42GEF associated with osteoarthritis	O15068	-
	VAV1 (2)	Acts as a RAC1/RHOAGEF; involved in cell differentiation & proliferation	P15498	30,31,64,65
	VAV2 (2)	Acts as a RAC1GEF; involved in angiogenesis & endothelial cell migration	P52735	-
	VAV3 (2)	Acts a RHOA/RHOGGEF; involved in angiogenesis & endothelial cell migration	Q9UKW4	-

3: Several or single SH3 plus other shared domains	ABI1 (1)	E3B1; binds Abl, spectrin & EPS8; regulate the dendritic outgrowth & branching	Q8IZP0	3,26 66,67
	ABI2 (1)	ArgBP1; component of the WAVE complex; involved in cell motility & adhesion	Q9NYB9	68
	ABI3 (1)	NESH; component of the WAVE complex, regulates dendritic Spine Morphology	Q9P2A4	69
	BAIAP2L1 (1)	IRTKS; IR substrate; RAC1 binding; promotes actin assembly & membrane protrusions	Q9UHR4	70-72
	BAIAP2L2 (1)	Pinkbar; formation of curved membrane structures	Q6UXY1	-
	BAIAP2 (1)	IRS58; links RAC1/CDC42 to downstream effectors, promotes filopodial protrusions	Q9UQB8	-
	RUSC1 (1)	NESCA; regulates MAPK & NFκB pathways, & NGF-dependent neurite outgrowth	Q9BVN2	-
	RUSC2 (1)	MRT61; IPORIN; acts as a RAB35 effector on intracellular vesicular trafficking	Q8N2Y8	-
	SH3YL1 (1)	RAY; involved in hair follicle development, cell migration, & dorsal ruffle formation	Q96HL8	73,74
	PEX13 (1)	PEROXIN13; NALD; involved in the import of peroxisomal biogenesis factors PTS1/2	Q92968	75,76
	MAPK8IP1 (1)	JIP1; IB1; involved as MAPK component in survival response	Q9UQF2	77
	MAPK8IP2 (1)	JIP2; IB2; involved as MAPK component in survival response	Q13387	-
	FUT8 (1)	CDGF1; a Golgi associated enzyme regulates adhesion, migration & invasion	Q9BYC5	-
	EFS (1)	HEFS, CAS3; SIN; acts as SRC activator on cell adhesion	O43281	78,79
	DBNL (1)	SH3P7; ABP1; CMAP; HIP55; involved endocytic pathways & podosome formation	Q9UJU6	-
	PPP1R13B (1)	ASPP1; regulates the DNA binding & transactivation function of p53	Q96KQ4	80,81
	TP53BP2 (1)	ASPP2; P53BP2; regulates cell growth & apoptosis by binding to p53 & BCL2	Q13625	80-82
	PPP1R13L (1)	IASPP; NKIP1; RIA4; inhibits p53 & NFκB; regulates apoptosis and transcription	Q8WUF5	-
	OSTF1 (1)	SH3P2; OSF; induces bone resorption & enhances osteoclast formation & activity	Q92882	83
	BIN1 (1)	AMPHL; SH3P9, membrane curvature & remodeling; negative regulator of endocytosis	O00499	84-87
	GAS7 (1)	KIAA0394; promotes maturation & morphological differentiation of cerebellar neurons	O60861	-
	AMPH (1)	Amphiphysin; involved in regulated endocytosis	P49418	88
	Endophilin A2 (1)	SH3GL1; SH3D2B; acts on membrane shaping & clathrin-independent endocytosis	Q99961	-
	Endophilin B2 (1)	SH3GLB2; RRIG1; involved in endocytosis	Q9NR46	-
	Endophilin B1 (1)	SH3GLB1; BIF1; involved in membrane fusion & in the regulation of autophagy	Q9Y371	-
	Endophilin 1 (1)	SH3GL2; SH3D2A; acts on membrane shaping & synaptic vesicle endocytosis	Q99962	-
	Endophilin 3 (1)	SH3GL3; SH3D2C; implicated in membrane shaping & endocytosis	Q99963	89
	STAC (2)	Involved in the modulation of calcium channel at the cell membrane	Q99469	-
	STAC2 (2)	24B2; involved in the modulation of calcium channel at the cell membrane	Q6ZMT1	-
	STAC3 (2)	MYPBB; NAM; Required for excitation-contraction coupling in skeletal muscle	Q96MF2	90
	DNMBP (6)	TUBA; ARHGEF36; links dynamin to actin regulatory proteins & is involved in adhesion	Q6XZF7	91-94
	ARHGEF37 (2)	FLJ41603; RHOGEF; clathrin-mediated endocytosis, GPCR & p75-NRT signaling	A1IGU5	-
	ARHGEF38 (2)	FLJ20184; RHOGEF; GPCR & p75-NRT signaling	Q9NXL2	-
	SH3BP4 (2)	EHB10; TTP; BOG25; controls clathrin-mediated endocytosis	Q9P0V3	95,96
	TSPOAP1 (3)	RIMBP1; RBP1; PRAX1; synchronizes and couples synaptic vesicle to the exocytic sites	O95153	97,98
	SH3PXD2A (5)	TKS5; SH3MD1; involved in ROS generation, podosome formation & ECM degradation	Q5TCZ1	99
	SH3PXD2B (4)	TSK4; FAD49; involved in ROS generation, podosome formation & ECM degradation	A1X283	99
	SH3RF1 (4)	POSH1; SH3MD2; involved in dynamin-dependent endocytosis & JNK activation	Q7Z6J0	100
	SH3RF3 (4)	POSH2; SH3MD4; is a RAC effector & mediates proteasomal degradation	Q8TEJ3	101,102
	SH3D19 (5)	EBP; EVE-1; acts on ADAMs/EGFR axis & suppresses RAS-induced cell transformation	Q5HYK7	-
	ITSN1 (5)	SH3D1A; SH3P17; acts as a CDC42GEF on actin nucleation & endocytosis	Q15811	103-109
	ITSN2 (5)	SH3P18; SWAP; acts as a CDC42GEF on actin nucleation & endocytosis	Q9NZM3	-
	CD2AP (3)	CMS; involved in receptor clustering & cytoskeletal polarity	Q9Y5K6	47,110
	NCK1 (3)	Acts as an RTK-associated protein on RAS signaling & dsRNA-induced PKR activation	P16333	63,111,112
	NCK2 (3)	GRB4; acts as an RTK-associated protein on RAS signaling & translational initiation	O43639	111
	RIMBP3B (3)	Plays a key role in sperm head morphogenesis during late stages of sperm development	A6NNM3	-
	RIMBP3C (3)	Plays a key role in sperm head morphogenesis during late stages of sperm development	A6NJZ7	-
	RIMBP3 (3)	RIMBP3A; plays a key role in sperm head morphogenesis during sperm development	Q9UFD9	-
	TSPOAP1 (3)	RIMBP1; RBP1; PRAX1; synchronizes and couples synaptic vesicle to the exocytic sites	O95153	97,98
	RIMBP2 (3)	RBP2, PPP1R133; synchronizes and couples synaptic vesicle to the sites of exocytosis	O15034	-
	SH3KBP1 (3)	CD2BP3; CIN85; HSB1; controls cell shape & migration, & stimulates B cell activation	Q96B97	-
	SH3RF2 (3)	POSH3; HEPP1; mediates TNFα signaling & proteasomal degradation	Q8TEC5	113
	SORBS1 (3)	SH3P12; FLAF2; CAP; involved in formation of actin stress fibers and focal adhesions	Q9BX66	114
	SORBS2 (3)	ARGBP2; forms complex with ABL1/CBL & promotes ABL1 ubiquitination & degradation	O94875	-
	SORBS3 (3)	VINEXIN; SH3D4; SCAM1; plays a role in cell spreading	O60504	115,116
4: PDZ and/or GuaKin domain	MPP2 (1)	DLG2, negatively regulates SRC function in epithelial cells	Q14168	117
	PALS2 (1)	MPP6; VAM1; act on receptor clustering by forming multiprotein complexes	Q9NZW5	-
	PALS1 (1)	MPP5; involved in adherens junction biogenesis & localization of the exocyst complex	Q8N3R9	-
	MPP3 (1)	DLG3, interact with the cytoskeleton & regulates intracellular junctions & cell proliferation	Q13368	-
	MPP7 (1)	Promotes epithelial cell polarity and tight junction formation	Q5T2T1	-
	CASK (1)	CSKP; FGS4; LIN2, HCASK, a Ca2+/CAM-dependent kinase involved in neurogenesis	O14936	-
	MPP4 (1)	DLG6; plays a role in retinal photoreceptors development.	Q96JB8	-
	MPP1 (1)	EMP55; AAG12; EMP55; as a MAGUK family proteins regulates neutrophil polarity	Q00013	-
	DLG3 (1)	MRX90; SAP102; XLMR; involved in NMDA receptor-mediated synaptic plasticity	Q92796	-
	DLG4 (1)	PSD95; SAP90; required for synaptic plasticity associated with NMDA receptor signaling	P78352	-
	DLG1 (1)	SAP97; DLGH1; involved in synaptogenesis & lymphocyte activation	Q12959	118
	DLG2 (1)	PSD93; binds NMDA receptor subunits & regulates excitatory synapses	Q15700	119
	DLG5 (1)	PDLG; involved in dendritic spine formation & synaptogenesis as well as ciliogenesis	Q8TDM6	-
	TJP1 (1)	ZO1; involved in tight junction organization, epithelial polarization and barrier formation	Q07157	120
	TJP2 (1)	ZO2; PFIC4; DFNA51; plays a role in tight junctions and adherents junctions	Q9UDY2	-
	TJP3 (1)	ZO3; links tight junction transmembrane proteins	O95049	-
	CACNB2 (1)	CACNLB2, CAVB2; MYSB; a subunit of voltage-dependent calcium channels	Q08289	121
	CACNB1 (1)	CACNLB1; CAB1, CCHLB1; regulates the activity of L-type calcium channels	Q02641	-

	CACNB3 (1)	CACNLB3; CAB3; a regulatory subunit of the voltage-gated calcium channel	P54284	-
	CACNB4 (1)	CACNLB4; CAB4, EJM4; a dihydropyridine-sensitive subunit of L-type calcium channel	O00305	-
	SHANK2 (1)	CORTBP1; involved in structural and functional organization of the dendritic spine	Q9UPX8	-
	SHANK1 (1)	SSTRIP; acts in GKAP/PSD95/HOMER complex on dendritic spine organization	Q9Y566	122
	SHANK3 (1)	PSAP2; acts on th dendritic spine and synapse formation, maturation and maintenance	Q9BYB0	123
5: FCH and/or RHOGAP domains	FCHSD1 (2)	NWK2; promotes SNX9WASL-mediated actin polymerization.	Q86WN1	-
	FCHSD2 (2)	NWK1; SH3MD3; promotes actin polymerization & internalization of surface receptors	O94868	-
	FNBP1 (1)	FBP17; Rapostlin; links RND2 signaling to F-actin & spine morphogenesis	Q96RU3	-
	NOSTRIN (1)	Multivalent adapter protein involved in NO metabolism by sequestering NOS3	Q8IVI9	124-126
	TRIP10 (1)	CIP4, STP; promotes CDC42(WASP-induced actin polymerization	Q15642	127,128
	FNBP1L (1)	TOCA1; binds CDC42/WASP; promote membrane tubulation & F-actin reorganization	Q5T0N5	-
	PACSIN1 (1)	SYNDAPIN1; recruits DNM1/2/3 to membranes; regulates neurite formation & branching	Q9BY11	129
	PACSIN2 (1)	SYNDAPIN2; involved in plasma membrane protein internalization by endocytosis	Q9UNF0	129
	PACSIN3 (1)	SYNDAPIN3; involved in cell-surface receptor internalization by endocytosis	Q9UKS6	129
	PSTPIP1 (1)	CD2BP1L; PAPAS; regulates WAS actin-bundling activity, endocytosis and cell migration	O43586	130-133
	PIK3R1 (1)	p85α; AMG7; regulates membrane binding & activity of p110 catalytic subunit of PI3K	P27986	134-137
	PIK3R2 (1)	P85β; MPPH1; regulates membrane binding & activity of p110 catalytic subunit of PI3K	O00459	136
	ARHGAP32 (1)	p200; GRIT; acts as a RHOGAP in the differentiation of neuronal cells	A7KAX9	-
	ARHGAP33 (1)	SNX26; TCGAP; acts as a GAP on RHO family proteins in intracellular trafficking	O14559	-
	ARHGAP4 (1)	RGC1; SRGAP4; acts as RHOGAP in hematopoietic cells	P98171	-
	SRGAP3 (1)	ARHGAP14; WRP; MEGAP; WAVE-associated Rac1/CDC42GAP	O43295	138,139
	SRGAP1 (1)	ARHGAP13; Acts as RHOA/CDC42GAP in neuronal migration	Q7Z6B7	138
	SRGAP2 (1)	ARHGAP34; regulates as a RAC1GAP cell migration and differentiation	O75044	140
6: UBA & HPhos	UBASH3A (1)	TULA1, STS2; as a T-cell ubiquitin ligand family member negatively act on T-cell signaling	P57075	141-144
	UBASH3B (1)	TULA2; STS1; as a T-cell ubiquitin ligand family member negatively act on T-cell signaling	Q8TF42	143,144
7: S-rich & CAS-C	CASS4 (1)	CAS4; HEFL; regulates focal adhesion integrity & cell spreading	Q9NQ75	-
	BCAR1 (1)	p130CAS; CAS1; CASS1; regulates cell adhesion & migration	P56945	1-3,25,145-147
	NEDD9 (1)	CAS2; CASL; CASS2; regulates cell adhesion & migration	Q14511	148,149
8: Myosin &/or MyTH4	MYO7A (1)	DFNB2; NSRD2; mediates in complex with USH1C/G & CDH23 mechanotransduction	Q13402	-
	MYO7B (1)	MYOVIIb; acts in the intermicrovillar adhesion complex on microvilli organization & length	Q6PIF6	-
	MYO15A (1)	DFNB3; unconventional MYO15 required for stereocilia formation in mature hair bundles.	Q9UKN7	-
	MYO15B (1)	MYO15BP; no functional motor domain	Q96JP2	-
	MYO1E (1)	FSGS6; HUNCM-IC; controls the movement of class II-containing cytoplasmic vesicles	Q12965	150-152
	MYO1F (1)	Acts with MYO1E on innate immunity in cell migration & phagocytosis	O00160	-
9: SAM* along with PTB and SLY	EPS8L1 (1)	DRC3; EPS8R1; involved in membrane ruffling & remodeling of the actin cytoskeleton	Q8TE68	112
	EPS8L2 (1)	DFNB106; required for stereocilia maintenance in adult hair cells	Q9H6S3	-
	EPS8L3 (2)	EPS8R3; function unknown	Q8TE67	-
	EPS8 (1)	DFNB102; regulates in complex with SOS1/ABI1 cell migration & invasion	Q12929	67,153-155
	SASH1 (1)	PEPE1; SH3D6A; Acts on TLR4/NFκB signaling & LPS-induced endothel. cell migration	O94885	156
	SAMSN1 (1)	HACS1; SH3D6B; acts on RAC1-dependent cell spreading & polarization	Q9NSI8	157
	SASH3 (1)	HACS2; SH3D6C; functions as a signaling adapter protein in lymphocytes	O75995	-
	CASKIN1 (1)	CSKI1; ANKS5A; links CASK to downstream intracellular effectors	Q8WXD9	-
	CASKIN2 (1)	CSKI2; ANKS5B; links CASK to downstream intracellular effectors	Q8WXE0	-
10: Diverse domains	NCF1B (2)	NCF1B; required for activation of the latent NADPH oxidase	A6NI72	-
	NCF1C (2)	NCF1C; required for activation of the latent NADPH oxidase	A8MVU1	-
	NCF1 (2)	p47phox; NOXO2; NCF1A; required for activation of the latent NADPH oxidase	P14598	158-160
	NCF4 (1)	p40phox; SH3PXD4; involved assembly & activation of the NADPH oxidase complex	Q15080	158-160
	NOXO1 (2)	SH3PXD5; p41NOX; activates together with NOX2 NOX1/3	Q8NFA2	158,161
	SNX18 (1)	SNAG1; SH3PX2; stimulates DNM2 GTPase activity; involved in endocytosis	Q96RF0	162,163
	SNX9 (1)	SH3PX1; SDP1; WISP; stimulates DNM2 GTPase activity; involved in endocytosis	Q9Y5X1	164-173
	SNX33 (1)	SH3PX2; reorganizes the cytoskeleton, endocytosis and cellular vesicle trafficking	Q8WV41	-
	NCF2 (2)	p67phox; NOXA2; required for activation of the latent NADPH oxidase	P19878	158-160
	SH3TC2 (2)	CMT4C; MNMN; involved as a RAB11 effector in axoglial interactions myelination	Q8TF17	174,175
	NOXA1 (1)	p51NOX; activates as a p67^{phox}-like factor NOX1/3 in the host defense & oxygen sensing	Q86UR1	158,161
	SH3TC1 (1)	Unknown function	Q8TE82	-
	NEBL (1)	LASP2; LIM-Nebulette; links sarcomeric actin to desmin around the Z-disk	O76041	176
	NEB (1)	NEBU; NEM2; NEB177B; binds & stabilize F-actin; involved in sarcomeric integrity	P20929	177
	LASP1 (1)	MLN50; regulates actin-associated ion transport activities	Q14847	176,178-182
	AHI1 (1)	JBTS3; involved in vesicle trafficking, ciliogenesis & WNT signaling	Q8N157	183
	PRMT2 (1)	ANM2; methylates arginines in STAT3, FBL, & H4; involved in growth regulation	P55345	184
	FYB (1)	SLAP130; THC3; binds FYN and LCP2 & regulates actin cytoskeleton in T-cells	O15117	49
	HCLS1 (1)	LCKBP1; HS1; CTTNL; involves in antigen receptor signaling in lymphoid cells	P14317	-
	CTTN (1)	SRC8; EMS1; Amplaxin; involved in the formation of lamellipodia and in cell migration	Q14247	-
	MACC1 (1)	SH3BP4L; 7A5; promotes HGF-MET signaling & cell motility, proliferation & metastasis	Q6ZN28	185,186
	MAP3K9 (1)	MLK1; MEKK9, activates JNK pathway; involved in the cytochrome-C release & apoptosis	P80192	-
	SGSM3 (1)	MAP; RUSC3; RABGAP5; involved in NF2-mediated growth suppression of cells	Q96HU1	-
	NCKIPSD (1)	SPIN90; WISH; WASLBP; stimulates N-WASP-induced ARP2/3 complex activation	Q9NZQ3	4,63,187
	STAM (1)	STAM1; HSE1H; involved in signal transduction mediated by cytokines and growth factors	Q92783	-
	STAM2 (1)	HBP; involved in signal transduction mediated by cytokines and growth factors	O75886	-

11: Spectrin and EF-hand domain	SPTA1 (1)	SPH3; EL2; forms the cytoskeletal superstructure of the erythrocyte plasma membrane	P02549	-
	SPTAN1 (1)	NEAS; EIEE5; involved in calcium-dependent cytoskeleton movement at the membrane	Q13813	188
	DSP (1)	DESP; Desmoplakin; is part of the desmosomal cadherin-plakoglobin complexes	P15924	-
	DST (1)	Dystonin; BPAG1; MACF2; acts as a cytoskeletal linker protein on axonal transport	Q03001	-
	MACF1 (1)	ACF7; LIS9; OFC4; involved in AXIN1/APC/CTNNB1/GSK3B complex translocation	Q9UPN3	-
12: DOCK & DHR domains	DOCK2 (1)	IMD40; involved as RAC1/2 GEF in lymphocyte migration	Q92608	189,190
	DOCK4 (1)	KIAA0716; with its RHOGEF function regulates cell migration	Q8N1I0	191
	DOCK1 (1)	DOCK180; as a GEF regulates cell spreading & migration	Q14185	3,25
	DOCK3 (1)	MOCA; PBP; activates as a RACGEF the WAVE complex & induces axonal outgrowth	Q8IZD9	-
	DOCK5 (1)	Associates with CRK/CRKL, & regulates epithelial cell spreading & migration	Q9H7D0	-
13: single SH3 domain	FYB2 (1)	ARAP; T-cell receptor signaling & integrin-mediated adhesion	Q5VWT5	-
	MIA (1)	MIA1; Associated with melanoma, glioma and neuroectodermal tumors	Q16674	
	MIA2 (1)	MGEA11; TALI; MEA6; involved in cholesterol & TAG homeostasis, & OL7A1 secretion	Q96PC5	-
	MIA3 (1)	TANGO; ARNT; required for membrane-bound ER-resident complexes consisting of MIA2	Q5JRA6	192
	NPHP1 (1)	NPH1; Nephrocystin-1; control together with PTK2B/PYK2 the epithelial cell polarity	O15259	193-195
	OTOR (1)	Otoraplin; MIAL1; FDP; functions in cartilage development and maintenance	Q9NRC9	-
	PRAM (1)	PRAM1; PMLRAR; involved in myeloid differentiation & integrin signaling in neutrophils	Q96QH2	-
	SH3D21 (1)	Unknown function	A4FU49	-

[a]To provide comprehensive alias information and interaction details, Gene Cards database was utilized.
[b]UniProt ID was included to better identify SH3DCPs due to their various names.

Table S2. List of protein domains found in SH3DCP (alphabetical order)

Domains	Full name
2'-5'_RNA_ligase2	2'-5' RNA ligase 2 domain
Abi_alpha	ABL interactor alpha domain
Abi_HHR	ABL interactor homeodomain homologous region
Ank	Ankyrin repeat
ARFGAP	ARF GTPase activating protein
ARHGEF5	RHO guanine nucleotide exchange factor 5
Baculo_p24	Baculovirus P24-like
BAR	Bin/amphiphysin/Rvs
BAR_3_WASP_bdg	BAR 3 domain of WASP interacting protein
betaPIX_CC	BetaPIX coiled-coil domain
BTK	Bruton tyrosine kinase
C1	Protein kinase C conserved region 1
C2	Protein kinase C conserved region 2
CAS_C	CRK-associated substrate C-terminal
Caskin1-CID	CASKIN1 carboxy-terminal interaction domain
Caskin-Pro-rich	CASKIN proline-rich domain
Caskin-tail	CASKIN carboxy-terminal domain
CH	Calponin homology domain
Cofilin_ADF	Cofilin-actin-depolymerizing factor
Cohesin_load	Cohesin loader N-terminal domain
CRAL_TRIO	CRAL-TRIO lipid binding domain
CSD	Cold-shock domain
CSD3_N	Cold shock domain 3, N-terminal domain
CTNNBL	Catenin-beta-like domain
CTV_P33	Citrus tristeza virus P33
CYYR1	Cysteine/tyrosine-rich 1 domain
dbPDZ_assoc	Unstructured region between two PDZ domains on Dlg5 or PDZ domain, Dlg/ZO-1-associated domain
DEDD_Tnp_IS110	Transposase for efficient DNA transposition or DEDD-like exonuclease TnpI-IS110 domain
DegS	Signal transduction histidine kinase DegS
DHR-2_Lobe_A	DHR-2 lobe A domain
DHR-2_Lobe_B	DHR-2 lobe B domain
DHR-2_Lobe_C	DHR-2 lobe C domain
DOCK_N	Dedicator of cytokinesis N-terminal domain
DOCK-C2	DOCK C2 domain
DUF1539	Domain of unknown function 1539
DUF1664	Domain of unknown function 1664
DUF1778	Domain of unknown function 1778
DUF2605	Domain of unknown function 2605
DUF4100	Domain of unknown function 4100
DUF4404	Domain of unknown function 4404
DUF6781	Domain of unknown function 6781
EF-hand	EF-hand calcium-binding domain
EFhand_Ca_insen	Ca^{2+} insensitive EF hand
EF-hand_like	EF-hand-like domain
ERM_helical	Ezrin/radixin/moesin, alpha-helical domain
Exonuc_VII_L	Exonuclease VII large subunit domain
F_actin_bind	F-actin binding domain
FCH	Fes-CIP4 homology
FERM_f0	FERM domain F0 subdomain
FERM_M	FERM domain M subdomain
Filamin	Actin-binding filamin domain
FlaC_arch	Archaeal flagellar accessory protein (FLaCa) domain
Flg_hook	Flagellin hook region
fn3	Fibronectin type III domain
FTZ	Fushi tarazu
FUT8_N_cat	Fucosyltransferase 8 N-terminal and catalytic domains
GAS2	Growth arrest-specific protein 2
GAT	GGA and Tom1 (GAT) domain
GDPD	Glycerophosphodiester phosphodiesterase
Glyco_hyd_101C	Glycosyl hydrolase family 101, subfamily C
GP3_package	Glycoprotein 3 (GP3) packaging domain
GrpE	Nucleotide exchange factor GrpE
GSH_synthase	Glutathione synthetase
GTPase_binding	GTPase binding domain
Guanylate_kin	Guanylate kinase domain
HAUS-augmin3	HAUS augmin-like complex subunit 3
His_Phos	Histidine phosphatase domain
HOIP-UBA	HOIL-1 interacting protein ubiquitin-associated domain
HR1	Homology region 1
HS1_rep	Repeat in HS1/Cortactin
hSH3	Helically-extended SH3 domain

Ig	Immunoglobulin domain
IMD	IRSp53/MIM homology domain
Inhibitor_Mig-6	Mitogen-activated protein kinase (MAPK) inhibitor-6 domain
INTAP	Intersectin and clathrin adaptor AP2 binding region
I-set	Immunoglobulin I-set domain
KxDL	KxDL domain
L27	L27 domain
L27_N	N-Terminal L27 domain
Laminin_II	Laminin Domain II
LANC_like	Lanthionine synthetase C-like protein domain
LIM	Lin-11/Isl-1/Mec-3
LMBR1	LMBR1 domain
Lzipper-MIP1	Leucine-zipper of ternary complex factor MIP1 domains
MAGUK_N_PEST	Membrane-associated guanylate kinase (MAGUK) N-terminal and Polyubiquitination (PEST) domains
MCU	Mitochondrial calcium uniporter domain
Methyltransf	Methyltransferase domain
MIC19_MIC25	Mitochondrial contact site and cristae organizing system (MICOS) subunits MIC19 and MIC25
MTS	Methyltransferase small domain
Myb_DNA-bind	Myb-like DNA-binding domain
Myosin_head	Myosin head domain
Myosin_TH1	Class I myosin tail homology domain
MyTH4	Myosin tail homology 4 (MYTH4) domain
NBCH_WD40	Neurobeachin, beta-propeller domain
Nebulin	Nebulin repeat domain
NECFESHC	SH3 terminal domain of 2nd SH3 on Neutrophil cytosol factor 1
NHS	Nance-Horan syndrome protein (NHS)
NPF	Asn-Pro-Phe domain
OmpH	Outer membrane protein (OmpH-like)
p47_phox_C	NADPH oxidase subunit p47Phox, C terminal domain
PB1	Phox and Bem1 domain
PDZ	PSD-95/Discs large/ZO-1
Peptidase_M1	Peptidase M1 domain
Peptidase_M50	Peptidase M50 domain
Peroxin-13_N	Peroxin-13 N-Terminal domain
PH	Pleckstrin homology domain
PI3K_P85_iSH2	Phosphatidylinositol 3-kinase regulatory subunit P85 inter-SH2 domain
PID	Phosphotyrosine interaction domain
Pilin_GH	Type IV pilin-like G and H, putative
PI-PLC-X	Phosphatidylinositol-specific phospholipase C X-domain
PI-PLC-Y	Phosphatidylinositol-specific phospholipase C Y-domain
PK_Tyr_Ser-Thr	Protein kinase Tyr/Ser/Thr domain
Pkinase	Protein kinase domain
Plectin	Plectin repeat
PTB	Phosphotyrosine binding domain
PX	Phox homology
RABGAP-TBC	RAB GTPase-activating protein TBC domain
RASGAP	RAS GTPase-activating protein
RHOGAP	RHO GTPase-activating protein
RHOGEF	RHO guanine nucleotide exchange factor
RHOGEF67_u1	Unstructured region one on RhoGEF 6 and 7
RHOGEF67_u2	Unstructured region two on RhoGEF 6 and 7
RNase_Y_N	Ribonuclease Y N-terminal domain
RPEL	RPEL (RPxxxEL) motif
RsgA_GTPase	RsgA GTPase
RUN	RPIP8/UNC-14/NESCA
SAM*	Sterile Alpha Motif (denoted as SAM* when regarded as a domain rather than a protein)
SAM_PNT	Sterile alpha motif (SAM)/Pointed domain
Serine_rich	Serine-rich domain
SH2	SRCc homology 2 domain
SH3BP5	SH3 domain-binding protein 5
SLY	SH3-domain containing protein expressed in lymphocytes
SNAP	synaptosome-associated protein 25kDa
Sorb	Sorbin homologous domain
Spectrin	Spectrin repeat
Spectrin_like	Spectrin-like domain
SPIN90_LRD	leucine-rich domain (LRD) within the C-terminal domain of SPIN90 (also known as NCK interacting protein with SH3 domain (NCKIPSD))
STAC2_u1	Unstructured on SH3 and cysteine-rich domain-containing protein 2
Takusan	Takusan ("many" in Japanese) protein family regulates synaptic activity
TcpQ	Toxin co-regulated pilus biosynthesis protein Q
Tetrabrachion	Tetrabrachion, parallel right-handed coiled coil domain
Tmemb_cc2	Transmembrane protein with coiled-coil domains 2
TPR	Tetratricopeptide repeat domain

TPR_MalT	Tetratricopeptide repeat domain-containing protein MALT or MalT-like TPR region
Trypan_PARP	Procyclic acidic repetitive protein (PARP)
UBA	Ubiquitin-associated domain
VGCC_beta4Aa_N	Voltage gated calcium channel subunit beta domain 4Aa N terminal
VHS	Vps27, Hrs, and STAM domain
WD40	WD40 repeat domain
WW	Two tryptophan (W) residues
YL1	YL1 protein domain or Vps72/YL1, C-terminal
Ysc84	Ysc84 actin-binding domain
zf-C3HC4	Zinc finger C3HC4 type (RING finger) domain
zf-C4H2	Zinc finger C4H2 type domain
zf-RING_UBOX	Zinc finger, RING-type
ZU5	Zona occludens protein 5 domain

Figure S1. Gene Ontology analysis of the superfamily of human SH3 domain-containing protein. Gene Ontology (GO) terms for the biological process, molecular function, and protein classes of human SH3 domain-containing protein were identified using the PANTHER 17.0 database. In this study, a file including UniProt ID of human SH3 domain-containing proteins were inputted into the PANTHER database. The analysis parameters were set to include Homo sapiens as the species of interest and to retrieve GO terms for functional classification viewed in pie chart. This analysis facilitated a comprehensive understanding of functional characteristics of the human SH3 domain-containing protein superfamily.

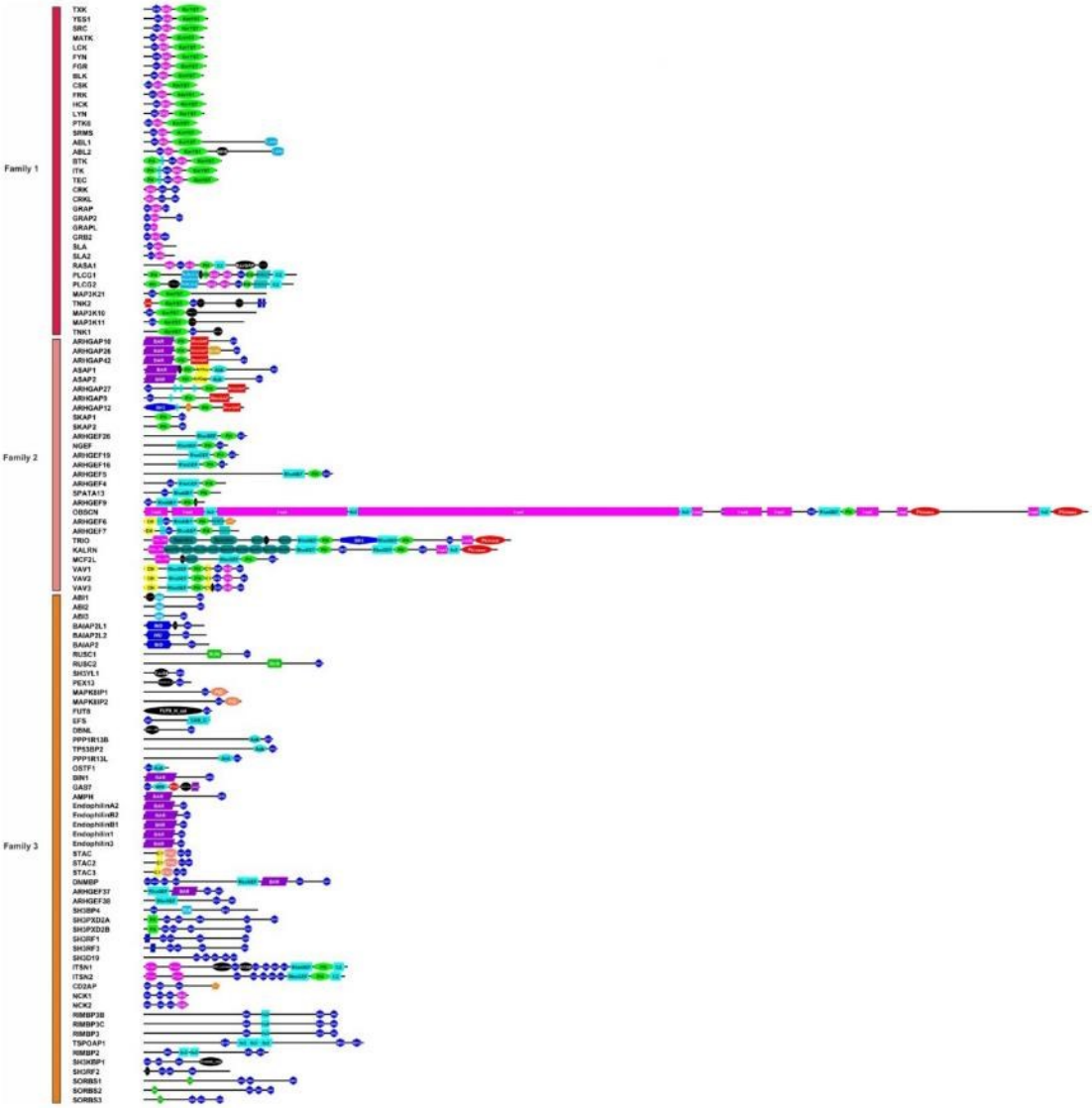
Family 1
Family 2
Family 3
TXK
YES1
SRC
MATK
LCK
FYN
FGR
BLK
CSK
FRK
HCK
LYN
PTK6
SRMS
ABL1
ABL2
BTK
ITK
TEC
CRK
CRKL
GRAP
GRAP2
GRAPL
GRB2
SLA
SLA2
RASA1
PLCG1
PLCG2
MAP3K21
TNK2
MAP3K10
MAP3K11
TNK1
ARHGAP10
ARHGAP26
ARHGAP42
ASAP1
ASAP2
ARHGAP27
ARHGAP5
ARHGAP12
SKAP1
SKAP2
ARHGEF26
NGEF
ARHGEF19
ARHGEF16
ARHGEF5
ARHGEF4
SPATA13
ARHGEF9
OBSCN
ARHGEF6
ARHGEF7
TRIO
KALRN
MCF2L
VAV1
VAV2
VAV3
ABI1
ABI2
ABI3
BAIAP2L1
BAIAP2L2
BAIAP2
RUSC1
RUSC2
SH3YL1
PEX13
MAPK8IP1
MAPK8IP2
FUT8
EFS
DBNL
PPP1R13B
TP53IP2
PPP1R13L
OSTF1
BIN1
GAB2
AMPH
EndophilinA2
EndophilinB2
EndophilinB1
Endophilin1
Endophilin2
STAC
STAC2
STAC3
DNMBP
ARHGEF37
ARHGEF38
SH3BP4
SH2PX2IA
SH2PX2B
SH3RF1
SH3RF3
SH3D19
ITSN1
ITSN2
CD2AP
NCK1
NCK2
RIMBP3B
RIMBP3C
RIMBP3
TSPOAP1
RIMBP2
SH3KBP1
SH3RF2
SORBS1
SORBS2
SORBS3

10

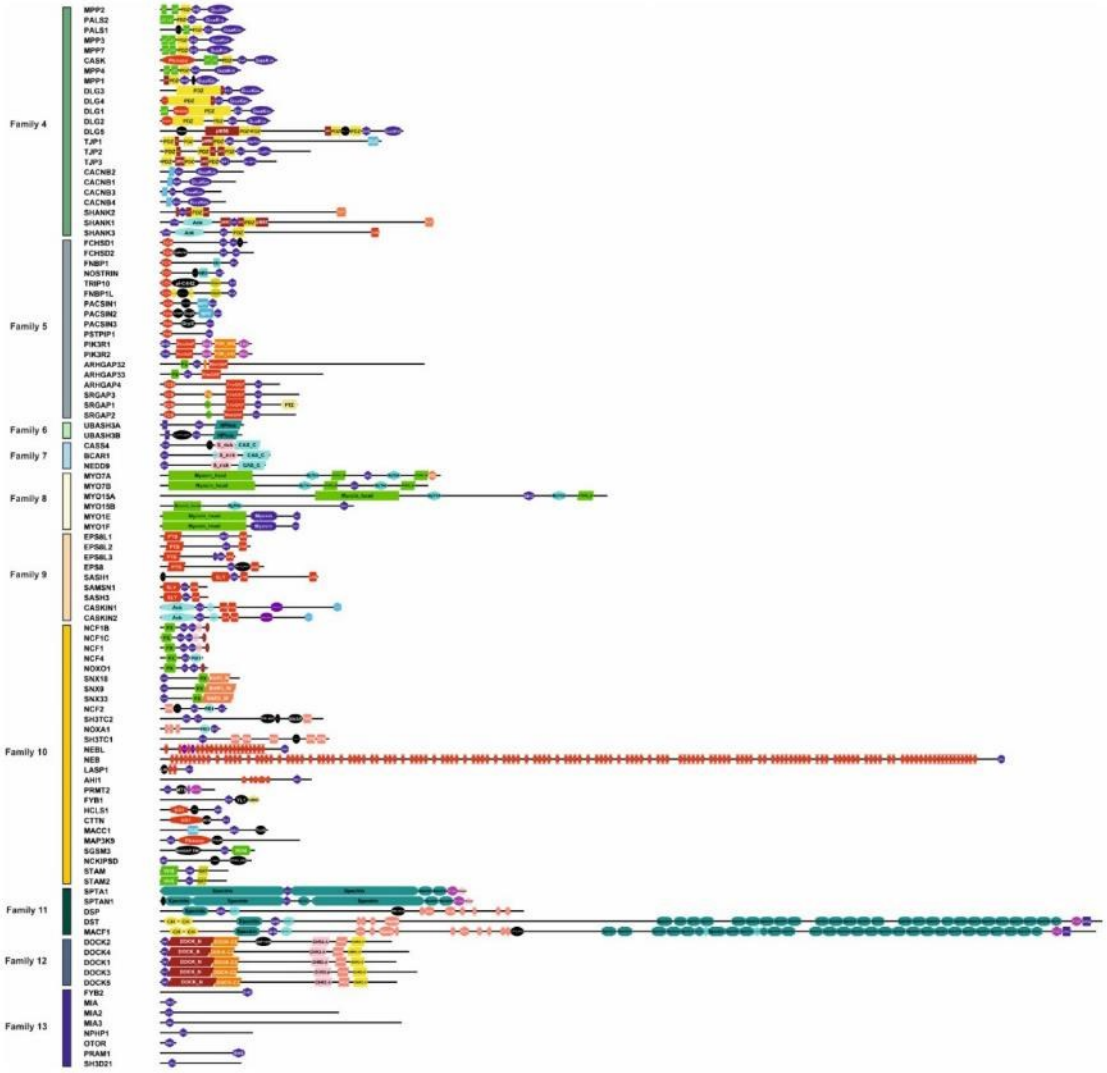

Figure S2. Domain organization of the SH3DCP superfamily. The SH3DCP families are organized based on the phylogenetic tree (Figure 3). Detailed information on all SH3DCPs and their respective domains can be found in Table S1.

References

1. Wallez Y, Mace PD, Pasquale EB, Riedl SJ. NSP-CAS protein complexes: emerging signaling modules in cancer. Genes & cancer. 2012;3(5-6):382-393.
2. Gemperle J, Hexnerová R, Lepšík M, et al. Structural characterization of CAS SH3 domain selectivity and regulation reveals new CAS interaction partners. Scientific reports. 2017;7(1):1-18.
3. Birge RB, Kalodimos C, Inagaki F, Tanaka S. Crk and CrkL adaptor proteins: networks for physiological and pathological signaling. Cell Communication and Signaling. 2009;7(1):1-23.
4. Rönty M, Taivainen A, Heiska L, et al. Palladin interacts with SH3 domains of SPIN90 and Src and is required for Src-induced cytoskeletal remodeling. Experimental Cell Research. 2007/07/15/ 2007;313(12):2575-2585.
5. Ortiz MA, Mikhailova T, Li X, Porter BA, Bah A, Kotula L. Src family kinases, adaptor proteins and the actin cytoskeleton in epithelial-to-mesenchymal transition. Cell Communication and Signaling. 2021/06/30 2021;19(1):67.
6. Silva CM. Role of STATs as downstream signal transducers in Src family kinase-mediated tumorigenesis. Oncogene. 2004/10/01 2004;23(48):8017-8023.
7. Rudd ML, Tua-Smith A, Straus DB. Lck SH3 domain function is required for T-cell receptor signals regulating thymocyte development. Molecular and cellular biology. 2006;26(21):7892-7900.
8. Umemori H, Satot S, Yagi T, Aizawal S, Yamamoto T. Initial events of myelination involve Fyn tyrosine kinase signalling. Nature. 1994;367(6463):572-576.
9. Klein C, Krämer E-M, Cardine A-M, Schraven B, Brandt R, Trotter J. Process outgrowth of oligodendrocytes is promoted by interaction of fyn kinase with the cytoskeletal protein tau. Journal of Neuroscience. 2002;22(3):698-707.
10. Matrone C, Petrillo F, Nasso R, Ferretti G. Fyn tyrosine kinase as harmonizing factor in neuronal functions and dysfunctions. International journal of molecular sciences. 2020;21(12):4444.
11. Lau DH, Hogseth M, Phillips EC, et al. Critical residues involved in tau binding to fyn: implications for tau phosphorylation in Alzheimer's disease. Acta neuropathologica communications. 2016;4(1):1-13.
12. Annerén C, Lindholm CK, Kriz V, Welsh M. The FRK/RAK-SHB signaling cascade: a versatile signal-transduction pathway that regulates cell survival, differentiation and proliferation. Current molecular medicine. 2003;3(4):313-324.
13. Stanglmaier M, Warmuth M, Kleinlein I, Reis S, Hallek M. The interaction of the Bcr-Abl tyrosine kinase with the Src kinase Hck is mediated by multiple binding domains. Leukemia. 2003;17(2):283-289.
14. Radha V, Sudhakar C, Ray P, Swarup G. Induction of cytochrome c release and apoptosis by Hck-SH3 domain-mediated signalling requires caspase-3. Apoptosis. 2002;7(3):195-207.
15. Hammond S, Wagenknecht-Wiesner A, Veatch SL, Holowka D, Baird B. Roles for SH2 and SH3 domains in Lyn kinase association with activated FcεRI in RBL mast cells revealed by patterned surface analysis. Journal of structural biology. 2009;168(1):161-167.
16. Zheng Y, Peng M, Wang Z, Asara JM, Tyner AL. Protein tyrosine kinase 6 directly phosphorylates AKT and promotes AKT activation in response to epidermal growth factor. Molecular and cellular biology. 2010;30(17):4280-4292.
17. Xue C, Wang X, Zhang L, Qu Q, Zhang Q, Jiang Y. Ibrutinib in B-cell lymphoma: single fighter might be enough? Cancer Cell International. 2020;20(1):1-13.
18. Kueffer LE, Joseph RE, Andreotti AH. Reining in BTK: interdomain interactions and their importance in the regulatory control of BTK. Frontiers in Cell and Developmental Biology. 2021;9:655489.
19. López-Herrera G, Vargas-Hernández A, González-Serrano ME, et al. Bruton's tyrosine kinase—an integral protein of B cell development that also has an essential role in the innate immune system. Journal of leukocyte biology. 2014;95(2):243-250.
20. Cory G, MacCarthy-Morrogh L, Banin S, et al. Evidence that the Wiskott-Aldrich syndrome protein may be involved in lymphoid cell signaling pathways. The Journal of Immunology. 1996;157(9):3791-3795.
21. Nore BF, Mohamed AJ, Vargas L, et al. The Role of Bruton's Tyrosine Kinase (Btk) in Phosphoinositide-Dependent Signaling. ACI International. 2000;12:3.
22. Akinleye A, Chen Y, Mukhi N, Song Y, Liu D. Ibrutinib and novel BTK inhibitors in clinical development. Journal of hematology & oncology. 2013;6(1):1-9.
23. Andersen TCB, Kristiansen PE, Huszenicza Z, et al. The SH3 domains of the protein kinases ITK and LCK compete for adjacent sites on T cell–specific adapter protein. Journal of Biological Chemistry. 2019;294(42):15480-15494.
24. Perez-Villar JJ, O'Day K, Hewgill DH, Nadler SG, Kanner SB. Nuclear localization of the tyrosine kinase Itk and interaction of its SH3 domain with karyopherin α (Rch1α). International immunology. 2001;13(10):1265-1274.
25. Lawson CD, Ridley AJ. Rho GTPase signaling complexes in cell migration and invasion. Journal of Cell Biology. 2018;217(2):447-457.
26. Hossain S, Dubielecka PM, Sikorski AF, Birge RB, Kotula L. Crk and ABI1: binary molecular switches that regulate abl tyrosine kinase and signaling to the cytoskeleton. Genes & cancer. 2012;3(5-6):402-413.
27. Feng G-S, Ouyang Y-B, Hu D-P, Shi Z-Q, Gentz R, Ni J. Grap Is a Novel SH3-SH2-SH3 Adaptor Protein That Couples Tyrosine Kinases to the Ras Pathway (∗). Journal of Biological Chemistry. 1996;271(21):12129-12132.
28. Schlessinger J. SH2/SH3 signaling proteins. Current opinion in genetics & development. 1994;4(1):25-30.
29. Kazemein Jasemi NS, Herrmann C, Magdalena Estirado E, et al. The intramolecular allostery of GRB2 governing its interaction with SOS1 is modulated by phosphotyrosine ligands. Biochemical Journal. 2021;478(14):2793-2809.
30. Boomer JS, Green JM. An enigmatic tail of CD28 signaling. Cold Spring Harb Perspect Biol. Aug 2010;2(8):a002436.

31. Nishida M, Nagata K, Hachimori Y, et al. Novel recognition mode between Vav and Grb2 SH3 domains. Embo j. Jun 15 2001;20(12):2995-3007.
32. Marton N, Baricza E, Érsek B, Buzás EI, Nagy G. The Emerging and Diverse Roles of Src-Like Adaptor Proteins in Health and Disease. Mediators Inflamm. 2015;2015:952536.
33. Sosinowski T, Pandey A, Dixit VM, Weiss A. Src-like adaptor protein (SLAP) is a negative regulator of T cell receptor signaling. The Journal of experimental medicine. 2000;191(3):463-474.
34. Lapinski PE, King PD. RASA1. In: Choi S, ed. Encyclopedia of Signaling Molecules. New York, NY: Springer New York; 2012:1601-1605.
35. Wang Y, Wu J, Wang Z. Akt binds to and phosphorylates phospholipase C-γ1 in response to epidermal growth factor. Molecular biology of the cell. 2006;17(5):2267-2277.
36. Rellahan BL, Graham LJ, Tysgankov AY, et al. A dynamic constitutive and inducible binding of c-Cbl by PLCγ1 SH3 and SH2 domains (negatively) regulates antigen receptor-induced PLCγ1 activation in lymphocytes. Experimental cell research. 2003;289(1):184-194.
37. Karpov OA, Fearnley GW, Smith GA, et al. Receptor tyrosine kinase structure and function in health and disease. AIMS Biophysics. 2015;2(4):476-502.
38. Chen D, Simons M. Emerging roles of PLCγ1 in endothelial biology. Science signaling. 2021;14(694):eabc6612.
39. Mahajan K, Mahajan NP. ACK1/TNK2 tyrosine kinase: molecular signaling and evolving role in cancers. Oncogene. 2015;34(32):4162-4167.
40. Mahajan K, Mahajan NP. Shepherding AKT and androgen receptor by Ack1 tyrosine kinase. Journal of cellular physiology. 2010;224(2):327-333.
41. Lucken-Ardjomande Häsler S, Vallis Y, Pasche M, McMahon HT. GRAF2, WDR44, and MICAL1 mediate Rab8/10/11–dependent export of E-cadherin, MMP14, and CFTR ΔF508. Journal of Cell Biology. 2020;219(5).
42. Lee S, Salazar SV, Cox TO, Strittmatter SM. Pyk2 signaling through Graf1 and RhoA GTPase is required for amyloid-β oligomer-triggered synapse loss. Journal of Neuroscience. 2019;39(10):1910-1929.
43. Doherty GJ, Ahlund MK, Howes MT, et al. The endocytic protein GRAF1 is directed to cell-matrix adhesion sites and regulates cell spreading. Molecular biology of the cell. 2011;22(22):4380-4389.
44. Bharti S, Inoue H, Bharti K, et al. Src-dependent phosphorylation of ASAP1 regulates podosomes. Molecular and cellular biology. 2007;27(23):8271-8283.
45. Brown MT, Andrade J, Radhakrishna H, Donaldson JG, Cooper JA, Randazzo PA. ASAP1, a phospholipid-dependent arf GTPase-activating protein that associates with and is phosphorylated by Src. Molecular and cellular biology. 1998;18(12):7038-7051.
46. Liu Y, Loijens JC, Martin KH, Karginov AV, Parsons JT. The association of ASAP1, an ADP ribosylation factor-GTPase activating protein, with focal adhesion kinase contributes to the process of focal adhesion assembly. Molecular biology of the cell. 2002;13(6):2147-2156.
47. Liu Y, Yerushalmi GM, Grigera PR, Parsons JT. Mislocalization or reduced expression of Arf GTPase-activating protein ASAP1 inhibits cell spreading and migration by influencing Arf1 GTPase cycling. Journal of Biological Chemistry. 2005;280(10):8884-8892.
48. Ba W, Selten MM, Van Der Raadt J, et al. ARHGAP12 functions as a developmental brake on excitatory synapse function. Cell reports. 2016;14(6):1355-1368.
49. Dadwal N, Mix C, Reinhold A, et al. The multiple roles of the cytosolic adapter proteins ADAP, SKAP1 and SKAP2 for TCR/CD3-mediated signaling events. Frontiers in immunology. 2021;12:703534.
50. Liu J, Kang H, Raab M, da Silva AJ, Kraeft SK, Rudd CE. FYB (FYN binding protein) serves as a binding partner for lymphoid protein and FYN kinase substrate SKAP55 and a SKAP55-related protein in T cells. Proc Natl Acad Sci U S A. Jul 21 1998;95(15):8779-8784.
51. Jin X, Chen Y, Sheng Z, et al. SKAP2 is downregulated in the villous tissues of patients with missed abortion and regulates growth and migration in trophoblasts through the WAVE2-ARP2/3 signaling pathway. Placenta. 2022/10/01/ 2022;128:100-111.
52. Takahashi T, Yamashita H, Nagano Y, et al. Identification and Characterization of a Novel Pyk2/Related Adhesion Focal Tyrosine Kinase-associated Protein That Inhibits α-Synuclein Phosphorylation*. Journal of Biological Chemistry. 2003/10/24/ 2003;278(43):42225-42233.
53. Bureau JF, Cassonnet P, Grange L, et al. The SRC-family tyrosine kinase HCK shapes the landscape of SKAP2 interactome. Oncotarget. Mar 2 2018;9(17):13102-13115.
54. Mitin N, Betts L, Yohe ME, Der CJ, Sondek J, Rossman KL. Release of autoinhibition of ASEF by APC leads to CDC42 activation and tumor suppression. Nature structural & molecular biology. 2007;14(9):814-823.
55. Hamann MJ, Lubking CM, Luchini DN, Billadeau DD. Asef2 functions as a Cdc42 exchange factor and is stimulated by the release of an autoinhibitory module from a concealed C-terminal activation element. Molecular and cellular biology. 2007;27(4):1380-1393.
56. Kawasaki Y, Sagara M, Shibata Y, Shirouzu M, Yokoyama S, Akiyama T. Identification and characterization of Asef2, a guanine–nucleotide exchange factor specific for Rac1 and Cdc42. Oncogene. 2007;26(55):7620-7627.
57. Young P, Ehler E, Gautel M. Obscurin, a giant sarcomeric Rho guanine nucleotide exchange factor protein involved in sarcomere assembly. The Journal of cell biology. 2001;154(1):123-136.

58. Feng Q, Baird D, Cerione RA. Novel regulatory mechanisms for the Dbl family guanine nucleotide exchange factor Cool-2/α-Pix. The EMBO journal. 2004;23(17):3492-3504.
59. Manser E, Loo T-H, Koh C-G, et al. PAK kinases are directly coupled to the PIX family of nucleotide exchange factors. Molecular cell. 1998;1(2):183-192.
60. Mott HR, Nietlispach D, Evetts KA, Owen D. Structural analysis of the SH3 domain of β-PIX and its interaction with α-p21 activated kinase (PAK). Biochemistry. 2005;44(33):10977-10983.
61. Hoelz A, Janz JM, Lawrie SD, Corwin B, Lee A, Sakmar TP. Crystal structure of the SH3 domain of βPIX in complex with a high affinity peptide from PAK2. Journal of molecular biology. 2006;358(2):509-522.
62. Simmons A, Gangadharan B, Hodges A, et al. Nef-mediated lipid raft exclusion of UbcH7 inhibits Cbl activity in T cells to positively regulate signaling. Immunity. 2005;23(6):621-634.
63. Lim CS, Kim SH, Jung JG, Kim J-K, Song WK. Regulation of SPIN90 phosphorylation and interaction with Nck by ERK and cell adhesion. Journal of Biological Chemistry. 2003;278(52):52116-52123.
64. Ye ZS, Baltimore D. Binding of Vav to Grb2 through dimerization of Src homology 3 domains. Proc Natl Acad Sci U S A. Dec 20 1994;91(26):12629-12633.
65. Cuadrado M, Robles-Valero J. VAV Proteins as Double Agents in Cancer: Oncogenes with Tumor Suppressor Roles. Biology (Basel). Sep 8 2021;10(9).
66. Steinestel K, Brüderlein S, Steinestel J, et al. Expression of Abelson interactor 1 (Abi1) correlates with inflammation, KRAS mutation and adenomatous change during colonic carcinogenesis. PLoS One. 2012;7(7):e40671.
67. Luo K, Zhang L, Liao Y, et al. Effects and mechanisms of Eps8 on the biological behaviour of malignant tumours. Oncology Reports. 2021;45(3):824-834.
68. Smith LG, Li R. Actin polymerization: riding the wave. Current Biology. 2004;14(3):R109-R111.
69. Sekino S, Kashiwagi Y, Kanazawa H, et al. The NESH/Abi-3-based WAVE2 complex is functionally distinct from the Abi-1-based WAVE2 complex. Cell Communication and Signaling. 2015;13(1):1-15.
70. Postema MM, Grega-Larson NE, Neininger AC, Tyska MJ. IRTKS (BAIAP2L1) elongates epithelial microvilli using EPS8-dependent and independent mechanisms. Current Biology. 2018;28(18):2876-2888. e2874.
71. Li L, Baxter SS, Zhao P, Gu N, Zhan X. Differential interactions of missing in metastasis and insulin receptor tyrosine kinase substrate with RAB proteins in the endocytosis of CXCR4. Journal of Biological Chemistry. 2019;294(16):6494-6505.
72. Wu C, Cui X, Huang L, et al. IRTKS promotes insulin signaling transduction through inhibiting SHIP2 phosphatase activity. International Journal of Molecular Sciences. 2019;20(11):2834.
73. Blessing AM, Ganesan S, Rajapakshe K, et al. Identification of a Novel Coregulator, SH3YL1, That Interacts With the Androgen Receptor N-Terminus. Mol Endocrinol. Oct 2015;29(10):1426-1439.
74. Hasegawa J, Jebri I, Yamamoto H, et al. SH3YL1 cooperates with ESCRT-I in the sorting and degradation of the EGF receptor. Journal of Cell Science. 2019;132(19):jcs229179.
75. Barnett P, Bottger G, Klein AT, Tabak HF, Distel B. The peroxisomal membrane protein Pex13p shows a novel mode of SH3 interaction. The EMBO Journal. 2000;19(23):6382-6391.
76. Pires JR, Hong X, Brockmann C, et al. The ScPex13p SH3 domain exposes two distinct binding sites for Pex5p and Pex14p. Journal of molecular biology. 2003;326(5):1427-1435.
77. Kim M, Ann E, Mo J, et al. JIP1 binding to RBP-Jk mediates cross-talk between the Notch1 and JIP1-JNK signaling pathway. Cell Death & Differentiation. 2010;17(11):1728-1738.
78. Ohba T, Ishino M, Aoto H, Sasaki T. Dot far-western blot analysis of relative binding affinities of the Src homology 3 domains of Efs and its related proteins. Analytical biochemistry. 1998;262(2):185-192.
79. Deneka A, Korobeynikov V, Golemis EA. Embryonal Fyn-associated substrate (EFS) and CASS4: The lesser-known CAS protein family members. Gene. 2015;570(1):25-35.
80. Patel S, George R, Autore F, Fraternali F, Ladbury JE, Nikolova PV. Molecular interactions of ASPP1 and ASPP2 with the p53 protein family and the apoptotic promoters PUMA and Bax. Nucleic acids research. 2008;36(16):5139-5151.
81. Benyamini H, Friedler A. The ASPP interaction network: electrostatic differentiation between pro-and anti-apoptotic proteins. Journal of molecular recognition. 2011;24(2):266-274.
82. Rotem-Bamberger S, Katz C, Friedler A. Regulation of ASPP2 interaction with p53 core domain by an intramolecular autoinhibitory mechanism. PLoS One. 2013;8(3):e58470.
83. Lyraki R, Lokaj M, Soares DC, et al. Characterization of a novel RP2–OSTF1 interaction and its implication for actin remodelling. Journal of cell science. 2018;131(4):jcs211748.
84. Sottejeau Y, Bretteville A, Cantrelle F-X, et al. Tau phosphorylation regulates the interaction between BIN1's SH3 domain and Tau's proline-rich domain. Acta neuropathologica communications. 2015;3(1):1-12.
85. Lasorsa A, Malki I, Cantrelle F-X, et al. Structural basis of tau interaction with BIN1 and regulation by tau phosphorylation. Frontiers in molecular neuroscience. 2018:421.
86. Picas L, Viaud J, Schauer K, et al. BIN1/M-Amphiphysin2 induces clustering of phosphoinositides to recruit its downstream partner dynamin. Nature Communications. 2014;5(1):1-12.
87. Mendes T. Identification of the modulators of and the molecular pathways involved in the BIN1-Tau interaction, Université de Lille; 2018.
88. Yoshida Y, Kinuta M, Abe T, et al. The stimulatory action of amphiphysin on dynamin function is dependent on lipid bilayer curvature. The EMBO journal. 2004;23(17):3483-3491.

89. Chen R, Zhao H, Wu D, Zhao C, Zhao W, Zhou X. The role of SH3GL3 in myeloma cell migration/invasion, stemness and chemo-resistance. Oncotarget. 2016;7(45):73101.
90. Campiglio M, Kaplan MM, Flucher BE. STAC3 incorporation into skeletal muscle triads occurs independent of the dihydropyridine receptor. Journal of cellular physiology. 2018;233(12):9045-9051.
91. Oda Y, Otani T, Ikenouchi J, Furuse M. Tricellulin regulates junctional tension of epithelial cells at tricellular contacts through Cdc42. Journal of cell science. 2014;127(19):4201-4212.
92. Salazar MA, Kwiatkowski AV, Pellegrini L, et al. Tuba, a novel protein containing bin/amphiphysin/Rvs and Dbl homology domains, links dynamin to regulation of the actin cytoskeleton. Journal of Biological Chemistry. 2003;278(49):49031-49043.
93. Polle L, Rigano LA, Julian R, Ireton K, Schubert W-D. Structural details of human tuba recruitment by InlC of Listeria monocytogenes elucidate bacterial cell-cell spreading. Structure. 2014;22(2):304-314.
94. Cestra G, Kwiatkowski A, Salazar M, Gertler F, De Camilli P. Tuba, a GEF for CDC42, links dynamin to actin regulatory proteins. Methods in enzymology. 2005;404:537-545.
95. Kim Y-M, Stone M, Hwang TH, et al. SH3BP4 is a negative regulator of amino acid-Rag GTPase-mTORC1 signaling. Molecular cell. 2012;46(6):833-846.
96. Kim Y-M, Kim D-H. dRAGging amino acid-mTORC1 signaling by SH3BP4. Molecules and cells. 2013;35(1):1-6.
97. Acuna C, Liu X, Gonzalez A, Südhof TC. RIM-BPs mediate tight coupling of action potentials to Ca2+-triggered neurotransmitter release. Neuron. 2015;87(6):1234-1247.
98. Mencacci NE, Brockmann MM, Dai J, et al. Biallelic variants in TSPOAP1, encoding the active-zone protein RIMBP1, cause autosomal recessive dystonia. J Clin Invest. Apr 1 2021;131(7).
99. Buschman MD, Bromann PA, Cejudo-Martin P, Wen F, Pass I, Courtneidge SA. The novel adaptor protein Tks4 (SH3PXD2B) is required for functional podosome formation. Molecular biology of the cell. 2009;20(5):1302-1311.
100. de Bock CE, Hughes MR, Snyder K, et al. Protein interaction screening identifies SH 3 RF 1 as a new regulator of FAT 1 protein levels. FEBS letters. 2017;591(4):667-678.
101. Zhang P, Liu Y, Lian C, et al. SH3RF3 promotes breast cancer stem-like properties via JNK activation and PTX3 upregulation. Nature Communications. 2020/05/19 2020;11(1):2487.
102. Kärkkäinen S, van der Linden M, Renkema GH. POSH2 is a RING finger E3 ligase with Rac1 binding activity through a partial CRIB domain. FEBS Lett. Sep 24 2010;584(18):3867-3872.
103. Okur MN, Ooi J, Fong CW, et al. Intersectin 1 enhances Cbl ubiquitylation of epidermal growth factor receptor through regulation of Sprouty2-Cbl interaction. Molecular and cellular biology. 2012;32(4):817-825.
104. Hussain NK, Jenna S, Glogauer M, et al. Endocytic protein intersectin-l regulates actin assembly via Cdc42 and N-WASP. Nature cell biology. 2001;3(10):927-932.
105. Keating DJ, Chen C, Pritchard MA. Alzheimer's disease and endocytic dysfunction: clues from the Down syndrome-related proteins, DSCR1 and ITSN1. Ageing research reviews. 2006;5(4):388-401.
106. Herrero-Garcia E, O'Bryan JP. Intersectin scaffold proteins and their role in cell signaling and endocytosis. Biochimica et Biophysica Acta (BBA)-Molecular Cell Research. 2017;1864(1):23-30.
107. Tong X-K, Hussain NK, Adams AG, O'Bryan JP, McPherson PS. Intersectin can regulate the Ras/MAP kinase pathway independent of its role in endocytosis. Journal of Biological Chemistry. 2000;275(38):29894-29899.
108. Jakob B, Kochlamazashvili G, Jäpel M, et al. Intersectin 1 is a component of the Reelin pathway to regulate neuronal migration and synaptic plasticity in the hippocampus. Proceedings of the National Academy of Sciences. 2017;114(21):5533-5538.
109. Gubar O, Morderer D, Tsyba L, et al. Intersectin: the crossroad between vesicle exocytosis and endocytosis. Frontiers in endocrinology. 2013;4:109.
110. Rouka E, Simister PC, Janning M, et al. Differential recognition preferences of the three Src homology 3 (SH3) domains from the adaptor CD2-associated protein (CD2AP) and direct association with Ras and Rab interactor 3 (RIN3). Journal of Biological Chemistry. 2015;290(42):25275-25292.
111. Frese S. Structural and biochemical analysis of Nck1 and Nck2 SH2 domains2005.
112. Kesti T, Ruppelt A, Wang J-H, et al. Reciprocal regulation of SH3 and SH2 domain binding via tyrosine phosphorylation of a common site in CD3ε. The Journal of Immunology. 2007;179(2):878-885.
113. Kim TW, Kang YK, Park ZY, et al. SH3RF2 functions as an oncogene by mediating PAK4 protein stability. Carcinogenesis. 2014;35(3):624-634.
114. Lin W-H, Huang C-J, Liu M-W, et al. Cloning, mapping, and characterization of the human sorbin and SH3 domain containing 1 (SORBS1) gene: a protein associated with c-Abl during insulin signaling in the hepatoma cell line Hep3B. Genomics. 2001;74(1):12-20.
115. Matsuyama M, Mizusaki H, Shimono A, et al. A novel isoform of Vinexin, Vinexin γ, regulates Sox9 gene expression through activation of MAPK cascade in mouse fetal gonad. Genes to Cells. 2005;10(5):421-434.
116. Akamatsu M, Aota S, Suwa A, et al. Vinexin forms a signaling complex with Sos and modulates epidermal growth factor-induced c-Jun N-terminal kinase/stress-activated protein kinase activities. J Biol Chem. Dec 10 1999;274(50):35933-35937.
117. Rademacher N, Schmerl B, Lardong JA, Wahl MC, Shoichet SA. MPP2 is a postsynaptic MAGUK scaffold protein that links SynCAM1 cell adhesion molecules to core components of the postsynaptic density. Scientific Reports. 2016;6(1):1-10.

118. Krishna Subbaiah V, Massimi P, Boon SS, et al. The invasive capacity of HPV transformed cells requires the hDlg-dependent enhancement of SGEF/RhoG activity. PLoS pathogens. 2012;8(2):e1002543.
119. Zhu J, Shang Y, Zhang M. Mechanistic basis of MAGUK-organized complexes in synaptic development and signalling. Nature Reviews Neuroscience. 2016;17(4):209-223.
120. McNeil E, Capaldo CT, Macara IG. Zonula occludens-1 function in the assembly of tight junctions in Madin-Darby canine kidney epithelial cells. Molecular biology of the cell. 2006;17(4):1922-1932.
121. Cruz Garcia Y. Interactome of the β2b subunit of L-type voltage-gated calcium channels in cardiomyocytes, Universität Würzburg; 2021.
122. Quitsch A, Berhörster K, Liew CW, Richter D, Kreienkamp H-J. Postsynaptic shank antagonizes dendrite branching induced by the leucine-rich repeat protein Densin-180. Journal of Neuroscience. 2005;25(2):479-487.
123. Bucher M, Niebling S, Han Y, et al. Autism-associated SHANK3 missense point mutations impact conformational fluctuations and protein turnover at synapses. Elife. 2021;10:e66165.
124. Chakraborty S, Ain R. Nitric-oxide synthase trafficking inducer is a pleiotropic regulator of endothelial cell function and signaling. Journal of Biological Chemistry. 2017;292(16):6600-6620.
125. Zimmermann K, Opitz N, Dedio J, Renné C, Müller-Esterl W, Oess S. NOSTRIN: a protein modulating nitric oxide release and subcellular distribution of endothelial nitric oxide synthase. Proceedings of the National Academy of Sciences. 2002;99(26):17167-17172.
126. Icking A, Matt S, Opitz N, Wiesenthal A, Müller-Esterl W, Schilling K. NOSTRIN functions as a homotrimeric adaptor protein facilitating internalization of eNOS. Journal of Cell Science. 2005;118(21):5059-5069.
127. Tian L, Nelson DL, Stewart DM. Cdc42-interacting protein 4 mediates binding of the Wiskott-Aldrich syndrome protein to microtubules. Journal of Biological Chemistry. 2000;275(11):7854-7861.
128. Richnau N, Aspenström P. Rich, a rho GTPase-activating protein domain-containing protein involved in signaling by Cdc42 and Rac1. Journal of Biological Chemistry. 2001;276(37):35060-35070.
129. Quan A, Robinson PJ. Syndapin–a membrane remodelling and endocytic F-BAR protein. The FEBS journal. 2013;280(21):5198-5212.
130. Marcos T, Ruiz-Martín V, de la Puerta ML, et al. Proline-serine-threonine phosphatase interacting protein 1 inhibition of T-cell receptor signaling depends on its SH 3 domain. The FEBS journal. 2014;281(17):3844-3854.
131. Cong F, Spencer S, Côté J-F, et al. Cytoskeletal protein PSTPIP1 directs the PEST-type protein tyrosine phosphatase to the c-Abl kinase to mediate Abl dephosphorylation. Molecular cell. 2000;6(6):1413-1423.
132. Shoham NG, Centola M, Mansfield E, et al. Pyrin binds the PSTPIP1/CD2BP1 protein, defining familial Mediterranean fever and PAPA syndrome as disorders in the same pathway. Proceedings of the National Academy of Sciences. 2003;100(23):13501-13506.
133. Wu Y, Spencer SD, Lasky LA. Tyrosine phosphorylation regulates the SH3-mediated binding of the Wiskott-Aldrich syndrome protein to PSTPIP, a cytoskeletal-associated protein. Journal of Biological Chemistry. 1998;273(10):5765-5770.
134. Ren S-y, Xue F, Feng J, Skorski T. Intrinsic regulation of the interactions between the SH3 domain of p85 subunit of phosphatidylinositol-3 kinase and the protein network of BCR/ABL oncogenic tyrosine kinase. Experimental hematology. 2005;33(10):1222-1228.
135. Yudowski GA, Efendiev R, Pedemonte CH, Katz AI, Berggren P-O, Bertorello AM. Phosphoinositide-3 kinase binds to a proline-rich motif in the Na+, K+-ATPase α subunit and regulates its trafficking. Proceedings of the National Academy of Sciences. 2000;97(12):6556-6561.
136. Ito Y, Vogt PK, Hart JR. Domain analysis reveals striking functional differences between the regulatory subunits of phosphatidylinositol 3-kinase (PI3K), p85α and p85β. Oncotarget. 2017;8(34):55863.
137. Ren S-y, Bolton E, Mohi MG, Morrione A, Neel BG, Skorski T. Phosphatidylinositol 3-kinase p85α subunit-dependent interaction with BCR/ABL-related fusion tyrosine kinases: molecular mechanisms and biological consequences. Molecular and cellular biology. 2005;25(18):8001-8008.
138. Ma Y, Mi Y-J, Dai Y-K, Fu H-L, Cui D-X, Jin W-L. The inverse F-BAR domain protein srGAP2 acts through srGAP3 to modulate neuronal differentiation and neurite outgrowth of mouse neuroblastoma cells. PloS one. 2013;8(3):e57865.
139. Bacon C, Endris V, Rappold GA. The cellular function of srGAP3 and its role in neuronal morphogenesis. Mechanisms of development. 2013;130(6-8):391-395.
140. Mason FM, Heimsath EG, Higgs HN, Soderling SH. Bi-modal regulation of a formin by srGAP2. Journal of Biological Chemistry. 2011;286(8):6577-6586.
141. Newman JRB, Concannon P, Ge Y. UBASH3A Interacts with PTPN22 to Regulate IL2 Expression and Risk for Type 1 Diabetes. Int J Mol Sci. May 12 2023;24(10).
142. Feshchenko EA, Smirnova EV, Swaminathan G, et al. TULA: an SH3- and UBA-containing protein that binds to c-Cbl and ubiquitin. Oncogene. Jun 10 2004;23(27):4690-4706.
143. Tsygankov AY. TULA-family proteins: an odd couple. Cell Mol Life Sci. Sep 2009;66(17):2949-2952.
144. Kowanetz K, Crosetto N, Haglund K, Schmidt MHH, Heldin CH, Dikic I. Suppressors of T-cell receptor signaling Sts-1 and Sts-2 bind to Cbl and inhibit endocytosis of receptor tyrosine kinases. J Biol Chem. Jul 30 2004;279(31):32786-32795.
145. Janoštiak R, Tolde O, Brůhová Z, et al. Tyrosine phosphorylation within the SH3 domain regulates CAS subcellular localization, cell migration, and invasiveness. Molecular biology of the cell. 2011;22(22):4256-4267.

146. Janoštiak R, Brábek J, Auernheimer V, et al. CAS directly interacts with vinculin to control mechanosensing and focal adhesion dynamics. Cellular and molecular life sciences. 2014;71(4):727-744.
147. Gemperle J, Dibus M, Koudelková L, Rosel D, Brábek J. The interaction of p130Cas with PKN 3 promotes malignant growth. Molecular oncology. 2019;13(2):264-289.
148. Tachibana K, Urano T, Fujita H, et al. Tyrosine phosphorylation of Crk-associated substrates by focal adhesion kinase: a putative mechanism for the integrin-mediated tyrosine phosphorylation of Crk-associated substrates. Journal of Biological Chemistry. 1997;272(46):29083-29090.
149. Suzuki T, Nakamoto T, Ogawa S, et al. MICAL, a novel CasL interacting molecule, associates with vimentin. Journal of Biological Chemistry. 2002;277(17):14933-14941.
150. Tanimura S, Hashizume J, Arichika N, et al. ERK signaling promotes cell motility by inducing the localization of myosin 1E to lamellipodial tips. Journal of Cell Biology. 2016;214(4):475-489.
151. Krendel M, Osterweil EK, Mooseker MS. Myosin 1E interacts with synaptojanin-1 and dynamin via its SH3 domain. FEBS letters. 2007;581(4):644.
152. Heim JB, Squirewell EJ, Neu A, et al. Myosin-1E interacts with FAK proline-rich region 1 to induce fibronectin-type matrix. Proceedings of the National Academy of Sciences. 2017;114(15):3933-3938.
153. Matoskova B, Wong WT, Nomura N, Robbins KC, Di Fiore PP. RN-tre specifically binds to the SH3 domain of eps8 with high affinity and confers growth advantage to NIH3T3 upon carboxy-terminal truncation. Oncogene. 1996;12(12):2679-2688.
154. Matoskova B, Wong WT, Salcini AE, Pelicci PG, Di Fiore PP. Constitutive phosphorylation of eps8 in tumor cell lines: relevance to malignant transformation. Molecular and Cellular Biology. 1995;15(7):3805-3812.
155. Maa M-C, Leu T-H. EPS8, an adaptor protein acts as an oncoprotein in human cancer. Carcinogenesis: IntechOpen; 2013.
156. Jaufmann J, Franke FC, Sperlich A, et al. The emerging and diverse roles of the SLy/SASH1-protein family in health and disease—Overview of three multifunctional proteins. The FASEB Journal. 2021;35(4):e21470.
157. Kwan JJ, Slavkovic S, Piazza M, et al. HACS1 signaling adaptor protein recognizes a motif in the paired immunoglobulin receptor B cytoplasmic domain. Communications Biology. 2020/11/13 2020;3(1):672.
158. Schroeder K, Weissmann N, Brandes RP. Organizers and activators: Cytosolic Nox proteins impacting on vascular function. Free Radical Biology and Medicine. 2017;109:22-32.
159. Wishart MJ, Taylor GS, Dixon JE. Phoxy lipids: revealing PX domains as phosphoinositide binding modules. Cell. 2001;105(7):817-820.
160. Ueno N, Takeya R, Miyano K, Kikuchi H, Sumimoto H. The NADPH oxidase Nox3 constitutively produces superoxide in a p22phox-dependent manner: its regulation by oxidase organizers and activators. Journal of Biological Chemistry. 2005;280(24):23328-23339.
161. Miyano K, Ueno N, Takeya R, Sumimoto H. Direct involvement of the small GTPase Rac in activation of the superoxide-producing NADPH oxidase Nox1. Journal of Biological Chemistry. 2006;281(31):21857-21868.
162. Nakazawa S, Gotoh N, Matsumoto H, Murayama C, Suzuki T, Yamamoto T. Expression of sorting nexin 18 (SNX18) is dynamically regulated in developing spinal motor neurons. Journal of Histochemistry & Cytochemistry. 2011;59(2):202-213.
163. Park J, Kim Y, Lee S, et al. SNX18 shares a redundant role with SNX9 and modulates endocytic trafficking at the plasma membrane. Journal of cell science. 2010;123(10):1742-1750.
164. Soulet F, Yarar D, Leonard M, Schmid SL. SNX9 regulates dynamin assembly and is required for efficient clathrin-mediated endocytosis. Molecular biology of the cell. 2005;16(4):2058-2067.
165. Shin N, Lee S, Ahn N, et al. Sorting nexin 9 interacts with dynamin 1 and N-WASP and coordinates synaptic vesicle endocytosis. Journal of Biological Chemistry. 2007;282(39):28939-28950.
166. Yeow-Fong L, Lim L, Manser E. SNX9 as an adaptor for linking synaptojanin-1 to the Cdc42 effector ACK1. FEBS letters. 2005;579(22):5040-5048.
167. Baumann C, Lindholm CK, Rimoldi D, Lévy F. The E3 ubiquitin ligase Itch regulates sorting nexin 9 through an unconventional substrate recognition domain. The FEBS journal. 2010;277(13):2803-2814.
168. Schulze WX, Mann M. A novel proteomic screen for peptide-protein interactions. Journal of Biological Chemistry. 2004;279(11):10756-10764.
169. Worby CA, Simonson-Leff N, Clemens JC, Kruger RP, Muda M, Dixon JE. The sorting nexin, DSH3PX1, connects the axonal guidance receptor, Dscam, to the actin cytoskeleton. Journal of Biological Chemistry. 2001;276(45):41782-41789.
170. Lundmark R, Carlsson SR. SNX9–a prelude to vesicle release. Journal of cell science. 2009;122(1):5-11.
171. Badour K, McGavin MK, Zhang J, et al. Interaction of the Wiskott–Aldrich syndrome protein with sorting nexin 9 is required for CD28 endocytosis and cosignaling in T cells. Proceedings of the National Academy of Sciences. 2007;104(5):1593-1598.
172. Bendris N, Schmid SL. Endocytosis, Metastasis and Beyond: Multiple Facets of SNX9. Trends Cell Biol. Mar 2017;27(3):189-200.
173. Howard L, Nelson KK, Maciewicz RA, Blobel CP. Interaction of the metalloprotease disintegrins MDC9 and MDC15 with two SH3 domain-containing proteins, endophilin I and SH3PX1. Journal of Biological Chemistry. 1999;274(44):31693-31699.

174. Lupo V, Galindo MI, Martínez-Rubio D, et al. Missense mutations in the SH3TC2 protein causing Charcot-Marie-Tooth disease type 4C affect its localization in the plasma membrane and endocytic pathway. Human Molecular Genetics. 2009;18(23):4603-4614.
175. Huang C, Yi H, Zhou Y, Zhang Q, Yao X. Pan-Cancer Analysis Reveals SH3TC2 as an Oncogene for Colorectal Cancer and Promotes Tumorigenesis via the MAPK Pathway. Cancers. 2022;14(15):3735.
176. Li B, Zhuang L, Trueb B. Zyxin interacts with the SH3 domains of the cytoskeletal proteins LIM-nebulette and Lasp-1. Journal of biological chemistry. 2004;279(19):20401-20410.
177. Ma K, Wang K. Interaction of nebulin SH3 domain with titin PEVK and myopalladin: implications for the signaling and assembly role of titin and nebulin. FEBS letters. 2002;532(3):273-278.
178. Mihlan S, Reiss C, Thalheimer P, et al. Nuclear import of LASP-1 is regulated by phosphorylation and dynamic protein–protein interactions. Oncogene. 2013;32(16):2107-2113.
179. Rachlin AS, Otey CA. Identification of palladin isoforms and characterization of an isoform-specific interaction between Lasp-1 and palladin. Journal of cell science. 2006;119(6):995-1004.
180. Keicher C, Gambaryan S, Schulze E, Marcus K, Meyer HE, Butt E. Phosphorylation of mouse LASP-1 on threonine 156 by cAMP-and cGMP-dependent protein kinase. Biochemical and biophysical research communications. 2004;324(1):308-316.
181. Orth MF, Cazes A, Butt E, Grunewald TG. An update on the LIM and SH3 domain protein 1 (LASP1): a versatile structural, signaling, and biomarker protein. Oncotarget. 2015;6(1):26.
182. Butt E, Raman D. New frontiers for the cytoskeletal protein LASP1. Frontiers in oncology. 2018;8:391.
183. Esmailzadeh S, Jiang X. AHI-1: a novel signaling protein and potential therapeutic target in human leukemia and brain disorders. Oncotarget. 2011;2(12):918.
184. Hou W, Nemitz S, Schopper S, Nielsen ML, Kessels MM, Qualmann B. Arginine methylation by PRMT2 controls the functions of the actin nucleator Cobl. Developmental Cell. 2018;45(2):262-275. e268.
185. Imbastari F, Dahlmann M, Sporbert A, et al. MACC1 regulates clathrin-mediated endocytosis and receptor recycling of transferrin receptor and EGFR in colorectal cancer. Cellular and Molecular Life Sciences. 2021;78(7):3525-3542.
186. Stein U, Walther W, Arlt F, et al. MACC1, a newly identified key regulator of HGF-MET signaling, predicts colon cancer metastasis. Nature medicine. 2009;15(1):59-67.
187. Kim H, Oh H, Oh YS, et al. SPIN90, an adaptor protein, alters the proximity between Rab5 and Gapex5 and facilitates Rab5 activation during EGF endocytosis. Experimental & Molecular Medicine. 2019/07/01 2019;51(7):1-14.
188. Ackermann A, Brieger A. The role of nonerythroid spectrin II in cancer. Journal of oncology. 2019;2019.
189. Guo X, Chen SY. Dedicator of cytokinesis 2 in cell signaling regulation and disease development. Journal of cellular physiology. 2017;232(8):1931-1940.
190. Sakurai T, Kukimoto-Niino M, Kunimura K, et al. A conserved PI (4, 5) P2–binding domain is critical for immune regulatory function of DOCK8. Life science alliance. 2021;4(4).
191. Huang M, Liang C, Li S, et al. Two autism/dyslexia linked variations of DOCK4 disrupt the gene function on rac1/rap1 activation, neurite outgrowth, and synapse development. Frontiers in cellular neuroscience. 2020:577.
192. Lei Y, Xu J, Li M, et al. MIA SH3 Domain ER Export Factor 3 Deficiency Prevents Neointimal Formation by Restoring BAT-Like PVAT and Decreasing VSMC Proliferation and Migration. Frontiers in Endocrinology. 2021;12.
193. Wodarczyk C, Distefano G, Rowe I, et al. Nephrocystin-1 forms a complex with polycystin-1 via a polyproline motif/SH3 domain interaction and regulates the apoptotic response in mammals. PloS one. 2010;5(9):e12719.
194. Mannella V, Quilici G, Nigro EA, et al. The N-Terminal Domain of NPHP1 Folds into a Monomeric Left-Handed Antiparallel Three-Stranded Coiled Coil with Anti-apoptotic Function. ACS Chemical Biology. 2019;14(8):1845-1854.
195. Benzing T, Simons M, Walz G. Wnt signaling in polycystic kidney disease. Journal of the American Society of Nephrology. 2007;18(5):1389-1398.

Chapter II. Functional Classification and Interaction Selectivity Landscape of the Human SH3 Domain Superfamily

Authors: *Neda S. Kazemein Jasemi*[*], ***Mehrnaz Mehrabipour***[*], *Eva Magdalena Estirado, Luc Brunsveld, Radovan Dvorsky, Mohammad R. Ahmadian*

*: These authors contributed equally to this work.

DOI: *10.3390/cells13020195*

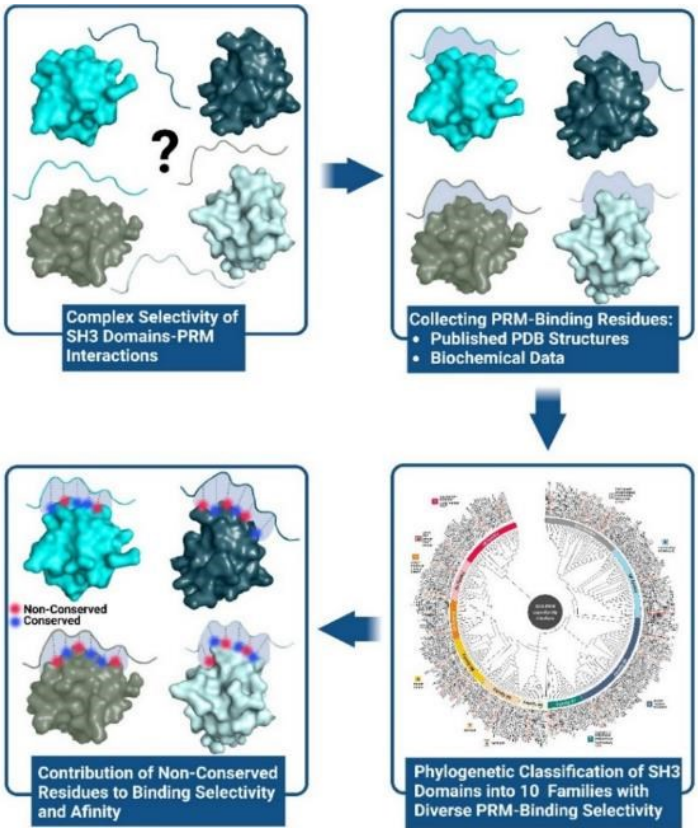

Status:	Published in January 2024
Journal:	Cells
JIF:	5.1
Contribution:	45% Responsible for writing the manuscript, collecting SH3-PRM biochemical and structural data, performing SH3 domain alignment, preparing the phylogenetic tree, classifying SH3 superfamily selectivity, conducting BLAST searches, carrying out cloning, cell culture, and immunoprecipitation (IP) experiments, as well as preparing and illustrating the figures.

cells

MDPI

Article

Functional Classification and Interaction Selectivity Landscape of the Human SH3 Domain Superfamily

Neda S. Kazemein Jasemi [1,†], Mehrnaz Mehrabipour [1,†], Eva Magdalena Estirado [2], Luc Brunsveld [2], Radovan Dvorsky [1] and Mohammad R. Ahmadian [1,*]

[1] Institute of Biochemistry and Molecular Biology II, Medical Faculty and University Hospital Düsseldorf, Heinrich Heine University Düsseldorf, 40225 Düsseldorf, Germany; neda.jasemi@hhu.de (N.S.K.J.); mehrnaz.mehrabipour@hhu.de (M.M.); radovan.dvorsky@gmail.com (R.D.)

[2] Laboratory of Chemical Biology, Department of Biomedical Engineering and Institute for Complex Molecular Systems (ICMS), Eindhoven University of Technology, P.O. Box 513, 5600MB Eindhoven, The Netherlands; evamagdalena2@gmail.com (E.M.E.); l.brunsveld@tue.nl (L.B.)

* Correspondence: reza.ahmadian@hhu.de; Tel.: +49-21-1811-2384

† These authors contributed equally to this work.

Abstract: SRC homology 3 (SH3) domains are critical interaction modules that orchestrate the assembly of protein complexes involved in diverse biological processes. They facilitate transient protein–protein interactions by selectively interacting with proline-rich motifs (PRMs). A database search revealed 298 SH3 domains in 221 human proteins. Multiple sequence alignment of human SH3 domains is useful for phylogenetic analysis and determination of their selectivity towards PRM-containing peptides (PRPs). However, a more precise functional classification of SH3 domains is achieved by constructing a phylogenetic tree only from PRM-binding residues and using existing SH3 domain–PRP structures and biochemical data to determine the specificity within each of the 10 families for particular PRPs. In addition, the C-terminal proline-rich domain of the RAS activator SOS1 covers 13 of the 14 recognized proline-rich consensus sequence motifs, encompassing differential PRP pattern selectivity among all SH3 families. To evaluate the binding capabilities and affinities, we conducted fluorescence dot blot and polarization experiments using 25 representative SH3 domains and various PRPs derived from SOS1. Our analysis has identified 45 interacting pairs, with binding affinities ranging from 0.2 to 125 micromolar, out of 300 tested and potential new SH3 domain-SOS1 interactions. Furthermore, it establishes a framework to bridge the gap between SH3 and PRP interactions and provides predictive insights into the potential interactions of SH3 domains with PRMs based on sequence specifications. This novel framework has the potential to enhance the understanding of protein networks mediated by SH3 domain–PRM interactions and be utilized as a general approach for other domain–peptide interactions.

Keywords: ARHGAP12; GRB2; NCK1; proline-rich motifs; protein–protein interaction; SH3 domain; signal transduction; SOS1; SRC homology 3; WRCH1/RHOU

check for updates

Citation: Kazemein Jasemi, N.S.; Mehrabipour, M.; Magdalena Estirado, E.; Brunsveld, L.; Dvorsky, R.; Ahmadian, M.R. Functional Classification and Interaction Selectivity Landscape of the Human SH3 Domain Superfamily. *Cells* **2024**, *13*, 195. https://doi.org/10.3390/cells13020195

Academic Editors: Alexander E. Kalyuzhny and Laszlo Buday

Received: 12 December 2023
Revised: 9 January 2024
Accepted: 17 January 2024
Published: 20 January 2024

1. Introduction

Protein–protein interactions are fundamental to the intricate machinery that controls virtually all biological processes. [1]. Among the diverse array of protein domains that facilitate these interactions, the SRC homology 3 (SH3) domains stand out as central modular units. These compact domains, consisting of approximately 60 amino acids with similar sequences that adopt a compact β-barrel fold made of five β-strands [2], are found predominantly in various signaling proteins and various protein families [3,4]. The selective interactions of the SH3 domain with proline-rich motifs (PRMs) are fundamental for the assembly and orchestration of multiprotein complexes [5]. It is rational that the SH3 domain-containing proteins (SH3DCPs) are involved in a wide variety of biological processes [4], subsequently leading to a substantial influence on a spectrum of diseases,

such as cancers [6], neurological disorders [7], kidney and urinary disorders [8,9], muscle and myopathy disorders [10,11], immune disorders [12,13], and genetic and developmental disorders [4,14,15].

To date, a series of seven types of PRM-binding modules have been reported, including SH3, WW (two highly conserved tryptophan amino acids), EVH1 (Ena/VASP homology domain 1), GYF (glycine-tyrosine-phenylalanine), Profilin, CAP-Gly (cytoskeleton-associated protein-glycine-rich), and UEV (ubiquitin E2 variant) [16,17]. Proline-rich target peptides possess core PRMs with unique properties that influence interaction selectivity. The diversity of PRMs results from the inclusion of one or more proline residues in various combinations within the peptide sequences. The proline side chains and carbonyl groups are exposed at regular intervals, allowing intermolecular hydrogen bonding with PRM-binding domains [16]. Interactions involving PRMs have a low entropic cost of binding due to the restricted rotational freedom of proline residues along the peptide backbone. This restricted flexibility contributes to a higher overall binding energy for complexes involving PRM-containing peptides (or PRPs). This property increases the affinity of PRM interactions and influences ligand recognition [16]. In addition, PRMs can interact with their binding partners in two distinct orientations; this is influenced by the arrangement of non-proline residues either located N- or C-terminal to the core motif, often involving positively charged counterparts (R or K) [16,18].

In the context of SH3 domain interaction with PRMs, a specific contact recognition occurs, where a positively charged PRM residue binds to conserved negatively charged residues in the variable loop region of the SH3 domain, resulting in moderate selectivity and affinity [5,16]. Comparative analysis of SH3 domain binding sites reveals remarkable variability and flexibility in the loop regions, contributing to the specificity and affinity of PRM binding [6,19]. The preference of the SH3 domain for specific PRMs is usually moderate, with affinities typically in the low micromolar range [20–22]. Furthermore, SH3 domains exhibit a broad spectrum of both conventional (PRM-based) and nonconventional selectivity, effectively recognizing a diverse array of protein interactors in a differentiated manner [4,5].

SH3DCPs play a pivotal role in biological processes by facilitating diverse protein–protein interactions that rely on their selectivity and affinity. The intricate nature of protein assembly orchestrated by SH3 domains raises significant questions regarding the underlying selectivity framework governing complex networks of SH3 domain–PRMs interactions [23]. Despite sharing a 25% sequence homology, accurate prediction of the selective PRM recognition by SH3 domains remains a formidable challenge [21,24,25]. In this study, we analyzed the phylogenetic and structure–function relationships of all 298 human SH3 domains, specifically focusing on the sequences of their PRM binding sites. We then performed classification based on their PRM-binding selectivity, organizing them into 10 distinct families. In addition, the distinctive recognition pattern of PRMs within SOS1, a well-established PRM-containing protein, caught our attention. This pattern of selectivity across all SH3 families led us to use SOS1 as a comprehensive model protein to elucidate the recognition mechanisms of established SH3 domains within the human proteome in our research. The binding capabilities and affinities of 25 representative SH3 domains toward 10 SOS1-derived PRPs and 2 reference peptides were carefully evaluated. The reference peptides, RP1, a derivative of SOS1 and part of P3, and RP2, a derivative of the RHO GTPase WRCH1, were used as controls. Our investigation using fluorescence dot blot and polarization techniques revealed a significant finding: out of 300 SH3 domain–peptide combinations, only 45 exhibited binding affinities, which ranged from 0.2 to 125 micromolar. This study pioneers the understanding of the selectivity and affinity of SH3 protein modules for specific PRMs, encompassing a wide range of proteins. This framework lays the foundation for a predictive matrix that enables the anticipation of SH3 domain–PRM-mediated protein–protein interactions within complex cell signaling networks.

2. Materials and Methods

2.1. Bioinformatics, Databases, and Structural Analysis

The sequences of the SH3DCPs were obtained from the UniProt database by combining full-text searches and sequence homology searches performed with the HMMER v3.4 software package. Isolated sequences of the SH3 domains were then extracted from the previously obtained proteins, again using the subprograms of HMMER. Alignment of the SH3 domain sequences was then performed using BioEdit 7.2.5 software, and the resulting phylogenetic tree was constructed using MEGA 10.2.6 software.

Available structures containing SH3 domains were retrieved from the Protein Data Bank (PDB) website using the BLAST program. To further analyze the SH3 domain structure and define its binding residues for interaction with PRMs, Python scripts were used to identify all residues in SH3 structures within 4.0 Å of the PRM bound to it. The information thus obtained was then projected onto the global sequence alignment of all SH3 domains, and only homologous residues potentially contacting PRMs were selected to define the alignment of the PRM-binding residues of SH3 domains. Finally, PRMs were collected from published articles available on the NCBI website. In addition, BLAST analysis of SOS1 PRMs was performed on the NCBI platform.

2.2. Constructs, Peptides, and Proteins

The constructs and peptides employed in our study are listed in Tables S1 and S2, respectively. All fluorescein-labeled PRPs were synthesized and used under the conditions described previously [22]. p3XFLAG-CMV ARHGAP12^{wt} [26] was used to generate a SH3 domain deletion (ARHGAP12$^{\Delta SH3}$). NCK1^{wt}, NCK1$^{\Delta SH3-3}$, and NCK1^{Set-1} (N205D, D206T, D226Q, and P227D) were ordered in pcDNA3.0-Flag vectors from BioCat GmbH., Heidelberg, Germany. HA-SOS1 in the pCGN vector was ordered from addgene (#32920). All SH3 domains of the proteins listed in Table S1 within the pGEX4-T1 vector were expressed in *Escherichia coli* strains CodonPlus, Rosetta, and BL21(DE3) and purified as GST-tagged fusion proteins. The purification process involved affinity chromatography on a glutathione Sepharose column [22]. For subsequent polarization analysis, a portion of these GST fusion proteins underwent cleavage of the GST tag using thrombin (#T6884-1KU, Sigma Aldrich, Taufkirchen, Germany) at 4 °C until achieving full digestion of the fusion protein. Following this cleavage step, the proteins were subjected to further purification and separation by employing size exclusion. All purified proteins underwent analysis via SDS-PAGE and were subsequently stored at −80 °C for further use.

2.3. Pull-Down and Fluorescence Dot Blot Analysis

Pull-down of 10 μM of FITC-labeled peptides (Table S2) with 5 μM of purified GST-SH3 domains (Table S1) was performed using 10 μL of glutathione Sepharose beads (GE Healthcare, Chalfont Saint Giles, UK) in a buffer containing 30 mM Tris-HCl at pH 7.5, 3 mM dithiothreitol, and 5 mM MgCl2 for 1 h at 4 °C. Purified GST was used as a negative control. After three washes, bound proteins were eluted by incubation in the same buffer containing 20 mM reduced glutathione for 15 min at 4 °C, and the beads were separated by centrifugation. Bound FITC-labeled peptides were detected by dot blot analysis using 1 μL of eluent at an emission wavelength of 600 nm and an Odyssey Fc imaging system (LI-COR Biosciences, Lincoln, NE, USA). Detected signals were quantified densitometrically using LI-COR Image Studio version 5.2 imaging software.

2.4. Fluorescence Polarization

The interaction between fluorescein-labeled proline-rich peptides (0.2 μM) and increasing concentrations of SH3 domains (ranging from 0 to 200 μM) was measured in a buffer (containing 30 mM Tris/HCl (pH 7.5), 5 mM $MgCl_2$, and 3 mM DTT at 25 °C) in a total volume of 200 μL using a Fluoromax 4 fluorimeter in polarization mode and a quartz glass fluorescence cuvette (Hellma Ultra-Micro Cuvette 105.250-QS, Thermo Fisher Scientific, Waltham, MA USA). Excitation was performed at 470 nm and emission

was measured at 560 nm. Dissociation constants (K_d) were determined by fitting the concentration-dependent binding curve to a quadratic ligand binding equation.

2.5. Trandfection and Immunoprecipitation Analysis

CHO-K1 cells were cultured in Dulbecco's modified Eagle's serum (DMEM, Gibco, Waltham, MA, USA) supplemented with 10% FBS (Gibco) and 1% penicillin/streptomycin (Genaxxon, Ulm, Germany). Cells were co-transfected with HA-tagged SOS1 full-length (FL) and FLAG-tagged $NCK1^{wt}$, $NCK1^{\Delta SH3-3}$, and $NCK1^{Set-1}$ or FLAG-tagged $ARHGAP12^{wt}$ $ARHGAP12^{\Delta SH3}$ using a Turbofect reagent (Thermo Fisher Scientific). To perform co-immunoprecipitation assays, the CHO-K1 cells were lysed on ice for 5 min employing a buffer containing 50 mM Tris/HCl (pH 7.4), 100 mM NaCl, 2 mM $MgCl_2$, 10% glycerol, 20 mM ß-glycerophosphate, 1 mM Na_3VO_4, 1% IGPAL (Thermo Fisher Scientific), and 1x protease inhibitor cocktail (Roche, Basel, Switzerland). Lysates were cleared by centrifugation (20,000× *g* at 4 °C for 5 min). Protein concentrations were determined using the Bradford assay. Lysates were then incubated overnight at 4 °C with either anti-Flag M2 agarose beads (Sigma Aldrich) or Protein A-Sepharose beads with anti-Flag antibody and anti-IgG as control. The beads were then washed three times with a wash buffer containing 50 mM Tris-HCl and 150 mM NaCl with 1 mM EDTA. Proteins bound to the beads were eluted with 2.5x Laemmli loading buffer and subjected to SDS-PAGE for further analysis. The primary antibodies used in Western blot analysis included anti-GST (own antibody), anti-Flag (1:1000 WB and 1:50 CO-IP, #F742; and #F3165, both from Sigma), anti-IgG (1:50; # sc-2025, Santa Cruz), anti-SOS1 (1:1000; #sc-256, Santa Cruz), and anti-Vinculin (1:1000; #V9131, Sigma). The secondary antibodies used were purchased from LI-COR (anti-mouse 700 nm: IRDye #926-32213; anti-rabbit 800 nm: IRDye #926-6807).

3. Results

3.1. Sequence–Structure–Function Classification of Human SH3 Domains

In our previous study, we performed a comprehensive survey in which we identified 298 SH3 domains within 221 SH3DCPs spanning a range of 13- to 720-kilodalton proteins [4]. This analysis included a phylogenetic assessment of human SH3DCPs based on their multidomain architecture, providing a convenient functional classification within different physiological pathways. However, this approach did not address the intrinsic PRM selectivity of the SH3 domain itself. Therefore, we set out to comparatively study the sequence–structure–function relationships of human SH3 domains with a focus on three key aspects: the amino acid sequence, three-dimensional (3D) structure, and spatial arrangement of PRM-binding sites, combining bioinformatics with experimental and structural biology.

As a first step, we focused on elucidating the critical aspects of the PRM binding properties of the SH3 domain. To achieve this, we obtained primary sequences covering a collection of 298 human SH3 domains from the UniProt database. These sequences were then aligned and used to construct a phylogenetic tree of the SH3 domain superfamily using MEGA software (version 10.2.6). The resulting phylogenetic tree, designated tree #1 (Figure S1), depicted the evolutionary relationships among human SH3 domains. Examination of this tree revealed a remarkable conservation of key regions essential for the 3D structure of SH3 domains (Figure S2). This finding underscored a robust and consistent sequence–structure relationship spanning specific parts of the SH3 domain responsible for PRP interactions in SH3DCP families [4]. However, a more complex scenario emerged when delving into the comprehensive analysis of SH3 domain–PRP interactions. Despite meticulous exploration of SH3 domain–PRP structures available in the protein database (Table S3) and a comprehensive review of published biochemical data on SH3 domain–PRP interactions (Table S4), no discernible structure–function relationship was revealed from tree #1. Strikingly, PRPs exhibit clustering patterns that are inconsistent with established SH3 domain families. Instead, they were distributed among distantly related families (Figure S1).

A different approach to characterize the SH3 domain–PRM interaction was to perform a second phylogenetic analysis focusing only on the active site regions of the SH3 domain, specifically the residues involved in PRM binding. Unlike the methodology for tree #1, which considered complete SH3 domain sequences, the second phylogenetic tree (tree #2) was constructed exclusively from the PRM-binding residues potentially involved in PRM interactions. The PRM-binding residues within the SH3 domains were inferred from the structures of the SH3 domains in complex with their specific PRPs (Table S3). It is noteworthy that tree #2 shows 10 different families of SH3 domains that can be very well assigned to their respective PRPs (Figures 1, S3 and S4). This strategic approach now allowed us to explore the intricate associations between individual SH3 domains and specific PRMs, as discussed in the following sections.

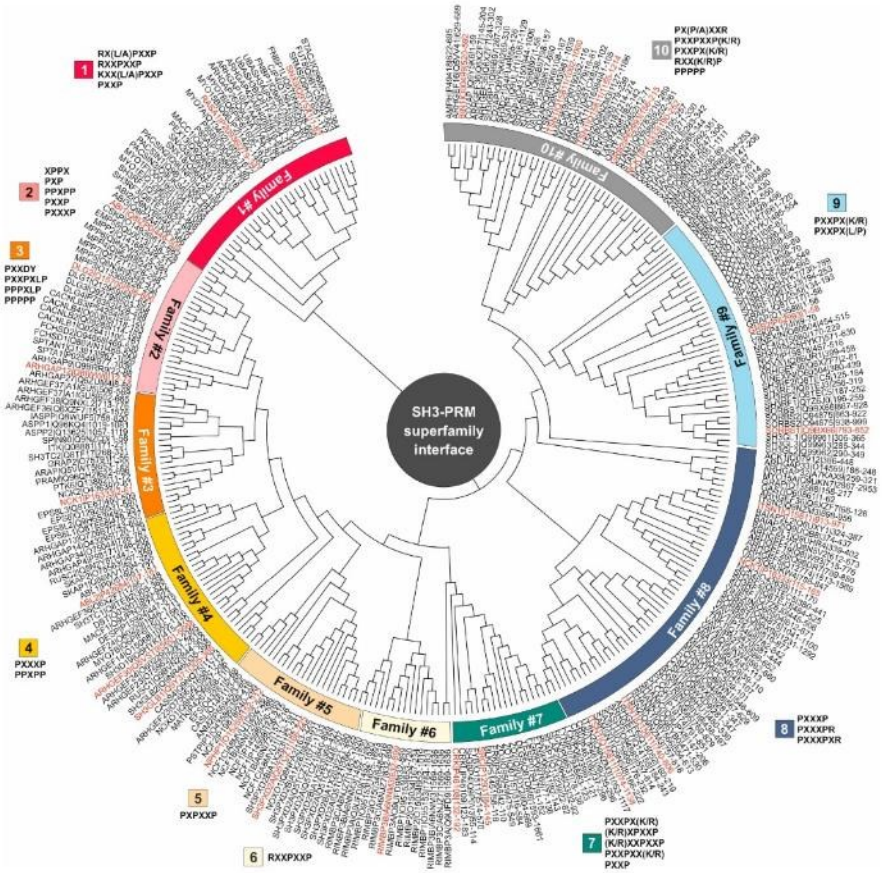

Figure 1. Evolutionary relationships among PRM-binding residues within SH3 domains. The phylogenetic tree (tree #2) was constructed by collecting PRM—binding residues from 298 human SH3 domains, using published SH3 domain-PRM structures (Table S3) and biochemical data (Table S4), and utilizing the MEGA7 software. SH3 domains were systematically classified into ten distinct families based on their interaction properties with specific PRMs as indicated by the color codes. SH3 domains highlighted in red were selected as representatives for further analysis in this study. The protein name is accompanied by the corresponding Uniprot ID and residue span for the SH3 domain.

3.2. PRM Selectivities of Different SH3 Families

Classification of PRMs into distinct families based on published structural and biochemical data (Tables S3 and S4) reveals specific sequence patterns that guide protein–protein interactions (Figure S5). Family 1 includes motifs such as RX(L/A)PXXP, RXXPXXP, KXX(L/A)PXXP, and PXXP, suggesting a diverse yet structured arrangement for interaction. Family 2, characterized by a PPXPPXP consensus, shows patterns such as XPPX, PXP, PPXPP, PXXP, and PXXXP, indicating a diverse but consistent motif profile. Family 3 sequences, including PXXDY, PXXPXLP, PPPXLP, and PPPPP, show specificity around proline and other residues such as D and Y. Family 4 follows a PXXXPPXPP consensus with specific motifs such as PXXXP and PPXPP. Family 5 has a specific PXPXXP motif. Notably, family 6 lacks structural and biochemical data. However, RIMBP1/2 (RIM-binding protein 1 and 2) can recognize a potential consensus of RXXPXXP and can likely bind to motifs such as the RQLPQL/VP, RLLPPTP, and RQLPQTP found in RIM1/2 (RAB3-interacting molecule 1 and 2). RIMBP1/2 has been shown to bind and couple RIM1/2 to voltage-gated Ca^{2+} channels [27]. Family 7 shows patterns such as PXXPX(K/R), (K/R)XPXXP, (K/R)XXPXXP, PXXPXX(K/R), and PXXP. Family 8 motifs, including PXXXP, PXXXPR, and PXXXPXR, highlight a selective array of proline-rich sequences. Family 9, characterized by PXXPX(K/R) and PXXPX(L/P), shows specificity for proline and amino acid residues such as K/R and L/P. Family 10 presents PX(P/A)XXR, PXXPXXP(K/R), PXXPX(K/R), RXX(K/R)P, and PPPPP motifs, illustrating a specific yet versatile proline-rich arrangement. These results highlight the complex yet diverse nature of PRMs across families controlling specific protein interactions and functions.

We observed an overlap of PRM sequences from families 5 and 6 with family 1, suggesting potential similarities and shared binding motifs within their respective SH3 domain interactions. In our phylogenetic classification based on SH3 domain specificity for PRM, family 1 interacts with RX(L/A)PXXP, RXXPXXP, KXX(L/A)PXXP, and PXXP motifs, whereas family 5 has specificity for PXPXXP and family 6 for RXXPXXP motifs. The biological interpretation of this overlap suggests a potential convergence or similarity in binding preferences among these families despite their specific motifs. Such overlapping PRM sequences imply a nuanced relationship in which different SH3 domain families may exhibit distinct specificities yet recognize certain common motifs. This observation may indicate functional redundancies, cooperative interactions, or shared regulatory pathways among these SH3 domain families in cellular processes.

3.3. Affinity and Selectivity of the SH3 Family Proteins for SOS1 PRP

The intriguing recognition pattern of PRMs observed in SOS1, a particularly PRM-rich protein, caught our attention. SOS1 shows co-occurrence of 13 out of a total of 14 PRMs (including sequences such as PPPP, XPPX, PXP, PXPXP, PPXPP, PXXP, PXXPX[KR], [KR]XXPXXP, PXXPXXP, PXXXP, PXXXPXXXP, PXXXPR, and PXXXXP), as shown in Table S5. This distinct pattern, showing selectivity across all SH3 families, motivated us to use SOS1 as a comprehensive model to uncover the recognition mechanisms of established SH3 proteins in the human proteome. Therefore, 25 SH3 domains from different SH3 families were selected (Figure 1), cloned, purified as GST fusion proteins, and used for PRP binding analysis (Table S1). We selected at least one representative SH3 domain per defined family concerning accessibility and experimental viability (see Tables S3 and S4). In addition, we selected 10 different PRPs from the proline-rich domain (RPD) of the SOS1 protein (Table S5). This collection was designed to cover the full spectrum of PRM types (P1-P10; Table S2). Two reference peptides were included as controls: RP1, a well-studied SOS1 derivative encompassing part of P3, and RP2, a peptide derived from the N-terminal extension of the RHO GTPase WRCH1/RHOU (Table S2). The 12 PRPs were labeled with FITC to assess their binding capacities with purified GST fusion proteins of the 25 SH3 domains using fluorescence dot blot and polarization analysis (Figure 2A).

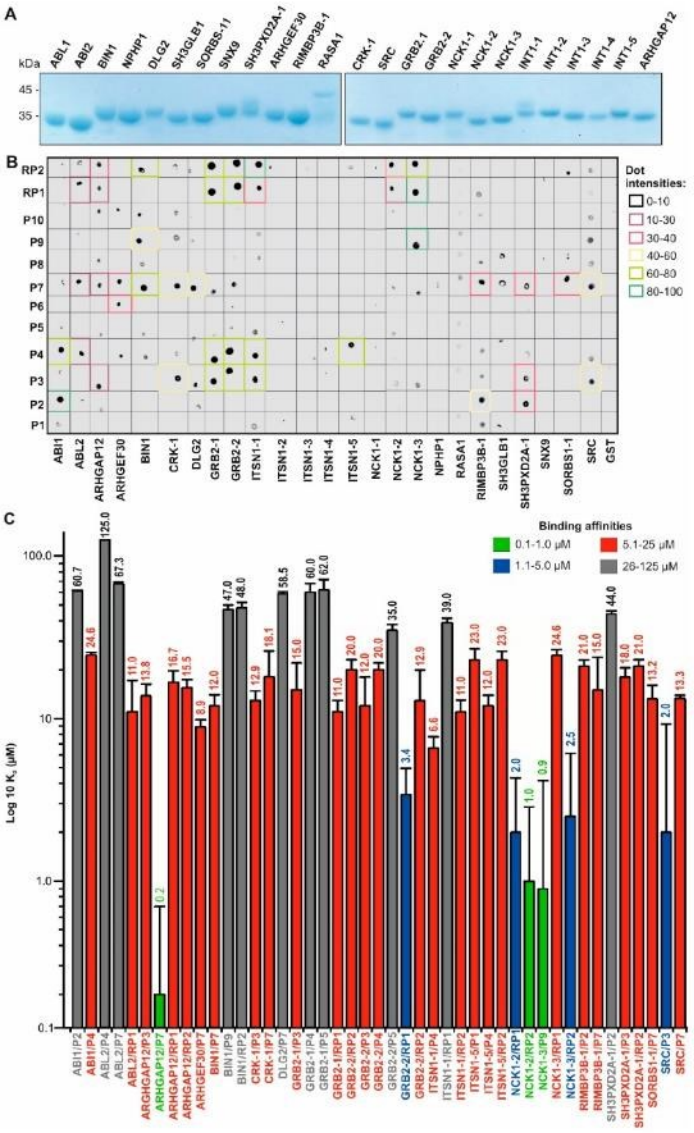

Figure 2. Evaluation of the binding selectivity of SH3 domain representatives with different PRP types. (**A**) Coomassie brilliant blue-stained SDS gels show purified SH3 domains as GST fusion proteins. (**B**) Fluorescence dot blots revealed the variable binding strengths of 12 fluorescent PRPs with 25 GST-SH3 domains. Dot intensities are categorized into five groups ranging from 0 (black) to 100 (dark green). (**C**) Bar graphs show the evaluated dissociation constants (K_d) for the selected SH3 domain–PRP interactions determined by fluorescence polarization (Table S6; Figure S6). The color codes indicate the K_d values, classified into high affinity (green), intermediate affinity (blue), low affinity (red), and very low affinity (black).

The binding of 12 FITC-labeled PRPs to 25 GST-SH3 domains was qualitatively analyzed by combining GST pull-down and dot blot assays. GST protein alone was used as a negative control. In a previous study [22], we showed that fluorescein labeling does not affect the interaction of proline-rich peptides with the SH3 domains. Different binding strengths were observed among the proteins tested, particularly with the P2, P3, P4, P7, and P9 peptides (Figure 2A). The strongest interactions (dot intensity >80) were between ABI1 and P2, ITSN1-1 and RP2, and NCK1-3 and P9 and RP1. In contrast, no PRP binding (dot intensity 0) was detected for NCK1-1, NPHP1, RASA1, SH3GLB-1, SNX9, ITSNS1-2, ITSNS1-3, and ITSNS1-4. These data provide valuable insight into the varying degrees of interaction across the panel of PRPs and SH3 domains tested (Figure 2A).

Fluorescence polarization measurements were performed to determine the binding affinities of SH3 domain–PRP interaction pairs from the dot blot analysis. SH3 proteins were titrated at increasing concentrations against fluorescent PRPs, which were kept at a constant concentration of 0.2 μM. GRB2-2^{W193K}, which is defective in the binding of PRPs such as RP1, was used as a negative control as previously described [22]. Interestingly, none of the PRPs we examined showed any binding for seven SH3 domains: ITSN1-2/-3/-4, NPHP1, RASA1, SH3GLB1, and SNX9 (Table S6). The resulting data (Figure S6) allowed the evaluation of equilibrium dissociation constants (K_d) for 45 interactions between the SH3 domains and the PRPs (Figure 2B; Table S6). In particular, the results confirmed that the peptides P2, P3, P4, P7, and P9 were associated with approximately 17 SH3 domains. The K_d values determined were categorized into four affinity levels (Figure 2B; Table S6): high (0.1 to 1.0 μM; green), intermediate (1.1 to 5 μM; blue), low (5.1 to 25 μM; red), and very low (26 to 125 μM; black). Whereas previously reported SH3 domain–PRM interactions exhibited micromolar affinities, our results revealed interactions with nanomolar affinities in some cases. The most notable and novel pairs of interaction were ARHGAP12/P7, NCK1-3/P9, and NCK1-2/RP2, which had affinities in the nanomolar range of 0.2, 09, and 1.0 μM, respectively.

3.4. Non-Conserved Residues Define the Selectivity and Affinity of SH3 Domain–PRM Interactions

To better understand the role of the residues of SH3 domains in selective binding to PRPs, we have generated a multiple sequence alignment (Figure S7). It highlights the conserved and variable residues that are likely to be critical for the selectivity and affinity of the SH3 domain–PRM interactions. The importance of variable residues was investigated by specifically selecting ARHGAP12 and NCK1-3 for mutational analysis due to their high binding affinities of 0.2 and 0.9 μM for P7 and P9, respectively. In contrast, ABL2 and BIN1 were selected for their very low affinity for P7 and P9, respectively. Two different sets of mutations were generated by substituting a combination of amino acids from ARHGAP12 and NCK1-3 for ABL2 and BIN1 and vice versa (Figure 3A; Table S1).

Comparative fluorescence polarization measurements between wt and mutant SH3 domains (Figure S8) revealed that variable residues determine selectivity and affinity. The determined K_d values of 14 and 23 μM showed a drastic reduction in the binding affinity of the Set-1 mutants of ARHGAP12 and NCK1 by 115-fold and 15.6-fold for P7 and P9, respectively (Figure 3B). This demonstrates the importance of the selected variable residues for the PRP interactions, especially because ABL2^{Set-1} and BIN1^{Set-1} showed a 9- and an 11-fold increase in binding to P7 and P9, respectively (Figure 3B). In light of this result, we decided to investigate another set of variable residues (Set-2; Figure 3A). The binding affinity for ARHGAP12^{Set-2} was reduced 47-fold, indicating the critical role of these residues in determining the selectivity and affinity of ARHGAP12 for P7 (Figure 3B). However, NCK1-3^{Set-2} did not differ from the NCK1-3^{wt} in terms of P9 binding, suggesting that the Set-2 residues are not critical for NCK1-3/P9 interaction (Figure 3B).

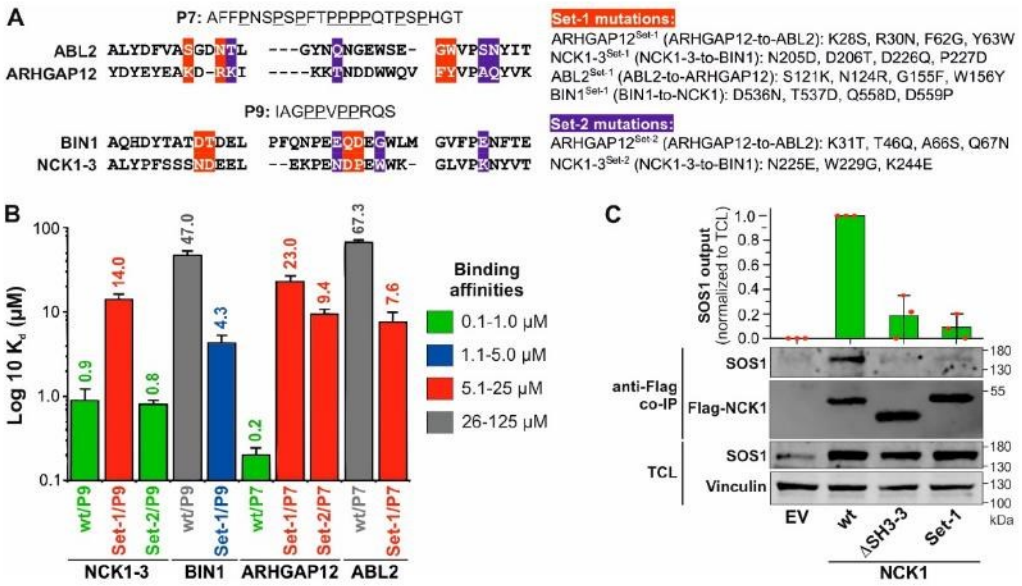

Figure 3. Variable residues determine the specificity and affinity of SH3 domain–PRP interactions. (**A**) A sequence alignment of the PRM-binding residues of ABL2, ARHGAP12, BIN1, and NCK1-3 is extracted from the alignment shown in Figure S7. Residues in red (Set-1) and blue (Set-2) are variable residues (left panel) and are the subject of mutation analysis (right panel). (**B**) K_d values determined by fluorescence polarization partially revealed shifts in the binding affinities of the investigated SH3 domain mutants for P7 and P9, respectively, with decreased affinity for ARHGAP12^{Set1} and ARHGAP12^{Set2}, and NCK1^{Set-1} and increased affinity for ABL2^{Set1} and BIN1^{Set-1}. NCK1^{Set-2} had the same K_d value as NCK1^{wt}. (**C**) SOS1 co-immunoprecipitated (Co-IP) with NCK1^{wt} but not with NCK1-3$^{\Delta SH3-3}$ and NCK1^{Set-1} overexpressed in CHO-K1 cells.

To investigate a potential SOS1 binding of ARHGAP12 and NCK1 and to assess the relevance of variable residues in the SH3 domain–PRMs interaction in cells, CHO-K1 cells were co-transfected with wt and mutant variants of NCK1 and ARHGAP12 together with HA-SOS1 containing P7 and P9 at its C-terminal PRD (Figure 4). Co-immunoprecipitation (Co-IP) with anti-Flag beads was performed to investigate the possible interaction of ARHGAP12 and NCK1 with HA-SOS1 (Figures S9 and S10). As shown in Figure 3C, all three NCK1 proteins, wt, ΔSH3-3, and Set-1, were immunoprecipitated, but SOS1 was only co-immunoprecipitated with NCK1^{wt} and not with NCK1$^{\Delta SH3-3}$ and NCK1^{Set-1} (Figure 3C). No ARHGA12-SOS1 interaction was observed in similar experiments (Figure S10). Taken together, our data not only highlight the essential role of these flanking residues in determining the selectivity and affinity of SH3 domains for their cognate PRPs but also provide unprecedented insight into a potential SOS1-NCK1 interaction in cells.

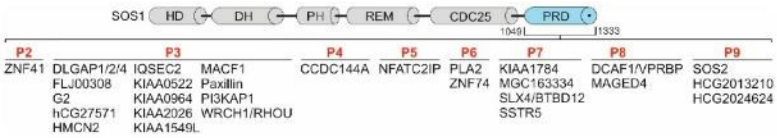

Figure 4. Proteins containing PRMs homologous to P2–P9 derived from the SOS1 PRD. BLAST searches with each SOS1 PRP identified several human proteins (see Table S7) with a high degree of sequence similarity to P2–P9. CDC25, cell division cycle 25; DH, DBL homology domain; HD, histone-like domain; PH, pleckstrin domain; REM, RAS exchange motif; PRD, proline-rich domain.

3.5. SH3 Domain–PRP Relationships beyond SOS1

We used the position-specific iterated BLAST (PSI-BLAST) algorithm to perform an analysis of the SOS1 PRPs in the human proteome using the NCBI (National Center for Biotechnology Information, Bethesda, MD, USA) database as a reference. Our goal was to identify homologous peptides from proteins other than SOS1 as potential interaction partners for the SH3 domains investigated in this study. In our analysis, we considered alignments with percentage identities ranging from 98% to 100% and with E values up to 10, which, although less stringent, may still indicate potential similarities between the SOS1 PRPs and other protein sequences. More than 30 proteins were found with partial sequence identities with P2 to P9 (Table S7; Figures 4 and S11) and 0 with P1 and P10 (Refer to Table S1). Some of these proteins contain multiple PRM repeats (Figure S11), for example, IQSEC2, paxillin, DLGAP1, PI3KAP1, and WRCH1/RHOU within P3 (Motif: PVPPPVP), SSTR5 and SLX4 within P7 (Motif: PPPPQTP), DCAF1 and MAGED4 within P8 (Motif: HLPSPP), and SOS2 and HCG2013210 within P9 (Motif: PPVPPRQ). This suggests that the SH3 interactions with the PRPs characterized in this study go beyond SOS1 as a binding partner, although the binding specificities of the listed proteins (Figure 4) remain to be investigated. However, several studies confirm the interactions of the identified proteins with SH3DCPs, including zinc finger proteins with p130Cas [28], MACF1 with Spectrin [29], DLGAP with DLG [30], WRCH1/RHOU with GRB2 [31,32], Paxillin with SRC [33,34], and SSTR5 with Homer, Dynamin, IRSp53, and Cortactin [35].

4. Discussion

SH3 domains are critical in multiple signaling pathways; they interact with diverse proteins involved in apoptosis, proteasomal degradation, endocytosis, and with SRC family protein tyrosine kinases, influencing downstream processes including proliferation, cell survival, growth, actin reorganization, and cell migration [4]. The broad influence of SH3 domains on cellular functions raises fundamental questions about the specificity of their interaction networks. Previous research has also highlighted the importance of proline amino acids in forming the polyproline type II helix (PPII) conformation, which provides a binding pocket for SH3 domain residues, particularly from the RT and n-SRC loops [17]. Despite the discovery of 14 PRM consensus sequences in the human proteome (Table S5), the specificity pattern of the interaction of SH3 domains with PRMs is still unclear. Understanding the molecular basis of SH3 domain–PRM interactions is crucial to gain insight into how these interactions regulate signaling pathways.

Interface residues often play an important role in the functional outcome of protein interactions. Many diseases, including cancer and neurodegenerative disorders, are associated with aberrant protein–protein interactions resulting from mutated interacting residues. Abnormal SH3 domain interactions in cancer fuel dysregulated signaling that drives uncontrolled cell proliferation, survival, tumor growth, metastasis, apoptosis evasion, and resistance to anticancer therapies [4,6]. In neurodegenerative diseases like Alzheimer's and Parkinson's, these interactions disrupt signaling pathways, leading to the accumulation of misfolded proteins and neuronal degeneration. Altered SH3 domain interactions in synaptic proteins affect neurotransmission and synaptic plasticity [7]. In autoimmune diseases, aberrant SH3 domain interactions contribute to immune cell activation and tissue

damage, as immune cells mistakenly target healthy tissues [12,13]. Understanding the interface residues involved in SH3 domain–PRM interactions can thus provide insight into disease mechanisms and potential targets for intervention. In drug development, knowledge of interface residues is essential for designing molecules that can disrupt or modulate specific protein–protein interactions. Targeting these residues can lead to the development of therapeutic agents for the treatment of various diseases.

In recent years, several studies have been devoted to elucidating the diverse nature of SH3 domain interactions. Cesareni and colleagues used a novel chip technology to perform high-throughput qualitative analyses, revealing a variety of human SH3 domains that fall into two categories: those characterized by classical proline-rich core motifs accompanied by positively charged amino acids and atypical ones lacking the core motif [20]. Nevertheless, the diversity of PRM selectivity patterns is evident among all human SH3 domains. Furthermore, a comprehensive analysis of SH3 domain interactions in the evolution of four yeast species, Saccharomyces cerevisiae, *Ashbya gossypii*, Candida albicans, and *Schizosaccharomyces*, revealed that nearly 75 percent of SH3 families identified within the phylogenetic tree have a conserved SH3 specificity profile over 400 million years of evolution [36]. Utilizing the evolutionary relationships of peptide recognition domains in eukaryotes, we identified common structural features and ancestry that allowed us to group SH3 domains into similar binding preference families. This comprehensive investigation aimed to clarify the specificity profiles of SH3 PRMs within the human proteome through categorization based on the phylogenetic tree of SH3DCPs.

To provide an accurate specificity map of SH3 domains, we performed deep phylogenetic analyses coupled with computational analysis of the related structural data. Initial evolutionary analysis of the sequence–structure–function of full-length SH3 domains was unsuccessful due to the presence of SH3 regions that do not interact with PRMs. Within these, each SH3 domain exhibited variation in binding specificity to PRMs, making the characterization of SH3DCPs infeasible. Instead of relying on full-length sequences, we focused on binding residues that directly interact with PRMs, as revealed by sequence alignments coupled with analysis of the published SH3 domain structures in complex with PRMs. This refined phylogenetic approach led to the identification of ten distinct families based on both the structural and biochemical assessments of SH3 domain–PRM interactions and their distribution within the phylogenetic tree. This approach facilitates the assessment of cross-reactivity among SH3 domain recognition sites for PRMs, a phenomenon also observed in previous studies examining the yeast SH3 domain peptide library [37] and including SH3 domains that recognize multiple PRMs. The findings of this study highlight the fact that each SH3 domain family interacts with different but distinct sets of PRMs.

Considering the significant involvement of SOS1 in interactions with SH3DCPs such as GRB2 [38], ITSN1 [39], NCK1 [40], and ABI1 [41], along with its comprehensive coverage of all known PRMs in the human proteome (Tables S2 and S5), we decided to use SOS1 as a model for in-depth exploration of SH3 domain specificity in the realm of polyproline interactions. We performed in vitro studies with 25 representative SH3 domains selected from the phylogenetic tree. We performed low-throughput analyses, including pull-down assays, dot blotting, and fluorescence polarization, to investigate SH3 domain–PRP interactions. These investigations revealed novel interactions that had nanomolar affinities, which were subsequently confirmed by mutational studies.

The general concept of protein association is essential for describing protein–protein interactions in complexes, especially those with weak affinities in the micromolar range or transient interactions such as the SH3 domain with PRMs [42]. Mayer and Saksela noted that the limited selectivity of SH3 domains for PRMs implies that SH3-domain-mediated interactions may be highly dependent on external environmental factors [43]. In certain scenarios, the presence of additional surfaces on either the SH3 domain or the ligand it recognizes, along with the presence of either multiple SH3 domains or different domains within the same protein, or even the co-localization of two partners within a multi-protein complex, can cooperatively enhance SH3 domain–PRM specificity to a

significant degree [44]. This suggests that the low-affinity-region results in our study may be compensated by these scenarios, ultimately increasing the affinity and specificity of SH3 domain–PRM interactions. It has also been reported that the moderate affinities of SH3-domain-mediated interactions imply that the interactions have a high dynamic remodeling potential (rapid off-rates), depending on the subcellular localization and accessible binding partners [43]. This observation is consistent with our polarization data, which showed high K_d values for many low-affinity interactions.

The question of how the specificity of SH3 domain–RPM networks is achieved has been addressed by various research groups. It has been postulated that specificity in cells is not solely encoded by isolated SH3 domain–PRM partners but rather by the context in which the partners are presented as full-length proteins. Dione et al. have shown that the identity of the host protein and the position of the SH3 domains within their host are critical for interaction specificity, cellular functions, and key biophysical processes such as phase separation [45]. In addition, Zarrinpar et al. have shown that isolated SH3 domains can determine the interaction specificity between host SH3 domains [46]. This may also be true for certain high-affinity SH3 domain–PRM interactions, as shown in this study for the newly discovered interactions of NCK1-2, NCK1-3, and ARHGAP12 with WRCH1/RHOU-derived RP2 and SOS1-derived P9 and P7, respectively. NCK1 has been shown to modulate ITSN1-CDC42-WASP-dependent actin polymerization [47]. WRCH1/RHOU, a CDC42 homologous protein, encompasses an extended N-terminus that contains RPMs specific for various adaptor proteins, including GRB2, CRK, and NCK1 [32]. The association of these proteins with WRCH1/RHOU may not only determine its signaling specificity but may also regulate its activity in cells [48]. However, it should be noted that, in some cases, a negative effect of other domains on SH3 domain–PRM binding was observed. Notably, NCK1-3 showed more extensive protein interaction than the full-length NCK1 in immunoprecipitation experiments, possibly indicating a detrimental effect of the C-terminal SH2 domain on specific SH3-domain-mediated interactions. Furthermore, the spectrum of proteins associated with NCK1-3 is not simply the cumulative sum of proteins associated with individual SH3 domains [49].

A closer examination of the PRMs revealed that the positioning of the proline residues plays a critical role in the recognition of the SH3 domain, providing the structural basis for defining interaction specificity. The current results indicate that residues −2, −1, +1, and +2 are critical for the recognition of SH3 PRMs. In addition, adjacent positively charged residues contribute additional features that help stabilize the transient interaction [50]. For example, structural studies of the PI3K SH3 domain in association with the peptide RKLPPRPSK provided evidence for the role of adjacent non-proline residues such as Arg-1, Leu-3, and Arg-6 in contributing to the SH3 domain interaction [51]. Arginine residues at positions R + 5, R + 6, and R + 7 are thought to play an important role in enhancing the affinity of GRB2-SH3 domains for SOS1-PRM by contributing to the overall free energy of the interaction [52]. While the majority of SH3 domains interact with PRMs, there have been documented cases where the SH3 domain deviates from the typical classical proline-rich interaction pattern [4]. For example, the RASA1 (or p120RASGAP) SH3 domain specifically interacts with the catalytic arginine finger of the RHOGAP domain of DLC1, thereby competitively and potently inhibiting its RHOGAP activity [53]. Interestingly, none of the PRPs we examined showed any binding for seven SH3 domains: ITSN1-2/-3/-4, NPHP1, RASA1, and SH3GLB1 (Table S6). While our study comprehensively highlights the major SH3 domain–PRM interactions in the human proteome, the specificity and mechanism of the PRM-independent interaction of SH3 domains remain to be elucidated in further studies.

In our study, SOS1 was used as a PRP model for biophysical and bioinformatic analysis of the SH3 domain–PRM interaction landscape because the SOS1 PRD contains 13 out of 14 different classified proline-rich consensus sequence motifs (Table S5). This alternative model reveals a spectrum of interactions between different SOS1 PRPs and a number of SH3DCPs, including ABI1, ABL2, ARHGAP12, ARHGEF30 (Obscurin/OBSCN),

BIN1, CRK-1, DLG2, GRB2, ITSN1, NCK1, SRC, SH3PXD2A-1, and SORBS1-1. Among them, ABI1 [54], ITSN1 [55], SRC [56], NCK1 [57], GRB2 [58], CRK [59], and SH3PXD2A (TKS5) [60] have been previously established as SOS1 binding partners in cells. ABL1, but not ABL2, has also been shown to interact with SOS1 [61]. Importantly, the precise binding sites for most of these proteins have yet to be investigated. Our study not only elucidates the binding sites of these established SOS1 partners but also uncovers novel interactions, including ABL2, BIN1, DLG2, SORBS1, ARHGEF30, and ARHGAP12. In particular, a high affinity (<0.5 μM) interaction was observed between ARHGAP12 and the P7 of SOS1, demonstrating the interplay between small GTPase regulators, GAPs, and GEFs. However, immunoprecipitation experiments with overexpressed ARHGAP12 in CHO-K1 cells did not confirm an interaction with SOS1 (Figure S10). The reliability of this result may depend on the expression level and affinity of other interaction partners, like accessory proteins, that could potentially bind more strongly and possibly in a multivalent manner. However, it is important to note that this result does not definitively rule out the existence of this interaction in cells, especially considering examples of reported GEF-GAP interactions. A study using immunoprecipitation and mass spectrometry unravels the intricate protein interaction networks involving the synaptic proteins SYNGAP1 (RASGAP), KALIRIN (RHOGEF), and AGAP2 (ARFGAP) in both the postsynaptic density (PSD) and non-PSD fractions of the adult mouse cortex. This investigation sheds light on their role in the organization of GAP and GEF protein families and their associations with proteins associated with intellectual disability and psychiatric disorders [62]. In conclusion, to confirm the significance and broader implications of these novel findings, additional studies within the cellular context are warranted.

Predicting the potential interaction of SH3 domains with PRMs by considering their sequence specificities, as we did in this study, is a promising approach in the field of molecular biology and protein–protein interactions. In pursuing this goal, we are faced with an interesting challenge: the identification of binding affinities between SH3 domains and peptides containing PRMs. The sequence specificity of these interactions is paramount, as SH3 domains exhibit diverse binding preferences that depend on the PRMs present in the peptides.

5. Conclusions

SH3 domains are small protein interaction modules that are involved in numerous fundamental cellular processes and associated with the development of several diseases, including Joubert syndrome, leukemia, lymphoma, Usher syndrome or non-syndromic deafness, centronuclear myopathy, schizophrenia, and other neurodevelopmental disorders [4]. Over the past three decades, researchers have focused on how members of the SH3DCP superfamily selectively recognize and bind to their associated PRM-containing proteins.

To systematically address this question, we first extracted 298 SH3 domains in 221 SH3DCPs ranging in size from 13 (small monodomain proteins) to 720 (large multidomain proteins) kilodaltons [4]. The subsequent evolutionary multidomain relationship of the SH3DCP superfamily not only allowed us to functionally classify them into thirteen families but also provided new insights into their diverse roles and interactions in cellular signaling processes, as well as their relevance to various diseases when exploiting the modular interactions of SH3 proteins as drug targets [4]. In the present study, we have incorporated the available sequence, structure, and interaction data into a phylogenetic tree (Figure 1) that groups 298 SH3 domains in the human proteome into 10 families related to the PRM binding interface. These families are aligned with the frames necessary for the interaction of their respective potential PRMs. Mutational analysis suggests the critical role of non-conserved sequences within each SH3 family in defining the specificity and affinity of their interactions with specific PRMs. This investigation highlights that the recognition mechanisms of SH3 proteins across the human proteome are not only influenced by PRMs but also by the core binding site within the SH3 domain. The study of the PRM-binding residues of SH3

domains revealed a significant relationship between individual SH3 domains and specific PRMs, culminating in a detailed map of their associations.

In this study, we performed a comprehensive analysis by comparing published biochemical interaction data, available structural information, and sequence alignments. The goal was to identify specificity-determining residues within PRMs that are critical for interacting with different SH3 domains. A phylogenetic tree based solely on the interacting interface of SH3 domains allowed us to categorize distinct families of SH3 domains within the human proteome, each interacting specifically with unique PRMs. Subsequent mutational analysis supported our categorization and hypothesis by demonstrating that the non-conserved interface sequences within each family are critical in defining the specificity of their interaction with PRMs. The different interface residues within each family were found to determine the affinity and specificity of each protein towards PRMs. In particular, the discovery of common PRMs in two different SH3 domain families underscores the importance of other residues (designated X) beyond proline in determining interaction specificity. It is generally accepted that prolines serve as recognition sites and the backbone of interactions, while X residues define specificities. A comparison of the PRM consensus sequences of the SOS1-homologous proteins reveals other common amino acids, such as V in P3 and P9, Q in P7 and P9, R in P3, P4, P5, and P9 (Figure S11). Notably, the third SH3 domain of NCK1 (NCK1-3) tightly bound P9 but none of the other PRPs tested in this study (Table S6); this implies that residues other than valine and arginine in P9 may dictate the specificity of the NCK1–P9 interaction. In addition, the sequence motif ^{224}ENDPEW of NCK1-3 (Figure 3A) contains three negatively charged residues that may be in electrostatic contact with the R in P9. In contrast, NCK1-1 and NCK1-2, which do not bind P9, contain a lysine instead of glutamate or aspartate within this sequence motif, which counteracts a P9 interaction. An important next step in elucidating the specificity of the interaction of the SH3 domain with the PRM at the atomic level is to analyze the nearly 800 available experimental structures containing SH3 domains. This will be performed by generating homology models and correlating and combining them with the measured affinities and known binding properties of SH3 domain–PRM complexes.

A total of 7 out of the 25 examined SH3 domains showed no interaction with any of the 12 selected PRPs (Table S6). The tested peptides cover 13 of the 14 recognized proline-rich consensus sequence motifs, suggesting that they may bind in a proline-independent manner. (Table S5). It is suggested that these SH3 domains may bind in a proline-independent manner. SH3 domains in several studies exhibit an extended repertoire of binding sequences, known as proline-independent binding, allowing SH3DCPs to mediate a broader array of interactions [4,5]. An example of atypical binding is the SH3 domain of RASA1, the RAS-specific GAP (p120RASGAP), which interacts with the catalytic GAP and kinase domains of DLC1, thereby inhibiting its activity [53,63]. Another example is the selective interaction of the GADS/GRAB2L SH3 domain with an RXXK motif of SLP-76 [64]. These types of SH3 interactions with a non-canonical binding mode add to the complexity of understanding protein–protein interactions involving SH3 domains.

The SH3 domains are modular building blocks across all five kingdoms of life and viruses and play a critical role in facilitating inter- and intramolecular interactions and functional interplay within domain-specific interaction networks. SH3DCPs, except the MIA family with a single SH3 domain, are multi-domain proteins [4]. Several recent studies have shown that SH3 domains have an extended repertoire of binding sequences, known as proline-independent binding [4,17,53]. This allows SH3DCPs to mediate a wider range of interactions. However, a quantitative description of the communication between two different sites in a multivalent protein is still challenging. In some cases, the task reaches another level of complexity, such as the interaction of the two SH3 domains of GRB2 with SOS1. Not only the association of the two functional SH3 domains of GRB2 with SOS1 but also the physical interactions between the two SH3 domains are required to allosterically control SOS1 activation [22]. Such a regulatory mechanism involves a series

of intramolecular interactions that are further amplified by the interaction of GRB2 with upstream ligands [65].

Supplementary Materials: The following supporting information can be downloaded at: https://www.mdpi.com/article/10.3390/cells13020195/s1; Table S1: Proteins used in this study; Table S2: Peptides used in this study; Table S3: Published structures of the SH3 domain–PRM complexes; Table S4: Published dissociation constants (K_d) determined for the SH3 domain–PRP interactions; Table S5: PRM classification and occurrence in SOS1 PRD; Table S6: Dissociation constants (K_d) for the SH3 domain–PRP interactions determined in this study; Table S7: Proteins containing PRMs homologous to peptides 2–9 derived from the SOS1 PR; Figure S1: Evolutionary sequence–structure–function relationships of SH3 domains; Figure S2: Alignment of SH3 domain sequences; Figure S3: PRM-binding residues in human SH3 domains; Figure S4: Exploring evolutionary connections of PRM-binding residues in SH3 domains; Figure S5: Analysis of SH3 domain–PRMs interaction specificity across various SH3 domain families in the human proteome; Figure S6: Fluorescence polarization measurements of SH3 domain interactions with SOS1 and reference peptides; Figure S7: Sequence alignment of PRM-binding residues in representative SH3 domains interacting with specific PRP; Figure S8: Mutational analysis of the SH3 domain–fluorescent PRP interactions using fluorescence polarization. Figure S9: Co-immunoprecipitation of NCK1 with SOS1 in CHO-K1 cells; Figure S10: No co-immunoprecipitation of SOS1 with ARHGAP12 in CHO-K1 cells; Figure S11: SOS1 homologous PRM sequences found in other human proteins.

Author Contributions: M.R.A. designed and coordinated the study. N.S.K.J., M.M. and M.R.A. designed the study and drafted the manuscript. E.M.E. and L.B. synthesized the peptides. N.S.K.J., M.M., R.D. and M.R.A. designed, performed, and analyzed the experiments. All authors have read and agreed to the published version of the manuscript.

Funding: This research was funded by the German Research Foundation (DFG; grant number: AH 92/8-1), the European Network on Noonan Syndrome and Related Disorders (NSEuroNet; grant number: 01GM1602B), and the Foundation for Ageing Research of the Heinrich Heine University (grant number 701.810.845).

Institutional Review Board Statement: Not applicable.

Informed Consent Statement: Not applicable.

Data Availability Statement: The data supporting the results of this study are available both as supplementary material and, upon reasonable request, are available from the corresponding author.

Acknowledgments: We thank our colleagues Doreen Floß, Roland Piekorz, and Jürgen Scheller for the discussions. We thank Soyoun Kim for providing the p3XFLAG-CMV ARHGAP12 plasmid.

Conflicts of Interest: The authors declare no conflicts of interest.

References

1. Mabonga, L.; Kappo, A.P. Protein-protein interaction modulators: Advances, successes and remaining challenges. *Biophys. Rev.* **2019**, *11*, 559–581. [CrossRef] [PubMed]
2. Musacchio, A.; Noble, M.; Pauptit, R.; Wierenga, R.; Saraste, M. Crystal structure of a Src-homology 3 (SH3) domain. *Nature* **1992**, *359*, 851–855. [CrossRef] [PubMed]
3. Stahl, M.L.; Ferenz, C.R.; Kelleher, K.L.; Kriz, R.W.; Knopf, J.L. Sequence similarity of phospholipase C with the non-catalytic region of src. *Nature* **1988**, *332*, 269–272. [CrossRef] [PubMed]
4. Mehrabipour, M.; Jasemi, N.S.K.; Dvorsky, R.; Ahmadian, M.R. A Systematic Compilation of Human SH3 Domains: A Versatile Superfamily in Cellular Signaling. *Cells* **2023**, *12*, 2054. [CrossRef] [PubMed]
5. Teyra, J.; Huang, H.; Jain, S.; Guan, X.; Dong, A.; Liu, Y.; Tempel, W.; Min, J.; Tong, Y.; Kim, P.M. Comprehensive analysis of the human SH3 domain family reveals a wide variety of non-canonical specificities. *Structure* **2017**, *25*, 1598–1610.e3. [CrossRef] [PubMed]
6. Berndt, S.; Gurevich, V.V.; Iverson, T. Crystal structure of the SH3 domain of human Lyn non-receptor tyrosine kinase. *PLoS ONE* **2019**, *14*, e0215140. [CrossRef] [PubMed]
7. Bircher, J.E.; Koleske, A.J. Trio family proteins as regulators of cell migration and morphogenesis in development and disease–mechanisms and cellular contexts. *J. Cell Sci.* **2021**, *134*, jcs248393. [CrossRef]
8. Hildebrandt, F.; Otto, E.; Rensing, C.; Nothwang, H.G.; Vollmer, M.; Adolphs, J.; Hanusch, H.; Brandis, M. A novel gene encoding an SH3 domain protein is mutated in nephronophthisis type 1. *Nat. Genet.* **1997**, *17*, 149–153. [CrossRef]

9. Saunier, S.; Calado, J.; Benessy, F.; Silbermann, F.; Heilig, R.; Weissenbach, J.; Antignac, C. Characterization of the NPHP1 locus: Mutational mechanism involved in deletions in familial juvenile nephronophthisis. *Am. J. Hum. Genet.* **2000**, *66*, 778–789. [CrossRef]
10. Wu, T.; Shi, Z.; Baumgart, T. Mutations in BIN1 associated with centronuclear myopathy disrupt membrane remodeling by affecting protein density and oligomerization. *PLoS ONE* **2014**, *9*, e93060. [CrossRef]
11. Hohendahl, A.; Roux, A.; Galli, V. Structural insights into the centronuclear myopathy-associated functions of BIN1 and dynamin 2. *J. Struct. Biol.* **2016**, *196*, 37–47. [CrossRef] [PubMed]
12. Manso, J.A.; Marcos, T.; Ruiz-Martín, V.; Casas, J.; Alcón, P.; Sánchez Crespo, M.; Bayón, Y.; de Pereda, J.M.; Alonso, A. PSTPIP1-LYP phosphatase interaction: Structural basis and implications for autoinflammatory disorders. *Cell Mol. Life Sci.* **2022**, *79*, 131. [CrossRef] [PubMed]
13. Starnes, T.W.; Bennin, D.A.; Bing, X.; Eickhoff, J.C.; Grahf, D.C.; Bellak, J.M.; Seroogy, C.M.; Ferguson, P.J.; Huttenlocher, A. The F-BAR protein PSTPIP1 controls extracellular matrix degradation and filopodia formation in macrophages. *Blood* **2014**, *123*, 2703–2714. [CrossRef] [PubMed]
14. Qin, Y.; Du, Y.; Chen, L.; Liu, Y.; Xu, W.; Liu, Y.; Li, Y.; Leng, J.; Wang, Y.; Zhang, X.Y.; et al. A recurrent SHANK1 mutation implicated in autism spectrum disorder causes autistic-like core behaviors in mice via downregulation of mGluR1-IP3R1-calcium signaling. *Mol. Psychiatry* **2022**, *27*, 2985–2998. [CrossRef] [PubMed]
15. Leblond, C.S.; Heinrich, J.; Delorme, R.; Proepper, C.; Betancur, C.; Huguet, G.; Konyukh, M.; Chaste, P.; Ey, E.; Rastam, M. Genetic and functional analyses of SHANK2 mutations suggest a multiple hit model of autism spectrum disorders. *PLoS Genet.* **2012**, *8*, e1002521. [CrossRef] [PubMed]
16. Ball, L.J.; Kühne, R.; Schneider-Mergener, J.; Oschkinat, H. Recognition of Proline-Rich Motifs by Protein–Protein-Interaction Domains. *Angew. Chem. Int. Ed.* **2005**, *44*, 2852–2869. [CrossRef] [PubMed]
17. Li, S.S.-C. Specificity and versatility of SH3 and other proline-recognition domains: Structural basis and implications for cellular signal transduction. *Biochem. J.* **2005**, *390*, 641–653. [CrossRef]
18. Cesareni, G.; Gimona, M. *Modular Protein Domains*; Wiley: Hoboken, NJ, USA, 2005.
19. Cámara-Artigas, A.; Martínez-Rodríguez, S.; Ortiz-Salmerón, E.; Martín-García, J.M. 3D domain swapping in a chimeric c-Src SH3 domain takes place through two hinge loops. *J. Struct. Biol.* **2014**, *186*, 195–203. [CrossRef]
20. Carducci, M.; Perfetto, L.; Briganti, L.; Paoluzi, S.; Costa, S.; Zerweck, J.; Schutkowski, M.; Castagnoli, L.; Cesareni, G. The protein interaction network mediated by human SH3 domains. *Biotechnol. Adv.* **2012**, *30*, 4–15. [CrossRef]
21. Panni, S.; Dente, L.; Cesareni, G. In vitro evolution of recognition specificity mediated by SH3 domains reveals target recognition rules. *J. Biol. Chem.* **2002**, *277*, 21666–21674. [CrossRef]
22. Kazemein Jasemi, N.S.; Herrmann, C.; Magdalena Estirado, E.; Gremer, L.; Willbold, D.; Brunsveld, L.; Dvorsky, R.; Ahmadian, M.R. The intramolecular allostery of GRB2 governing its interaction with SOS1 is modulated by phosphotyrosine ligands. *Biochem. J.* **2021**, *478*, 2793–2809. [CrossRef] [PubMed]
23. Mayer, B.J. SH3 domains: Complexity in moderation. *J. Cell Sci.* **2001**, *114*, 1253–1263. [CrossRef] [PubMed]
24. Kay, B.K. SH3 domains come of age. *FEBS Lett.* **2012**, *586*, 2606–2608. [CrossRef]
25. Landgraf, C.; Panni, S.; Montecchi-Palazzi, L.; Castagnoli, L.; Schneider-Mergener, J.; Volkmer-Engert, R.; Cesareni, G. Protein interaction networks by proteome peptide scanning. *PLoS Biol.* **2004**, *2*, e14. [CrossRef] [PubMed]
26. Bae, D.J.; Seo, J.; Kim, S.Y.; Park, S.Y.; Do Yoo, J.; Pyo, J.H.; Cho, W.; Cho, J.Y.; Kim, S.; Kim, I.S. ArhGAP12 plays dual roles in Stabilin-2 mediated efferocytosis: Regulates Rac1 basal activity and spatiotemporally turns off the Rac1 to orchestrate phagosome maturation. *Biochim. Biophys. Acta Mol. Cell Res.* **2019**, *1866*, 1595–1607. [CrossRef] [PubMed]
27. Hibino, H.; Pironkova, R.; Onwumere, O.; Vologodskaia, M.; Hudspeth, A.J.; Lesage, F. RIM binding proteins (RBPs) couple Rab3-interacting molecules (RIMs) to voltage-gated Ca(2+) channels. *Neuron* **2002**, *34*, 411–423. [CrossRef] [PubMed]
28. Nakamoto, T.; Yamagata, T.; Sakai, R.; Ogawa, S.; Honda, H.; Ueno, H.; Hirano, N.; Yazaki, Y.; Hirai, H. CIZ, a zinc finger protein that interacts with p130(cas) and activates the expression of matrix metalloproteinases. *Mol. Cell Biol.* **2000**, *20*, 1649–1658. [CrossRef]
29. Salem, D.; Fecek, R.J. Role of microtubule actin crosslinking factor 1 (MACF1) in bipolar disorder pathophysiology and potential in lithium therapeutic mechanism. *Transl. Psychiatry* **2023**, *13*, 221. [CrossRef]
30. Rasmussen, A.H.; Rasmussen, H.B.; Silahtaroglu, A. The DLGAP family: Neuronal expression, function and role in brain disorders. *Mol. Brain* **2017**, *10*, 43. [CrossRef]
31. Bustelo, X.R.; Sauzeau, V.; Berenjeno, I.M. GTP-binding proteins of the Rho/Rac family: Regulation, effectors and functions in vivo. *Bioessays* **2007**, *29*, 356–370. [CrossRef]
32. Risse, S.L.; Vaz, B.; Burton, M.F.; Aspenström, P.; Piekorz, R.P.; Brunsveld, L.; Ahmadian, M.R. SH3-mediated targeting of Wrch1/RhoU by multiple adaptor proteins. *Biol. Chem.* **2013**, *394*, 421–432. [CrossRef] [PubMed]
33. López-Colomé, A.M.; Lee-Rivera, I.; Benavides-Hidalgo, R.; López, E. Paxillin: A crossroad in pathological cell migration. *J. Hematol. Oncol.* **2017**, *10*, 50. [CrossRef] [PubMed]
34. Webb, D.J.; Schroeder, M.J.; Brame, C.J.; Whitmore, L.; Shabanowitz, J.; Hunt, D.F.; Horwitz, A.R. Paxillin phosphorylation sites mapped by mass spectrometry. *J. Cell Sci.* **2005**, *118*, 4925–4929. [CrossRef] [PubMed]

35. Kreienkamp, H.-J.; Liew, C.W.; Bächner, D.; Mameza, M.-G.; Soltau, M.; Quitsch, A.; Christenn, M.; Wente, W.; Richter, D. Physiology of somatostatin receptors: From genetics to molecular analysis. In *Somatostatin*; Springer: Berlin/Heidelberg, Germany, 2004; pp. 185–202.
36. Verschueren, E.; Spiess, M.; Gkourtsa, A.; Avula, T.; Landgraf, C.; Mancilla, V.T.; Huber, A.; Volkmer, R.; Winsor, B.; Serrano, L. Evolution of the SH3 domain specificity Landscape in Yeasts. *PLoS ONE* **2015**, *10*, e0129229. [CrossRef] [PubMed]
37. Cesareni, G.; Panni, S.; Nardelli, G.; Castagnoli, L. Can we infer peptide recognition specificity mediated by SH3 domains? *FEBS Lett.* **2002**, *513*, 38–44. [CrossRef]
38. Chook, Y.M.; Gish, G.D.; Kay, C.M.; Pai, E.F.; Pawson, T. The Grb2-mSos1 complex binds phosphopeptides with higher affinity than Grb2. *J. Biol. Chem.* **1996**, *271*, 30472–30478. [CrossRef]
39. Herrero-Garcia, E.; O'Bryan, J.P. Intersectin scaffold proteins and their role in cell signaling and endocytosis. *Biochim. Biophys. Acta (BBA)-Mol. Cell Res.* **2017**, *1864*, 23–30. [CrossRef]
40. Alfaidi, M.; Scott, M.L.; Orr, A.W. Sinner or Saint?: Nck adaptor proteins in vascular biology. *Front. Cell Dev. Biol.* **2021**, *9*, 688388. [CrossRef]
41. Yu, X.; Liang, C.; Zhang, Y.; Zhang, W.; Chen, H. Inhibitory short peptides targeting EPS8/ABI1/SOS1 tri-complex suppress invasion and metastasis of ovarian cancer cells. *BMC Cancer* **2019**, *19*, 878. [CrossRef]
42. Hahn, S.; Kim, D. Transient protein-protein interaction of the SH3-peptide complex via closely located multiple binding sites. *PLoS ONE* **2012**, *7*, e32804. [CrossRef]
43. Mayer, B.J.; Saksela, K. SH3 domains. In *Modular Protein Domains*; Wiley: Hoboken, NJ, USA, 2005; pp. 37–58.
44. Dionne, U.; Percival, L.J.; Chartier, F.J.; Landry, C.R.; Bisson, N. SRC homology 3 domains: Multifaceted binding modules. *Trends Biochem. Sci.* **2022**, *47*, 772–784. [CrossRef] [PubMed]
45. Dionne, U.; Bourgault, É.; Dubé, A.K.; Bradley, D.; Chartier, F.J.M.; Dandage, R.; Dibyachintan, S.; Després, P.C.; Gish, G.D.; Pham, N.T.H.; et al. Protein context shapes the specificity of SH3 domain-mediated interactions in vivo. *Nat. Commun.* **2021**, *12*, 1597. [CrossRef] [PubMed]
46. Zarrinpar, A.; Park, S.-H.; Lim, W.A. Optimization of specificity in a cellular protein interaction network by negative selection. *Nature* **2003**, *426*, 676–680. [CrossRef]
47. Humphries, A.C.; Donnelly, S.K.; Way, M. Cdc42 and the Rho GEF intersectin-1 collaborate with Nck to promote N-WASP-dependent actin polymerisation. *J. Cell Sci.* **2014**, *127 Pt 3*, 673–685. [CrossRef] [PubMed]
48. Shutes, A.; Berzat, A.C.; Cox, A.D.; Der, C.J. Atypical mechanism of regulation of the Wrch-1 Rho family small GTPase. *Curr. Biol.* **2004**, *14*, 2052–2056. [CrossRef] [PubMed]
49. Lettau, M.; Pieper, J.; Gerneth, A.; Lengl-Janssen, B.; Voss, M.; Linkermann, A.; Schmidt, H.; Gelhaus, C.; Leippe, M.; Kabelitz, D.; et al. The adapter protein Nck: Role of individual SH3 and SH2 binding modules for protein interactions in T lymphocytes. *Protein Sci.* **2010**, *19*, 658–669. [CrossRef] [PubMed]
50. Ahmad, M.; Gu, W.; Helms, V. Mechanism of fast peptide recognition by SH3 domains. *Angew. Chem. Int. Ed.* **2008**, *47*, 7626–7630. [CrossRef]
51. Yu, H.; Chen, J.K.; Feng, S.; Dalgarno, D.C.; Brauer, A.W.; Schrelber, S.L. Structural basis for the binding of proline-rich peptides to SH3 domains. *Cell* **1994**, *76*, 933–945. [CrossRef]
52. McDonald, C.B.; Seldeen, K.L.; Deegan, B.J.; Farooq, A. SH3 domains of Grb2 adaptor bind to PXψPXR motifs within the Sos1 nucleotide exchange factor in a discriminate manner. *Biochemistry* **2009**, *48*, 4074–4085. [CrossRef]
53. Jaiswal, M.; Dvorsky, R.; Amin, E.; Risse, S.L.; Fansa, E.K.; Zhang, S.-C.; Taha, M.S.; Gauhar, A.R.; Nakhaei-Rad, S.; Kordes, C. Functional cross-talk between ras and rho pathways: A Ras-specific GTPase-activating protein (p120RasGAP) competitively inhibits the RhoGAP activity of deleted in liver cancer (DLC) tumor suppressor by masking the catalytic arginine finger. *J. Biol. Chem.* **2014**, *289*, 6839–6849. [CrossRef]
54. Fan, P.-D.; Goff, S.P. Abl interactor 1 binds to sos and inhibits epidermal growth factor-and v-Abl-induced activation of extracellular signal-regulated kinases. *Mol. Cell. Biol.* **2000**, *20*, 7591–7601. [CrossRef] [PubMed]
55. Tong, X.K.; Hussain, N.K.; de Heuvel, E.; Kurakin, A.; Abi-Jaoude, E.; Quinn, C.C.; Olson, M.F.; Marais, R.; Baranes, D.; Kay, B.K.; et al. The endocytic protein intersectin is a major binding partner for the Ras exchange factor mSos1 in rat brain. *EMBO J.* **2000**, *19*, 1263–1271. [CrossRef] [PubMed]
56. Qian, X.; Esteban, L.; Vass, W.C.; Upadhyaya, C.; Papageorge, A.G.; Yienger, K.; Ward, J.M.; Lowy, D.R.; Santos, E. The Sos1 and Sos2 Ras-specific exchange factors: Differences in placental expression and signaling properties. *Embo J.* **2000**, *19*, 642–654. [CrossRef] [PubMed]
57. Hu, Q.; Milfay, D.; Williams, L.T. Binding of NCK to SOS and activation of ras-dependent gene expression. *Mol. Cell Biol.* **1995**, *15*, 1169–1174. [CrossRef] [PubMed]
58. Chardin, P.; Camonis, J.H.; Gale, N.W.; Van Aelst, L.; Schlessinger, J.; Wigler, M.H.; Bar-Sagi, D. Human Sos1: A guanine nucleotide exchange factor for Ras that binds to GRB2. *Science* **1993**, *260*, 1338–1343. [CrossRef] [PubMed]
59. Birge, R.B.; Kalodimos, C.; Inagaki, F.; Tanaka, S. Crk and CrkL adaptor proteins: Networks for physiological and pathological signaling. *Cell Commun. Signal.* **2009**, *7*, 13. [CrossRef] [PubMed]
60. Rufer, A.C.; Rumpf, J.; von Holleben, M.; Beer, S.; Rittinger, K.; Groemping, Y. Isoform-selective interaction of the adaptor protein Tks5/FISH with Sos1 and dynamins. *J. Mol. Biol.* **2009**, *390*, 939–950. [CrossRef]

61. Sini, P.; Cannas, A.; Koleske, A.J.; Di Fiore, P.P.; Scita, G. Abl-dependent tyrosine phosphorylation of Sos-1 mediates growth-factor-induced Rac activation. *Nat. Cell Biol.* **2004**, *6*, 268–274. [CrossRef]
62. Wilkinson, B.; Li, J.; Coba, M.P. Synaptic GAP and GEF complexes cluster proteins essential for GTP signaling. *Sci. Rep.* **2017**, *7*, 5272. [CrossRef]
63. Chau, J.E.; Vish, K.J.; Boggon, T.J.; Stiegler, A.L. SH3 domain regulation of RhoGAP activity: Crosstalk between p120RasGAP and DLC1 RhoGAP. *Nat. Commun.* **2022**, *13*, 4788. [CrossRef]
64. Berry, D.M.; Nash, P.; Liu, S.K.; Pawson, T.; McGlade, C.J. A high-affinity Arg-X-X-Lys SH3 binding motif confers specificity for the interaction between Gads and SLP-76 in T cell signaling. *Curr. Biol.* **2002**, *12*, 1336–1341. [CrossRef] [PubMed]
65. Kazemein Jasemi, N.S.; Ahmadian, M.R. Allosteric regulation of GRB2 modulates RAS activation. *Small GTPases* **2022**, *13*, 282–286. [CrossRef] [PubMed]

Supplementary information

Functional classification and interaction selectivity landscape of the human SH3 domain superfamily*

Neda S. Kazemein Jasemi, Mehrnaz Mehrabipour, Eva Magdalena Estirado, Luc Brunsveld, Radovan Dvorsky, Mohammad R. Ahmadian

Institute of Biochemistry and Molecular Biology II, Medical Faculty and University Hospital Düsseldorf, Heinrich Heine University Düsseldorf, Universitätsstrasse 1, 40225 Düsseldorf, Germany

Table S1. Proteins used in this study

SH3 domains[1]	Construct (aa)	UniProt ID
ABI1	446-505	Q8IZP0
ABL2	107-167	P42684
ABL2^{Set-1} (S121K, N124R, G155F, W156Y)		
ARHGAP12	12-74	Q8IWW6
ARHGAP12^{Set-1} (K28S, R30N, F62G, Y63W)		
ARHGAP12^{Set-2} (K31T, T46Q, A66S, Q67N)		
ARHGEF30 (OBSCN)	5600-5667	Q5VST9
BIN1	520-593	O00499
BIN1^{Set-1} (D536N, T537D, Q558D, D559P)		
CRK-1	132-192	P46108
DLG2	536-606	Q15700
GRB2-1	1-58	P62993
GRB2-2	158-215	
ITSN1-1	740-806	Q15811
ITSN1-2	913-971	
ITSN1-3	1002-1060	
ITSN1-4	1070-1138	
ITSN1-5	1155-1214	
NCK1-1	2-61	P16333
NCK1-2	106-165	
NCK1-3	190–252	
NCK1-3^{Set-1} (N205D, D206T, D226Q, P227D)	190–252	
NCK1-3^{Set-2} (N225E, W229G, K244E)	190–252	
RASA1	279–341	P20936
RIMBP3B-1	832-899	A6NNM3
SRC	77-140	P12931
SH3GLB1	305-365	Q9Y371
SH3PXD2A-1	166-225	Q5TCZ1
SORBS1-1	793-852	Q9BX66
SNX9	1-62	Q9Y5X1

[1] Expressed in the *Escherichia coli* strains CodonPlus, Rosetta, and BL21(DE3) with the use of pGEX4T-1.

Table S2. List of peptides used in this study.

Peptide name	Peptide sequence
P1[1]	[1078]SAPNSPRTPLTPPPAS[1063]
P2	[1124]VTLPHGPRSA[1133]
P3	[1146]EVPVPPPVPPRRRPESAPAESSPSKI[1171]
P4	[1176]LDSPPAIPPRQPTSK[1190]
P5	[1204]ISDPPESPPLLPPREPVRTPDV[1225]
P6	[1227]SSSPLHLQPPPLGKK[1241]
P7	[1247]AFFPNSPSPFTPPPPQTPSPHGT[1269]
P8	[1271]RHLPSPPLTQ[1280]
P9	[1287]IAGPPVPPRQS[1297]
P10	[1300]QHIPKLPPKTY[1310]
RP1[2]	[1147]VPVPPPVPPRRR[1158]
RP2[3]	[13]RCEAPPVPPRRERG[26]

[1] P represents peptides derived from SOS1.
[2] RP1 is the reference peptide1 derived from peptide 3 (P3).
[3] RP1 is the reference peptide 2 derived from WRCH1/RHOU.

Table S3. Published structures of the SH3-PRM complexes.

Fam. no.	SH3/PRM structures[1]	PRM sequence[2]	Proposed Consensus PRM (current study)	Consensus published PRM	PDB code	Ref.[3]
1	PACSIN3/TRPV4	TKGPAPNPPPILKVW	KXX(L/A)PXXP	KXXAPXXXPX	6F55	[1]
	SNX9/EEEV nsP3 peptide	AERLIPRRPAPPVPVPA RIPSPR	RX(L/A)PXXP	RXAPXXP	7OJ9	[2]
	P85A/peptide	KRPLPPLPS	RX(L/A)PXXP	LPX(L/A)P	3I5R	[3]
2	SPTAN1/P41 peptide	APSYSPPPPP	PPXPPXP	------	2JMA	[4]
	SPTAN1/P41 peptide	PPPVPP	PPXPPXP	PXPXP	3THK	[5]
3	NCK2-1/CD3epsilon	KERPPPVPNPDY	PXXDY	PXXDY	2JXB	[6]
	EPS8L1/CD3epsilon	PPVPNPDYEPIR	PXXDY	PXXDY	2ROL	[7]
	TUBA-6 (ARHGEF36-6)/NWASP	PPPALPSSAPSG	PPPXLP	PPPXLPS	4CC2	[8]
	TUBA-6 (ARHGEF36-6)/NWASP	PPPALPSSAPSG	PPPXLP	PPPXLPS	4CC7	[8]
	TUBA-6 (ARHGEF36-6)/MENA	PPPPLPSGPAYA	PPPXLP	PPPXLPS	4CC3	[8]
4	ABL1 mutant (N114A)/P17	APTYSPPLPP	PXXXPPXPP	------	4J9E	TBP
	ABL1 mutant (H59Q-N96T)/P17	APTYSPPLPP	PXXXPPXPP	------	4J9C	TBP
	ABL1/P17	APTYSPPLPP	PXXXPPXPP	------	4J9I	TBP
	ABL1/P7	APTYPPPPPP	PXXXPPXPP	------	4J9G 4J9H	TBP
	ABL1 mutant (N114A)/P41	APSYSPPPPP	PXXXPPXPP	PXXP	2O88	[9]
	ABL1/P41 peptide	APSYSPPPPP	PXXXPPXPP	PXXP	1BBZ 3EG1	[10, 11]
	ABL1 mutant (N114A)/P0	APTYPPPLPP	PXXXPPXPP	------	4J9D	TBP
	ABL1/P0	APTYPPPLPP	PXXXPPXPP	------	4J9F	TBP
	ABL1/3BP-1	APTMPPPLPP	PXXXPPXPP	PXXXPPXPP	1ABO	[12]
5	NCF1-2(p47phox)/p22phox	QPPSNPPPRPP	PXPXXP	PXPXXP	1OV3	[13]
	NCF1-2(p47phox)/p22phox	GPLGSKQPPSNPPPRP PAEARKKPS	PXPXXP	PPPRPPAEAR	1WLP	[14]
7	CRKII-1 (CRK-1)/C3G	DNSPPPALPPKKRQSY	PXXPX(K/R)	------	5L23	TBP
	CRK-1 (C-CRK)/C3G	PPPALPPKKR	PXXPX(K/R)	PXLPXK	1CKA	[15]
	CRKII-1 (CRK-1)/C-ABL	YEKPALPRKR	PXXPX(K/R)	PXLPXK	5IH2	[16]
	CRK-1/peptide inhibitor	YEVPGPVPPRRR	PXXPX(K/R)	PXXPXR	1B07	[17]
	CRK-1 (C-CRK)/SOS peptide	PPPVPPRR	PXXPX(K/R)	PXXPXR	1CKB	[15]
	HCK/synthetic peptide	HSKYPLPPLPSL	(K/R)XPXXP	LPX(L/A)P	2OJ2 2OI3	[18]
	FYN/synthetic peptide	VSLARRPLPPLP	(K/R)XPXXP	RXPXXP	4EIK	[19]
	FYN/synthetic peptide	APPLPPRNRPRL	PXXPXX(K/R)	PXXPXXR	4ZNX	[19]
	FYN/3BP-2	PPAYPPPPVP	PXXP	------	1FYN	[12]
	FYN/P2Lsynthetic peptide(PI3K-P85)	PPRPLPVAPGSSKT	(K/R)XXPXXP	RPLPVAP	1A0N 1AZG	[20]
	FYN/NS5A	APPIPPPR	PXXPX(K/R)	XPXXPX(K/R)	3UA7	[21]
	LYN/TIP	WDPGMPTPPLPPRPAN LGERQA	PXXPX(K/R)	PPLPPR	1WA7	[22]
	SRC/VSL12	VSLARRPLPPLP	(K/R)XXPXXP	RXLPPXP	1QWF	[23]
	SRC(C-SRC)/APP12	APPLPPRNRPRL	PXXPX(K/R)	XPPLPXR	1QWE	[23]
	SRC mutant (T98D)(C-SRC)/APP12	APPLPPRNRP	PXXPX(K/R)	XPXXPXR	4HVU	[24]
	SRC mutant (T98E)(C-SRC)/APP12	APPLPPRNRP	PXXPX(K/R)	XPXXPXR	4HVV 4HVW	[24]
	SRC/tyrosine phosphatase PEP	IPPPLPERTPESFIVVEE	PXXPX(K/R)	PXXPXR	1JEG	[25]
	SRC(C-SRC)/NL1	PLPPLP	PXXP	PXXP	1NLO	[26]
	SRC(C-SRC)/NL2	PLPPLP	PXXP	PXXP	1NLP	[26]
	SRC(C-SRC)/PLR1	AFAPPLPRR	PXXPX(K/R)	XPPLPXR	1PRM 1PRL	[27]
	SRC(C-SRC)/PLR2	RALPPLPRY	(K/R)XXPXXP	RXLPPLP	1RLP 1RLQ	[27]
	SRC(C-SRC)/NS5A	APPIPPPR	PXXPX(K/R)	PXXPXR	4QT7	[28]
8	ITSN1-2/synthetic peptide	WRDSSGYVMGPW	Exceptional	[W/F][R/W]XSX[A/G][F/Y][L/V]XGP[W/L]	4IIM	[29]
	ITSN2-2/synthetic peptide	WRGSLSYLKGPL	Exceptional	[W/F][R/W]XSX[A/G][F/Y][L/V]XGP[W/L]	4IIO	[29]
	betaPIX (ARHGEF7)/alphaPAK	DATPPPVIAPRPEHTKS VYTRS	PXXXPR	XPXXXPXR	1ZSG	[30]
	betaPIX (ARHGEF7)/CBL-b	RPPKPRPR	PXXXPR	PXXXPR	2AK5	[31]
	betaPIX(ARHGEF7)/AIP4	GGFKPSRPPRPSRPPP PTPRRPASV	PXXXPR	PXXXPR	2P4R	[32]
	betaPIX (ARHGEF7)/ITCH	GSGGGKPSRPPRPSRP PPPTPRRPASY	PXXXPR	PXXPXXR	5SXP	[33]
	betaPIX (ARHGEF7)/PAK2	PPVIAPRPEHTKSIYTRS	PXXXPR	PXXXPR	2DF6	[34]
	IRTKaS(BAIAP2L1)/EspFu-R47	HIPPAPNWPAPTPPVQ N	PXXXP	IPxZPxxxZPxZP (wherein Z is P, A, I, L, or V)	2KXC	[35]

	PLCG1/SLP-76	QPPVPPQRPM	PXXXPXR	XPXXPXRP	1YWO	[36]
9	GRB2-1 mutant (Y7V,C32S)/SOS1	VPPPVPPRRR	PXXPX(K/R)	------	1AZE	[37]
	GRB2-1/SOS1	VPPPVPPRRR	PXXPX(K/R)	------	1GBQ 3GBQ 4GBQ	[38]
	DOCK2/ELMO1	RLLDLENIQIPDAPPPIP KEPSNYDFVY	PXXPX(L/P)	------	2RQR	[39]
	DOCK2/ELMO1	PDAPPPIP	PXXPX(L/P)	------	3A98	[39]
	p67phox-2 (NCF2-2)/p47phox (NCF1)	SKPQPAVPPRPSADLIL NRCSESTKRKLASAV	PXXPX(K/R)	PXXPXR	1K4U	[40]
	P40phox (NCF4)/p47phox (NCF1)	KPQPAVPPRPSAD	PXXPX(K/R)	------	1W70	[41]
	Cortactin (SRC8)/AMAP1	KRPPPPPPG	PXXPX(L/P)	RXXPXXP	2D1X	[42]
	Cortactin (SRC8)/Arg nonreceptor tyrosine kinase	SSVVPYLPRLPIL	PXXPX(L/P)	------	3ULR	[43]
	Ponsin-2(SORBS1-2)/Paxillin	VPPPVPPPPS	PXXPX(L/P)	------	2O9V	[44]
	CAP-2 (SORBS1-2)/Vinculin	ELAPPKPPLPE	PXXPX(L/P)	XPXXPXL	4LN2	[45]
	CAP-1(SORBS1-1)/Vinculin	VPPPRPPPPE	PXXPX(L/P)	XPXXPXX	4LNP	[45]
	NEBL/XIRP2	PPPTLPKPKLPKH	PXXPX(L/P)	PPXXXPKP	4F14	[46]
10	GRB2-2/synthetic peptide	RHYRPLPPLP	RXX(K/R)P	------	1IO6	TBP
	GRB2-2/SOS1 peptide	APPPRPPKP	RXX(K/R)P	RXXKP	2W0Z	[47]
	GRB2-2/Gab2	IQPPPVNRNLKPDR	RXX(K/R)P	PXXXRXXKP	2VWF	[48]
	CD2AP-2/ARAP1	PTPRPVPMKRHIFR	PX(P/A)XXR	PX(P/A)XXR	4X1V	[49]
	CD2AP-2/RIN3	TAKQPPVPPPRKKRIS	PX(P/A)XXR+ PXXPX(K/R)	PX(P/A)XXR	3U23	[49]
	CD2AP-1/RIN3	AKKNLPTAPPRRRVSE	PX(P/A)XXR + PXXPX(K/R)	PX(P/A)XXR	4WCI	[49]
	CD2AP-1/CBL-B	PPKPRPRR	PX(P/A)XXR	PXXXPR	2J6F	[50]
	CMS-1(CD2AP1-1)/CD2	PLPRPRV	PX(P/A)XXR	PXXXPR	2J6O	[50]
	CMS-1(CD2AP1-1)/CD2	KGPPLPRPRV	PX(P/A)XXR	PXXXPR	2J7I	[50]
	CIN85-1(SH3KBP1-1)/CBL-b	PARPPKPRPRR	PX(P/A)XXR + RXX(K/R)P +PXXPX(K/R)	PXXXPR	2BZ8	[31]
	STAM2/AMSH	AKPPVVDRSLKPGA	RXX(K/R)P	PX(V/I)(D/N)RXXKP	5IXF	[51]
	STAM2/UBPY-derived peptide	TPMVNRENKPP	RXX(K/R)P	PX(V/I)(D/N)RXXKP	1UJ0	[52]
	BIN1/C-MYC	LLPTPPLSPSRRSG	PXXPX(K/R)	PXXPXR	1MV0	[53]
	GRAP2-2 (Mona/Gads)/HPK1	GQPPLVPPRKEKMRGK	PXXPX(K/R)	PXVPXRXXK	1UTI	[54]
	GRAP2-2 (Mona/Gads)/ phosphatase-like protein HD-PTP	PPPRPTAPKPLL	PXXPXXP(K/R)	RXXXXK	2W10	[48]
	GRAP2-2/Lymphocyte cytosolic protein2(SLP-76)	APSIDRSTKPPL	RXX(K/R)P	PXXDRXXKP	1OEB 1H3H	[55, 56]
	GRAP2-2/SLP-76	PSIDRSTKP	RXX(K/R)P	PXXXRXXKP	2D0N	[57]
	ASAP1/MICAL1	GPGSEPPPKPPRS	PXXPX(K/R)	XPXKPXR	8HLO	[58]
	STAC2/CaV1.1	EPEIPLSPRP	PXXPXXP(K/R)	------	6B27	[59]

[1] Names in parentheses represent aliases.

[2] The underlined residues in the second column represent motifs associated with the published consensus PRMs, while the residues highlighted in green represent the proposed consensus PRM identified in the current study.

[3] TBP stands for to be published. This means that the molecular structure is available in the Protein Data Bank (PDB), but the corresponding research article is not yet publicly available.

Table S4. Published dissociation constants (K_d) determined for the SH3-PRP interactions

Fam. no.	SH3DCP	PRM	peptide Sequence[1]	proposed Consensus PRM (current study)	consensus published PRM	K_d (μM)	Method[2]	Ref.
1	SNX9	EEEV nsP3	AERLIPRRPAPPVPVPARI PSPR	RX(L/A)PXXP	RXAPXXP	0.3	ITC	[2]
	PACSIN1	Itch	PEDAGAGENRRVSGNNS PSLSNGGFK PSRPPRPSRPPPPTPRRP ASVNGSPS ATSESDGSSTG	RXXPXXP	K/RXXPXXPXK/R	4.33	ITC	[60]
		TRPV4	TKGPAPNPPPVLKV	KXX(L/A)PXXP	KXXAPXXXPX	51.6	HSQC	[61]
	PACSIN2	TRPV4	TKGPAPNPPPVLKV	KXX(L/A)PXXP	KXXAPXXXPX	12.7	HSQC	
	PACSIN3	TRPV4	TKGPAPNPPPVLKV	KXX(L/A)PXXP	KXXAPXXXPX	68.6	HSQC	
	p85A	Synthetic peptide	RKLPPRPSK	RX(L/A)PXXP	RXLPPRPXX	9.1	FL	[62]
		PD1R	HSKRPLPPLPSL	RX(L/A)PXXP	LPX(L/A)P	40	SPR	[3]
		PD1	HSKYPLPPLPSL	KXX(L/A)PXXP	------	120		
2	SPTAN1	Peptide41	ASYPPVPPP	PPXPPXP	------	160	FL	[63]
3	NCK1-1	N-WASP	1.LRRQAPPPPPPS 2.APPPPPPSRGG 3.GPPPPPARGRGA 4.TAAPPPPPPSRP 5.SAPSGPPPPPPSVL	PPPPP	------	>1 MM	HSQC	[64]
	EPS8	E3b1	PPPPPVDYEDEE	PPPPP+PXXDY	PXXDY	35	ELISA	[65]
	EPS8L1	CD3ε	PPVPNPDYEPIR	PXXDY	PXXDY	24	ITC	[7]
	ITK	TSAD	LLRPKPPIPAKPQLP	PXXPXLP	------	150 mM	HSQC	[66]
			LLRPKPPIPAKPQLPPEVY TIPVPRHR	PXXPXLP	------	123 mM		
4	ABL1	P4	APSYSPPPPP	PXXXPPXPP	------	1.5	FL	[67]
		P4	APTYSPPPPP	PXXXPPXPP	------	0.4		
		P8	APTYPPPAPP	PXXXPPXPP	------	5±		
		3BP-1	RAPTMPPPLPP	PXXXPPXPP		34		
5	SH3PXD2 B-1/2	SH3PXD 2B	GSHMGDAKQRSPKMRQR PPPRRD	PXPXXP	PPPRR	15	MST	[68]
			MTIPRGLNLPKPPIPPQVE			11	FL	
	NCF1-2 (p47^{phox})	p22phox	QPPSNPPPRPPAEAR	PXPXXP	------	8.67	FL	[14]
			QPPSNPPPRPPAEARKKP SE	PXPXXP	RKKPSE	0.64		
7	CRK-1	C3G	PPPALPPKKR	PXXPX(K/R)	PXXPXK	1.9	FL	[15]
			PPPALPPKKR	PXXPX(K/R)	XXPXLPXKXX	1.89	FL	[69]
			DNSPPPALPPKKRQSAPS	PXXPX(K/R)	PXLPXK	~2	ITC	[70]
		DOCK180	DVADVPPPLPLKGSVADY GNLMENQDLLGSPTPPPP PPHQRHLPPPLPSKT	PXXPX(K/R)	PPXLPXK	0.35	SPR	[71]
		ST12	SLPGPLTPVAEGQEIGMN TETSGTSAREK ELSPPPGLPSKIGSISRQS SL	PXXPX(K/R)		0.91		
		SOS1	YEVPPPVPPRRR	PXXPX(K/R)	PXXPXR	6	FL	[17]
			PPPVPPRRRR	PXXPX(K/R)		5.2	FL	[15]
	SRC	VSL12	VSLARRPLPPLP	(K/R)XPXXP	+XPpXP	0.45	FL	[23]
		APP12	APPLPPRNRPRL	PXXPX(K/R)	XPpXP+	1.2		
		Synthetic peptide	RALPPLPRY	(K/R)XXPXXP	RXLPPLPRX	7.8	FL	[62]
		SOS1	YEVPPPVPPRRR	PXXPX(K/R)	PXXPXR	25	FL	[17]
	HCK	Nef	PVRPQVPLRPMT	PXXPX(K/R)	PXXP	91	SPR	[72]
	FYN	Nef	PVRPQVPLRPMT	PXXPX(K/R)	PXXP	202	SPR	[72]
		PI3K-p85α	KRISPPTPKPRPPR	(K/R)XXPXXP	------	3 mM	HSQC	[73]
			PPRPLPVAPGSSKA	(K/R)XXPXXP	RXXPXXP	50		
			PPRPTPVAPGSSKA	(K/R)XXPXXP	RXXPXXP	300		
		P2L	PPRPLPVAPGSSKT	(K/R)XXPXXP	------	50	NMR	[20]
						28	CD	
						16	ITC	
	LCK	Tip	ATLDPGMPTPPLPPRPAN LG	PXXPX(K/R)	------	16.80	FL	[74]
		TSAD	LLRPKPPIPAKPQLP	PXXPX(K/R)	------	69 mM	HSQC	[66]
			LLRPKPPIPAKPQLPPEVY TIPVPRHR	PXXPX(K/R)	XPXPXX(R/K)	161 mM		
8	βPIX (ARH GEF7)	Itch	KPSRPPRPSRPPPPTPRR PAS	PXXXPR	RPXPPXPR	1.59	ITC	[33]
			PEDAGAGENRRVSGNNS PSLSNGGFK	PXXXPR	K/RXXPXXPXK/R	1.44	ITC	[60]

			PSRPPRPSRPPPTPRRP ASVNGSPS ATSESDGSSTG					
		PAK2	EETAPPVIAPRPDHTKSIY TRSVI	PXXXPR	PXXXPR	1.05	ITC	[34]
	ITSN1-2	Synthetic peptide	WRDSSGYVMGPW	Exceptional	[W/F][R/W]xSx[A/G][F/Y][L/V]xGP[W/L]	53	ITC	[29]
	NCK1-2	N-WASP	GPPPPPARGRGA	PXXXPXR	------	147	HSQC	[64]
			VAVPPPPPNRMY	PXXXPXR		199		
	PLCG1	SOS1	AAPVPPPVPPRRRP	PXXXPR	------	0.20mM	SPR	[75]
			AADSPPAIPPRQPT	PXXXPR		0.40mM		
			AAESPPLLPPREPV	PXXXPR		0.70mM		
			AAIAGPPVPPRQST	PXXXPR		0.28mM		
	BAIAP2L1 (IRTKS)	$EspF_UR4_S$	IPPAPNWPAPTPP	PXXXP	------	0.5 nM	ITC	[76]
9	SORBS2-1	Synthetic peptide	LRTGEAYLRYVD	Exceptional	XRXGXAYLXYVX	38	ITC	[29]
		Synthetic peptide	RLPLRPPLPHTS	PXXPX(L/P)	PXXPXXP	121	ITC	[29]
	GRB2-1	C3G	PPPALPPKKR	PXXPX(K/R)	PXXPXK	142	FL	[15]
		SOS1	PPPVPPRRRR	PXXPX(K/R)	PXXPXR	3.5	FL	
			VPPPVPPRRR	PXXPX(K/R)	PXXPPR	5.6	FL	[77]
			PVPPPVPPRRRP	PXXPX(K/R)	PPVPPR	38.64	ITC	[78]
			PVPPPVPPRRRP	PXXPX(K/R)	PX(V/L/I)PXR	39	ITC	[79]
			DSPPAIPPRQPT			55		
			ESPPLLPPREPV			117		
			IAGPPVPPRQST			82		
			YEVPPPVPPRRR	PXXPX(K/R)	PXXPXR	5	FL	[17]
			PKPLPRFPKK	PXXPX(K/R)	PXPXPRXPKK(S suggested core: PXXPXK)	250	NMR	[47]
			PVPPPVPPRRRP	PXXPX(K/R)	PXXPXR	37	NMR	
			PSPHGTRRHLPSPP	Exceptional	RR	208	NMR	
			APNSPRTPLTPPPAYS	PXXPX(L/P)	PXXPRXPXXP	280	NMR	
	SH3GL2 (Endophilin-A1)	Itch	PEDAGAGENRRVSGNNS PSLSNGGFK PSRPPRPSRPPPPTPRRP ASVNGSPS ATSESDGSSTG	PXXPX(K/R) + PXXPX(L/P)	(K/R)XXPXXPX(K/R)	0.457	ITC	[60]
10	STAM2	UBPY	TPMVNRENKPP	RXX(K/R)P	PX(V/I)(D/N)RXXKP	27	FL	[52]
	NCK1-3	N-WASP	VAVPPPPPNRMY	PX(P/A)XXR	------	~1mM	HSQC	[64]
			1.NRMYPPPPPALP 2.SAPSGPPPPPPPSVL 3.VAPPPPPPPPPPPG 4.PGPPPPPGLPSD	PPPPP	------	>>1 mM	HSQC	
	AMPH	Dynamin-I	PSRPNR	PXXPX(K/R)	PXRPXR(H)R(H)	0.19	γ-radiation	[80]
	GRB2-2	SOS1	PVPPPVPPRRRP	PX(P/A)XXR + PXXPX(K/R)	PPVPPR	117	ITC	[78]
			PVPPPVPPRRRP	PX(P/A)XXR + PXXPX(K/R)	PX(V/L/I)PXR	125	ITC	[79]
			DSPPAIPPRQPT	PXXPX(K/R)		1,396		
			ESPPLLPPREPV	PXXPX(K/R)		1.718		
			IAGPPVPPRQST	PXXPX(K/R)		1.318		
			PVPPPVPPRRRP	PX(P/A)XXR + PXXPX(K/R)	PXXPXR	142	NMR	[47]
			PKLPPKTYKREH	PXXPX(K/R)	PXXPXKXXKR	156		
		SLP-76	PAPSIDRSTKPPL	RXX(K/R)P	PX3RX2KP	9.7	ITC	[55]
		Gab2b	IQPPPVNRNLKPDRK	PX(P/A)XXR + RXX(K/R)P	PX3RX2KP	17.4	ITC	[48]
	GRAP2-2	SLP-76	PAPSIDRSTKPPL	RXX(K/R)P	PX3RX2KP	0.181	ITC	[55]
			APSIDRSTKPP	RXX(K/R)P	PX3RX2KP	0.675	ITC	
			PSIDRSTKP	RXX(K/R)P	PX3RX2KP	30	ITC	[57]
	BIN1	Tau	SRTPSLPTPPTREPKKVA VVRTPPKSPSSAK	PX(P/A)XXR + PXXPX(K/R)	PXPPXR and RXPPXXP	44	NMR	[81]
	STAC1	CaV1.1	EDEPEIPLSPRPRP	PXXPXXP(K/R)	------	3.92	ITC	[59]
			NVNEVKDPYPSADFPGDD	PXXPXXP(K/R)		0.78		
	STAC2		EEDEPEIPLSP RPRPLAELQLKEKAVPIPE			1.85		
			EDEPEIPLSPRPRP	PXXPXXP(K/R)		9.31		
		CaV1.2	NENEDKSPYPNPETTGEE DEEEPEMPVGP	PXXPXXP(K/R)		19.3		

			RPRPLSELHLKEKAVPMPE					
	CD2AP-1 (CMS)	CD2	QKGPPLPRPRVQPKPPHG	PX(P/A)XXR	PXXXPR	100	SPR	[50, 82]
	SH3KBP1-1 (CIN85)							

[1] The underlined residues in the second column represent motifs associated with the published consensus PRMs, while the residues highlighted in green represent the proposed consensus PRM identified in the current study.
[2] CD: Circular Dichroism Spectroscopy FL: fluorescence-based titrations; HSQC: Heteronuclear Single Quantum Coherence; ITC: Isothermal titration calorimetry; MST: microscale thermophoresis

Table S5. PRM classification and occurrence in SOS1 PRD.

No.	ID	Consensus sequences	Ref.	Peptides[1]											
				P1	P2	P3	P4	P5	P6	P7	P8	P9	P10	RP1	RP2
1	0X1	PPPP	[83]	-	-	-	-	-	-	+	-	-	-	-	-
2	0X2	XPPX	[84]	+	-	+	+	+	+	+	+	+	+	+	+
3	1X1	PXP	[85]	+	-	+	-	-	+	+	+	+	-	+	+
4	1X2	PXPXP	[86]	-	-	+	-	-	-	-	-	-	-	+	-
5	1X3	PPXPP	[87]	-	-	+	+	+	-	-	-	+	-	+	+
6	2X1	PXXDY	[7]	-	-	-	-	-	-	-	-	-	-	-	-
7	2X2	PXXP	[62]	+	+	+	+	+	-	+	+	+	+	+	+
8	2X3	PXXPX[KR]	[88]	-	-	+	+	+	-	-	-	+	-	+	+
9	2X4	[KR]XXPXXP	[88]	-	-	-	-	-	-	-	+	-	-	-	-
10	2X5	PXXPXXP	[89]	+	-	+	-	-	-	-	-	-	-	+	-
11	3X1	PXXXP	[90]	+	-	+	+	+	+	+	-	+	+	+	+
12	3X2	PXXXPXXXP	[91]	-	-	+	+	+	-	-	-	-	-	-	-
13	3XP	PXXXPR	[92]	-	-	+	+	+	-	-	-	+	-	+	+
14	4XP	PXXXXP	[93]	+	-	+	+	+	-	+	-	-	-	+	-

[1] The amino acid sequences of the peptides are listed in Table S2. + Presence of consensus sequence in peptides; - Absence of consensus sequence in peptides.

Table S6. Dissociation constants (K_d)[1] for the SH3-PRP interactions determined in this study.

SH3	Peptides[4]											
Domains[2,3]	**P1**	**P2**	**P3**	**P4**	**P5**	**P6**	**P7**	**P8**	**P9**	**P10**	**RP1**	**RP2**
ABI1	-	60.7	-	24.6	-	-	-	-	-	-	-	-
ABL2	-	-	-	125	-	-	67.3	-	-	-	11	-
ARHGAP12	-	-	13.8	-	-	-	0.2	-	-	-	16.7	15.5
ARHGEF30	-	-	-	-	-	-	8.9	-	-	-	-	-
BIN1	-	-	-	-	-	-	12.0	-	47.0	-	-	48.0
CRK-1	-	-	12.9	-	-	-	18.1	-	-	-	-	-
DLG2	-	-	-	-	-	-	58.5	-	-	-	-	-
GRB2-1	-	-	15.0	60	62	-	-	-	-	-	11.0	20.0
GRB2-2	-	-	12.0	20	35	-	-	-	-	-	3.4	12.9
ITSN1-1	-	-	-	6.6	-	-	-	-	-	-	39	11.0
ITSN1-2	-	-	-	-	-	-	-	-	-	-	-	-
ITSN1-3	-	-	-	-	-	-	-	-	-	-	-	-
ITSN1-4	-	-	-	-	-	-	-	-	-	-	-	-
ITSN1-5	23.0	-	-	12.0	-	-	-	-	-	-	-	23.0
NCK1-1	-	-	-	-	-	-	-	-	-	-	-	-
NCK1-2	-	-	-	-	-	-	-	-	-	-	2.0	1.0
NCK1-3	-	-	-	-	-	-	-	-	0.9	-	24.6	2.5
NPHP1	-	-	-	-	-	-	-	-	-	-	-	-
RASA1	-	-	-	-	-	-	-	-	-	-	-	-
RIMBP3B-1	-	21.0	-	-	-	-	15.0	-	-	-	-	-
SH3GLB1	-	-	-	-	-	-	-	-	-	-	-	-
SH3PXD2A-1	-	44.0	18.0	-	-	-	-	-	-	-	-	21.0
SNX9	-	-	-	-	-	-	-	-	-	-	-	-
SORBS1-1	-	-	-	-	-	-	13.2	-	-	-	-	-
SRC	-	-	2.0	-	-	-	13.3	-	-	-	-	-

[1] The dissociation constants (K_d) were determined by analyzing the fluorescence polarization data (Figure S6) shown as bar charts in Figure 2B. The evaluated K_d values were categorized into different affinity levels: high affinity (0.1 to 1.0 μM; green), intermediate affinity (1.1 to 5.0 μM; blue), low affinity (5.1 to 25 μM; red), and very low affinity (26 to 125 μM; black). No binding is indicated by a dash (-).

[2] SH3DCPs with two or more SH3 domains are indicated by a dash followed by the SH3 domain number.

[3] Proteins in bold: Seven proteins did not bind to any of the 12 peptides that were tested under the conditions of this study.

[4] Amino acid sequences of the peptides are provided in Table S2.

Table S7. Proteins containing PRMs homologous to peptides 2-9 derived from the SOS1 PRD.[1]

Abbreviation/Alias	Protein Names	Accession no.
CCDC144A	Coiled-coil domain-containing protein 144A	XP_016880918.1
DCAF1/VPRBP	DDB1- and CUL4-associated factor 1/Vpr (HIV-1) binding protein (VPRBP)	NP_001336097.1
DLGAP1/2/4	Disks large-associated protein 1/2/4	NP_001385456.1, NP_001333739.1, NP_055717.2
HMCN2	Hemicentin-2	XP_011516769.1
IQSEC2	IQ motif and SEC7 domain-containing protein 2	NP_001104595.1
MACF1	Microtubule-actin cross-linking factor 1	NP_001384402.1
MAGED4	Melanoma antigen family D, 4	EAW62887.1
NFATC2IP	NFATC2-interacting protein	NP_116204.3
PI3KAP1	Phosphoinositide-3-kinase adaptor protein 1	NP_689522.2
PLA2	Phospholipase A2	BAD92387.1
SLX4/BTBD12	Structure-specific endonuclease subunit/ BTB (POZ) domain containing 12	NP_115820.2
SSTR5	Somatostatin receptor subtype 5B	ABE27002.1
WRCH1/RHOU	Wnt-responsive CDC42 homologue/RHO-related GTP-binding protein	NP_067028.1
ZNF41	Zinc finger protein 41	NP_001311071.1
ZNF74	Zinc finger protein 74	KAI2596768.1

[1] See Figure 4 for more details.

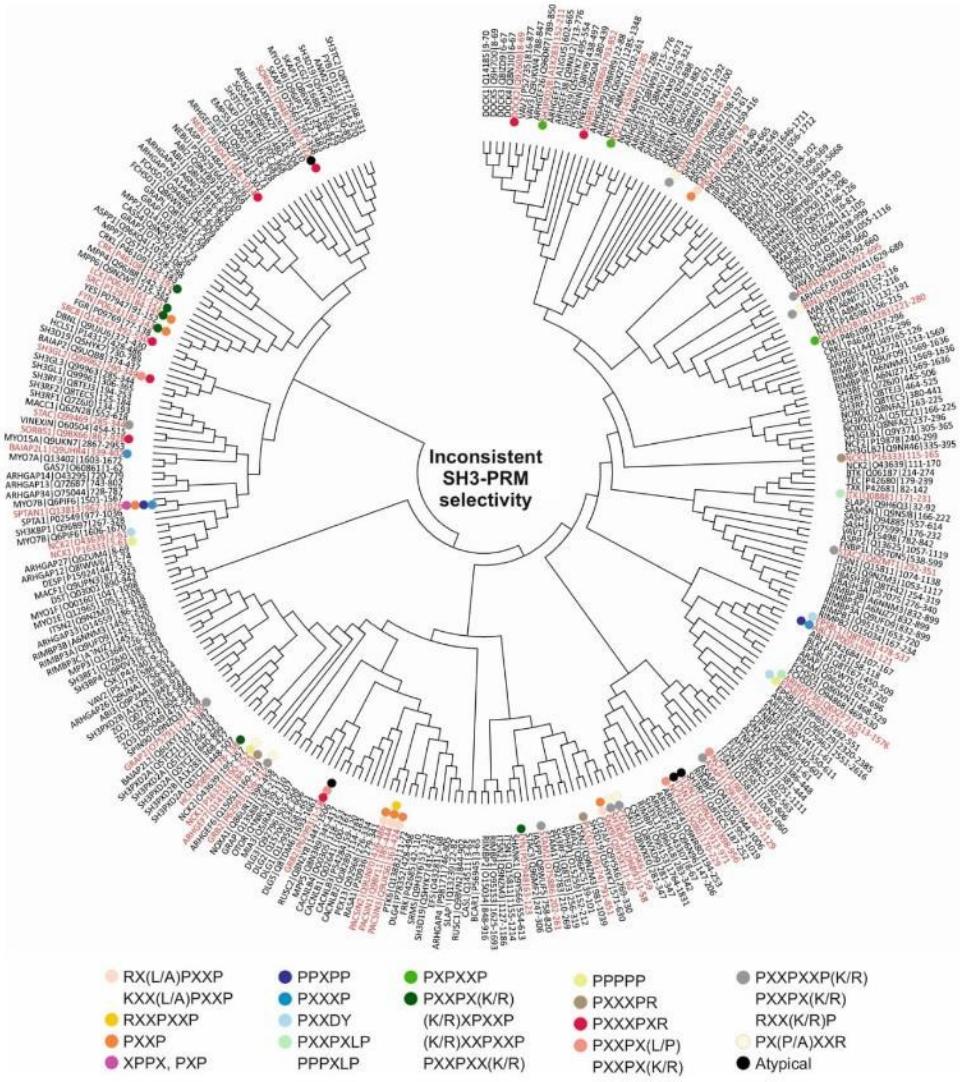

Figure S1. Evolutionary sequence-structure-function relationships of SH3 domains. A whole-sequence phylogenetic tree (tree #1) encompassing 298 human SH3 domains was constructed using the MEGA software (version 10.2.6). Using the structures and biochemical information of SH3 domains, presented in Tables S3 and S4, the interactions between PRMs and their corresponding SH3s are visually represented in the tree. The distinct preferences of SH3 domains for specific PRMs are represented by colored circles, each denoting a PRM preference, while the corresponding SH3 domains are highlighted in red. Interestingly, the PRMs exhibit clustering patterns that are inconsistent with established SH3 domain families.

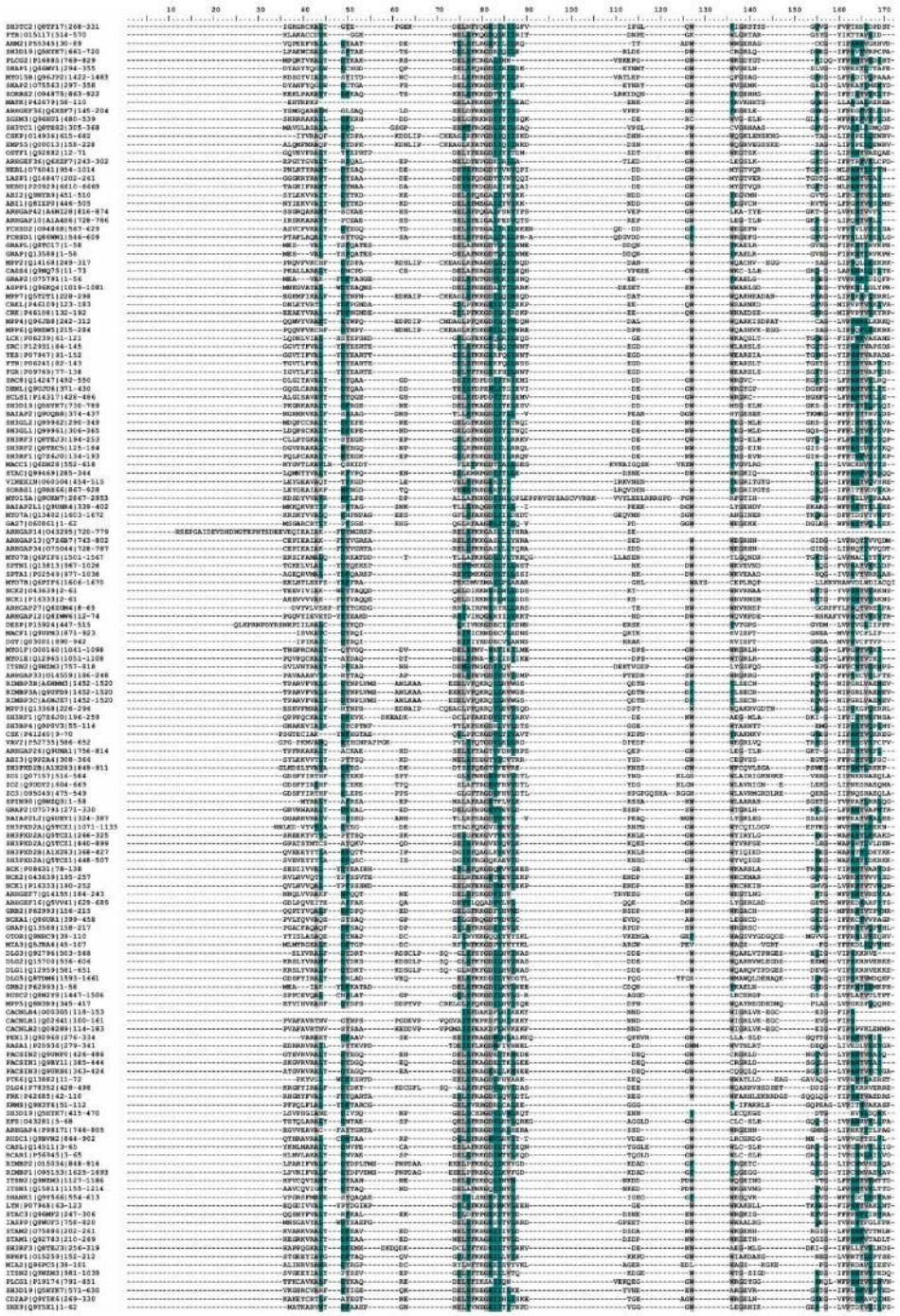

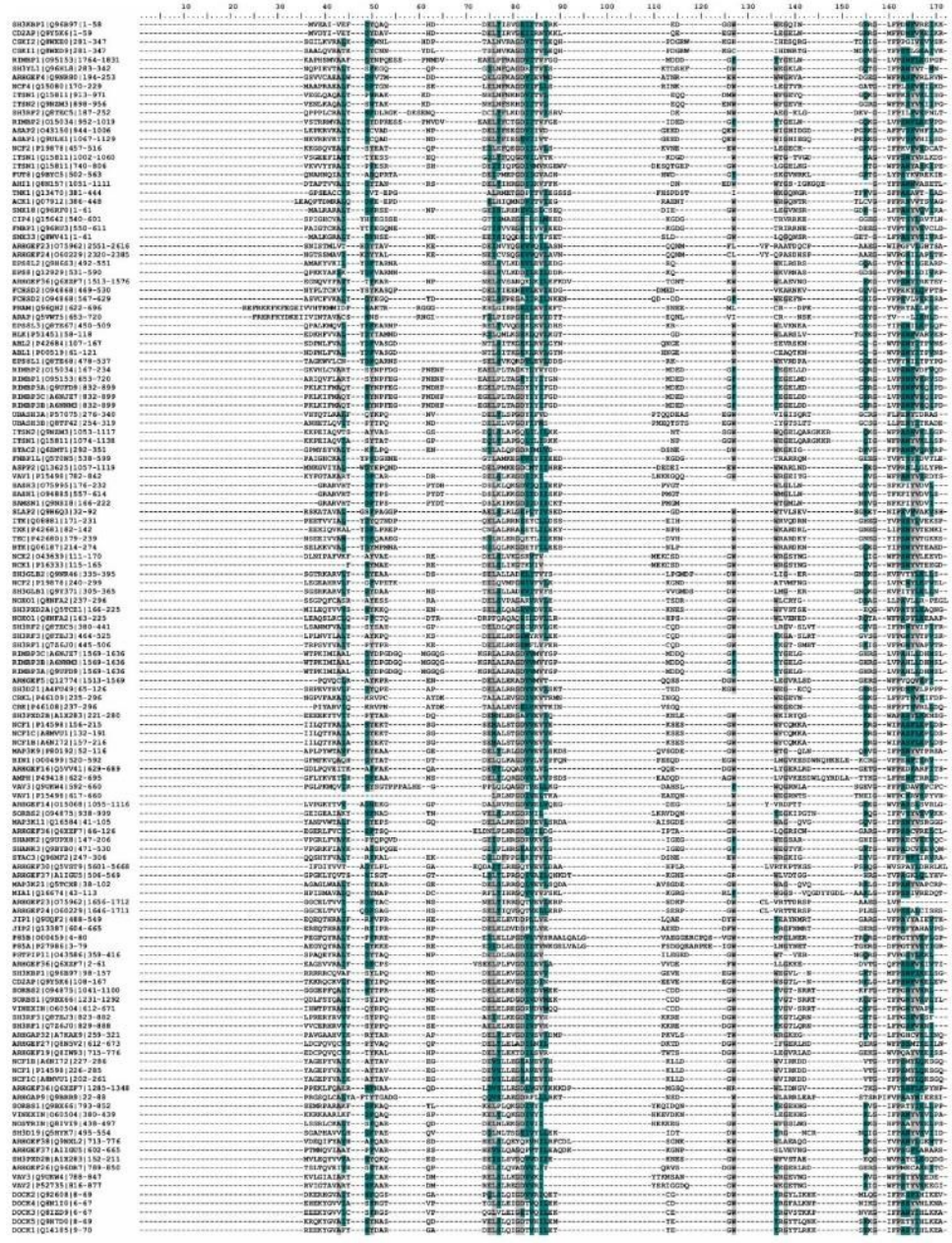

Figure S2. Alignment of SH3 domain sequences. The multiple sequence alignment of the SH3 domains was generated using the BioEdit program by CLUSTALW. Amino acids that are either identical or similar are indicated by gray and green shading, respectively. Gaps are shown as dashed lines.

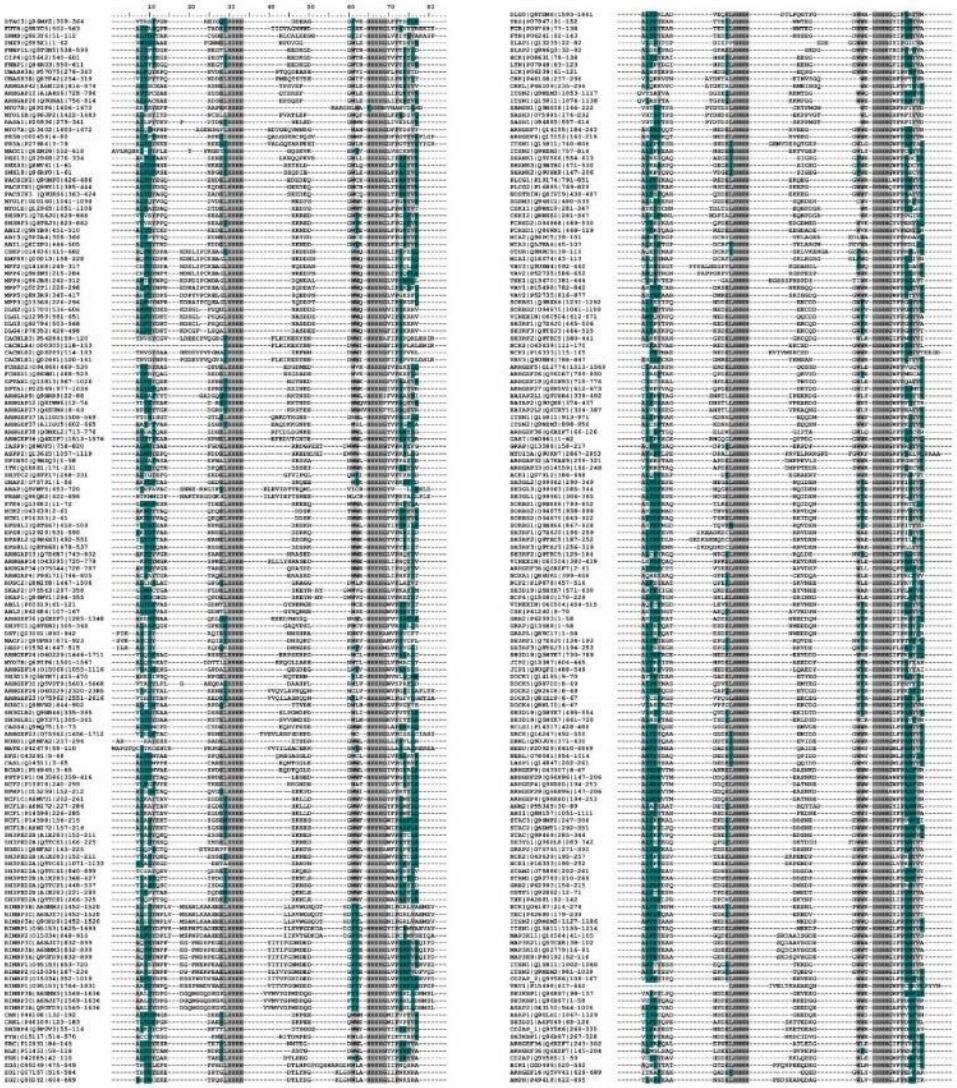

Figure S1. PRM-binding residues in human SH3 domains. The multiple sequence alignment of PRM-binding residues in SH3 domains is generated using ClustalW multiple alignments in BioEdit 7.2.5 software. Amino acids that are either identical or similar are shaded in gray and green, respectively. H-repeats indicate deleted parts of the SH3 domains.

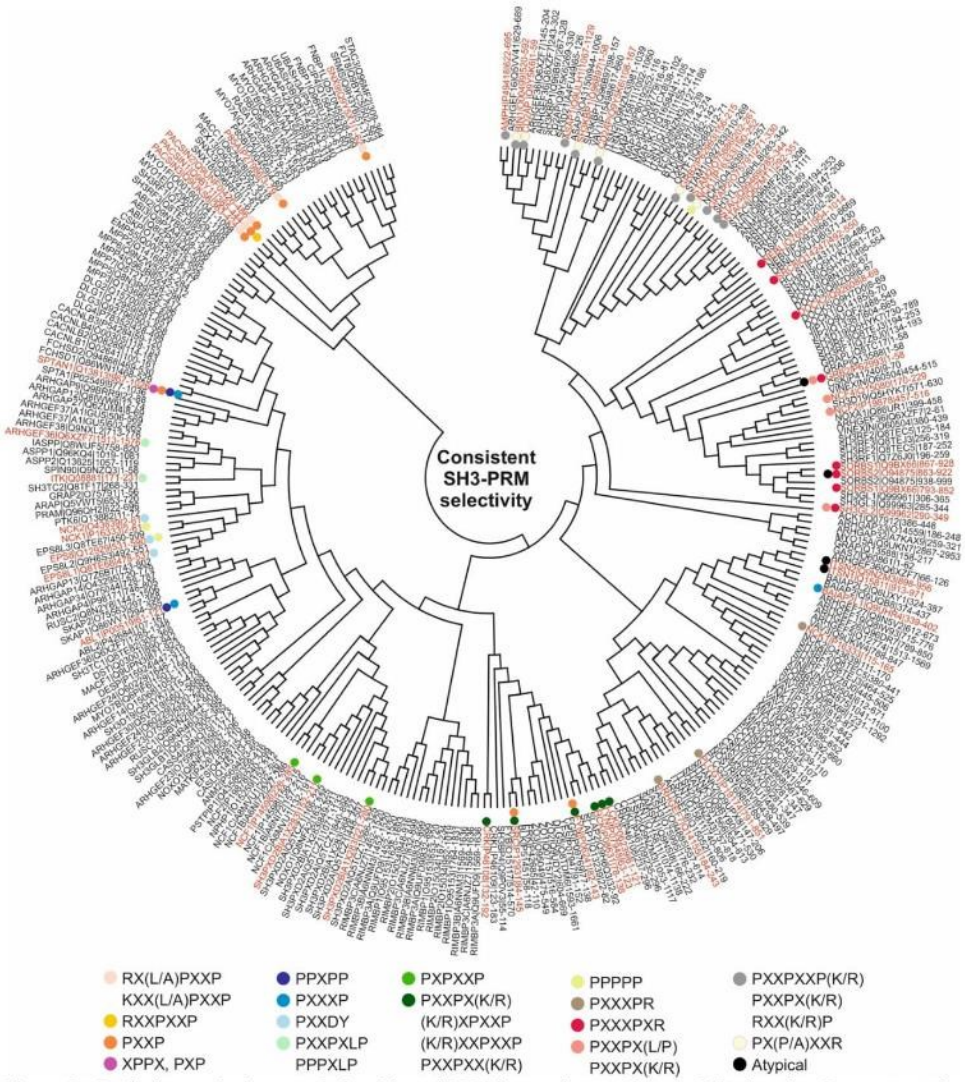

Figure S2. Exploring evolutionary relationships of PRM-interacting residues in SH3 domains. To construct the phylogenetic tree (tree #2), we meticulously examined PRM-interacting residues derived from 298 human SH3 domains, using the MEGA software (version 10.2.6). Using structural and biochemical data from SH3 domains (detailed in Tables S3 and S4), the graphical representation in the tree illustrates interactions between PRMs and their corresponding SH3s. Specific PRM preferences of SH3 domains are highlighted by colored circles, while the related SH3 domains are emphasized in red. Remarkably, the PRMs exhibit clustering patterns consistent with established SH3 domain families, allowing us to systematically categorize them into ten distinct families, each associated with specific PRMs, as shown below (Figure 1).

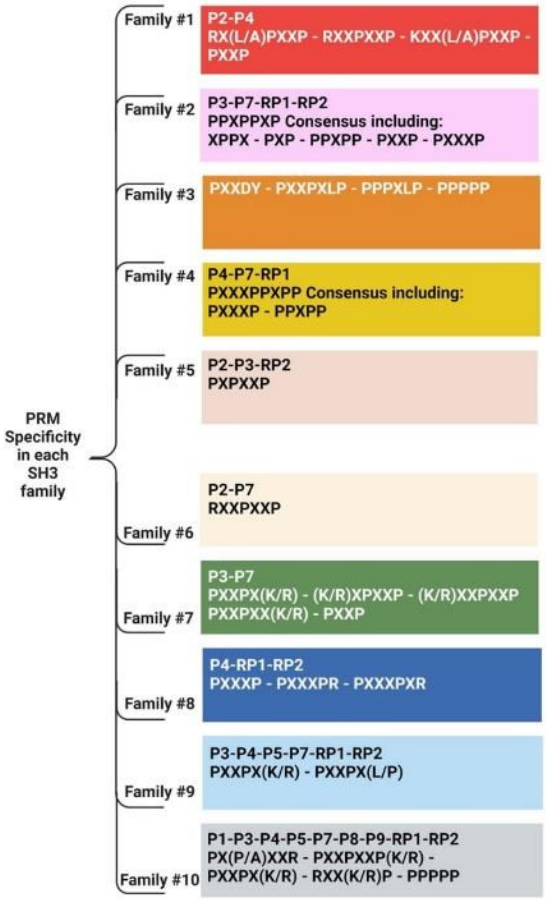

Figure S5. Analysis of SH3-PRM interaction specificity across different SH3 domain families within the human proteome. The top line illustrates the specificity of PRMs interacting with individual SH3 domain families represented by SH3 representatives from P1 to P10 and RP1 to RP2. The lower line delineates the specificity of the PRM motif within each family by evaluating structural and functional analyses of SH3 domains associated with PRMs as documented in published data (Tables S3 and S4).

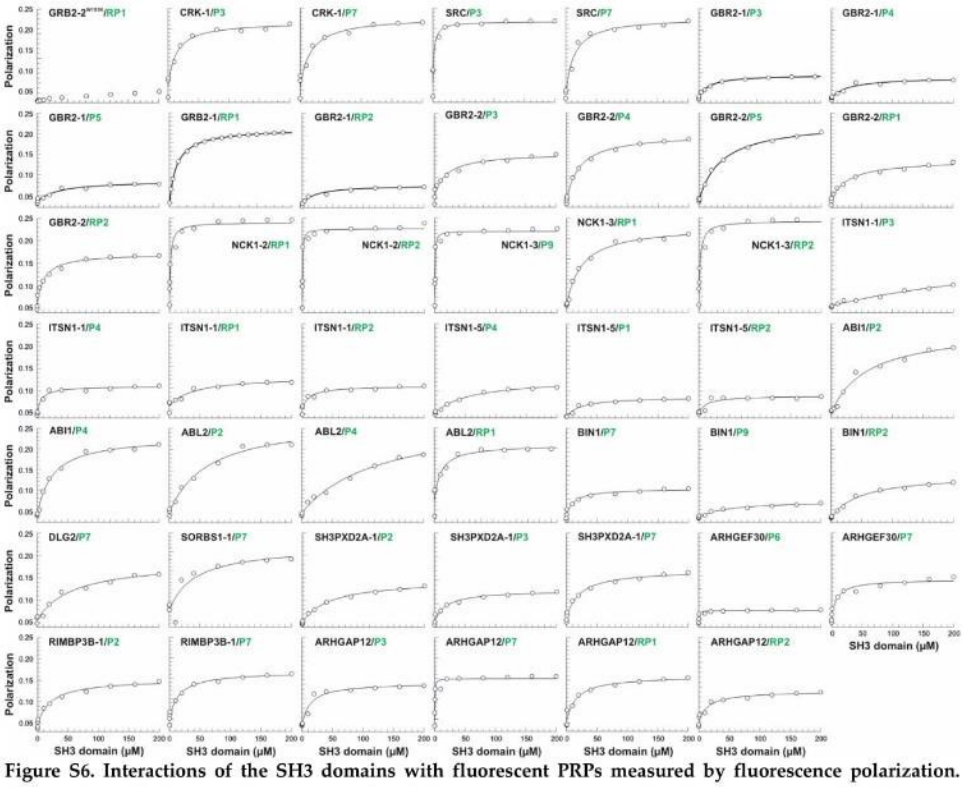

Figure S6. Interactions of the SH3 domains with fluorescent PRPs measured by fluorescence polarization. Fluorescent peptides (0.2 μM) were titrated with increasing concentrations of the corresponding SH3 domains. GRB2-2^{W193K}, defective in the binding of PRPs such as RP1, was used as a negative control as previously described [94]. The x-axis represents SH3 domain concentrations as GST fusion proteins in μM, while the y-axis represents fluorescence polarization. The equilibrium dissociation constants (K_d) for the respective measurements were determined by fitting the titration curves to a quadratic ligand-binding equation (solid lines). All K_d values are summarized in Figure 2B and Table S6. Error bars are derived from the fitting errors.

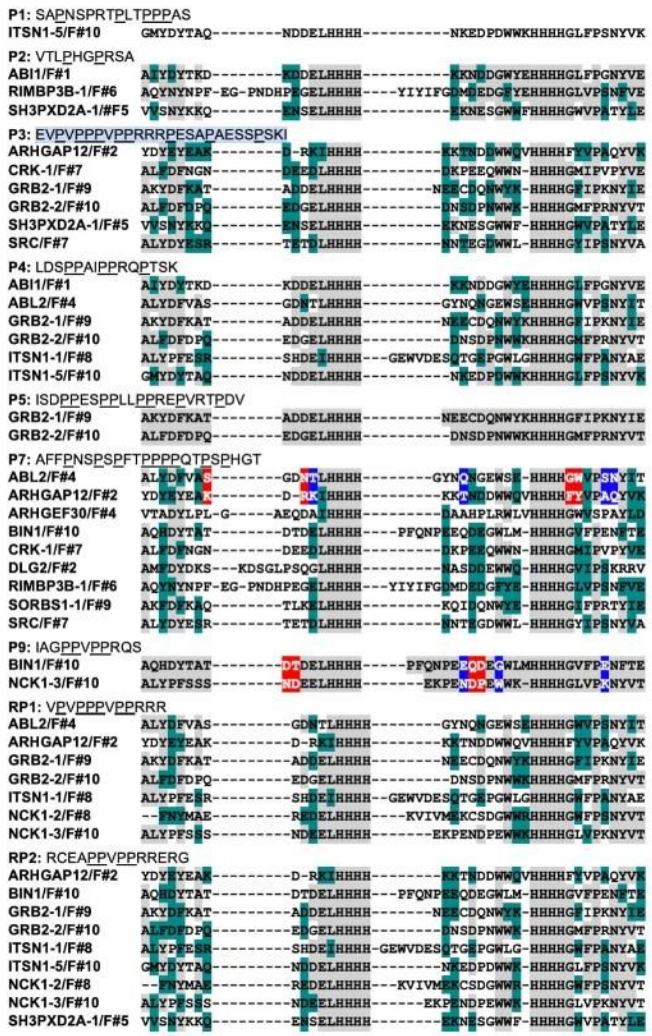

Figure S7. Sequence alignment of PRM-binding residues in representative SH3 domains interacting with specific PRPs. Conserved residues crucial for these interactions are highlighted. H-repeats indicate deleted portions of the SH3 domains. The proteins are also assigned to their respective families according to Figure 1. Residues in red (Set-1) and in blue (Set-2) are non-conserved residues and are the subjects of mutational analysis.

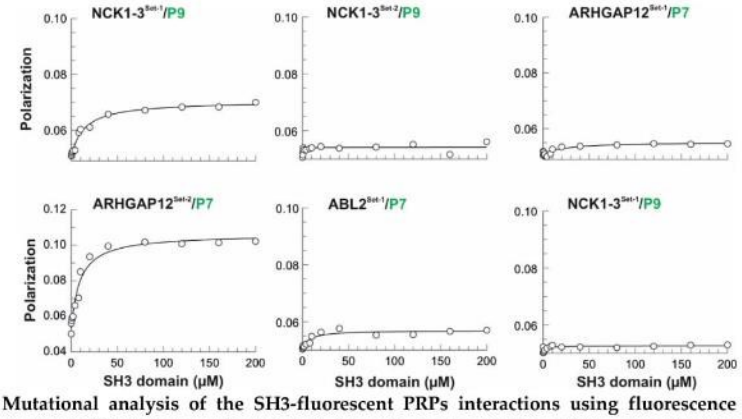

Figure S8. Mutational analysis of the SH3-fluorescent PRPs interactions using fluorescence polarization. Fluorescent peptides (0.2 μM) were titrated with increasing concentrations of the corresponding SH3 domain mutants (see Figure 3A and Table S1). The x-axis represents SH3 domain concentrations as GST fusion proteins in μM, while the y-axis represents fluorescence polarization. The equilibrium dissociation constants (K_d) for the respective measurements were determined by fitting the titration curves to a quadratic ligand-binding equation (solid lines). All K_d values are summarized in Figure 3B. Error bars are derived from the fitting errors.

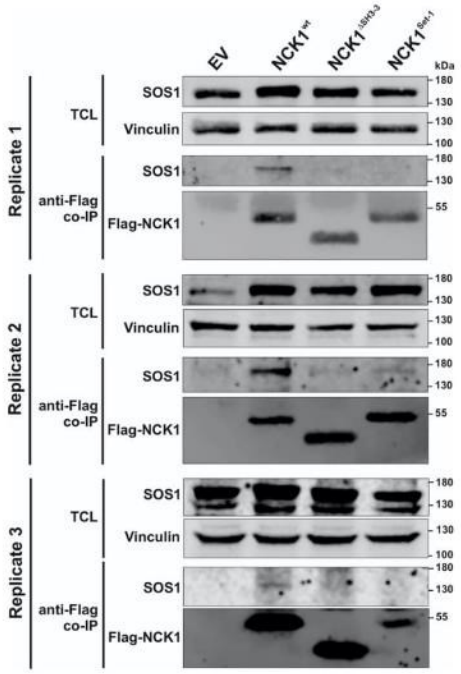

Figure S9. Co-immunoprecipitation of NCK1 with SOS1 in CHO-K1 cells. Experimental replicates of co-immunoprecipitation (co-IP) assays were conducted in CHO-K1 cells, co-transfected with HA-tagged SOS1 and Flag-tagged NCK1^{wt}, NCK1$^{\Delta SH3-3}$, and NCK1^{Set-1}. Co-IP was performed using anti-Flag beads to investigate potential interactions between NCK1 and SOS1 in the cellular context. The immunoblot analysis was performed using anti-SOS1 (1:1000; #sc-256, Santa Cruz) and anti-Flag (#F742, Sigma) antibodies. All three replicates showed co-immunoprecipitation of SOS1 with NCK1^{wt} but not NCK1$^{\Delta SH3-3}$, or NCK1^{Set-1}.

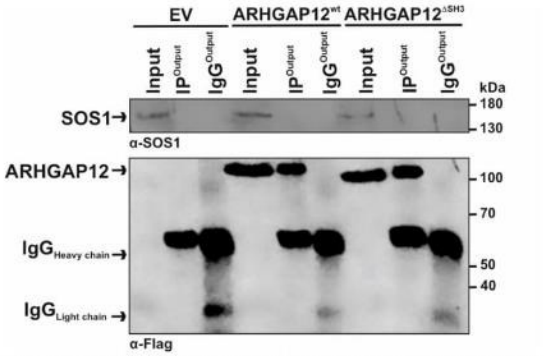

Figure S10. No co-immunoprecipitation of SOS1 with ARHGAP12 in CHO-K1 cells. Co-immunoprecipitation (co-IP) assay was conducted in CHO-K1 cells, co-transfected with HA-tagged SOS1 and Flag-tagged ARHGAP12^{wt}, and ARHGAP12$^{\Delta SH3-3}$. Co-IP was performed using protein A beads to investigate potential interactions between ARHGAP12 and SOS1 in the cellular context. Lysates from these transfected cells were subjected to Co-IP using anti-Flag (1:50; #F3165, Sigma) and anti-IgG (1:50; # sc-2025, Santa Cruz) antibodies coupled to protein A beads. The immunoblot analysis was performed using anti-SOS1 (1:1000; #sc-256, Santa Cruz) and anti-Flag (#F742, Sigma) antibodies. immunoblot analysis using anti-SOS1 (1:1000; #sc-256, Santa Cruz) and anti-Flag (#F742, Sigma) antibodies revealed no interaction neither ARHGAP12^{wt} nor ARHGAP12$^{\Delta SH3}$ with HA-SOS1.

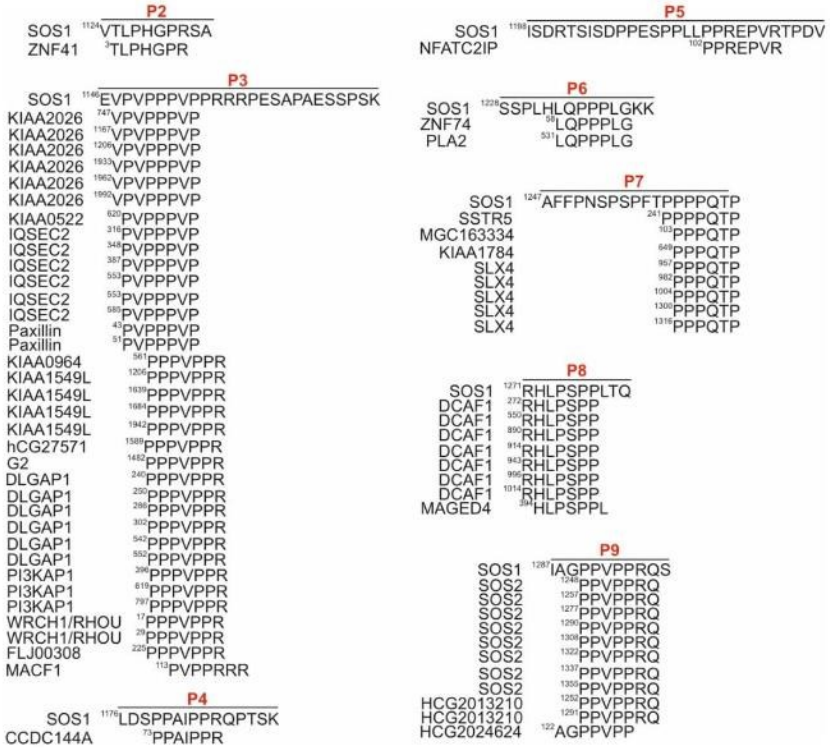

Figure S11. SOS1 homologous PRM sequences found in other human proteins. BLAST searches associated with each SOS1 PRD peptide identified homologous sequences in other human proteins (See also Table S7 and Figure 4).

References

1. Goretzki, B., N. A. Glogowski, E. Diehl, E. Duchardt-Ferner, C. Hacker, R. Gaudet, and U. A. Hellmich. "Structural Basis of Trpv4 n Terminus Interaction with Syndapin/Pacsin1-3 and Pip(2)." *Structure* 26, no. 12 (2018): 1583-93.e5.
2. Tossavainen, Helena, Hasan Uğurlu, Mikael Karjalainen, Maarit Hellman, Lina Antenucci, Riku Fagerlund, Kalle Saksela, and Perttu Permi. "Structure of Snx9 Sh3 in Complex with a Viral Ligand Reveals the Molecular Basis of Its Unique Specificity for Alanine-Containing Class I Sh3 Motifs." *Structure* 30, no. 6 (2022): 828-39. e6.
3. Batra-Safferling, R., J. Granzin, S. Mödder, S. Hoffmann, and D. Willbold. "Structural Studies of the Phosphatidylinositol 3-Kinase (Pi3k) Sh3 Domain in Complex with a Peptide Ligand: Role of the Anchor Residue in Ligand Binding." *Biol Chem* 391, no. 1 (2010): 33-42.
4. Casares, S., E. Ab, H. Eshuis, O. Lopez-Mayorga, N. A. van Nuland, and F. Conejero-Lara. "The High-Resolution Nmr Structure of the R21a Spc-Sh3:P41 Complex: Understanding the Determinants of Binding Affinity by Comparison with Abl-Sh3." *BMC Struct Biol* 7 (2007): 22.
5. Gushchina, L. V., A. G. Gabdulkhakov, S. V. Nikonov, and V. V. Filimonov. "High-Resolution Crystal Structure of Spectrin Sh3 Domain Fused with a Proline-Rich Peptide." *J Biomol Struct Dyn* 29, no. 3 (2011): 485-95.
6. Takeuchi, Koh, Hailin Yang, Elise Ng, Sungh-youk Park, Zhen-Yu J Sun, Ellis L Reinherz, and Gerhard Wagner. "Structural and Functional Evidence That Nck Interaction with Cd3ε Regulates T-Cell Receptor Activity." *Journal of molecular biology* 380, no. 4 (2008): 704-16.
7. Aitio, Olli, Maarit Hellman, Tapio Kesti, Iivari Kleino, Olga Samuilova, Kimmo Pääkkönen, Helena Tossavainen, Kalle Saksela, and Perttu Permi. "Structural Basis of Pxxdy Motif Recognition in Sh3 Binding." *Journal of Molecular Biology* 382, no. 1 (2008): 167-78.
8. Polle, Lilia, Luciano A Rigano, Rowan Julian, Keith Ireton, and Wolf-Dieter Schubert. "Structural Details of Human Tuba Recruitment by Inlc of Listeria Monocytogenes Elucidate Bacterial Cell-Cell Spreading." *Structure* 22, no. 2 (2014): 304-14.
9. Cámara-Artigas, A., A. Palencia, J. C. Martínez, I. Luque, J. A. Gavira, and J. M. García-Ruiz. "Crystallization by Capillary Counter-Diffusion and Structure Determination of the N114a Mutant of the Sh3 Domain of Abl Tyrosine Kinase Complexed with a High-Affinity Peptide Ligand." *Acta Crystallogr D Biol Crystallogr* 63, no. Pt 5 (2007): 646-52.
10. Grover, Prerna, Haibin Shi, Matthew Baumgartner, Carlos J Camacho, and Thomas E Smithgall. "Fluorescence Polarization Screening Assays for Small Molecule Allosteric Modulators of Abl Kinase Function." *PLoS One* 10, no. 7 (2015): e0133590.
11. Palencia, A., A. Camara-Artigas, M. T. Pisabarro, J. C. Martinez, and I. Luque. "Role of Interfacial Water Molecules in Proline-Rich Ligand Recognition by the Src Homology 3 Domain of Abl." *J Biol Chem* 285, no. 4 (2010): 2823-33.
12. Musacchio, Andrea, Matti Saraste, and Matthias Wilmanns. "High-Resolution Crystal Structures of Tyrosine Kinase Sh3 Domains Complexed with Proline-Rich Peptides." *Nature structural biology* 1, no. 8 (1994): 546-51.
13. Groemping, Y., K. Lapouge, S. J. Smerdon, and K. Rittinger. "Molecular Basis of Phosphorylation-Induced Activation of the Nadph Oxidase." *Cell* 113, no. 3 (2003): 343-55.
14. Ogura, K., I. Nobuhisa, S. Yuzawa, R. Takeya, S. Torikai, K. Saikawa, H. Sumimoto, and F. Inagaki. "Nmr Solution Structure of the Tandem Src Homology 3 Domains of P47phox Complexed with a P22phox-Derived Proline-Rich Peptide." *J Biol Chem* 281, no. 6 (2006): 3660-8.
15. Wu, Xiaodong, Beatrice Knudsen, Stephan M. Feller, Jie Zheng, Andrej Sali, David Cowburn, Hidesaburo Hanafusa, and John Kuriyan. "Structural Basis for the Specific Interaction of Lysine-Containing Proline-Rich Peptides with the N-Terminal Sh3 Domain of C-Crk." *Structure* 3, no. 2 (1995): 215-26.
16. Bhatt, Veer S, Danyun Zeng, Inna Krieger, James C Sacchettini, and Jae-Hyun Cho. "Binding Mechanism of the N-Terminal Sh3 Domain of Crkii and Proline-Rich Motifs in Cabl." *Biophysical journal* 110, no. 12 (2016): 2630-41.
17. Nguyen, Jack T., Christoph W. Turck, Fred E. Cohen, Ronald N. Zuckermann, and Wendell A. Lim. "Exploiting the Basis of Proline Recognition by Sh3 and Ww Domains: Design of N-Substituted Inhibitors." *Science* 282, no. 5396 (1998): 2088-92.
18. Schmidt, Holger, Silke Hoffmann, Tuyen Tran, Matthias Stoldt, Thomas Stangler, Katja Wiesehan, and Dieter Willbold. "Solution Structure of a Hck Sh3 Domain Ligand Complex Reveals Novel Interaction Modes." *Journal of molecular biology* 365, no. 5 (2007): 1517-32.
19. Camara-Artigas, Ana, Emilia Ortiz-Salmeron, Montserrat Andujar-Sánchez, Julio Bacarizo, and Jose Manuel Martin-Garcia. "The Role of Water Molecules in the Binding of Class I and Ii Peptides to the Sh3 Domain of

the Fyn Tyrosine Kinase." *Acta Crystallographica Section F: Structural Biology Communications* 72, no. 9 (2016): 707-12.

20. Renzoni, D. A., D. J. Pugh, G. Siligardi, P. Das, C. J. Morton, C. Rossi, M. D. Waterfield, I. D. Campbell, and J. E. Ladbury. "Structural and Thermodynamic Characterization of the Interaction of the Sh3 Domain from Fyn with the Proline-Rich Binding Site on the P85 Subunit of Pi3-Kinase." *Biochemistry* 35, no. 49 (1996): 15646-53.
21. Martin-Garcia, J. M., I. Luque, J. Ruiz-Sanz, and A. Camara-Artigas. "The Promiscuous Binding of the Fyn Sh3 Domain to a Peptide from the Ns5a Protein." *Acta Crystallogr D Biol Crystallogr* 68, no. Pt 8 (2012): 1030-40.
22. Schweimer, K., S. Hoffmann, F. Bauer, U. Friedrich, C. Kardinal, S. M. Feller, B. Biesinger, and H. Sticht. "Structural Investigation of the Binding of a Herpesviral Protein to the Sh3 Domain of Tyrosine Kinase Lck." *Biochemistry* 41, no. 16 (2002): 5120-30.
23. Feng, S., C. Kasahara, R. J. Rickles, and S. L. Schreiber. "Specific Interactions Outside the Proline-Rich Core of Two Classes of Src Homology 3 Ligands." *Proc Natl Acad Sci U S A* 92, no. 26 (1995): 12408-15.
24. Bacarizo, J., and A. Camara-Artigas. "Atomic Resolution Structures of the C-Src Sh3 Domain in Complex with Two High-Affinity Peptides from Classes I and Ii." *Acta Crystallogr D Biol Crystallogr* 69, no. Pt 5 (2013): 756-66.
25. Ghose, R., A. Shekhtman, M. J. Goger, H. Ji, and D. Cowburn. "A Novel, Specific Interaction Involving the Csk Sh3 Domain and Its Natural Ligand." *Nat Struct Biol* 8, no. 11 (2001): 998-1004.
26. Feng, Sibo, Tarun M. Kapoor, Fumiyuki Shirai, Andrew P. Combs, and Stuart L. Schreiber. "Molecular Basis for the Binding of Sh3 Ligands with Non-Peptide Elements Identified by Combinatorial Synthesis." *Chemistry & Biology* 3, no. 8 (1996): 661-70.
27. Feng, S., J. K. Chen, H. Yu, J. A. Simon, and S. L. Schreiber. "Two Binding Orientations for Peptides to the Src Sh3 Domain: Development of a General Model for Sh3-Ligand Interactions." *Science* 266, no. 5188 (1994): 1241-7.
28. Bacarizo, J., S. Martínez-Rodríguez, and A. Cámara-Artigas. "Structure of the C-Src-Sh3 Domain in Complex with a Proline-Rich Motif of Ns5a Protein from the Hepatitis C Virus." *J Struct Biol* 189, no. 1 (2015): 67-72.
29. Teyra, Joan, Haiming Huang, Shobhit Jain, Xinyu Guan, Aiping Dong, Yanli Liu, Wolfram Tempel, Jinrong Min, Yufeng Tong, and Philip M Kim. "Comprehensive Analysis of the Human Sh3 Domain Family Reveals a Wide Variety of Non-Canonical Specificities." *Structure* 25, no. 10 (2017): 1598-610. e3.
30. Mott, Helen R, Daniel Nietlispach, Katrina A Evetts, and Darerca Owen. "Structural Analysis of the Sh3 Domain of B-Pix and Its Interaction with A-P21 Activated Kinase (Pak)." *Biochemistry* 44, no. 33 (2005): 10977-83.
31. Jozic, Daniela, Nayra Cárdenes, Yonathan Lissanu Deribe, Gabriel Moncalián, Daniela Hoeller, Yvonne Groemping, Ivan Dikic, Katrin Rittinger, and Jerónimo Bravo. "Cbl Promotes Clustering of Endocytic Adaptor Proteins." *Nature structural & molecular biology* 12, no. 11 (2005): 972-79.
32. Janz, Jay M, Thomas P Sakmar, and K Christopher Min. "A Novel Interaction between Atrophin-Interacting Protein 4 and B-P21-Activated Kinase-Interactive Exchange Factor Is Mediated by an Sh3 Domain." *Journal of Biological Chemistry* 282, no. 39 (2007): 28893-903.
33. Desrochers, Guillaume, Laurent Cappadocia, Mathieu Lussier-Price, Anh-Tien Ton, Riham Ayoubi, Adrian Serohijos, James G Omichinski, and Annie Angers. "Molecular Basis of Interactions between Sh3 Domain-Containing Proteins and the Proline-Rich Region of the Ubiquitin Ligase Itch." *Journal of Biological Chemistry* 292, no. 15 (2017): 6325-38.
34. Hoelz, A., J. M. Janz, S. D. Lawrie, B. Corwin, A. Lee, and T. P. Sakmar. "Crystal Structure of the Sh3 Domain of Betapix in Complex with a High Affinity Peptide from Pak2." *J Mol Biol* 358, no. 2 (2006): 509-22.
35. Aitio, Olli, Maarit Hellman, Arunas Kazlauskas, Didier F Vingadassalom, John M Leong, Kalle Saksela, and Perttu Permi. "Recognition of Tandem Pxxp Motifs as a Unique Src Homology 3-Binding Mode Triggers Pathogen-Driven Actin Assembly." *Proceedings of the National Academy of Sciences* 107, no. 50 (2010): 21743-48.
36. Deng, L., C. A. Velikovsky, C. P. Swaminathan, S. Cho, and R. A. Mariuzza. "Structural Basis for Recognition of the T Cell Adaptor Protein Slp-76 by the Sh3 Domain of Phospholipase Cgamma1." *J Mol Biol* 352, no. 1 (2005): 1-10.
37. Vidal, Michel, Nathalie Goudreau, Fabrice Cornille, Didier Cussac, Edith Gincel, and Christiane Garbay. "Molecular and Cellular Analysis of Grb2 Sh3 Domain Mutants: Interaction with Sos and Dynamin." *Journal of molecular biology* 290, no. 3 (1999): 717-30.
38. Wittekind, M., C. Mapelli, V. Lee, V. Goldfarb, M. S. Friedrichs, C. A. Meyers, and L. Mueller. "Solution Structure of the Grb2 N-Terminal Sh3 Domain Complexed with a Ten-Residue Peptide Derived from Sos: Direct Refinement against Noes, J-Couplings and 1h and 13c Chemical Shifts." *J Mol Biol* 267, no. 4 (1997): 933-52.
39. Hanawa-Suetsugu, Kyoko, Mutsuko Kukimoto-Niino, Chiemi Mishima-Tsumagari, Ryogo Akasaka, Noboru Ohsawa, Shun-ichi Sekine, Takuhiro Ito, Naoya Tochio, Seizo Koshiba, and Takanori Kigawa. "Structural

Basis for Mutual Relief of the Rac Guanine Nucleotide Exchange Factor Dock2 and Its Partner Elmo1 from Their Autoinhibited Forms." *Proceedings of the National Academy of Sciences* 109, no. 9 (2012): 3305-10.

40. Kami, Keiichiro, Ryu Takeya, Hideki Sumimoto, and Daisuke Kohda. "Diverse Recognition of Non-Pxxp Peptide Ligands by the Sh3 Domains from P67phox, Grb2 and Pex13p." *The EMBO Journal* 21, no. 16 (2002): 4268-76.
41. Massenet, Claire, Sylvie Chenavas, Claudine Cohen-Addad, Marie-Claire Dagher, Gérard Brandolin, Eva Pebay-Peyroula, and Franck Fieschi. "Effects of P47phox C Terminus Phosphorylations on Binding Interactions with P40phox and P67phox: Structural and Functional Comparison of P40phox and P67phox Sh3 Domains." *Journal of Biological Chemistry* 280, no. 14 (2005): 13752-61.
42. Hashimoto, Shigeru, Mayumi Hirose, Ari Hashimoto, Masaki Morishige, Atsuko Yamada, Harumi Hosaka, Ken-ichi Akagi, Eiji Ogawa, Chitose Oneyama, and Tsutomu Agatsuma. "Targeting Amap1 and Cortactin Binding Bearing an Atypical Src Homology 3/Proline Interface for Prevention of Breast Cancer Invasion and Metastasis." *Proceedings of the National Academy of Sciences* 103, no. 18 (2006): 7036-41.
43. Liu, W., S. M. MacGrath, A. J. Koleske, and T. J. Boggon. "Lysozyme Contamination Facilitates Crystallization of a Heterotrimeric Cortactin-Arg-Lysozyme Complex." *Acta Crystallogr Sect F Struct Biol Cryst Commun* 68, no. Pt 2 (2012): 154-8.
44. Gehmlich, Katja, Nikos Pinotsis, Katrin Hayeß, Peter FM van der Ven, Hendrik Milting, Aly El Banayosy, Reiner Körfer, Matthias Wilmanns, Elisabeth Ehler, and Dieter O Fürst. "Paxillin and Ponsin Interact in Nascent Costameres of Muscle Cells." *Journal of molecular biology* 369, no. 3 (2007): 665-82.
45. Zhao, Debiao, Xuejuan Wang, Junhui Peng, Chongyuan Wang, Fudong Li, Qianqian Sun, Yibo Zhang, Jiahai Zhang, Gang Cai, and Xiaobing Zuo. "Structural Investigation of the Interaction between the Tandem Sh3 Domains of C-Cbl-Associated Protein and Vinculin." *Journal of structural biology* 187, no. 2 (2014): 194-205.
46. Eulitz, Stefan, Florian Sauer, Marie-Cecile Pelissier, Prisca Boisguerin, Sibylle Molt, Julia Schuld, Zacharias Orfanos, Rudolf A Kley, Rudolf Volkmer, and Matthias Wilmanns. "Identification of Xin-Repeat Proteins as Novel Ligands of the Sh3 Domains of Nebulin and Nebulette and Analysis of Their Interaction During Myofibril Formation and Remodeling." *Molecular biology of the cell* 24, no. 20 (2013): 3215-26.
47. Liao, Tsung-Jen, Hyunbum Jang, Ruth Nussinov, and David Fushman. "High-Affinity Interactions of the Nsh3/Csh3 Domains of Grb2 with the C-Terminal Proline-Rich Domain of Sos1." *Journal of the American Chemical Society* 142, no. 7 (2020): 3401-11.
48. Harkiolaki, M., T. Tsirka, M. Lewitzky, P. C. Simister, D. Joshi, L. E. Bird, E. Y. Jones, N. O'Reilly, and S. M. Feller. "Distinct Binding Modes of Two Epitopes in Gab2 That Interact with the Sh3c Domain of Grb2." *Structure* 17, no. 6 (2009): 809-22.
49. Rouka, Evgenia, Philip C Simister, Melanie Janning, Joerg Kumbrink, Tassos Konstantinou, João RC Muniz, Dhira Joshi, Nicola O'Reilly, Rudolf Volkmer, and Brigitte Ritter. "Differential Recognition Preferences of the Three Src Homology 3 (Sh3) Domains from the Adaptor Cd2-Associated Protein (Cd2ap) and Direct Association with Ras and Rab Interactor 3 (Rin3)." *Journal of Biological Chemistry* 290, no. 42 (2015): 25275-92.
50. Moncalián, Gabriel, Nayra Cárdenes, Yonathan Lissanu Deribe, Mercedes Spínola-Amilibia, Ivan Dikic, and Jerónimo Bravo. "Atypical Polyproline Recognition by the Cms N-Terminal Src Homology 3 Domain." *Journal of Biological Chemistry* 281, no. 50 (2006): 38845-53.
51. Hologne, Maggy, François-Xavier Cantrelle, Gwladys Riviere, Florence Guillière, Xavier Trivelli, and Olivier Walker. "Nmr Reveals the Interplay among the Amsh Sh3 Binding Motif, Stam2, and Lys63-Linked Diubiquitin." *Journal of molecular biology* 428, no. 22 (2016): 4544-58.
52. Kaneko, Tomonori, Takashi Kumasaka, Tadashi Ganbe, Takao Sato, Keiji Miyazawa, Naomi Kitamura, and Nobuo Tanaka. "Structural Insight into Modest Binding of a Non-Pxxp Ligand to the Signal Transducing Adaptor Molecule-2 Src Homology 3 Domain." *Journal of Biological Chemistry* 278, no. 48 (2003): 48162-68.
53. Pineda-Lucena, A., C. S. Ho, D. Y. Mao, Y. Sheng, R. C. Laister, R. Muhandiram, Y. Lu, B. T. Seet, S. Katz, T. Szyperski, L. Z. Penn, and C. H. Arrowsmith. "A Structure-Based Model of the C-Myc/Bin1 Protein Interaction Shows Alternative Splicing of Bin1 and C-Myc Phosphorylation Are Key Binding Determinants." *J Mol Biol* 351, no. 1 (2005): 182-94.
54. Lewitzky, M., M. Harkiolaki, M. C. Domart, E. Y. Jones, and S. M. Feller. "Mona/Gads Sh3c Binding to Hematopoietic Progenitor Kinase 1 (Hpk1) Combines an Atypical Sh3 Binding Motif, R/Kxxk, with a Classical Pxxp Motif Embedded in a Polyproline Type Ii (Ppii) Helix." *J Biol Chem* 279, no. 27 (2004): 28724-32.
55. Harkiolaki, M., M. Lewitzky, R. J. Gilbert, E. Y. Jones, R. P. Bourette, G. Mouchiroud, H. Sondermann, I. Moarefi, and S. M. Feller. "Structural Basis for Sh3 Domain-Mediated High-Affinity Binding between Mona/Gads and Slp-76." *Embo j* 22, no. 11 (2003): 2571-82.
56. Liu, Q., D. Berry, P. Nash, T. Pawson, C. J. McGlade, and S. S. Li. "Structural Basis for Specific Binding of the Gads Sh3 Domain to an Rxxk Motif-Containing Slp-76 Peptide: A Novel Mode of Peptide Recognition." *Mol Cell* 11, no. 2 (2003): 471-81.

57. Dimasi, N. "Crystal Structure of the C-Terminal Sh3 Domain of the Adaptor Protein Gads in Complex with Slp-76 Motif Peptide Reveals a Unique Sh3-Sh3 Interaction." *Int J Biochem Cell Biol* 39, no. 1 (2007): 109-23.
58. Jia, X., L. Lin, S. Xu, L. Li, Z. Wei, C. Yu, and F. Niu. "Crystal Structure of the Sh3 Domain of Asap1 in Complex with the Proline Rich Motif (Prm) of Mical1 Reveals a Unique Sh3/Prm Interaction Mode." *Int J Mol Sci* 24, no. 2 (2023).
59. Wong King Yuen, Siobhan M., Marta Campiglio, Ching-Chieh Tung, Bernhard E. Flucher, and Filip Van Petegem. "Structural Insights into Binding of Stac Proteins to Voltage-Gated Calcium Channels." *Proceedings of the National Academy of Sciences* 114, no. 45 (2017): E9520-E28.
60. Desrochers, Guillaume, Mathieu Lussier-Price, James G. Omichinski, and Annie Angers. "Multiple Src Homology 3 Binding to the Ubiquitin Ligase Itch Conserved Proline-Rich Region." *Biochemistry* 54, no. 50 (2015): 7345-54.
61. Goretzki, Benedikt, Nina A Glogowski, Erika Diehl, Elke Duchardt-Ferner, Carolin Hacker, Rachelle Gaudet, and Ute A Hellmich. "Structural Basis of Trpv4 N Terminus Interaction with Syndapin/Pacsin1-3 and Pip2." *Structure* 26, no. 12 (2018): 1583-93. e5.
62. Yu, Hongtao, James K Chen, Sibo Feng, David C Dalgarno, Andrew W Brauer, and Stuart L Schrelber. "Structural Basis for the Binding of Proline-Rich Peptides to Sh3 Domains." *Cell* 76, no. 5 (1994): 933-45.
63. Gushchina, LV, AG Gabdulkhakov, and VV Filimonov. "Design and Structural Thermodynamic Studies of the Chimeric Protein Derived from Spectrin Sh3 Domain." *Molecular biology* 43 (2009): 444-52.
64. Banjade, Sudeep, Qiong Wu, Anuradha Mittal, William B Peeples, Rohit V Pappu, and Michael K Rosen. "Conserved Interdomain Linker Promotes Phase Separation of the Multivalent Adaptor Protein Nck." *Proceedings of the National Academy of Sciences* 112, no. 47 (2015): E6426-E35.
65. Mongioví, A. M., P. R. Romano, S. Panni, M. Mendoza, W. T. Wong, A. Musacchio, G. Cesareni, and P. P. Di Fiore. "A Novel Peptide-Sh3 Interaction." *Embo j* 18, no. 19 (1999): 5300-9.
66. Andersen, Thorny Cesilie Bie, Per Eugen Kristiansen, Zsuzsa Huszenicza, Maria U. Johansson, Ramakrishna Prabhu Gopalakrishnan, Hanna Kjelstrup, Scott Boyken, Vibeke Sundvold-Gjerstad, Stine Granum, Morten Sørli, Paul Hoff Backe, D. Bruce Fulton, B. Göran Karlsson, Amy H. Andreotti, and Anne Spurkland. "The Sh3 Domains of the Protein Kinases Itk and Lck Compete for Adjacent Sites on T Cell–Specific Adapter Protein." *Journal of Biological Chemistry* 294, no. 42 (2019): 15480-94.
67. Pisabarro, MT, and L Serrano. "Rational Design of Specific High-Affinity Peptide Ligands for the Abl-Sh3 Domain." *Biochemistry* 35, no. 33 (1996): 10634-40.
68. Merő, B., K. Koprivanacz, A. Cserkaszky, L. Radnai, V. Vas, G. Kudlik, G. Gógl, P. Sok, L. Póti Á, B. Szeder, L. Nyitray, A. Reményi, M. Geiszt, and L. Buday. "Characterization of the Intramolecular Interactions and Regulatory Mechanisms of the Scaffold Protein Tks4." *Int J Mol Sci* 22, no. 15 (2021).
69. Knudsen, B. S., J. Zheng, S. M. Feller, J. P. Mayer, S. K. Burrell, D. Cowburn, and H. Hanafusa. "Affinity and Specificity Requirements for the First Src Homology 3 Domain of the Crk Proteins." *Embo j* 14, no. 10 (1995): 2191-8.
70. Sarkar, P., C. Reichman, T. Saleh, R. B. Birge, and C. G. Kalodimos. "Proline Cis-Trans Isomerization Controls Autoinhibition of a Signaling Protein." *Mol Cell* 25, no. 3 (2007): 413-26.
71. Matsuda, Michiyuki, Satoshi Ota, Ryuji Tanimura, Haruki Nakamura, Koozi Matuoka, Tadaomi Takenawa, Kazuo Nagashima, and Takeshi Kurata. "Interaction between the Amino-Terminal Sh3 Domain of Crk and Its Natural Target Proteins*." *Journal of Biological Chemistry* 271, no. 24 (1996): 14468-72.
72. Lee, C. H., B. Leung, M. A. Lemmon, J. Zheng, D. Cowburn, J. Kuriyan, and K. Saksela. "A Single Amino Acid in the Sh3 Domain of Hck Determines Its High Affinity and Specificity in Binding to Hiv-1 Nef Protein." *Embo j* 14, no. 20 (1995): 5006-15.
73. Morton, Craig J, David JR Pugh, Emma LJ Brown, Jan D Kahmann, Debora AC Renzoni, and Iain D Campbell. "Solution Structure and Peptide Binding of the Sh3 Domain from Human Fyn." *Structure* 4, no. 6 (1996): 705-14.
74. Bauer, Finn, and Heinrich Sticht. "A Proline to Glycine Mutation in the Lck Sh3-Domain Affects Conformational Sampling and Increases Ligand Binding Affinity." *FEBS letters* 581, no. 8 (2007): 1555-60.
75. Zeng, Longhui, Ivan Palaia, Anđela Šarić, and Xiaolei Su. "Plcγ1 Promotes Phase Separation of T Cell Signaling Components." *Journal of Cell Biology* 220, no. 6 (2021).
76. Aitio, O., M. Hellman, A. Kazlauskas, D. F. Vingadassalom, J. M. Leong, K. Saksela, and P. Permi. "Recognition of Tandem Pxxp Motifs as a Unique Src Homology 3-Binding Mode Triggers Pathogen-Driven Actin Assembly." *Proc Natl Acad Sci U S A* 107, no. 50 (2010): 21743-8.
77. Goudreau, N, F Cornille, M Duchesne, F Parker, B Tocque, C Garbay, and BP Roques. "Nmr Structure of the N-Terminal Sh3 Domain of Grb2 and Its Complex with a Proline-Rich Peptide from Sos." *Nature structural biology* 1, no. 12 (1994): 898-907.

78. McDonald, Caleb B, Kenneth L Seldeen, Brian J Deegan, and Amjad Farooq. "Structural Basis of the Differential Binding of the Sh3 Domains of Grb2 Adaptor to the Guanine Nucleotide Exchange Factor Sos1." *Archives of biochemistry and biophysics* 479, no. 1 (2008): 52-62.
79. ———. "Sh3 Domains of Grb2 Adaptor Bind to Pxψpxr Motifs within the Sos1 Nucleotide Exchange Factor in a Discriminate Manner." *Biochemistry* 48, no. 19 (2009): 4074-85.
80. Grabs, Detlev, Vladimir I Slepnev, Zhou Songyang, Carol David, Mary Lynch, Lewis C Cantley, and Pietro De Camilli. "The Sh3 Domain of Amphiphysin Binds the Proline-Rich Domain of Dynamin at a Single Site That Defines a New Sh3 Binding Consensus Sequence." *Journal of Biological Chemistry* 272, no. 20 (1997): 13419-25.
81. Lasorsa, Alessia, Krishnendu Bera, Idir Malki, Elian Dupré, François-Xavier Cantrelle, Hamida Merzougui, Davy Sinnaeve, Xavier Hanoulle, Jozef Hritz, and Isabelle Landrieu. "Conformation and Affinity Modulations by Multiple Phosphorylation Occurring in the Bin1 Sh3 Domain Binding Site of the Tau Protein Proline-Rich Region." *Biochemistry* 62, no. 11 (2023): 1631-42.
82. Hutchings, Nicholas J, Nicholas Clarkson, Robert Chalkley, A Neil Barclay, and Marion H Brown. "Linking the T Cell Surface Protein Cd2 to the Actin-Capping Protein Capz Via Cms and Cin85." *Journal of Biological Chemistry* 278, no. 25 (2003): 22396-403.
83. Fang, Nancy N, Gerard T Chan, Mang Zhu, Sophie A Comyn, Avinash Persaud, Raymond J Deshaies, Daniela Rotin, Joerg Gsponer, and Thibault Mayor. "Rsp5/Nedd4 Is the Main Ubiquitin Ligase That Targets Cytosolic Misfolded Proteins Following Heat Stress." *Nature cell biology* 16, no. 12 (2014): 1227-37.
84. Peil, Lauri, Agata L Starosta, Jürgen Lassak, Gemma C Atkinson, Kai Virumäe, Michaela Spitzer, Tanel Tenson, Kirsten Jung, Jaanus Remme, and Daniel N Wilson. "Distinct Xppx Sequence Motifs Induce Ribosome Stalling, Which Is Rescued by the Translation Elongation Factor Ef-P." *Proceedings of the National Academy of Sciences* 110, no. 38 (2013): 15265-70.
85. Hupp, Ted R, and Malcolm Walkinshaw. "Multienzyme Assembly of a P53 Transcription Complex." *Nature structural & molecular biology* 14, no. 10 (2007): 885-87.
86. Dornan, David, Harumi Shimizu, Lindsay Burch, Amanda J Smith, and Ted R Hupp. "The Proline Repeat Domain of P53 Binds Directly to the Transcriptional Coactivator P300 and Allosterically Controls DNA-Dependent Acetylation of P53." *Molecular and cellular biology* 23, no. 23 (2003): 8846-61.
87. Guruprasad, L, V Dhanaraj, D Timm, TL Blundell, I Gout, and MD Waterfield. "The Crystal Structure of the N-Terminal Sh3 Domain of Grb2." *Journal of molecular biology* 248, no. 4 (1995): 856-66.
88. Tan, Soon-Heng, Willy Hugo, Wing-Kin Sung, and See-Kiong Ng. "A Correlated Motif Approach for Finding Short Linear Motifs from Protein Interaction Networks." *BMC bioinformatics* 7, no. 1 (2006): 502.
89. Rader, Katherine, Robert A Orlando, Xiaojing Lou, and Marilyn Gist Farquhar. "Characterization of Ankra, a Novel Ankyrin Repeat Protein That Interacts with the Cytoplasmic Domain of Megalin." *Journal of the American Society of Nephrology* 11, no. 12 (2000): 2167-78.
90. Menon, Rajesh P, and R Colin Hughes. "Determinants in the N-Terminal Domains of Galectin-3 for Secretion by a Novel Pathway Circumventing the Endoplasmic Reticulum–Golgi Complex." *European journal of biochemistry* 264, no. 2 (1999): 569-76.
91. Beltrao, Pedro, and Luis Serrano. "Comparative Genomics and Disorder Prediction Identify Biologically Relevant Sh3 Protein Interactions." *PLoS computational biology* 1, no. 3 (2005).
92. Kowanetz, Katarzyna, Koraljka Husnjak, Daniela Holler, Marcin Kowanetz, Philippe Soubeyran, Dianne Hirsch, Mirko HH Schmidt, Kresimir Pavelic, Pietro De Camilli, and Paul A Randazzo. "Cin85 Associates with Multiple Effectors Controlling Intracellular Trafficking of Epidermal Growth Factor Receptors." *Molecular biology of the cell* 15, no. 7 (2004): 3155-66.
93. D'erchia, AM, G Pesole, A Tullo, C Saccone, and E Sbisa. "Guinea Pig P53 Mrna: Identification of New Elements in Coding and Untranslated Regions and Their Functional and Evolutionary Implications." *Genomics* 58, no. 1 (1999): 50-64.
94. Kazemein Jasemi, Neda S., Christian Herrmann, Eva Magdalena Estirado, Lothar Gremer, Dieter Willbold, Luc Brunsveld, Radovan Dvorsky, and Mohammad R. Ahmadian. "The Intramolecular Allostery of Grb2 Governing Its Interaction with Sos1 Is Modulated by Phosphotyrosine Ligands." *Biochemical Journal* 478, no. 14 (2021): 2793-809.

Chapter III. Membrane-Binding Modules: Key Players in Cellular Function, Disease Pathogenesis, and Therapeutic Targets

Authors: ***Mehrnaz Mehrabipour***, *Vanshika Garg, Mohammad R. Ahmadian*

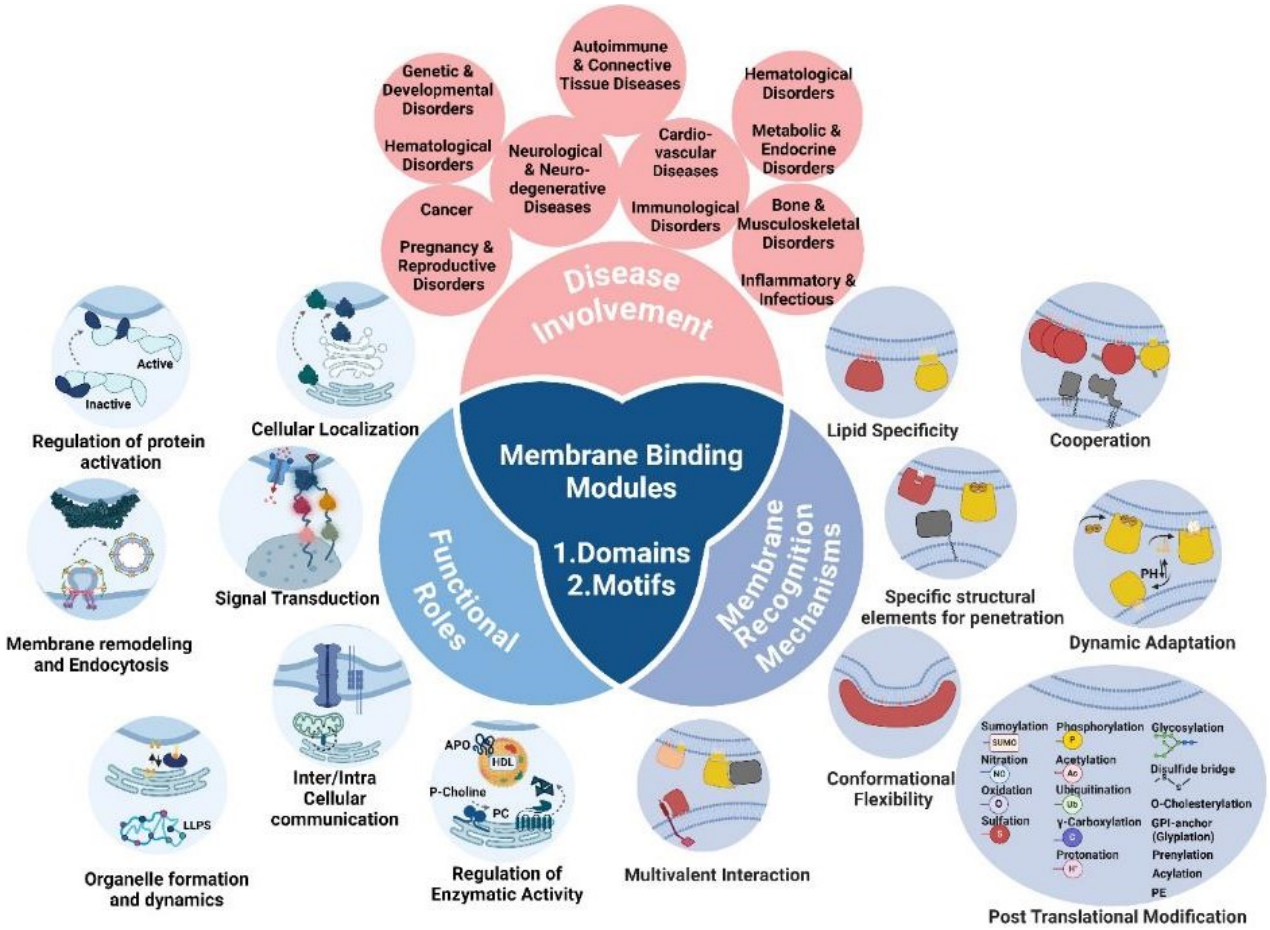

Status:	Submitted in August 2024
Journal:	FEBS Journal
JIF:	5.5
Contribution:	70%

Responsible for conceptualizing, drafting, and writing the manuscript, as well as collecting data and creating figures.

Membrane-binding modules: key players in cellular function, disease pathogenesis, and therapeutic targets

Mehrnaz Mehrabipour[1], Vanshika Garg[1], Mohammad R. Ahmadian[1@]

[1]Institute of Biochemistry and Molecular Biology II, Medical Faculty and University Hospital Düsseldorf, Heinrich Heine University Düsseldorf, Universitätsstrasse 1, 40225 Düsseldorf, Germany

[@]Corresponding authors: reza.ahmadian@hhu.de

Abstract
The intricate linkage between extracellular stimuli and intracellular signaling pathways is a multifaceted process essential for the orchestration of cellular functions. Among the key steps in signal transduction, the association of proteins with intracellular membranes is facilitated by membrane-binding modules. In addition to initiating intracellular signaling, membrane-binding modules are critical for modulating membrane dynamics and forming protein complexes at the right time and in the right subcellular localization. While a large number of membrane-binding modules with a variety of structures and mechanisms of membrane recognition have been characterized, their pivotal roles in signaling pathways and their impact on human disease are still in need of greater emphasis. This review explores the diverse roles of membrane-binding modules in cellular functions, scrutinizes their dysregulation in various human diseases, and highlights their potential as promising therapeutic drug targets.

Keywords: Membrane-binding modules; protein complex assembly; signal transduction; subcellular localization; therapeutic potential.

1. Introduction

Membrane-protein interactions are essential for a wide range of cellular functions, from signaling and trafficking to maintaining structural integrity. They are either defined motifs or distinct domains within a protein and are responsible for the association of proteins with intracellular membranes. In essence, while all membrane binding modules are involved in the interaction between proteins and cellular membranes, they differ in size, specificity, and structural characteristics. Motifs are characterized by smaller and more specific sequences, while domains are larger, well-structured functional units within proteins. One type of motif comprises polybasic groups containing multiple basic amino acids that interact with membrane phospholipids via electrostatic interactions. Another type of motif consists of specific amino acid sequences serving as recognition signals for enzymes involved in lipidation processes. These sequences guide proteins through lipidation events, including prenylation (such as farnesylation and geranylgeranylation), myristoylation, palmitoylation, cholesteroylation, GPI anchoring (glypiation), and PE addition (Table 1). For example, members of the Src family kinases (such as Lyn, Fyn, and Src) utilize myristoylation and palmitoylation [1], while RAS proteins employ prenylation and palmitoylation to associate with the cell membrane [2]. In the case of the HRAS, KRAS4A, and NRAS paralogs, a motif for palmitoylation provides an additional anchoring site to the inner leaflet of the plasma

membrane besides prenylation [3]. In contrast, KRAS4B features a polylysine motif within its C-terminal hypervariable region (HVR), distinct from the prenylation observed in other paralogs [3]. Furthermore, the human proteome encompasses various membrane-binding domains, including GRAM, GLA, Annexin, FERM, C1, C2, PH, FYVE, PX, ENTH, BAR, PDZ, SH2, SMP, PHD, ANTH/CALM, GOLPH3, IMD, KA1, PTB, Tubby, M domain of CTP:phosphocholine cytidylyltransferase, membrane binding of Dystrophin protein, GLUE, TPR repeat, Transmembrane domain (TMD), PLAT, MH2, VHS, C domain of β-arrestin, and PROPPINs (Table S1). These domains play critical roles in mediating interactions between proteins and cellular membranes, exhibiting distinct lipid recruitment strategies. They contribute to the spatial organization and functional modulation of proteins within the cellular membrane environment and, in some cases, to the generation and/or stabilization of membrane curvature. In the following, we provide an overview of functional classification of membrane binding modules, membrane recognition mechanisms with a focus on post-translational modifications (Table 2), and their significance in mutations associated with various diseases (Table 3).

2. The multiple roles of membrane-binding modules in cellular dynamics and functionality

Cellular Localization. Membrane-binding modules are primarily studied for their role in determining cellular localization. Concerning membrane binding motifs, covalent attachment of lipophilic groups to proteins, such as myristoylation, palmitoylation, and prenylation, influences protein targeting within different membrane subdomains [4]. Specifically, NRAS and HRAS undergo farnesylation and palmitoylation at specific cysteine residues. The reversible process of palmitoylation plays a key role in regulating the localization and intracellular trafficking of NRAS and HRAS between the plasma membrane (PM) and Golgi apparatus [5, 6]. In contrast, KRAS4B lacks palmitoylation but features a polybasic motif consisting of six lysine residues (Lys 175-180) just before its farnesylation site. Unlike its counterparts, KRAS4B does not localize to the Golgi apparatus, opting instead for a different route [6]. Instead, farnesylated KRAS4B molecules detach from the endoplasmic reticulum (ER) and diffuse cytosolically with the aid of phosphodiesterase δ (PDEδ), which encloses the farnesyl anchor of KRAS4B in the cytosol through its prenyl-binding pocket [7]. In addition, protein domains such as the extensively studied PH domain in the AKT protein facilitate its specific targeting to the plasma membrane where it undergoes phosphorylation and activation by PDK1 [8]. Similarly, C1 and C2 domains are typically found in members of the protein kinase C (PKC) family, which are involved in membrane targeting and activation [9]. The PROPPINs' membrane-binding domain, characterized by their β-propeller structure with PtdIns3P- and PtdIns(3,5)P2-binding sites, plays a crucial role in their localization to cellular membranes, which is important for autophagy processes [10].

Signal Transduction. Another function is in signal transduction, exemplified by the TMD of receptor tyrosine kinases (RTKs), where it plays a pivotal role in tightly controlling the monomer-dimer equilibrium critical for the regulation of RTKs in vital biochemical processes [11]. Additionally, TMD domains in other signaling proteins, such as G protein-coupled receptors (GPCRs) and ion channels, mediate crucial signal transduction events by facilitating receptor-ligand interactions and modulating membrane potential, respectively [12]. Studies have also demonstrated how membrane binding motifs can facilitate non-overlapping protein assembly for functional signaling events. For instance, RAS proteins exhibit distinct clustering behavior attributed to variations in lipid modifications. These nanoclusters serve as exclusive sites for effector recruitment and activation [5]. Specifically, HRAS is anchored to the plasma

membrane via a lipid-modified C terminus containing a polyunsaturated farnesyl and two saturated palmitoyls. In contrast, NRAS and KRAS4A lacks the second palmitoyl, while KRAS4B has a polybasic lipid-anchor without palmitoylation [5]. Despite their structural similarity, these differences in lipid modifications lead to the formation of differential plasma membrane (PM) clustering may contribute to the functional differences observed in Ras-mediated signaling pathways, such as cell differentiation, proliferation, and survival. For example, both HRAS NRAS and monopalmitoylation supports correct GTP/GDP regulated lateral segregation between cholesterol-dependent and cholesterol-independent microdomains at membrane [13, 14]. K-RAS, on the other hand, clusters within the cholesterol-depleted liquid-disordered (Ld) (cholesterol independent) microdomains at membrane [14]. These distinct clustering behaviors among Ras proteins suggest differential plasma membrane (PM) clustering may contribute to the functional differences observed in RAS-mediated signaling pathways, such as cell differentiation, proliferation, and survival.

Cellular communication. Another important role is in inter-cellular communication, where the TMD of GAP junction proteins, such as connexin, form channels that allow the exchange of ions and small molecules between neighboring cells [15]. Additionally, Intra-cellular communication can be facilitated by lipid-binding proteins at membrane contact sites (MCS). These proteins are involved in interactions between the endoplasmic reticulum (ER) and various organelles, including the plasma membrane, mitochondria, peroxisomes, lipid particles, trans-Golgi network (TGN), endosomes, and lysosomes. The ORP (oxysterol-binding protein (OSBP) related proteins) family functions at membrane contact sites, where the PH domain aids in targeting to these specific membrane regions [16].

Regulation of Enzymatic Activity. In addition, membrane-binding modules can regulate metabolic processes. The membrane-binding domain in HMG-CoA reductase plays a critical role in sensing membrane sterol levels and ultimately initiating reactions that lead to sterol-accelerated degradation of the enzyme via the 26S proteasome pathway [17]. In another example, CTP:phosphocholine cytidylyltransferase (CCT) plays a pivotal role in phosphatidylcholine (PC) synthesis, vital for maintaining cellular lipid homeostasis. This enzyme, crucial in the CDP-choline pathway, is intricately regulated, notably through reversible membrane binding (by amphipathic α-helix called M domain), which acts as a unique lipid compositional sensor [18, 19]. By actively modulating phospholipid compositions and influencing membrane curvature, CCT ensures cellular membrane integrity and function [19]. Another recent paper in 2021 investigates the crucial role of apolipoprotein E (apoE) in regulating cholesterol and triglyceride homeostasis, with a particular focus on its structural domains and their involvement in lipid metabolism. The study highlights how the NT domain, characterized by a stable 4-helix bundle structure, influences the spatial disposition of the CT domain within lipid-associated states, such as those found in reconstituted high-density lipoprotein (rHDL) particles[20]. This interaction with lipids within rHDL particles affects the protein's function in lipid binding and cellular clearance mechanisms, shedding light on fundamental mechanisms governing cholesterol metabolism.

Regulation of protein activation. Membrane binding domain contribute to protein auto-regulation, where the PH domain of the SOS protein, together with its DH domain, plays a role in regulating its function to inhibit RAS-specific exchange factor activity [21], and the interaction

of the PH domain with its DH domain controls RAC activation [22]. Another example is the BAR domain of the RHOGAPs of the GRAF family that binds to the GAP domain and inhibits its activity [23]. In an alternative scenario, the FERM domain within ERM proteins undergoes a transition from an inactive state where it engages with the internal C-terminal ERMAD domain to an active state triggered by kinase activation of the ERMAD domain [24]. This activation allows the FERM domain to bind to the membrane. Investigations of the ARF family have also revealed the impact of membrane association on nucleotide affinity. The controlled exposure and membrane binding of a myristoylated N-terminal α-helix may facilitate the exchange of GDP for GTP, thus serving as a crucial regulatory mechanism for ARF by directly connecting nucleotide exchange to its membrane binding and translocation [25].

Membrane remodeling and Endocytosis. In addition to its role in regulating protein activation, the FERM domain interacts not only with the membrane but also with the cytoplasmic extensions of membrane proteins such as integrins, GPCRs, cadherins, and adhesion molecules, acting as a linker between the membranes and the cortical actin cytoskeleton [24]. This illustrates how membrane binding contributes significantly to cell structure and the regulation of membrane remodeling. In addition, dynamin, a GTPase, binds to the neck of budding vesicles on the plasma membrane through the PH domain and plays a critical role in vesicle scission during endocytosis [26]. The interaction between ANTH and ENTH domains, coupled with PIP_2 binding, forms a stable and highly organized protein-lipid-protein complex that enhances membrane anchoring and promotes efficient endocytosis [27]. In addition, the ENTH domain binds to $PI(4,5)P_2$, which promotes vesicle curvature during endocytosis [28]. Similarly, the BAR domain senses membrane curvature without specific lipid recognition but interacts with acidic phospholipids to complement and support membrane curvature [23, 29, 30].

Organelle formation and dynamics. Membrane binding domains are also involved in lipid exchange between membranes and may be involved in membrane organization. The function of the SMP domain involves shuttling between the tubular ER and the acidic lipid-enriched PM, facilitating lipid exchange via its tip region, which contains positively charged residues to interact with acidic lipids [31]. Furthermore, proteins with phase separation properties can bind to the two lipid layers and potentially enhance lipid phase separation [32]. Membrane-binding domains, such as PLAT, a protein domain commonly found in membrane-associated proteins when attached to the lipid membrane of the cell, interact with proteins such as GRB2 and SOS1. This interaction triggers liquid-liquid phase separation (LLPS), creating distinct phases either on the membrane or independently in solution, driven by the interplay of these proteins [33].

3. Membrane recognition mechanisms

Lipid specificity. Membrane-binding modules employ a variety of tactics, including lipid specificity in membrane recognition. Several papers have investigated the membrane binding specificity of various membrane-binding modules. These investigations revealed that protein domains often hinges on the presence or absence of the target lipid within membranes and exhibit distinct preferences for specific phospholipids [34]. For example, the ENTH domain within mammalian HIP1 shows a preference for binding to $PtdIns(3,4)P_2$ and $PtdIns(3,5)P_2$ [35]. The PH domain was found to bind specifically to various PIPs (phosphoinositides) [36]. The majority of PX domains had a preferential affinity for PtdIns3P [37]. On the other hand, annexin domains can interact with a wide range of lipids, including phosphatidylserine (PS),

phosphatidic acid (PA), phosphatidylinositol (PI), PtdIns(4,5)P_2, various fatty acids, ceramides, and lipid-derived metabolites [38]. Lipidations, as membrane-binding motifs, can also influence lipid preference, resulting in non-overlapping nano clusters, as previously discussed (refer to the section "Signal Transduction"). The polybasic domain of KRAS plays a pivotal role in the selective sorting of lipid headgroups. When combined with prenylation, the polybasic domain of KRAS significantly contributes to the specificity of lipid headgroups within KRAS nanoclusters. These findings indicate that KRAS nanoclusters preferentially accumulate phosphatidylserine (PS) and phosphatidic acid (PA), while not exhibiting enrichment for PIP2, PIP3, or cholesterol [39].

Specific structural elements for membrane penetration. Another strategy, in addition to lipid selectivity through specific membrane-binding modules, is membrane penetration facilitated by hydrophobic residues. Typical C1 domains interact with the lipid messenger diacylglycerol (DAG) and DAG mimetics such as phorbol esters via a polar binding pocket. This pocket is surrounded by hydrophobic and aromatic residues that are critical for their penetration into membranes for efficient anchoring of DAG [40, 41]. In addition, PH domains, which have been described for their binding to a variety of phosphoinositides (PIs), exhibit diverse membrane binding mechanisms. In particular, the extent of membrane penetration varies among PH domains, influenced in part by the distinct distribution of hydrophobic residues in their membrane-binding loops upon PI docking [42]. FYVE domain binding to PtdIns(3)P induces membrane penetration of hydrophobic surface residues. This is likely due to local conformational changes and neutralization of the positive electrostatic potential around hydrophobic loop residues, facilitating membrane entry [43]. The same mechanism is observed in PX domains, where PtdIns(3)P binding acts as an electrostatic penalty during membrane penetration of hydrophobic residues [44]. Certain adapter proteins, such as those with ENTH and ANTH domains from the CALM protein subfamily, have this additional membrane binding mode. They insert an N-terminal helix into the plasma membrane, which is proposed to occur when binding to PIP_2 induces the N-terminal portion to fold into an α-helix, contributing to membrane penetration [45]. In another example, the C2 domain of the discoidin family (factor V) contains a basic patch and aromatic/aliphatic side chains, suggesting membrane insertion [34]. Additionally, in certain scenarios, the C2 domain exhibits Ca^{2+}-dependent binding to phosphatidylserine, suggesting mechanisms for membrane interaction and penetration, as observed for the C2 domain of PKCα [34]. Further research on other proteins has revealed the contribution of protein lipidation to membrane insertion. A review paper from 2007 describes how the varying insertion levels of HRAS proteins into the inner leaflet of the membrane result in a difference in area between the two leaflets, leading to localized membrane curvature that stabilizes specific domains in the plasma membrane [14]. Another study elucidated the molecular mechanism of membrane insertion for lipidated LC3 protein, vital in autophagy initiation, revealing that its reversible conjugation to phosphatidylethanolamine (PE) enables stable association with the autophagosome membrane. Molecular dynamics simulations highlighted that basic charged amino acids, particularly Lys65, Arg68, and Arg69, drive the insertion of the protein-lipid anchor into the membrane, as validated by live-cell imaging, signifying a critical step in understanding the insertion process of lipidated proteins [46].

Conformational flexibility. Conformational flexibility in membrane-binding modules is essential for their effective interaction with diverse cell membranes, allowing shape adaptation, specific target recognition, and multifunctional roles through structural changes. For example, the BAR and amphipathic helices of the N-BAR domains in endophilin A1 cooperatively

promote membrane curvature, enabling its role in membrane deformation during endocytosis [47]. A/ENTH domains also function in the development of membrane curvature through lipid remodeling during the formation of clathrin-coated vesicles [48]. PROPPINs also contribute to the category of membrane recognition mechanisms related to curvature dependence. This is evident from their ability to bind to specific phospholipids, such as PtdIns3P and PtdIns(3,5)P2, in a manner that is dependent on membrane curvature, as indicated by their higher affinity for small unilamellar vesicles compared to large ones [10].

Multivalent interaction. Multivalent interactions refer to the ability of membrane binding modules to simultaneously engage multiple lipid sites, thereby increasing both the specificity and strength of the interaction between the protein and the cell membrane. Notable examples include the SLM1 PH domain adjacent binding site for PtdIns(4,5)P_2 and dihydro-phingosine-1-phosphate [49]. The SOS1 PH domain binds specifically to PtdIns(4,5)P_2 [50], and the p47^{phox} PX domain interacts with PtdIns(3,4)P_2 [51]. Both domains use an adjacent basic patch, a similar structural feature in PH and PX domains, to interact with phosphatidic acid (PA) [51-53]. This interaction with PA may increase their binding affinity to membrane PIs. Similarly, the PKCα C2 domain simultaneously binds to PS and PtdIns(4,5)P_2 [54]. In addition, multivalent interactions play a role in spatiotemporal regulation, allowing for appropriate interaction with the membrane and maintenance of proper physiological functions. An example of this concept is the FAPP1 PH domain, which binds both PIs like PtdIns(4)P and ARF1 to facilitate Golgi localization [55]. Similarly, the DAB1 PTB domain accommodates both the ApoER2 NPXY peptide and a PI headgroup binding and plays a critical role in transmitting essential positional signals to migrating neurons [56].

Cooperation of multiple domains/other proteins. The idea of cooperation in membrane binding encompasses several interactions, including instances where membrane modules act as dimers binding to the membrane. The annexin domain, which has been proposed to promote cooperative membrane aggregation, is not limited to a monomeric interaction with a membrane through the N-terminus after calcium-dependent binding to another membrane. Rather, it is proposed that other cooperative processes involve the formation of dimers or the assembly of heterotetramers consisting of two annexins and two S100 proteins. All of these interactions are facilitated in a calcium-dependent manner and contribute to the bridging of two membranes [57]. Another example of the cooperative binding mechanism is observed in the crystal structure of the EEA1-FYVE domain homodimer in PtdIns(3)P2 binding, which supports a multivalent mechanism that amplifies weak affinity and modest specificity for enhanced endosomal tethering [58]. In addition, the PH domain of dynamin is required in a dimeric or tetrameric structure for significantly enhanced membrane binding [59]. Cooperation of multiple domains in a protein for membrane recruitment is also seen in phospholipase C-γ (PLCγ), where the N-terminal SH2 domain forms complexes with activated RTKs, while the C2 and PH domains cooperate with the SH2 domain to direct PLCγ to the plasma membrane [60]. A more complex cooperative binding is evident in the retromer complex during late endosome-mediated tubule formation. The SNX-PX domain dimer serves as a critical anchor to the membrane, and the SNX-BAR dimer induces curvature, resulting in the formation of tubular extensions. Completion of this process requires further cooperation, as the N-terminal sequence of SNX works with the Vps26-Vps35-Vps29 trimer to recognize and interact with cargo molecules [61].Another example is the cooperative engagement of different lipid anchor motifs. These include the farnesyl moiety present in all three paralogs of H/K/NRAS in addition

to the palmitoyl group of NRAS, two palmitoyl groups in HRAS, and a polylysine motif in KRAS4B [62].

Dynamic adaptation to cellular conditions. Proteins can modulate their interactions in response to cellular cues. Changes in cofactor, lipid composition, pH, or the presence of signaling molecules can alter the behavior of the protein or its affinity for the membrane. This is evident in the case of RASAL and PKCγ upon stimulation of G protein-coupled receptors. Studies on conventional PKC isoforms have revealed a frequency-dependent activation mechanism that depends on oscillatory contacts with the plasma membrane coupled to variations in intracellular Ca^{2+} (via the C2 domain) and DAG (via the C1 domain) levels [63]. In addition, RASAL undergoes rhythmic oscillations, shuttling between the plasma membrane and the cytosol in synchrony with repetitively measured Ca^{2+} spikes [64]. Local pH variations at the cellular level play a crucial role, especially in processes such as cell migration [65] and within mitochondria [66]. The acid-base properties of membrane lipids make them directly sensitive to pH, resulting in chemical modifications that have broad physical effects on the cell membrane. In particular, one study showed that changing pH induces local membrane dynamic deformations, vesicle migration, global deformation, and polarization in vesicles with phase-separated membrane domains [67]. Importantly, these dynamic changes may have implications for protein-membrane recruitment. A putative model for pH-triggered membrane insertion of helices is described in the annexin XII monomer, where at neutral pH or in the presence of Ca^{2+}, helices D and E form a helical hairpin at the membrane surface, and upon pH decrease, protonation of carboxylate groups leads to their insertion into the bilayer as a transmembrane helix [68]. In addition, annexins exhibit coordinated Ca^{2+}-induced translocations in living cells, with different calcium sensitivities among family members, suggesting their potential as a sophisticated Ca^{2+}-sensing system influencing various signaling pathways [69].

Regulation via posttranslational modifications.

Lipidation. Posttranslational modifications (PTMs) can effectively regulate proteins recruitment to the membranes. Among these modifications, lipidations such as prenylation, myristoylation, palmitoylation, cholesteroylation, GPI anchoring, and PE addition are well-characterized PTMs occurring on a protein membrane binding motif with a recognition site that facilitate protein targeting to membranes (As detailed in the motifs undergoing PTMs in Table1).

Phosphorylation. Phosphorylation can, in many cases, control the membrane binding and localization of membrane-binding proteins. One example is Annexin proteins which initially identified as substrates for PKC with several potential PKC binding sites, it has been discovered that PKC-mediated phosphorylation affects the localization, membrane binding affinity, and functional properties of annexins. Conversely, annexins ANXA1, A2, A5, and A6 also play a role in modulating PKC localization and signaling [70]. One example is the phosphorylation of S-27 residue in the N-terminal of ANXA1 protein, which facilitates its translocation to cellular membrane [71]. In addition, phosphorylation of Y20 in ANXA1 plays a critical role in membrane remodeling, leading to subsequent proteolytic cleavage that releases the ANXA1 dimer and contributes to membrane fission and internal vesicle release [72]. The dependence of phosphorylation of Y23 on ANXA2 to effectively bind and stabilize association with lipid raft regions of the plasma membrane is also suggested [73]. In addition, it is shown that the differential distribution of ANXA2 is likely influenced by the phosphorylation of either S-25 or Y23 [74]. Furthermore, the data suggest that annexin VI function may be subject to growth-dependent regulation by an uncharacterized phosphorylation (on serine and, to a

lesser extent, threonine) [75]. Similarly, tyrosine phosphorylation of ANXA7/ANXA1 has been reported without further elucidation of its physiological consequences, and the potential impact of this modification on membrane recruitment remains to be explored [76]. Moreover, phosphorylation of ANTH domain in CALM and AP180 proteins regulates their interactions and functions in synaptic vesicle endocytosis [77]. Other examples include phosphorylation of endophilin A1 on T14 by Rho kinase plays a crucial role in regulating its recruitment to activated EGF receptors during clathrin-mediated endocytosis [78, 79]. This modification affects the formation of protein complexes necessary for receptor internalization, rather than the protein's ability to bind to membranes, and may also influence endophilin's auto-regulatory mechanisms [79]. Additionally, phosphorylation of endophilin A1 at S75, within the central insert region of the BAR-domain dimer, by LRRK2 is essential for synaptic vesicle endocytosis and neurotransmission, reducing its membrane affinity and tubulating activity [79, 80]. A similar change in membrane-binding properties and tubulating activity has been observed in Pacsin 1 protein upon phosphorylation at S76 and T181 within the BAR domain [81]. S76 phosphorylation may alter the curvature of the F-BAR dimer, while T181 phosphorylation may interfere with the tip-to-tip inter-dimer association necessary for filament assembly [79]. Phosphorylation of Arfaptin proteins, notably Arfaptin-1 at S132 and Arfaptin-2 at S260, respectively regulates granule fission by disrupting the arfaptin1-vesicle neck interaction and demonstrates neuroprotective effects [79]. Research indicates that PKCδ undergoes multiple phosphorylation events for the regulation of its activation and translocation in various cellular processes [82]. For instance, phosphorylation of tyrosine residues Tyr311 and Tyr332 in response to apoptotic stimuli enables caspase 3 to cleave PKCδ. This proteolytic cleavage by caspase 3 produces a 40 kDa catalytically active fragment of PKCδ, which can then translocate to the mitochondria and/or nucleus, where it facilitates apoptosis [83]. Several studies have indicated that phosphorylation of the C-terminal tail leads to a conformational change in PTEN, favoring a closed and stabilized state, thereby reducing its interaction with membrane phospholipids [84]. In another example, WNK1 phosphorylates synaptotagmin 2 within its C2 domain, thereby augmenting the threshold of Ca2+ needed for membrane binding [85]. Similarly, phosphorylation of C2 domain of human tricalbin at Y1009 could alter the charge of the region, potentially affecting its ability to interact with lipids [86]. Phosphorylation at Ezrin residues S66 and Y270, located near the putative FERM interface, could impact the FERM–membrane interaction [87]. Additionally, Ezrin phosphorylation at T567 site may enhance protein affinity for PI(4,5)P2 [87]. Other phosphorylation sites of Ezrin and moesin at C-term (T576 and T558, respectively) play a crucial role in the precise regulation of the connection between the plasma membrane and the actin cytoskeleton [88]. There is additional threonine phosphorylation in the FERM membrane-binding domain that are proposed to regulate the activation of these proteins. However, their effects on membrane binding activity still need to be functionally validated. In a comparable manner, phosphorylated H58 and Y194 in the FERM domain of the FAK protein influence its activation and regulation[89]. However, the potential role of lipid binding to the FAK-FERM domain requires further investigation. Furthermore, the effect of TYK2-FERM domain phosphorylation on lipid binding, aside from its activation consequences, needs to be investigated. Another protein whose localization is regulated by phosphorylation of S13 at the N-terminus is Merlin. This phosphorylation is essential for the proper loading of Merlin onto adherens junctions during the formation of functional junctions [90]. It has been suggested that phosphorylation of residues within the membrane insertion region of FGD family proteins could regulate its multidomain membrane binding. This This process may create induce enough electrostatic repulsion to remove these proteins from membranes or potentially modify interdomain dynamics [91]. Mass spectrometry results

confirm phosphorylation of hLst at residue T870 on FYVE domain, but its role in lipid binding requires further investigation [92]. Another uncharacterized FYVE membrane-binding domain in Spir2 proteins involves phosphorylation at S636. Further investigation is needed to understand the role of this phosphorylation site in membrane targeting and intracellular membrane transport [93]. Another interesting PTM effect involves GOLPH3. Upon DNA damage, DNA-PK phosphorylates GOLPH3 at threonine residues 143 and 148 within a TQ motif. This modification strengthens GOLPH3's interaction with MYO18A, enhancing its pulling force on the Golgi apparatus. Consequently, the Golgi becomes fragmented and disperses across the cytoplasm [94]. Moreover, the two novel phosphorylation of the KA1 membrane binding-domain of Chk1 still requires further characterization regarding its interaction with phospholipids, beyond its known roles in kinase activation and rapid proteasomal degradation [95]. Phosphorylation of PTEN at the PDZ-binding domain by ATM triggers its export from the nucleus [96] and increases cellular sensitivity to DNA damage [97]. Additionally, recent studies indicate that this phosphorylation impacts PTEN dimerization [84, 98]. Other examples include serine phosphorylation of PDZ domain-containing proteins such as SAP-97, PSD-95, and NHERF-1, which may disrupt PDZ protein-protein interactions [99]. A proposed regulatory mechanism for the formation and stabilization of protein complexes involves the binding of multiple PDZ domains to lipid membranes containing phosphoinositides [99-101]. Further studies on the effect of these phosphorylations on lipid binding are necessary. The phosphorylation of the PH domain is also observed in certain cases, such as the AKT protein at T72. However, research only demonstrates the role of this phosphorylation in enhancing AKT kinase activity [102]. The potential impact of this phosphorylation on the membrane anchoring of the AKT-PH domain remains to be investigated. Similarly, the phosphorylation of AGAP2-PH at sites K80, K81, and K103 has been proposed to regulate cell cycle, proliferation, and cell death [103]. However, the exact mechanism by which the phosphorylated PH domain influences its membrane interaction/association needs further investigation.

Acetylation. Acetylation as another PTM can help directly or indirectly in membrane-binding of proteins. The ANXA2-S100A10 complex plays a key regulatory role because it is the only form that can stably anchor to the plasma membrane [104]. This anchoring is vital for the complex's function in targeting and recruiting specific ion channels and receptors to the membrane. Crucially, the N-terminal acetylation of ANXA2 is essential for binding with S100A10 [104], underscoring the significance of this modification in the formation and functionality of the complex at the membrane. Another indirect effect involves PTEN, which is acetylated by the p300–CREB-binding protein (CBP) at K402, a site in the C-terminal PDZ domain-binding motif [84, 105]. This acetylation potentially might affect PTEN's interactions with other proteins, including its binding with plasma membrane proteins that regulate PTEN's membrane localization [84, 105]. Moreover, the acetylation of IRS1 and IRS2 is suggested to impair insulin signaling by diminishing tyrosine phosphorylation, which is essential for the recruitment of downstream mediators to the plasma membrane [106, 107]. Notably, the presence of some of these acetylation sites such as K80, K81, and K103 on the PH domain might impede its activity by inhibiting its plasma membrane recruitment. Further elucidation is needed to understand this mechanism.

sumoylation. In many plasma membrane proteins, sumoylation serves as another PTM, but its precise functional significance often remains unclear in many instances. According to in vitro studies by Schmidt et al., the B-cell restricted factor, Bright, binds to the lipid raft of resting B cells by Palmitoylation. After BCR ligation, Bright becomes sumoylated and dissociates from the lipid raft. The amount of Bright in the lipid raft regulates the threshold of BCR signaling; less Bright bound to the lipid raft results in stronger BCR signaling [108]. This suggests

sumoylation's role in modulating membrane-association of Bright protein. Moreover, sumoylation has been found to silence the plasma membrane leak potassium channel K2P1 [109]. In another example, membrane-localized metabotropic glutamate receptors (mGluRs) are targeted by sumoylation [110], but the exact function of this modification in regulating their targeting needs to be understood. Moreover, sumoylation directly affects the localization of proteins such as PTEN. Specifically, sumoylation of the C2 domain at K266 increases its association with the plasma membrane [111], while sumoylation at lysine K254 promotes nuclear import [97]. Furthermore, findings suggest that sumoylation of the FAK-FERM domain at the K152 residue in the presence of PIAS1 significantly enhances FAK autophosphorylation, leading to its activation and predominantly sumoylated presence in the nuclear fraction [112]. While it is observed that sumoylated FAK is concentrated in the nucleus, alternative research suggests that the sumoylation of FAK at K152 does not play a crucial role in facilitating its translocation into the nucleus [113]. In addition, sumoylation of Merlin at K76 within FERM domain is essential for its tumor-suppressive activity, mediating intra/intermolecular binding activities, and modulating its cellular localization by regulating cytoplasmic/nuclear trafficking [114]. Another example is the sumoylation of the Anx domain of ANXA1, which has been shown to directly enhance its ligase activity [115]. However, given sumoylation's role in regulating nucleo-cytoplasmic trafficking, this modification may also alter the localization of ANXA1.

Ubiquitination. Ubiquitination is another common occurring PTM as a covalent modifier to target proteins for proteasome-mediated degradation or to modulate their functions. The type of ubiquitin modification determines its function. For instance, monoubiquitination does not lead to protein degradation but allows the protein to interact with other proteins, change subcellular localization, and alter structural and targeting properties through ubiquitin-binding proteins and receptors. Conversely, polyubiquitination can serve various roles depending on the type of linkage, such as activating kinases or providing scaffolds for signaling processes, without necessarily targeting the protein for degradation [116]. In this regard, studies have revealed the presence of monoubiquitinated ANXA1, specifically within its Anx domain, in the nuclei. This highlights the likely importance of this post-translational modification in its translocation, alongside its established role in the DNA damage response [115]. Another example is AKT-mediated phosphorylation, which leads to Merlin degradation through polyubiquitination of its FERM domain, with the fragment containing residues 1–133 being robustly ubiquitinated [114]. Furthermore, PTEN regulation involves both polyubiquitylation for proteasomal degradation, and monoubiquitylation at K13 (N-term) and K289 (C2 domain) enhances its nuclear import [84]. Considering the ubiquitination of membrane-binding domains such as Anx, FERM, and C2 in the examples mentioned above, further investigation into the impact of this modification on direct membrane binding is needed.

Another less common PTM observed is S-glutathiolation on the N-terminal of ANXA2 at the C8 residue. Considering ANXA2's involvement in membrane trafficking events, which may necessitate aggregation activity, it is crucial to investigate the relationship between this modification and its role in membrane-related functions, particularly in terms of aggregation activity or potential interference with necessary conformational changes [72]. Another instance involves the N-terminal domains of ANXA1, which include a glutamine residue at position 18, where transglutaminase can facilitate the formation of cross-links between ANXA1 chains. This process results in the formation of ANXA1 homodimers, which display increased sensitivity to calcium ions for binding to phospholipids [117].

Nitration. Furthermore, protein tyrosine nitration is a form of PTM that results in permanent structural changes [118]. Nitration has been detected in the ANTH membrane-binding domain

of the AP180 protein [119]. However, its specific function in membrane binding and its broader influence on regulating other functions are not yet fully understood. Tyrosine nitration plays a pivotal role in modulating synaptic vesicle dynamics and neurotransmitter release. There are several nitration sites within the C2A and C2B domains of Syt1, a calcium sensor crucial for SNARE-mediated, Ca2+-triggered synaptic vesicle fusion in neurons. Syt1 exhibits interactions with membranes in both Ca2+-dependent and -independent manners, and these nitrations could potentially influence its ability to bind to membranes. In particular, the nitrated residue Y311, situated near the lysine-rich region of the C2B domain, might affects various aspects of synaptic vesicle exocytosis and endocytosis, including Syt1 oligomerization, Ca2+ affinity, and interactions with syntaxin/SNAP-25. Similarly, the nitration of Tyr364 within the C2B domain's Ca2+-binding motif could alter Ca2+ binding and consequently impact synaptic vesicle fusion. Additionally, nitration of Tyr380, positioned in the loop associated with SNARE interaction, may modulate Syt1's interaction with SNARE proteins. Furthermore, nitration of tyrosine residues in the C2A domain, such as Tyr151, Tyr216, and Tyr229, could influence Ca2+-mediated synaptic vesicle fusion and neurotransmitter release by altering the conformation of the Ca2+-binding loop [120]. Overall, these findings suggest that tyrosine nitration of synaptotagmin isoforms may disrupt crucial interactions and conformational changes, thus affecting Ca2+-triggered synaptic vesicle exo- and endocytosis processes.

Oxidation. Moreover, oxidative protein modification can produce stable PTMs on proteins. The activation of PKCγ by H_2O_2 is modulated through the oxidation of cysteine residues within the C1 domain, suggesting that an oxidative mechanism plays a role in inducing the translocation of protein kinase C gamma (PKCγ) via its C1 domain [121]. Similarly, for other isoforms of PKCα, PKCβ, PKCδ, and PKCε, reactive oxygen species (ROS), at low concentrations, have been shown to directly activate and induce the translocation to the plasma membrane through the oxidation of cysteines in the zinc fingers within their regulatory domains (C1 Domain) [122, 123]. However, under the same conditions, PKCζ translocates to the nucleus [124].

Glycosylation. Another striking PTM difference is glycosylation found in FVIII, a cofactor in the blood coagulation cascade, with glycosylation of the N residues in functional A and C1 domains [125]. One study noted that the lipid-binding region 2303–2332 of recombinant FVIII is essential for its membrane binding and proper function, with changes in this region initiating aggregation. Biochemical analysis indicated that deglycosylation, particularly the removal of N-glycan at positions N-1823 (A3 domain) and N-2131 (C1 domain), resulted in loss of activity, aggregation and impaired lipid interaction, possibly impacting the conformation of the lipid-binding region or the accessibility of this epitope [126]. However, other studies on the glycosylation of FVa suggest that glycosylation at N2181 in the C2 domain, which is essential for membrane binding, reduces the affinity for phospholipid membranes, especially at low phospholipid concentrations, resulting in decreased pro-coagulant activity [127]. Another investigation argues that the N-glycosylation site N292 within the classical PTEN structure lies adjacent to an ubiquitination site within the C2 phosphatase domain, which is pivotal for regulating PTEN's nuclear localization [128] and stability [129]. Consequently, N-glycosylation at N292 has the potential to impact both the stability and functionality of PTEN [130]. However, the direct effect of this glycan on the membrane binding of the C2 domain remains uncertain. In another instance, two N-glycosylation sites on the C2 domain of the TPIP (TPTE and PTEN homologous inositol lipid phosphatase) protein have been identified[85], yet further characterization of the role of this glycosylation remains lacking.

Sulfation. Furthermore, sulfation is a PTM that occurs in the trans-Golgi apparatus and has been observed in the B and C2 domain of FV. Studies have indicated that inhibiting sulfation by increasing sodium chloride leads to reduced FV activity, highlighting the importance of

sulfation for efficient thrombin activation [131]. However, due to the C2 domain's requirement for membrane binding, the effect of sulfation on membrane binding has not been demonstrated.

Protonation. PTM by protons can directly influence interactions with other molecules or drive changes in protein structure and dynamics, thereby impacting function [132]. For example, in the activation of FAK, H58 deprotonation within the FERM-F1 lobe occurs in response to increased intracellular pH, leading to conformational changes that expose the FAK linker region and enable autophosphorylation of Y397. This process involves a complex interplay of molecular events, including Src binding and phosphorylation within the kinase domain, ultimately resulting in full FAK activation [89]. Crucially, the F2 loop of the FERM domain, situated near the F1 loop, plays a significant role in receptor and/or phosphatidylinositol 4,5-P2 interaction during the activation process [89]. It is worth exploring how this protonation might affect the interaction between the F2 loop and the membrane.

γ-Carboxylation. The function of MGP depends on a post-translational modification in which specific glutamate residues within the GLA domain undergo γ-carboxylation by a vitamin K-dependent carboxylase. MGP, with its γ-carboxylated glutamate and phosphorylated serine motifs, inhibits calcification by binding to the cell surface and vesicle-like structures, particularly under high calcium concentrations [133]. Similarly, PRRG4 undergoes γ-carboxylation modification in its GLA domain. Data indicate that the absence of this γ-carboxylation affects its function, leading to the accumulation of a slower migrating form of PRRG4 [134]. Importantly, the GLA domain in the family of γ-carboxyglutamic (GLA) domain-containing proteins facilitates calcium-dependent association with anionic phospholipid-containing membranes [135]. However, further investigation is necessary to fully understand the precise mechanism by which this PTM modulates their membrane binding capacity and ultimately impacts their function. This modification is also present in coagulation proteins within their GLA domain, as outlined in Table 2 and play a crucial role in calcium binding to phospholipid membranes and in the formation of coagulation complexes, which are essential for the generation of thrombin [136].

Disulfide bridge. Evidence suggests that the inhibition of PTEN activity relies on the binding of TRX-1 to PTEN, facilitated by a disulfide bond formation between the active site C32 of Trx-1 and C212 of PTEN's C2 domain. This interaction leads to steric hindrance at the PTEN phosphatase catalytic site and inhibits the lipid membrane binding activity of its C2 domain [137].

4. Disease Involvement and Challenges in Drug Development for Targeting Membrane-Binding Modules

Mutations and dysregulation of membrane-binding modules significantly contribute to the pathogenesis of various human diseases due to their diverse functionalities (as explained in part 2. The potential mechanisms by which mutations or dysregulation in protein modules can lead to **(a) mutations affecting folding and/or oligomerization:** mutations in proteins can disrupt their proper folding and/or assembly into functional complexes (oligomerization). This disruption can interfere with the protein's trafficking within the cell. For example, proteins may fail to fold correctly in the endoplasmic reticulum (ER), leading to ER retention or misfolding. Misfolded proteins may then undergo proteasomal degradation as a quality control mechanism. **(b) impact on protein function:** Mutant proteins may reach their intended cellular destinations even if they fail to fold properly, forming dysfunctional complexes at the plasma membrane.

This impairment can disrupt their normal function, potentially contributing to disease progression. **(c) regulation of protein expression**: Dysfunctions in protein modules can also arise from changes in the regulation of protein expression levels. Upregulation or downregulation) of proteins containing these modules can disrupt normal cellular processes. Overall, the resulting pathologies can be broadly categorized into several major disease classes, including neurodegenerative diseases, cancers, cardiovascular diseases, autoimmune disorders, and metabolic syndromes. Table3 elaborates a detailed exploration of how these alterations contribute to different disease categories. As explained in Table 3, there are many examples of mutations in membrane binding modules that have not yet been characterized.

Given the prevalence of membrane-binding domains in numerous diseases, the discovery and development of drugs targeting these domains is of paramount importance for advancing therapeutic interventions. However, the development of drugs targeting membrane-binding modules faces several significant challenges. Firstly, accessibility is major concerns as membrane-bound domains are often embedded within the cell membrane, making them less accessible for drug molecules. This limitation arises due to the essential requirement for a solvent-accessible surface area, which serves as a hallmark of druggability [138]. Secondly, ensuring that a drug specifically targets the intended domain without affecting other essential membrane-bound proteins is a complex task. Thirdly, the diversity and complexity of membrane-binding domains or motifs, which exhibit a wide range of structures and functions, complicate the design of a single drug that can effectively target the various motifs or domains found in different proteins. However, despite these challenges, recent advances offer promising solutions. The development of exogenous probes specifically designed to study molecular recognition within membranes, the folding of membrane proteins, cell signal transduction, the formation of membrane lipid rafts, and interactions between proteins and lipids is crucial for advancing our understanding of membrane proteins [139]. Additionally, the dynamic nature of interactions between membrane-bound proteins and lipid bilayers presents another layer of complexity, implying that lipid bilayer can significantly influence the mechanism of drug binding. Kiriakidi et al. explored the conformational features of the candesartan, AT1 receptor blocker drug, and its localization within the membrane core using molecular dynamics, suggesting that the lipid bilayer significantly influences the drug's binding mechanism. This implies that the lipid bilayer restricts the ligand's degrees of freedom present in an aqueous environment, thereby inducing conformational changes in the drug [140]. Finally, regulatory hurdles further complicate the process, as stringent approval processes for drugs targeting novel protein-lipid interactions require extensive preclinical and clinical studies to ensure safety and efficacy, adding both time and complexity to drug development. Addressing these challenges requires a deep understanding of the structural and functional aspects of membrane-binding domains, along with novel drug development strategies and innovative technologies. Technological advances in imaging techniques, structural biology, and computational modeling [141] can offer deeper insights into molecular interactions between membrane-binding domains and lipids, aiding in drug design.

Based on a comprehensive review of drug-target development, membrane proteins are prevalent among drug targets, with receptors constituting the largest group. Specifically, 193 proteins, or 44% of human drug targets, are receptors, and of these, 82 (19%) are G protein-coupled receptors (GPCRs). Approximately 36% of all drugs target GPCRs, which are commonly targeted by antihypertensive and anti-allergic drugs [142]. GPCRs comprise seven TMD helices. Interestingly, experimentally determined structures of receptor-bound peptides and non-peptide ligands, including approved and under-development drugs, generally show that most of them bind to the transmembrane domains of GPCRs [143, 144]. Moreover, ligand-gated ion channels, the second-largest receptor target class, are frequently targeted by hypnotic drugs and sedatives, while receptor tyrosine kinases, the third-largest class, are often targeted by anticancer drugs. Additionally, transporter proteins make up 15% of drug targets, facilitating the movement of specific substrates across membranes and being commonly targeted by drugs like antihypertensives, diuretics, anesthetics, and anti-arrhythmics [142].

Strategies to counteract the membrane-binding modules dysfunctional effect include **(a) restore trafficking**: rescuing the partially functional mutant protein from stringent quality control mechanisms, despite its misfolding. For instance, many mutations in the TMD of the CFTR ion channel cause cystic fibrosis [145]. A study examined four CFTR mutants in the transmembrane domain (G85E, E92K, L1077P, and M1101K) and found that a combination of the correctors C4 and C18 can rescue CFTR expression and function in three of them (E92K, L1077P, and M1101K). These correctors mitigate the interactions of the mutants with proteostasis components and reduce ubiquitination, allowing the functional protein to reach the cell surface [146]. **(b) rescue folding/stability defect:** To rescue the folding or stability defects of membrane protein modules caused by a mutation, several strategies can be employed, such as assistance from chaperone proteins or pharmacological chaperones—small molecules designed for this purpose. A study focused on mutations in PMP22 linked to peripheral neuropathies such as CMT1A. These mutations cause misfolding of PMP22 in the ER, resulting in toxic accumulation of mutants that contributes to disease. Researchers analyzed two mutant forms, G150D and L16P, finding they folded similarly to the wild type but were unstable, especially L16P. They discovered wild type PMP22 binds zinc and copper, essential for stability. Importantly, zinc supplementation restored stability in the mutant forms, suggesting a potential therapy for neuropathies caused by protein folding defects [147]. In another study, treatment with an antagonist was found to restore both cell surface expression and signaling activity of disease-linked mutants of V2R in nephrogenic diabetes insipidus (NDI). These antagonists act as pharmacological chaperones by binding to and stabilizing partially folded mutant receptors intracellularly, thereby promoting their proper folding and maturation [148]. In general, pharmacological chaperones, typically selective lipophilic ligands, enter cells and bind to partially folded receptors early in biosynthesis. This binding alters the protein's folding equilibrium, favoring correct folding, thereby allowing the receptor to evade ER quality control and increase functional receptor levels at the cell surface without globally inhibiting the quality control system [149]. This implies that

pharmacological chaperones can support both the rescue of protein folding and the subsequent restoration of proper trafficking to the cell surface. Other examples of GPCRs targeted by pharmacological chaperones include the GnRH receptor, the δ-opioid receptor, and rhodopsin [149]. **(c) pharmacological inhibition/ modulation:** It involves using exogenous molecules (such as drugs or small molecules) to interfere with the activity or function of a protein that is causing undesired effects in a specific context or scenario. For example, a study identified a critical GxxxA motif within the γ6 subunit's TMD1 that is essential for inhibiting Cav3.1 current. An eight-amino acid peptide containing this motif acts as a novel pharmacological inhibitor of Cav3.1 current, binding dynamically to the channel in a concentration-dependent and voltage-independent manner [150]. Moreover, peptide-based strategies targeting the TMDs of receptors such as ErbB family proteins [151] and Neuropilins [152], to inhibit their dimerization and activation, offer a promising anti-cancer therapeutic approach. Such approache is demonstrated in another study that disrupting the lipid-exposed face of transmembrane segment IV (TM IV) of the Class II G protein-coupled secretin receptor impedes its oligomerization and reduces its ability to stimulate intracellular cAMP, suggesting that similar approaches may be effective for other transmembrane proteins and GPCRs implicated in cancer [153]. Additionally, targeting the lipidations of RAS proteins to interfere with their pathogenic functions has also been explored. Statins exhibit pleiotropic effects due to their inhibition of the enzyme 3-hydroxy-3-methylglutaryl-CoA reductase in the mevalonate pathway, which is essential for cholesterol and isoprenoid synthesis. These off-target effects interfere with the prenylation of RAS proteins [154]. A review study described diverse compounds, including GPI anchor inhibitors (e.g., Gepinacin), myristoylation inhibitors (e.g., PF-03402623), and prenylation inhibitors (e.g., lonafarnib), that target the membrane binding modules of pathogenic proteins to inhibit their function [155]. **(d) gene therapy and read-through compounds:** Gene therapy offers a potential solution by directly correcting genetic defects at the DNA level. Comprehensive preclinical data in rodents strongly support the clinical advancement of intrathecal adeno-associated viral (AAV) gene therapy targeting MFSD8, a multi-pass membrane lysosomal protein, for CLN7 (neuronal ceroid lipofuscinosis type 7) disease with mutations of D368H (within the extracellular region) and i6SVA insertion (leading to translational termination) [156]. This gene therapy approach shows promise for addressing other disorders related to MFSD8 mutations within its TMD and other membrane-binding domains. Additionally, read-through compounds represent another potential strategy to bypass premature termination codons (PTCs), allowing for the production of full-length, functional proteins. A recent study identified 180 compounds with read-through activity from a screen of over 771,000 compounds, including SRI-37240 and its more potent derivative, SRI-41315. SRI-41315 effectively suppressed PTCs associated with cystic fibrosis in CFTR protein receptor by prolonging translation at stop codons and reducing the termination factor eRF1 [157]. Combining such readthrough agents targeting different parts of the translation process shows promise as a treatment strategy for PTC-related diseases.

5. Conclusion

This review has reframed (a) our understanding of membrane-binding modules by compiling an extensive collection of these domains and motifs (b) biological comprehension of how these modules mediate their functions, (c) diverse strategies employed by membrane binding modules to interact with membranes, and (d) significance of mutations in membrane-binding modules and their association with various diseases and challenges and opportunities for developing druggable therapeutic modalities targeting these modules.

Acknowledgments: We are grateful to our colleagues from the Institute of Biochemistry and Molecular Biology II of the Medical Faculty of the Heinrich-Heine University, Düsseldorf, for their support, helpful advice, and stimulating discussions.

Conflict of interest: The authors declare no competing financial interest.

Author Contributions: M.M. was responsible for conceiving, drafting, and approving the manuscript. V.G. assisted in creating tables and editing. M.R.A. coordinated, edited the manuscript, and approved the final submission.

Funding: This study was supported by the Foundation for Ageing Research of Heinrich Heine University (grant number: 701.810.845), and the German Research Foundation (Deutsche Forschungsgemeinschaft or DFG; grant number: AH 92/8-3).

Institutional Review Board Statement: Not applicable.

Informed Consent Statement: Not applicable.

Data Availability Statement: It is affirmed that no new data were generated while compiling this review manuscript. All referenced data sources are openly accessible and appropriately cited within the manuscript. Please do not hesitate to contact the corresponding author if any additional information or clarification is required.

Conflicts of Interest: The authors declare no conflict of interest.

Disclosure Statement: The authors are unaware of any affiliations, memberships, funding, or financial holdings that might be perceived as affecting the objectivity of this review.

Abbreviations:

Abbreviation	Full name
GPI	Glycosylphosphatidylinositol
HVR	Hypervariable region
TMD	Transmembrane domain
PM	Plasma membrane
ER	Endoplasmic reticulum
PDEδ	Phosphodiesterase δ
PKC	Protein kinase C
RTKs	Receptor tyrosine kinases

GPCRs	G protein-coupled receptors
Ld	Liquid-disordered
MCS	Membrane contact sites
TGN	Trans-Golgi network
ORP	Oxysterol-binding protein (OSBP) related proteins
CCT	CTP:phosphocholine cytidylyltransferase
apoE	apolipoprotein E
rHDL	reconstituted high-density lipoprotein
PLCγ	phospholipase C-γ
PTMs	Posttranslational modifications
PC	Phosphatidylcholine
PS	phosphatidylserine
PA	Phosphatidic acid
PE	phosphatidylethanolamine
DAG	Diacylglycerol
PIPs	Phosphoinositides
PI	phosphatidylinositol
Bright	B-cell restricted factor
BCR	B cell receptor
mGluRs	membrane-localized metabotropic glutamate receptors
ROS	Reactive oxygen species
TPIP	TPTE and PTEN homologous inositol lipid phosphatase
TMH	Transmembrane helix
5′ss	5′ splice site
ER	Endoplasmic reticulum
NDI	Nephrogenic diabetes insipidus

References

1. Salter, M.W. and L.V. Kalia, *Src kinases: a hub for NMDA receptor regulation.* Nature Reviews Neuroscience, 2004. **5**(4): p. 317-328.
2. Cox, A.D., C.J. Der, and M.R. Philips, *Targeting RAS Membrane Association: Back to the Future for Anti-RAS Drug Discovery?* Clin Cancer Res, 2015. **21**(8): p. 1819-27.
3. Simanshu, D.K., D.V. Nissley, and F. McCormick, *RAS proteins and their regulators in human disease.* Cell, 2017. **170**(1): p. 17-33.
4. Resh, M.D., *Membrane Targeting of Lipid Modified Signal Transduction Proteins*, in *Membrane Dynamics and Domains: Subcellular Biochemistry*, P.J. Quinn, Editor. 2004, Springer US: Boston, MA. p. 217-232.
5. Zhou, Y., A.A. Gorfe, and J.F. Hancock, *RAS Nanoclusters Selectively Sort Distinct Lipid Headgroups and Acyl Chains.* Front Mol Biosci, 2021. **8**: p. 686338.
6. Ahearn, I.M., et al., *Regulating the regulator: post-translational modification of RAS.* Nature Reviews Molecular Cell Biology, 2012. **13**(1): p. 39-51.
7. Schmick, M., et al., *KRas Localizes to the Plasma Membrane by Spatial Cycles of Solubilization, Trapping and Vesicular Transport.* Cell, 2014. **157**(2): p. 459-471.
8. Yoshizaki, H., et al., *Akt-PDK1 complex mediates epidermal growth factor-induced membrane protrusion through Ral activation.* Mol Biol Cell, 2007. **18**(1): p. 119-28.

9. Giorgione, J.R., et al., *Increased membrane affinity of the C1 domain of protein kinase Cδ compensates for the lack of involvement of its C2 domain in membrane recruitment.* Journal of Biological Chemistry, 2006. **281**(3): p. 1660-1669.
10. Busse, R.A., et al., *Characterization of PROPPIN-Phosphoinositide Binding and Role of Loop 6CD in PROPPIN-Membrane Binding.* Biophys J, 2015. **108**(9): p. 2223-34.
11. Li, E. and K. Hristova, *Role of receptor tyrosine kinase transmembrane domains in cell signaling and human pathologies.* Biochemistry, 2006. **45**(20): p. 6241-51.
12. Inanobe, A. and Y. Kurachi, *Membrane channels as integrators of G-protein-mediated signaling.* Biochimica et Biophysica Acta (BBA) - Biomembranes, 2014. **1838**(2): p. 521-531.
13. Roy, S., et al., *Individual palmitoyl residues serve distinct roles in H-ras trafficking, microlocalization, and signaling.* Mol Cell Biol, 2005. **25**(15): p. 6722-33.
14. Abankwa, D., A.A. Gorfe, and J.F. Hancock, *Ras nanoclusters: molecular structure and assembly.* Semin Cell Dev Biol, 2007. **18**(5): p. 599-607.
15. León-Fuentes, I.M., et al., *Connexins in Cancer, the Possible Role of Connexin46 as a Cancer Stem Cell-Determining Protein.* Biomolecules, 2023. **13**(10): p. 1460.
16. Runfola, M., et al., *The N-terminal Acetylation of α-Synuclein Changes the Affinity for Lipid Membranes but not the Structural Properties of the Bound State.* Scientific Reports, 2020. **10**(1): p. 204.
17. DeBose-Boyd, R.A., *Feedback regulation of cholesterol synthesis: sterol-accelerated ubiquitination and degradation of HMG CoA reductase.* Cell Res, 2008. **18**(6): p. 609-21.
18. Dunne, S.J., et al., *Structure of the membrane binding domain of CTP: phosphocholine cytidylyltransferase.* Biochemistry, 1996. **35**(37): p. 11975-11984.
19. Cornell, R.B. and N.D. Ridgway, *CTP:phosphocholine cytidylyltransferase: Function, regulation, and structure of an amphitropic enzyme required for membrane biogenesis.* Progress in Lipid Research, 2015. **59**: p. 147-171.
20. Kothari, S., et al., *The LDL receptor binding domain of apolipoprotein E directs the relative orientation of its C-terminal segment in reconstituted nascent HDL.* Biochim Biophys Acta Biomembr, 2021. **1863**(7): p. 183618.
21. Jun, J.E., I. Rubio, and J.P. Roose, *Regulation of ras exchange factors and cellular localization of ras activation by lipid messengers in T cells.* Front Immunol, 2013. **4**: p. 239.
22. Nimnual, A. and D. Bar-Sagi, *The Two Hats of SOS.* Science's STKE, 2002. **2002**(145): p. pe36-pe36.
23. Eberth, A., et al., *A BAR domain-mediated autoinhibitory mechanism for RhoGAPs of the GRAF family.* Biochem J, 2009. **417**(1): p. 371-7.
24. Jiang, L., et al., *CLIC proteins, ezrin, radixin, moesin and the coupling of membranes to the actin cytoskeleton: A smoking gun?* Biochimica et Biophysica Acta (BBA) - Biomembranes, 2014. **1838**(2): p. 643-657.
25. Seidel, R.D., 3rd, et al., *Conformational changes in human Arf1 on nucleotide exchange and deletion of membrane-binding elements.* J Biol Chem, 2004. **279**(46): p. 48307-18.
26. Anggono, V. and P.J. Robinson, *Dynamin*, in *Encyclopedia of Neuroscience*, L.R. Squire, Editor. 2009, Academic Press: Oxford. p. 725-735.
27. Lizarrondo, J., et al., *Structure of the endocytic adaptor complex reveals the basis for efficient membrane anchoring during clathrin-mediated endocytosis.* Nature Communications, 2021. **12**(1): p. 2889.

28. Ford, M.G., et al., *Curvature of clathrin-coated pits driven by epsin.* Nature, 2002. **419**(6905): p. 361-6.
29. Peter, B.J., et al., *BAR domains as sensors of membrane curvature: the amphiphysin BAR structure.* Science, 2004. **303**(5657): p. 495-499.
30. Mim, C. and V.M. Unger, *Membrane curvature and its generation by BAR proteins.* Trends Biochem Sci, 2012. **37**(12): p. 526-33.
31. Wang, Y., et al., *Insights into membrane association of the SMP domain of extended synaptotagmin.* Nature Communications, 2023. **14**(1): p. 1504.
32. Lee, I.H., et al., *Lipid Raft Phase Modulation by Membrane-Anchored Proteins with Inherent Phase Separation Properties.* ACS Omega, 2019. **4**(4): p. 6551-6559.
33. Ditlev, J.A., *Membrane-associated phase separation: organization and function emerge from a two-dimensional milieu.* J Mol Cell Biol, 2021. **13**(4): p. 319-324.
34. Lemmon, M.A., *Membrane recognition by phospholipid-binding domains.* Nature Reviews Molecular Cell Biology, 2008. **9**(2): p. 99-111.
35. Hyun, T.S., et al., *HIP1 and HIP1r stabilize receptor tyrosine kinases and bind 3-phosphoinositides via epsin N-terminal homology domains.* Journal of Biological Chemistry, 2004. **279**(14): p. 14294-14306.
36. Singh, N., et al., *Redefining the specificity of phosphoinositide-binding by human PH domain-containing proteins.* Nature Communications, 2021. **12**(1): p. 4339.
37. Chandra, M., et al., *Classification of the human phox homology (PX) domains based on their phosphoinositide binding specificities.* Nature communications, 2019. **10**(1): p. 1-14.
38. Bandorowicz-Pikula, J., M. Wos, and S. Pikula, *Do annexins participate in lipid messenger mediated intracellular signaling? A question revisited.* Mol Membr Biol, 2012. **29**(7): p. 229-42.
39. Zhou, Y. and J.F. Hancock, *Lipid Profiles of RAS Nanoclusters Regulate RAS Function.* Biomolecules, 2021. **11**(10): p. 1439.
40. Colón-González, F. and M.G. Kazanietz, *C1 domains exposed: From diacylglycerol binding to protein–protein interactions.* Biochimica et Biophysica Acta (BBA) - Molecular and Cell Biology of Lipids, 2006. **1761**(8): p. 827-837.
41. Stahelin, R.V., *Lipid binding domains: more than simple lipid effectors.* Journal of lipid research, 2009. **50**(Supplement): p. S299-S304.
42. Manna, D., et al., *Mechanistic Basis of Differential Cellular Responses of Phosphatidylinositol 3,4-Bisphosphate- and Phosphatidylinositol 3,4,5-Trisphosphate-binding Pleckstrin Homology Domains*.* Journal of Biological Chemistry, 2007. **282**(44): p. 32093-32105.
43. Stahelin, R.V., et al., *Phosphatidylinositol 3-phosphate induces the membrane penetration of the FYVE domains of Vps27p and Hrs.* Journal of Biological Chemistry, 2002. **277**(29): p. 26379-26388.
44. Stahelin, R.V., et al., *Membrane Binding Mechanisms of the PX Domains of NADPH Oxidase p40phox and p47phox*.* Journal of Biological Chemistry, 2003. **278**(16): p. 14469-14479.
45. Garcia-Alai, M.M., et al., *Epsin and Sla2 form assemblies through phospholipid interfaces.* Nature Communications, 2018. **9**(1): p. 328.
46. Ray, A., N. Jatana, and L. Thukral, *Lipidated proteins: Spotlight on protein-membrane binding interfaces.* Progress in Biophysics and Molecular Biology, 2017. **128**: p. 74-84.

47. Gallop, J.L., et al., *Mechanism of endophilin N-BAR domain-mediated membrane curvature.* Embo j, 2006. **25**(12): p. 2898-910.
48. Legendre-Guillemin, V., et al., *ENTH/ANTH proteins and clathrin-mediated membrane budding.* Journal of cell science, 2004. **117**(1): p. 9-18.
49. Gallego, O., et al., *A systematic screen for protein–lipid interactions in Saccharomyces cerevisiae.* Molecular systems biology, 2010. **6**(1): p. 430.
50. Zheng, J., et al., *The solution structure of the pleckstrin homology domain of human SOS1: a possible structural role for the sequential association of diffuse B cell lymphoma and pleckstrin homology domains.* Journal of Biological Chemistry, 1997. **272**(48): p. 30340-30344.
51. Karathanassis, D., et al., *Binding of the PX domain of p47^{phox} to phosphatidylinositol 3,4‐bisphosphate and phosphatidic acid is masked by an intramolecular interaction.* The EMBO Journal, 2002. **21**(19): p. 5057-5068-5068.
52. Zhao, C., et al., *Phospholipase D2-generated phosphatidic acid couples EGFR stimulation to Ras activation by Sos.* Nature cell biology, 2007. **9**(6): p. 707-712.
53. Moravcevic, K., Camilla L. Oxley, and Mark A. Lemmon, *Conditional Peripheral Membrane Proteins: Facing up to Limited Specificity.* Structure, 2012. **20**(1): p. 15-27.
54. Guerrero-Valero, M., et al., *Structural and mechanistic insights into the association of PKCα-C2 domain to PtdIns(4,5)P₂.* Proceedings of the National Academy of Sciences, 2009. **106**(16): p. 6603-6607.
55. He, J., et al., *Molecular basis of phosphatidylinositol 4-phosphate and ARF1 GTPase recognition by the FAPP1 pleckstrin homology (PH) domain.* J Biol Chem, 2011. **286**(21): p. 18650-7.
56. Stolt, P.C., et al., *Origins of Peptide Selectivity and Phosphoinositide Binding Revealed by Structures of Disabled-1 PTB Domain Complexes.* Structure, 2003. **11**(5): p. 569-579.
57. Lizarbe, M.A., et al., *Annexin-phospholipid interactions. Functional implications.* International journal of molecular sciences, 2013. **14**(2): p. 2652-2683.
58. Dumas, J.J., et al., *Multivalent Endosome Targeting by Homodimeric EEA1.* Molecular Cell, 2001. **8**(5): p. 947-958.
59. Prichard, K.L., et al., *Role of clathrin and dynamin in clathrin mediated endocytosis/synaptic vesicle recycling and implications in neurological diseases.* Frontiers in Cellular Neuroscience, 2022. **15**: p. 754110.
60. Lemmon, M.A. and J. Schlessinger, *Cell signaling by receptor tyrosine kinases.* Cell, 2010. **141**(7): p. 1117-34.
61. Trousdale, C. and K. Kim, *Retromer: Structure, function, and roles in mammalian disease.* European Journal of Cell Biology, 2015. **94**(11): p. 513-521.
62. Gorfe, A.A., *Mechanisms of allostery and membrane attachment in Ras GTPases: implications for anti-cancer drug discovery.* Current medicinal chemistry, 2010. **17**(1): p. 1-9.
63. Oancea, E. and T. Meyer, *Protein kinase C as a molecular machine for decoding calcium and diacylglycerol signals.* Cell, 1998. **95**(3): p. 307-318.
64. Walker, S.A., et al., *Identification of a Ras GTPase-activating protein regulated by receptor-mediated Ca2+ oscillations.* Embo j, 2004. **23**(8): p. 1749-60.
65. Martin, C., et al., *Intracellular pH gradients in migrating cells.* American Journal of Physiology-Cell Physiology, 2011. **300**(3): p. C490-C495.

66. Davies, K.M., et al., *Macromolecular organization of ATP synthase and complex I in whole mitochondria.* Proceedings of the National Academy of Sciences, 2011. **108**(34): p. 14121-14126.
67. Angelova, M.I., et al., *pH sensing by lipids in membranes: The fundamentals of pH-driven migration, polarization and deformations of lipid bilayer assemblies.* Biochimica et Biophysica Acta (BBA) - Biomembranes, 2018. **1860**(10): p. 2042-2063.
68. Hawkins, T.E., C.J. Merrifield, and S.E. Moss, *Calcium signaling and annexins.* Cell Biochemistry and Biophysics, 2000. **33**: p. 275-296.
69. Monastyrskaya, K., et al., *Annexins as intracellular calcium sensors.* Cell Calcium, 2007. **41**(3): p. 207-219.
70. Hoque, M., et al., *Annexins—Scaffolds modulating PKC localization and signaling.* Cellular signalling, 2014. **26**(6): p. 1213-1225.
71. Solito, E., et al., *Post-translational modification plays an essential role in the translocation of annexin A1 from the cytoplasm to the cell surface.* Faseb j, 2006. **20**(9): p. 1498-500.
72. Benz, J. and A. Hofmann, *Annexins: From structure to function.* Biological Chemistry, 1997. **378**(3-4): p. 177-183.
73. Valapala, M. and J.K. Vishwanatha, *Lipid raft endocytosis and exosomal transport facilitate extracellular trafficking of annexin A2.* Journal of Biological Chemistry, 2011. **286**(35): p. 30911-30925.
74. Grindheim, A.K., J. Saraste, and A. Vedeler, *Protein phosphorylation and its role in the regulation of Annexin A2 function.* Biochimica et Biophysica Acta - General Subjects, 2017. **1861**(11): p. 2515-2529.
75. Moss, S.E., et al., *A growth-dependent post-translational modification of annexin VI.* Biochimica et Biophysica Acta (BBA)/Protein Structure and Molecular, 1992. **1160**(1): p. 120-126.
76. Furge, L.L., K. Chen, and S. Cohen, *Annexin VII and annexin XI are tyrosine phosphorylated in peroxovanadate-treated dogs and in platelet-derived growth factor-treated rat vascular smooth muscle cells.* J Biol Chem, 1999. **274**(47): p. 33504-9.
77. Moshkanbaryans, L., L.S. Chan, and M.E. Graham, *The biochemical properties and functions of CALM and AP180 in clathrin mediated endocytosis.* 2014, MDPI AG. p. 388-413.
78. Kaneko, T., et al., *Rho mediates endocytosis of epidermal growth factor receptor through phosphorylation of endophilin A1 by Rho-kinase.* Genes to Cells, 2005. **10**(10): p. 973-987.
79. Salzer, U., J. Kostan, and K. Djinović-Carugo, *Deciphering the BAR code of membrane modulators.* Cellular and Molecular Life Sciences 2017 74:13, 2017. **74**(13): p. 2413-2438.
80. Matta, S., et al., *LRRK2 controls an EndoA phosphorylation cycle in synaptic endocytosis.* Neuron, 2012. **75**(6): p. 1008-21.
81. Quan, A., et al., *Phosphorylation of syndapin I F-BAR domain at two helix-capping motifs regulates membrane tubulation.* Proc Natl Acad Sci U S A, 2012. **109**(10): p. 3760-5.
82. Salzer, E., et al., *Protein Kinase C δ: a Gatekeeper of Immune Homeostasis.* Journal of Clinical Immunology, 2016. **36**(7): p. 631-640.
83. Steinberg, S.F., *Distinctive activation mechanisms and functions for protein kinase Cdelta.* Biochem J, 2004. **384**(Pt 3): p. 449-59.

84. Lee, Y.R., M. Chen, and P.P. Pandolfi, *The functions and regulation of the PTEN tumour suppressor: new modes and prospects.* Nature Reviews Molecular Cell Biology, 2018. **19**(9): p. 547-562.
85. Mishra, R.R., J.K. Chaudhary, and P.C. Rath, *Cell cycle arrest and apoptosis by expression of a novel TPIP (TPIP-C2) cDNA encoding a C2-domain in HEK-293 cells.* Molecular Biology Reports, 2012. **39**(7): p. 7389-7402.
86. Jiménez, J.L., et al., *A systematic comparative and structural analysis of protein phosphorylation sites based on the mtcPTM database.* Genome Biology, 2007. **8**(5): p. R90-R90.
87. Michie, K.A., et al., *Two Sides of the Coin: Ezrin/Radixin/Moesin and Merlin Control Membrane Structure and Contact Inhibition.* 2019, NLM (Medline).
88. García-Ortiz, A. and J.M. Serrador, *ERM proteins at the crossroad of leukocyte polarization, migration and intercellular adhesion.* International Journal of Molecular Sciences, 2020. **21**(4): p. 1502.
89. Lawson, C. and D.D. Schlaepfer, *Phocal adhesion kinase regulation is on a FERM foundation.* Journal of Cell Biology, 2013. **202**(6): p. 833-836.
90. Dimarco Hewitt, P., *Regulation of Cell Adhesion by the FERM Proteins, PTPN14 and Merlin.* 2015.
91. Eitzen, G., et al., *Structure and function of the Fgd family of divergent FYVE domain proteins.* Biochemistry and Cell Biology, 2019. **97**(3): p. 257-264.
92. Mosesson, Y., et al., *Monoubiquitinylation Regulates Endosomal Localization of Lst2, a Negative Regulator of EGF Receptor Signaling.* Developmental Cell, 2009. **16**(5): p. 687-698.
93. *POST-TRANSLATIONAL MODIFICATION AND REGULATION OF HUMAN SPIR PROTEIN.* 2011.
94. Sechi, S., et al., *Oncogenic roles of GOLPH3 in the physiopathology of cancer.* International Journal of Molecular Sciences, 2020. **21**(3).
95. Gong, E.-Y., et al., *Chk1 KA1 domain auto-phosphorylation stimulates biological activity and is linked to rapid proteasomal degradation.* Scientific reports, 2018. **8**(1): p. 1-11.
96. Gil, A., et al., *Nuclear localization of PTEN by a Ran-dependent mechanism enhances apoptosis: Involvement of an N-terminal nuclear localization domain and multiple nuclear exclusion motifs.* Mol Biol Cell, 2006. **17**(9): p. 4002-13.
97. Bassi, C., et al., *Nuclear PTEN controls DNA repair and sensitivity to genotoxic stress.* Science, 2013. **341**(6144): p. 395-9.
98. Papa, A., et al., *Cancer-associated PTEN mutants act in a dominant-negative manner to suppress PTEN protein function.* Cell, 2014. **157**(3): p. 595-610.
99. Lee, H.J. and J.J. Zheng, *PDZ domains and their binding partners: Structure, specificity, and modification.* Cell Communication and Signaling, 2010. **8**(May).
100. Zimmermann, P., *The prevalence and significance of PDZ domain–phosphoinositide interactions.* Biochimica et Biophysica Acta (BBA) - Molecular and Cell Biology of Lipids, 2006. **1761**(8): p. 947-956.
101. Gallardo, R., et al., *Structural Diversity of PDZ–Lipid Interactions.* ChemBioChem, 2010. **11**(4): p. 456-467.
102. Li, X., et al., *Autophosphorylation of Akt at threonine 72 and serine 246: A potential mechanism of regulation of Akt kinase activity.* Journal of Biological Chemistry, 2006. **281**(19): p. 13837-13843.

103. Navarro-corcuera, A., et al., *AGAP2: Modulating TGFβ1-signaling in the regulation of liver fibrosis*. 2020, MDPI AG. p. 1400-1400.
104. Nazmi, A.R., et al., *N-terminal acetylation of annexin A2 is required for S100A10 binding*. Biological Chemistry, 2012. **393**(10): p. 1141-1150.
105. Ikenoue, T., et al., *PTEN Acetylation Modulates Its Interaction with PDZ Domain.* Cancer Research, 2008. **68**(17): p. 6908-6912.
106. Peng, J. and L. He, *IRS posttranslational modifications in regulating insulin signaling.* Journal of Molecular Endocrinology, 2018. **60**(1): p. R1-R8.
107. Guo, S., *Insulin signaling, resistance, and the metabolic syndrome: insights from mouse models into disease mechanisms.* J Endocrinol, 2014. **220**(2): p. T1-t23.
108. Schmidt, C., et al., *Signalling of the BCR is regulated by a lipid rafts-localised transcription factor, Bright*. Embo j, 2009. **28**(6): p. 711-24.
109. Rajan, S., et al., *Sumoylation silences the plasma membrane leak K+ channel K2P1*. Cell, 2005. **121**(1): p. 37-47.
110. Tang, Z., et al., *Pias1 Interaction and Sumoylation of Metabotropic Glutamate Receptor 8*.* Journal of Biological Chemistry, 2005. **280**(46): p. 38153-38159.
111. Huang, J., et al., *SUMO1 modification of PTEN regulates tumorigenesis by controlling its association with the plasma membrane*. Nature Communications, 2012. **3**(1): p. 911.
112. Kadaré, G., et al., *PIAS1-mediated Sumoylation of Focal Adhesion Kinase Activates Its Autophosphorylationn**. Journal of Biological Chemistry, 2003. **278**(48): p. 47434-47440.
113. Lim, S.T., et al., *Nuclear FAK promotes cell proliferation and survival through FERM-enhanced p53 degradation.* Mol Cell, 2008. **29**(1): p. 9-22.
114. Qi, Q., et al., *Merlin sumoylation is required for its tumor suppressor activity.* Oncogene, 2014. **33**(41): p. 4893-4903.
115. Hirata, F., L.M. Thibodeau, and A. Hirata, *Ubiquitination and SUMOylation of annexin A1 and helicase activity*. Biochimica et Biophysica Acta (BBA) - General Subjects, 2010. **1800**(9): p. 899-905.
116. Huang, T.T. and A.D. D'Andrea, *Regulation of DNA repair by ubiquitylation.* Nature Reviews Molecular Cell Biology, 2006. **7**(5): p. 323-334.
117. Ando, Y., et al., *Calcium-induced intracellular cross-linking of lipocortin I by tissue transglutaminase in A431 cells. Augmentation by membrane phospholipids*. Journal of Biological Chemistry, 1991. **266**(2): p. 1101-1108.
118. Li, H., Z. Yang, and Z. Gao, *Chapter Four - Protein tyrosine nitration: Chemistry and role in diseases*, in *Advances in Molecular Toxicology*, J.C. Fishbein and J.M. Heilman, Editors. 2019, Elsevier. p. 109-128.
119. Zhan, X. and D.M. Desiderio, *The human pituitary nitroproteome: detection of nitrotyrosyl-proteins with two-dimensional Western blotting, and amino acid sequence determination with mass spectrometry*. Biochemical and Biophysical Research Communications, 2004. **325**(4): p. 1180-1186.
120. Vrljic, M., et al., *Post-translational modifications and lipid binding profile of insect cell-expressed full-length mammalian synaptotagmin 1*. Biochemistry, 2011. **50**(46): p. 9998-10012.
121. Lin, D. and D.J. Takemoto, *Oxidative Activation of Protein Kinase Cγ through the C1 Domain: EFFECTS ON GAP JUNCTIONS**. Journal of Biological Chemistry, 2005. **280**(14): p. 13682-13693.

122. Bahia, P.K., et al., *Antimycin A increases bronchopulmonary C-fiber excitability via protein kinase C alpha.* Respiratory Physiology & Neurobiology, 2020. **278**: p. 103446.
123. Knapp, L.T. and E. Klann, *Superoxide-induced stimulation of protein kinase C via thiol modification and modulation of zinc content.* Journal of Biological Chemistry, 2000. **275**(31): p. 24136-24145.
124. Giorgi, C., et al., *Redox control of protein kinase C: cell- and disease-specific aspects.* Antioxid Redox Signal, 2010. **13**(7): p. 1051-85.
125. Kannicht, C., et al., *Characterisation of the post-translational modifications of a novel, human cell line-derived recombinant human factor VIII.* Thrombosis research, 2013. **131**(1): p. 78-88.
126. Kosloski, M.P., R.D. Miclea, and S.V. Balu-Iyer, *Role of glycosylation in conformational stability, activity, macromolecular interaction and immunogenicity of recombinant human factor VIII.* The AAPS journal, 2009. **11**: p. 424-431.
127. Nicolaes, G.A.F., B.O. Villoutreix, and B. Dahlbäck, *Partial Glycosylation of Asn2181 in Human Factor V as a Cause of Molecular and Functional Heterogeneity. Modulation of Glycosylation Efficiency by Mutagenesis of the Consensus Sequence for N-Linked Glycosylation.* Biochemistry, 1999. **38**(41): p. 13584-13591.
128. Trotman, L.C., et al., *Ubiquitination Regulates PTEN Nuclear Import and Tumor Suppression.* Cell, 2007. **128**(1): p. 141-156.
129. Wang, X., et al., *NEDD4-1 Is a Proto-Oncogenic Ubiquitin Ligase for PTEN.* Cell, 2007. **128**(1): p. 129-139.
130. K.M. Ip, C., et al., *Genomic-Glycosylation Aberrations in Tumor Initiation, Progression and Management.* AIMS Medical Science, 2016. **3**(4): p. 386-416.
131. Pittman, D.D., et al., *Posttranslational Sulfation of Factor V Is Required for Efficient Thrombin Cleavage and Activation and for Full Procoagulant Activity.* Biochemistry, 1994. **33**(22): p. 6952-6959.
132. Schönichen, A., et al., *Considering protonation as a posttranslational modification regulating protein structure and function.* Annu Rev Biophys, 2013. **42**: p. 289-314.
133. Schurgers, L.J., et al., *Post-translational modifications regulate matrix Gla protein function: Importance for inhibition of vascular smooth muscle cell calcification.* Journal of Thrombosis and Haemostasis, 2007. **5**(12): p. 2503-2511.
134. Yazicioglu, M.N., et al., *Cellular localization and characterization of cytosolic binding partners for gla domain-containing proteins PRRG4 and PRRG2.* Journal of Biological Chemistry, 2013. **288**(36): p. 25908-25914.
135. Kulman, J.D., et al., *Identification of two novel transmembrane gamma-carboxyglutamic acid proteins expressed broadly in fetal and adult tissues.* Proc Natl Acad Sci U S A, 2001. **98**(4): p. 1370-5.
136. Zwaal, R.F.A., P. Comfurius, and E.M. Bevers, *Lipid–protein interactions in blood coagulation.* Biochimica et Biophysica Acta (BBA) - Reviews on Biomembranes, 1998. **1376**(3): p. 433-453.
137. Meuillet, E.J., et al., *Thioredoxin-1 binds to the C2 domain of PTEN inhibiting PTEN's lipid phosphatase activity and membrane binding: a mechanism for the functional loss of PTEN's tumor suppressor activity.* Archives of Biochemistry and Biophysics, 2004. **429**(2): p. 123-133.
138. Cheng, A.C., et al., *Structure-based maximal affinity model predicts small-molecule druggability.* Nature biotechnology, 2007. **25**(1): p. 71-75.

139. Yin, H., *Exogenous Agents that Target Transmembrane Domains of Proteins.* Angewandte Chemie International Edition, 2008. **47**(15): p. 2744-2752.
140. Kiriakidi, S., et al., *Exploring the role of the membrane bilayer in the recognition of candesartan by its GPCR AT1 receptor.* Biochimica et Biophysica Acta (BBA) - Biomembranes, 2020. **1862**(3): p. 183142.
141. Róg, T., M. Girych, and A. Bunker, *Mechanistic Understanding from Molecular Dynamics in Pharmaceutical Research 2: Lipid Membrane in Drug Design.* Pharmaceuticals, 2021. **14**(10): p. 1062.
142. Rask-Andersen, M., M.S. Almén, and H.B. Schiöth, *Trends in the exploitation of novel drug targets.* Nature Reviews Drug Discovery, 2011. **10**(8): p. 579-590.
143. Davenport, A.P., et al., *Advances in therapeutic peptides targeting G protein-coupled receptors.* Nature Reviews Drug Discovery, 2020. **19**(6): p. 389-413.
144. Zhang, M., et al., *G protein-coupled receptors (GPCRs): advances in structures, mechanisms, and drug discovery.* Signal Transduction and Targeted Therapy, 2024. **9**(1): p. 88.
145. Estabrooks, S. and J.L. Brodsky, *Regulation of CFTR Biogenesis by the Proteostatic Network and Pharmacological Modulators.* Int J Mol Sci, 2020. **21**(2).
146. Lopes-Pacheco, M., et al., *Combination of Correctors Rescues CFTR Transmembrane-Domain Mutants by Mitigating their Interactions with Proteostasis.* Cell Physiol Biochem, 2017. **41**(6): p. 2194-2210.
147. Myers, J.K., C.K. Mobley, and C.R. Sanders, *The peripheral neuropathy-linked Trembler and Trembler-J mutant forms of peripheral myelin protein 22 are folding-destabilized.* Biochemistry, 2008. **47**(40): p. 10620-9.
148. Morello, J.P., et al., *Pharmacological chaperones rescue cell-surface expression and function of misfolded V2 vasopressin receptor mutants.* Journal of Clinical Investigation, 2000. **105**(7): p. 887-895.
149. Bernier, V., D.G. Bichet, and M. Bouvier, *Pharmacological chaperone action on G-protein-coupled receptors.* Current Opinion in Pharmacology, 2004. **4**(5): p. 528-533.
150. Chen, R.S. and P.M. Best, *A small peptide inhibitor of the low voltage-activated calcium channel Cav3.1.* Mol Pharmacol, 2009. **75**(5): p. 1042-51.
151. Arpel, A., et al., *Transmembrane domain targeting peptide antagonizing ErbB2/Neu inhibits breast tumor growth and metastasis.* Cell Rep, 2014. **8**(6): p. 1714-1721.
152. Nasarre, C., et al., *Peptide-based interference of the transmembrane domain of neuropilin-1 inhibits glioma growth in vivo.* Oncogene, 2010. **29**(16): p. 2381-2392.
153. Harikumar, K.G., D.I. Pinon, and L.J. Miller, *Transmembrane Segment IV Contributes a Functionally Important Interface for Oligomerization of the Class II G Protein-coupled Secretin Receptor*.* Journal of Biological Chemistry, 2007. **282**(42): p. 30363-30372.
154. Konstantinopoulos, P.A., M.V. Karamouzis, and A.G. Papavassiliou, *Post-translational modifications and regulation of the RAS superfamily of GTPases as anticancer targets.* Nature Reviews Drug Discovery, 2007. **6**(7): p. 541-555.
155. Ganesan, L. and I. Levental, *Pharmacological Inhibition of Protein Lipidation.* J Membr Biol, 2015. **248**(6): p. 929-41.
156. Chen, X., et al., *AAV9/MFSD8 gene therapy is effective in preclinical models of neuronal ceroid lipofuscinosis type 7 disease.* J Clin Invest, 2022. **132**(5).
157. Sharma, J., et al., *A small molecule that induces translational readthrough of CFTR nonsense mutations by eRF1 depletion.* Nature Communications, 2021. **12**(1): p. 4358.

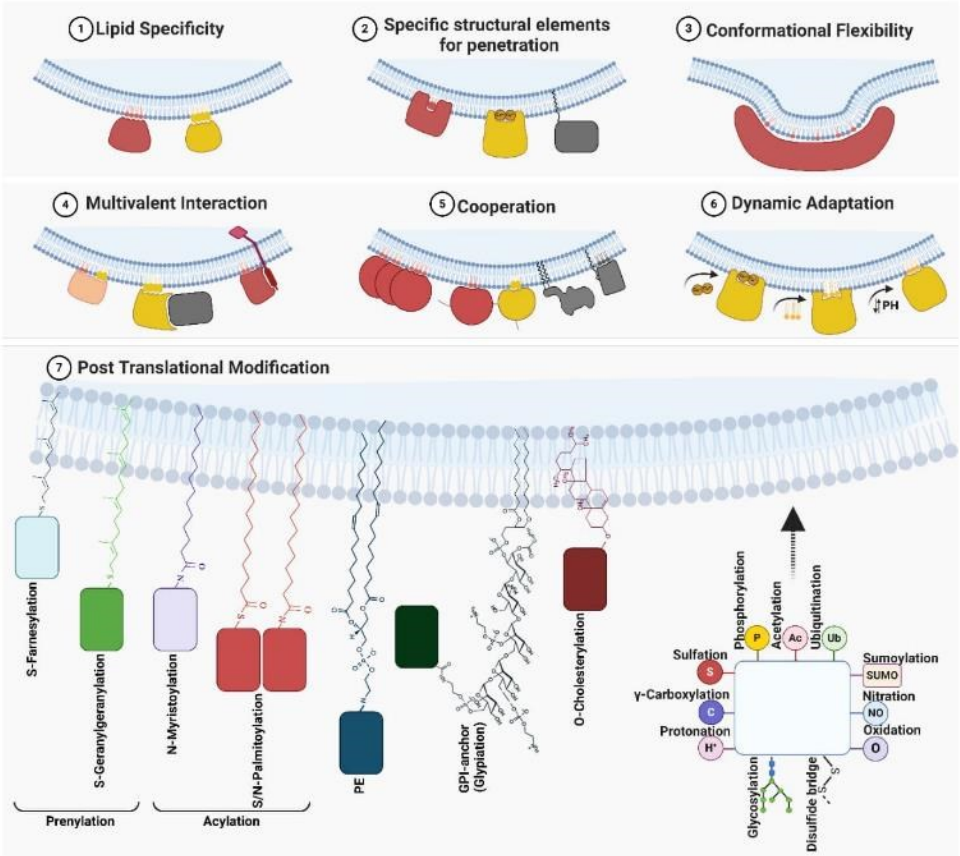

Figure 1. Schematic representation of membrane binding strategies (1-7). (1) Lipid specificity: Membrane binding domains exhibit specificity for certain lipids. (2) Specific structural elements for membrane penetration include the use of hydrophobic residues for membrane insertion. In certain cases, calcium ions facilitate structural changes that promote membrane interaction. In addition, lipidation enhances membrane insertion by facilitating in stable association with membranes. (3) Conformational flexibility: Protein domains adapt their structure to promote membrane curvature. (4) Multivalent interaction refers to the ability of membrane-binding proteins to simultaneously engage with multiple targets within the same domain, such as different lipid species, other proteins, or receptor proteins. This simultaneous engagement enhances the regulatory potential of their interactions with cell membranes. (5) Cooperation of multiple modules: Cooperative mechanisms include domain oligomerization to facilitate robust membrane association or the engagement of multiple modules (domains or motifs) within the same protein, such as two membrane binding domains or two lipidations or a combination of a membrane binding domain with lipidations. (6) Dynamic adaptation to cellular conditions: Membrane interactions are in some cases modulated by cellular factors such as cofactor availability, lipid composition, and pH changes. (7) Regulation by post-translational modifications (PTMs) in membrane binding. PTMs such as lipidations (e.g., prenylation, acylation, PE addition, GPI anchoring, cholesterylation) facilitate protein recruitment to membranes. Other PTMs that modulate membrane interaction include phosphorylation, acetylation, ubiquitination, sumoylation, nitration, oxidation, sulfation, γ-carboxylation, protonation, glycosylation, and disulfide bridge.

Table 1, Lipid-binding motifs.

Lipid-binding Motifs	Modification	Sub-Categories	Proteins	Motif Sequence	Comments	Ref.
Polybasic group	----	----	Src	N_{term}- MGSNKSKPKDASQRRSLEPD	In addition to myristoylation and S-palmitoylation	[1]
			K-Ras 4B	KMSKDGKKKKKSKTKCVIM-C_{term}		[1]
			MARKCS	N_{term}- MGAFSKTAAK …*(polybasic ed)*…	In addition to myristoylation	[1]
			Rap1a	NRKTPVDKKKPKKKSCLLL-C_{term}	In addition to geranylgeranylation	[1]
			Rit	KNSVWKRLKSPFRKKKDSVT-C_{term}		[1]
Motifs with recognition signal	Prenylation	Farnesylation	N-Ras	LNSSDDGTQGCMGLPCVVM-C_{term}		[1, 2]
			H-Ras	LNPPDESGPGCMSCKCVLS -C_{term}		[1, 2]
			Paralemmin	DMKKHRCKCCSIM-C_{term}		[1, 3]
			K-Ras 4A	KKISKEEKTPGCVKIKKCIIM-C_{term}		[4]
			K-Ras 4B	KMSKDGKKKKKSKTKCVIM-Cterm		[1]
			p21rho	----	In addition to Geranylgeranylation	[5]
			Rheb	----		[6]
		Geranylgeranylation	Rab8	GVKITPDQQKRSSFFRCVLL-C_{term}		[1]
			Rab5a	GGGVDLTEPTQPTRNQCCSN-C_{term}	Dual geranylgeranylation	[1]
			Rab14	EPIKLDKNDRAKASAESCSC-C_{term}	Dual geranylgeranylation	[1]
			Rap2b	NTAAQSNGDEGCCSACVIL-C_{term}		[1]
			Rap1a	NRKTPVDKKKPKKKSCLLL-C_{term}	In addition to protein- based polybasic group	[1]
			p21rho	---	In addition to Farnesylation	[5]
	Myristoylation		Lyn	N_{term}- M**G**CIKSKGKDSLSDDG···	Underlined G-2 residues are sites for N-myristoylation	[1, 7, 8]
			$G_{i\alpha1}$	N_{term}- MGCTLSAEDK		[1]
			Fyn	N_{term}- M**G**CVQCKDKEATKLTE····	Underlined G-2 residues are sites for N-myristoylation	[1, 7, 8]
			Src	N_{term}- M**G**SNKSKPKDASQRRR···	Underlined G-2 residues are sites for N-myristoylation, In addition to protein-based polybasic group and S-palmitoylation	[1, 7, 8]
			MARKCS	N_{term}- MGAFSKTAAK …*(polybasic ed)*…	In addition to protein- based polybasic group	[1]
			Yes	N_{term}- M**G**CIKSKENKSPAIKY···	Underlined G-2 residues are sites for N-myristoylation	[7, 8]
			Fgr	N_{term}- M**G**CVFCKKLEPVATAK···	Underlined G-2 residues are sites for N-myristoylation	[7]
			Lck	N_{term}-M**G**CGCSSHPEDDWMEN···	Underlined G-2 residues are sites for N-myristoylation	[7, 8]
			Hck	N_{term}-M**G**GRSSCEDPGCPRDE···	Underlined G-2 residues are sites for N-myristoylation	[7]
			Blk	N_{term}-M**G**LVSSKKPDKEKPIK···	Underlined G-2 residues are sites for N-myristoylation	[7]
			ARF	-----	N-myristoylation	[9]

			Annexin A13a and A13b	-----	N-myristoylation	[10]
	Palmitoylation	S-Palmitoylation	N-Ras	LNSSDDGTQGCMGLPCVVM-C_{term}		[1, 2]
			H-Ras	LNPPDESGPGCMSCKCVLS -C_{term}	Reversible S-Palmitoylation	[1, 2]
			K-Ras 4A	KKISKEEKTPGCVKIKKCIIM-C_{term}		[4]
			GAP-43	N_{term}- MLCCMRRTKQV	Reversible S-Palmitoylation	[1, 11]
			PSD-95	N_{term}- MDCLCIVTTKKY	Reversible S-Palmitoylation	[1, 12]
			ABP-L	N_{term}- MRGWLRRNLALCLQRPLP		[1, 13]
			$G_{s\alpha}$	N_{term}- N-GCLGNSKTE	Reversible S-Palmitoylation	[1, 14]
			Lyn	N_{term}- MGCIKSKGKD		[1, 8]
			$G_{i\alpha1}$	N_{term}- MGCTLSAEDK		[1]
			Fyn	N_{term}-MGCVQCKDKEATKLTE		[1, 8]
			Src	N_{term}- MGSNKSKPKDASQRRSLEPD	In addition to protein- based polybasic group and myristoylation	[1, 8]
			Rap2b	NTAAQSNGDEGCCSACVIL-C_{term}		[1]
			Paralemmin	DMKKHRCKCCSIM-C_{term}		[1, 3]
			Bright	C342		[15]
		N-palmitoylation	Hedgehog	N_{term}-N-CGPGP….G-C_{term}	Modification with cholestrol and palmitate at same time	[1, 2, 16]
			OprM	---	N-palmitoylated cysteine	[17]
			$G_{s\alpha}$	N_{term}- N-GCLGNSKTE	Reversible N-Palmitoylation	[1, 14]
	Cholesteroylation		Hedgehog	N_{term}-N-CGPGP….G-C_{term}	Modification with cholestrol and palmitate at same time	[1, 2, 16]
	GPI-anchor (Glypiation)		PrP	Position 230 at the C-terminal		[1, 18, 19]
			CD59	---		[20]
	Phosphatidylethanolamine (PE) Conjugation		LC3	C-terminal glycine		[21]

Table 2. Posttranslational modification in membrane integration

Post translational Modification	Protein	Common Residue (Location)	Ref.
phosphorylation	ANXA1	Y20, T24, S27, S28 (N-term)	[10, 22, 23]
	ANXA2	S11, S25 and Y23 (N-term)	[10, 23-25]
	ANXA4	T6	[23]
	Annexin VI	S and Lesser extent T, S15 (N-term), T356 (C-term)	[23, 26]
	ANXA7	T275, T286 (Anx Domain)	[23]

	ANXA7/ANXA11	Y (N-term)	[27]
	CALM/AP180	S107 (ANTH Domain)	[28]
	Endophilin A1	T14 (Membrane-binding amphipathic helix)	[29, 30]
		S75 (BAR Domain)	[29, 31]
	Pacsin 1	S76 and T181 (BAR Domain)	[29, 32]
	Arfaptin-1	S132 (close to the N-terminus of BAR domain)	[29]
	Arfaptin-2	S260 (BAR domain)	
	PKCδ	S, T, Y	[33]
	PTEN	S229, T319, T321, T232, Y336 (C2 Domain) and S362, T366, S370, S380, T382, T383, S385 (C-terminal phosphorylation)	[34, 35]
	TPIP	76-78(SIR)and 112-114(TDK) (C2 Domian)	[36]
	Synaptotagmin2	(C2 Domian)	[37]
	Tricalbin	Y1009, Y822 (C2 Domian)	[38]
	Ezrin	S66, Y270 (near the putative FERM Domain)	[39, 40]
		T567 (C-term)	[39, 41]
		Y145, T235 (FERM Domain) and T576 (C-ERMAF)	[42]
	Moesin	Y145, T235 (FERM Domain) and T558 (C-ERMAF)	
	FAK	H58, Y194 (FERM Domain)	[43]
	TYK2	Y292, Y433 (FERM Domain)	[44]
	Merlin	S (N-term)	[45]
	FGD3	S547, T549 (FYVE Domain)	[46]
	hLst2	T870 (FYVE Domain)	[47]
	Spir2	S636 (FYVE Domain)	[48]
	GOLPH3	T143 and T148 (TQ Motif)	[49]
	Chk1	T378, T382 (KA1)	[50]
	PTEN	T398 (PDZ-Binding Domain)	[35]
	SAP-97	S232 (PDZ1 Domain)	[51]
	PSD-95	S73 (PDZ1 Domain)	[51]
	NHERF-1	S77 (PDZ1 Domain), S162 (PDZ2 Domian)	[51]
	AKT	T72 (PH Domain)	[52]
	AGAP2	S351, S377, S472 (PH Domain)	[53]
	FGD3	S446 (PH1 Domain)	[46]
	FGD4	S702 (PH2 Domain)	
	FGD5	Y1142, Y1199 (PH1 Domain)	
Acetylation	ANXA2	S2 (N-term)	[54]
	PTEN	K402 (PDZ-Binding Domain)	[35]
	IRS2	K80, K81, K103 (PH Domain)	[55]
Sumoylation	Bright	-----	[15]
	K2P1	K274 (C-term)	[56]
	mGluRs	K882 (Cterm)	[57]
	PTEN	K254, K266 (C2 Domain)	[35]
	FAK	K152 (FERM Domain)	[58]
	Merlin	K76 (FERM Domain)	[59]
	ANXA1	160LKRD (Anx Domain)	[60]
Ubiquination	ANXA1	K58, K166 and K276 (Anx Domain)	[60, 61]
	PTEN	K13 (N-term), K289 (C2 Domain)	[35]
	Merlin	1–133 (FERM Domain)	[59]
S-glutathiolation	ANXA2	C8 (N-term)	[10]
Transglutaminase-mediated cross-linking	ANXA1	Q18 (N-term)	[62]
Nitration	AP180	Y237 (ANTH)	[63]
	Syt1	Y151, Y216, Y229 (C2A domain), and Y311, Y364, and Y380 (C2B domain)	[64]
Oxidation	PKCα/β/γ/δ/ε/ζ	C (C1 Domain)	[65-68]
N-linked Glycosylation	FVIII	N residues (A and C1 Domains)	[69, 70]
	FV	N residues (A, C1, C2 Domians)	[71, 72]
	PTEN	N292 (C2 Domain)	[73]
	TPIP	N residues at 103NCSI106 and 152NTSF155 sites (C2 Domain)	[36]
Sulfation	FV	Y (B and C2 Domains)	[71, 74]
Deprotonation	FAK	H58 (FERM)	[43]
γ -Carboxylation	MGP	35-54 residues (GLA Domain)	[75]
	PRRG4	-----(GLA Domain)	[76]
	Factor VII	E6, E7, E14, E16, E19, E20, E25, E26, E29, E35(GLA Domain)	[71, 77]
	Factor X	E6, E7, E14, E16, E19, E20, E25, E26, E29, E32, E39 (GLA Domain)	[71, 77]
	Protein S	E6, E7, E14, E16, E19, E20, E25, E26, E29, E32, E36 (GLA Domain)	[71, 77]
	Prothrombin	E6, E7, E14, E16, E19, E20, E25, E26, E29, E32 (GLA Domain)	[71, 77]
	Protein C	E6, E7, E14, E16, E19, E20, E25, E26, E29 (GLA Domain)	[71, 77]
	Protein Z	E7, E8, E11, E15, E17, E20, E21, E26, E27, E30, E33, E35, E40 (GLA Domain)	[71, 77]

	Factor IX	E7, E8, E15, E17, E20, E21, E26, E27, E30, E33, E36, E40 (GLA Domain)	[71, 77]
Disulfide bridge	PTEN	C32 of TRX-1 with C212 of PTEN (C2 domain)	[78]

Table 3. Lipid binding domain mutations associated with human diseases

Domain	Pathology	Protein	Amino acid change	Description	Ref.
Annexin	ALS (Amyotrophic lateral sclerosis)	ANXA11	R235Q, R346(S229R, R302(R302C, G491R, A293V, I307M		[79-83]
	Ovarian Cancer	ANXA11	---		[84]
	Breast Cancer, Ovarian Cancer, Colorectal Cancer	ANXA11	---		[85]
	SLE (systemic lupus erythematosus), undifferentiated connective tissue disease, rheumatoid arthritis and APS (anti-phospholipid togliere antibodies syndrome)	ANXA11	---		[85]
	Sarcoidosis	ANXA11	SNP in R230C		[86]
	Inflammation(Cystic fibrosis), cancer progression	ANXA11	---		[87, 88]
	prostate cancer	Annexin A7/A1	---		[89]
	heart disease	annexin A2/A6/A5 /A7/A1	---		[89-92]
	lung cancer	annexin A2	---		[93]
	coagulopathy of acute promyelocytic leukemia, antiphospholipid syndrome, cerebral thrombosis, and possibly preeclampsia, stroke and avascular osteonecrosis of bone	annexin A2	---		[94]
	hypercholesterolemia, an important risk factor for atherosclerosis and coronary artery disease (CAD)	AnxA2	V98L		[95, 96]
	Alzheimer's disease	AnxA2 & AnxA6	---		[97]
	rheumatoid arthritis	Annexin V	---		[98]
	Systemic lupus erythematosus (SLE)	Annexin V	---		[99]
	antiphospholipid syndrome, autosomal dominant polycystic kidney disease	ANXA5			[89]
	recurrent pregnancy loss (RPL)	ANXA5	---		[100]
	associated with carotid atherosclerosis and contributed to cardiovascular disease (CVD) risk in patients with familial hypercholesterolemia (FH)	ANXA5	---		[101]
	Niemann-Pick type C disease	AnxA6	---		[102]
ANTH/CALM	SNPs in AD, somatic mutation/gene fusion in ALL and AML	CALM (PICALM)	---		[103-105]
	growth retardation, cognitive defects, and Alzheimer's disease	CALM/PICALM	---		[106]

	late-onset Alzheimer disease (LOAD), familial AD and Down syndrome	CALM/PICALM, AP180	---	[106-110]
	Link to psychotic bipolar disorder and to ASDs; downregulated in gliomas	AP180 (SNAP91)	---	[103]
BAR	autosomal recessive centronuclear myopathy	amphiphysin 2 (BIN1)	---	[111, 112]
	autoinflammatory disease (PAPA- Pyogenic Arthritis, Pyoderma gangrenosum, and Acne-syndrome)	PSTPIP1	E250Q, A230T	[113-115]
	hyperzincemia and hypercalprotectinemia (Hz/Hc)	PSTPIP1	E250K, E257K	[115, 116]
	centronuclear myopathy (CNM)	BIN1	K35N, D151N, R154Q	[117-119]
	Parkinson's disease	Endophilin A (LRRK2-dependent EndoA phosphorylation on Ser75)	---	[31, 115]
C1	Hypertrophic cardiomyopathy (HCM)	cMyBP-C	R177H, A216T, E258K	[120]
		cMyBP-C	Y235S	[121]
	Lung	PKC	G61W, Q62H	[122]
	head and neck	PKC	W58L	[122]
	colorectal	PKC	H75Q	[122]
	hemophilia A	Factor VIIIa	---	[123]
	Dyskinesia	ADCY5	A726T, R418W, R418Q	[124, 125]
	atypical hemolytic uremic syndrome (aHUS)	DGKE	R63E, W158Lfs*8, V163Sfs*3	[126, 127]
	Hereditary coagulation factor V deficiency (bleeding disorder)	Factor V	Nonsense mutation (R1133X) and a novel in-frame 6-bp deletion (6116-6121delGAAC) corresponding to the amino-acid deletion N1982-S1983)	[128]
		Factor V	Gln2031stop	[129]
	Spinocerebellar ataxia type 14 (SCA14)	PKCγ	---	[130-133]
		PKCγ	H101Y, G118D, S119P, G128D	[134]
	lymphoproliferative syndrome	PKCγ domain	G248S in C1B	[131]
	Von Willebrand Disease	VWF	R2313H	[135]
		VWF	C2283R, C2327W	[136]
		VWF	---	[137, 138]
	Spinocerebellar ataxia (SCA)	PRKCG	G128D	[139, 140]
C2	Spinocerebellar ataxia type 14 (SCA14)	PKCγ	I173S, H174P	[132]
	Dyskinesia	ADCY5	M1029K	[124, 125]
	hypertrophic cardiomyopathy (HCM)	cMyBP-C	V375E, E542Q	[141]
	colorectal and ovarian cancers and in melanoma	PKC	D193N	[122]
	Stomach cancer	PKC	T218M	[122]
	endometrial/ovarian cancer	PKC	D254N	[122]
	Lung cancer	PKC	G257V	[122]
	nonsyndromic mental retardation	Cc2d1a	---	[142]
	Joubert syndrome	CC2D2A	---	[143, 144]
	Joubert syndrome (JS) and Jeune asphyxiating thoracic dystrophy (JATD)	CEP120	V194A, A199P in C2B	[145]
	non-syndromic hearing loss in humans (DFNB9 deafness)	Otoferlin	P490Q, I515T, L1011P, R1520Q, R1607W, E1733K,	[146, 147]

			F1795C, E1804del, P1852A, R1856Q, D1767G	
	limb-girdle muscular dystrophy and Miyoshi myopathy	Dysferlin	---	[147-150]
	cancer cell invasiveness and muscle development	myoferlin	---	[147, 151, 152]
	extrahepatic biliary atresia (EHBA)	Jagged-1	---	[153]
	Von Willebrand Disease	VWF	---	[135, 137, 138]
	Endometrial Cancer	p110α and p110β	---	[154, 155]
	Cancer	P85	D560K and N564K	[155]
	familial hemophagocytic lymphohistiocytosis type 3	Munc13-4	D127N & D133N in C2A D941N & D947N in C2B	[156]
	parahemophilia	Factor V	R2074H	[157]
	hemophilia A	Factor VIII (fVIII)	E2181D, A2201P, L2210F, L2210P, V2223M, W2229C, M2238V, D2288A, P2300L, P2300S, R2304C, R2304G, R2304H, R2304L, R2307G, R2307Q, R2307L, Q2311P, W2313R, C2326S	[158, 159]
	Leber congenital amaurosis (LCA) syndrome	RPGRIP1 and RPGRIP1L	---	[160]
	cancer, complex immune disorders, inflammation (further implicated in other diseases such as cancer and steroid-sensitive nephrotic syndrome) as well as Alzheimer's and related neurodegenerative diseases	PLCγ1	E1163K & D1165H (deletion of 1161-11(& 1164-1170)	[161]
	Sézary Syndrome	PLCG1	R1158H, E1163K, D1165H	[162]
	antibody deficiency & immune dysregulation (APLAID) syndrome and pediatric common variable immunodeficiency (CVID)	PLCγ2	M1141K, M1141R	[163]
	Chronic lymphocytic leukemia	PLCG2 + BTK	R665W, S707F, L845F, L845V in PLCG & C481 IN BTK	[164]
	Horizontal Gaze Palsy with Progressive Scoliosis (HGPPS	ROBO 3	---	[165, 166]
	AP2M1 mutation (epileptic encephalopathy); AP2S1 mutation (familial hypocalciuric hypercalcemia type 3); AP-2α, AP-2β, AP-2σ downregulated in gliomas; AP2A1, AP2A2 association with AD	AP-2	---	[103]
	lung cancer	PTEN	S294N	[167]
CTP protein (An amphipathic R-helix between	hereditary spastic paraplegia	CTP	H244Y	[168]
	congenital lipodystrophy and fatty liver disease (CLD-FL)	PCYT1A	E280del	[169-171]

residues 235 & 298 (domain M))	Leber Congenital Amaurosis (LCA)	PCYT1A	c.897+1G>A	[169]
	Retinal dystrophy	CCTα	R283-STOP (R283*)	[171]
	spondylometaphyseal dysplasia with cone-rod dystrophy (SMD-CRD)	CCTα	Y240H	[171]
		PCYT1A	R283*	[169, 170]
CRIB	Diverse Developmental Phenotypes	CDC42	I21, Y23 & E171	[172]
	Neurodegenerative diseases involving neuronal apoptosis	MLK3	CRIB(−)	[173]
	hereditary and sporadic MSI gastrointestinal tumours and colorectal cancer cell lines	MLK3	c.493 G>T	[174]
	development, progression, and metastasis of several forms of cancer	Ack1	H464D	[175]
	Wiskott-Aldrich syndrome (WAS)	WASP	---	[176, 177]
Dystrophin protein (Subdomins' of CR, R1-3, R10-12 & CT)	Duchenne muscular dystrophy (DMD), Becker muscular dystrophy (BMD), intermediate muscular dystrophy (IMD)	Dystrophin	---	[178-184]
	Familial dilated cardiomyopathy (DCM)	Dystrophin	---	[185]
Discoidin	Spondylo-meta-epiphyseal Dysplasia (SMED)	DDR2	---	[186]
		DDR2	E113K	[140]
	Schizophrenia	DDR1	---	[187]
	Lung Adenocarcinoma, Melanoma, Stomach	DDR1	---	[188]
	lung cancer	DDR2	R105S, L63V, I120M, D125Y, S131C, A21G, E85X, N134K, M117V, D171Y, P197Q, G253C, L239R	[189-195]
	Promotes tumor cell Proliferation and invasion.	DDR2	S131C	[194]
	autosomal recessive human growth disorder SMED-SL	DDR2	E113K	[195]
	Retinoschisis	Retinoschisin	---	[196]
	juvenile X-linked retinoschisis (XLRS)	retinoschisin (RS1)	G70S, E72K, Y89C, W92C, W96R, R102W N104K, F108C, G109R G109E, C110Y, W112C L113F, R141H, R141G R141C, C142W, D143V R182C, P203L, H207Q R209H, R213W, C219G C219R	[197-200]
	head and neck squamous cell carcinoma (HNSCC)	DDR2	---	[201]
	parahemophilia and hemophilia A	factor V and VIII	---	[196]
ENTH	---	---	---	---
FERM	Adult T-cell Leukemia/Lymphoma	JAK3	---	[202]
	Spontaneous coronary artery dissection (SCAD)	talin 1	R297H	[203]

	Autosomal Recessive Nonsyndromic Hearing Loss	MYO15A	---		[204]
	congenital motor nystagmus	FRMD7	---		[205, 206]
	Myeloproliferative neoplasms (MPNs), leukemia-like disease	JAK2	---		[207, 208]
	X-linked primary immunodeficiency	moesin (MSN)	---		[209]
	Chronic myeloproliferative neoplasms (CMPNs)	JAK2	---		[210]
	myeloproliferative disease or cancer, compromised immune function	JAK1, JAK2, JAK3 and TYK2	---		[211]
	Neurofibromatosis type 2 (NF2) , Schwannomas, Meningiomas, malignant mesothelioma (MM).	Merlin	---		[212-215]
	Severe combined immunodeficiency (SCID)	Jak3	---		[216]
		Jak2	---		[211]
	Kindler syndrome	Kindlerin	---		[217]
	type I Usher syndrome, nonsyndromic deaf	myo7a	---		[218-220]
	X-linked intellectual disability and disrupt dendritic spine morphogenesis	FRMPD4	---		[221]
FYVE	myotubular myopathy and Charcot-Marie-Tooth disease	MTMR3 and MTMR4	---		[222, 223]
	Charcot–Marie–Tooth disease	FGD4	M566I		[224]
	faciogenital dysplasia	FGD1	---		[225, 226]
	*NCI-60 Cancer	FGD1	R806H, R738C		[227]
	*Uterine Cancer	FGD1	R749C, R738C, V772I, R749C		[227]
	*ccRCC Cancer	FGD1	R777C		[227]
	*Pancreas Cancer	FGD1	R749C		[227]
	*Testicular Cancer	FGD1	N714I		[227]
	*Head & Neck Cancer	FGD1	S715F		[227]
	Alzheimer's Disease	RUFY1	---		[228]
Gla	anticoagulant activity and increased phospholipid binding	Protein C	---		[229, 230]
	thrombotic disease, purpura fulminans, antiinflammatory and antiapoptotic	protein C	---	Not directly related in GLA domain	[231]
	arterial and venous thrombosis	type II protein C	E20A & V34M		[232]
	venous thrombosis and pulmonary embolism	type II protein C	E26K		[233]
	Antiphospholipid syndrome	Prothrombin	---		[234]
	hemophilia B	factor IX	---		[235-238]
	thrombosise (with co-existence of other genetic factors)	protein S	R2L, R1H, K9E		[239]
	antithrombin–heparin inhibition reaction	Fxa	---		[240]
	severe bleeding diathesis	factor X	G11V		[241]
	protein S deficiency and thrombosis	Protein S	G11D & T37M		[242]
	ischemic stroke	Protein S	F72C		[243]
	low coagulative activity	Factor VII	S23P		[244]
GOLPH3	connective tissue tumors	GOLPH3	---		[245]
	muscle-eye-brain disease	GOLPH3	---		[245]
	Hepatocellular carcinoma	GOLPH3	---		[246]
	Renal cell carcinoma	GOLPH3	---		[247]

	epithelial ovarian carcinoma	GOLPH3	---	[248]
	Colorectal cancer	GOLPH3	---	[249]
	Gastric cancer	GOLPH3	---	[250]
	Esophageal squamous cell carcinoma	GOLPH3	---	[251]
	Prostate cancer	GOLPH3	---	[252]
	Oral tongue cancer	GOLPH3	---	[253]
	Breast cancer	GOLPH3	---	[245, 254]
	Rhabdomyosarcoma	GOLPH3	---	[255]
	Pancreatic ductal adenocarcinoma	GOLPH3	---	[256]
	Non-small cell lung cancer	GOLPH3	---	[245, 257]
	Glioma	GOLPH3	---	[245, 258]
	melanoma	GOLPH3	---	[245]
	lung cancer	GOLPH3	---	[259]
	neurodegenerative diseases, including amyotrophic lateral sclerosis, Parkinson's disease, and Alzheimer's disease	GOLPH3	---	[260]
	lysosomal storage disorder mucolipidosis III	GOLPH3	---	[261]
GRAM	Charcot–Marie–Tooth disease (CMT)	MTMR2	---	[119, 262]
		myotubularin-related proteins	---	
		dynamin 2	---	
		SBF2	---	[263]
	gastric cancer	GRAMD1B	---	[264]
	centronuclear myopathy (XLCNM) and CMT	MTM1, MTMR2, MTMR13	---	[119]
	neurological syndromes and neuropathies	myotubularin, amphiphysin 2 (BIN1), and dynamin 2	---	[119]
	tissue-specific disorders	MTM1, MTMR2, DNM2, BIN1	---	[119]
	autosomal dominant centronuclear myopathy (ADCNM)	Dynamin	---	[119]
	Stiff-man syndrome	AMPH1	---	[265]
	CMT neuropathy	Myotubularin	---	[119]
	autosomal recessive form of CNM (ARCNM)	Amphiphysin	---	[119]
	X-linked myotubular myopathy(centronuclear myopathy) -XLCNM	Myotubularin (MTM1)	---	[119, 266, 267]
IMD(I-BAR)	bladder cancer	MIM	---	[268]
	tumorigenesis, several neurological disorders including learning defects, attention deficit disorder, autism spectrum disorder, schizophrenia, and Alzheimer's disease	IRSp53	---	[269]
	developmental delay, oligodactyly and subcutaneous edema, and died of severely impaired cardiac and placental development, exacerbated placental abnormalities.	IRSp53	---	[270]
	progressive kidney disease	MIM	---	[113]
	tumor progression and secretion for cellular proliferation	IRSp53	---	[271]
KA1	Alzheimer	MARK/PAR1 kinases	---	[272-276]
	Cancer	MARK/PAR1 kinases	---	[272-274]

	diabetes	MARK/PAR1 kinases	---	[272, 273]
	Autism	MARK/PAR1 kinases	---	[272, 273]
PDZ	Alzheimer	MAGI2, MPP7	---	[277]
		PICK1	---	[278]
	Charcot-Marie-Tooth (CMT) disease	L-periaxin	---	[279]
	the regulation of insulin production in diabetes and the modulation of rates of cellular replication and/or apoptosis.	Bridge-1	---	[280]
	renal cell carcinoma	PDZK1	---	[281]
	Cervical cancer	HPV-PDZ interactions	---	[282]
	mental retardation	Shank-3 PDZ/GKAP	---	[283]
	Autism spectrum disorder (ASD)	PSD-95 and additional PDZ domain-containing proteins (SHANK2, SHANK3, SNTG2), SHANK	---	[277, 283, 284]
		CASK PDZ/NRXN PSD-95 PDZ3/NLGN Syntrophin PDZ/NLGN3	---	[283]
	Depressive disorder	PSD-95	---	[277]
		PICK-1 PDZ/ErbB2 PICK-1 PDZ/AMPA GluR2 PICK-1 PDZ/dopamine transporter (DAT)	---	[283]
	Non-specific neurodegenerative disorders		---	[277]
	Cystic Fibrosis	CAL	---	[277, 285]
		NHEFR2 PDZ domain/ LPA (lysophosphatidic acids	---	[283]
	infectious disease (HTLV-1, HPV, Ad)	--	---	[277]
	melanoma, glioblastoma, breast cancer, and urothelial cell cancer	Syntenin	---	[286]
	Glioblastoma multiforme cancer and melanoma	Syntenin1 PDZ1/ c-Src tyrosine kinase	---	[283]
	Colon and skin cancer, and leukemia	Dvl PDZ domain/ Frizzed-7	---	[283]
	Acute lymphoblastic leukemia, breast cancer, and prostate cancer	AF-6 PDZ/ Bcr LARG PDZ/ CD44 Tiam1 PDZ/ sydecan1	---	[283]
	cancers of various forms, especially skin, uterine, stomach, and lung cancers	GRIP1, *SCRIB*, membrane-associated guanylate kinase, MAGI1 and MAGI2, PATJ, PDZD2, and MPDZ/MUPP1	---	[277]
	Epithelial-to-mesenchymal transition in tumor progression	Par-6 PDZ/ Par-3 Par-3 PDZ/ PTEN Dlg1 PDZ1/ β-catenin	---	[283, 287]
	Non-specific neurodevelopmental disorders	RIMS1, PARD3B, CASK, DLG4, PSD-95	---	[277, 288]
	Smith–Magenis syndrome-like developmental disorder	CASK	---	[277, 289]
	Parkinson's disease	CNKSR3, MPP2, serine protease HTRA2, NOS1, PICK1	---	[277]

	hearing and vision loss disorders, including Usher syndrome	USH1C, WHRN, GIPC3, TJP2, PDZD7	---	[277, 290]
	retinitis pigmentosa	USH1C, WHRN, PDZD7 and RIMS1	---	[277]
	abnormalities in brain morphology	GRIP	---	[277]
	kidney stones	SLC9A3R1	---	[277]
	schizophrenia	PDZRN, PSD-95, PICK1, SHANK	---	[277, 291]
		PICK-1 PDZ/ErbB2 PICK-1 PDZ/AMPA GluR2 PICK-1 PDZ/dopamine transporter (DAT)	---	[283]
	intellectual disability	SHANK	---	[277]
	fibrosis, neurodegeneration, hepatocellular carcinoma, hepatoblastoma, colorectal cancer, acute myeloid leukemia (AML), chronic myeloid leukemia (CML), multiple myeloma, and gastric cancer	Dvl	---	[277]
	colorectal cancer	whirlin isoform 2	---	[292]
	cryptophthalmossyndrome	GRIP	---	[277]
	Mental retardation	CASK	---	[277, 289]
	metabolic diseases such as 3-methylglutaconic aciduria	HTRA2	---	[277]
	chronic pain, epilepsy	PICK1	---	[277]
	stroke	PICK1	---	[277]
		PSD95 PDZ1/ NMDAR PSD95 PDZ2/nNOS	---	[283]
	heart muscle disease cardiomyopathy	LDB PDLIM3	---	[277]
		ZASP	---	[293]
		PDZK1	---	[294]
	Neuropathic pain	PSD95 PDZ1/ Serotonin receptor (5-HT_{2A})	---	[283]
		PICK-1 PDZ/ErbB2 PICK-1 PDZ/AMPA GluR2 PICK-1 PDZ/dopamine transporter (DAT)	---	
	cerebral ischemic damage	PSD95 PDZ1/ NMDAR PSD95 PDZ2/ nNOS	---	[283]
	hepatitis C virus infection	PDZK1	---	[294]
	hypercholanemia	TJP2	---	[277]
PH	Aarskog-Scott syndrome (AAS)	FGD1	---	[295]
	centronuclear myopathy & Charcot–Marie–Tooth neuropathy	DNM2	---	[119, 296]
	centronuclear myopathy (XLCNM) and CMT	MTM1, MTMR2, MTMR13	---	[119]
	Autism	Trio-9	V2220L	[297]
	Neurodevelopmental disorder	Trio-9	exon deletion	[297]
	Sézary Syndrome	PLCG1	R48W	[162]
	Wiskott-Aldrich syndrome (WAS)	WASP	---	[298]
	breast, colorectal and ovarian cancer	Akt1	---	[299]
		Akt1	E17K	[140]
	hypoinsulinemic hypoglycemia and hemihypertrophy	AKT2	---	[300]

	hemimegalencephaly (HME)	AKT3	---	[301]
	Proteus syndrome	Akt1	---	[302]
	ovarian cancer	mSin1	---	[303]
	breast cancer	PAR1&2	---	[304]
	epithelial malignancies	PAR1&2	---	[305]
	X-linked agammaglobulinemia (XLA)	BTK	---	[306, 307]
		BTK	P33T & D113V	[140]
	Alzheimer	APPL1	---	[308, 309]
	leukaemia	Bcr-Abl	---	[310]
	Obesity and Diabets	PDK1	---	[311, 312]
	Charcot-Marie-Tooth disease (CMT), lower motor neuron disease (LMND)	PLEKHG5	---	[313]
	Lymphoproliferative syndrome	ITK	---	[314]
		ITK	R29H	[140]
PHD	T-B-NK+ Severe Combined Immunodeficieny (SCID) and Omenn syndrome	RAG2	---	[315]
	Autoimmune polyendocrinopathy candidiasis ectodermal dystrophy (APECED), also known as Autoimmune polyglandular syndrome type 1 (APS-1)	AIRE	---	[316, 317]
	Breast cancer, melanoma, esophageal squamous cell carcinoma (SSC), head and neck SSC	ING1	---	[318]
	ovarian carcinomas	SPOC1	---	[319]
	Myeloid leukemia	JARID1A (RBP2)	---	[320]
		PHF23	---	[321]
		NSD1, NSD3	---	[322, 323]
	T-cell lymphoblastic leukaemia	MLL	---	[324]
	Endometrial stromal sarcoma	PHF1	---	[325]
	Childhood overgrowth syndromes such as Sotos syndrome and Weaver syndrome	NSD1	---	[326]
	Various X-linked mental retardation disorders, including Alpha-Thalassemia and Mental Retardation, X-linked (ATRX) Syndrome	ATRX	---	[327]
	renal cancer	JADE1	---	[328]
	Rubenstein-Taybi Syndrome (RTS)	CBP	---	[329]
	Borjeson-Forssman-Lehmann Syndrome (BFLS)	PHF6	---	[330]
PX	Chronic granulomatous disease	NCF4	R105Q	[331]
		p47phox	---	[332, 333]
	Aβ production (AD)-Alzheimer	SNX1, SNX6, SNX9, SNX33, SH3PXD2A (SH3MD1, FISH, Tks5), SNX17, PLD1, PLD2	---	[334-342]
	Up-regulated in endometrial cancer cells	PLD1	---	[343]
	Down-regulated in colon cancer	SNX1	---	[344]
	Tumour metastasis	SH3PXD2A (SH3MD1, FISH, Tks5)	---	[345]

	Invasion by metastatic breast cancer cells	PLD2, PLD1	---	[346]
	Lymphoma cell proliferation	PLD2	---	[347]
	Colon cancer	PLD2, PLD1	---	[348, 349]
	Down-regulated in ovarian cancer	SNX1	---	[334, 335]
	Candidate gene involved in Jacobsen syndrome	SNX19	---	[350]
	Transcriptionally up-regulated in thyroid oncocytic tumours	SNX19	---	[351]
	Genetic risk factor in myocardial infarction	SNX19	---	[352]
	Potential oncogene in myeloid leukaemia	SNX19	---	[353]
	Homozygous deletion of 3_ exons found in B-cell non-Hodgkin's lymphoma cell lines	SNX25	---	[354]
	Akt-independent cancer cell survival	SGK3 (CISK, SGKL)	---	[355]
	Prostate cancer risk	PIK3C2B (PI3K-C2β)	---	[356]
	Up-regulated in some glioblastoma brain tumours	PIK3C2B (PI3K-C2β)	---	[357]
	Up-regulated and promotes cell survival in oestrogen-receptor-positive breast cancer	SGK3 (CISK, SGKL)	---	[358]
	osteopetrosis	SNX10	---	[359]
	May be a chondrogenic factor in osteoarthritis	SNX19	---	[360]
	Gefitinib-sensitive non-small lung cancer	SNX1	---	[335]
	An effector of lithium treatment for bipolar disorder, and a regulator of neurite outgrowth	SNX3	---	[361]
	Oestrogen-regulated expression in breast cancer cell lines	SNX24	---	[362]
	Familial essential tremor	HS1BP3	---	[363]
	Metastatic mammary adenocarcinoma	SNX15, PLD2	---	[364]
	Differential expression used as a biomarker in bladder cancer	SNX16	---	[365]
	Undergoes alternative splicing in certain melanoma cell lines	SNX16	---	[366]
	pathogen invasion	SNX1, SNX2, SNX3, SNX15, SNX6, SNX9 and SNX33 p47phox, p40phox, NOXO1, SNX8, SNX5, SNX16	---	[334, 335, 367-371]
	inflammation	SNX17, SNX20, SNX27, SNX21	---	[335]
	MMEP (microcephaly, microphthalmia, ectrodactyly and prognathism)	SNX3	---	[372]
	SLE (systemic lupus erythematosus)	PXK (MONaKA)	---	[373]
	epilepsy	SNX2	---	[374]
PTB	Autosomal recessive hypercholesterolemia	ARH	---	[375]
	Cerebral cavernous malformation	OSM (CCM2)	---	[375]
	coronary artery disease	IRS-1	---	[375]
	Alzheimer's disease	Fe65	---	[375, 376]
	Downregulated in cancers (bladder, breast, colorectal,	Dab2	---	[103]

	oesophageal, ovarian, prostate)			
	Type 2 diabetes mellitus	IRS-1 IRS-2 JIP-1	---	[375]
SH2	Severe combined immunodeficiency (SCID)	ZAP-70	---	[377]
	Sézary Syndrome	PLCG1	S520F	[162]
	Noonan syndrome	SHP-2	---	[377, 378]
		PTPN11	---	[378, 379]
	Noonan-like/multiple giant-cell lesion syndrome	SHP-2	---	[377]
	Juvenile myelomonocytic leukaemia (JMML)	SHP-2	---	[377]
	Severe insulin deficiency	P85α	---	[377]
		RASA1	---	[379]
	Basal cell carcinoma (BCC)	RasGAP	---	[377]
	STAT1 deficiency, complete	STAT1	---	[377]
	Growth hormone insensitivitywith immunodeficiency	STAT5B	---	[377, 380]
	Myeloproliferative neoplasms (MPNs)	LNK	---	[381]
	Chronic myelogeneous leukemia (CML), acute lymphoblastic leukemia (ALL), myelogenous leukemia (AML)	ABL1	---	[140, 379]
	Acute myeloid leukemia	ABL2	---	[379]
	Human immunodeficiency, Pre-B-cell acute lymphoblastic leukemia (ALL)	BLNK	---	[379]
	X-linked agammaglobulinemia (XLA)	BTK	---	[379, 382] [377, 383]
		BTK	Y361C	[140]
	Acute myeloid leukemia, Acute leukemia, B cell lymphoma, Ewing sarcoma	CBL	---	[379]
	Isolated lissencephaly sequence (ILS) to Miller-Dieker syndrome (MDS)	CRK	---	[379]
	Peripheral T cell lymphoma	ITK	---	[379]
	Acute lymphoblastic leukemia, Chronic myelogenous leukemia, Polycythemia vera and myeloproliferative disorders	JAK2	---	[379]
	SCID, lymphopenia	JAK3	---	[379]
	T cell acute lymphoblastic leukemia, SCID	LCK	---	[379]
	Multiple lentigines (ML)/Leopard syndrome (LS)	PTPN11	---	[379]
	Basal cell carcinoma, Capillary malformation-arteriovenous malformation	RASA1	---	[379]
	X-linked lymphoproliferative syndrome (XLP)	SH2D1A(SAP)	---	[379, 384, 385] [377]
	Cherubism	SH3BP2	---	[379]
	Lymphoproliferative syndrome	BG loop of the SH2 domain	R335W	[140, 314]

	Type 2 diabetes, hypertension	SHIP2	---		[379, 386]
	Advanced colon cancer	SRC	---		[379]
	Susceptibility to mycobacterial and viral disease	STAT1	---		[379]
	Growth hormone insensitivity with immunodeficiency, Acute promyeloyctic leukemia (APL)	STAT5B	---		[379]
	Myelodysplastic syndrome (MDS), Peripheral T cell lymphoma	SYK	---		[379]
	Systemic lupus erythematosus (SLE)	TYK2	---		[379]
	SCID (T cell defect)	ZAP70	---		[379, 387]
SMP	neurological disorders	E-Syt	---		[388-390]
	neurological and psychiatric diseases	TMEM24	---		[389]
	Alzheimer	ERMES	---		[390]
Tubby	Ciliopathic Polycystic Kidney Disease	Tulp3	K407I		[391, 392]
	retinitis pigmentosa	TULP1, *TULP2*	---		[393, 394]
	hearing loss	TULPs	---		[395]
	obesity	TULPs	---		[395]
TMD	Charcot–Marie–Tooth (CMT)	Peripheral Myelin Protein 22 (PMP22)	L16P (TMD1); G150D (TMD4)	cause destabilization of the TMD and toxic accumulation of mutants	[396-398]
			S79C (TMD2); T118M , L105R (TMD3); L147R (TMD4)	Impaired intracellular trafficking	
			G107V, 5'ss (TMD3)	Not characterized	
		Myelin Protein Zero (MPZ)	Y154-stop		[396]
			G163R	Missense mutation cause disruption of TMD homodimerization	[399, 400]
	Dejerine–Sottas Syndrome (DSS)		G167R	Missense mutation cause disruption of TMD homodimerization, ER accumulation and activation of the unfolded protein Response (UPR)	[396, 400, 401]
			frameshift codon172, 167, 174		[396]
		Peripheral Myelin Protein 22 (PMP22)	H12Q, L19P (TMD1); M69K, S72L, S72W, S72P, S76I, S79P, frameshift codon80, L80P, and F84del (TMD2); G100R, G100E (TMD3); G150D, G150C (TMD4)		[396]
	Hereditary Neuropathy with liability to Pressure Palsies (HNPP)		Frameshift codon7, 5'ss (TMD1)		
	Familial Hyperthyroidism	Thyrotrophin Receptor (TSH-R)	V509A	Variant cause disruption of interactions between TMH3 and TMH5, leading to increased flexibility and	[402]

			constant activation of the TSH-R	
Cystic Fibrosis (CF)	CFTR	R117H (TMD1)	Variant cause misfolded CFTR and prevents its proper maturation and transport to the cell surface and abnormal gating	[403]
		G178R (TMD1)	Variant cause abnormal gating, and reduced ion pore conductance	
		R334W, T338I, R347H, R352Q (TMD1); S977F, L927P, G970R, G1069R, F1052V, D1152H (TMD2)	Variant leading to no folding defect	[404]
		P67L, R74W, E56K, D110H, H192G, G178R, V232D, F311del, I336K, Q359K, T360K, R117C, R117H, R347P, S341P, I336K (TMD1); S945L, R1070Q, R1070W (TMD2)	Variant causes mild folding defect	
		G85E, E92K, G91R, H199Y, P205S, L206W, L227R (TMD1); L1065P, R1066C, R1066H, L1077P, M1101K (TMD2)	Variant cause severe folding defect	
Deafness	Connexin26	30delG, 35delG, I20T, I35S, I82M, L90P, Y136X, V153I, L214P, E147K, F142L	Variant prevent the formation of gap junctions	[405]
		W24X, I33T, M34 T, V37I, A40V, W77R, T135A	Variant cause non-functional gap junctions	
		S19T, M34A, F83L, V84L, A88S, V95M, N206S	Variants impair biochemical coupling mediated by gap junctions	
		R143W, Q80R, V27I, V37I, I203T, M34T, A40A	No functional effects	
		R32C,31del14, , S199F, C202F, F142L, 176–191 del (16), L81V, M195V, Q80K, S199F, D159V	Not characterized	
Obesity	MC4R	G55V, G55D, S136F, and A303T	Mutant strengthened helix–helix interactions, preventing movement during receptor activation, impaired cAMP production	[406]
		L54P, E61K, I69T, S136P, M161T, T162I, and I269N	Impaired cell surface trafficking, reduced αMSH binding, and diminished cAMP generation.	
Breast cancer	ErbB2	I655V	increases the active conformation of the receptor dimer.	[407]

References

1. Fivaz, M. and T. Meyer, *Specific localization and timing in neuronal signal transduction mediated by protein-lipid interactions.* Neuron, 2003. **40**(2): p. 319-330.
2. Linder, M.E. and R.J. Deschenes, *Palmitoylation: policing protein stability and traffic.* Nat Rev Mol Cell Biol, 2007. **8**(1): p. 74-84.
3. Kutzleb, C., et al., *Paralemmin, a prenyl-palmitoyl-anchored phosphoprotein abundant in neurons and implicated in plasma membrane dynamics and cell process formation.* J Cell Biol, 1998. **143**(3): p. 795-813.
4. Amendola, C.R., et al., *KRAS4A directly regulates hexokinase 1.* Nature, 2019. **576**(7787): p. 482-486.
5. Adamson, P., et al., *Post-translational modifications of p21rho proteins.* J Biol Chem, 1992. **267**(28): p. 20033-8.
6. Ismail, S.A., et al., *Arl2-GTP and Arl3-GTP regulate a GDI-like transport system for farnesylated cargo.* Nature Chemical Biology, 2011. **7**(12): p. 942-949.
7. Kinoshita-Kikuta, E., et al., *Protein-N-myristoylation-dependent phosphorylation of serine 13 of tyrosine kinase Lyn by casein kinase 1γ at the Golgi during intracellular protein traffic.* Scientific Reports, 2020. **10**(1): p. 16273.
8. Salter, M.W. and L.V. Kalia, *Src kinases: a hub for NMDA receptor regulation.* Nature Reviews Neuroscience, 2004. **5**(4): p. 317-328.
9. Liu, Y., R.A. Kahn, and J.H. Prestegard, *Structure and membrane interaction of myristoylated ARF1.* Structure, 2009. **17**(1): p. 79-87.
10. Benz, J. and A. Hofmann, *Annexins: From structure to function.* Biological Chemistry, 1997. **378**(3-4): p. 177-183.
11. McLaughlin, R.E. and J.B. Denny, *Palmitoylation of GAP-43 by the ER-Golgi intermediate compartment and Golgi apparatus.* Biochim Biophys Acta, 1999. **1451**(1): p. 82-92.
12. Fukata, M., et al., *Identification of PSD-95 Palmitoylating Enzymes.* Neuron, 2004. **44**(6): p. 987-996.
13. DeSouza, S., et al., *Differential palmitoylation directs the AMPA receptor-binding protein ABP to spines or to intracellular clusters.* J Neurosci, 2002. **22**(9): p. 3493-503.
14. Iiri, T., et al., *Reciprocal regulation of Gs alpha by palmitate and the beta gamma subunit.* Proc Natl Acad Sci U S A, 1996. **93**(25): p. 14592-7.
15. Schmidt, C., et al., *Signalling of the BCR is regulated by a lipid rafts-localised transcription factor, Bright.* Embo j, 2009. **28**(6): p. 711-24.
16. Zhang, Y. and P.A. Beachy, *Cellular and molecular mechanisms of Hedgehog signalling.* Nature Reviews Molecular Cell Biology, 2023. **24**(9): p. 668-687.
17. Monlezun, L., et al., *New OprM structure highlighting the nature of the N-terminal anchor.* Front Microbiol, 2015. **6**: p. 667.
18. Puig, B., H. Altmeppen, and M. Glatzel, *The GPI-anchoring of PrP: implications in sorting and pathogenesis.* Prion, 2014. **8**(1): p. 11-8.
19. Rudd, P.M., et al., *Glycosylation and prion protein.* Current Opinion in Structural Biology, 2002. **12**(5): p. 578-586.
20. Fletcher, C.M., et al., *Structure of a soluble, glycosylated form of the human complement regulatory protein CD59.* Structure, 1994. **2**(3): p. 185-99.
21. Li, W., et al., *Phospholipid peroxidation inhibits autophagy via stimulating the delipidation of oxidized LC3-PE.* Redox Biology, 2022. **55**: p. 102421.

22. Solito, E., et al., *Post-translational modification plays an essential role in the translocation of annexin A1 from the cytoplasm to the cell surface.* Faseb j, 2006. **20**(9): p. 1498-500.
23. Hoque, M., et al., *Annexins—Scaffolds modulating PKC localization and signaling.* Cellular signalling, 2014. **26**(6): p. 1213-1225.
24. Grindheim, A.K., J. Saraste, and A. Vedeler, *Protein phosphorylation and its role in the regulation of Annexin A2 function.* Biochimica et Biophysica Acta - General Subjects, 2017. **1861**(11): p. 2515-2529.
25. Valapala, M. and J.K. Vishwanatha, *Lipid raft endocytosis and exosomal transport facilitate extracellular trafficking of annexin A2.* Journal of Biological Chemistry, 2011. **286**(35): p. 30911-30925.
26. Moss, S.E., et al., *A growth-dependent post-translational modification of annexin VI.* Biochimica et Biophysica Acta (BBA)/Protein Structure and Molecular, 1992. **1160**(1): p. 120-126.
27. Furge, L.L., K. Chen, and S. Cohen, *Annexin VII and annexin XI are tyrosine phosphorylated in peroxovanadate-treated dogs and in platelet-derived growth factor-treated rat vascular smooth muscle cells.* J Biol Chem, 1999. **274**(47): p. 33504-9.
28. Moshkanbaryans, L., L.S. Chan, and M.E. Graham, *The biochemical properties and functions of CALM and AP180 in clathrin mediated endocytosis.* 2014, MDPI AG. p. 388-413.
29. Salzer, U., J. Kostan, and K. Djinović-Carugo, *Deciphering the BAR code of membrane modulators.* Cellular and Molecular Life Sciences 2017 74:13, 2017. **74**(13): p. 2413-2438.
30. Kaneko, T., et al., *Rho mediates endocytosis of epidermal growth factor receptor through phosphorylation of endophilin A1 by Rho-kinase.* Genes to Cells, 2005. **10**(10): p. 973-987.
31. Matta, S., et al., *LRRK2 controls an EndoA phosphorylation cycle in synaptic endocytosis.* Neuron, 2012. **75**(6): p. 1008-21.
32. Quan, A., et al., *Phosphorylation of syndapin I F-BAR domain at two helix-capping motifs regulates membrane tubulation.* Proc Natl Acad Sci U S A, 2012. **109**(10): p. 3760-5.
33. Salzer, E., et al., *Protein Kinase C δ: a Gatekeeper of Immune Homeostasis.* Journal of Clinical Immunology, 2016. **36**(7): p. 631-640.
34. Brito, M.B., E. Goulielmaki, and E.A. Papakonstanti, *Focus on PTEN regulation.* Frontiers in Oncology, 2015. **5**(JUL): p. 1-15.
35. Lee, Y.R., M. Chen, and P.P. Pandolfi, *The functions and regulation of the PTEN tumour suppressor: new modes and prospects.* Nature Reviews Molecular Cell Biology, 2018. **19**(9): p. 547-562.
36. Mishra, R.R., J.K. Chaudhary, and P.C. Rath, *Cell cycle arrest and apoptosis by expression of a novel TPIP (TPIP-C2) cDNA encoding a C2-domain in HEK-293 cells.* Molecular Biology Reports, 2012. **39**(7): p. 7389-7402.
37. Leonard, T.A., *C2 Domain Proteins.* 2013, Springer New York. p. 309-318.
38. Jiménez, J.L., et al., *A systematic comparative and structural analysis of protein phosphorylation sites based on the mtcPTM database.* Genome Biology, 2007. **8**(5): p. R90-R90.
39. Michie, K.A., et al., *Two Sides of the Coin: Ezrin/Radixin/Moesin and Merlin Control Membrane Structure and Contact Inhibition.* 2019, NLM (Medline).
40. Cd, P.-t.A., I. Stamenkovic, and Q. Yu, *CD44 Meets Merlin and Ezrin: Their Interplay Mediates the Pro-Tumor Activity of CD44 and Tumor-Suppressing Effect of Merlin.* 2009: p. 71-87.

41. Bosk, S., et al., *Activation of F-actin binding capacity of ezrin: synergism of PIP_2 interaction and phosphorylation*. Biophys J, 2011. **100**(7): p. 1708-17.
42. García-Ortiz, A. and J.M. Serrador, *ERM proteins at the crossroad of leukocyte polarization, migration and intercellular adhesion*. International Journal of Molecular Sciences, 2020. **21**(4): p. 1502.
43. Lawson, C. and D.D. Schlaepfer, *Phocal adhesion kinase regulation is on a FERM foundation*. Journal of Cell Biology, 2013. **202**(6): p. 833-836.
44. Leitner, N.R., et al., *Tyrosine kinase 2 – Surveillant of tumours and bona fide oncogene*. 2017, Academic Press. p. 209-218.
45. Dimarco Hewitt, P., *Regulation of Cell Adhesion by the FERM Proteins, PTPN14 and Merlin.* 2015.
46. Eitzen, G., et al., *Structure and function of the Fgd family of divergent FYVE domain proteins.* Biochemistry and Cell Biology, 2019. **97**(3): p. 257-264.
47. Mosesson, Y., et al., *Monoubiquitinylation Regulates Endosomal Localization of Lst2, a Negative Regulator of EGF Receptor Signaling.* Developmental Cell, 2009. **16**(5): p. 687-698.
48. *POST-TRANSLATIONAL MODIFICATION AND REGULATION OF HUMAN SPIR PROTEIN.* 2011.
49. Sechi, S., et al., *Oncogenic roles of GOLPH3 in the physiopathology of cancer.* International Journal of Molecular Sciences, 2020. **21**(3).
50. Gong, E.-Y., et al., *Chk1 KA1 domain auto-phosphorylation stimulates biological activity and is linked to rapid proteasomal degradation.* Scientific reports, 2018. **8**(1): p. 1-11.
51. Lee, H.J. and J.J. Zheng, *PDZ domains and their binding partners: Structure, specificity, and modification.* Cell Communication and Signaling, 2010. **8**(May).
52. Li, X., et al., *Autophosphorylation of Akt at threonine 72 and serine 246: A potential mechanism of regulation of Akt kinase activity.* Journal of Biological Chemistry, 2006. **281**(19): p. 13837-13843.
53. Navarro-corcuera, A., et al., *AGAP2: Modulating TGFβ1-signaling in the regulation of liver fibrosis*. 2020, MDPI AG. p. 1400-1400.
54. Nazmi, A.R., et al., *N-terminal acetylation of annexin A2 is required for S100A10 binding.* Biological Chemistry, 2012. **393**(10): p. 1141-1150.
55. Peng, J. and L. He, *IRS posttranslational modifications in regulating insulin signaling.* Journal of Molecular Endocrinology, 2018. **60**(1): p. R1-R8.
56. Rajan, S., et al., *Sumoylation silences the plasma membrane leak K+ channel K2P1.* Cell, 2005. **121**(1): p. 37-47.
57. Tang, Z., et al., *Pias1 Interaction and Sumoylation of Metabotropic Glutamate Receptor 8*.* Journal of Biological Chemistry, 2005. **280**(46): p. 38153-38159.
58. Kadaré, G., et al., *PIAS1-mediated Sumoylation of Focal Adhesion Kinase Activates Its Autophosphorylationn*.* Journal of Biological Chemistry, 2003. **278**(48): p. 47434-47440.
59. Qi, Q., et al., *Merlin sumoylation is required for its tumor suppressor activity.* Oncogene, 2014. **33**(41): p. 4893-4903.
60. Hirata, F., L.M. Thibodeau, and A. Hirata, *Ubiquitination and SUMOylation of annexin A1 and helicase activity.* Biochimica et Biophysica Acta (BBA) - General Subjects, 2010. **1800**(9): p. 899-905.
61. Araújo, T.G., et al., *Annexin A1 as a regulator of immune response in cancer.* Cells, 2021. **10**(9): p. 2245.
62. Ando, Y., et al., *Calcium-induced intracellular cross-linking of lipocortin I by tissue transglutaminase in A431 cells. Augmentation by membrane phospholipids.* Journal of Biological Chemistry, 1991. **266**(2): p. 1101-1108.

63. Zhan, X. and D.M. Desiderio, *The human pituitary nitroproteome: detection of nitrotyrosyl-proteins with two-dimensional Western blotting, and amino acid sequence determination with mass spectrometry.* Biochemical and Biophysical Research Communications, 2004. **325**(4): p. 1180-1186.
64. Vrljic, M., et al., *Post-translational modifications and lipid binding profile of insect cell-expressed full-length mammalian synaptotagmin 1.* Biochemistry, 2011. **50**(46): p. 9998-10012.
65. Lin, D. and D.J. Takemoto, *Oxidative Activation of Protein Kinase Cγ through the C1 Domain: EFFECTS ON GAP JUNCTIONS*.* Journal of Biological Chemistry, 2005. **280**(14): p. 13682-13693.
66. Bahia, P.K., et al., *Antimycin A increases bronchopulmonary C-fiber excitability via protein kinase C alpha.* Respiratory Physiology & Neurobiology, 2020. **278**: p. 103446.
67. Knapp, L.T. and E. Klann, *Superoxide-induced stimulation of protein kinase C via thiol modification and modulation of zinc content.* Journal of Biological Chemistry, 2000. **275**(31): p. 24136-24145.
68. Giorgi, C., et al., *Redox control of protein kinase C: cell- and disease-specific aspects.* Antioxid Redox Signal, 2010. **13**(7): p. 1051-85.
69. Kannicht, C., et al., *Characterisation of the post-translational modifications of a novel, human cell line-derived recombinant human factor VIII.* Thrombosis research, 2013. **131**(1): p. 78-88.
70. Kosloski, M.P., R.D. Miclea, and S.V. Balu-Iyer, *Role of glycosylation in conformational stability, activity, macromolecular interaction and immunogenicity of recombinant human factor VIII.* The AAPS journal, 2009. **11**: p. 424-431.
71. Hansson, K. and J. Stenflo, *Post-translational modifications in proteins involved in blood coagulation.* Journal of Thrombosis and Haemostasis, 2005. **3**(12): p. 2633-2648.
72. Nicolaes, G.A.F., B.O. Villoutreix, and B. Dahlbäck, *Partial Glycosylation of Asn2181 in Human Factor V as a Cause of Molecular and Functional Heterogeneity. Modulation of Glycosylation Efficiency by Mutagenesis of the Consensus Sequence for N-Linked Glycosylation.* Biochemistry, 1999. **38**(41): p. 13584-13591.
73. K.M. Ip, C., et al., *Genomic-Glycosylation Aberrations in Tumor Initiation, Progression and Management.* AIMS Medical Science, 2016. **3**(4): p. 386-416.
74. Pittman, D.D., et al., *Posttranslational Sulfation of Factor V Is Required for Efficient Thrombin Cleavage and Activation and for Full Procoagulant Activity.* Biochemistry, 1994. **33**(22): p. 6952-6959.
75. Schurgers, L.J., et al., *Post-translational modifications regulate matrix Gla protein function: Importance for inhibition of vascular smooth muscle cell calcification.* Journal of Thrombosis and Haemostasis, 2007. **5**(12): p. 2503-2511.
76. Yazicioglu, M.N., et al., *Cellular localization and characterization of cytosolic binding partners for gla domain-containing proteins PRRG4 and PRRG2.* Journal of Biological Chemistry, 2013. **288**(36): p. 25908-25914.
77. Bandyopadhyay, P.K., *Vitamin K-Dependent γ-Glutamylcarboxylation: An Ancient Posttranslational Modification.* Vitamins and Hormones, 2008. **78**(07): p. 157-184.
78. Meuillet, E.J., et al., *Thioredoxin-1 binds to the C2 domain of PTEN inhibiting PTEN's lipid phosphatase activity and membrane binding: a mechanism for*

the functional loss of PTEN's tumor suppressor activity. Archives of Biochemistry and Biophysics, 2004. **429**(2): p. 123-133.
79. Smith, B.N., et al., *Mutations in the vesicular trafficking protein annexin A11 are associated with amyotrophic lateral sclerosis.* Science translational medicine, 2017. **9**(388).
80. Lillebostad, P.A.G., et al., *Structure of the ALS Mutation Target Annexin A11 Reveals a Stabilising N-Terminal Segment.* Biomolecules, 2020. **10**(4).
81. Liu, X., et al., *Two rare variants of the ANXA11 gene identified in Chinese patients with amyotrophic lateral sclerosis.* Neurobiol Aging, 2019. **74**: p. 235.e9-235.e12.
82. Liao, Y.-C., et al., *RNA granules hitchhike on lysosomes for long-distance transport, using annexin A11 as a molecular tether.* 2019. **179**(1): p. 147-164. e20.
83. Smith, B.N., et al., *Mutations in ANXA11 cause familial and sporadic amyotrophic lateral sclerosis.* 2014. **17**(5): p. 664-6.
84. Song, J., et al., *Annexin XI is associated with cisplatin resistance and related to tumor recurrence in ovarian cancer patients.* 2007. **13**(22): p. 6842-6849.
85. Wang, J., et al., *Annexin A11 in disease.* 2014. **431**: p. 164-168.
86. Mirsaeidi, M., et al., *Annexins family: insights into their functions and potential role in pathogenesis of sarcoidosis.* 2016. **14**(1): p. 1-9.
87. Boudhraa, Z., et al., *Annexin A1 localization and its relevance to cancer.* 2016. **130**(4): p. 205-220.
88. Bensalem, N., et al., *Down-regulation of the anti-inflammatory protein annexin A1 in cystic fibrosis knock-out mice and patients.* 2005. **4**(10): p. 1591-1601.
89. Gerke, V. and S.E.J.P.r. Moss, *Annexins: from structure to function.* 2002. **82**(2): p. 331-371.
90. Camors, E., V. Monceau, and D.J.C.r. Charlemagne, *Annexins and Ca2+ handling in the heart.* 2005. **65**(4): p. 793-802.
91. Kusters, D., *Annexin A1 and annexin A5 in cardiovascular disease.* 2015.
92. Simpkins, B., *Molecular Dynamics Studies of Point Mutations of Cardiac Troponin C and Annexin.* 2015.
93. Huang, Y., et al., *Involvement of Annexin A2 in p53 induced apoptosis in lung cancer.* 2008. **309**(1-2): p. 117-123.
94. Hedhli, N., et al., *The Annexin A2/S100A10 System in Health and Disease: Emerging Paradigms.* Journal of Biomedicine and Biotechnology, 2012. **2012**: p. 406273.
95. Seidah, N.G., et al., *Annexin A2 is a natural extrahepatic inhibitor of the PCSK9-induced LDL receptor degradation.* PloS one, 2012. **7**(7): p. e41865-e41865.
96. Mayer, G., S. Poirier, and N.G. Seidah, *Annexin A2 is a C-terminal PCSK9-binding protein that regulates endogenous low density lipoprotein receptor levels.* J Biol Chem, 2008. **283**(46): p. 31791-801.
97. Gauthier-Kemper, A., et al., *Annexins A2 and A6 interact with the extreme N terminus of tau and thereby contribute to tau's axonal localization.* 2018. **293**(21): p. 8065-8076.
98. Rodríguez-García, M.I., et al., *Annexin V autoantibodies in rheumatoid arthritis.* Ann Rheum Dis, 1996. **55**(12): p. 895-900.
99. Nielsen, C.T., *Circulating microparticles in systemic Lupus Erythematosus.* Dan Med J, 2012. **59**(11): p. B4548.

100. Bogdanova, N., et al., *A common haplotype of the annexin A5 (ANXA5) gene promoter is associated with recurrent pregnancy loss.* Human Molecular Genetics, 2007. **16**(5): p. 573-578.
101. Hiddink, L., et al., *Annexin A5 haplotypes in familial hypercholesterolemia: lack of association with carotid intima-media thickness and cardiovascular disease risk.* 2015. **238**(2): p. 195-200.
102. Domoń, M., *Annexin A6 involvement in the organization of cholesterol-rich membrane microdomains: evidence from cells of the Niemann-Pick type C disease patients and biomimetic lipid monolayers*. 2011.
103. Azarnia Tehran, D., T. López-Hernández, and T. Maritzen, *Endocytic Adaptor Proteins in Health and Disease: Lessons from Model Organisms and Human Mutations.* Cells, 2019. **8**(11): p. 1345.
104. Dreyling, M., et al., *The t (10; 11)(p13; q14) in the U937 cell line results in the fusion of the AF10 gene and CALM, encoding a new member of the AP-3 clathrin assembly protein family.* 1996. **93**(10): p. 4804-4809.
105. Moshkanbaryans, L., L.-S. Chan, and M.E.J.M. Graham, *The biochemical properties and functions of CALM and AP180 in clathrin mediated endocytosis.* 2014. **4**(3): p. 388-413.
106. Miller, Sharon E., et al., *The Molecular Basis for the Endocytosis of Small R-SNAREs by the Clathrin Adaptor CALM.* Cell, 2011. **147**(5): p. 1118-1131.
107. Ando, K., et al., *Clathrin adaptor CALM/PICALM is associated with neurofibrillary tangles and is cleaved in Alzheimer's brains.* 2013. **125**(6): p. 861-878.
108. Koo, S.J., et al., *SNARE motif-mediated sorting of synaptobrevin by the endocytic adaptors clathrin assembly lymphoid myeloid leukemia (CALM) and AP180 at synapses.* 2011. **108**(33): p. 13540-13545.
109. Silkov, A., et al., *Genome-wide structural analysis reveals novel membrane binding properties of AP180 N-terminal homology (ANTH) domains.* 2011. **286**(39): p. 34155-34163.
110. Kanatsu, K., et al., *Partial loss of CALM function reduces Aβ42 production and amyloid deposition in vivo.* 2016. **25**(18): p. 3988-3997.
111. Nicot, A.-S., et al., *Mutations in amphiphysin 2 (BIN1) disrupt interaction with dynamin 2 and cause autosomal recessive centronuclear myopathy.* 2007. **39**(9): p. 1134-1139.
112. Stanishneva-Konovalova, T., et al., *The role of BAR domain proteins in the regulation of membrane dynamics.* Acta Naturae (англоязычная версия), 2016. **8**(4 (31)).
113. Safari, F. and S. Suetsugu, *The BAR Domain Superfamily Proteins from Subcellular Structures to Human Diseases.* Membranes, 2012. **2**(1): p. 91-117.
114. Wise, C.A., et al., *Mutations in CD2BP1 disrupt binding to PTP PEST and are responsible for PAPA syndrome, an autoinflammatory disorder.* Hum Mol Genet, 2002. **11**(8): p. 961-9.
115. Salzer, U., J. Kostan, and K. Djinović-Carugo, *Deciphering the BAR code of membrane modulators.* Cellular and Molecular Life Sciences, 2017. **74**(13): p. 2413-2438.
116. Holzinger, D., et al., *Single amino acid charge switch defines clinically distinct proline-serine-threonine phosphatase-interacting protein 1 (PSTPIP1)–associated inflammatory diseases.* 2015. **136**(5): p. 1337-1345.
117. Wu, T., Z. Shi, and T. Baumgart, *Mutations in BIN1 Associated with Centronuclear Myopathy Disrupt Membrane Remodeling by Affecting Protein Density and Oligomerization.* PLOS ONE, 2014. **9**(4): p. e93060.

118. Hohendahl, A., A. Roux, and V. Galli, *Structural insights into the centronuclear myopathy-associated functions of BIN1 and dynamin 2.* Journal of Structural Biology, 2016. **196**(1): p. 37-47.
119. Cowling, B.S., et al., *Defective membrane remodeling in neuromuscular diseases: insights from animal models.* 2012. **8**(4): p. e1002595.
120. Gajendrarao, P., et al., *Molecular modeling of disease causing mutations in domain C1 of cMyBP-C.* PLoS One, 2013. **8**(3).
121. Doh, C.Y., et al., *The HCM-causing Y235S cMyBPC mutation accelerates contractile function by altering C1 domain structure.* Biochimica et biophysica acta. Molecular basis of disease, 2019. **1865**(3): p. 661-677.
122. Antal, C.E., et al., *Cancer-associated protein kinase C mutations reveal kinase's role as tumor suppressor.* Cell, 2015. **160**(3): p. 489-502.
123. Liu, M.-L., et al., *Hemophilic factor VIII C1-and C2-domain missense mutations and their modeling to the 1.5-angstrom human C2-domain crystal structure.* 2000. **96**(3): p. 979-987.
124. Chen, D.-H., et al., *ADCY5-related dyskinesia.* Broader spectrum and genotype–phenotype correlations, 2015. **85**(23): p. 2026-2035.
125. Waalkens, A.J.E., et al., *Expanding the ADCY5 phenotype toward spastic paraparesis: A mutation in the M2 domain.* Neurology. Genetics, 2018. **4**(1): p. e214-e214.
126. Córdoba, S.R.d., et al., *Genetics of atypical hemolytic uremic syndrome (aHUS).* 2014. **40 4**: p. 422-30.
127. Baldanzi, G. and M.J.I.J.o.M.S. Malerba, *DGKα in Neutrophil Biology and Its Implications for Respiratory Diseases.* 2019. **20**(22): p. 5673.
128. Song, J., et al., *A novel in-frame deletion in the factor V C1 domain associated with severe coagulation factor V deficiency in a Korean family.* 2009. **20**(2): p. 150-156.
129. Wang, Y., et al., *Factor V deficiency caused by a novel nonsense mutation (Gln2031stop) in a Chinese patient.* Blood Coagulation & Fibrinolysis, 2014. **25**(3).
130. Verbeek, D.S., et al., *PKCγ mutations in spinocerebellar ataxia type 14 affect C1 domain accessibility and kinase activity leading to aberrant MAPK signaling.* 2008. **121**(14): p. 2339-2349.
131. Newton, A.C., *Protein kinase C as a tumor suppressor.* Seminars in cancer biology, 2018. **48**: p. 18-26.
132. Wong, M.M., et al., *Neurodegeneration in SCA14 is associated with increased PKCγ kinase activity, mislocalization and aggregation.* 2018. **6**(1): p. 1-14.
133. Verbeek, D., et al., *Protein kinase C gamma mutations in spinocerebellar ataxia 14 increase kinase activity and alter membrane targeting.* 2005. **128**(2): p. 436-442.
134. Lin, D. and D.J.J.J.o.B.C. Takemoto, *Oxidative activation of protein kinase Cγ through the C1 domain effects on gap junctions.* 2005. **280**(14): p. 13682-13693.
135. Vangenechten, I., et al., *Analysis of von Willebrand Disease in the South Moravian Population (Czech Republic): Results from the BRNO-VWD Study.* Thromb Haemost, 2019. **119**(4): p. 594-605.
136. Yadegari, H., et al., *Insights into pathological mechanisms of missense mutations in C-terminal domains of von Willebrand factor causing qualitative or quantitative von Willebrand disease.* 2013. **98**(8): p. 1315-1323.
137. Gadisseur, A., et al., *Laboratory Diagnosis of von Willebrand Disease Type 1/2E (2A Subtype IIE), Type 1 Vicenza and Mild Type 1 Caused by Mutations*

in the D3, D4, B1–B3 and C1–C2 Domains of the von Willebrand Factor Gene. 2009. **121**(2-3): p. 128-138.
138. Michiels, J.J., et al., *Changing insights in the diagnosis and classification of autosomal recessive and dominant von Willebrand diseases 1980-2015.* 2016. **5**(3): p. 61-74.
139. Morita, H., et al., *A Japanese case of SCA14 with the Gly128Asp mutation.* 2006. **51**(12): p. 1118-1121.
140. Rakshambikai, R., et al., *Typical and atypical domain combinations in human protein kinases: functions, disease causing mutations and conservation in other primates.* 2015. **5**(32): p. 25132-25148.
141. McNamara, J.W., et al., *MYBPC3 mutations are associated with a reduced super-relaxed state in patients with hypertrophic cardiomyopathy.* 2017. **12**(6): p. e0180064.
142. Al-Tawashi, A., et al., *Protein implicated in nonsyndromic mental retardation regulates protein kinase A (PKA) activity.* 2012. **287**(18): p. 14644-14658.
143. Gorden, N.T., et al., *CC2D2A is mutated in Joubert syndrome and interacts with the ciliopathy-associated basal body protein CEP290.* 2008. **83**(5): p. 559-571.
144. Bachmann-Gagescu, R., et al., *Genotype–phenotype correlation in CC2D2A-related Joubert syndrome reveals an association with ventriculomegaly and seizures.* 2012. **49**(2): p. 126-137.
145. Joseph, N., et al., *Disease-associated mutations in CEP120 destabilize the protein and impair ciliogenesis.* 2018. **23**(9): p. 2805-2818.
146. Ramakrishnan, N.A., et al., *Calcium regulates molecular interactions of otoferlin with soluble NSF attachment protein receptor (SNARE) proteins required for hair cell exocytosis.* 2014. **289**(13): p. 8750-8766.
147. Marty, N.J., et al., *The C2 domains of otoferlin, dysferlin, and myoferlin alter the packing of lipid bilayers.* 2013. **52**(33): p. 5585-5592.
148. Liu, J., et al., *Dysferlin, a novel skeletal muscle gene, is mutated in Miyoshi myopathy and limb girdle muscular dystrophy.* 1998. **20**(1): p. 31-36.
149. Wein, N., et al., *Efficient bypass of mutations in dysferlin deficient patient cells by antisense-induced exon skipping.* 2010. **31**(2): p. 136-142.
150. Vincent, A.E., et al., *Dysferlin mutations and mitochondrial dysfunction.* 2016. **26**(11): p. 782-788.
151. Zhu, W., et al., *Myoferlin, a multifunctional protein in normal cells, has novel and key roles in various cancers.* Journal of cellular and molecular medicine, 2019. **23**(11): p. 7180-7189.
152. Eisenberg, M.C., et al., *Mechanistic modeling of the effects of myoferlin on tumor cell invasion.* Proc Natl Acad Sci U S A, 2011. **108**(50): p. 20078-83.
153. Shilo, B.Z. and D.J.T.E.j. Sprinzak, *The lipid-binding side of Notch ligands.* 2017. **36**(15): p. 2182-2183.
154. Mazloumi Gavgani, F., et al., *Class I phosphoinositide 3-Kinase PIK3CA/p110α and PIK3CB/p110β isoforms in endometrial cancer.* 2018. **19**(12): p. 3931.
155. Wu, H., et al., *Regulation of Class IA PI 3-kinases: C2 domain-iSH2 domain contacts inhibit p85/p110α and are disrupted in oncogenic p85 mutants.* 2009. **106**(48): p. 20258-20263.
156. Bin, N.-R., et al., *C2 domains of Munc13-4 are crucial for Ca2+-dependent degranulation and cytotoxicity in NK cells.* 2018. **201**(2): p. 700-713.
157. Schrijver, I., et al., *Novel factor V C2-domain mutation (R2074H) in two families with factor V deficiency and bleeding.* 2002. **87**(02): p. 294-299.

158. Spiegel, P.C., P. Murphy, and B.L.J.J.o.B.C. Stoddard, *Surface-exposed hemophilic mutations across the factor VIII C2 domain have variable effects on stability and binding activities.* 2004. **279**(51): p. 53691-53698.
159. Spiegel Jr, P.C., et al., *Structure of a factor VIII C2 domain–immunoglobulin G4κ Fab complex: identification of an inhibitory antibody epitope on the surface of factor VIII.* 2001. **98**(1): p. 13-19.
160. Remans, K., et al., *C2 domains as protein-protein interaction modules in the ciliary transition zone.* 2014. **8**(1): p. 1-9.
161. Liu, Y., et al., *Structural insights and activating mutations in diverse pathologies define mechanisms of deregulation for phospholipase C gamma enzymes.* 2020. **51**: p. 102607.
162. Patel, V.M., et al., *Frequent and Persistent PLCG1 Mutations in Sézary Cells Directly Enhance PLCγ1 Activity and Stimulate NFκB, AP-1, and NFAT Signaling.* 2020. **140**(2): p. 380-389. e4.
163. Novice, T., et al., *A Germline Mutation in the C2 Domain of PLCγ2 Associated with Gain-of-Function Expands the Phenotype for PLCG2-Related Diseases.* 2020. **40**(2): p. 267-276.
164. Jones, D., et al., *PLCG2 C2 domain mutations co-occur with BTK and PLCG2 resistance mutations in chronic lymphocytic leukemia undergoing ibrutinib treatment.* 2017. **31**(7): p. 1645-1647.
165. Ungaro, C., et al., *The Spectrum of ROBO3 Mutations in Horizontal Gaze Palsy with Progressive Scoliosis: An Update.* 2018. **9**(4): p. 187-197.
166. Ortiz, F.W. and Y.V.J.S.r. Sergeev, *Global computational mutagenesis of domain structures associated with inherited eye disease.* 2019. **9**(1): p. 1-12.
167. Trigka, E.A., et al., *A detailed immunohistochemical analysis of the PI3K/AKT/mTOR pathway in lung cancer: correlation with PIK3CA, AKT1, K-RAS or PTEN mutational status and clinicopathological features.* Oncology reports, 2013. **30**(2): p. 623-636.
168. Vaz, F.M., et al., *Mutations in PCYT2 disrupt etherlipid biosynthesis and cause a complex hereditary spastic paraplegia.* 2019. **142**(11): p. 3382-3397.
169. Testa, F., et al., *Mutations in the PCYT1A gene are responsible for isolated forms of retinal dystrophy.* 2017. **25**(5): p. 651-655.
170. Payne, F., et al., *Mutations disrupting the Kennedy phosphatidylcholine pathway in humans with congenital lipodystrophy and fatty liver disease.* 2014. **111**(24): p. 8901-8906.
171. Cornell, R.B., et al., *Disease-linked mutations in the phosphatidylcholine regulatory enzyme CCTα impair enzymatic activity and fold stability.* 2019. **294**(5): p. 1490-1501.
172. Martinelli, S., et al., *Functional dysregulation of CDC42 causes diverse developmental phenotypes.* The American Journal of Human Genetics, 2018. **102**(2): p. 309-320.
173. Mota, M., et al., *Evidence for a role of mixed lineage kinases in neuronal apoptosis.* 2001. **21**(14): p. 4949-4957.
174. Velho, S., et al., *Mixed lineage kinase 3 gene mutations in mismatch repair deficient gastrointestinal tumours.* Hum Mol Genet, 2010. **19**(4): p. 697-706.
175. Prieto-Echagüe, V. and W.T. Miller, *Regulation of Ack-Family Nonreceptor Tyrosine Kinases.* Journal of Signal Transduction, 2011. **2011**: p. 742372.
176. Burns, S., et al., *Mechanisms of WASp-mediated hematologic and immunologic disease.* 2004. **104**(12): p. 3454-3462.
177. Kato, M., et al., *Wiskott-Aldrich syndrome protein induces actin clustering without direct binding to Cdc42.* 1999. **274**(38): p. 27225-27230.

178. Juan-Mateu, J., et al., *DMD mutations in 576 dystrophinopathy families: a step forward in genotype-phenotype correlations.* 2015. **10**(8): p. e0135189.
179. Mercier, S., et al., *Genetic and clinical specificity of 26 symptomatic carriers for dystrophinopathies at pediatric age.* 2013. **21**(8): p. 855-863.
180. Nicolas, A., et al., *Assessment of the structural and functional impact of in-frame mutations of the DMD gene, using the tools included in the eDystrophin online database.* 2012. **7**(1): p. 1-15.
181. Aartsma-Rus, A., I.B. Ginjaar, and K.J.J.o.m.g. Bushby, *The importance of genetic diagnosis for Duchenne muscular dystrophy.* 2016. **53**(3): p. 145-151.
182. Acsadi, G., et al., *Novel mutation in spectrin-like repeat 1 of dystrophin central domain causes protein misfolding and mild Becker muscular dystrophy.* J Biol Chem, 2012. **287**(22): p. 18153-62.
183. Takeshima, Y., et al., *Mutation spectrum of the dystrophin gene in 442 Duchenne/Becker muscular dystrophy cases from one Japanese referral center.* 2010. **55**(6): p. 379-388.
184. Torella, A., et al., *One hundred twenty-one dystrophin point mutations detected from stored DNA samples by combinatorial denaturing high-performance liquid chromatography.* 2010. **12**(1): p. 65-73.
185. Pioner, J.M., et al., *Advances in Stem Cell Modeling of Dystrophin-Associated Disease: Implications for the Wider World of Dilated Cardiomyopathy.* 2020. **11**.
186. Ali, B.R., et al., *Trafficking defects and loss of ligand binding are the underlying causes of all reported DDR2 missense mutations found in SMED-SL patients.* 2010. **19**(11): p. 2239-2250.
187. Roig, B., et al., *The discoidin domain receptor 1 as a novel susceptibility gene for schizophrenia.* 2007. **12**(9): p. 833-841.
188. Ambrogio, C., et al., *A putative role for Discoidin Domain Receptor 1 in cancer chemoresistance.* 2018. **12**(4): p. 394-397.
189. Ford, C.E., et al., *Expression and mutation analysis of the discoidin domain receptors 1 and 2 in non-small cell lung carcinoma.* British journal of cancer, 2007. **96**(5): p. 808-814.
190. Lee, M.-S., et al., *Prevalence of mutations in discoidin domain-containing receptor tyrosine kinase 2 (DDR2) in squamous cell lung cancers in Korean patients.* 2017. **49**(4): p. 1065.
191. Miao, L., et al., *Identification of novel driver mutations of the discoidin domain receptor 2 (DDR2) gene in squamous cell lung cancer of Chinese patients.* 2014. **14**(1): p. 1-10.
192. Hammerman, P.S., et al., *Mutations in the DDR2 kinase gene identify a novel therapeutic target in squamous cell lung cancer.* 2011. **1**(1): p. 78-89.
193. Ricordel, C., et al., *Mutational Landscape of DDR2 Gene in Lung Squamous Cell Carcinoma Using Next-generation Sequencing.* Clin Lung Cancer, 2018. **19**(2): p. 163-169 e4.
194. Rammal, H., et al., *Discoidin Domain Receptors: Potential Actors and Targets in Cancer.* Front Pharmacol, 2016. **7**: p. 55.
195. Li, Y., et al., *Small molecule discoidin domain receptor kinase inhibitors and potential medical applications.* J Med Chem, 2015. **58**(8): p. 3287-301.
196. Abdulhussein, R., et al., *Exploring the collagen-binding site of the DDR1 tyrosine kinase receptor.* J Biol Chem, 2004. **279**(30): p. 31462-70.
197. Wu, J.W., H.-L.J.J.o.B.S. Liu, and Dynamics, *In silico investigation of the disease-associated retinoschisin C110Y and C219G mutants.* 2012. **29**(5): p. 937-959.

198. Wang, T., et al., *Molecular pathology of X linked retinoschisis: mutations interfere with retinoschisin secretion and oligomerisation.* 2006. **90**(1): p. 81-86.
199. Wang, T., et al., *Intracellular retention of mutant retinoschisin is the pathological mechanism underlying X-linked retinoschisis.* 2002. **11**(24): p. 3097-3105.
200. Molday, R.S., et al., *X-linked juvenile retinoschisis: clinical diagnosis, genetic analysis, and molecular mechanisms.* 2012. **31**(3): p. 195-212.
201. Hedberg, M.L., et al., *Genetic landscape of metastatic and recurrent head and neck squamous cell carcinoma.* 2016. **126**(1): p. 169-180.
202. Elliott, N.E., et al., *FERM domain mutations induce gain of function in JAK3 in adult T-cell leukemia/lymphoma.* Blood, The Journal of the American Society of Hematology, 2011. **118**(14): p. 3911-3921.
203. Turley, T.N., et al., *Rare Missense Variants in TLN1 Are Associated With Familial and Sporadic Spontaneous Coronary Artery Dissection.* 2019. **12**(4): p. e002437.
204. Xia, H., et al., *Identification of a novel MYO15A mutation in a Chinese family with autosomal recessive nonsyndromic hearing loss.* 2015. **10**(8): p. e0136306.
205. Jia, X., et al., *Novel mutations of FRMD7 in Chinese patients with congenital motor nystagmus.* 2017. **16**(2): p. 1753-1758.
206. Watkins, R.J., et al., *The Role of FRMD7 in Idiopathic Infantile Nystagmus.* Journal of Ophthalmology, 2012. **2012**: p. 460956.
207. Eder-Azanza, L., et al., *p. Y317H is a new JAK2 gain-of-function mutation affecting the FERM domain in a myelofibrosis patient with CALR mutation.* 2017. **102**(8): p. e328.
208. Wernig, G., et al., *The Jak2V617F oncogene associated with myeloproliferative diseases requires a functional FERM domain for transformation and for expression of the Myc and Pim proto-oncogenes.* Blood, 2008. **111**(7): p. 3751-3759.
209. Lagresle-Peyrou, C., et al., *X-linked primary immunodeficiency associated with hemizygous mutations in the moesin (MSN) gene.* J Allergy Clin Immunol, 2016. **138**(6): p. 1681-1689 e8.
210. Aranaz, P., et al., *A new potential oncogenic mutation in the FERM domain of JAK2 in BCR/ABL1-negative and V617F-negative chronic myeloproliferative neoplasms revealed by a comprehensive screening of 17 tyrosine kinase coding genes.* 2010. **199**(1): p. 1-8.
211. McNally, R., A.V. Toms, and M.J.J.P.O. Eck, *Crystal structure of the FERM-SH2 module of human Jak2.* 2016. **11**(5): p. e0156218.
212. Kang, B.S., et al., *The structure of the FERM domain of merlin, the neurofibromatosis type 2 gene product.* Acta Crystallographica Section D Biological Crystallography, 2002. **58**(3): p. 381-391.
213. Sato, T. and Y. Sekido, *NF2/Merlin Inactivation and Potential Therapeutic Targets in Mesothelioma.* Int J Mol Sci, 2018. **19**(4).
214. Shimizu, T., et al., *Structural basis for neurofibromatosis type 2. Crystal structure of the merlin FERM domain.* J Biol Chem, 2002. **277**(12): p. 10332-6.
215. Havranek, B. and S.M. Islam, *Prediction and evaluation of deleterious and disease causing non-synonymous SNPs (nsSNPs) in human NF2 gene responsible for neurofibromatosis type 2 (NF2).* J Biomol Struct Dyn, 2020: p. 1-12.

216. Zhou, Y.-J., et al., *Unexpected effects of FERM domain mutations on catalytic activity of Jak3: structural implication for Janus kinases.* 2001. **8**(5): p. 959-969.
217. Jobard, F., et al., *Identification of mutations in a new gene encoding a FERM family protein with a pleckstrin homology domain in Kindler syndrome.* Human Molecular Genetics, 2003. **12**(8): p. 925-935.
218. Li, J., et al., *Structure of Myo7b/USH1C complex suggests a general PDZ domain binding mode by MyTH4-FERM myosins.* Proceedings of the National Academy of Sciences, 2017: p. 201702251.
219. Schwander, M., et al., *A novel allele of myosin VIIa reveals a critical function for the C-terminal FERM domain for melanosome transport in retinal pigment epithelial cells.* 2009. **29**(50): p. 15810-15818.
220. Jacobson, S.G., et al., *Retinal disease course in Usher syndrome 1B due to MYO7A mutations.* 2011. **52**(11): p. 7924-7936.
221. Piard, J., et al., *FRMPD4 mutations cause X-linked intellectual disability and disrupt dendritic spine morphogenesis.* Human Molecular Genetics, 2017. **27**(4): p. 589-600.
222. Stefan, C., A. Audhya, and S.D. Emr, *FYVE Domains in Membrane Trafficking and Cell Signaling*, in *Handbook of Cell Signaling*. 2010, Elsevier. p. 1111-1121.
223. Laporte, J., et al., *Myotubularins, a large disease-associated family of cooperating catalytically active and inactive phosphoinositides phosphatases.* Human Molecular Genetics, 2003. **12**(suppl_2): p. R285-R292.
224. Eitzen, G., et al., *Structure and function of the Fgd family of divergent FYVE domain proteins (1).* Biochem Cell Biol, 2019. **97**(3): p. 257-264.
225. Bedoyan, J.K., et al., *First case of deletion of the faciogenital dysplasia 1 (FGD1) gene in a patient with Aarskog–Scott syndrome.* European Journal of Medical Genetics, 2009. **52**(4): p. 262-264.
226. Kutateladze, T.G., et al., *Phosphatidylinositol 3-phosphate recognition by the FYVE domain.* Molecular cell, 1999. **3**(6): p. 805-811.
227. Pedigo, N.G., et al., *Minireview: Role of genetic changes of faciogenital dysplasia protein 1 in human disease.* Physiol Genomics, 2016. **48**(7): p. 446-54.
228. Char, R. and P. Pierre, *The RUFYs, a Family of Effector Proteins Involved in Intracellular Trafficking and Cytoskeleton Dynamics.* 2020. **8**(779).
229. Sun, Y.-H., L. Shen, and B.r.J.B. Dahlbäck, The Journal of the American Society of Hematology, *Gla domain–mutated human protein C exhibiting enhanced anticoagulant activity and increased phospholipid binding.* 2003. **101**(6): p. 2277-2284.
230. Christiansen, W.T., A. Tulinsky, and F.J.J.B. Castellino, *Functions of Individual. gamma.-Carboxyglutamic Acid (Gla) Residues of Human Protein C. Determination of Functionally Nonessential Gla Residues and Correlations with Their Mode of Binding to Calcium.* 1994. **33**(50): p. 14993-15000.
231. Dahlback, B. and B.O. Villoutreix, *Regulation of blood coagulation by the protein C anticoagulant pathway: novel insights into structure-function relationships and molecular recognition.* Arterioscler Thromb Vasc Biol, 2005. **25**(7): p. 1311-20.
232. Kd, T., *Protein CVermont: Symptomatic Type I1 Protein C Deficiency Associated With Two GLA Domain Mutations.*
233. SHIRAKAWA, M., et al., *Gene Analysis of an Abnormal Protein C with a Mutation of GAG for Glu26 to AAG for Lys.* 1996. **7**(1): p. 36-43.

234. Atsumi, T., O. Amengual, and T. Koike, *Antiphospholipid syndrome: pathogenesis*, in *Systemic lupus erythematosus*. 2011, Elsevier. p. 945-965.
235. Rallapalli, P., et al., *An interactive mutation database for human coagulation factor IX provides novel insights into the phenotypes and genetics of hemophilia B.* 2013. **11**(7): p. 1329-1340.
236. Lam, K., et al., *A Novel Missense Mutation of F9 Gene in Hemophilia B Patients*. 2017. **8**(383): p. 2.
237. *The Factor IX γ-Carboxyglutamic Acid (Gla) Domain is Involved in*

Interactions between Factor IX and Factor XI.
238. Yi, S., et al., *A novel missense mutation in F9 gene causes hemophilia B in a family with clinical variability*. 2020. **31**(2): p. 121-126.
239. Gandrille, S., et al., *Scientific and Standardization Committee Communication: Protein S Deficiency: A Database of Mutations-FIRST UPDATE*.
240. Whinna, H., et al., *Role of the γ-carboxyglutamic acid domain of activated factor X in the presence of calcium during inhibition by antithrombin–heparin.* 2004. **2**(7): p. 1127-1134.
241. Chafa, O., et al., *Characterization of a homozygous Gly11Val mutation in the Gla domain of coagulation factor X*. Thromb Res, 2009. **124**(1): p. 144-8.
242. Rezende, S.M., et al., *Protein S Gla-domain mutations causing impaired Ca2+-induced phospholipid binding and severe functional protein S deficiency*. 2002. **100**(8): p. 2812-2819.
243. Pilli, V.S., W. Plautz, and R. Majumder, *The Journey of Protein S from an Anticoagulant to a Signaling Molecule.* JSM biochemistry and molecular biology, 2016. **3**(1): p. 1014.
244. Shahbazi, S. and R. Mahdian, *Factor VII Gene Defects: Review of Functional Studies and Their Clinical Implications*. Iranian biomedical journal, 2019. **23**(3): p. 165-174.
245. Pereira, N.A., et al., *Golgi phosphoprotein 3 mediates the Golgi localization and function of protein O-linked mannose β-1,2-N-acetlyglucosaminyltransferase 1.* The Journal of biological chemistry, 2014. **289**(21): p. 14762-14770.
246. XiaoJie, M., et al., *GOLP3 is a predictor of survival in patients with hepatocellular carcinoma*. 2014. **37**(4): p. E233-E242.
247. Xue, Y., et al., *GOLPH3 is a novel marker of poor prognosis and a potential therapeutic target in human renal cell carcinoma.* 2014. **110**(9): p. 2250-2260.
248. Ma, Y., et al., *High GOLPH3 expression is associated with a more aggressive behavior of epithelial ovarian carcinoma.* 2014. **464**(4): p. 443-452.
249. Wang, Z., et al., *GOLPH3 predicts survival of colorectal cancer patients treated with 5-fluorouracil-based adjuvant chemotherapy.* 2014. **12**(1): p. 15.
250. Peng, J., et al., *Mechanisms of GOLPH3 associated with the progression of gastric cancer: a preliminary study.* 2014. **9**(10): p. e107362.
251. Wang, J.-H., et al., *High expression of GOLPH3 in esophageal squamous cell carcinoma correlates with poor prognosis.* 2012. **7**(10): p. e45622.
252. Hua, X., et al., *Increased expression of Golgi phosphoprotein-3 is associated with tumor aggressiveness and poor prognosis of prostate cancer.* 2012. **7**(1): p. 127.
253. Li, H., et al., *GOLPH3 overexpression correlates with tumor progression and poor prognosis in patients with clinically N0 oral tongue cancer.* 2012. **10**(1): p. 1-8.

254. Tokuda, E., et al., *Phosphatidylinositol 4-phosphate in the Golgi apparatus regulates cell-cell adhesion and invasive cell migration in human breast cancer.* Cancer Res, 2014. **74**(11): p. 3054-66.
255. Kunigou, O., et al., *Role of GOLPH3 and GOLPH3L in the proliferation of human rhabdomyosarcoma.* 2011. **26**(5): p. 1337-1342.
256. Zhang, L.J., et al., *Overexpression of GOLPH3 is associated with poor prognosis and clinical progression in pancreatic ductal adenocarcinoma.* BMC Cancer, 2014. **14**: p. 571.
257. Zhang, Y., M. Ma, and B.J.T.B. Han, *GOLPH3 high expression predicts poor prognosis in patients with resected non-small cell lung cancer: an immunohistochemical analysis.* 2014. **35**(11): p. 10833-10839.
258. Zhang, X., et al., *GOLPH3 promotes glioblastoma cell migration and invasion via the mTOR-YB1 pathway in vitro.* Mol Carcinog, 2015. **54**(11): p. 1252-63.
259. Sechi, S., et al., *The multiple cellular functions of the oncoprotein Golgi phosphoprotein 3.* Oncotarget, 2015. **6**(6): p. 3493-3506.
260. Buschman, M.D., M. Xing, and S.J. Field, *The GOLPH3 pathway regulates Golgi shape and function and is activated by DNA damage.* 2015. **9**(362).
261. Liu, L., B. Doray, and S. Kornfeld, *Recycling of Golgi glycosyltransferases requires direct binding to coatomer.* Proc Natl Acad Sci U S A, 2018. **115**(36): p. 8984-8989.
262. Berger, P., et al., *Membrane association of myotubularin-related protein 2 is mediated by a pleckstrin homology-GRAM domain and a coiled-coil dimerization module.* 2003. **100**(21): p. 12177-12182.
263. Senderek, J., et al., *Mutation of the SBF2 gene, encoding a novel member of the myotubularin family, in Charcot-Marie-Tooth neuropathy type 4B2/11p15.* Hum Mol Genet, 2003. **12**(3): p. 349-56.
264. Khanna, P., et al., *GRAM domain-containing protein 1B (GRAMD1B), a novel component of the JAK/STAT signaling pathway, functions in gastric carcinogenesis.* 2017. **8**(70): p. 115370.
265. De Camilli, P., et al., *The synaptic vesicle-associated protein amphiphysin is the 128-kD autoantigen of Stiff-Man syndrome with breast cancer.* 1993. **178**(6): p. 2219-2223.
266. Tsujita, K., et al., *Myotubularin regulates the function of the late endosome through the gram domain-phosphatidylinositol 3, 5-bisphosphate interaction.* 2004. **279**(14): p. 13817-13824.
267. Doerks, T., et al., *GRAM, a novel domain in glucosyltransferases, myotubularins and other putative membrane-associated proteins.* 2000. **25**(10): p. 483-485.
268. Lee, Y.-G., et al., *MIM, a potential metastasis suppressor gene in bladder cancer.* Neoplasia (New York, N.Y.), 2002. **4**(4): p. 291-294.
269. Kast, D.J. and R.J.M.b.o.t.c. Dominguez, *IRSp53 coordinates AMPK and 14-3-3 signaling to regulate filopodia dynamics and directed cell migration.* 2019. **30**(11): p. 1285-1297.
270. Chou, A.M., et al., *Redundant functions of I-BAR family members, IRSp53 and IRTKS, are essential for embryonic development.* Scientific Reports, 2017. **7**(1): p. 40485.
271. Hu, H.T., et al., *Involvement of I-BAR protein IRSp53 in tumor cell growth via extracellular microvesicle secretion.* 2020: p. 2020.04.20.050492.
272. Moravcevic, K., et al., *Kinase associated-1 domains drive MARK/PAR1 kinases to membrane targets by binding acidic phospholipids.* Cell, 2010. **143**(6): p. 966-977.

273. Emptage, R.P., M.A. Lemmon, and K.M. Ferguson, *Molecular determinants of KA1 domain-mediated autoinhibition and phospholipid activation of MARK1 kinase.* The Biochemical journal, 2017. **474**(3): p. 385-398.
274. Emptage, R.P., et al., *Structural basis for MARK1 kinase autoinhibition by its KA1 domain.* 2018. **26**(8): p. 1137-1143. e3.
275. Timm, T., et al., *Structure and regulation of MARK, a kinase involved in abnormal phosphorylation of Tau protein.* 2008. **9**(2): p. 1-6.
276. Matenia, D. and E.-M.J.T.i.b.s. Mandelkow, *The tau of MARK: a polarized view of the cytoskeleton.* 2009. **34**(7): p. 332-342.
277. Christensen, N.R., et al., *PDZ domains as drug targets.* 2019. **2**(7): p. 1800143.
278. Lin, E.Y.S., et al., *Potent PDZ-Domain PICK1 Inhibitors that Modulate Amyloid Beta-Mediated Synaptic Dysfunction.* Scientific Reports, 2018. **8**(1): p. 13438.
279. Sherman, D.L., et al., *Specific disruption of a schwann cell dystrophin-related protein complex in a demyelinating neuropathy.* 2001. **30**(3): p. 677-687.
280. Lee, J.H., et al., *Interactions with p300 enhance transcriptional activation by the PDZ-domain coactivator Bridge-1.* J Endocrinol, 2005. **187**(2): p. 283-92.
281. Zheng, J., et al., *Low level of PDZ domain containing 1 (PDZK1) predicts poor clinical outcome in patients with clear cell renal cell carcinoma.* 2017. **15**: p. 62-72.
282. Nagasaka, K., et al., *PDZ Domains and Viral Infection: Versatile Potentials of HPV-PDZ Interactions in relation to Malignancy.* BioMed Research International, 2013. **2013**: p. 369712.
283. Liu, X. and E.J. Fuentes, *Emerging Themes in PDZ Domain Signaling: Structure, Function, and Inhibition.* International review of cell and molecular biology, 2019. **343**: p. 129-218.
284. Bourgeron, T.J.N.R.N., *From the genetic architecture to synaptic plasticity in autism spectrum disorder.* 2015. **16**(9): p. 551-563.
285. Guggino, W.B.J.P.o.t.A.T.S., *The cystic fibrosis transmembrane regulator forms macromolecular complexes with PDZ domain scaffold proteins.* 2004. **1**(1): p. 28-32.
286. Kegelman, T.P., et al., *Targeting tumor invasion: the roles of MDA-9/Syntenin.* 2015. **19**(1): p. 97-112.
287. Giallourakis, C., et al., *A molecular-properties-based approach to understanding PDZ domain proteins and PDZ ligands.* 2006. **16**(8): p. 1056-1072.
288. Stessman, H.A., et al., *Targeted sequencing identifies 91 neurodevelopmental-disorder risk genes with autism and developmental-disability biases.* 2017. **49**(4): p. 515-526.
289. Daniels, D.L., et al., *Crystal structure of the hCASK PDZ domain reveals the structural basis of class II PDZ domain target recognition.* Nature Structural Biology, 1998. **5**(4): p. 317-325.
290. Moinuddin, M., W. Aftab, and A. Memic, *A Novel Computational Framework to Predict the Impact of a Point Mutation on PDZ Domain Classification.* 2018: p. 244251.
291. Lu, Z., et al., *Regulation of synaptic growth and maturation by a synapse-associated E3 ubiquitin ligase at the neuromuscular junction.* 2007. **177**(6): p. 1077-1089.
292. Toiyama, Y., et al., *Overexpression of the signal peptide whirlin isoform 2 is related to disease progression in colorectal cancer patients.* Int J Oncol, 2009. **35**(4): p. 709-15.

293. Fratev, F., E. Mihaylova, and I. Pajeva, *Combination of Genetic Screening and Molecular Dynamics as a Useful Tool for Identification of Disease-Related Mutations: ZASP PDZ Domain G54S Mutation Case*. Journal of Chemical Information and Modeling, 2014. **54**(5): p. 1524-1536.
294. Tsukamoto, K., et al., *Challenges in using cultured primary rodent hepatocytes or cell lines to study hepatic HDL receptor SR-BI regulation by its cytoplasmic adaptor PDZK1*. 2013. **8**(7): p. e69725.
295. Orrico, A., et al., *A mutation in the pleckstrin homology (PH) domain of the FGD1 gene in an Italian family with faciogenital dysplasia (Aarskog–Scott syndrome)*. FEBS letters, 2000. **478**(3): p. 216-220.
296. Zhao, M., N. Maani, and J.J. Dowling, *Dynamin 2 (DNM2) as Cause of, and Modifier for, Human Neuromuscular Disease*. Neurotherapeutics, 2018. **15**(4): p. 966-975.
297. Sadybekov, A., et al., *An autism spectrum disorder-related de novo mutation hotspot discovered in the GEF1 domain of Trio*. Nature Communications, 2017. **8**(1): p. 601.
298. Jin, Y., et al., *Mutations of the Wiskott-Aldrich Syndrome Protein (WASP): hotspots, effect on transcription, and translation and phenotype/genotype correlation*. Blood, 2004. **104**(13): p. 4010-9.
299. Carpten, J.D., et al., *A transforming mutation in the pleckstrin homology domain of AKT1 in cancer*. Nature, 2007. **448**(7152): p. 439-444.
300. Hussain, K., et al., *An activating mutation of AKT2 and human hypoglycemia*. 2011. **334**(6055): p. 474-474.
301. Lee, J.H., et al., *De novo somatic mutations in components of the PI3K-AKT3-mTOR pathway cause hemimegalencephaly*. 2012. **44**(8): p. 941-945.
302. Lindhurst, M.J., et al., *A mosaic activating mutation in AKT1 associated with the Proteus syndrome*. 2011. **365**(7): p. 611-619.
303. Liu, P., et al., *PtdIns(3,4,5)P₃-Dependent Activation of the mTORC2 Kinase Complex*. Cancer Discovery, 2015. **5**(11): p. 1194.
304. Kancharla, A., et al., *PH motifs in PAR1&2 endow breast cancer growth*. Nat Commun, 2015. **6**: p. 8853.
305. Bar-Shavit, R., et al., *Protease-activated receptors (PARs) in cancer: Novel biased signaling and targets for therapy*. Methods Cell Biol, 2016. **132**: p. 341-58.
306. Vihinen, M.J.I.t., *BTKbase: a database of XLA-causing mutations*. 1995. **16**(10): p. 460-465.
307. Lu, D., et al., *Molecular dynamic simulation to explore the molecular basis of Btk-PH domain interaction with Ins(1,3,4,5)P4*. TheScientificWorldJournal, 2013. **2013**: p. 580456-580456.
308. Ogawa, A., et al., *Characterization and distribution of adaptor protein containing a PH domain, PTB domain and leucine zipper motif (APPL1) in Alzheimer's disease hippocampus: an immunohistochemical study*. Brain Res, 2013. **1494**: p. 118-24.
309. Orrico, A., et al., *A mutation in the pleckstrin homology (PH) domain of the FGD1 gene in an Italian family with faciogenital dysplasia (Aarskog-Scott syndrome)*. FEBS Lett, 2000. **478**(3): p. 216-20.
310. Miroshnychenko, D., et al., *Novel role of pleckstrin homology domain of the Bcr-Abl protein: analysis of protein-protein and protein-lipid interactions*. Exp Cell Res, 2010. **316**(4): p. 530-42.

311. Bayascas, J.R., et al., *Mutation of the PDK1 PH domain inhibits protein kinase B/Akt, leading to small size and insulin resistance.* Mol Cell Biol, 2008. **28**(10): p. 3258-72.
312. Manna, P. and S.K. Jain, *Phosphatidylinositol-3,4,5-Triphosphate and Cellular Signaling: Implications for Obesity and Diabetes.* Cellular Physiology and Biochemistry, 2015. **35**(4): p. 1253-1275.
313. Kim, H.J., et al., *Mutations in the PLEKHG5 gene is relevant with autosomal recessive intermediate Charcot-Marie-Tooth disease.* Orphanet Journal of Rare Diseases, 2013. **8**(1): p. 104.
314. Linka, R., et al., *Loss-of-function mutations within the IL-2 inducible kinase ITK in patients with EBV-associated lymphoproliferative diseases.* 2012. **26**(5): p. 963-971.
315. Matthews, A.G., et al., *RAG2 PHD finger couples histone H3 lysine 4 trimethylation with V (D) J recombination.* 2007. **450**(7172): p. 1106-1110.
316. Org, T., et al., *The autoimmune regulator PHD finger binds to non-methylated histone H3K4 to activate gene expression.* 2008. **9**(4): p. 370-376.
317. Villaseñor, J., C. Benoist, and D.J.I.r. Mathis, *AIRE and APECED: molecular insights into an autoimmune disease.* 2005. **204**(1): p. 156-164.
318. Gong, W., et al., *Function of the ING family of PHD proteins in cancer.* 2005. **37**(5): p. 1054-1065.
319. Kinkley, S., et al., *SPOC1: a novel PHD-containing protein modulating chromatin structure and mitotic chromosome condensation.* J Cell Sci, 2009. **122**(Pt 16): p. 2946-56.
320. van Zutven, L.J., et al., *Identification of NUP98 abnormalities in acute leukemia: JARID1A (12p13) as a new partner gene.* 2006. **45**(5): p. 437-446.
321. Reader, J., et al., *A novel NUP98-PHF23 fusion resulting from a cryptic translocation t (11; 17)(p15; p13) in acute myeloid leukemia.* 2007. **21**(4): p. 842-844.
322. Cerveira, N., et al., *Frequency of NUP98-NSD1 fusion transcript in childhood acute myeloid leukaemia.* 2003. **17**(11): p. 2244-2247.
323. Rosati, R., et al., *NUP98 is fused to the NSD3 gene in acute myeloid leukemia associated with t (8; 11)(p11. 2; p15).* 2002. **99**(10): p. 3857-3860.
324. Ayton, P.M. and M.L.J.O. Cleary, *Molecular mechanisms of leukemogenesis mediated by MLL fusion proteins.* 2001. **20**(40): p. 5695-5707.
325. Micci, F., et al., *Consistent rearrangement of chromosomal band 6p21 with generation of fusion genes JAZF1/PHF1 and EPC1/PHF1 in endometrial stromal sarcoma.* 2006. **66**(1): p. 107-112.
326. Tatton-Brown, K., et al., *Genotype-phenotype associations in Sotos syndrome: an analysis of 266 individuals with NSD1 aberrations.* 2005. **77**(2): p. 193-204.
327. Argentaro, A., et al., *Structural consequences of disease-causing mutations in the ATRX-DNMT3-DNMT3L (ADD) domain of the chromatin-associated protein ATRX.* 2007. **104**(29): p. 11939-11944.
328. Musselman, C.A. and T.G. Kutateladze, *PHD fingers: epigenetic effectors and potential drug targets.* Mol Interv, 2009. **9**(6): p. 314-23.
329. Kalkhoven, E., et al., *Loss of CBP acetyltransferase activity by PHD finger mutations in Rubinstein–Taybi syndrome.* 2003. **12**(4): p. 441-450.
330. Lower, K.M., et al., *Mutations in PHF6 are associated with Börjeson–Forssman–Lehmann syndrome.* 2002. **32**(4): p. 661-665.
331. Matute, J.D., et al., *A new genetic subgroup of chronic granulomatous disease with autosomal recessive mutations in p40phox and selective defects in neutrophil NADPH oxidase activity.* Blood, 2009. **114**(15): p. 3309-3315.

332. Bravo, J., et al., *The crystal structure of the PX domain from p40phox bound to phosphatidylinositol 3-phosphate.* 2001. **8**(4): p. 829-839.
333. Noack, D., et al., *Autosomal recessive chronic granulomatous disease caused by defects in NCF-1, the gene encoding the phagocyte p47-phox: mutations not arising in the NCF-1 pseudogenes.* 2001. **97**(1): p. 305-311.
334. Chandra, M., et al., *Classification of the human phox homology (PX) domains based on their phosphoinositide binding specificities.* Nature Communications, 2019. **10**(1): p. 1528.
335. Teasdale, Rohan D. and Brett M. Collins, *Insights into the PX (phox-homology) domain and SNX (sorting nexin) protein families: structures, functions and roles in disease.* Biochemical Journal, 2011. **441**(1): p. 39-59.
336. Oliveira, T.G., et al., *Phospholipase d2 ablation ameliorates Alzheimer's disease-linked synaptic dysfunction and cognitive deficits.* 2010. **30**(49): p. 16419-16428.
337. Liu, Y., et al., *Intracellular trafficking of presenilin 1 is regulated by β-amyloid precursor protein and phospholipase D1.* 2009. **284**(18): p. 12145-12152.
338. Lee, J., et al., *Adaptor protein sorting nexin 17 regulates amyloid precursor protein trafficking and processing in the early endosomes.* 2008. **283**(17): p. 11501-11508.
339. Ha, S.H., et al., *PLD2 forms a functional complex with mTOR/raptor to transduce mitogenic signals.* 2006. **18**(12): p. 2283-2291.
340. Yarar, D., C.M. Waterman-Storer, and S.L.J.D.c. Schmid, *SNX9 couples actin assembly to phosphoinositide signals and is required for membrane remodeling during endocytosis.* 2007. **13**(1): p. 43-56.
341. Ahn, B.-H., et al., *Phospholipase D is activated and phosphorylated by casein kinase-II in human U87 astroglioma cells.* 2006. **38**(1): p. 55-62.
342. Jin, J.K., et al., *Phospholipase D1 is up-regulated in the mitochondrial fraction from the brains of Alzheimer's disease patients.* Neurosci Lett, 2006. **407**(3): p. 263-7.
343. Shen, Q., et al., *Morphoproteomic analysis reveals an overexpressed and constitutively activated phospholipase D1-mTORC2 pathway in endometrial carcinoma.* 2011. **4**(1): p. 13.
344. Katso, R.M., et al., *Phosphoinositide 3-Kinase C2beta regulates cytoskeletal organization and cell migration via Rac-dependent mechanisms.* Mol Biol Cell, 2006. **17**(9): p. 3729-44.
345. Zhao, Y., I. Gaidarov, and J.H.J.J.o.B.C. Keen, *Phosphoinositide 3-kinase C2α links clathrin to microtubule-dependent movement.* 2007. **282**(2): p. 1249-1256.
346. Henkels, K.M., et al., *Cell invasion of highly metastatic MTLn3 cancer cells is dependent on phospholipase D2 (PLD2) and Janus kinase 3 (JAK3).* 2011. **408**(5): p. 850-862.
347. Knoepp, S.M., et al., *Effects of active and inactive phospholipase D2 on signal transduction, adhesion, migration, invasion, and metastasis in EL4 lymphoma cells.* 2008. **74**(3): p. 574-584.
348. Saito, M., et al., *Expression of phospholipase D2 in human colorectal carcinoma.* 2007. **18**(5): p. 1329-1334.
349. Kang, D.W., et al., *Phorbol ester up-regulates phospholipase D1 but not phospholipase D2 expression through a PKC/Ras/ERK/NFκB-dependent pathway and enhances matrix metalloproteinase-9 secretion in colon cancer cells.* 2008. **283**(7): p. 4094-4104.

350. Ji, T., et al., *Diagnosis and fine mapping of a deletion in distal 11q in two Chinese patients with developmental delay.* 2010. **55**(8): p. 486-489.
351. Jacques, C., et al., *Two-step differential expression analysis reveals a new set of genes involved in thyroid oncocytic tumors.* 2005. **90**(4): p. 2314-2320.
352. Bare, L.A., et al., *Five common gene variants identify elevated genetic risk for coronary heart disease.* 2007. **9**(10): p. 682-689.
353. Tyybäkinoja, A., et al., *Amplified, lost, and fused genes in 11q23–25 amplicon in acute myeloid leukemia, an array-CGH study.* 2006. **45**(3): p. 257-264.
354. Mestre-Escorihuela, C., et al., *Homozygous deletions localize novel tumor suppressor genes in B-cell lymphomas.* 2007. **109**(1): p. 271-280.
355. Vasudevan, K.M., et al., *AKT-independent signaling downstream of oncogenic PIK3CA mutations in human cancer.* 2009. **16**(1): p. 21-32.
356. Koutros, S., et al., *Pooled analysis of phosphatidylinositol 3-kinase pathway variants and risk of prostate cancer.* 2010. **70**(6): p. 2389-2396.
357. Traer, C.J., et al., *Are class II phosphoinositide 3-kinases potential targets for anticancer therapies?* 2006. **93**(5): p. 10053-10058.
358. Wang, Y., et al., *SGK3 is an estrogen-inducible kinase promoting estrogen-mediated survival of breast cancer cells.* 2011. **25**(1): p. 72-82.
359. Xu, J., et al., *Structure of sorting nexin 11 (SNX11) reveals a novel extended phox homology (PX) domain critical for inhibition of SNX10-induced vacuolation.* J Biol Chem, 2013. **288**(23): p. 16598-605.
360. Kan, A., et al., *Screening of chondrogenic factors with a real-time fluorescence-monitoring cell line ATDC5-C2ER: Identification of sorting nexin 19 as a novel factor.* 2009. **60**(11): p. 3314-3323.
361. Mizutani, R., et al., *Sorting nexin 3, a protein upregulated by lithium, contains a novel phosphatidylinositol-binding sequence and mediates neurite outgrowth in N1E-115 cells.* 2009. **21**(11): p. 1586-1594.
362. Wright, P.K., et al., *Estrogen regulates vesicle trafficking gene expression in EFF-3, EFM-19 and MCF-7 breast cancer cells.* 2009. **2**(5): p. 463.
363. Higgins, J.J., et al., *HS1-BP3 gene variant is common in familial essential tremor.* 2006. **21**(3): p. 306-309.
364. Król, M., et al., *Transcriptomic signature of cell lines isolated from canine mammary adenocarcinoma metastases to lungs.* 2010. **51**(1): p. 37-50.
365. Osman, I., et al., *Novel blood biomarkers of human urinary bladder cancer.* 2006. **12**(11): p. 3374-3380.
366. Watahiki, A., et al., *Libraries enriched for alternatively spliced exons reveal splicing patterns in melanocytes and melanomas.* 2004. **1**(3): p. 233-239.
367. Popoff, V., et al., *Analysis of articulation between clathrin and retromer in retrograde sorting on early endosomes.* 2009. **10**(12): p. 1868-1880.
368. Le Blanc, I., et al., *Endosome-to-cytosol transport of viral nucleocapsids.* 2005. **7**(7): p. 653-664.
369. Braun, V., et al., *Sorting nexin 3 (SNX3) is a component of a tubular endosomal network induced by Salmonella and involved in maturation of the Salmonella-containing vacuole.* 2010. **12**(9): p. 1352-1367.
370. Hanson, B.J. and W.J.J.o.B.C. Hong, *Evidence for a role of SNX16 in regulating traffic between the early and later endosomal compartments.* 2003. **278**(36): p. 34617-34630.
371. Shin, N., et al., *Sorting nexin 9 interacts with dynamin 1 and N-WASP and coordinates synaptic vesicle endocytosis.* J Biol Chem, 2007. **282**(39): p. 28939-50.

372. Kumar, R.A., et al., *Absence of mutations in NR2E1 and SNX3in five patients with MMEP (microcephaly, microphthalmia, ectrodactyly, and prognathism) and related phenotypes.* 2007. **8**(1): p. 48.
373. Harley, J.B., et al., *Genome-wide association scan in women with systemic lupus erythematosus identifies susceptibility variants in ITGAM, PXK, KIAA1542 and other loci.* 2008. **40**(2): p. 204-210.
374. Takeuchi, H., et al., *Characterization of PXK as a protein involved in epidermal growth factor receptor trafficking.* Mol Cell Biol, 2010. **30**(7): p. 1689-702.
375. Uhlik, M.T., et al., *Structural and evolutionary division of phosphotyrosine binding (PTB) domains.* 2005. **345**(1): p. 1-20.
376. Margolis, B.J.T.i.E. and Metabolism, *The PTB domain: the name doesn't say it all.* 1999. **10**(7): p. 262-267.
377. Lappalainen, I., et al., *Genome wide analysis of pathogenic SH2 domain mutations.* Proteins: Structure, Function, and Bioinformatics, 2008. **72**(2): p. 779-792.
378. Müller, P.J., et al., *Protein tyrosine phosphatase SHP2/PTPN11 mistargeting as a consequence of SH2-domain point mutations associated with Noonan Syndrome and leukemia.* 2013. **84**: p. 132-147.
379. Liu, B.A., et al., *The human and mouse complement of SH2 domain proteins—establishing the boundaries of phosphotyrosine signaling.* 2006. **22**(6): p. 851-868.
380. Scaglia, P.A., et al., *A Novel Missense Mutation in the SH2 Domain of the STAT5B Gene Results in a Transcriptionally Inactive STAT5b Associated with Severe IGF-I Deficiency, Immune Dysfunction, and Lack of Pulmonary Disease.* The Journal of Clinical Endocrinology & Metabolism, 2012. **97**(5): p. E830-E839.
381. Oh, S.T., et al., *Novel mutations in the inhibitory adaptor protein LNK drive JAK-STAT signaling in patients with myeloproliferative neoplasms.* Blood, 2010. **116**(6): p. 988-92.
382. Kaneko, T., et al., *Phosphotyrosine recognition domains: the typical, the atypical and the versatile.* Cell Communication and Signaling, 2012. **10**(1): p. 32.
383. Mattsson, P.T., et al., *Six X-linked agammaglobulinemia-causing missense mutations in the Src homology 2 domain of Bruton's tyrosine kinase: phosphotyrosine-binding and circular dichroism analysis.* 2000. **164**(8): p. 4170-4177.
384. Li, S.-C., et al., *Novel mode of ligand binding by the SH2 domain of the human XLP disease gene product SAP/SH2D1A.* 1999. **9**(23): p. 1355-1362.
385. Li, C., et al., *Disease-causing SAP mutants are defective in ligand binding and protein folding.* Biochemistry, 2003. **42**(50): p. 14885-92.
386. Kaisaki, P.J., et al., *Polymorphisms in Type II SH2 domain–containing inositol 5-phosphatase (INPPL1, SHIP2) are associated with physiological abnormalities of the metabolic syndrome.* 2004. **53**(7): p. 1900-1904.
387. Chan, A.C., et al., *ZAP-70 deficiency in an autosomal recessive form of severe combined immunodeficiency.* 1994. **264**(5165): p. 1599-1601.
388. Yu, H., et al., *Extended synaptotagmins are Ca2+-dependent lipid transfer proteins at membrane contact sites.* 2016. **113**(16): p. 4362-4367.
389. Sun, E.W., et al., *Lipid transporter TMEM24/C2CD2L is a Ca2+-regulated component of ER–plasma membrane contacts in mammalian neurons.* 2019. **116**(12): p. 5775-5784.

390. Hirabayashi, Y., et al., *ER-mitochondria tethering by PDZD8 regulates Ca2+ dynamics in mammalian neurons.* 2017. **358**(6363): p. 623-630.
391. Nelson, C.P., S.R. Nahorski, and R.J. Challiss, *Temporal profiling of changes in phosphatidylinositol 4, 5-bisphosphate, inositol 1, 4, 5-trisphosphate and diacylglycerol allows comprehensive analysis of phospholipase C-initiated signalling in single neurons 1.* Journal of neurochemistry, 2008. **107**(3): p. 602-615.
392. Short, B.J.T.J.o.C.B., *Tubby proteins prove their adaptability.* 2017. **216**(3): p. 527.
393. Mukhopadhyay, S. and P.K.J.G.b. Jackson, *The tubby family proteins.* 2011. **12**(6): p. 1-9.
394. North, M.A., et al., *Molecular characterization of TUB, TULP1, and TULP2, members of the novel tubby gene family and their possible relation to ocular diseases.* 1997. **94**(7): p. 3128-3133.
395. Boggon, T.J., et al., *Implication of tubby proteins as transcription factors by structure-based functional analysis.* 1999. **286**(5447): p. 2119-2125.
396. Nelis, E., N. Haites, and C. Van Broeckhoven, *Mutations in the peripheral myelin genes and associated genes in inherited peripheral neuropathies.* Human mutation, 1999. **13**(1): p. 11-28.
397. Myers, J.K., C.K. Mobley, and C.R. Sanders, *The Peripheral Neuropathy-Linked Trembler and Trembler-J Mutant Forms of Peripheral Myelin Protein 22 Are Folding-Destabilized.* Biochemistry, 2008. **47**(40): p. 10620-10629.
398. Naef, R., *A common disease mechanism for hereditary neuropathies due to point mutations in the peripheral myelin protein 22.* 2000, ETH Zurich.
399. Eggers, S.D., et al., *Clinical and genetic description of a family with Charcot–Marie–Tooth disease type 1b from a transmembrane MPZ mutation.* Muscle & Nerve: Official Journal of the American Association of Electrodiagnostic Medicine, 2004. **29**(6): p. 867-869.
400. Marinko, J.T., et al., *Folding and Misfolding of Human Membrane Proteins in Health and Disease: From Single Molecules to Cellular Proteostasis.* Chem Rev, 2019. **119**(9): p. 5537-5606.
401. Bai, Y., et al., *Myelin protein zero mutations and the unfolded protein response in Charcot Marie Tooth disease type 1B.* Ann Clin Transl Neurol, 2018. **5**(4): p. 445-455.
402. Karges, B., et al., *TSH receptor mutation V509A causes familial hyperthyroidism by release of interhelical constraints between transmembrane helices TMH3 and TMH5.* Journal of Endocrinology, 2005. **186**(2): p. 377-385.
403. Shteinberg, M., et al., *Cystic fibrosis.* The Lancet, 2021. **397**(10290): p. 2195-2211.
404. Estabrooks, S. and J.L. Brodsky, *Regulation of CFTR Biogenesis by the Proteostatic Network and Pharmacological Modulators.* Int J Mol Sci, 2020. **21**(2).
405. Hoang Dinh, E., et al., *Diverse deafness mechanisms of connexin mutations revealed by studies using in vitro approaches and mouse models.* Brain Res, 2009. **1277**: p. 52-69.
406. Tan, K., et al., *Functional Characterization and Structural Modeling of Obesity Associated Mutations in the Melanocortin 4 Receptor.* Endocrinology, 2009. **150**(1): p. 114-125.
407. Cymer, F. and D. Schneider, *Transmembrane helix-helix interactions involved in ErbB receptor signaling.* Cell adhesion & migration, 2010. **4**(2): p. 299-312.

Supplementary information

Membrane-binding modules: key players in cellular function, disease pathogenesis, and therapeutic targets

Mehrnaz Mehrabipour[1], Vanshika Garg[1], Mohammad R. Ahmadian[1@]

[1]Institute of Biochemistry and Molecular Biology II, Medical Faculty and University Hospital Düsseldorf, Heinrich Heine University Düsseldorf, Universitätsstrasse 1, 40225 Düsseldorf, Germany

[@]Corresponding authors: reza.ahmadian@hhu.de

Table S 1. List of Lipid-Binding Domains: Reported versus Accepted Counts.

Domain Name	status in UniProtKB (Reviewed-unreviewed)	Ref.
GRAM (glucosyltransferases, Rablike GTPase activators, and myotubularins)	21-40	[1]
GLA	14-51	[2]
Annexin	0-5	[3]
FERM (4.1, ezrin, radixin, and moesin)	52-263	[4]
C1 (protein kinase C (PKC) conserved 1)	47-72	[5]
C2 (protein kinase C (PKC) conserved 2)	490-637	[5]
PH (Pleckstrin Homology)	287-1015	[6]
FYVE (Fab1p, YOTB, Vac1p, and EEA1)	0-113	[7]
PX (Phox homology)	51-173	[8]
ENTH (Epsin N-terminal homology)	10-46	[9]
BAR (Bin, Amphiphysin, and Rvs)	57-209	[10]
PDZ (PSD-95, Discs Large, and ZO-1)	155-657	[11]
SH2	109-434	[12]
SMP (Synaptotagmin-like Mitochondrial-lipid-binding Protein)	7-14	[13]
PHD	0-409	[14]
ANTH/CALM (AP180 N-terminal homology)	0-2	[9]
GOLPH3	11-3	[15]
IMD	5-29	[15]
KA1	5-43	[15]
PTB (phosphotyrosine-binding)	22-61	[15]
Tubby	0-17	[16]
M domain of CTP:phosphocholine cytidylyltransferase	2-11	[17]
CR (cysteine-rich), spectrin-like repeats (R)1-3, R10-12 and C-terminus (CT) of Dystrophin	---	[18]
GLUE (GRAM-like ubiquitin-binding in EAP45)	1-1	[19]
TPR repeat (Tetratricopeptide Repeat)	0-9	[20]
Transmembrane domain (TMD)	36-1087	[21]
PLAT (polycystin-1, lipoxygenase, and α-toxin)	21-66	[22]
MH2 (MAD homology 2)	8-19	[23]
VHS (Vps-27, Hrs, and STAM)	9-85	[24]
C domain of β-arrestin	0-25	[25]
PROPPINs (β–propellers that bind phosphoinositides)	4-33	[26]

References

1. Ercan, B., et al., *Molecular basis of accessible plasma membrane cholesterol recognition by the GRAM domain of GRAMD1b.* Embo j, 2021. **40**(6): p. e106524.
2. Huang, M., et al., *Structural basis of membrane binding by Gla domains of vitamin K–dependent proteins.* Nature Structural & Molecular Biology, 2003. **10**(9): p. 751-756.
3. Lizarbe, M.A., et al., *Annexin-phospholipid interactions. Functional implications.* International journal of molecular sciences, 2013. **14**(2): p. 2652-2683.
4. Hamada, K., et al., *Structural basis of the membrane-targeting and unmasking mechanisms of the radixin FERM domain.* The EMBO journal, 2000. **19**(17): p. 4449-4462.
5. Johnson, J.E., J. Giorgione, and A.C. Newton, *The C1 and C2 domains of protein kinase C are independent membrane targeting modules, with specificity for phosphatidylserine conferred by the C1 domain.* Biochemistry, 2000. **39**(37): p. 11360-11369.
6. Lemmon, M.A., *Membrane recognition by phospholipid-binding domains.* Nature reviews Molecular cell biology, 2008. **9**(2): p. 99-111.
7. Kutateladze, T.G., et al., *Phosphatidylinositol 3-phosphate recognition by the FYVE domain.* Molecular cell, 1999. **3**(6): p. 805-811.
8. Stahelin, R.V., et al., *Structural and membrane binding analysis of the Phox homology domain of phosphoinositide 3-kinase-C2α.* Journal of Biological Chemistry, 2006. **281**(51): p. 39396-39406.
9. Legendre-Guillemin, V., et al., *ENTH/ANTH proteins and clathrin-mediated membrane budding.* Journal of cell science, 2004. **117**(1): p. 9-18.
10. Stanishneva-Konovalova, T., et al., *The role of BAR domain proteins in the regulation of membrane dynamics.* Acta Naturae (англоязычная версия), 2016. **8**(4 (31)).
11. Erlendsson, S. and K.L. Madsen, *Membrane binding and modulation of the PDZ domain of PICK1.* Membranes, 2015. **5**(4): p. 597-615.
12. Park, M.-J., et al., *SH2 domains serve as lipid-binding modules for pTyr-signaling proteins.* Molecular cell, 2016. **62**(1): p. 7-20.
13. Toulmay, A. and W.A. Prinz, *A conserved membrane-binding domain targets proteins to organelle contact sites.* Journal of cell science, 2012. **125**(1): p. 49-58.
14. DiNitto, J.P., T.C. Cronin, and D.G. Lambright, *Membrane recognition and targeting by lipid-binding domains.* Sci. Stke, 2003. **2003**(213): p. re16-re16.
15. Nastou, K.C., et al., *MBPpred: Proteome-wide detection of membrane lipid-binding proteins using profile Hidden Markov Models.* Biochimica et Biophysica Acta (BBA)-Proteins and Proteomics, 2016. **1864**(7): p. 747-754.
16. Mukhopadhyay, S. and P.K. Jackson, *The tubby family proteins.* Genome biology, 2011. **12**(6): p. 225.
17. Dunne, S.J., et al., *Structure of the membrane binding domain of CTP: phosphocholine cytidylyltransferase.* Biochemistry, 1996. **35**(37): p. 11975-11984.
18. Zhao, J., et al., *Dystrophin contains multiple independent membrane-binding domains.* Human molecular genetics, 2016. **25**(17): p. 3647-3653.
19. Pemberton, J.G. and T. Balla, *Polyphosphoinositide-binding domains: Insights from peripheral membrane and lipid-transfer proteins.* 2019.

20. Clairfeuille, T., et al., *Structure and Membrane Binding Properties of the Endosomal Tetratricopeptide Repeat (TPR) Domain-containing Sorting Nexins SNX20 and SNX21*. J Biol Chem, 2015. **290**(23): p. 14504-17.
21. Wayne Albers, R.R.W., *Chapter 2 - Cell Membrane Structures and Functions*, in *Basic Neurochemistry (Eighth Edition)*, S.T. Brady, et al., Editors. 2012, Academic Press: New York. p. 26-39.
22. Xu, Y., et al., *The Polycystin-1, Lipoxygenase, and α-Toxin Domain Regulates Polycystin-1 Trafficking.* J Am Soc Nephrol, 2016. **27**(4): p. 1159-73.
23. Buwaneka, P., et al., *Phosphoinositide-binding activity of Smad2 is essential for its function in TGF-β signaling.* J Biol Chem, 2021. **297**(5): p. 101303.
24. Zouhar, J. and M. Sauer, *Helping hands for budding prospects: ENTH/ANTH/VHS accessory proteins in endocytosis, vacuolar transport, and secretion.* Plant Cell, 2014. **26**(11): p. 4232-44.
25. Staus, D.P., et al., *Structure of the M2 muscarinic receptor–β-arrestin complex in a lipid nanodisc.* Nature, 2020. **579**(7798): p. 297-302.
26. Busse, R.A., et al., *Characterization of PROPPIN-Phosphoinositide Binding and Role of Loop 6CD in PROPPIN-Membrane Binding.* Biophys J, 2015. **108**(9): p. 2223-34.

Chapter IV. SIRT4 as a Novel Interactor and Candidate Suppressor of CRAF Kinase in MAPK Signaling

Authors: Mehrnaz Mehrabipour, Saeideh Nakhaei-Rad, Radovan Dvorsky, Alexander Lang, Patrick Verhülsdonk, Mohammad Reza Ahmadian and Roland P. Piekorz

DOI: 10.26508/lsa.202302507

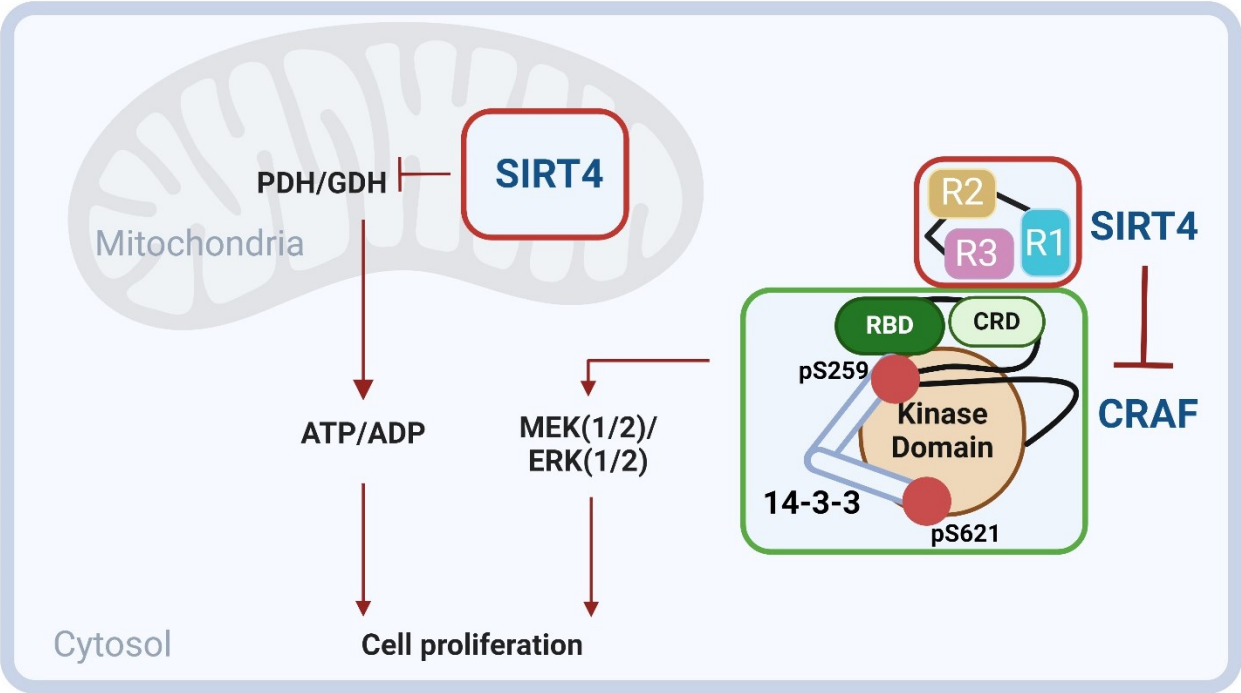

Status:	Published in March 2024
Journal:	Life Science Alliance
JIF:	3.3
Contribution:	70%

Responsible for conceptualization, data preparation, protein purification, cell culture, mutational analysis, protein interaction analysis (including co-immunoprecipitation and pull-down assays), molecular docking, structural and binding site analysis, writing the original draft, reviewing and editing, and creating figures.

Published Online: 18 March, 2024 | Supp Info: http://doi.org/10.26508/lsa.202302507

Research Article

TRANSPARENT PROCESS SOURCE DATA OPEN ACCESS

Life Science Alliance

SIRT4 as a novel interactor and candidate suppressor of C-RAF kinase in MAPK signaling

Mehrnaz Mehrabipour[1], Saeideh Nakhaei-Rad[2], Radovan Dvorsky[1], Alexander Lang[1], Patrick Verhülsdonk[1], Mohammad R Ahmadian[1,*], Roland P Piekorz[1,*]

Cellular responses leading to development, proliferation, and differentiation depend on RAF/MEK/ERK signaling, which integrates and amplifies signals from various stimuli for downstream cellular responses. C-RAF activation has been reported in many types of tumor cell proliferation and developmental disorders, necessitating the discovery of potential C-RAF protein regulators. Here, we identify a novel and specific protein interaction between C-RAF among the RAF kinase paralogs, and SIRT4 among the mitochondrial sirtuin family members SIRT3, SIRT4, and SIRT5. Structurally, C-RAF binds to SIRT4 through the N-terminal cysteine-rich domain, whereas SIRT4 predominantly requires the C-terminus for full interaction with C-RAF. Interestingly, SIRT4 specifically interacts with C-RAF in a pre-signaling inactive (serine 259–phosphorylated) state. Consistent with this finding, the expression of SIRT4 in HEK293 cells results in an up-regulation of pS259-C-RAF levels and a concomitant reduction in MAPK signaling as evidenced by strongly decreased phospho-ERK signals. Thus, we propose an additional extra-mitochondrial function of SIRT4 as a cytosolic tumor suppressor of C-RAF-MAPK signaling, besides its metabolic tumor suppressor role of glutamate dehydrogenase and glutamate levels in mitochondria.

DOI 10.26508/lsa.202302507 | Received 4 December 2023 | Revised 6 March 2024 | Accepted 7 March 2024 | Published online 18 March 2024

Introduction

C-RAF (often also called RAF1) belongs to the RAF kinase family (A-RAF, B-RAF, and C-RAF), which transfers proliferative and growth signals to downstream activation of MEK/ERK kinases. These RAF paralogs share several structural properties (Rezaei Adariani et al, 2018; Nakhaei-Rad et al, 2023b), yet they differ in terms of activity levels and functional roles (Desideri et al, 2015). Among them, C-RAF exhibits moderate activity, less than B-RAF, but more than A-RAF, and is associated with cancer and developmental disorders (Blasco et al, 2011; Karreth et al, 2011; Gelb et al, 2015; Degirmenci et al, 2020). There are three conserved regions (CR) within RAF proteins that are important for their respective regulatory functions (CR1 and CR2) and kinase activity (CR3) (Rezaei Adariani et al, 2018). CR1 contains a RAS-binding domain (RBD), mediating a RAS interaction, and a cysteine-rich domain (CRD), which mediates membrane binding and enhances RAS/RBD affinity at the membrane (Fang et al, 2020; Tran et al, 2021; Nguyen et al, 2022). CR2 is enriched by several Ser/Thr residues, including serine 259 (S259), which is an important site for inhibitory phosphorylation and 14-3-3 binding that regulates RAF kinase activation (Dhillon et al, 2002). When phosphorylated by upstream kinases such as AKT, PKA, or LATS1, CR2 acts as an inhibitory domain that keeps C-RAF in an inactive state (Zimmermann & Moelling, 1999; Dumaz & Marais, 2003; Romano et al, 2014). Dephosphorylation of CR2 by protein phosphatases, such as PP2A or PP1, relieves this autoinhibition on the kinase domain and activates C-RAF (Jaumot & Hancock, 2001). CR3 functions as a catalytic C-terminal region, constituting a putative phosphorylation segment for kinase activation (Chong et al, 2001). Thus, C-RAF cycles between a close inactive and an open active conformation, which is regulated by different phosphorylation and dephosphorylation events (Lavoie & Therrien, 2015). Overall, phosphorylation, feedback/autoinhibition, and protein–protein interaction occur in C-RAF regulation in response to signaling events (Wimmer & Baccarini, 2010; Cseh et al, 2014; Romano et al, 2014; Lavoie & Therrien, 2015; Varga et al, 2017; Okamoto & Sako, 2023). In particular, RAS and 14-3-3 binding are major regulatory events of RAF activation, membrane recruitment, and stabilization (Matallanas et al, 2011; Li et al, 2018; Jang et al, 2020; Tran et al, 2021). Addressing the molecular control of C-RAF by interacting regulators and the underlying molecular and structural mechanisms is still necessary for understanding the complex landscape of MAPK network signaling. Several proteins that bind and regulate C-RAF have been identified, including RKIP (RAF1 kinase inhibitor protein), which functions as an anti-metastatic tumor suppressor and is down-regulated in various cancers (Yesilkanal & Rosner, 2018; Touboul et al, 2021; Cessna et al,

[1]Institute of Biochemistry and Molecular Biology II, Medical Faculty and University Hospital Düsseldorf, Heinrich Heine University, Düsseldorf, Germany [2]Stem Cell Biology, and Regenerative Medicine Research Group, Institute of Biotechnology, Ferdowsi University of Mashhad, Mashhad, Iran

Correspondence: Reza.Ahmadian@hhu.de; Roland.Piekorz@hhu.de
Alexander Lang's present address is Department of Cardiology, Pulmonology, and Vascular Medicine, Medical Faculty and University Hospital Düsseldorf, Heinrich Heine University, Düsseldorf, Germany
*Mohammad R Ahmadian and Roland P Piekorz contributed equally to this work

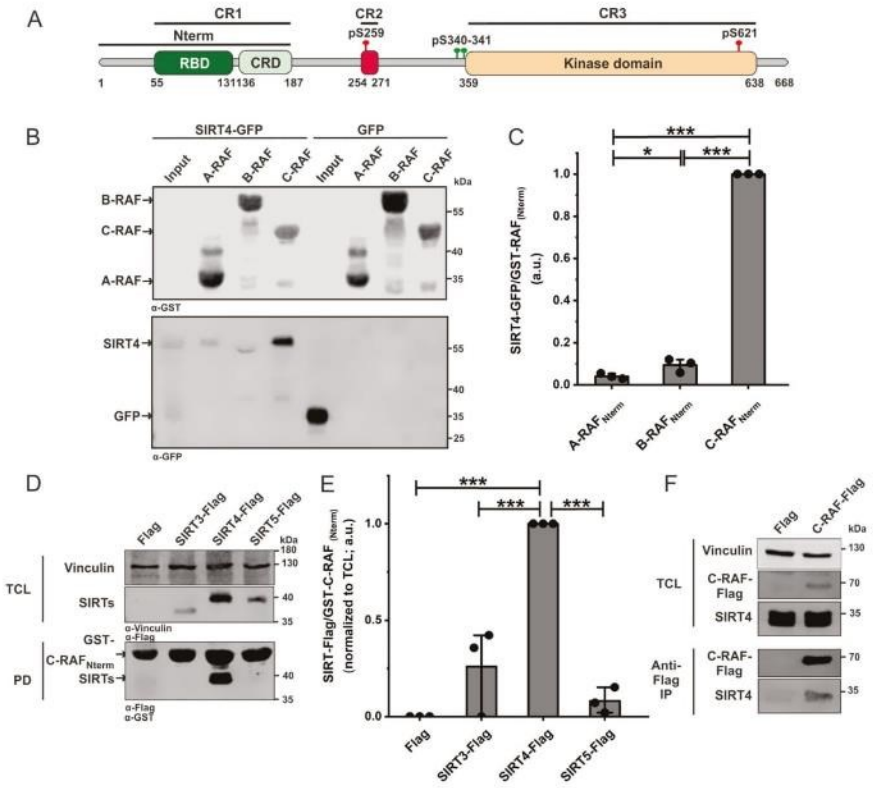

Figure 1. Identification of a selective interaction between SIRT4 and C-RAF within the RAF kinase and SIRT paralogs.
(A) Domain organization of C-RAF including the RAS-binding domain and cysteine-rich domain, which are parts of the N-terminal region (Nterm). Phosphorylation sites regulating the activity of C-RAF (pS259: inactive form; pY340/341: active form) are indicated. **(B)** Total cell lysates (TCL) from SIRT4-eGFP– or eGFP-expressing HEK293 cells were subjected to pull-down experiments using normalized bacterial lysates containing the GST-fused Nterm region of A-RAF, B-RAF, or C-RAF. **(C)** Densitometric quantification of immunoblot signals of binding of SIRT4-eGFP to the N-RBD-CRD of C-RAF as compared to A-RAF and B-RAF. Data were subjected to statistical one-way ANOVA (mean ± S.D.; $^*P < 0.05$; $^{***}P < 0.001$). **(D)** TCL from HEK293 cells expressing Flag-tagged versions of SIRT3, SIRT4, or SIRT5 were subjected to pull-down (PD) experiments using the GST-fused Nterm region of C-RAF. **(E)** Densitometric quantification of immunoblot signals of binding of the Nterm region of C-RAF to SIRT4 as compared to SIRT3 and SIRT5. Data were subjected to statistical one-way ANOVA (mean ± S.D.; $^{***}P < 0.001$). **(F)** Co-immunoprecipitation analysis (anti-Flag Co-IP) of endogenous SIRT4 was performed using TCL from Flag-C-RAF–expressing COS7 cells.
Source data are available for this figure.

2022; Moghaddam et al, 2023). RKIP binds to the N-terminal region of C-RAF and therefore inhibits C-RAF–mediated phosphorylation and activation of MEK1/2 (Rath et al, 2008).

The family of human sirtuins comprises seven members, of which SIRT3, SIRT4, and SIRT5 function as bona fide metabolic regulators in mitochondria (Ji et al, 2022). In particular, SIRT4 inhibits, as a tumor suppressor, the metabolic gatekeepers pyruvate dehydrogenase and glutamate dehydrogenase (Haigis et al, 2006; Mathias et al, 2014), with particular significance for the regulation of glutamine metabolism in tumor cells. Recent findings uncovered novel extra-mitochondrial roles of SIRT4 in microtubule dynamics and regulation of mitotic cell cycle progression, WNT/β-catenin and Hippo signaling, and SNARE complex formation required for autophagosome–lysosome fusion (Bergmann et al, 2020; Wang et al, 2022; Yang et al, 2022; Huang et al, 2023). Interestingly, proteomic analysis of the SIRT4 interactome identified C-RAF as a potential binding partner of SIRT4, indicating a novel role of SIRT4 in the regulation of the RAF-MAPK signaling pathway (Bergmann et al, 2020). Consistent with this idea, recent studies have demonstrated that (i) the tumor suppressor SIRT4 is down-regulated in most human solid tumor types and cell lines (Bai et al, 2020; Tomaselli et al, 2020; Wang et al, 2020), and (ii) the ectopic expression of SIRT4 down-regulates pERK1/2 levels and hence inhibits MAPK signaling and cell proliferation (Fu et al, 2017; Chen et al, 2019; Hu et al, 2019; Bai et al, 2020; Tomaselli et al, 2020; Wang et al, 2020). Considering these interrelated findings, in this study we investigated the

molecular and functional interaction between the proto-oncogene C-RAF and the tumor suppressor SIRT4 in the context of MAPK signaling inhibition.

Results

Identification of a selective SIRT4-C-RAF interaction among SIRT and RAF protein family members

In a previous study, we employed mass spectrometry and proteomic analysis to identify novel SIRT4-interacting proteins (Bergmann et al, 2020). Interestingly, C-RAF kinase (often referred to by its gene name *Raf1*), a major component of the MAPK signaling pathway, emerged as a novel SIRT4-binding protein as confirmed by nanobody-based co-immunoprecipitation analysis (Fig S1). Considering the presence of N-terminal regulatory (CR1, CR2) and C-terminal catalytic (CR3) domains in C-RAF (Fig 1A), we hypothesized that the N-terminal CR1 regulatory segment, consisting of the RBD (RAS-binding domain) and CRD, might be involved in SIRT4 interaction.

Accordingly, we addressed the specificity of SIRT4-C-RAF interaction by protein pull-down analysis using bacterially expressed GST-fused N-terminal (Nterm) regions of A-RAF, B-RAF, or C-RAF, each containing the respective RBD and CRD. Normalized amounts of GST-RAF lysates were coupled to GSH (glutathione) beads followed by incubation with total cell lysates from HEK293 cells expressing SIRT4-GFP or GFP as a control. As indicated in Figs 1B and C and S2A, a strong physical interaction with SIRT4 was only observed for C-RAF$_{Nterm}$, but not for A-RAF$_{Nterm}$ or B-RAF$_{Nterm}$. In complementary pull-down experiments, we used total cell lysates from HEK293 cells stably expressing C-terminally Flag-tagged SIRT3, SIRT4, or SIRT5. Only SIRT4 exhibited a robust interaction with C-RAF$_{Nterm}$, but not SIRT3 or SIRT5 (Figs 1D and E and S2B). Finally, we immunoprecipitated Flag-tagged C-RAF from COS7 cell lysates and could demonstrate co-immunoprecipitation of endogenous SIRT4 (Figs 1F and S2C). Overall, our data suggest that within the sirtuin and RAF family members studied, only C-RAF and SIRT4 undergo a unique interaction.

The CRD of C-RAF and the C-terminus of SIRT4 are major determinants of the interaction between SIRT4 and C-RAF

In the next step, we sought to determine the regions or subdomains of C-RAF and SIRT4 that are directly involved in the interaction between these two proteins. We expressed GST-C-RAF-Nterm, RBD, and CRD in *Escherichia coli* and used them to pull down SIRT4-Flag from total cell lysates of HEK293 cells. As indicated in Fig S3A–C, C-RAF$_{Nterm}$ and interestingly CRD alone (C-RAF$_{CRD}$) bound to SIRT4-Flag, although with a higher efficiency seen for C-RAF$_{Nterm}$. However, no or only a slight interaction with SIRT4-Flag could be observed for the RBD (C-RAF$_{RBD}$) (Figs 2A and B and S3A–D). These results suggest that the CRD is the major SIRT4-binding domain of C-RAF.

In order to get insight into molecular aspects of SIRT4 binding to C-RAF, we set out to inspect the structures of these proteins and analyze their putative complex. We first generated a homology model of human SIRT4 using the 3D structure of SIRT4 from *Xenopus tropicalis* (PDB: 5OJ7) (Pannek et al, 2017) as a template. Given that SIRT4, but neither SIRT3 nor SIRT5, binds to C-RAF$_{Nterm}$ (Fig 1B and C), we have scrutinized their sequences and compared our model structure of SIRT4 with the structure of human SIRT5 (PDB: 4G1C) (Fig S4A and B). This analysis revealed three regions in SIRT4 that differ from SIRT5, that is, R1$_{(69–98)}$, R2$_{(165–229)}$, and R3$_{(255–314)}$ (Figs 2C and D and S4). The corresponding SIRT4 deletion mutants SIRT4(Δ69–98; ΔR1), SIRT4(Δ165–229; ΔR2), and SIRT4(Δ255–314; ΔR3) were generated as C-terminal GFP-tagged proteins, stably expressed in HEK293 cells, and tested for C-RAF$_{Nterm}$ binding in pull-down experiments. As shown in Figs 2E and F and S3E, SIRT4(ΔR3) strikingly showed the weakest interaction with C-RAF$_{Nterm}$, whereas ΔR1 and ΔR2 were not significantly different from wild-type SIRT4. Moreover, SIRT4(ΔN28), which lacks the N-terminal mitochondrial translocation signal (Lang et al, 2017), as well as the catalytically inactive mutant SIRT4(H161Y) (Lang et al, 2017), bound C-RAF$_{Nterm}$ comparable to WT SIRT4 (Figs 2E and F and S5A–C). Taken together, C-RAF$_{CRD}$ and the C-terminus of SIRT4, encompassing residues 255–314, are involved in SIRT4-C-RAF interaction, which is independent of the first 28 a.a. of SIRT4 and therefore its mitochondrial localization and of the catalytic activity of SIRT4. Our findings also add a new function to the C-terminus of SIRT4 besides its role in proteasomal degradation and stability regulation of SIRT4 (Hampel et al, 2023).

Mutational analysis of the interaction between C-RAF$_{CRD}$ and SIRT4

We generated nine single mutations and three sets of combined mutations of C-RAF$_{CRD}$ based on the multiple sequence alignment of amino acid deviations of C-RAF$_{CRD}$ in comparison with the CRD of A-RAF and B-RAF (Fig 3A and B). All mutants were expressed and purified as GST-fusion proteins and subjected to pull-down assays using total cell lysates from SIRT4-Flag–expressing HEK293 cells. As indicated in Figs 3C and E and S6, and quantitatively analyzed in Fig 3D and F, none of the single or combined mutants analyzed a decreased interaction of C-RAF$_{CRD}$ with SIRT4-Flag. Rather, we observed significantly stronger binding for the CRD mutants Q156R, Set1 (E174Q/H175R/T178S/K179E/T182L), and Set2 (Q156R/F158L/L160F) (Fig 3C–F).

To identify residues of the C-RAF$_{CRD}$-SIRT4-binding interface and obtain a more detailed insight into their intermolecular interplay, we performed molecular docking analysis between C-RAF$_{CRD}$ (PDB: 1FAQ) and full-length SIRT4 (Q9Y6E7) using the ClusPro 2.0 server. The 3D surface structure (Fig 3G) highlights the binding between C-RAF$_{CRD}$ and R3 of SIRT4, along with certain parts of R1. For a more detailed understanding of this intermolecular binding, analysis of the binding surface using BIOVIA software revealed an interacting network (Fig 3H), in which the stability of the C-RAF$_{CRD}$-SIRT4 complex is the result of a combination of various interaction types, that is, hydrogen bonds, electrostatic interactions, and hydrophobic contacts (Table S1). For example, the C-RAF$_{CRD}$ residue K157 and the SIRT4 residue D236 form a hydrogen/electrostatic bond with a distance of 1.8 Å, indicative of a strong interaction. C-RAF$_{CRD}$ residues R143, K157, H175, T178, K179, Q156, E174, S177, N161, and I154, and SIRT4 residues R75, R97, T274, H92, T237, D236, Q264, Q91, R270, R291, G93, G235, and Y266 further contribute to the binding stability

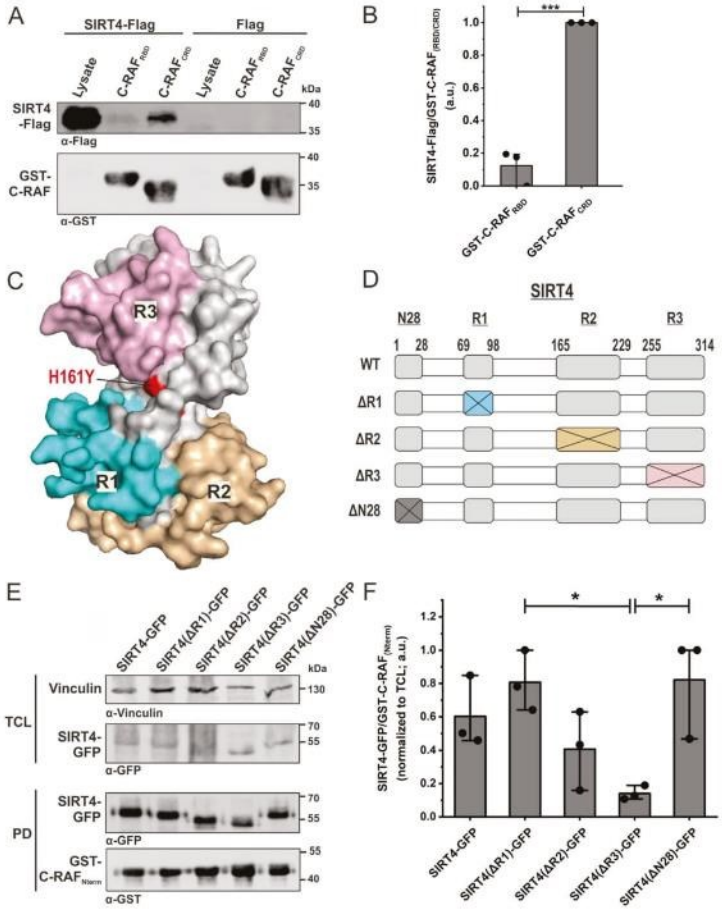

Figure 2. Identification of a selective interaction between the cysteine-rich domain of C-RAF and the very C-terminal region of SIRT4.
(A) Identification of the CRD of C-RAF as the primary SIRT4-interacting domain. Total cell lysates from HEK293 cells stably expressing SIRT4-Flag were subjected to pull-down experiments using GST or the GST-fused N-terminal RBD or CRD subdomains of C-RAF. **(B)** Densitometric quantification of immunoblot signals of the relative binding of RBD and CRD subdomains of C-RAF to SIRT4-Flag. Data were subjected to statistical one-way ANOVA (mean ± S.D.; ***$P < 0.001$). **(C)** Predicted functional surface of SIRT4 was obtained from comparative homology modeling with SIRT5 (see Fig S4A and B). Three regions (R1, R2, and R3), which are different between SIRT4 and SIRT5, are highlighted in the 3D-modeled SIRT4 structure. Replacement of histidine 161 by tyrosine creates the catalytically inactive SIRT4. **(D)** Schematic representation of SIRT4 deletion mutants, including ΔR1, ΔR2, ΔR3, and ΔN28 lacking the N-terminal mitochondrial translocation sequence. **(E)** Equal amounts of total cell lysates from HEK293 cells expressing the SIRT4-eGFP of the indicated deletion mutants were subjected to pull-down (PD) analysis using the GST-fused C-RAF$_{Nterm}$. **(F)** Densitometric quantification of immunoblot signals of the relative binding of SIRT4-GFP deletion mutants to the GST-fused C-RAF$_{Nterm}$. Data were subjected to statistical one-way ANOVA (mean ± S.D.; *$P < 0.05$).
Source data are available for this figure.

via hydrogen bonds. Notably, electrostatic interactions were observed between C-RAF$_{CRD}$ residues R143, E174, and F141, and SIRT4 residues E277, R270, and R291, respectively (Fig 3H; Table S1). Moreover, hydrophobic interactions were identified involving residues of C-RAF$_{CRD}$ (H175, L160, F163, R143) and SIRT4 (V232, F234, P240, Y266, R270).

Because the C-RAF$_{CRD}$ Set1 and Set2 mutations resulted in stronger binding to SIRT4-Flag (Fig 3C–F), further molecular docking analysis was performed for these C-RAF$_{CRD}$ gain-of-function mutations. Comparing the cluster scores of WT C-RAF$_{CRD}$ interacting with SIRT4 shows a weighted score of −716 for both the middle and the lowest energy. In contrast, Set1 and Set2 have lower, more stable cluster scores: −738.7 and −795 for the center and the lowest energy in the case of Set1, and −744 for both the center and the lowest energy in the case of Set2. The combined mutations in Set1, particularly the E174Q, H175R, T175S, K179E, and T182L mutations, alter the interaction profile of C-RAF$_{CRD}$ with SIRT4, thereby forming new hydrogen bonds, as well as electrostatic and hydrophobic contacts, which potentially enhance complex stability (Fig S7D and Table S2). Although some interactions are lost in Set1 compared with WT C-RAF$_{CRD}$ (Table S2), considering the cluster score and the mode of binding, we propose also new platforms of interactions. These involve a new set of C-RAF$_{CRD}$ residues, that is, D153, Y170, P181, L182, M183, and V185, that might collectively increase the binding affinity of Set1 to SIRT4 (Fig S7D and Table S2). Moreover, compared with WT C-RAF$_{CRD}$, the mutations within Set1 induce a modified interaction pattern with SIRT4, characterized by an increased interaction of C-RAF$_{CRD}$ residues with R1 of SIRT4 while exhibiting a reduced interaction with R3 and the SIRT4 gray area (which lacks R1, R2, and R3) (Fig S7A–D).

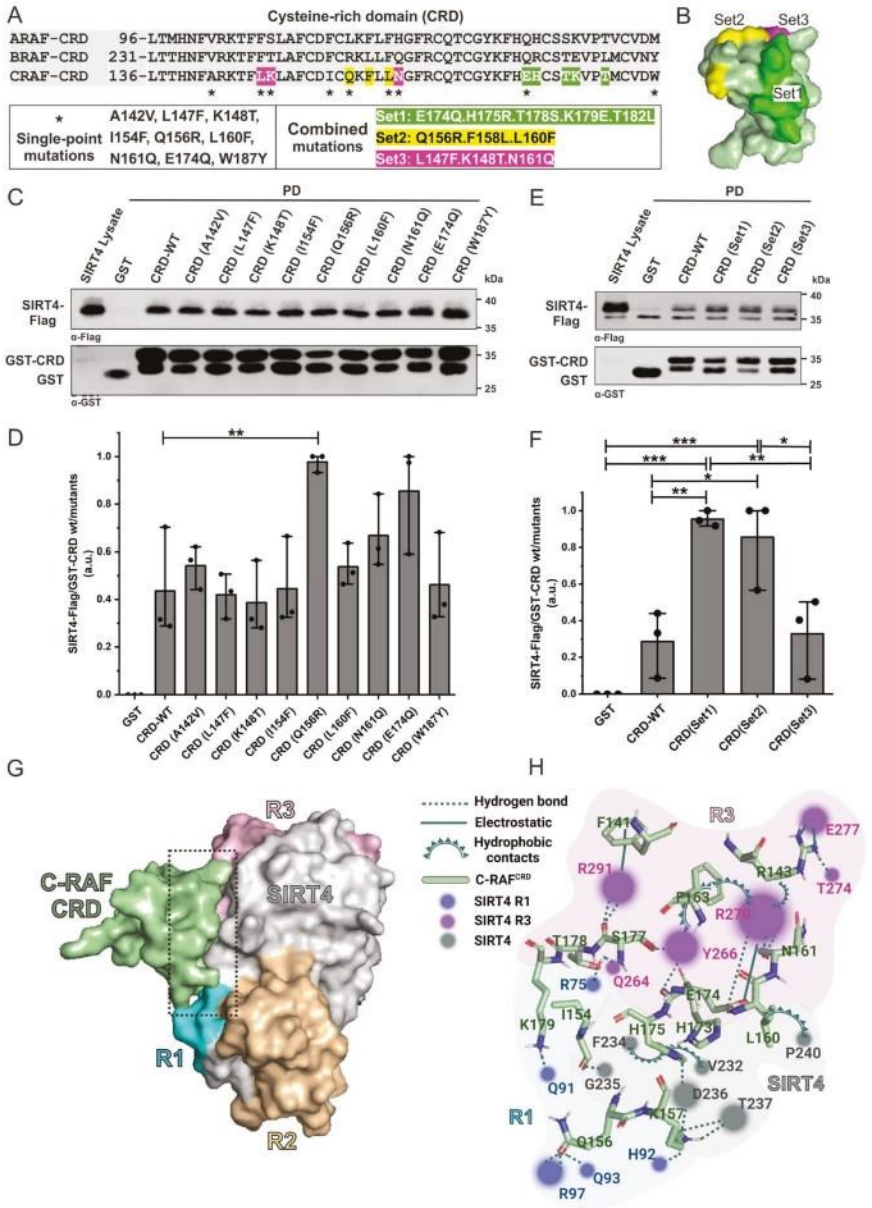

Figure 3. Mapping the SIRT4-binding site of C-RAF.
(A) Multiple sequence alignment highlights amino acid deviations of the CRD of C-RAF as compared to the CRD of A-RAF and B-RAF and is the basis for single-point and combined mutations of C-RAF generated in this study. **(B)** 3D model of the three sets of combined mutations in the CRD of C-RAF. **(A, C, E)** Total cell lysates from HEK293 cells stably expressing SIRT4-Flag were subjected to pull-down experiments using GST, GST-CRD (WT), or GST-CRD harboring single-point mutations (C) or combined mutations (E) as indicated in (A). **(D, F)** Densitometric quantification of immunoblot signals of the relative binding of WT and mutated CRD subdomains of C-RAF to

Similar to C-RAF$_{CRDSet1}$, Set2 mutations in the C-RAF$_{CRD}$ region also introduce new interactions, as well as changes in the type and distance of existing interactions with the respective SIRT4 regions (Fig S7E and F). For instance, the F158L mutation leads to the formation of a new hydrogen bond with T237 of SIRT4, and the L160F mutation results in the interaction with both P240 and V243 of SIRT4, leading to a higher involvement of CRD-Set2 residues (Fig S7F and Table S2). Notably, in the case of C-RAF$_{CRDSet2}$, the C-RAF$_{CRD}$ residues C155, L158, F172, and H173 undergo novel hydrogen bonds with SIRT4 residues, suggesting a restructuring of the binding interface and thereby increasing the stability of the C-RAF$_{CRD}$-SIRT4 interaction in the case of C-RAF$_{CRDSet2}$ (Fig S7F and Table S2).

SIRT4 binds selectively to the inactive state of C-RAF characterized by phosphorylation of serine 259

C-RAF exists in two distinct forms. Its closed, monomeric, autoinhibited form is stabilized by phosphorylation at serines 259 and 621 (pS259/pS621), and subsequent association with the 14-3-3 dimer (Rommel et al, 1996; Matallanas et al, 2011). The C-RAF activation involves a series of complex processes, including dephosphorylation (pS259) and phosphorylation (pY340/pY341) events, conformational changes, dimerization, and association with RAS, 14-3-3, and the membrane, ultimately stabilizing the open, dimeric, active form of C-RAF (Emerson et al, 1995; Diaz et al, 1997; Jaumot & Hancock, 2001; Harding et al, 2003; Terai & Matsuda, 2005; Takahashi et al, 2017). Thus, we addressed whether SIRT4 interacts with C-RAF in its active or inactive state. As indicated in Figs 4A and S8A, endogenously expressed C-RAF could be immunoprecipitated from total cell lysates of HEK293 cells expressing SIRT4-Flag. However, when using specific antibodies against pS259-C-RAF (closed, inactive form) and pY340/341-C-RAF (open, active form), only pS259-C-RAF was detected in the immunoprecipitates (Fig 4A). These findings are consistent with homology modeling of C-RAF$_{CRD}$ in the inactive form of C-RAF (Fig 4B), in which the putative SIRT4-binding region remains accessible as part of the C-RAF$_{CRD}$ domain (indicated in pale green). Furthermore, co-immunoprecipitation of KRAS within the SIRT4-Flag-C-RAF–interacting complex could not be detected (Figs 4A and S8A), supporting the notion that C-RAF exclusively exists in its autoinhibited form in complex with SIRT4. Overall, this is consistent with an interaction of KRAS only with the active form of C-RAF, which requires dephosphorylation of S259 and unmasking of the RBD and CRD to allow KRAS binding to C-RAF at the membrane (reviewed in Matallanas et al [2011]). Further structural analysis provides additional evidence that the SIRT4-binding region of C-RAF$_{CRD}$ contains residues required for KRAS–membrane interaction (Fig 4B).

SIRT4-C-RAF interaction is associated with the inhibition of the MAPK signaling pathway

It is well established in the literature that SIRT4 overexpression inhibits cell proliferation, among other cellular responses, in several tumor cell lines, most likely through inhibition of the MAPK pathway (Fu et al, 2017; Chen et al, 2019; Hu et al, 2019; Bai et al, 2020; Tomaselli et al, 2020; Wang et al, 2020). Here, we addressed the regulatory affect of ectopic SIRT4 expression on ERK1/2 phosphorylation. As shown in Figs 4C and D and S8B, the ectopic expression of SIRT4 led to a clear accumulation of the levels of inactive C-RAF phosphorylated at S259. At the same time, MAPK signaling was strongly inhibited as evidenced by an ~80% reduction in p-ERK1/2 levels as compared to Flag-expressing control cells. Overall, these data suggest that SIRT4 both interacts with and possibly sequesters the inactive form of C-RAF. Thus, the extra-mitochondrial function of SIRT4 on C-RAF-MAPK signaling may provide a novel control mechanism for tumor suppression (Fig 4E).

Discussion

The work presented in this study has identified a novel interaction of SIRT4, a tumor suppressor sirtuin, with C-RAF, a key regulatory kinase and a component of the oncogenic MAPK pathway. The results indicate that (i) among the RAF kinases (A-RAF, B-RAF, and C-RAF) and sirtuin proteins (SIRT3, SIRT4, and SIRT5) analyzed, C-RAF selectively interacts with SIRT4; (ii) this interaction involves the N-terminal CRD of C-RAF and the C-terminal region 3 (R3) of SIRT4 as revealed by pull-down and molecular docking analyses; (iii) mutational analysis of C-RAF$_{CRD}$ so far identified gain-of-function mutations with improved SIRT4 binding, thus highlighting the importance of these residues in the C-RAF$_{CRD}$-SIRT4 interaction; (iv) in particular, SIRT4 specifically interacts with C-RAF in its inactive state (C-RAF^{pS259}); and (v) the ectopic expression of functional SIRT4 leads to accumulation of pS259-C-RAF levels, which is associated with inhibition of MAPK signaling as shown by greatly reduced p-ERK1/2 levels. Thus, our data highlight a novel extra-mitochondrial, anti-proliferative function of SIRT4 in binding and potentially sequestering C-RAF from its substrate MEK1/2 and consequently interfering with ERK1/2 activation.

The MAPK signaling pathway plays a critical role in the regulation of various cellular processes such as differentiation, survival, and, in particular, proliferation (Zhang & Liu, 2002; Guo et al, 2020; Ullah et al, 2022). Dysregulation of this pathway is frequently associated with the initiation and progression of human diseases, including cancer (Degirmenci et al, 2020) and developmental disorders such as RASopathies (Dar & Brady, 2022), the latter exemplified by the RAF1^{S257L} mutation causing cardiomyopathy (Dhandapany

SIRT4-Flag. Data were subjected to statistical one-way ANOVA (mean ± S.D.; *P < 0.05; **P < 0.01; ***P < 0.001). **(G)** Molecular docking and binding site analyses between the CRD of C-RAF and specified regions of SIRT4. The predicted interaction between the CRD of C-RAF and the C-terminal region R3 of SIRT4, along with a smaller part of R1, is depicted in this 3D model. **(H)** Schematic, magnified view of the CRD-SIRT4–interacting surface and the involved amino acid residues. The binding types, that is, hydrogen bonds, electrostatic interactions, and hydrophobic contacts, are indicated. The colored circles mark SIRT4 residues, with the size of the circles indicating the number of interactions with the CRD.
Source data are available for this figure.

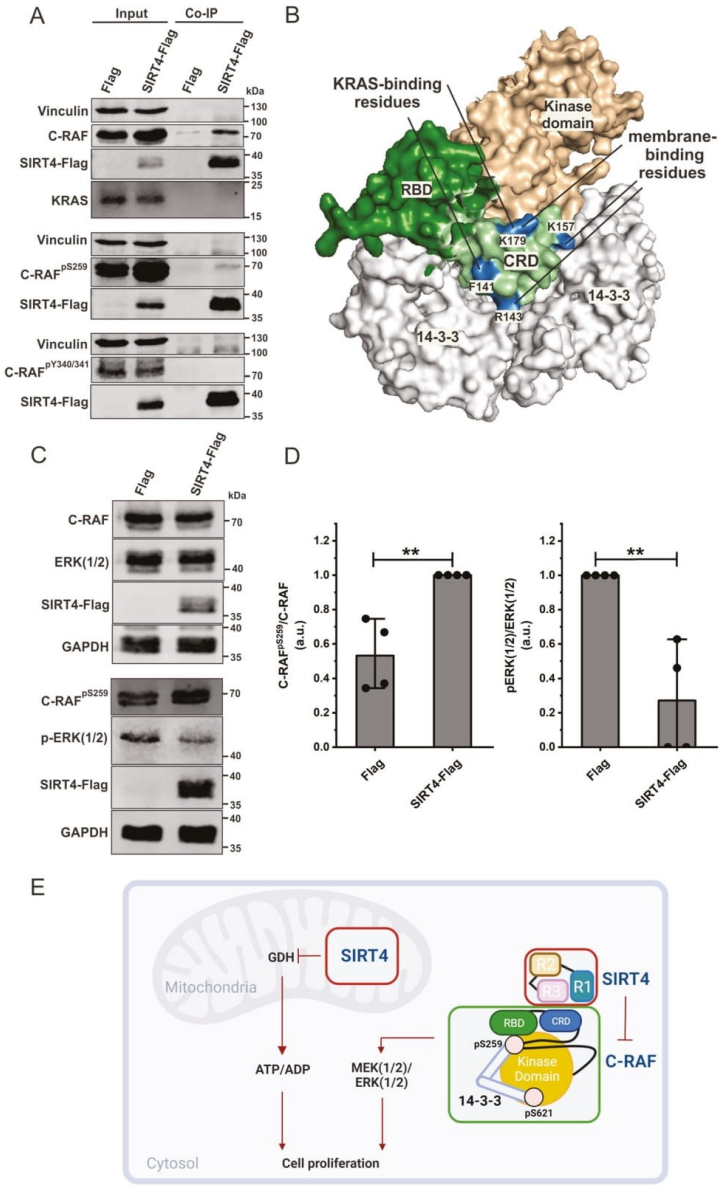

Figure 4. SIRT4 interacts with and up-regulates the inactive form of C-RAF phosphorylated at serine 259 (S259).
(A) Co-immunoprecipitation analysis using total cell lysates (Input) from HEK293 cells expressing Flag or SIRT4-Flag shows the SIRT4 interaction specifically with C-RAF in its autoinhibited state (pS259-C-RAF) but not with pY340/341-C-RAF in its active state. Moreover, KRAS did not co-immunoprecipitate with the SIRT4-pS259-C-RAF complex. **(B)** Homology model of the closed, inactive C-RAF structure in complex with the 14-3-3 dimer (light gray) was built using the crystal structure of B-RAF as a template. The accessibility of the CRD in its inactive form is represented (pale green). The model depicts regions highlighted in blue that are crucial for KRAS binding and membrane interaction in the active state of C-RAF. The amino acids involved are indicated. **(C)** Total cell lysates from HEK293 cells expressing Flag or SIRT4-Flag were subjected to immunoblot analysis of pS259-C-RAF and pERK1/2 levels. The ectopic expression of SIRT4 in HEK293 cells increased the levels of inactive pS259-C-RAF and reduced ERK1/2 phosphorylation. **(D)** Densitometric immunoblot analysis of the levels of pS259-C-RAF (left panel) and pERK1/2 (right panel) upon Flag or SIRT4-Flag expression was subjected to statistical one-way ANOVA (mean ± S.D.; $^{**}P < 0.01$). **(E)** Hypothetical model summarizing the two anti-proliferative axes of SIRT4. SIRT4 displays bifunctional activities in inhibiting glutamate dehydrogenase in mitochondria and C-RAF-MAPK signaling in the cytosol. For further explanation, see Discussion.
Source data are available for this figure.

et al, 2014; Jaffre et al, 2019; Nakhaei-Rad et al, 2023a). As a key component of the MAPK pathway, C-RAF is activated by upstream receptor–RAS signaling and subsequently activates several downstream effectors, particularly MEK1/2 kinases and subsequently ERK1/2 signaling (Wimmer & Baccarini, 2010; Matallanas et al, 2011; Ullah et al, 2022). Several studies have highlighted the molecular mechanism of C-RAF regulation underlying post-translational modifications through phosphorylation and dephosphorylation,

autoinhibition, and conformational changes associated with stabilized protein–protein interaction (Romano et al, 2014; Lavoie & Therrien, 2015; Varga et al, 2017; Okamoto & Sako, 2023). Classically, RAS proteins and 14-3-3 binding are major regulators of RAF activation, membrane recruitment of C-RAF, and its stability (Matallanas et al, 2011; Tran et al, 2021). The complexity of C-RAF regulation is further highlighted by its heterodimerization with B-RAF, which acts as an allosteric inducer of C-RAF in normal and cancer cells in a RAS-independent manner (Garnett et al, 2005).

Recent findings have identified and characterized additional C-RAF regulators. SHOC2 serves as a scaffold protein for C-RAF that recruits together with MRAS protein phosphatase 1 to dephosphorylate inactive C-RAF at S259, thereby facilitating the C-RAF interaction with RAS at the plasma membrane (Matsunaga-Udagawa et al, 2010; Boned Del Rio et al, 2019; Kwon et al, 2022). In another example, SHOC2 serves as a regulatory factor for C-RAF and has been shown to accelerate the interaction between RAS and C-RAF, ultimately influencing the spatiotemporal patterns of the RAS-ERK signaling pathway (Matsunaga-Udagawa et al, 2010). Moreover, RKTG (RAF kinase trapping to Golgi) has been suggested to regulate the spatial localization of C-RAF by trapping it to the Golgi, thereby altering the interaction of C-RAF with RAS and MEK1 and inhibiting ERK signaling (Feng et al, 2007). Another regulator of C-RAF is RKIP (Yesilkanal & Rosner, 2018; Touboul et al, 2021; Cessna et al, 2022; Moghaddam et al, 2023), which binds to the N-terminal region of C-RAF, thereby inhibiting C-RAF–mediated phosphorylation and activation of MEK1/2 (Park et al, 2006; Rath et al, 2008). Interestingly, a comparison between RKIP and SIRT4 reveals cellular and functional similarities: (i) both proteins are tumor suppressors (Jeong et al, 2013; Moghaddam et al, 2023) that inhibit/prevent C-RAF activation, and their expression is usually down-regulated in cancer (Yesilkanal & Rosner, 2018; Bai et al, 2020; Tomaselli et al, 2020; Wang et al, 2020), although the underlying mechanisms for SIRT4 are still unclear; (ii) SIRT4 and RKIP are both involved in the regulation of mitotic cell division. SIRT4 achieves this through centrosomal localization and potential control of microtubule dynamics (Bergmann et al, 2020), whereas RKIP achieves this through interaction with Aurora-B and control of the mitotic checkpoint (Eves et al, 2006); and finally, (iii) both SIRT4 (Lang et al, 2017; Li et al, 2023) and RKIP are linked to the regulation of autophagy. RKIP is involved in LC3 processing and presumably contributes to autophagosome formation upon starvation (Noh et al, 2016; Wang & Bonavida, 2018). The role of the SIRT4-C-RAF axis in the regulation of these cellular responses requires further characterization.

Interestingly, analogous to our finding, the role of C-RAF$_{CRD}$ interaction in an isoform-specific manner with another C-RAF regulator to inhibit the MAPK pathway has been demonstrated for RAP1 (Nussinov et al, 2020). Here, RAP1 inhibits MAPK signaling via interaction with C-RAF$_{CRD}$ by reducing the number of clustered oncogenic Ras molecules, thereby suppressing C-RAF (but not B-RAF) activation and MAPK signaling. The presence of RAP1 within the nanoclusters competes with RAS for C-RAF as a common target, resulting in the suppression of C-RAF activation. However, whereas RAP1 interacts with the open form of C-RAF at the cell membrane, our data suggest that SIRT4 binds to the autoinhibited (closed) form of C-RAF. Regardless, similar to RAP1, SIRT4 may functionally hijack and inhibit C-RAF via its CRD.

The intermolecular interplay within the C-RAF$_{CRD}$-SIRT4-binding interface remains to be determined at the residual level. The single and combined C-RAF$_{CRD}$ mutations, defined by homology comparison with the CRD of A-RAF and B-RAF (which do not interact with SIRT4), did not negatively interfere with the C-RAF$_{CRD}$-SIRT4 interaction (Fig 3). Therefore, molecular docking experiments of C-RAF$_{CRD}$ on SIRT4 were performed to determine their putative binding interface. In addition to the residues identified in the mutational analysis of the C-RAF$_{CRD}$ domain (Fig 3), these analyses revealed other candidate residues that may be critical for the interaction with SIRT4 (Fig 3H and Table S1). In addition, candidate residues within the R3 and R1 regions of SIRT4 were identified, whose function also needs to be tested by mutational analysis.

Interestingly, the SIRT4-binding region of C-RAF$_{CRD}$ contains residues that are also required for KRAS and membrane interaction of C-RAF$_{CRD}$ (Fig 4B). Previous results identified seven essential basic residues within the CRD (R143, K144, K148, K157, R164, K171, and K179) that are critical for membrane interaction, with particular emphasis on the key basic residues R143, K144, and K148 (Li et al, 2018). R143, K157, and K179 are accessible in the inactive state of C-RAF and are part of the SIRT4 interaction surface, whereas the remaining residues are located on the opposite side and are shielded by 14-3-3 dimers (Fig 4B). In terms of KRAS binding, F141 and K179 are critical for the interaction between KRAS and C-RAF during the activation process (Tran et al, 2021). In the inactive state of C-RAF, in addition to K179, F141 (Fig 4B) is also accessible in the CRD, consistent with the involvement of these two residues in SIRT4 binding as revealed by docking analysis.

At the level of the functional C-RAF-SIRT4 interplay, it is currently unknown whether C-RAF is regulated by an acetylation/deacetylation cycle and whether C-RAF is an enzymatic target of SIRT4. SIRT4 itself exhibits several NAD^+-dependent enzymatic activities, including ADP-ribosylation, deacylation, and deacetylation (Betsinger & Cristea, 2019), with recent findings indeed uncovering several new SIRT4 deacetylation targets not only inside, but also outside of the mitochondria (Wang et al, 2022; Zhang et al, 2022). In this context, there is a paradigm for the regulation of B-RAF by SIRT1. Acetylation of B-RAF at lysine 601 by the p300 acetyltransferase promotes B-RAF kinase activity, thereby enhancing the proliferation of melanoma and resistance to B-RAF^{V600E} inhibitors (Dai et al, 2022). On the contrary, SIRT1 deacetylates B-RAF at K601 and therefore inhibits proliferation. Thus, SIRT1 mediates hypoacetylation of B-RAF and therefore (finely) regulates its downstream MAPK signaling activity.

Our results add another layer of complexity to the regulatory network of C-RAF and MAPK signaling by identifying SIRT4 as a C-RAF binder specifically in its inactive state. As summarized in Fig 4E, in mitochondria, SIRT4 inhibits anaplerosis and ultimately ATP generation via inhibition of glutamate dehydrogenase (Haigis et al, 2006). Outside of the mitochondria, SIRT4 interacts, seemingly via its C-terminal R3, with the inactive "closed" form of C-RAF, in which the kinase domain is concealed through 14-3-3 binding to pS259 and pS621. SIRT4 binding to the CRD of C-RAF potentially stabilizes pS259/pS621-C-RAF, thereby preventing membrane recruitment, which is followed by RAS binding and activation of C-RAF.

Consequently, an association of SIRT4 with C-RAF interferes with the activation of downstream MEK/ERK signaling, consistent with findings showing the SIRT4-mediated inhibition of the MAPK pathway (Fu et al, 2017; Chen et al, 2019; Hu et al, 2019; Bai et al, 2020; Tomaselli et al, 2020; Wang et al, 2020).

To date, only the MEK1/2 kinases have been well characterized as substrates of C-RAF. However, there is evidence for kinase-independent functions/activities of C-RAF, including regulation of apoptosis, cell cycle progression, and migration (Nolan et al, 2021). In this context, there is a broad spectrum of C-RAF targets that could interact either directly or indirectly with active (pSer-338) or inactive (pSer-259) forms of C-RAF. This interaction could also be RAS-dependent or RAS-independent. For example, the interaction between MST2 and C-RAF (pSer-259) prevents MST2 dimerization (Romano et al, 2014) and consequently modulates the strength of mitotic and apoptotic signaling. Notably, we also observed an effect of ectopic SIRT4 expression on the Hippo tumor suppressor pathway, which, in addition to the MAPK pathway, also regulates cell proliferation (Ehmer & Sage, 2016; Zinatizadeh et al, 2021). In particular, the increase in pS259-C-RAF levels upon SIRT4 expression (Fig 4C and D) was associated with a decrease in the pYAP/YAP ratio (unpublished results). Taken together, we describe a novel SIRT4-C-RAF axis that negatively affects both MAPK and Hippo-YAP signaling. Another example is ASK1, which normally activates the pro-apoptotic JNK and p38 pathways, and is negatively regulated by C-RAF (Alavi et al, 2007). C-RAF phosphorylated at residue 338 interacts with the N-terminal domain of ASK1 in a kinase-independent and HRAS-dependent manner (Du et al, 2004). The C-RAF-ASK1 complex formed in mitochondria is disrupted by oxidative stress (Matsuzawa et al, 2002). Whether SIRT4 plays a role in this process remains to be investigated. Other C-RAF activities that may be affected by SIRT4 include stimulation of negative regulation of cell migration through direct interaction with ROCKα (Ehrenreiter et al, 2005), promotion of the cell cycle progression through interaction with Polo-like kinase 1 and Aurora kinase A at the mitotic spindle, and the regulation of the DNA damage response through interaction with checkpoint kinase 2 (Mielgo et al, 2011; Zannini et al, 2014; Advani et al, 2015; Joukov & De Nicolo, 2018).

The functional implications of the SIRT4-C-RAF interaction can be extended to apoptosis. Interestingly, C-RAF plays an inhibitory role in mitochondrial apoptosis by promoting BCL-2 and inhibiting BAD (Bajia et al, 2022; Riaud et al, 2024). The latter is characterized by C-RAF–mediated phosphorylation and consequent inactivation of the PKCθ-BAD complex in the control of anti-apoptosis responses (Hindley & Kolch, 2007). In this line, binding of RKIP to C-RAF inhibits its translocation to mitochondria and phosphorylation of BAD, thereby triggering apoptosis as shown in the case of HBx-mediated hepatocarcinogenesis (Kim et al, 2011).

Our study has several limitations. Obtaining structural insights into the effects of the C-RAF$_{CRD}$ mutants in a liquid environment and dynamic system would enhance our understanding of the atomic changes in a more comprehensive manner. However, because of the unavailability of a complete structure of C-RAF (in contrast to B-RAF), we were only able to examine the interactions between SIRT4 and RBD-CRD, and could not address the autoinhibited versus closed conformation of the entire C-RAF protein. Furthermore, targeted inhibition of the SIRT4-C-RAF$_{CRD}$ interaction is required to functionally demonstrate the inhibitory role of SIRT4 overexpression on C-RAF–regulated pathways. This should include both C-RAF kinase–dependent and C-RAF kinase–independent functions, given that C-RAF deficiency causes embryonic lethality in mice (Wojnowski et al, 1998; Huser et al, 2001; Mikula et al, 2001), whereas kinase-deficient C-RAF knock-in mice are viable (Riaud et al, 2024). Therefore, further in-depth characterization of the interaction between SIRT4 and C-RAF$_{CRD}$ at the molecular and cellular/functional levels is required.

Materials and Methods

Plasmid constructs

The N-terminal RBD-CRD, RBD, and CRD of RAF kinases were cloned into the pGEX-4T1 vector (BioCat GmbH). Upon transformation into *E. coli*, lysates containing GST-tagged proteins were prepared as previously described (Hemsath & Ahmadian, 2005). The SIRT4 deletion mutants SIRT4(Δ69–98) (Δ1), SIRT4(Δ165–229) (Δ2), and SIRT4(Δ255–314) (Δ3) were generated by PCR-mediated mutagenesis and cloned into pcDNA-3.1 for eukaryotic expression as C-terminal eGFP fusion proteins. The expression construct for N-terminally Flag-tagged C-RAF was kindly provided by Dr. Motta (Genetics and Rare Diseases Research Division, Rome).

Cell culture and generation of stable cell lines

HEK293 cells were maintained in DMEM serum (Thermo Fisher Scientific) supplemented with 10% FBS (Gibco) and 1% penicillin–streptomycin (Genaxxon). HEK293 cell lines stably expressing eGFP or C-terminally tagged SIRT4-eGFP or SIRT4(ΔN28)-eGFP have been previously described (Lang et al, 2017). In addition, HEK293 cell lines expressing Flag M2 as control or C-terminally Flag M2–tagged SIRT3, SIRT4, or SIRT5 proteins have been described (Bergmann et al, 2020). HEK293 cell lines stably expressing SIRT4(Δ69–98)-eGFP (Δ1), SIRT4(Δ165–229)-eGFP (Δ2), or SIRT4(Δ255–314)-eGFP (Δ3) were generated by transfection using the TurboFect reagent (Thermo Fisher Scientific). Stable HEK293 cell lines were cultured in selection media containing either G418/Geneticin (400 μg/ml; Genaxxon) or puromycin (1.5 μg/ml; Thermo Fisher Scientific). The expression of all SIRT4 constructs was regularly controlled by flow cytometry and/or Western blot analysis.

Preparing total cell lysates for immunoblot analysis

Cells were lysed on ice for 5 min employing a buffer containing 50 mM Tris–HCl (pH 7.4), 100 mM NaCl, 2 mM $MgCl_2$, 10% glycerol, 20 mM ß-glycerophosphate, 1 mM Na_3VO_4, 1% IGEPAL (Thermo Fisher Scientific), and 1x protease inhibitor cocktail (Roche). Lysates were cleared by centrifugation (20.000*g* at 4°C for 5 min). Protein concentrations were determined using the Bradford assay.

Antibodies for immunoblot analysis

Primary antibodies used in Western blot analysis include anti-GST (own antibody); anti-GFP (1:1,000; #PA1-980; Thermo Fisher

Scientific); anti-Flag (1:1,000; #F742 and #F3165; both from Merck); anti-C-RAF-N-terminal (1:1,000; #ab181115; Abcam); anti-C-RAF-pS259 (1:1,000; #ab173539; Abcam), anti-C-RAF-pY340/341 (1:1,000; #sc-16806; Santa Cruz Biotechnology); anti-vinculin (1:1,000; #V9131; Merck); anti-SIRT4 (1:1,000; #69786; Cell Signaling); anti-ERK(1/2) (1:1,000; #9102; Cell Signaling); anti-p-ERK(1/2) (1:1,000; #4370; Cell Signaling); and anti-KRAS (1:1,000; 11H35L14; Thermo Fisher Scientific). Secondary antibodies employed were from LI-COR (anti-mouse 700 nm: IRDye #926-32213; anti-rabbit 800 nm: IRDye #926-6807).

Protein purification

The CRD of C-RAF, fused with GST, was cloned individually for each single-point mutation (A142V, L147F, K148T, I154F, Q156R, L160F, N161Q, E174Q, W187Y) and for distinct mutants within Set1 (E174Q, H175R, T178S, K179E, T182L), Set2 (Q156R, F158L, L160F), and Set3 (L147F, K148T, N161Q), using the pGEX-4T1 vector (BioCat GmbH). Fusion proteins were expressed in *E. coli* and subsequently purified using Glutathione High-Capacity Magnetic Agarose Beads (Merck Millipore GmbH) following the manufacturer's guidelines.

Pull-down assay using GST-fused proteins

Pull-down experiments using GST-fused proteins were performed using glutathione–agarose beads (Macherey-Nagel). The beads were incubated with the GST-fused proteins for 1 h, at 4°C under rotation and centrifuged at 500*g* followed by three times of washing with ice-cold buffer (30 mM Tris–HCl, 150 mM NaCl, 5 mM $MgCl_2$, and 3 mM DTT). In the next step, samples were incubated with total cell lysates from HEK293 cells stably expressing the indicated Flag-tagged sirtuins or SIRT4-eGFP wild-type and mutants overnight at 4°C followed by three washing steps with ice-cold buffer as indicated above. The protein samples were mixed with Laemmli loading buffer and analyzed by SDS–PAGE and immunoblotting.

Co-immunoprecipitation analysis

Total cell lysates of HEK293 cells stably expressing C-terminally Flag M2–tagged SIRT4 were incubated overnight at 4°C with anti-Flag M2 agarose beads (Merck). The beads were washed three times with washing buffer (50 mM Tris–HCl, 150 mM NaCl, and 1 mM EDTA). The beads were mixed with Laemmli loading buffer, and co-immunoprecipitation of SIRT4-Flag and endogenous C-RAF proteins was analyzed by SDS–PAGE and immunoblotting. Co-immunoprecipitation of SIRT4-eGFP and endogenous C-RAF using the anti-eGFP nanobody protocol was performed essentially as previously described (Bergmann et al, 2020).

Densitometric analysis of specific immunoblot protein signals followed by statistical evaluation

Intensities of specific protein bands were determined using Image Studio Lite version 5.2 software. Pull-down data were normalized to the respective total cell lysate signals to ensure an accurate comparison of target protein levels across various samples as previously described (Hsu et al, 2012). Data are presented as the mean ± S.D., and one-way ANOVA statistical evaluation was performed using Origin data analysis software (OriginLab 2021b). Results with at least $P \leq 0.05$ were considered significant (* $P \leq 0.05$; ** $P \leq 0.01$; and *** $P \leq 0.001$).

Structural analysis

We created a structural homology model of human SIRT4 based on the X-ray diffraction structure of SIRT4 from *X. tropicalis* (PDB: 5OJ7) and compared it with human SIRT5 (PDB: 4G1C) for mutational analysis using PyMOL (version 4.6.0). Moreover, because of the absence of a complete structure of inactive C-RAF, we employed a comparative approach by superimposing the structures of inactive B-RAF (full-length; PDB: 6NYB) to gain insights into the potential structure of inactive C-RAF (Park et al, 2019) in complex with 14-3-3. The three-dimensional structure of the resulting inactive state of C-RAF was analyzed and visualized using PyMOL (version 4.6.0).

Molecular docking simulations

The crystal structures of the $C\text{-}RAF_{CRD}$ (PDB: 1FAQ) and $KRAS\text{-}C\text{-}RAF_{RBD\text{-}CRD}$ complex (PDB: 6XHB) were obtained from the Protein Data Bank (PDB), and the human full-length SIRT4(AF-Q9Y6E7) structure was obtained from the AlphaFold database (https://alphafold.ebi.ac.uk/). Molecular docking simulations were performed using default mode settings available in the molecular docking ClusPro 2.0 server (Kozakov et al, 2017). From the refined selection of proposed structures, a configuration exhibiting optimal binding energies was chosen, aligning it with experimental data. After the docking simulations, the resulting structures were meticulously examined to identify significant molecular interactions using BIOVIA software.

Supplementary Information

Supplementary Information is available at https://doi.org/10.26508/lsa.202302507

Acknowledgements

We are grateful to our colleagues from the Institute of Biochemistry and Molecular Biology II for their support, helpful advice, and fruitful discussions. We thank Dr. Motta (Genetics and Rare Diseases Research Division, Rome) for providing the Flag-C-RAF expression vector. This study was supported by the German Research Foundation (DFG; grant AH 92/8-3 to MR Ahmadian), by the European Network on Noonan Syndrome and Related Disorders (NSEuroNet; grant 01GM1602B to MR Ahmadian), and in part by the Foundation for Ageing Research of the Heinrich Heine University (grants 701.810.783 to RP Piekorz, and 701.810.845 to MR Ahmadian).

Author Contributions

M Mehrabipour: conceptualization, data curation, software, formal analysis, validation, investigation, visualization, methodology, and writing—original draft, review, and editing.

S Nakhaei-Rad: software, formal analysis, investigation, methodology, and writing—review and editing.
R Dvorsky: software, formal analysis, investigation, methodology, and writing—review and editing.
A Lang: resources, investigation, methodology, and writing—review and editing.
P Verhülsdonk: formal analysis, investigation, and methodology.
MR Ahmadian: conceptualization, resources, data curation, formal analysis, supervision, funding acquisition, validation, investigation, visualization, methodology, project administration, and writing—original draft, review, and editing.
RP Piekorz: conceptualization, resources, data curation, formal analysis, supervision, funding acquisition, validation, investigation, visualization, methodology, project administration, and writing—original draft, review, and editing.

Conflict of Interest Statement

The authors declare that they have no conflict of interest.

References

Advani SJ, Camargo MF, Seguin L, Mielgo A, Anand S, Hicks AM, Aguilera J, Franovic A, Weis SM, Cheresh DA (2015) Kinase-independent role for craf-driving tumour radioresistance via chk2. *Nat Commun* 6: 8154. doi:10.1038/ncomms9154

Alavi AS, Acevedo L, Min W, Cheresh DA (2007) Chemoresistance of endothelial cells induced by basic fibroblast growth factor depends on raf-1-mediated inhibition of the proapoptotic kinase, ask1. *Cancer Res* 67: 2766–2772. doi:10.1158/0008-5472.CAN-06-3648

Bai Y, Yang J, Cui Y, Yao Y, Wu F, Liu C, Fan X, Zhang Y (2020) Research progress of sirtuin4 in cancer. *Front Oncol* 10: 562950. doi:10.3389/fonc.2020.562950

Bajia D, Bottani E, Derwich K (2022) Effects of noonan syndrome-germline mutations on mitochondria and energy metabolism. *Cells* 11: 3099. doi:10.3390/cells11193099

Bergmann L, Lang A, Bross C, Altinoluk-Hambuchen S, Fey I, Overbeck N, Stefanski A, Wiek C, Kefalas A, Verhulsdonk P, et al (2020) Subcellular localization and mitotic interactome analyses identify sirt4 as a centrosomally localized and microtubule associated protein. *Cells* 9: 1950. doi:10.3390/cells9091950

Betsinger CN, Cristea IM (2019) Mitochondrial function, metabolic regulation, and human disease viewed through the prism of sirtuin 4 (sirt4) functions. *J Proteome Res* 18: 1929–1938. doi:10.1021/acs.jproteome.9b00086

Blasco RB, Francoz S, Santamaría D, Cañamero M, Dubus P, Charron J, Baccarini M, Barbacid M (2011) C-raf, but not b-raf, is essential for development of k-ras oncogene-driven non-small cell lung carcinoma. *Cancer Cell* 19: 652–663. doi:10.1016/j.ccr.2011.04.002

Boned Del Rio I, Young LC, Sari S, Jones GG, Ringham-Terry B, Hartig N, Rejnowicz E, Lei W, Bhamra A, Surinova S, et al (2019) Shoc2 complex-driven raf dimerization selectively contributes to erk pathway dynamics. *Proc Natl Acad Sci U S A* 116: 13330–13339. doi:10.1073/pnas.1902658116

Cessna H, Baritaki S, Zaravinos A, Bonavida B (2022) The role of rkip in the regulation of emt in the tumor microenvironment. *Cancers (Basel)* 14: 4596. doi:10.3390/cancers14194596

Chen Z, Lin J, Feng S, Chen X, Huang H, Wang C, Yu Y, He Y, Han S, Zheng L, et al (2019) Sirt4 inhibits the proliferation, migration, and invasion abilities of thyroid cancer cells by inhibiting glutamine metabolism. *Onco Targets Ther* 12: 2397–2408. doi:10.2147/OTT.S189536

Chong H, Lee J, Guan KL (2001) Positive and negative regulation of raf kinase activity and function by phosphorylation. *EMBO J* 20: 3716–3727. doi:10.1093/emboj/20.14.3716

Cseh B, Doma E, Baccarini M (2014) "Raf" neighborhood: Protein-protein interaction in the raf/mek/erk pathway. *FEBS Lett* 588: 2398–2406. doi:10.1016/j.febslet.2014.06.025

Dai X, Zhang X, Yin Q, Hu J, Guo J, Gao Y, Snell AH, Inuzuka H, Wan L, Wei W (2022) Acetylation-dependent regulation of braf oncogenic function. *Cell Rep* 38: 110250. doi:10.1016/j.celrep.2021.110250

Dar AC, Brady DC (2022) Rasopathy mutations open new insights into the mechanism of braf activation. *Mol Cell* 82: 4192–4193. doi:10.1016/j.molcel.2022.10.034

Degirmenci U, Wang M, Hu J (2020) Targeting aberrant ras/raf/mek/erk signaling for cancer therapy. *Cells* 9: 198. doi:10.3390/cells9010198

Desideri E, Cavallo AL, Baccarini M (2015) Alike but different: Raf paralogs and their signaling outputs. *Cell* 161: 967–970. doi:10.1016/j.cell.2015.04.045

Dhandapany PS, Razzaque MA, Muthusami U, Kunnoth S, Edwards JJ, Mulero-Navarro S, Riess I, Pardo S, Sheng J, Rani DS, et al (2014) Raf1 mutations in childhood-onset dilated cardiomyopathy. *Nat Genet* 46: 635–639. doi:10.1038/ng.2963

Dhillon AS, Meikle S, Yazici Z, Eulitz M, Kolch W (2002) Regulation of raf-1 activation and signalling by dephosphorylation. *EMBO J* 21: 64–71. doi:10.1093/emboj/21.1.64

Diaz B, Barnard D, Filson A, MacDonald S, King A, Marshall M (1997) Phosphorylation of raf-1 serine 338-serine 339 is an essential regulatory event for ras-dependent activation and biological signaling. *Mol Cell Biol* 17: 4509–4516. doi:10.1128/mcb.17.8.4509

Du J, Cai SH, Shi Z, Nagase F (2004) Binding activity of h-ras is necessary for in vivo inhibition of ask1 activity. *Cell Res* 14: 148–154. doi:10.1038/sj.cr.7290214

Dumaz N, Marais R (2003) Protein kinase a blocks raf-1 activity by stimulating 14-3-3 binding and blocking raf-1 interaction with ras. *J Biol Chem* 278: 29819–29823. doi:10.1074/jbc.C300182200

Ehmer U, Sage J (2016) Control of proliferation and cancer growth by the hippo signaling pathway. *Mol Cancer Res* 14: 127–140. doi:10.1158/1541-7786.MCR-15-0305

Ehrenreiter K, Piazzolla D, Velamoor V, Sobczak I, Small JV, Takeda J, Leung T, Baccarini M (2005) Raf-1 regulates rho signaling and cell migration. *J Cell Biol* 168: 955–964. doi:10.1083/jcb.200409162

Emerson SD, Madison VS, Palermo RE, Waugh DS, Scheffler JE, Tsao KL, Kiefer SE, Liu SP, Fry DC (1995) Solution structure of the ras-binding domain of c-raf-1 and identification of its ras interaction surface. *Biochemistry* 34: 6911–6918. doi:10.1021/bi00021a001

Eves EM, Shapiro P, Naik K, Klein UR, Trakul N, Rosner MR (2006) Raf kinase inhibitory protein regulates aurora b kinase and the spindle checkpoint. *Mol Cell* 23: 561–574. doi:10.1016/j.molcel.2006.07.015

Fang Z, Lee KY, Huo KG, Gasmi-Seabrook G, Zheng L, Moghal N, Tsao MS, Ikura M, Marshall CB (2020) Multivalent assembly of kras with the ras-binding and cysteine-rich domains of craf on the membrane. *Proc Natl Acad Sci U S A* 117: 12101–12108. doi:10.1073/pnas.1914076117

Feng L, Xie X, Ding Q, Luo X, He J, Fan F, Liu W, Wang Z, Chen Y (2007) Spatial regulation of raf kinase signaling by rktg. *Proc Natl Acad Sci U S A* 104: 14348–14353. doi:10.1073/pnas.0701298104

Fu L, Dong Q, He J, Wang X, Xing J, Wang E, Qiu X, Li Q (2017) Sirt4 inhibits malignancy progression of nsclcs, through mitochondrial dynamics mediated by the erk-drp1 pathway. *Oncogene* 36: 2724–2736. doi:10.1038/onc.2016.425

Garnett MJ, Rana S, Paterson H, Barford D, Marais R (2005) Wild-type and mutant b-raf activate c-raf through distinct mechanisms involving

heterodimerization. *Mol Cell* 20: 963–969. doi:10.1016/j.molcel.2005.10.022

Gelb BD, Roberts AE, Tartaglia M (2015) Cardiomyopathies in noonan syndrome and the other rasopathies. *Prog Pediatr Cardiol* 39: 13–19. doi:10.1016/j.ppedcard.2015.01.002

Guo YJ, Pan WW, Liu SB, Shen ZF, Xu Y, Hu LL (2020) Erk/mapk signalling pathway and tumorigenesis. *Exp Ther Med* 19: 1997–2007. doi:10.3892/etm.2020.8454

Haigis MC, Mostoslavsky R, Haigis KM, Fahie K, Christodoulou DC, Murphy AJ, Valenzuela DM, Yancopoulos GD, Karow M, Blander G, et al (2006) Sirt4 inhibits glutamate dehydrogenase and opposes the effects of calorie restriction in pancreatic beta cells. *Cell* 126: 941–954. doi:10.1016/j.cell.2006.06.057

Hampel N, Georgy J, Mehrabipour M, Lang A, Lehmkuhl I, Scheller J, Ahmadian MR, Floss DM, Piekorz RP (2023) $Cocl_2$-triggered pseudohypoxic stress induces proteasomal degradation of sirt4 *via* polyubiquitination of lysines k78 and k299. *FEBS Open Bio* 13: 2187–2199. doi:10.1002/2211-5463.13715

Harding A, Hsu V, Kornfeld K, Hancock JF (2003) Identification of residues and domains of raf important for function in vivo and in vitro. *J Biol Chem* 278: 45519–45527. doi:10.1074/jbc.M303106200

Hemsath L, Ahmadian MR (2005) Fluorescence approaches for monitoring interactions of rho gtpases with nucleotides, regulators, and effectors. *Methods* 37: 173–182. doi:10.1016/j.ymeth.2005.05.014

Hindley A, Kolch W (2007) Raf-1 and b-raf promote protein kinase c theta interaction with bad. *Cell Signal* 19: 547–555. doi:10.1016/j.cellsig.2006.08.004

Hsu P-H, Miaw S-C, Chuang C-C, Chang P-Y, Fu S-J, Jow G-M, Chiu M-M, Jeng C-J (2012) 14-3-3θ is a binding partner of rat eag1 potassium channels. *PLoS One* 7: e41203. doi:10.1371/journal.pone.0041203

Hu Y, Lin J, Lin Y, Chen X, Zhu G, Huang G (2019) Overexpression of sirt4 inhibits the proliferation of gastric cancer cells through cell cycle arrest. *Oncol Lett* 17: 2171–2176. doi:10.3892/ol.2018.9877

Huang H, Ouyang Q, Mei K, Liu T, Sun Q, Liu W, Liu R (2023) Acetylation of scfd1 regulates snare complex formation and autophagosome-lysosome fusion. *Autophagy* 19: 189–203. doi:10.1080/15548627.2022.2064624

Huser M, Luckett J, Chiloeches A, Mercer K, Iwobi M, Giblett S, Sun XM, Brown J, Marais R, Pritchard C (2001) Mek kinase activity is not necessary for raf-1 function. *EMBO J* 20: 1940–1951. doi:10.1093/emboj/20.8.1940

Jaffre F, Miller CL, Schanzer A, Evans T, Roberts AE, Hahn A, Kontaridis MI (2019) Inducible pluripotent stem cell-derived cardiomyocytes reveal aberrant extracellular regulated kinase 5 and mitogen-activated protein kinase kinase 1/2 signaling concomitantly promote hypertrophic cardiomyopathy in raf1-associated noonan syndrome. *Circulation* 140: 207–224. doi:10.1161/CIRCULATIONAHA.118.037227

Jang H, Zhang M, Nussinov R (2020) The quaternary assembly of kras4b with raf-1 at the membrane. *Comput Struct Biotechnol J* 18: 737–748. doi:10.1016/j.csbj.2020.03.018

Jaumot M, Hancock JF (2001) Protein phosphatases 1 and 2a promote raf-1 activation by regulating 14-3-3 interactions. *Oncogene* 20: 3949–3958. doi:10.1038/sj.onc.1204526

Jeong SM, Xiao C, Finley LW, Lahusen T, Souza AL, Pierce K, Li YH, Wang X, Laurent G, German NJ, et al (2013) Sirt4 has tumor-suppressive activity and regulates the cellular metabolic response to DNA damage by inhibiting mitochondrial glutamine metabolism. *Cancer Cell* 23: 450–463. doi:10.1016/j.ccr.2013.02.024

Ji Z, Liu GH, Qu J (2022) Mitochondrial sirtuins, metabolism, and aging. *J Genet Genomics* 49: 287–298. doi:10.1016/j.jgg.2021.11.005

Joukov V, De Nicolo A (2018) Aurora-plk1 cascades as key signaling modules in the regulation of mitosis. *Sci Signal* 11: eaar4195. doi:10.1126/scisignal.aar4195

Karreth FA, Frese KK, DeNicola GM, Baccarini M, Tuveson DA (2011) C-Raf is required for the initiation of lung cancer by K-Ras(G12D). *Cancer Discov* 1: 128–136. doi:10.1158/2159-8290.CD-10-0044

Kim SY, Park SG, Jung H, Chi SW, Yu DY, Lee SC, Bae KH (2011) Rkip downregulation induces the hbx-mediated raf-1 mitochondrial translocation. *J Microbiol Biotechnol* 21: 525–528. doi:10.4014/jmb.1012.12023

Kozakov D, Hall DR, Xia B, Porter KA, Padhorny D, Yueh C, Beglov D, Vajda S (2017) The cluspro web server for protein-protein docking. *Nat Protoc* 12: 255–278. doi:10.1038/nprot.2016.169

Kwon JJ, Hajian B, Bian Y, Young LC, Amor AJ, Fuller JR, Fraley CV, Sykes AM, So J, Pan J, et al (2022) Structure-function analysis of the shoc2-mras-pp1c holophosphatase complex. *Nature* 609: 408–415. doi:10.1038/s41586-022-04928-2

Lang A, Anand R, Altinoluk-Hambuchen S, Ezzahoini H, Stefanski A, Iram A, Bergmann L, Urbach J, Bohler P, Hansel J, et al (2017) Sirt4 interacts with opa1 and regulates mitochondrial quality control and mitophagy. *Aging (Albany NY)* 9: 2163–2189. doi:10.18632/aging.101307

Lavoie H, Therrien M (2015) Regulation of raf protein kinases in erk signalling. *Nat Rev Mol Cell Biol* 16: 281–298. doi:10.1038/nrm3979

Li S, Jang H, Zhang J, Nussinov R (2018) Raf-1 cysteine-rich domain increases the affinity of k-ras/raf at the membrane, promoting mapk signaling. *Structure* 26: 513–525.e2. doi:10.1016/j.str.2018.01.011

Li J, Zhan H, Ren Y, Feng M, Wang Q, Jiao Q, Wang Y, Liu X, Zhang S, Du L, et al (2023) Sirtuin 4 activates autophagy and inhibits tumorigenesis by upregulating the p53 signaling pathway. *Cell Death Differ* 30: 313–326. doi:10.1038/s41418-022-01063-3

Matallanas D, Birtwistle M, Romano D, Zebisch A, Rauch J, von Kriegsheim A, Kolch W (2011) Raf family kinases: Old dogs have learned new tricks. *Genes Cancer* 2: 232–260. doi:10.1177/1947601911407323

Mathias RA, Greco TM, Oberstein A, Budayeva HG, Chakrabarti R, Rowland EA, Kang Y, Shenk T, Cristea IM (2014) Sirtuin 4 is a lipoamidase regulating pyruvate dehydrogenase complex activity. *Cell* 159: 1615–1625. doi:10.1016/j.cell.2014.11.046

Matsunaga-Udagawa R, Fujita Y, Yoshiki S, Terai K, Kamioka Y, Kiyokawa E, Yugi K, Aoki K, Matsuda M (2010) The scaffold protein shoc2/sur-8 accelerates the interaction of ras and raf. *J Biol Chem* 285: 7818–7826. doi:10.1074/jbc.M109.053975

Matsuzawa A, Nishitoh H, Tobiume K, Takeda K, Ichijo H (2002) Physiological roles of ask1-mediated signal transduction in oxidative stress- and endoplasmic reticulum stress-induced apoptosis: Advanced findings from ask1 knockout mice. *Antioxid Redox Signal* 4: 415–425. doi:10.1089/15230860260196218

Mielgo A, Seguin L, Huang M, Camargo MF, Anand S, Franovic A, Weis SM, Advani SJ, Murphy EA, Cheresh DA (2011) A mek-independent role for craf in mitosis and tumor progression. *Nat Med* 17: 1641–1645. doi:10.1038/nm.2464

Mikula M, Schreiber M, Husak Z, Kucerova L, Ruth J, Wieser R, Zatloukal K, Beug H, Wagner EF, Baccarini M (2001) Embryonic lethality and fetal liver apoptosis in mice lacking the c-raf-1 gene. *EMBO J* 20: 1952–1962. doi:10.1093/emboj/20.8.1952

Moghaddam M, Vivarelli S, Falzone L, Libra M, Bonavida B (2023) Cancer resistance via the downregulation of the tumor suppressors rkip and pten expressions: Therapeutic implications. *Explor Target Antitumor Ther* 4: 170–207. doi:10.37349/etat.2023.00128

Nakhaei-Rad S, Haghighi F, Bazgir F, Dahlmann J, Busley AV, Buchholzer M, Kleemann K, Schanzer A, Borchardt A, Hahn A, et al (2023a) Molecular and cellular evidence for the impact of a hypertrophic cardiomyopathy-associated raf1 variant on the structure and function of contractile machinery in bioartificial cardiac tissues. *Commun Biol* 6: 657. doi:10.1038/s42003-023-05013-8

Nakhaei-Rad S, Janatifard F, Dvorsky R, Ahmadian MR, Housaindokht MR (2023b) Molecular analyses of the c-terminal craf variants associated

with cardiomyopathy reveal their opposing impacts on the active conformation of the kinase domain. *J Biomol Struct Dyn* 41: 15328–15338. doi:10.1080/07391102.2023.2187221

Nguyen K, López CA, Neale C, Van QN, Carpenter TS, Di Natale F, Travers T, Tran TH, Chan AH, Bhatia H, et al (2022) Exploring crd mobility during ras/raf engagement at the membrane. *Biophys J* 121: 3630–3650. doi:10.1016/j.bpj.2022.06.035

Noh HS, Hah YS, Zada S, Ha JH, Sim G, Hwang JS, Lai TH, Nguyen HQ, Park JY, Kim HJ, et al (2016) Pebp1, a raf kinase inhibitory protein, negatively regulates starvation-induced autophagy by direct interaction with lc3. *Autophagy* 12: 2183–2196. doi:10.1080/15548627.2016.1219013

Nolan AA, Aboud NK, Kolch W, Matallanas D (2021) Hidden targets in raf signalling pathways to block oncogenic ras signalling. *Genes (Basel)* 12: 553. doi:10.3390/genes12040553

Nussinov R, Jang H, Zhang M, Tsai CJ, Sablina AA (2020) The mystery of rap1 suppression of oncogenic ras. *Trends Cancer* 6: 369–379. doi:10.1016/j.trecan.2020.02.002

Okamoto K, Sako Y (2023) Two closed conformations of craf require the 14-3-3 binding motifs and cysteine-rich domain to be intact in live cells. *J Mol Biol* 435: 167989. doi:10.1016/j.jmb.2023.167989

Pannek M, Simic Z, Fuszard M, Meleshin M, Rotili D, Mai A, Schutkowski M, Steegborn C (2017) Crystal structures of the mitochondrial deacylase sirtuin 4 reveal isoform-specific acyl recognition and regulation features. *Nat Commun* 8: 1513. doi:10.1038/s41467-017-01701-2

Park S, Rath O, Beach S, Xiang X, Kelly SM, Luo Z, Kolch W, Yeung KC (2006) Regulation of rkip binding to the n-region of the raf-1 kinase. *FEBS Lett* 580: 6405–6412. doi:10.1016/j.febslet.2006.10.054

Park E, Rawson S, Li K, Kim BW, Ficarro SB, Pino GG, Sharif H, Marto JA, Jeon H, Eck MJ (2019) Architecture of autoinhibited and active braf-mek1-14-3-3 complexes. *Nature* 575: 545–550. doi:10.1038/s41586-019-1660-y

Rath O, Park S, Tang HH, Banfield MJ, Brady RL, Lee YC, Dignam JD, Sedivy JM, Kolch W, Yeung KC (2008) The rkip (raf-1 kinase inhibitor protein) conserved pocket binds to the phosphorylated n-region of raf-1 and inhibits the raf-1-mediated activated phosphorylation of mek. *Cell Signal* 20: 935–941. doi:10.1016/j.cellsig.2008.01.012

Rezaei Adariani S, Buchholzer M, Akbarzadeh M, Nakhaei-Rad S, Dvorsky R, Ahmadian MR (2018) Structural snapshots of raf kinase interactions. *Biochem Soc Trans* 46: 1393–1406. doi:10.1042/bst20170528

Riaud M, Maxwell J, Soria-Bretones I, Dankner M, Li M, Rose AAN (2024) The role of craf in cancer progression: From molecular mechanisms to precision therapies. *Nat Rev Cancer* 24: 105–122. doi:10.1038/s41568-023-00650-x

Romano D, Nguyen LK, Matallanas D, Halasz M, Doherty C, Kholodenko BN, Kolch W (2014) Protein interaction switches coordinate raf-1 and mst2/hippo signalling. *Nat Cell Biol* 16: 673–684. doi:10.1038/ncb2986

Rommel C, Radziwill G, Lovrić J, Noeldeke J, Heinicke T, Jones D, Aitken A, Moelling K (1996) Activated ras displaces 14-3-3 protein from the amino terminus of c-raf-1. *Oncogene* 12: 609–619.

Takahashi M, Li Y, Dillon TJ, Kariya Y, Stork PJS (2017) Phosphorylation of the c-raf n region promotes raf dimerization. *Mol Cell Biol* 37: e00132-17. doi:10.1128/mcb.00132-17

Terai K, Matsuda M (2005) Ras binding opens c-raf to expose the docking site for mitogen-activated protein kinase kinase. *EMBO Rep* 6: 251–255. doi:10.1038/sj.embor.7400349

Tomaselli D, Steegborn C, Mai A, Rotili D (2020) Sirt4: A multifaceted enzyme at the crossroads of mitochondrial metabolism and cancer. *Front Oncol* 10: 474. doi:10.3389/fonc.2020.00474

Touboul R, Baritaki S, Zaravinos A, Bonavida B (2021) Rkip pleiotropic activities in cancer and inflammatory diseases: Role in immunity. *Cancers (Basel)* 13: 6247. doi:10.3390/cancers13246247

Tran TH, Chan AH, Young LC, Bindu L, Neale C, Messing S, Dharmaiah S, Taylor T, Denson J-P, Esposito D, et al (2021) Kras interaction with raf1 ras-binding domain and cysteine-rich domain provides insights into ras-mediated raf activation. *Nat Commun* 12: 1176. doi:10.1038/s41467-021-21422-x

Ullah R, Yin Q, Snell AH, Wan L (2022) Raf-mek-erk pathway in cancer evolution and treatment. *Semin Cancer Biol* 85: 123–154. doi:10.1016/j.semcancer.2021.05.010

Varga A, Ehrenreiter K, Aschenbrenner B, Kocieniewski P, Kochanczyk M, Lipniacki T, Baccarini M (2017) Raf1/braf dimerization integrates the signal from ras to erk and roka. *Sci Signaling* 10: eaai8482. doi:10.1126/scisignal.aai8482

Wang Y, Bonavida B (2018) A new linkage between the tumor suppressor rkip and autophagy: Targeted therapeutics. *Crit Rev Oncog* 23: 281–305. doi:10.1615/CritRevOncog.2018027211

Wang C, Liu Y, Zhu Y, Kong C (2020) Functions of mammalian sirt4 in cellular metabolism and research progress in human cancer. *Oncol Lett* 20: 11. doi:10.3892/ol.2020.11872

Wang Y, Yue J, Xiao M, Lu X, Chin YE (2022) SIRT4-Catalyzed deacetylation of Axin1 modulates the Wnt/β-Catenin signaling pathway. *Front Oncol* 12: 872444. doi:10.3389/fonc.2022.872444

Wimmer R, Baccarini M (2010) Partner exchange: Protein-protein interactions in the raf pathway. *Trends Biochem Sci* 35: 660–668. doi:10.1016/j.tibs.2010.06.001

Wojnowski L, Stancato LF, Zimmer AM, Hahn H, Beck TW, Larner AC, Rapp UR, Zimmer A (1998) Craf-1 protein kinase is essential for mouse development. *Mech Dev* 76: 141–149. doi:10.1016/s0925-4773(98)00111-7

Yang S, Xu W, Liu C, Jin J, Li X, Jiang Y, Zhang L, Meng X, Zhan J, Zhang H (2022) Lats1 k751 acetylation blocks activation of hippo signalling and switches lats1 from a tumor suppressor to an oncoprotein. *Sci China Life Sci* 65: 129–141. doi:10.1007/s11427-020-1914-3

Yesilkanal AE, Rosner MR (2018) Targeting raf kinase inhibitory protein regulation and function. *Cancers (Basel)* 10: 306. doi:10.3390/cancers10090306

Zannini L, Delia D, Buscemi G (2014) Chk2 kinase in the DNA damage response and beyond. *J Mol Cell Biol* 6: 442–457. doi:10.1093/jmcb/mju045

Zhang W, Liu HT (2002) Mapk signal pathways in the regulation of cell proliferation in mammalian cells. *Cell Res* 12: 9–18. doi:10.1038/sj.cr.7290105

Zhang F, Wang D, Li J, Su Y, Liu S, Lei QY, Yin M (2022) Deacetylation of mthfd2 by sirt4 senses stress signal to inhibit cancer cell growth by remodeling folate metabolism. *J Mol Cell Biol* 14: mjac020. doi:10.1093/jmcb/mjac020

Zimmermann S, Moelling K (1999) Phosphorylation and regulation of raf by akt (protein kinase b). *Science* 286: 1741–1744. doi:10.1126/science.286.5445.1741

Zinatizadeh MR, Miri SR, Zarandi PK, Chalbatani GM, Raposo C, Mirzaei HR, Akbari ME, Mahmoodzadeh H (2021) The hippo tumor suppressor pathway (yap/taz/tead/mst/lats) and egfr-ras-raf-mek in cancer metastasis. *Genes Dis* 8: 48–60. doi:10.1016/j.gendis.2019.11.003

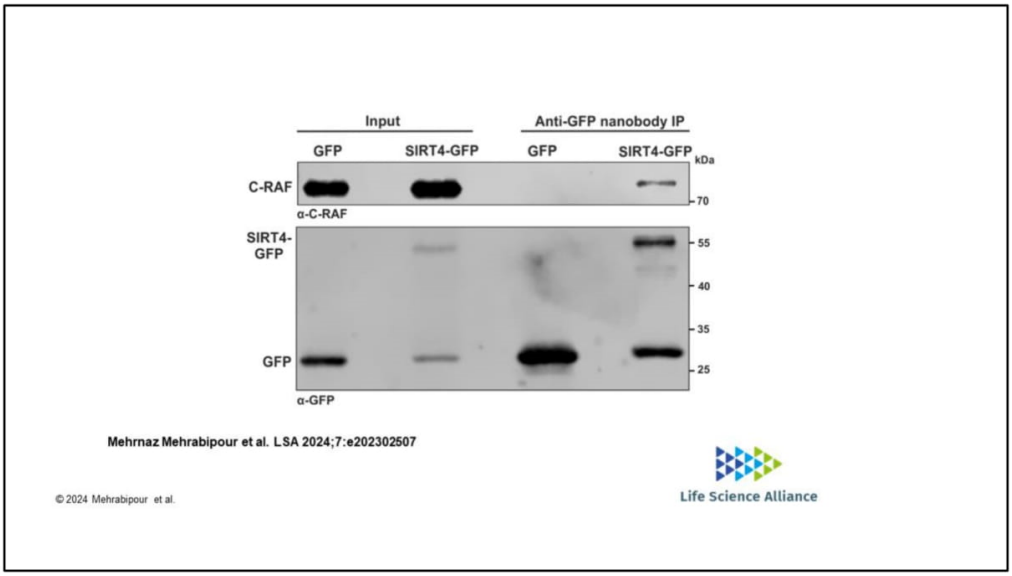

Figure S1.Validation of C-RAF as SIRT4-interacting protein.Total cell lysates of HEK293 cells stably expressing SIRT4-GFP or GFP as control were subjected to co-immunoprecipitation (IP) analysis using the anti-GFP nanobody method followed by immunoblotting for endogenous C-RAF using an Abcam antibody (#ab181115).

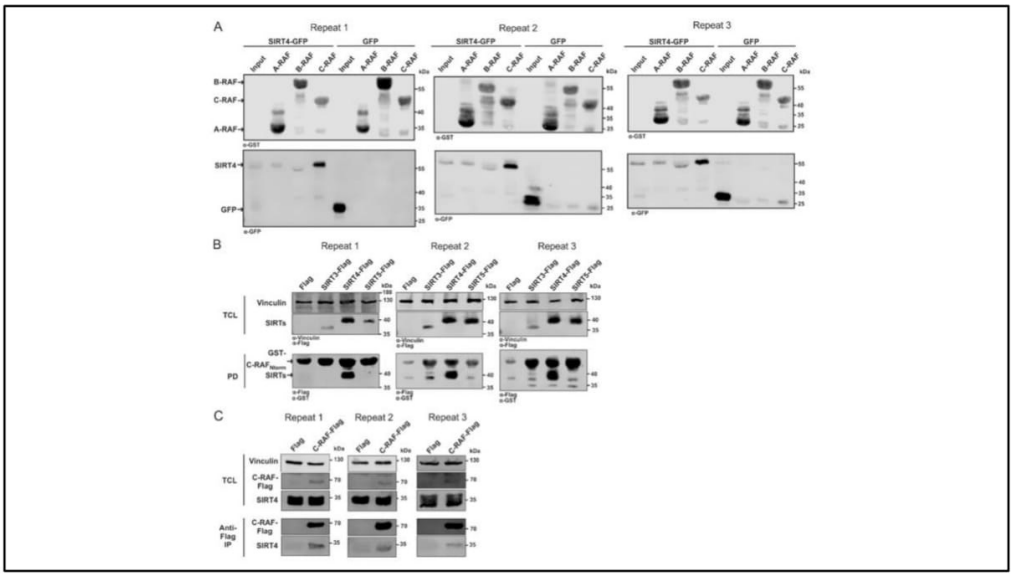

Figure S2.Independent experimental repeats statistically analyzed in Fig 1B–F are depicted.(A) Single experiments related to Fig 1B and C. (B) Single experiments related to Fig 1D and E. (C) Single experiments related to Fig 1F.

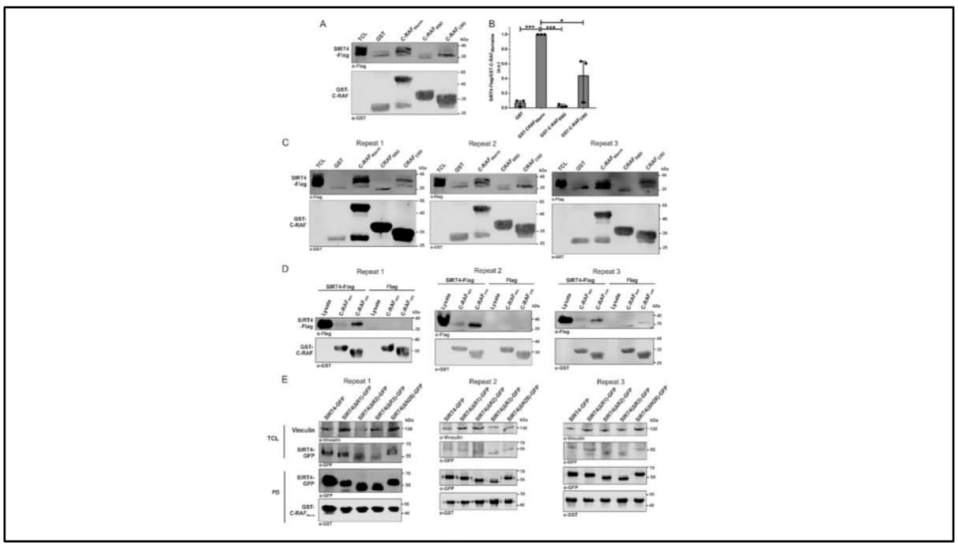

Figure S3.CRD within the N-terminus of C-RAF interacts with SIRT4.(A) Total cell lysates from HEK293 cells stably expressing SIRT4-Flag were subjected to pull-down experiments using GST, GST-C-RAF$_{Nterm}$, GST-C-RAF$_{RBD}$, or GST-C-RAF$_{CRD}$. (B) Densitometric quantification of immunoblot signals of binding of N-RBD-CRD subdomains of C-RAF to SIRT4-Flag. Data were subjected to statistical one-way ANOVA (mean ± S.D.; $*P < 0.05$; $***P < 0.001$). (C) Three independent experimental repeats statistically analyzed in Fig S2A and B are depicted. (D) Three independent experimental repeats analyzed in Fig 2A and B are depicted. (E) Three independent experimental repeats statistically analyzed in Fig 2E and F are depicted.

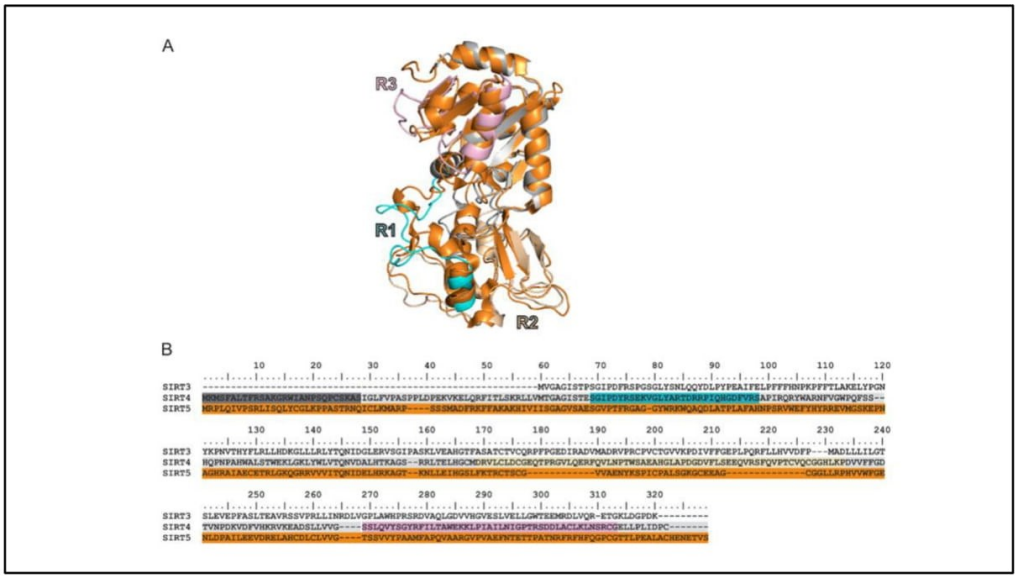

Figure S4.Homology modeling of human SIRT4 and SIRT5 proteins.(A) 3D homology comparison between SIRT5 (orange mesh) and SIRT4 (light gray mesh). (B) SIRT4 regions are highlighted in colors corresponding to (B). (B) Sequence alignment of human SIRT3, SIRT4, and SIRT5. The alignment highlights the initial N-terminal 28 amino acids of SIRT4 in gray. These amino acids are not represented in the structure. In addition, regions R1, R2, and R3 are indicated by cyan, mustard, and pink frames, respectively.

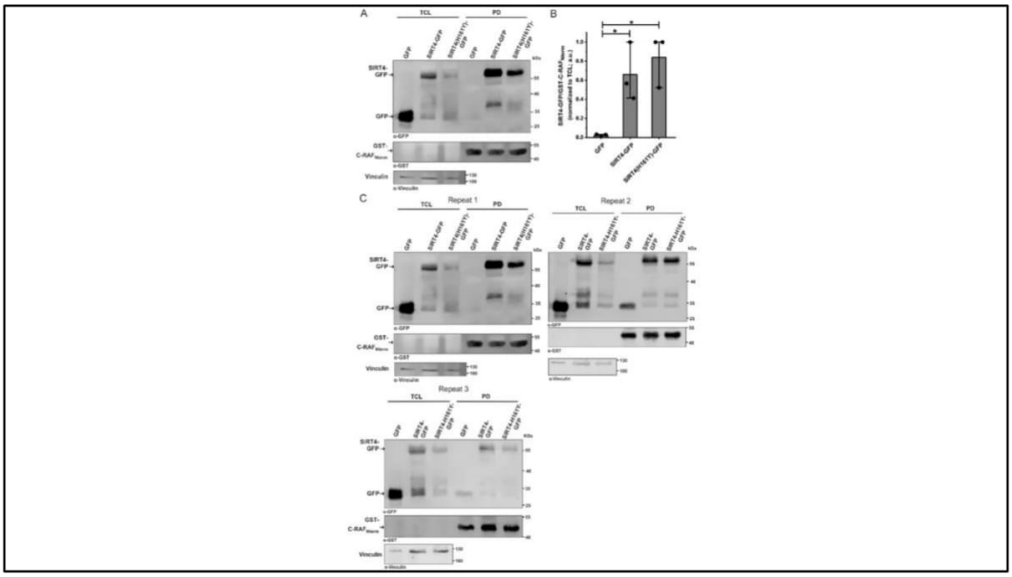

Figure S5.Interaction between SIRT4 and C-RAF is independent of the catalytic activity of SIRT4.(A) Total cell lysates from HEK293 cells expressing GFP, SIRT4-GFP, or the catalytically inactive mutant SIRT4(H161Y)-GFP were subjected to pull-down (PD) experiments using the GST-fused Nterm domain of C-RAF. (B) Densitometric quantification of immunoblot signals of binding of the Nterm domain of C-RAF to GFP, SIRT4-GFP, or SIRT4(H161Y)-GFP. Data were subjected to statistical one-way ANOVA (mean ± S.D.; $*P < 0.05$). (B, C) Three independent experimental repeats statistically analyzed in (B) are depicted.

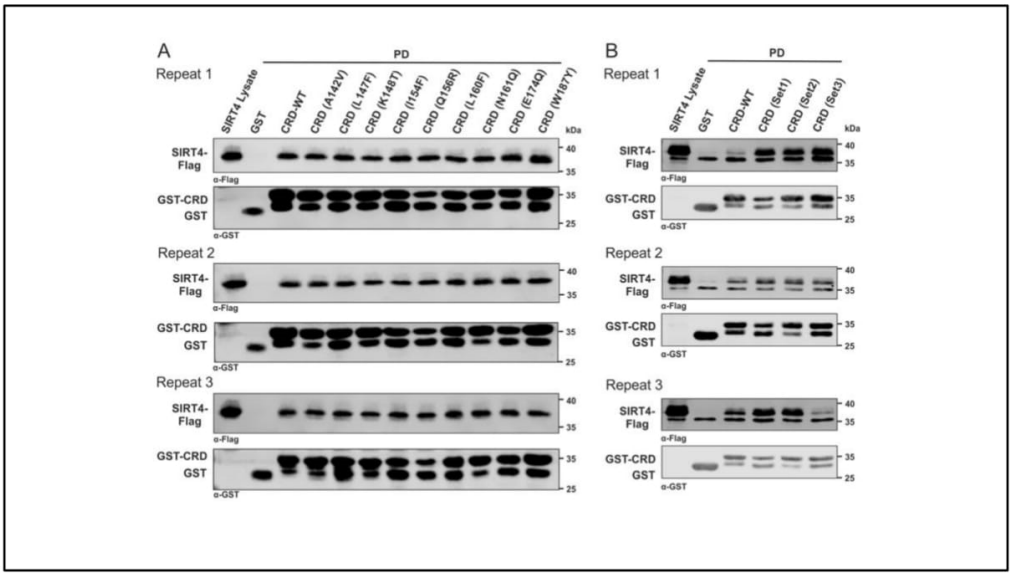

Figure S6.Three independent experimental repeats statistically analyzed in Fig 3 are depicted.(A) Analysis of CRD single-point mutants (Fig 3C and D). (B) Analysis of CRD forms with combined mutations (Fig 3E and F).

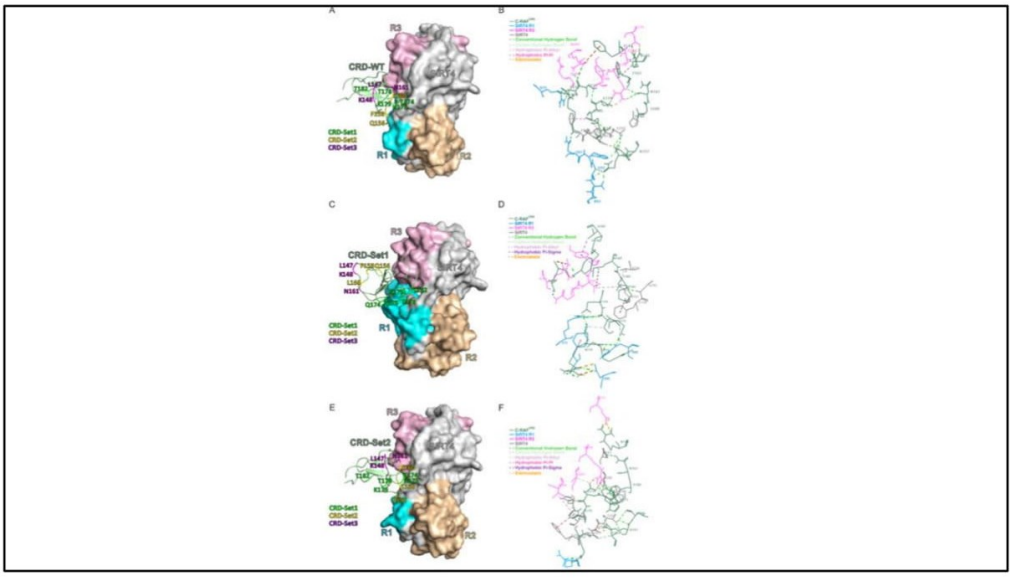

Figure S7.Analysis of WT C-RAF$_{CRD}$ and its gain-of-function (GOF) mutations Set1 and Set2, illustrating their structural influence and the resulting changes in the binding site pattern between C-RAF$_{CRD}$ and SIRT4.(A, B, C, D, E, F) Molecular docking and binding site analyses were performed between SIRT4 and WT C-RAF$_{CRD}$ (A, B), and the mutated forms of C-RAF$_{CRD}$, that is, Set1 (C, D) and Set2 (E, F). R1, R2, and R3 are specific regions of SIRT4 and indicated by color. (B, D, F) Magnified binding interfaces are depicted in (B, D, F). The binding types, that is, conventional hydrogen bonds, carbon–hydrogen interactions, various hydrophobic contacts, and electrostatic interactions, are indicated by colored dashed lines.

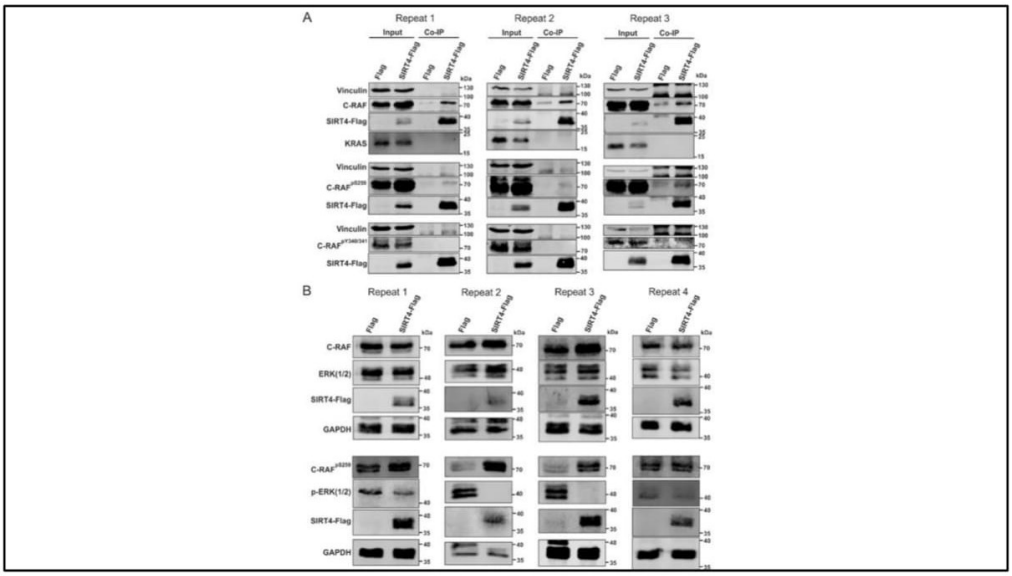

Figure S8.Experimental repeats statistically analyzed in Fig 4 are depicted.(A) Interaction of SIRT4 with the inactive form of C-RAF phosphorylated at serine 259 (S259) (Fig 4A). (B) SIRT4 expression up-regulates protein levels of C-RAF phosphorylated at serine 259 (S259) and down-regulates pERK1/2 levels (Fig 4C).

Chapter V. CoCl2-Triggered Pseudohypoxic Stress Induces Proteasomal Degradation of SIRT4 via Polyubiquitination of Lysines K78 and K299

Authors: Nils Hampel, Jacqueline Georgy, **Mehrnaz Mehrabipour**, Alexander Lang, Isabell Lehmkuhl, Jürgen Scheller, Mohammad R. Ahmadian, Doreen M. Floss, Roland P. Piekorz

DOI: 10.1002/2211-5463.13715

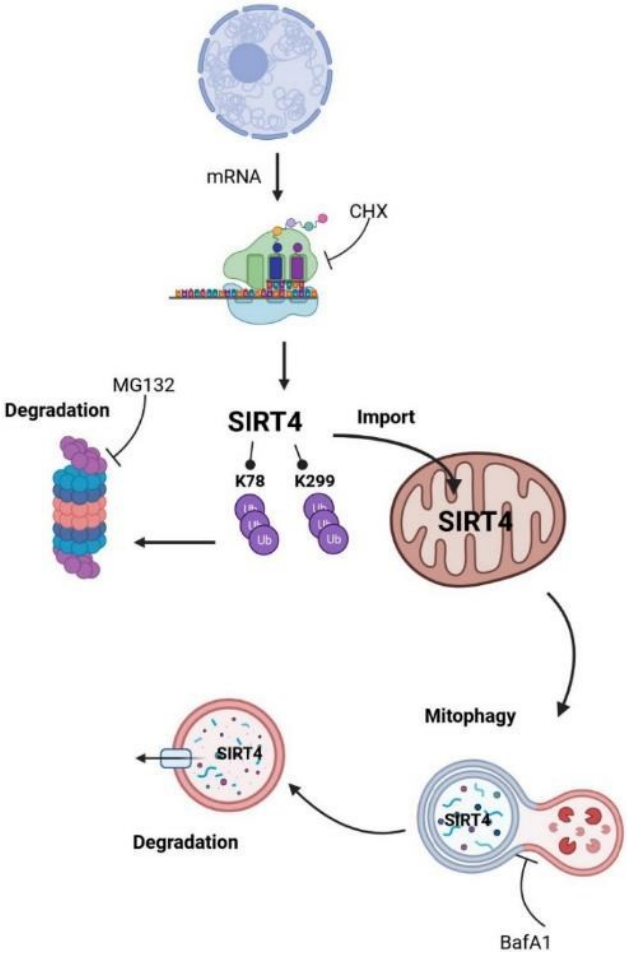

Status:	Published in October 2023
Journal:	FEBS Open bio
JIF:	2.8
Contribution:	20%
	Performed evolutionary analysis using Clustal W alignment to study the conservation of K78 and K299 in the sirtuin protein family and SIRT4 homologs across vertebrates.

FEBS openbio

FEBS PRESS
science publishing by scientists

RESEARCH ARTICLE

$CoCl_2$-triggered pseudohypoxic stress induces proteasomal degradation of SIRT4 via polyubiquitination of lysines K78 and K299

Nils Hampel, Jacqueline Georgy, Mehrnaz Mehrabipour, Alexander Lang*, Isabell Lehmkuhl, Jürgen Scheller, Mohammad R. Ahmadian, Doreen M. Floss and Roland P. Piekorz

Institute of Biochemistry and Molecular Biology II, Medical Faculty, Heinrich Heine University Düsseldorf, Universitätsstrasse 1, Düsseldorf, 40225, Germany

Keywords
autophagy; proteasome; pseudohypoxia; SIRT4; sirtuin; ubiquitination

Correspondence
R. P. Piekorz, Institute of Biochemistry and Molecular Biology II, Medical Faculty, Heinrich Heine University Düsseldorf, Universitätsstrasse 1, Düsseldorf, 40225, Germany
E-mail: roland.piekorz@hhu.de

Present address
*Department of Cardiology, Pulmonology, and Vascular Medicine, Medical Faculty, Heinrich Heine University Düsseldorf, Germany

(Received 17 May 2023, revised 24 August 2023, accepted 4 October 2023)

doi:10.1002/2211-5463.13715

Edited by Ivana Novak

SIRT4, together with SIRT3 and SIRT5, comprises the mitochondrially localized subgroup of sirtuins. SIRT4 regulates mitochondrial bioenergetics, dynamics (mitochondrial fusion), and quality control (mitophagy) via its NAD^+-dependent enzymatic activities. Here, we address the regulation of SIRT4 itself by characterizing its protein stability and degradation upon $CoCl_2$-induced pseudohypoxic stress that typically triggers mitophagy. Interestingly, we observed that of the mitochondrial sirtuins, only the protein levels of SIRT4 or ectopically expressed SIRT4-eGFP decrease upon $CoCl_2$ treatment of HEK293 cells. Co-treatment with BafA1, an inhibitor of autophagosome–lysosome fusion required for autophagy/mitophagy, or the use of the proteasome inhibitor MG132, prevented $CoCl_2$-induced SIRT4 downregulation. Consistent with the proteasomal degradation of SIRT4, the lysine mutants SIRT4(K78R) and SIRT4(K299R) showed significantly reduced polyubiquitination upon $CoCl_2$ treatment and were more resistant to pseudohypoxia-induced degradation as compared to SIRT4. Moreover, SIRT4(K78R) and SIRT4(K299R) displayed increased basal protein stability as compared to wild-type SIRT4 when subjected to MG132 treatment or cycloheximide (CHX) chase assays. Thus, our data indicate that stress-induced protein degradation of SIRT4 occurs through two mechanisms: (a) via mitochondrial autophagy/mitophagy, and (b) as a separate process via proteasomal degradation within the cytoplasm.

Sirtuins comprise a group of proteins initially defined through the identification of the NAD^+-dependent histone deacetylase Sir2 in yeast [1]. Sirtuins can be subdivided into five distinct phylogenetic branches by analysis of conserved catalytic core domain sequences. In human, seven sirtuins have been identified grouping them into four phylogentic branches, i.e., class 1 (sirtuins 1–3), class 2 (SIRT4), class 3 (SIRT5), and class 4 (sirtuins 6 and 7) [2,3]. These proteins function in epigenetic regulation and gene expression control in the nucleus (SIRT1, 2, 6, and 7; [4]), microtubule dynamics (SIRT2, SIRT4; [5–7]), proliferation/cell survival, senescence and aging (e.g. SIRT4 and SIRT6; [8,9]), life-span regulation (e.g. SIRT6; [9,10]), and regulation of mitochondrial metabolism (SIRT3, 4, 5; [11,12]). Mitochondrial sirtuins like SIRT3 represent potential targets for the treatment of aging-associated diseases [13,14]. This is further emphasized by recent

Abbreviations
BafA1, bafilomycin A1; CHX, cycloheximide; MPP^+, 1-methyl-4-phenylpyridinium; poly-Ub, polyubiquitination; SIRT, sirtuin.

data indicating an involvement of SIRT4 in the onset and development of Parkinson's disease [15].

Human sirtuins localize in multiple subcellular compartments, functioning across them [16–20]. E.g., SIRT4 is distributed between the cytoplasm, nucleus, and in particular mitochondria [5,21], the latter based on an N-terminal mitochondrial targeting sequence typical for mitochondrial sirtuins [22–24]. Functionally, SIRT4 has been characterized in mitochondria as tumor suppressor and inhibitor of the metabolic gatekeeper enzymes pyruvate dehydrogenase (PDH; [25]) and glutamate dehydrogenase (GDH; [26,27]) as well as based on its deacetylase activity as a regulator of leucine metabolism and insulin secretion [28]. Moreover, several recent reports attributed novel extramitochondrial roles to SIRT4 in microtubule dynamics and regulation of mitotic cell cycle progression, WNT/β-Catenin and Hippo signaling, and SNARE complex formation required for autophagosome–lysosome fusion [5,29–31].

The expression of SIRT4 is regulated both at the gene/mRNA and protein level. Regarding the latter, the degradation of sirtuins is mediated by two major cellular pathways, macroautophagy and presumably the ubiquitin-proteasome pathway. Mitochondrially localized sirtuins are degraded by macroautophagy in neuronal LUHMES cells, a M. Parkinson disease model, upon MPP^+ (1-methyl-4-phenylpyridinium) induced oxidative stress [32]. This degradation of oxidized sirtuins could be prevented by treatment with Bafilomycin A1 (BafA1), an inhibitor of autophagosome–lysosome fusion and therefore (macro)autophagy, whereas treatment with MG132, a widely used proteasome inhibitor, failed to preclude reduction of sirtuin protein levels [32].

Interestingly, within human SIRT4 comprehensive proteome mapping identified the putative Ubiquitin target lysine residues K78 and K299 [33,34], thus indicating that SIRT4 may indeed undergo ubiquitination and possibly polyubiquitination, given its subcellular distribution not only in mitochondria, but also in the cytoplasm and nucleus [5,21]. Polyubiquitination occurs via the internal lysine residue K48 of Ubiquitin (K48-polyUb), which is required to tag target proteins by multiple Ubiquitin molecules for subsequent proteasomal degradation in the cytoplasm [35–37]. Interestingly, hypoxia leads to the downregulation of SIRT4 at the protein level [38,39] by unknown mechanism(s). Therefore, in the present study we employed a chemical hypoxia model using $CoCl_2$ treatment [40] to address the role of the SIRT4 lysine residues K78 and K299 [33,34] in basal protein stability and stress-induced polyubiquitination and proteasomal degradation of SIRT4.

Materials and methods

Reagents

$CoCl_2$, Bafilomycin A1, Cycloheximide (CHX), and MG132 were obtained from Roth (Karlsruhe, Germany), Cayman Chemical (Biomol GmbH, Hamburg, Germany), Sigma-Aldrich (Taufkirchen, Germany), and Selleck Chemicals (Köln, Germany) respectively. Primary antibodies were directed against SIRT3 (#5490; Cell Signaling, Frankfurt am Main, Germany), SIRT4 (#66543-1-Ig; Proteintech), SIRT5 (#8782; Cell Signaling, Frankfurt am Main, Germany), eGFP (#11814460001; Roche), Ubiquitin (#12986-1-AP; Proteintech, Planegg/Martinsried, Germany; and #3933; Cell Signaling, Frankfurt am Main, Germany), and α-Tubulin (#ab52866; Abcam, Cambridge, UK; and #11224-1-AP; Proteintech, Planegg/Martinsried, Germany). Primary antibodies were detected using anti-mouse (700 nm; LI-COR IRDye #926-32213; Bad Homburg, Germany) or anti-rabbit (800 nm; LI-COR IRDye #926-68072) secondary antibodies.

Cell culture

Parental and SIRT4 wild-type/mutant expressing HEK293 cell lines were cultured at 37 °C and 5% CO_2 in DMEM (Dulbecco's Modified Eagle Medium) containing high glucose (4.5 $g \cdot L^{-1}$; Thermo Fisher Scientific, Oberhausen, Germany) with 10% FBS (Thermo Fisher Scientific, Oberhausen, Germany) and penicillin (100 $units \cdot mL^{-1}$)/streptomycin (100 $\mu g \cdot mL^{-1}$) (Genaxxon, Ulm, Germany). HEK293 cells were obtained from the German Collection of Microorganisms and Cell Cultures GmbH (DSMZ, Braunschweig, Germany) (HEK293: ACC 305). HEK293-eGFP and HEK293-SIRT4-eGFP cell lines have been described previously [5,41].

shRNA-mediated depletion of SIRT4

HEK293 cells were transfected with the pLKO.1 vector control or the pLKO.1_948 vector (TRCN0000018948; Merck, Darmstadt, Germany) using the Lipofectamine 3000 reagent (Thermo Fisher Scientific, Oberhausen, Germany). pLKO.1_948 expresses a shRNA targeting the sequence 5′-CCAGCGGTACTGGGCGAGAAA-3′ of the human SIRT4 mRNA. Stable cell lines were obtained and maintained in selection media containing puromycin (InvivoGen, Toulouse, France; 1.5 $\mu g \cdot mL^{-1}$).

Site-directed mutagenesis

Primers to generate SIRT4 mutations K78R and K299R were obtained from Eurofins Genomics (Ebersberg, Germany). The sequences of the oligonucleotides used in this study will be provided upon request. The pcDNA3.1 vector

FEBS Open Bio 13 (2023) 2187–2199 © 2023 The Authors. *FEBS Open Bio* published by John Wiley & Sons Ltd on behalf of Federation of European Biochemical Societies.

containing SIRT4-eGFP was used as a template for PCR-based site-directed mutagenesis using 100 picomoles of forward and reverse primers, 10–20 ng of template plasmid, and 1 µL of Phusion High-Fidelity DNA Polymerase (Thermo Fisher Scientific, Oberhausen, Germany). PCR reactions were performed for 15 cycles at a denaturation temperature of 98 °C (1 min), an annealing temperature of 55 °C (1 min), and an extension temperature of 72 °C (3 min). Methylated template DNA was digested by DpnI afterward. SIRT4 point mutations were confirmed by sequencing (MicroSynth Seqlab GmbH, Göttingen, Germany).

Generation of SIRT4 expressing cell lines

HEK293 cell lines stably expressing the mutated SIRT4-eGFP variants (K78R, K299R, or K78R/K299R) have been generated using the Turbofect transfection reagent (Thermo Fisher Scientific) and cultured in media containing 400 $\mu g \cdot mL^{-1}$ Geneticin/G418 (Genaxxon, Ulm, Germany) as a permanent selection agent. The expression of SIRT4-eGFP fusion constructs was validated by immunoblotting and flow cytometry. Generation of HEK293-SIRT (H161Y)-eGFP and HEK293-SIRT4(ΔN28)-eGFP cell lines has been previously described [5,41].

Treatment of HEK293 cell lines with the pseudohypoxia agent $CoCl_2$

HEK293 cell lines were grown to a cell density of approximately 80% and then subjected to a chemical hypoxia model [40] using $CoCl_2$ treatment at concentrations of 250 and 400 µM for 24 or 36 h.

Pulse-chase protein stability assay using cycloheximide

To determine basal protein stability of SIRT4 and mutants thereof, HEK293 cell lines were treated at a cell density of approximately 80% with the protein biosynthesis inhibitor cycloheximide for 4, 8, and 24 h. Based on this chase kinetics, linear regression was employed to calculate the protein half-life of SIRT4 variants.

Preparation of total cell lysates and immunoblot analysis

Cleared cell lysates were generated using lysis buffer containing 0.3% CHAPS (3-[(3-Cholamidopropyl) dimethylammonio]-1-propanesulfonate), 50 mM Tris–HCl (pH 7.4), 150 mM NaCl, 1 mM Na_3VO_4, 10 mM NaF, 1 mM EDTA, 1 mM EGTA, 2.5 mM $Na_4O_7P_2$, and 1 µM DTT. The cOmplete™ protease inhibitor cocktail (Sigma-Aldrich) was used to prevent the degradation of proteins in the lysates. The latter were cleared by centrifugation (11 000 ***g*** at 4 °C for 20 min) and the protein concentration of the supernatants (total cell lysates) was determined using the Bradford assay (Roth). Relative quantification of protein levels (as compared to α-Tubulin or β-Actin loading controls) was performed by IMAGEJ-based (Rasband, W.S., ImageJ, U.S. National Institutes of Health, Bethesda, Maryland, USA, https://imageJ.nih.gov/ij) densitometric analysis of specific immunoblot signals.

Immunoprecipitation of ubiquitinated SIRT4-eGFP wild-type and mutant proteins

Total cell lysates were obtained as described above and subjected to immunoprecipitation analysis using single-domain anti-eGFP antibodies (nanobody method based on [42]) essentially as described [5,41]. Polyubiquitination of wild-type and mutant SIRT4-eGFP forms was detected using Ubiquitin-specific antibodies.

Phylogenetic analysis

Sequences were obtained from the UniProt database (www.uniprot.org) and further analysis was performed using the CLUSTALW multiple alignment method (Thompson et al., PMID 7984417) followed by the sequence alignment editor software BIOEDIT 7.2.5 (Tom Hall, Ibis Biosciences, Carlsbad, USA).

Statistical analysis

Data are presented as mean ± SD. Multiple comparisons were analyzed by one-way or two-way analysis of variance (ANOVA) followed by Tukey's *post-hoc* test to identify group differences in variance analysis using the GRAPHPAD PRISM software (GraphPad Software, Boston, USA). Statistical significance was set at the level of $P \leq 0.05$ ($^{*}P \leq 0.05$, $^{**}P \leq 0.01$, $^{***}P \leq 0.001$).

Results

The protein levels of SIRT4, but not SIRT3 and SIRT5, decrease upon induction of pseudohypoxia

Given that hypoxia leads to the downregulation of SIRT4 at the protein level [38,39], we tested the impact of $CoCl_2$-induced pseudohypoxia on all three mitochondrial sirtuins in HEK293 cells. As shown in Fig. 1, $CoCl_2$ treatment at concentrations of 250 and 400 µM for 24 h resulted in a decrease of endogenous SIRT4 protein levels by up to 50%. The specificity of the anti-SIRT4 antibody was confirmed by immunoblot analysis of SIRT4-depleted HEK293 cells (Fig. S1). In contrast, under the same conditions, total cell protein quantities of SIRT3 and SIRT5 did not

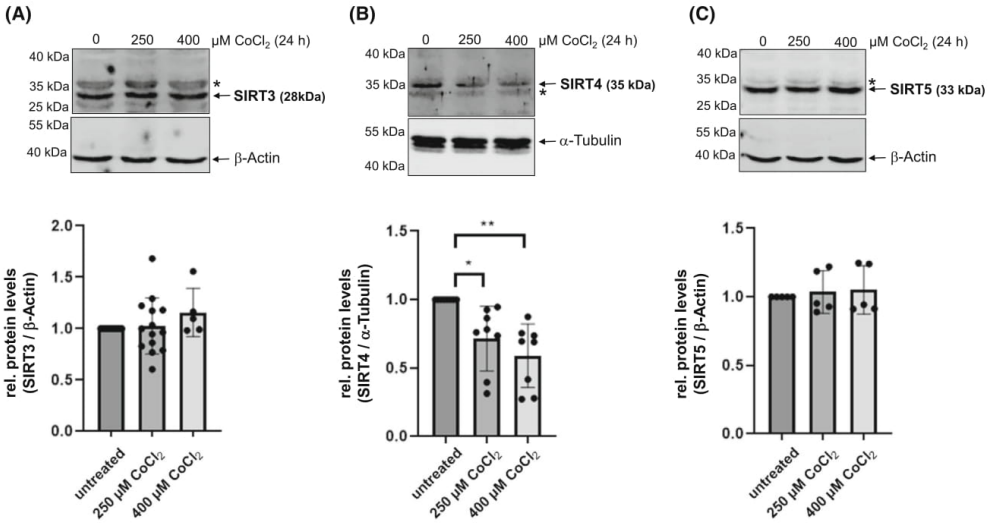

Fig. 1. Protein levels of SIRT4, but not SIRT3 and SIRT5, are downregulated upon $CoCl_2$-induced pseudohypoxia. HEK293 cells were subjected to $CoCl_2$ treatment for 24 h followed by analysis of endogenous protein levels of SIRT3 (n = 5–14) (A), SIRT4 (n = 8) (B), and SIRT5 (n = 5) (C). Relative quantification of immunoblot signals was performed using IMAGEJ-based densitometric evaluation and α-Tubulin levels as loading control. Unspecific bands are marked (*). To determine statistical significance, a One-Way ANOVA test followed by Tukey's test was employed (mean ± SD; $*P < 0.05$; $**P < 0.01$).

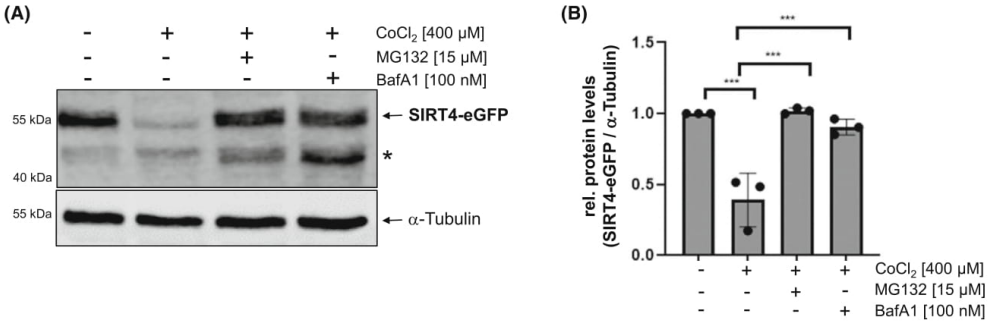

Fig. 2. Co-treatment of HEK293-SIRT4-eGFP cells with MG132 or Bafilomycin A1 (BafA1) inhibits degradation of SIRT4-eGFP during $CoCl_2$-induced pseudohypoxia. SIRT4-eGFP expressing HEK293 cells were subjected to $CoCl_2$ treatment for 24 h in the presence or absence of the proteasome inhibitor MG132 or BafA1, which prevents autophagosome–lysosome fusion. SIRT4-eGFP protein levels were analyzed by immunoblotting using anti-eGFP antibodies (A) and IMAGEJ-based densitometric evaluation using α-Tubulin levels as loading control (B). Unspecific bands are marked (*). To determine statistical significance, a One-Way ANOVA test followed by Tukey's test was employed (n = 3; mean ± SD; $***P < 0.001$).

alter significantly. Thus, within the family of mitochondrial sirtuins, the expression of SIRT4 is specifically downregulated at the protein level upon pseudohypoxic stress, presumably independent of altered SIRT4 gene expression as evident from the study by Pecher *et al.* [39].

Inhibition of the proteasome or autophagic degradation prevents protein degradation of SIRT4 in $CoCl_2$-induced pseudohypoxia

Consistent with the findings for endogenous SIRT4 (Fig. 1), the protein levels of ectopically expressed SIRT4-eGFP (Fig. 2A,B), but not eGFP as control (Fig. S2), were also reduced by approximately 60% upon $CoCl_2$-treatment. Interestingly, this reduction of SIRT4-eGFP levels could be prevented by treatment with either BafA1 or MG132, indicating that both macroautophagy/mitophagy and the proteasome, respectively, are involved in pseudohypoxic stress-induced SIRT4 degradation. MG132 mediated inhibition of the proteasome led also to the stabilization of the catalytically inactive mutant SIRT4(H161Y) and the N-terminal deletion mutant SIRT4(ΔN28) that lacks the mitochondrial translocation sequence (Fig. S3). Thus, proteasomal degradation of SIRT4 is independent of its enzymatic activity and occurs extra-mitochondrially in the cytoplasm.

The SIRT4 lysine mutants K78R and K299R are stabilized in $CoCl_2$-induced pseudohypoxia

Proteome-wide mapping identified within human SIRT4 the putative Ubiquitin target lysine residues K78 and K299 [33,34]. Thus, to further characterize the role of ubiquitination and proteasomal degradation in stress-induced regulation of SIRT4 levels, we generated HEK293 cell lines stably expressing the Lysine to Arginine mutated SIRT4 variants K78R, K299R, or the double mutant K78R/K299R (Fig. S4), therefore preventing ubiquitination of these lysine residues. We subjected these cell lines to $CoCl_2$ induced pseudohypoxic stress followed by the analysis of wild-type and mutated SIRT4 protein levels. As indicated in Fig. 3, $CoCl_2$ treatment for 24 h resulted in a significant reduction of SIRT4-eGFP protein levels by approximately 45%, whereas the mutants K78R, K299R, and K78R/K299R were stable with no overtly quantitative changes. Longer $CoCl_2$ treatment for 36 h ameliorated this phenotype and resulted in significant degradation of all three mutants, although K299R still retained an increased stability. Thus, both lysine residues K78 and K299 regulate the protein stability of SIRT4 upon pseudohypoxic stress.

The SIRT4 lysine mutants K78R and K299R undergo decreased polyubiquitination upon $CoCl_2$ induced pseudohypoxia

Polyubiquitination (poly-Ub) functions as a precursor and initiator of proteasome-mediated protein degradation [43]. We next subjected wild-type and mutated SIRT4-eGFP from untreated and $CoCl_2$-treated cells to immunoprecipitation using anti-eGFP nanobody beads followed by the analysis of the degree of SIRT4 polyubiquitination using anti-Ubiquitin immunoblotting. Consistent with the previous findings, the

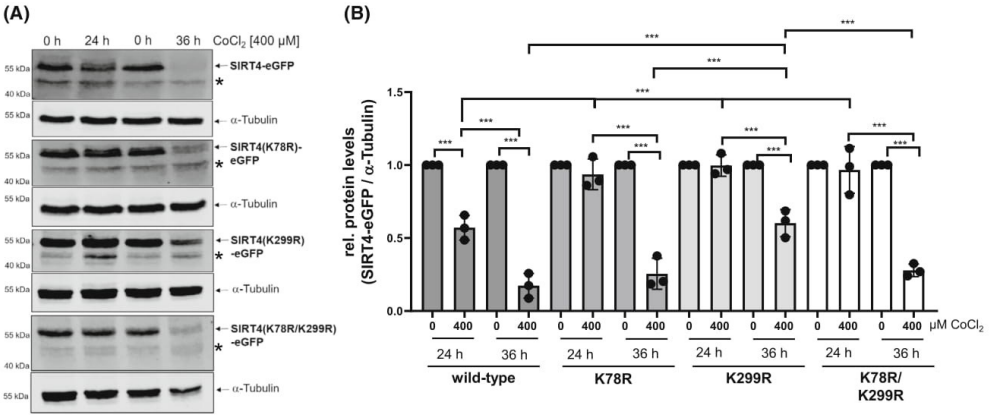

Fig. 3. The SIRT4 mutants K78R and K299R are more resistant to $CoCl_2$-induced degradation. HEK293 cell lines expressing SIRT4-eGFP or the indicated SIRT4 mutants thereof were subjected to $CoCl_2$-induced pseudohypoxia for 24 and 36 h followed by immunoblot analysis of the respective SIRT4-eGFP/mutant SIRT4-eGFP levels using anti-eGFP antibodies (A) and IMAGEJ based densitometric evaluation using α-Tubulin levels as loading control (B). Unspecific bands are marked (*). To determine statistical significance, a Two-Way ANOVA test followed by Tukey's test was employed ($n = 3$; mean ± SD; ***$P < 0.001$).

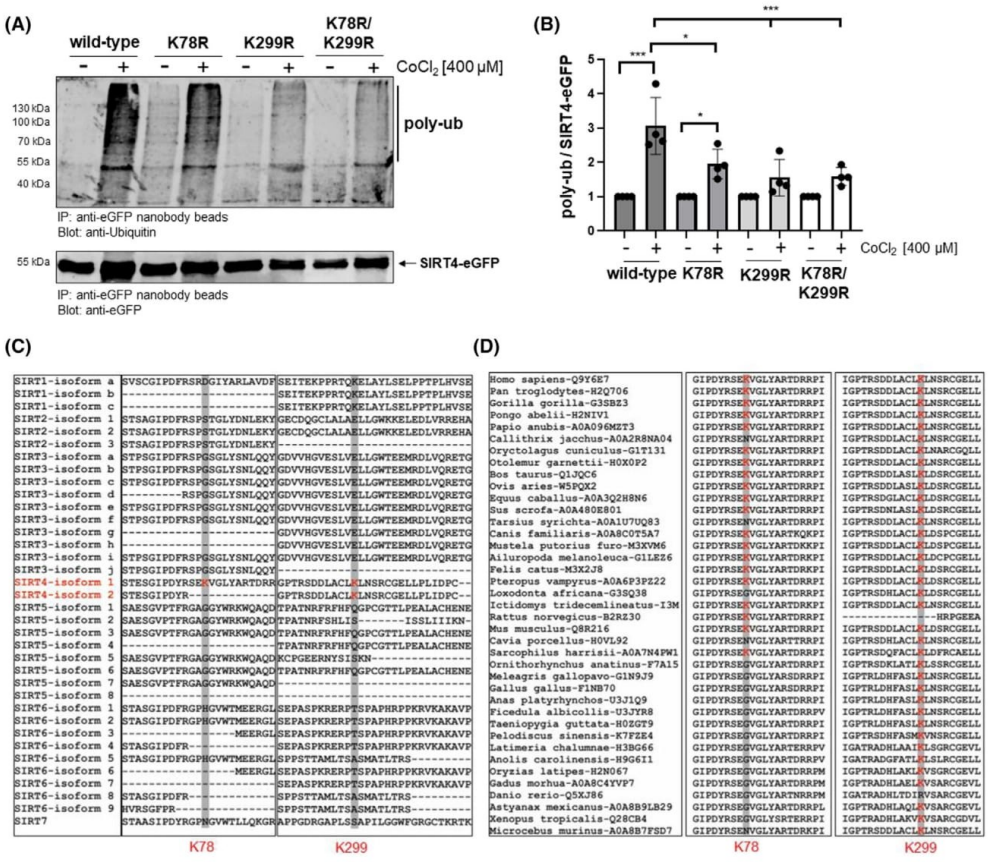

Fig. 4. The SIRT4 mutants K78R and K299R show a decreased polyubiquitination upon $CoCl_2$-induced pseudohypoxia. (A) HEK293 cell lines expressing SIRT4-eGFP or the indicated SIRT4-eGFP mutants thereof were either untreated or subjected to $CoCl_2$-induced pseudohypoxia for 24 h. SIRT4 variants were immunoprecipitated using anti-eGFP nanobody beads and further analyzed for the degree of polyubiquitination (poly-ub) using anti-Ubiquitin immunoblotting (upper panel). Immunoprecipitated SIRT4-eGFP proteins were detected on the same membrane using anti-eGFP antibodies (lower panel). (B) Relative quantification of polyubiquitination of SIRT4-eGFP mutants compared to wild-type SIRT4-eGFP using IMAGEJ-based densitometric evaluation. To determine statistical significance, a Two-Way ANOVA test followed by Tukey's test was employed ($n = 4$; mean ± SD; $*P < 0.05$; $***P < 0.001$). (C) SIRT4-specific conservation of lysines K78 and K299 (marked in red) within the human Sirtuin protein family. (D) Analysis of evolutionary conservation of K78 and K299 (marked in red) in SIRT4 homologs of vertebrates. Sequences in (C) and (D) were obtained from the UniProt database (www.uniprot.org). Sequence analysis was performed using the CLUSTALW multiple alignment method followed by the sequence alignment editor software BIOEDIT 7.2.5.

stress-induced polyubiquitination of all three SIRT4 variants K78R, K299R, and K78R/K299R was significantly lower as compared to wild-type SIRT4, the latter showing a 3-fold induction in poly-Ub levels (Fig. 4A,B). Next, we explored the conservation of lysine residues K78 and K299 of human SIRT4 both within the mammalian sirtuins and evolutionary within known SIRT4 homologs. As indicated in Fig. 4C, both K78 and K299 are unique for SIRT4 among all seven human sirtuin family members, in particular the mitochondrial sirtuins. The only exception is K299 which is also found in all known SIRT1 isoforms, but this lysine residue does not seem to be involved in SIRT1 ubiquitination [44]. At the level of SIRT4 homologs, K78 seems highly conserved in mammals but is absent in phylogenetically more

distant species like *Xenopus tropicalis* (Fig. 4D). In contrast, lysine K299 is completely conserved throughout the vertebrates indicating that K299 plays an evolutionary more conserved role in the regulation of stress-induced proteasomal degradation of SIRT4. Overall, these findings identify the SIRT4 residues K78 and K299 as conserved polyubiquitination targets and indicate that the level of polyubiquitination of SIRT4 negatively correlates with its protein stability upon pseudohypoxic stress.

The SIRT4 lysine mutants K78R and K299R display an increased basal protein stability

Pulse-chase assays are established to analyze the degree of basal protein stability upon cycloheximide (CHX)

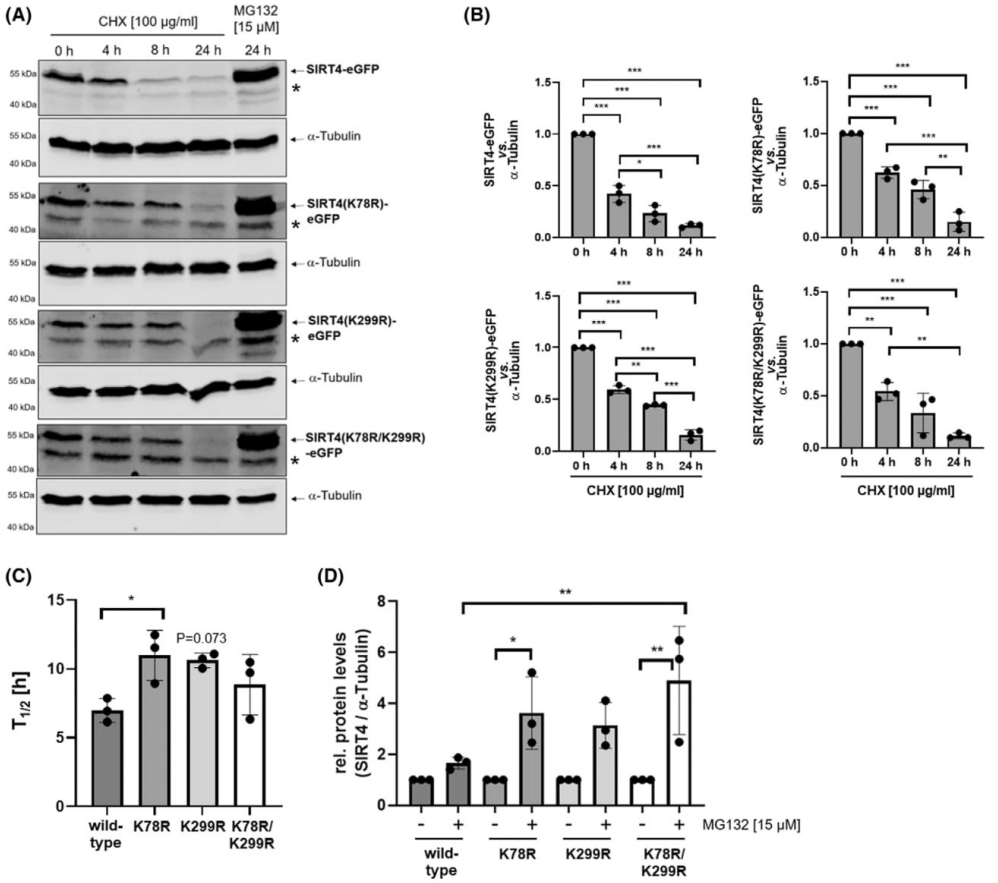

Fig. 5. The SIRT4 mutants K78R and K299R display increased protein stability. HEK293 cells stably expressing SIRT4-eGFP or the indicated SIRT4-eGFP mutants thereof were subjected to cycloheximide (CHX) chase assays for 4, 8, and 24 h or treatment with the proteasome inhibitor MG132 for 24 h. Expression of SIRT4-eGFP or the SIRT4-eGFP mutants thereof was analyzed by immunoblotting using anti-eGFP antibodies (A) and IMAGEJ-based densitometric evaluation using α-Tubulin levels as loading control (B). Unspecific bands are marked (*). (C) Determination of the protein half-life ($T_{1/2}$) of SIRT4-eGFP as compared to SIRT4(K78R)-eGFP and SIRT4(K299R)-eGFP analyzed in CHX chase assays. (D) MG132 mediated inhibition of the proteasome increases the stability of SIRT4(K78R)-eGFP, SIRT4(K299R)-eGFP, and the double mutant SIRT4(K78R/K299R)-eGFP as compared to wild-type SIRT4-eGFP. Immunoblots were subjected to IMAGEJ-based densitometric evaluation using α-Tubulin levels as loading control. To determine statistical significance, Two-Way ANOVA tests followed by Tukey's tests were employed ($n = 3$; mean ± SD; $*P < 0.05$; $**P < 0.01$; $***P < 0.001$).

mediated inhibition of protein translation [45]. Therefore, HEK293 cell lines expressing wild-type SIRT4 or the mutants K78R, K299R, or K78R/K299R, were subjected to a time kinetics of CHX treatment for up to 24 h. Interestingly, all three mutants displayed a delayed decrease in protein levels as compared to wild-type SIRT4 (Fig. 5A,B). To further examine differences in stability between wild-type SIRT4 and its mutants we calculated their protein half-lives ($T_{1/2}$) (Fig. 5C). The $T_{1/2}$ for SIRT4(K78R) was approximately 1.6-fold increased as compared to wild-type SIRT4, whereas its difference to SIRT4(K299R) was nearly significant. To address whether these SIRT4 mutants are more resistant to proteasomal degradation under basal conditions, we treated SIRT4 wild-type/mutant-expressing cell lines for 24 h with MG132. As indicated in Fig. 5A,D, in contrast to wild-type SIRT4, all SIRT4 variants showed a clear increase in protein levels upon MG132 treatment, with the biggest significant effect on the double mutant K78/K299.

Discussion

This study provides novel insights into the posttranscriptional regulation of SIRT4 protein levels under stress, i.e., pseudohypoxia-induced conditions. Our findings indicate that (a) pseudohypoxia-induced degradation of SIRT4 is mediated by two mechanisms, via macroautophagy/mitophagy upon mitochondrial translocation of SIRT4, and moreover as a separate process via proteasomal degradation within the cytoplasm; (b) the latter mechanism depends on two conserved polyubiquitination targets of SIRT4, i.e., lysine residues K78 and K299; and (c) within the group of mitochondrial sirtuins, SIRT4 is the only sirtuin which protein levels decrease upon $CoCl_2$ induced pseudohypoxic stress. Consistent with this, downregulation of SIRT4 by hypoxia (1–2% O_2) at the protein level occurs also under more physiological conditions in H9c2 cardio-myoblast and endothelial HUVEC cells [38,39]. This may result in an attenuated ROS response, given that increased SIRT4 can elevate mitochondrial H_2O_2 levels [41]. In contrast, dependent on the cell model analyzed, the modulation of SIRT3 by hypoxia results in either decrease or rather an increase of SIRT3 protein levels as summarized in [46]. E.g., a 2% O_2 hypoxic condition leads to an increase of SIRT3 in endothelial HUVEC cells that preserves via deacetylation of FOXO3 bioenergetics and cell survival under hypoxia [47].

The expression of SIRT4 is regulated at both the gene/mRNA and protein level. At the transcriptional level, mTORC1 functions as a negative regulator by repressing *Sirt4* gene expression via degradation of the transcription factor CREB2 [48,49]. Moreover, the *Sirt4* gene is directly repressed by the lysine-specific demethylase 1 (Lsd1) [50]. Positive regulators of *Sirt4* gene expression include E2F1 [51], and interestingly also SIRT6, whose target genes *Sirt3* and *Sirt4* are downregulated upon SIRT6 deficiency resulting in mitochondrial dysfunction [52]. Lastly, several microRNAs (miR-15a-5p, miR-15b, miR-130b-5p, and miR-497) bind SIRT4 transcripts and thereby modulate SIRT4 protein levels under basal as well as stress-induced and cell aging conditions [8,53–55].

The mechanism(s) involved in the direct protein degradation of mitochondrial sirtuins have only been recently addressed in closer detail by Baeken *et al.* [32]. The authors showed that MPP^+ induced oxidative stress in neuronal LUHMES cells, a M. Parkinson disease model, results in the degradation of SIRT4. This could be prevented by treatment with BafA1, an inhibitor of autophagosome–lysosome fusion and therefore (macro)autophagy. Consistent with this, MPP^+ treatment resulted in an increased sub-cellular co-localization of SIRT4 with LC3B positive autophagic structures [32]. In contrast, in the authors' MPP^+ model, the reduction of protein levels of oxidized SIRT4 was insensitive to treatment with the proteasome inhibitor MG132. This is in different from the rescue effect of MG132 treatment toward $CoCl_2$-induced degradation of SIRT4 (Fig. 2), and surprising, given that both MPP^+, an inhibitor of mitochondrial complex I [56], and hypoxia, an inhibitor of complex III [57], lead to the accumulation of the mitochondrial ROS species H_2O_2. These contrary results could be based on the different cell models analyzed and/or due to different extents of ROS generated by MPP_+ *vs.* $CoCl_2$. In this regard, and given the dynamic subcellular distribution pattern of SIRT4 [5,21], one can speculate that lower to medium mitochondrial H_2O_2 levels target predominantly mitochondrially localized SIRT4, whereas high cellular H_2O_2 levels also lead to oxidation of cytosolically localized SIRT4. The latter would then require the proteasome besides (macro)autophagy for efficient SIRT4 degradation. However, it needs to be analyzed to which extent $CoCl_2$ treatment mediates SIRT4 degradation via ROS generation and subsequent SIRT4 oxidation.

Polyubiquitination of SIRT4 has been previously observed [58,59], but the ubiquitination site(s) of SIRT4 were not analyzed. Consistent with our data, recent work by Zhao *et al.* [60] identified lysine residue K78 of SIRT4 as a polyubiquitination target under basal, i.e., non-stress conditions. The authors' data

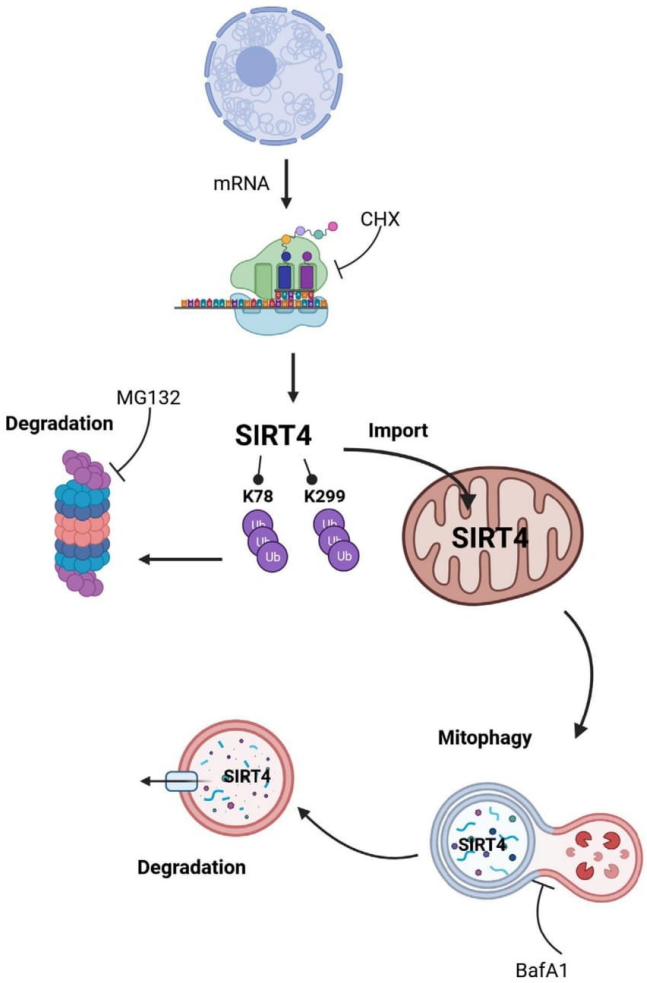

Fig. 6. Model overview about the cellular pathways involved in protein degradation of SIRT4. Given the significantly increased protein half-life of SIRT4(K78R) (Fig. 5C) and the greater stability of SIRT4(K299R) under pseudohypoxic stress (Fig. 3), it is tempting to speculate that K78 and K299 play some divergent roles in basal *vs.* stress-induced degradation of SIRT4, respectively.

indicate that the mTORC1-c-Myc regulated E3-Ubiquitin protein ligase TRIM32 targets SIRT4 via polyubiquitination of lysine K78 for proteasomal degradation [60]. However, this mechanism may not be relevant under (pseudo)hypoxic conditions given that hypoxia downregulates TRIM32 protein levels as shown in pulmonary artery smooth muscle cells [61]. Thus, it remains to be determined (a) whether other SIRT4 interacting E3-Ubiquitin protein ligases, including RNF138 [60] or TRIM28 ([60] and own unpublished results), are involved in proteasomal degradation of SIRT4, and (b) which of the lysine residues K78 and K299 are targeted by these E3-Ubiquitin ligases. Overall, our findings indicate that lysine K78 regulates protein half-life under basal conditions (Fig. 5C), whereas polyubiquitination of lysine K299 mediates SIRT4 degradation upon cellular stress (Figs 3 and 4).

In eukaryotes, polyubiquitination-dependent proteasomal degradation of proteins takes place in the cytoplasm and in the nucleus [62]. Interestingly, recent findings identified a mitochondrial E3-ubiquitin ligase involved in the degradation of the mitophagy receptors BNIP3 and NIX [63] and further uncovered ubiquitin-dependent degradation of mitochondrial proteins at the inner mitochondrial membrane [64]. Given these

observations one could speculate that polyubiquitination and proteasomal degradation of SIRT4 occurs not in the cytoplasm, but during/after mitochondrial translocation. Although we can exclude this possibility, the MG132-mediated stabilization of the ectopically expressed N-terminal deletion mutant SIRT4(ΔN28) (Fig. S3), which cannot be imported into mitochondria, supports the existence of an extramitochondrial polyubiquitination and degradation mechanism for SIRT4.

Conclusions

We propose a model in which stress-induced degradation of SIRT4 is regulated by and dependent on its subcellular localization, i.e., macroautophagy of mitochondrially localized SIRT4 and the ubiquitin-proteasome mediated degradation of extra-mitochondrial/cytoplasmatic SIRT4 (Fig. 6). Both degradation systems regulate cytoplasmatic *vs.* mitochondrial SIRT4 levels and therefore the respective subcellular functions of SIRT4. In the former case, SIRT4, a *bona fide* tumor suppressor protein, interacts with the mitotic spindle apparatus and negatively regulates cell cycle progression [5]. Here, downregulation of SIRT4 upon (pseudo)hypoxia would favor the proliferation of, e.g., stem cells or tumor cells in hypoxic niches [65,66]. In the latter case, mitochondrial SIRT4 interacts with the GTPase OPA1 thereby favoring mitochondrial fusion and thus counteracting mitophagy [41,67]. Here, the downregulation of SIRT4 would promote mitophagy and prevent the accumulation of defective mitochondria due to hypoxia. These models need to be tested in the future.

Acknowledgements

We thank Ursula Duerkop and Yvonne Arlt for expert technical assistance, Björn Stork for providing tools for polyubiquitination analysis, Sebastian Krüger for help with flow cytometry, Natascia Ventura for advice regarding the use of $CoCl_2$ in pseudohypoxia, and Laura Bergmann for discussion. This work was funded in part by the Stiftung für Altersforschung (grant 701.810.783) of the Heinrich Heine-University Düsseldorf (to RPP), and by the Deutsche Forschungsgemeinschaft (DFG, German Research Foundation) project AH 92/8-3 (to MRA). Open Access funding enabled and organized by Projekt DEAL.

Conflict of interest

The authors declare no conflict of interest.

Peer review

The peer review history for this article is available at https://www.webofscience.com/api/gateway/wos/peer-review/10.1002/2211-5463.13715.

Data accessibility

The data that supports the findings of this study are available in Figs 1–5 and the Supporting Information of this article.

Author contributions

NH and RPP initiated the project and designed the study. NH, JG, MM, AL, IL, DMF, and RPP designed, performed, and analyzed the experiments. JS, MRA, and DMF provided expertise, tools, and essential reagents for mutational and nanobody-based co-immunoprecipitation analysis. NH and RPP wrote the manuscript. All authors read, discussed, critically corrected, and approved the final version of the manuscript.

References

1 Imai S, Armstrong CM, Kaeberlein M and Guarente L (2000) Transcriptional silencing and longevity protein Sir2 is an NAD-dependent histone deacetylase. *Nature* **403**, 795–800.
2 Frye RA (2000) Phylogenetic classification of prokaryotic and eukaryotic Sir2-like proteins. *Biochem Biophys Res Commun* **273**, 793–798.
3 Gold DA and Sinclair DA (2022) Sirtuin evolution at the dawn of animal life. *Mol Biol Evol* **39**, msac192.
4 Mendes KL, Lelis DF and Santos SHS (2017) Nuclear sirtuins and inflammatory signaling pathways. *Cytokine Growth Factor Rev* **38**, 98–105.
5 Bergmann L, Lang A, Bross C, Altinoluk-Hambuchen S, Fey I, Overbeck N, Stefanski A, Wiek C, Kefalas A, Verhlsdonk P *et al.* (2020) Subcellular localization and mitotic interactome analyses identify SIRT4 as a centrosomally localized and microtubule associated protein. *Cells* **9**, 1950.
6 Skoge RH, Dolle C and Ziegler M (2014) Regulation of SIRT2-dependent alpha-tubulin deacetylation by cellular NAD levels. *DNA Repair (Amst)* **23**, 33–38.
7 Skoge RH and Ziegler M (2016) SIRT2 inactivation reveals a subset of hyperacetylated perinuclear microtubules inaccessible to HDAC6. *J Cell Sci* **129**, 2972–2982.
8 Lang A, Grether-Beck S, Singh M, Kuck F, Jakob S, Kefalas A, Altinoluk-Hambuchen S, Graffmann N, Schneider M, Lindecke A *et al.* (2016) MicroRNA-15b

regulates mitochondrial ROS production and the senescence-associated secretory phenotype through sirtuin 4/SIRT4. *Aging (Albany NY)* **8**, 534–559.
9 Mostoslavsky R, Chua KF, Lombard DB, Pang WW, Fischer MR, Gellon L, Liu P, Mostoslavsky G, Franco S, Murphy MM *et al.* (2006) Genomic instability and aging-like phenotype in the absence of mammalian SIRT6. *Cell* **124**, 315–329.
10 Kawahara TL, Michishita E, Adler AS, Damian M, Berber E, Lin M, McCord RA, Ongaigui KC, Boxer LD, Chang HY *et al.* (2009) SIRT6 links histone H3 lysine 9 deacetylation to NF-kappaB-dependent gene expression and organismal life span. *Cell* **136**, 62–74.
11 Jaiswal A, Xudong Z, Zhenyu J and Saretzki G (2021) Mitochondrial sirtuins in stem cells and cancer. *FEBS J* **289**, 3393–3415.
12 Ji Z, Liu GH and Qu J (2022) Mitochondrial sirtuins, metabolism, and aging. *J Genet Genomics* **49**, 287–298.
13 Zhang J, Xiang H, Liu J, Chen Y, He RR and Liu B (2020) Mitochondrial Sirtuin 3: new emerging biological function and therapeutic target. *Theranostics* **10**, 8315–8342.
14 He L, Wang J, Yang Y, Li J and Tu H (2022) Mitochondrial sirtuins in Parkinson's disease. *Neurochem Res* **47**, 1491–1502.
15 Weng H, Song W, Fu K, Guan Y, Cai G, Huang E, Chen X, Zou H and Ye Q (2022) Proteomic profiling reveals the potential mechanisms and regulatory targets of sirtuin 4 in 1-methyl-4-phenyl-1,2,3,6-tetrahydropyridine-induced Parkinson's mouse model. *Front Neurosci* **16**, 1035444.
16 Budayeva HG and Cristea IM (2016) Human sirtuin 2 localization, transient interactions, and impact on the proteome point to its role in intracellular trafficking. *Mol Cell Proteomics* **15**, 3107–3125.
17 Eldridge MJG, Pereira JM, Impens F and Hamon MA (2020) Active nuclear import of the deacetylase sirtuin-2 is controlled by its C-terminus and importins. *Sci Rep* **10**, 2034.
18 Osborne B, Bentley NL, Montgomery MK and Turner N (2016) The role of mitochondrial sirtuins in health and disease. *Free Radic Biol Med* **100**, 164–174.
19 Shoba B, Lwin ZM, Ling LS, Bay BH, Yip GW and Kumar SD (2009) Function of sirtuins in biological tissues. *Anat Rec (Hoboken)* **292**, 536–543.
20 Tanno M, Sakamoto J, Miura T, Shimamoto K and Horio Y (2007) Nucleocytoplasmic shuttling of the NAD+-dependent histone deacetylase SIRT1. *J Biol Chem* **282**, 6823–6832.
21 Ramadani-Muja J, Gottschalk B, Pfeil K, Burgstaller S, Rauter T, Bischof H, Waldeck-Weiermair M, Bugger H, Graier WF and Malli R (2019) Visualization of sirtuin 4 distribution between mitochondria and the nucleus, based on bimolecular fluorescence self-complementation. *Cells* **8**, 1583.
22 Ahuja N, Schwer B, Carobbio S, Waltregny D, North BJ, Castronovo V, Maechler P and Verdin E (2007) Regulation of insulin secretion by SIRT4, a mitochondrial ADP-ribosyltransferase. *J Biol Chem* **282**, 33583–33592.
23 Schwer B, North BJ, Frye RA, Ott M and Verdin E (2002) The human silent information regulator (Sir)2 homologue hSIRT3 is a mitochondrial nicotinamide adenine dinucleotide-dependent deacetylase. *J Cell Biol* **158**, 647–657.
24 Michishita E, Park JY, Burneskis JM, Barrett JC and Horikawa I (2005) Evolutionarily conserved and nonconserved cellular localizations and functions of human SIRT proteins. *Mol Biol Cell* **16**, 4623–4635.
25 Mathias RA, Greco TM, Oberstein A, Budayeva HG, Chakrabarti R, Rowland EA, Kang Y, Shenk T and Cristea IM (2014) Sirtuin 4 is a lipoamidase regulating pyruvate dehydrogenase complex activity. *Cell* **159**, 1615–1625.
26 Drews L, Zimmermann M, Westhoff P, Brilhaus D, Poss RE, Bergmann L, Wiek C, Brenneisen P, Piekorz RP, Mettler-Altmann T *et al.* (2020) Ammonia inhibits energy metabolism in astrocytes in a rapid and glutamate dehydrogenase 2-dependent manner. *Dis Model Mech* **13**, dmm047134.
27 Haigis MC, Mostoslavsky R, Haigis KM, Fahie K, Christodoulou DC, Murphy AJ, Valenzuela DM, Yancopoulos GD, Karow M, Blander G *et al.* (2006) SIRT4 inhibits glutamate dehydrogenase and opposes the effects of calorie restriction in pancreatic beta cells. *Cell* **126**, 941–954.
28 Anderson KA, Huynh FK, Fisher-Wellman K, Stuart JD, Peterson BS, Douros JD, Wagner GR, Thompson JW, Madsen AS, Green MF *et al.* (2017) SIRT4 is a lysine deacylase that controls leucine metabolism and insulin secretion. *Cell Metab* **25**, 838–855.e15.
29 Huang H, Ouyang Q, Mei K, Liu T, Sun Q, Liu W and Liu R (2023) Acetylation of SCFD1 regulates SNARE complex formation and autophagosome-lysosome fusion. *Autophagy* **19**, 189–203.
30 Wang Y, Yue J, Xiao M, Lu X and Chin YE (2022) SIRT4-catalyzed deacetylation of axin1 modulates the Wnt/beta-catenin signaling pathway. *Front Oncol* **12**, 872444.
31 Yang S, Xu W, Liu C, Jin J, Li X, Jiang Y, Zhang L, Meng X, Zhan J and Zhang H (2022) LATS1 K751 acetylation blocks activation of hippo signalling and switches LATS1 from a tumor suppressor to an oncoprotein. *Sci China Life Sci* **65**, 129–141.
32 Baeken MW, Schwarz M, Kern A, Moosmann B, Hajieva P and Behl C (2021) The selective degradation of sirtuins via macroautophagy in the MPP(+) model of Parkinson's disease is promoted by conserved oxidation sites. *Cell Death Discov* **7**, 286.
33 Akimov V, Barrio-Hernandez I, Hansen SVF, Hallenborg P, Pedersen AK, Bekker-Jensen DB, Puglia

M, Christensen SDK, Vanselow JT, Nielsen MM *et al.* (2018) UbiSite approach for comprehensive mapping of lysine and N-terminal ubiquitination sites. *Nat Struct Mol Biol* **25**, 631–640.
34 Udeshi ND, Svinkina T, Mertins P, Kuhn E, Mani DR, Qiao JW and Carr SA (2013) Refined preparation and use of anti-diglycine remnant (K-epsilon-GG) antibody enables routine quantification of 10,000s of ubiquitination sites in single proteomics experiments. *Mol Cell Proteomics* **12**, 825–831.
35 Nguyen LK, Dobrzynski M, Fey D and Kholodenko BN (2014) Polyubiquitin chain assembly and organization determine the dynamics of protein activation and degradation. *Front Physiol* **5**, 4.
36 Pohl C and Dikic I (2019) Cellular quality control by the ubiquitin-proteasome system and autophagy. *Science* **366**, 818–822.
37 van Wijk SJ, Fulda S, Dikic I and Heilemann M (2019) Visualizing ubiquitination in mammalian cells. *EMBO Rep* **20**, e46520.
38 Liu B, Che W, Xue J, Zheng C, Tang K, Zhang J, Wen J and Xu Y (2013) SIRT4 prevents hypoxia-induced apoptosis in H9c2 cardiomyoblast cells. *Cell Physiol Biochem* **32**, 655–662.
39 Pecher SJ, Potthast AB, von Versen-Hoynck F and Das AM (2020) Impact of short-term hypoxia on sirtuins as regulatory elements in HUVECs. *J Clin Med* **9**, 2604.
40 Munoz-Sanchez J and Chanez-Cardenas ME (2019) The use of cobalt chloride as a chemical hypoxia model. *J Appl Toxicol* **39**, 556–570.
41 Lang A, Anand R, Altinoluk-Hambuchen S, Ezzahoini H, Stefanski A, Iram A, Bergmann L, Urbach J, Bohler P, Hnsel J *et al.* (2017) SIRT4 interacts with OPA1 and regulates mitochondrial quality control and mitophagy. *Aging (Albany NY)* **9**, 2163–2189.
42 Rothbauer U, Zolghadr K, Muyldermans S, Schepers A, Cardoso MC and Leonhardt H (2008) A versatile nanotrap for biochemical and functional studies with fluorescent fusion proteins. *Mol Cell Proteomics* **7**, 282–289.
43 Pickart CM (2001) Mechanisms underlying ubiquitination. *Annu Rev Biochem* **70**, 503–533.
44 Peng L, Yuan Z, Li Y, Ling H, Izumi V, Fang B, Fukasawa K, Koomen J, Chen J and Seto E (2015) Ubiquitinated sirtuin 1 (SIRT1) function is modulated during DNA damage-induced cell death and survival. *J Biol Chem* **290**, 8904–8912.
45 Elgendy M (2017) Assessment of modulation of protein stability using pulse-chase method. *Bio Protoc* **7**, e2443.
46 Marcus JM and Andrabi SA (2018) SIRT3 regulation under cellular stress: making sense of the ups and downs. *Front Neurosci* **12**, 799.
47 Tseng AH, Wu LH, Shieh SS and Wang DL (2014) SIRT3 interactions with FOXO3 acetylation, phosphorylation and ubiquitinylation mediate endothelial cell responses to hypoxia. *Biochem J* **464**, 157–168.
48 Csibi A, Fendt SM, Li C, Poulogiannis G, Choo AY, Chapski DJ, Jeong SM, Dempsey JM, Parkhitko A, Morrison T *et al.* (2013) The mTORC1 pathway stimulates glutamine metabolism and cell proliferation by repressing SIRT4. *Cell* **153**, 840–854.
49 Csibi A, Fendt SM, Li C, Poulogiannis G, Choo AY, Chapski DJ, Jeong SM, Dempsey JM, Parkhitko A, Morrison T *et al.* (2021) The mTORC1 pathway stimulates glutamine metabolism and cell proliferation by repressing SIRT4. *Cell* **184**, 2256.
50 Castex J, Willmann D, Kanouni T, Arrigoni L, Li Y, Friedrich M, Schleicher M, Wohrle S, Pearson M, Kraut N *et al.* (2017) Inactivation of Lsd1 triggers senescence in trophoblast stem cells by induction of Sirt4. *Cell Death Dis* **8**, e2631.
51 Hong J, Li S, Wang X, Mei C and Zan L (2018) Study of expression analysis of SIRT4 and the coordinate regulation of bovine adipocyte differentiation by SIRT4 and its transcription factors. *Biosci Rep* **38**, BSR20181705.
52 Smirnov D, Eremenko E, Stein D, Kaluski S, Jasinska W, Cosentino C, Martinez-Pastor B, Brotman Y, Mostoslavsky R, Khrameeva E *et al.* (2023) SIRT6 is a key regulator of mitochondrial function in the brain. *Cell Death Dis* **14**, 35.
53 Deng J, Wang H, Liang Y, Zhao L, Li Y, Yan Y, Zhao H, Zhang X and Zou F (2022) miR-15a-5p enhances the malignant phenotypes of colorectal cancer cells through the STAT3/TWIST1 and PTEN/AKT signaling pathways by targeting SIRT4. *Cell Signal* **101**, 110517.
54 Wang H, Wang Z, Wang Y, Li X, Yang W, Wei S, Shi C, Qiu J, Ni M, Rao J *et al.* (2021) miRNA-130b-5p promotes hepatic stellate cell activation and the development of liver fibrosis by suppressing SIRT4 expression. *J Cell Mol Med* **25**, 7381–7394.
55 Xiao Y, Zhang X, Fan S, Cui G and Shen Z (2016) MicroRNA-497 inhibits cardiac hypertrophy by targeting Sirt4. *PLoS One* **11**, e0168078.
56 Murphy MP, Krueger MJ, Sablin SO, Ramsay RR and Singer TP (1995) Inhibition of complex I by hydrophobic analogues of N-methyl-4-phenylpyridinium (MPP+) and the use of an ion-selective electrode to measure their accumulation by mitochondria and electron-transport particles. *Biochem J* **306** (Pt 2), 359–365.
57 Chandel NS, McClintock DS, Feliciano CE, Wood TM, Melendez JA, Rodriguez AM and Schumacker PT (2000) Reactive oxygen species generated at mitochondrial complex III stabilize hypoxia-inducible factor-1alpha during hypoxia: a mechanism of O_2 sensing. *J Biol Chem* **275**, 25130–25138.

58 Iwahara T, Bonasio R, Narendra V and Reinberg D (2012) SIRT3 functions in the nucleus in the control of stress-related gene expression. *Mol Cell Biol* **32**, 5022–5034.
59 Li T, Li Y, Liu T, Hu B, Li J, Liu C, Liu T and Li F (2020) Mitochondrial PAK6 inhibits prostate cancer cell apoptosis via the PAK6-SIRT4-ANT2 complex. *Theranostics* **10**, 2571–2586.
60 Zhao L, Su H, Liu X, Wang H, Feng Y, Wang Y, Chen H, Dai L, Lai S, Xu S *et al.* (2022) mTORC1-c-Myc pathway rewires methionine metabolism for HCC progression through suppressing SIRT4 mediated ADP ribosylation of MAT2A. *Cell Biosci* **12**, 183.
61 Hu Z, Song Q, Ma H, Guo Y, Zhang T, Xie H and Luo X (2021) TRIM32 inhibits the proliferation and migration of pulmonary artery smooth muscle cells through the inactivation of PI3K/Akt pathway in pulmonary arterial hypertension. *J Bioenerg Biomembr* **53**, 309–320.
62 Chowdhury M and Enenkel C (2015) Intracellular dynamics of the ubiquitin-proteasome-system. *F1000Res* **4**, 367.
63 Cao Y, Zheng J, Wan H, Sun Y, Fu S, Liu S, He B, Cai G, Cao Y, Huang H *et al.* (2023) A mitochondrial SCF-FBXL4 ubiquitin E3 ligase complex degrades BNIP3 and NIX to restrain mitophagy and prevent mitochondrial disease. *EMBO J* **42**, e113033.
64 Lavie J, De Belvalet H, Sonon S, Ion AM, Dumon E, Melser S, Lacombe D, Dupuy JW, Lalou C and Benard G (2018) Ubiquitin-dependent degradation of mitochondrial proteins regulates energy metabolism. *Cell Rep* **23**, 2852–2863.
65 Druker J, Wilson JW, Child F, Shakir D, Fasanya T and Rocha S (2021) Role of hypoxia in the control of the cell cycle. *Int J Mol Sci* **22**, 4874.
66 Hubbi ME and Semenza GL (2015) Regulation of cell proliferation by hypoxia-inducible factors. *Am J Physiol Cell Physiol* **309**, C775–C782.
67 Lang A and Piekorz RP (2018) Novel role of the SIRT4-OPA1 axis in mitochondrial quality control. *Cell Stress* **2**, 1–3.

Supporting information

Additional supporting information may be found online in the Supporting Information section at the end of the article.

Fig. S1. shRNA-mediated depletion of SIRT4 in HEK293 cells.

Fig. S2. $CoCl_2$ treatment of HEK293-eGFP cells does not lead to downregulation of eGFP levels.

Fig. S3. Stabilization of SIRT4(H161Y) and SIRT4 (DN28) mutants by treatment with the proteasome inhibitor MG132.

Fig. S4. Flow cytometry-based analysis of expression of SIRT4 and SIRT4 mutants.

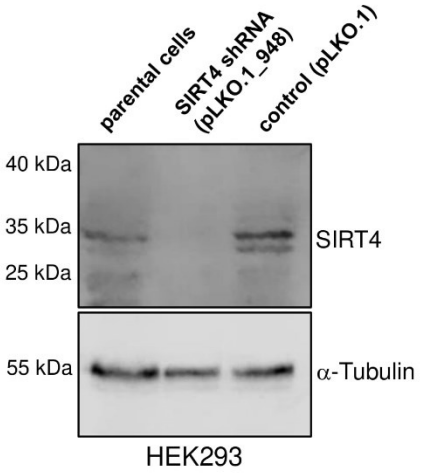

Figure S1. shRNA-mediated depletion of SIRT4 in HEK293 cells. HEK293 cell lines were generated which either express the control pLKO.1 vector or pLKO.1_948 that targets the human SIRT4 mRNA. Parental and transgenic cell lines were subjected to immunoblot analysis using a SIRT4 specific antibody.

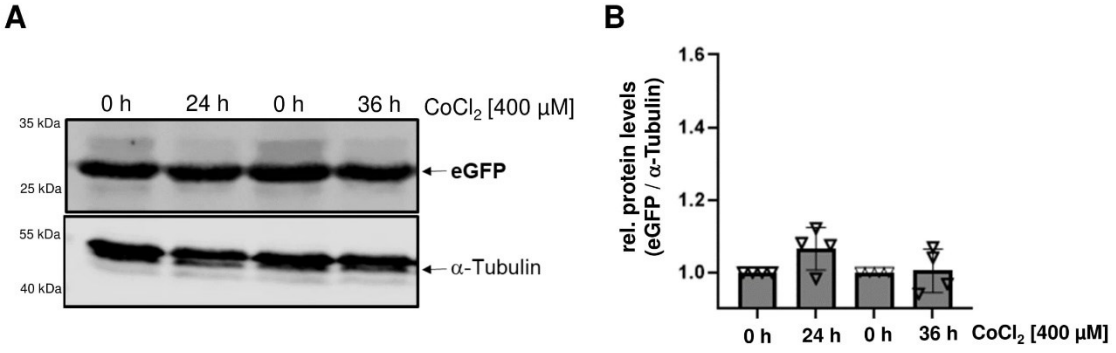

Figure S2. $CoCl_2$ treatment of HEK293-eGFP cells does not lead to downregulation of eGFP levels. (**A**) HEK293 cells stably expressing eGFP were subjected to $CoCl_2$ treatment for 24 h and 36 h followed by immunoblot analysis. (**B**) Relative quantification of eGFP immunoblot signals was performed using ImageJ based densitometric evaluation and α-Tubulin levels as loading control. To test statistical significances, a One-Way ANOVA test followed by Tukey´s Test was employed (n=4; mean ± S.D.).

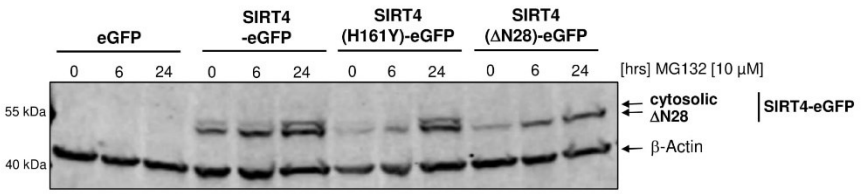

Figure S3. Stabilization of SIRT4(H161Y) and SIRT4(ΔN28) mutants by treatment with the proteasome inhibitor MG132. HEK293 cell lines expressing eGFP, SIRT4-eGFP, the catalytically inactive mutant H161Y, or the N-terminal deletion mutant SIRT4(ΔN28) that does not translocate into mitochondria, were subjected to MG132 treatment for 6 h and 24 h followed by immunoblot analysis of the respective SIRT4-eGFP/mutant SIRT4-eGFP levels. β-Actin staining served as loading control.

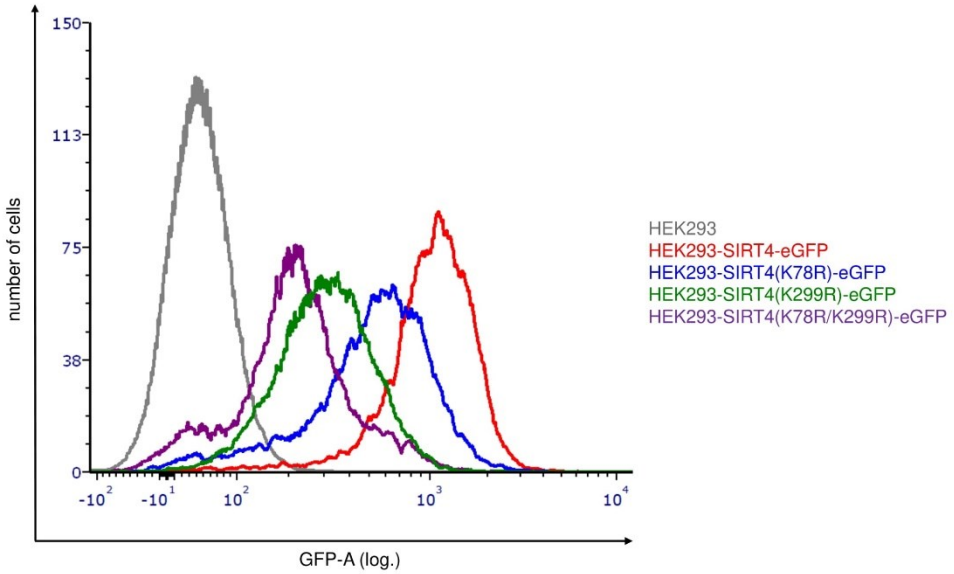

Figure S4. Flow cytometry-based analysis of expression of SIRT4 and SIRT4 mutants. Parental HEK293 cells as negative control and HEK293 cell lines stably expressing SIRT4-eGFP or SIRT4 mutants thereof were subjected to flow cytometry-based (GFP-A) expression analysis.

Chapter VI. SOS1 Delins Identified in Extracranial AVM Expand Genotypic Landscape: Implications for MAPK Hyperactivation and Targeted Inhibitor Efficacy

Authors: **Mehrnaz Mehrabipour***, Friedrich Kapp, Radovan Dvorsky, Annegret Holm, Mohammad R. Ahmadian and Whitney Margaret Eng

*: These authors contributed equally to this work.

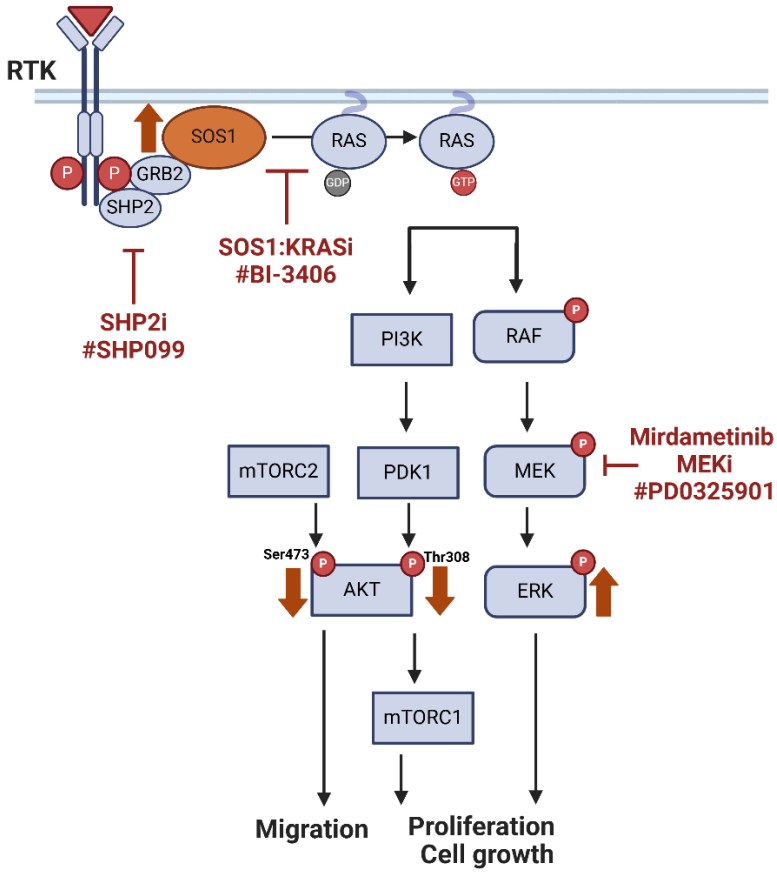

Status:	Ready for submission
Journal:	----
JIF:	----
Contribution:	50% Responsible for cloning patient mutant SOS1 constructs, performing downstream signaling analysis, evaluating the effects of drug treatments, conducting purification and RAS pull-down assays, creating figures, and preparing first draft.

SOS1 Delins Identified in Extracranial AVM Expand Genotypic Landscape: Implications for MAPK Hyperactivation and Targeted Inhibitor Efficacy

Mehrnaz Mehrabipour[1], Friedrich Kapp[2], Radovan Dvorsky[1], Annegret Holm[3], Mohammad R. Ahmadian[1@] and Whitney Margaret Eng[4@]

[1]Institute of Biochemistry and Molecular Biology II, Medical Faculty and University Hospital Düsseldorf, Heinrich Heine University Düsseldorf, Universitätsstrasse 1, 40225 Düsseldorf, Germany
[2]Division of Pediatric Hematology and Oncology, Department of Pediatrics and Adolescent Medicine, Medical Center-University of Freiburg, Faculty of Medicine, University of Freiburg, VASCERN VASCA European Reference Centre, 79106 Freiburg, Germany
[3]Vascular Biology Program, Department of Surgery, Boston Children's Hospital, Seattle, WA, USA
[4]Division of Hematology/Oncology, Seattle Children's Hospital, Boston, MA, USA
[@]Corresponding authors: reza.ahmadian@hhu.de; Whitney.Eng@seattlechildrens.org

Abstract

Arteriovenous malformations (AVMs) are high-flow vascular abnormalities that can cause recurrent bleeding, varying widely in complexity and severity. In our study, using ultra-deep sequencing, we identified new somatic SOS1 delins variants in the AVM tissues of three patients. SOS1 (Son of Sevenless homolog 1), encodes a protein that acts as a guanine nucleotide exchange factor (GEF) for RAS proteins, which are crucial in regulating the RAS-MAPK signaling pathway. Our study represents the first biochemical analysis of AVM-associated SOS1 mutations by introducing variants into HEK293T cells, revealing that these mutations lead to aberrant GEF activity of SOS1, which results in elevated RAS-GTP levels and subsequent hyperactivation of the downstream RAS-MAPK signaling pathway, as evidenced by increased p-ERK levels. These SOS1 variants notably impair AKT activation by reducing phosphorylation at T308, a critical site for its initial activation, and at S473, which is essential for full activation. Moreover, therapeutic potentials by assessing the efficacy of various inhibitors: SHP2i (SHP099), KRAS:SOS1 inhibitor (BI-3406), and MEK inhibitor (PD0325901) were explored all of which demonstrated significant reductions in p-ERK levels. In particular, the MEK inhibitor Trametinib led to a substantial reduction in bleeding and AVM size in two of the patients. These results point to SOS1's involvement in AVM pathogenesis and highlight the potential for targeted therapies in future clinical trials.

Introduction

Arteriovenous malformations (AVMs) are fast-flow vascular anomalies characterized by abnormal blood shunting that bypasses the capillary network. This disruption leads to tissue ischemia, ulceration, and frequent bleeding, making AVMs both progressive and resistant to conventional treatments [1]. Most AVMs are sporadic and primarily involve activation of the RAS-MAPK pathway, while rare familial cases affect the PI3K-AKT pathway [2, 3]. Despite the known involvement of somatic mutations in components of the RAS-MAPK pathway, such as HRAS [4], KRAS, BRAF [5], MEK1 (MAP2K1) [6], and RASA1 [7, 8], the identification of a definitive causative variant remains challenging, thus making genotype-phenotype correlation elusive. In these cases, identifying optimal targeted medical therapy can be difficult. We identified novel somatic mutations in the SOS1 gene in patients with complex extracranial AVMs using Oncopanel, a next-generation sequencing tool that evaluates 447 cancer-associated genes. SOS1 functions as a guanine nucleotide exchange factor (GEF), facilitating the activation of RAS proteins from their inactive

GDP-bound state to their active GTP-bound form, which is crucial for MAPK pathway signaling [9]. Although SOS1 has been linked to various RASopathies, including Noonan Syndrome (NS) [10], Hereditary Gingival Fibromatosis-1 (HGF-1) [11], Costello Syndrome (CS) [12], and Leopard Syndrome (LPRD), and is involved in several cancers [13], its role in AVMs has not been previously documented.

Our findings reveal that SOS1 variants lead to aberrant GEF activity, resulting in elevated RAS-GTP levels and hyperactivation of the downstream MAPK signaling pathway, as indicated by increased p-ERK levels. These SOS1 mutations notably diminished AKT phosphorylation at T308 and caused a significant reduction at S473, collectively impairing AKT activation. We also assessed the therapeutic potential of targeted inhibitors: SHP2i (SHP099), KRAS:SOS1 inhibitor (BI-3406), and MEK inhibitor (PD0325901). All inhibitors demonstrated significant reductions in p-ERK levels *in vitro*. Particularly, the oral MEK inhibitor Trametinib showed notable clinical benefits, including a substantial reduction in bleeding in two patients. Our report expands the genetic landscape of extracranial AVMs and describes the clinical features, treatment approaches, and characterization of SOS1 delins.

Results

Clinical Manifestations of Novel SOS1 Delins Variants in AVM Tissue from Three Patients

Using Oncopanel, a targeted next-generation sequencing test evaluating 447 genes implicated in cancer, we identified somatic mutations in the SOS1 gene in patients with complex extracranial AVM. We report clinical features (Figure 1), treatment approach, and response to targeted therapy with the oral MEK inhibitor Trametinib in these patients.

Patient one was an 18-year-old male who presented with AVM affecting his right cheek and jaw, characterized by marked redness and swelling, along with frequent bleeding episodes. Genetic analysis revealed a novel SOS1 variant, c.1306delins46, with a variant allele frequency (VAF) of 5.6% and sequencing coverage of 312x. From ages 1 to 9, the patient experienced recurrent gingival bleeding, necessitating seven embolization procedures. At age 13, he required another embolization due to a large bleed, which led to a tracheostomy. Propranolol treatment (1.5 mg/kg/day) was introduced, which improved the frequency of bleeding but did not prevent recurrent episodes. At age 14, the patient underwent surgical debulking with laser, reconstruction of the left temporomandibular joint (TMJ), and sclerotherapy. Despite these interventions, he faced a significant oropharyngeal hemorrhage at age 15, requiring emergent ligation and embolization. The patient was treated with Trametinib at a dosage of 1mg orally daily, which led to a noticeable reduction in swelling and bleeding episodes. However, the treatment was associated with side effects, including acne, rash, and swelling of the hands.

The second patient was a 25-year-old female who exhibited an AVM in the left jaw and temporomandibular joint, experiencing frequent bleeding episodes. The SOS1 variant identified was harboring c.1457_1459delins33 mutation with a VAF of 12% and unspecified sequencing coverage. Over the years, the patient has undergone a series of treatments: at age 8, she had an attempted operative resection; between ages 10 and 11, she underwent six embolizations; from ages 16 to 21, she received sclerotherapy, embolization, and cryoablation in five separate procedures. At age 21, she had temporomandibular joint arthroscopy and arthrocentesis, CO2 laser treatment to a neck scar, and an attempted transection of the right mandibular nerve. At age 22, she continued with sclerotherapy and CO2 laser treatment to her neck and chin. Further treatments at age 23 included additional sclerotherapy and embolization, and at age 24, she had

an excisional biopsy and release of a neck contracture. Currently, she is being treated with Trametinib at a daily oral dosage of 1.5 mg, which has successfully reduced the frequency of her bleeding episodes. However, this medication has also led to side effects, including acne and rash. Patient three was a 28-year-old male who had an extensive AVM involving the right pelvis, gluteal region, and lower extremity, accompanied by significant lymphedema of the scrotum and a non-healing ulcer on the hip and leg. The patient also experienced recurrent bleeding episodes with a hemoglobin nadir of 5.5 ng/mL and suffered a life-threatening hemorrhage following a wound debridement of the hip wound. His condition has necessitated multiple transfusions, and frequent admissions to the ICU, and has been complicated by continued bleeding, chronic anemia, and frequent infections with multi-drug resistant organisms, resulting in a very poor quality of life. The genetic variant identified was SOS1 c.1465_1466ins39 with a VAF of 10.0% and sequencing coverage of 179x. Treatment with Trametinib at 0.5mg orally daily was initiated but had to be discontinued due to the development of significant lymphedema.

Functional Domains of SOS1 Affected in delins

The variant identified in patient1, delins1, resulted in the replacement of G^{1306} with a 46-nucleotide sequence (CATTGGACAGTGTTGTTCAGAAGAATATTGATGGTTGGGAGGGAAA), leading to the deletion of amino acid D^{436} and the insertion of a 16-amino acid sequence HWTVLFRRILMVGREN, situated near the SOS1-PH domain after the DH domain. In Patient 2, the delins2 variant replaced G^{1456}-A^{1461} with a 33-nucleotide sequence (GTCTTAAAGAAAAGTTTTTTTAAAAGAAAGCAA), resulting in the deletion of A^{486}-E^{487} and the insertion of an 11-amino acid sequence VLKKSFFKRKQ, located within the PH domain. In Patient 3, the delins3 variant caused the addition of 39 nucleotides (TTAAAGAAAAGTTTTTAAGAAAAGTTTTAAAGAAAAAAA) between C^{1465}-G^{1466}, leading to the deletion of R^{489} and the insertion of a 14-amino acid sequence LKEKFLRKVLKKKS, also located within the PH domain. Delins mutations include alterations that are predicted to promote conformational rearrangements of the PH domains, as illustrated in Figure 2.

SOS1 Mutations Associated with AVM Elevate p-ERK Levels

To further investigate the impact of three distinct SOS1 delins on RAS-triggered downstream signaling, we analyzed the phosphorylation levels of key downstream effectors in the MAPK and PI3K/AKT pathways, including p-ERK, p-AKT(T308), and p-AKT(S473). p-AKT(T308) is phosphorylated by PDK1, while p-AKT(S473) is regulated by mTORC2, which is crucial for the full activation of AKT (Figure S1). The signaling outcomes of the SOS1 delins variants in P1, P2, and P3 were compared to the wild-type SOS1 full-length protein in HEK293 cells. As shown in Figures 3A and 3B, increased levels of p-ERK were observed in all SOS1 mutants compared to the wild-type SOS1 full-length protein. In contrast, SOS1 variants led to a decrease in the phosphorylation of AKT at T308 and S473 (Figure 3).

SOS1 Mutants Exhibit Gain-of-Function Effects Leading to Increased RAS Activation

Next, we assessed whether the expression of these SOS1 mutants altered MAPK signal transduction through RAS. A pulldown assay was performed to isolate GTP-bound RAS (active RAS) using GST-RAF-RBD. HEK293 cells were transfected with either wild-type SOS1 full-length protein or one of the three mutant SOS1 variants (P1, P2, and P3). After 48 hours, cells were lysed, and active RAS was isolated using a GST-RAF-RBD affinity probe. The levels of active

RAS were analyzed by Western blot. Additionally, the phosphorylation levels of p-ERK for each variant were compared to wild-type SOS1. The results showed that the SOS1 mutants caused essentially constitutive RAS activation compared to the wild-type (Figure 4A and 4B). Furthermore, the extent of RAS activation was positively correlated with ERK activation for each SOS1 mutant (Figures 4A and 4C).

Pharmacological Inhibition Reverses ERK Hyperphosphorylation Induced by SOS1 Delins

Additionally, to investigate the effect of inhibitors on downstream signaling mediated by SOS1 variants, we employed three inhibitors targeting different stages of the signaling pathway. The first inhibitor, SHP099, targets SHP2 upstream of SOS1. The second inhibitor, BI-3406, selectively inhibits the interaction between KRAS and SOS1, acting at the level of SOS1. The third inhibitor, PD0325901, known as Mirdametinib MEK inhibitor, acts downstream in the pathway by inhibiting MEK (Figure S1). All delins showed a notable decrease in p-ERK phosphorylation levels when treated with SHP2, SOS1-KRAS, and MEK inhibitors, as indicated by statistical significance (Figures 5A and 5B). The results for the empty vector (EV) and wild-type SOS1 (SOS1 wt) upon inhibitor treatment are shown in Figure S2.

Conclusion

Our study identifies novel somatic SOS1 mutations in extracranial AVMs, offering new insights into their genetic basis. By demonstrating that these mutations lead to aberrant SOS1 activity and hyperactivation of the RAS-MAPK pathway, we highlight a crucial mechanism in AVM pathogenesis. We detail the efficacy of three inhibitors: SHP099 (targeting SHP2), BI-3406 (blocking KRAS-SOS1 interaction), and PD0325901 (Mirdametinib, a MEK inhibitor) in attenuating MAPK activation. Moreover, we report clinical features, treatment approach, and response to targeted therapy with the oral MEK inhibitor Trametinib in these patients. The effectiveness of the oral MEK inhibitor Trametinib in reducing bleeding in two patients as well as three additional in vitro analyzed inhibitors demonstrates their potential as treatment strategies. As molecular diagnostics improve and targeted therapeutics for vascular anomalies expand, it will be important for clinicians to consider SOS1 as a potential causative gene for AVM patients, as identifying these mutations may have important diagnostic and therapeutic implications.

Methods

Cell Culture, Transfection, and Drug Treatment

Human embryonic kidney 293 (HEK293) cells were cultured by seeding 1,000,000 cells in 10 cm cell culture plates containing Dulbecco's Modified Eagle Medium (DMEM) supplemented with 10% fetal bovine serum (FBS; Gibco) and 1% Penicillin/Streptomycin (Genaxxon). Cells were allowed to adhere for 24 hours before transfection. Upon reaching approximately 70% confluency, cells were transfected using Turbofect reagent (Thermo Fisher Scientific). The transfection included HA-tagged SOS1 wild-type (pCMV construct from addgene plasmid #32920), along with delins1, delins2, and delins3 variants that were cloned into pCMV constructs, alongside an empty vector (EV) serving as a negative control. The medium was refreshed the next day at the 24-hour time point with 10μM of SHP2 inhibitor (SHP099; Selleckchem #S6388), 10μM KRAS-SOS1 inhibitor (BI-3406; MedChemExpress #HY-125817), and 1μM Mirdametinib MEK inhibitor (PD0325901; Selleckchem #S1036). Additionally, DMSO was included as a control, with a final concentration of almost 0.1%.

Cell Lysis and Protein Extraction

At 48 hours post-transfection, cells were washed with ice-cold phosphate-buffered saline (PBS) and then lysed in ice-cold lysis buffer for 5 minutes. The lysis buffer composition included 50 mM Tris/HCl (pH 7.4), 100 mM NaCl, 2 mM MgCl2, 10% glycerol, 20 mM ß-glycerophosphate, 1 mM Na3VO4, 1% IGPAL (Thermo Fisher Scientific), and 1x protease inhibitor cocktail (Roche). The cell lysates were cleared by centrifugation at 20,000 x g at 4°C for 5 minutes. Protein concentrations in the lysates were determined using the Bradford assay.

RAS Activation Assay

The RAS-binding domain (RBD) of CRAF (amino acids 55-131) was cloned into the pGEX-4T1 vector (BioCat GmbH) and transformed into E. coli. The expressed GST-fused RAF-RBD proteins were isolated from bacterial lysates using glutathione–agarose beads (Macherey-Nagel). For the RAS activation assay, the GST-fused RAF-RBD beads were used to pull down GTP-bound RAS (active RAS) from total cell lysates of HEK293 cells transfected with HA-SOS1-wt, HA-SOS1-P1, HA-SOS1-P2, and HA-SOS1-P3. The lysates were incubated with the beads for 1 hour at 4°C under rotation, followed by centrifugation at 500g. The beads were washed three times with ice-cold buffer (30 mM Tris–HCl, 150 mM NaCl, 5 mM MgCl2, and 3 mM DTT). Protein samples were mixed with Laemmli loading buffer and analyzed by SDS-PAGE, followed by immunoblotting to assess the levels of active RAS.

SDS-PAGE and Immunoblotting

1x Laemmli sample buffer was added to the protein samples, and the samples were subjected to sodium SDS-PAGE using 12.5% polyacrylamide gels. Following electrophoresis, the separated proteins were transferred to a membrane for immunoblotting.

Antibodies and Detection

Immunoblotting was performed using the following primary antibodies: anti-GST(own antibody), anti-ERK (1/2) (1:1000; #9102, Cell Signaling), anti-p-ERK (1/2) (1:1000; #4370, Cell Signaling), anti-Vinculin (1:1000; #V9131, Sigma), anti-AKT (1:1000; #2920, Cell Signaling), anti-p-AKT(T308) (1:500; #2965, Cell Signaling), anti-p-AKT(S473) (1:1000; #4060, Cell Signaling). Secondary antibodies used for detection: anti-mouse 700 nm: IRDye #926-32213, and anti-rabbit 800 nm: IRDye #926-6807. The protein bands were visualized using an LI-COR imaging system. All experiments were carried out in triplicate, and statistical analyses were performed to assess the significance of the results.

Statistical Evaluation of Downstream Signaling Pathways in Response to SOS1 Delins

Immunoblot protein signals were quantified using Image Studio Lite Version 5.2 software. Signal intensities were normalized to loading controls, and for accurate downstream signaling comparison, data were further normalized to total SOS1 expression across samples. Results are presented as mean ± S.D. One-way ANOVA analysis was conducted with Origin data analysis software (OriginLab-2021b). Significance was denoted as follows: *, $p \leq 0.05$; **, $p \leq 0.01$; ***, $p \leq 0.001$.

References

1. Liu, A.S., et al., *Extracranial arteriovenous malformations: natural progression and recurrence after treatment.* Plast Reconstr Surg, 2010. **125**(4): p. 1185-1194.
2. Barbosa Do Prado, L., et al., *Recent Advances in Basic Research for Brain Arteriovenous Malformation.* International Journal of Molecular Sciences, 2019. **20**(21): p. 5324.
3. Maddy, K., et al., *An updated review on the genetics of arteriovenous malformations.* Gene & protein in disease, 2023. **2**(2): p. 0312.
4. Konczyk, D.J., et al., *Arteriovenous malformation associated with a HRAS mutation.* Hum Genet, 2019. **138**(11-12): p. 1419-1421.
5. Hong, T., et al., *High prevalence of KRAS/BRAF somatic mutations in brain and spinal cord arteriovenous malformations.* Brain, 2019. **142**(1): p. 23-34.
6. Couto, J.A., et al., *Somatic MAP2K1 Mutations Are Associated with Extracranial Arteriovenous Malformation.* The American Journal of Human Genetics, 2017. **100**(3): p. 546-554.
7. Lapinski, P.E., et al., *Somatic second hit mutation of RASA1 in vascular endothelial cells in capillary malformation-arteriovenous malformation.* Eur J Med Genet, 2018. **61**(1): p. 11-16.
8. Sánchez-Espino, L.F., et al., *Single dominant lesion in capillary malformation-arteriovenous malformation (CM-AVM) syndrome.* Pediatric Dermatology. **n/a**(n/a).
9. Jun, J.E., I. Rubio, and J.P. Roose, *Regulation of ras exchange factors and cellular localization of ras activation by lipid messengers in T cells.* Frontiers in immunology, 2013. **4**: p. 239.
10. Lepri, F., et al., *SOS1 mutations in Noonan syndrome: molecular spectrum, structural insights on pathogenic effects, and genotype–phenotype correlations.* Human mutation, 2011. **32**(7): p. 760-772.
11. Strzelec, K., et al., *Clinics and genetic background of hereditary gingival fibromatosis.* Orphanet J Rare Dis, 2021. **16**(1): p. 492.
12. Tumurkhuu, M., et al., *A novel SOS1 mutation in Costello/CFC syndrome affects signaling in both RAS and PI3K pathways.* J Recept Signal Transduct Res, 2013. **33**(2): p. 124-8.
13. Baltanás, F.C., et al., *SOS GEFs in health and disease.* Biochimica et Biophysica Acta (BBA)-Reviews on Cancer, 2020. **1874**(2): p. 188445.

Figure Legends

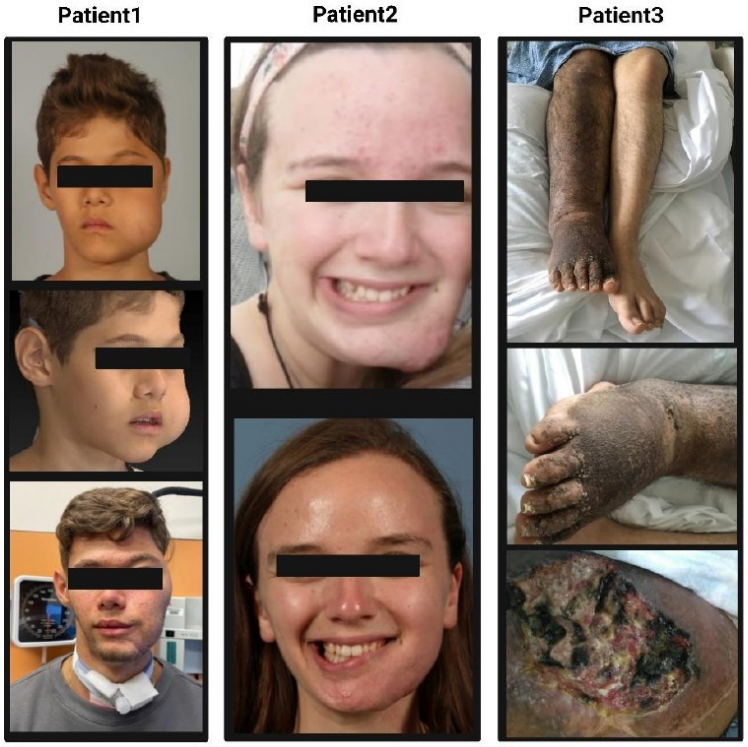

Figure 1. clinical presentation of AVM patients with SOS1 delins. This figure illustrates the clinical presentations of three patients with novel SOS1 delins variants identified in AVM. Patient 1, an 18-year-old male, had AVM affecting the right cheek and jaw with significant swelling and bleeding. Patient 2, a 25-year-old female, presented with AVM in the left jaw and temporomandibular joint, also experiencing frequent bleeding episodes. Patient 3, a 28-year-old male, had an extensive AVM involving the right pelvis, gluteal region, and lower extremity, complicated by severe lymphedema and non-healing ulcers.

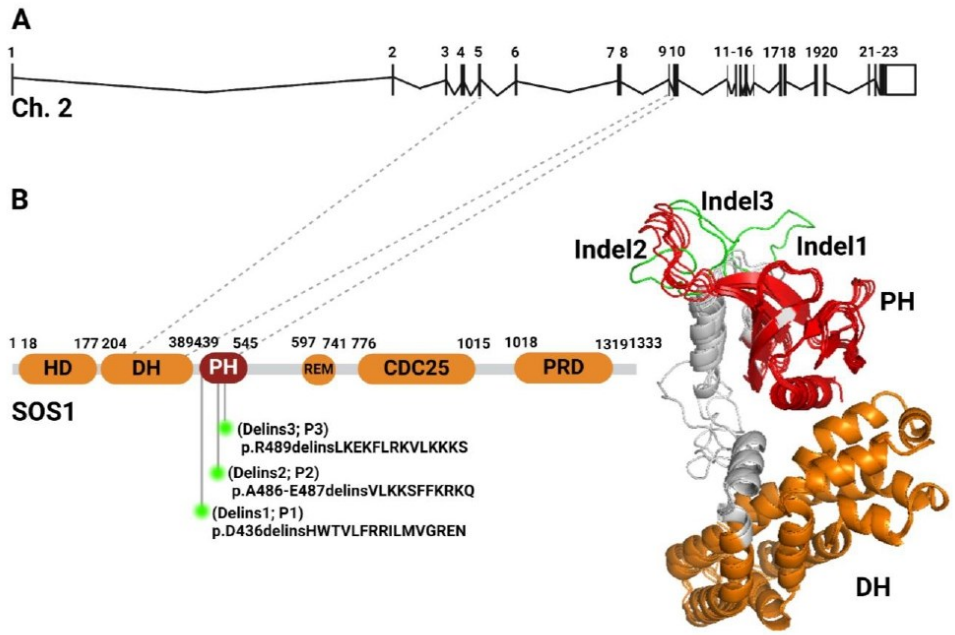

Figure 2. SOS1 genomic structure, domain organization, and location of residues altered in AVM. (A) Genomic structure and intron/exon distribution of the human SOS1 gene, with coding exons depicted as solid vertical boxes and non-coding exons as empty boxes. (B) Domain architecture of the SOS1 protein, including the HD (Histone-like Domain), DH (DBL Homology), PH (Pleckstrin Homology), REM (RAS Exchange Motif), CDC25 (Cell Division Cycle 25), and PRD (Proline-Rich domain). Additionally, a 3D structural alignment of the wild-type SOS1 with three mutants is presented, marking the locations of each delins in green to show their specific positions and potential impacts on protein structure.

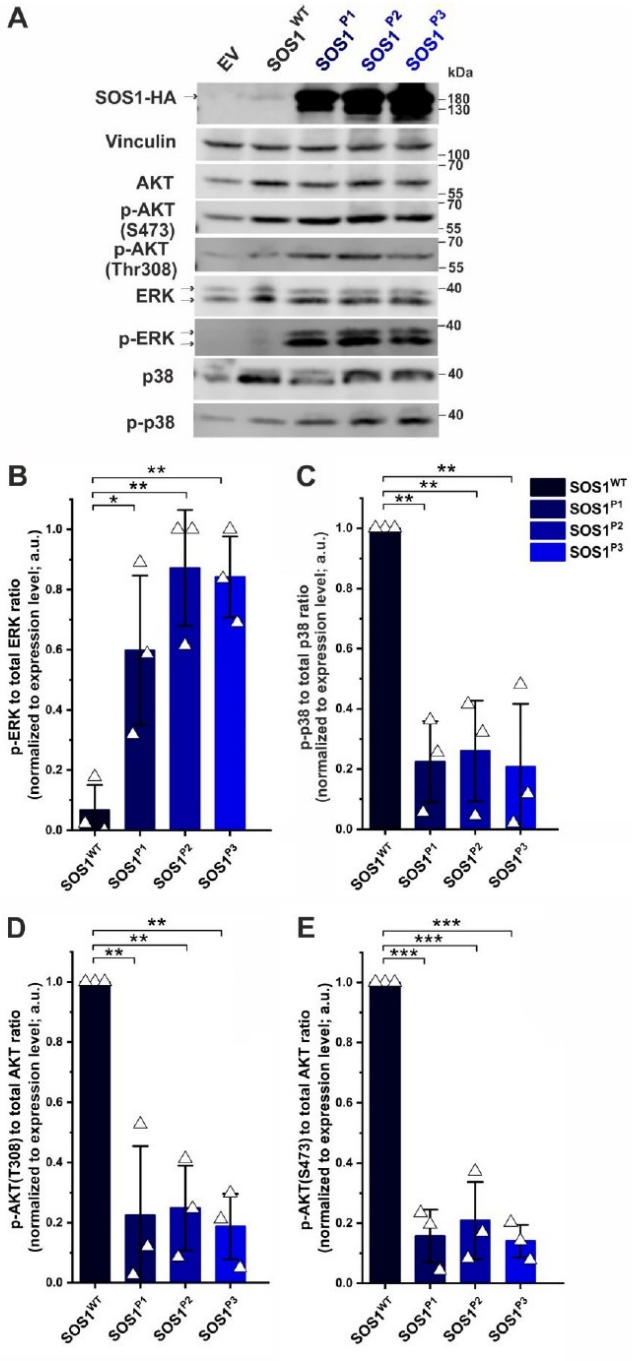
A
EV
SOS1 WT
SOS1 P1
SOS1 P2
SOS1 P3
kDa
SOS1-HA
180
130
Vinculin
100
AKT
70
55
p-AKT (S473)
70
55
p-AKT (Thr308)
70
55
ERK
40
p-ERK
40
p38
40
p-p38
40
B
p-ERK to total ERK ratio (normalized to expression level; a.u.)
C
p-p38 to total p38 ratio (normalized to expression level; a.u.)
SOS1WT
SOS1P1
SOS1P2
SOS1P3
D
p-AKT(T308) to total AKT ratio (normalized to expression level; a.u.)
E
p-AKT(S473) to total AKT ratio (normalized to expression level; a.u.)

9

Figure 3. Downstream signaling effects of SOS1 delins. (A) Immunoblot analysis of downstream signaling pathways in HEK293 cells transfected with empty vector (EV), HA-tagged SOS1 wild-type (SOS1-wt), P1, P2, and P3 variants. (B) Increased levels of phosphorylated ERK (p-ERK) were observed across all variants. (C) Phosphorylation levels of p38 showed a significant decrease difference between wild-type and delins. (D and E) Phosphorylation of AKT at T308 and S473 exhibited a significant decrease in all mutants compared to wild-type SOS1. Densitometric immunoblot analysis of the levels of p-ERK, p-AKT(T308), and p-AKT(S473) were subjected to statistical one-way ANOVA (mean ± S.D.; *P < 0.05; **P < 0.01; ***P < 0.001).

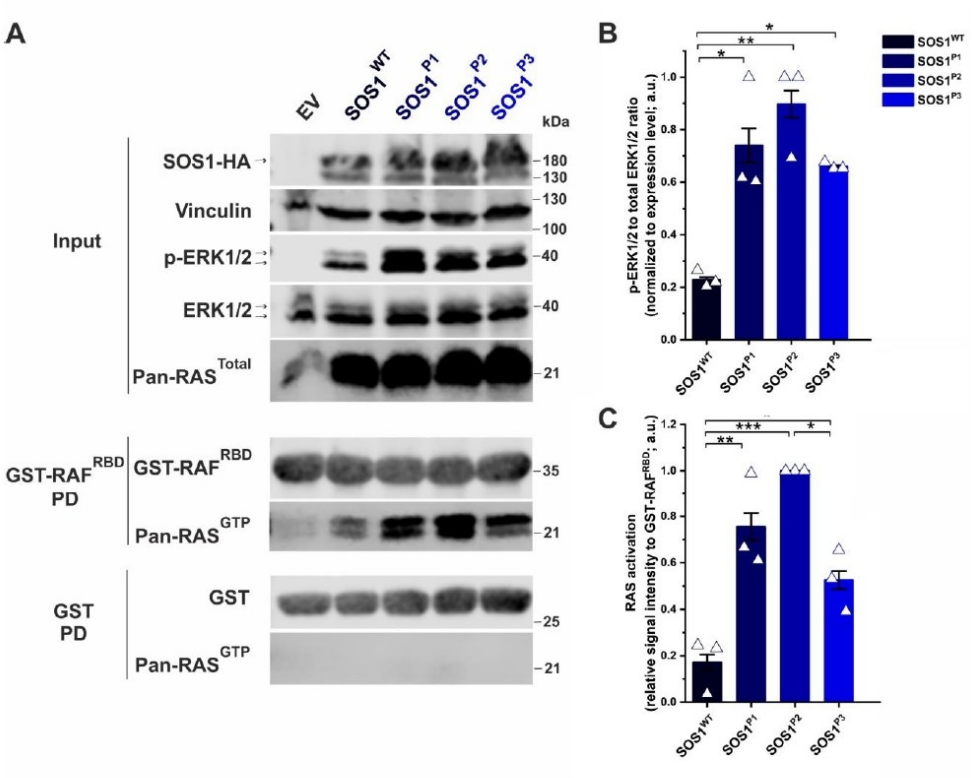

Figure 4. RAS activation assay. (A) HEK293 cells were transfected with full-length HA-tagged SOS1 wild-type (SOS1-wt), P1, P2, and P3. The binding of active RAS to GST-RAF-RBD was assessed to evaluate the effect of SOS1 variants on RAS-mediated downstream activation. RAS activation levels in cells expressing mutant SOS1 variants were compared to those in cells expressing wild-type SOS1, based on three independent replicates. A significant increase in RAS activation was observed for all mutant variants compared to the wild-type. Correspondingly, p-ERK levels also increased, showing a similar correlation with RAS activation. (B) and (C) Densitometric analysis of immunoblots for RAS activation and p-ERK levels was conducted. Statistical significance was determined using one-way ANOVA (mean ± S.D.; *P < 0.05; **P < 0.01; ***P < 0.001).

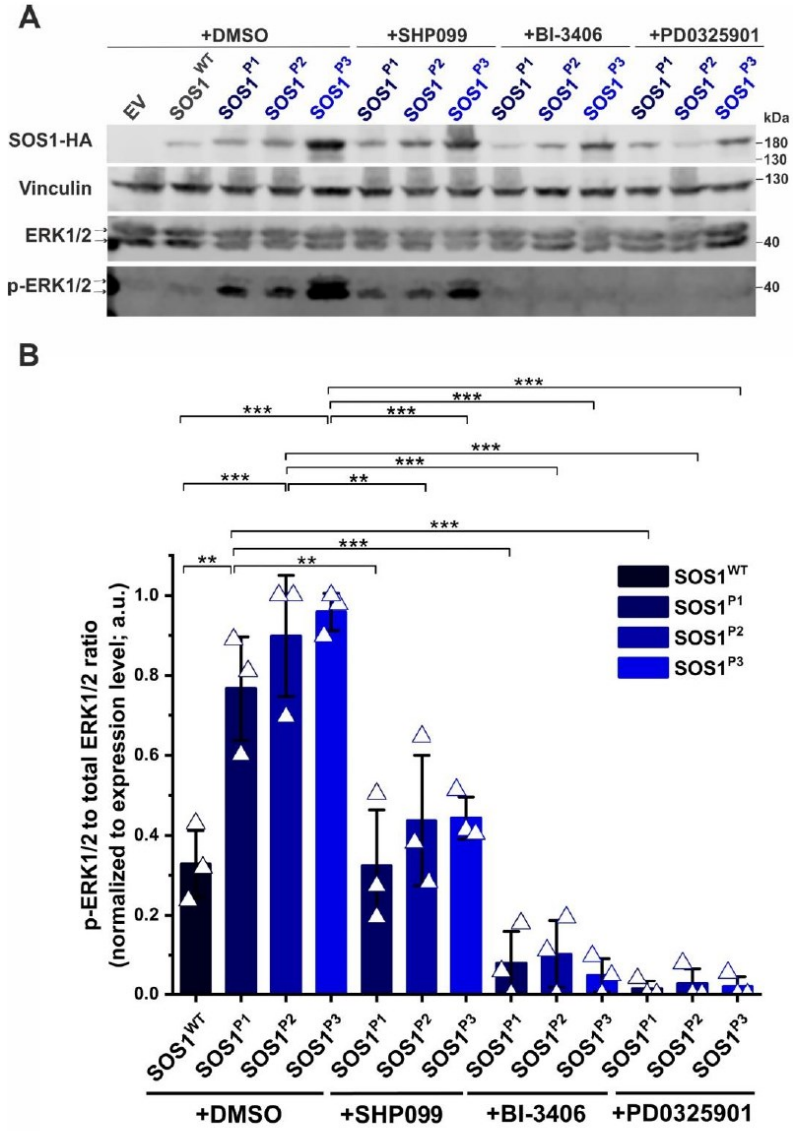

Figure 5. Impact of Inhibitors on p-ERK Phosphorylation in SOS1 Mutants. (A) HEK293 cells expressing SOS1 delins (P1, P2, and P3) were treated with three inhibitors: SHP099 (targeting SHP2), BI-3406 (blocking KRAS-SOS1 interaction), and PD0325901 (Mirdametinib, a MEK inhibitor). Additionally, cells transfected with empty vector (EV), HA-tagged SOS1 wild-type (SOS1 wt), P1, P2, and P3 variants were treated with DMSO as control. p-ERK phosphorylation levels were measured post-treatment. Significant reductions in p-ERK phosphorylation were observed for all SOS1 delins variants with each inhibitor, indicating effective modulation of ERK signaling (B). Densitometric analysis of immunoblots was performed, with data analyzed by one-way ANOVA (mean ± S.D.; *P < 0.05; **P < 0.01; ***P < 0.001).

Supporting Information

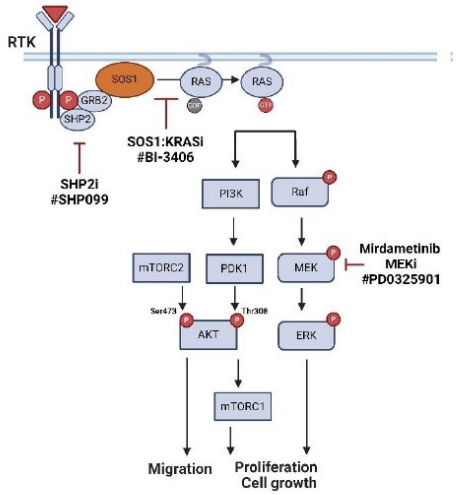

Figure S1. SOS signaling pathway. The figure illustrates the downstream signaling pathways activated by SOS1-RAS, highlighting the MAPK and PI3K-AKT pathways. It shows the phosphorylation of key signaling components: p-ERK, p-AKT(T308) (essential for partial AKT activation and mediated by PDK1), and p-AKT(S473) (crucial for full AKT activation and mediated by mTORC2). The pathways are depicted with red blunt arrows indicating the targets of the inhibitors used in this study: SHP099 (which inhibits SHP2 upstream of SOS1), BI-3406 (which blocks the KRAS-SOS1 interaction), and PD0325901 (Mirdametinib, a MEK inhibitor acting downstream).

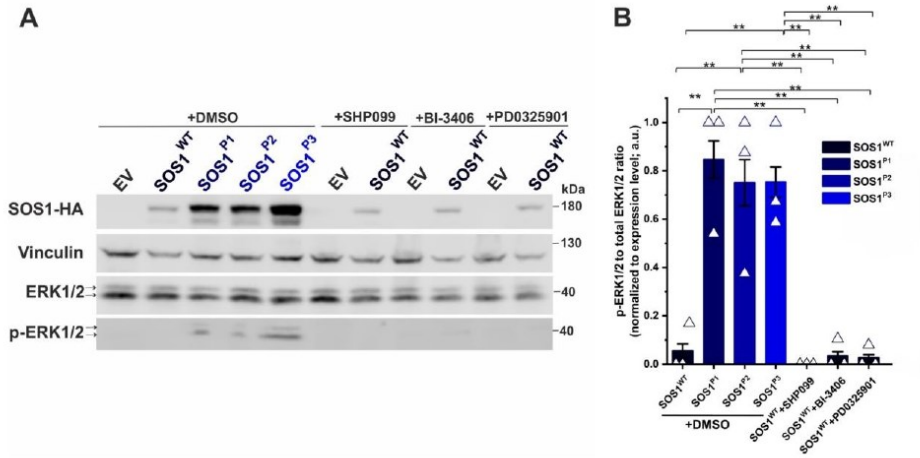

Figure S2. Impact of Inhibitors on p-ERK Phosphorylation in EV and SOS1-wt (A) HEK293 cells expressing SOS1 wild type and delins (P1, P2, and P3) were treated with DMSO as a control. Additionally, the effects of SHP099 (targeting SHP2), BI-3406 (blocking KRAS-SOS1 interaction), and PD0325901 (Mirdametinib, a MEK inhibitor) were analyzed on cells expressing empty vector (EV) and wild-type SOS1 (SOS1-wt) to assess downstream phosphorylation of ERK. p-ERK phosphorylation levels were measured post-treatment. (B) Densitometric analysis of immunoblots was performed, with data analyzed by one-way ANOVA (mean ± S.D.; *P < 0.05; **P < 0.01; ***P < 0.001).

Western Blot Replicates

Source data for Figure 3.

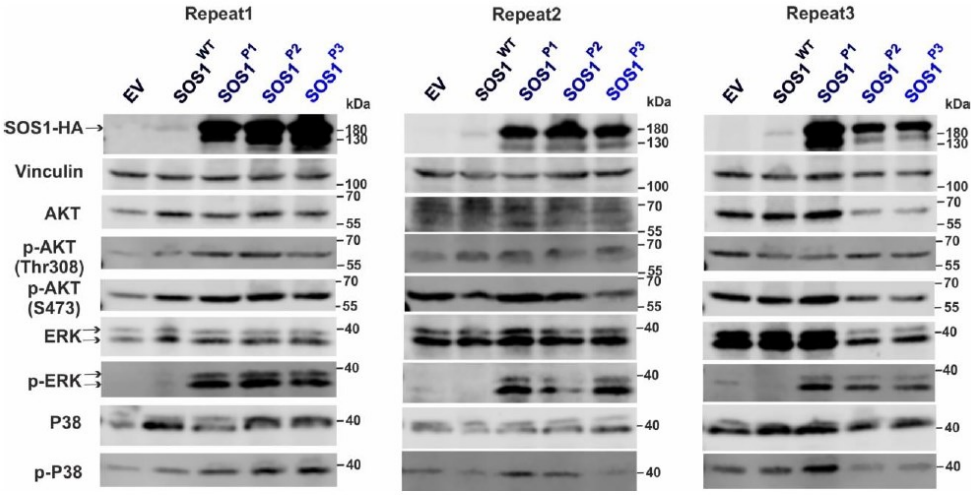

Source data for Figure 4.

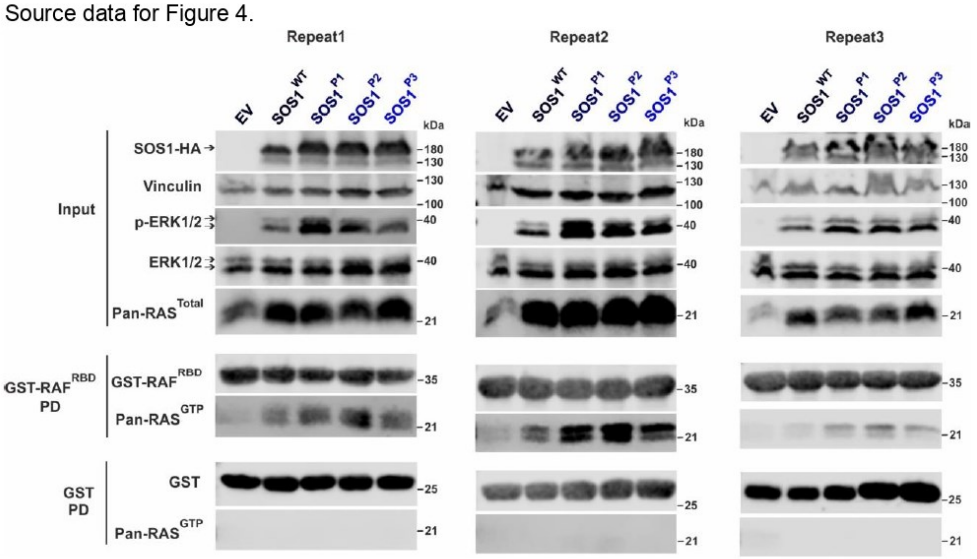

Source data for Figures 5 and S2.

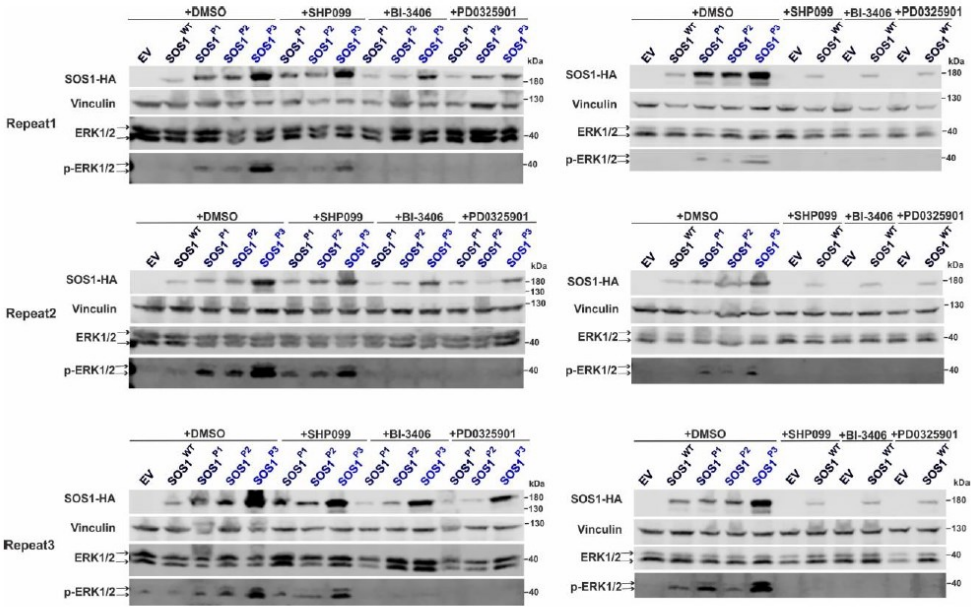

Chapter VII Somatic RIT1 Delins in Arteriovenous Malformations Hyperactivate RAS-MAPK Signaling Amenable to MEK Inhibition

Authors: Friedrich G Kapp*, Farhad Bazgir*, Nagi Mahammadzade*, **Mehrnaz Mehrabipour**, Erik Vassella, Sarah M Bernhard, Yvonne Döring, Annegret Holm, Axel Karow, Caroline Seebauer, Natascha Platz Batista da Silva, Walter A Wohlgemuth, Aviv Oppenheimer, Pia Kröning, Charlotte M Niemeyer, Denny Schanze, Martin Zenker, Whitney Eng, Mohammad R Ahmadian, Iris Baumgartner and Jochen Rössler

*: These authors contributed equally to this work.

DOI: 10.1007/s10456-024-09934-8

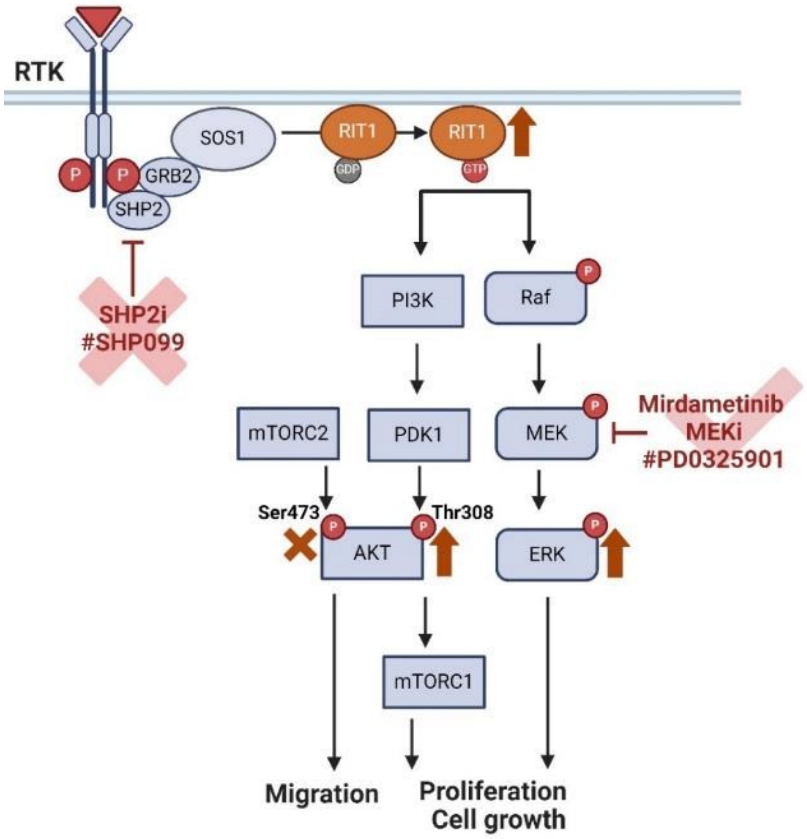

Status:	Published in July 2024
Journal:	Angiogenesis
JIF:	9.2
Contribution:	15% Responsible for performing downstream PI3K-AKT signaling analysis and creating the associated figures.

Angiogenesis
https://doi.org/10.1007/s10456-024-09934-8

ORIGINAL PAPER

Somatic RIT1 delins in arteriovenous malformations hyperactivate RAS-MAPK signaling amenable to MEK inhibition

Friedrich G. Kapp[1] · Farhad Bazgir[2] · Nagi Mahammadzade[1] · Mehrnaz Mehrabipour[2] · Erik Vassella[3] · Sarah M. Bernhard[4,5] · Yvonne Döring[4,5,6] · Annegret Holm[1,7] · Axel Karow[8] · Caroline Seebauer[9] · Natascha Platz Batista da Silva[10] · Walter A. Wohlgemuth[11] · Aviv Oppenheimer[1] · Pia Kröning[12] · Charlotte M. Niemeyer[1] · Denny Schanze[13] · Martin Zenker[13] · Whitney Eng[14] · Mohammad R. Ahmadian[2] · Iris Baumgartner[4,5] · Jochen Rössler[1,15,16]

Received: 19 January 2024 / Accepted: 18 June 2024

Abstract

Arteriovenous malformations (AVM) are benign vascular anomalies prone to pain, bleeding, and progressive growth. AVM are mainly caused by mosaic pathogenic variants of the RAS-MAPK pathway. However, a causative variant is not identified in all patients. Using ultra-deep sequencing, we identified novel somatic *RIT1* delins variants in lesional tissue of three AVM patients. *RIT1* encodes a RAS-like protein that can modulate RAS-MAPK signaling. We expressed *RIT1* variants in HEK293T cells, which led to a strong increase in ERK1/2 phosphorylation. Endothelial-specific mosaic overexpression of *RIT1* delins in zebrafish embryos induced AVM formation, highlighting their functional importance in vascular development. Both ERK1/2 hyperactivation in vitro and AVM formation in vivo could be suppressed by pharmacological MEK inhibition. Treatment with the MEK inhibitor trametinib led to a significant decrease in bleeding episodes and AVM size in one patient. Our findings implicate *RIT1* in AVM formation and provide a rationale for clinical trials with targeted treatments.

Keywords Vascular anomalies · Vascular malformation · Arteriovenous malformation · RIT1 · RAS-MAPK pathway · Trametinib

Abbreviations

AVM	Arteriovenous malformation
CSF	Cerebrospinal fluid
dpf	Days post fertilization
hpf	Hours post fertilization
PTU	1-Phenyl 2-thiourea
ISSVA	International Society for the Study of Vascular Anomalies
MRI	Magnetic resonance imaging
NGS	Next generation sequencing
VP	Ventriculoperitoneal

Friedrich G. Kapp, Farhad Bazgir and Nagi Mahammadzade have contributed equally to this work.

Extended author information available on the last page of the article

Introduction

Vascular anomalies are classified according to the Classification of the International Society for the Study of Vascular Anomalies (ISSVA) and are subdivided into vascular tumors and vascular malformations [1, 2]. While vascular tumors show increased cell proliferation, vascular malformations are thought to represent mainly non-proliferative lesions that originate from errors in vascular development. Most vascular malformations are caused by a somatic mosaic mutation in the affected tissue. Activation of the PI3K-AKT-mTOR pathway are thought to predominate in slow-flow malformations such as venous and lymphatic malformations [3–5], whereas variants activating the RAS-MAPK pathway are typically associated with fast-flow malformations such as AVM [6–9].

Extracranial AVM can occur anywhere in the body, most often in the soft tissue of extremities as well as the head and neck [10, 11]. AVM may become symptomatic with swelling, pain, pulsations, and bleeding. AVM located in the face may lead to major disfigurement and life-threatening

Published online: 05 July 2024

complications [12]. Almost all AVM progress over time [13, 14], which may lead to tissue necrosis, bleeding complications, and hyperdynamic heart failure. Treatment is mainly interventional (embolization) and/or surgical resection; however, invasive therapies can activate the lesion and often lead to relapse [14]. However, the exact pathomechanism of AVM development and progression are poorly understood. Taken together, AVM belongs to the most aggressive vascular anomalies and are often difficult to treat, highlighting the need for novel treatment strategies.

In this project, we identified novel mosaic delins variants in *RIT1* that were found in the lesional tissue of three patients with extracranial AVM. *RIT1* acts as modulator of the RAS-MAPK pathway and has so far not been implicated in the development of AVM. We characterized these variants by assessing their effect on ERK phosphorylation in vitro, on vascular development in vivo in a zebrafish model, and the response to MEK inhibition. We further present data on the off-label use of trametinib in one patient.

Results

Novel *RIT1* delins variants identified in AVM tissue from three patients

To identify underlying genotypic changes, a total of 691 samples of patients with vascular anomalies underwent next generation sequencing at three different centers for vascular anomalies. Out of these 691 samples, approximately 100 were from patients with an AVM. Three patients with an extracranial AVM were found to harbor a *RIT1* mutation.

Patient 1 (P1) was a 3-year-old girl with an AVM of the right face. A capillary anomaly and swelling of the right cheek were noticed at birth (Fig. 1A). A diagnosis of an infantile hemangioma was initially made at an external hospital and propranolol was initiated at one month of age. The lesion did not respond to this therapy and a first episode of epistaxis occurred at 6 months of age, eventually leading to the diagnosis of a facial AVM on magnetic resonance angiography (MRA) (Fig. 1B, C). Following this bleeding event, a first catheter embolization with Onyx was performed. Two additional embolizations followed until the age of 22 months, the last intervention of which was combined with bleomycin electro-sclerotherapy [15]. The lesion did not respond to either therapy and the AVM progressed with intermittent life-threatening bleeding episodes (Online Resource 1). Due to progressive symptoms, the patient was then treated with extensive Onyx embolization of the AVM, and a biopsy was obtained for genetic analysis. These interventions, including the removal of a molar that was rooted within the AVM, alleviated the symptoms only slightly. Due to the nature and course of the disease, a hemimaxillectomy was considered. However, infiltration of the AVM into the orbit made a cure by this very invasive approach seem unlikely. We thus initiated off-label treatment with thalidomide (25 mg per day) when the patient was 2 years of age. Under this treatment—and after the last extensive embolization—the severity of bleeding episodes decreased over the next months before deteriorating again. Genetic testing of the biopsy of affected tissue identified a *RIT1* delins variant (c.246_248delinsCCCTCT p.T83delinsPL (referred to as $RIT1^{P1}$, hereafter)), with a variant allele frequency (VAF) of 3.3%.

Patient 2 (P2) was a 42-year-old man with a first episode of neck pain at the age of 35 years. A continuously growing and pulsating vascular lesion was detected (Fig. 1D). MRA showed an isolated intramuscular AVM connected to the subclavian and the thyrocervical trunk on the right side with disfiguring diffuse muscle involvement including the splenius capitis muscle (Fig. 1E, F). Therapy with sirolimus was initiated but had to be discontinued due to suppurative osteomyelitis of the jaw within 3 weeks. At the age of 39 years, the patient received three direct intraarterial ethanol embolizations at monthly intervals without success. Although the initially dominating nidus of the AVM was completely shut down, there was a massive proliferation of microfistular AV shunts and an increase in tissue volume as a result. One year after embolization, debulking surgery was performed after the situation had stabilized. Histopathology showed typical findings of a diffuse intramuscular microfistular AVM. Ten months later, progression of the AVM was noted again and a combined approach with Onyx embolization and gross total resection was performed. Since then, the patient has been without complaints with stable disease and minimal radiological residuum. A *RIT1* delins variant was identified in the resected tissue (c.242_248delinsTCCCTCT p.E81_T83delinsVPL (referred to as $RIT1^{P2}$, hereafter) with a VAF of 6.0%.

P3 was a 17-year-old girl, who presented with a persistent prominence in the left forearm that was first noted one year before (Fig. 1G). At the time of the initial presentation, there was no associated pain, no functional deficit, no overlying skin changes, and only minimal swelling. An initial ultrasound was notable for a 5.4 cm × 1.1 cm × 4.7 cm intramuscular mass in the left forearm with diffuse internal vascularity seen on Doppler examination. An MRI of the lesion was notable for a solid enhancing mass in the left pronator teres muscle with imaging findings consistent with a solid neoplasm (Fig. 1H). She underwent an IR-guided biopsy of the lesion. Histopathology was consistent with an intramuscular fast-flow vascular anomaly. She was followed for the next two years and had progressive growth of the lesion associated with pain. Given the worsening of her symptoms, she underwent resection of the lesion. There were no complications and she has had minimal pain since. In the resected tissue, a *RIT1* delins variant

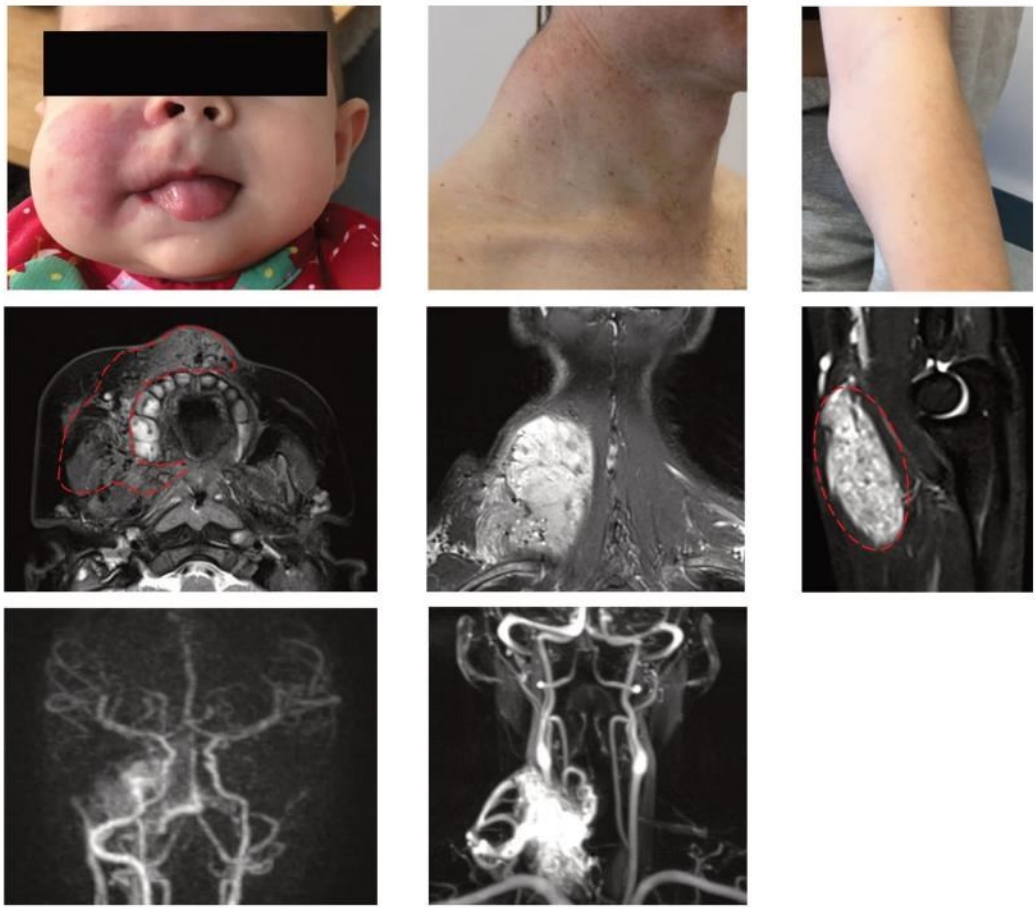

Fig. 1 Three patients with somatic *RIT1* variants identified in AVM tissue. **a** Patient P1 displays a capillary malformation and swelling of the right side of the face. **b** MRI of P1 at the age of 4 months, the image of a transversal T2 TSE sequence, in which an AVM could be detected; the extent of the lesion is labelled with red dashed line indicating soft tissue edema and flow-voids. **c** The MR angiography shows increased perfusion on the right side of the face (left side within the panel). **d** Patient P2 shows a prominent mass of the left cervical/nuchal area. **e** MR imaging (coronal T2 sequence with fat saturation), which shows the hyperintense isolated intramuscular lesion, flow-voids seen within the lesion representing high AVM flow, and disfiguring overgrowth. **f** MR angiography, which shows the large AVM connected to the subclavian and the thyrocervical trunk with multi-chambered central nidus. **g** Clinical aspect of the Patient P3 with swelling on the left forearm, close to the medial side of the elbow. **h** T2W sagittal images demonstrating a well-defined fusiform shaped hyperintense lesion involving the flexor muscle (pronator teres) of the forearm. Flow voids (red dashed line) are seen within the lesion representing arterial blood vessels. *MRI* Magnetic Resonance Imaging

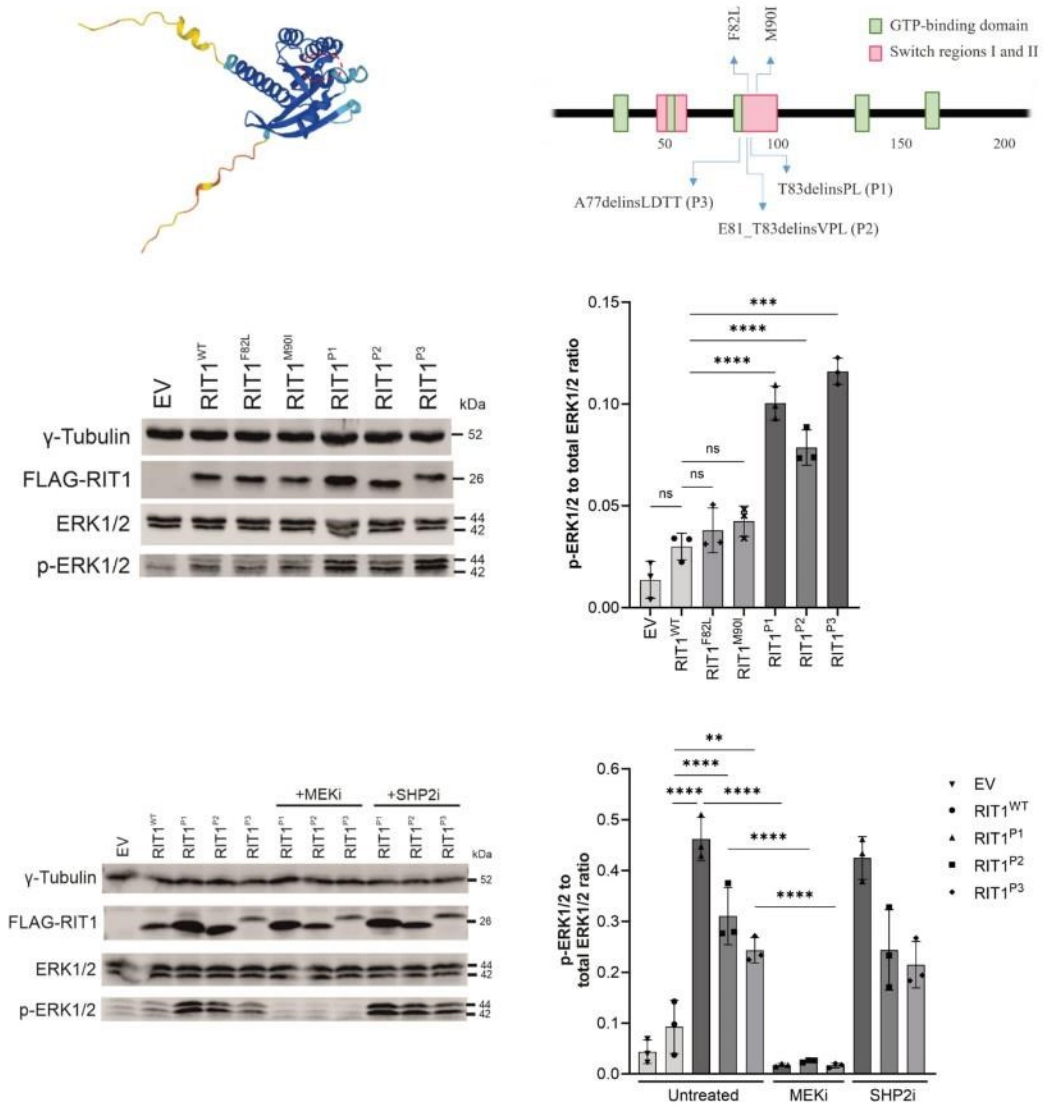

Fig. 2 ERK phosphorylation after expression of *RIT1* variants in vitro in HEK293T cells. **a** Protein structure of RIT1 predicted by AlphaFold, accessed through ensemble.org. The area labelled by the dashed red line indicates the switch 2 domain. **b** Schematic drawing of *RIT1* functional domains of human RIT1 protein (green boxes = GTP-binding regions; red boxes = switch domain 1 and 2; blue arrows (upward) = two mutations typically found in Noonan syndrome; blue arrows (downward) = mutations identified in P1-P3. **c** Western blot after expression of *RIT1* variants to assess RAS-MAPK pathway activation. Gamma tubulin served as loading control, FLAG-RIT1 confirms the expression of the construct, total ERK levels serve as a control to exclude the differential expression of ERK, and p-ERK measures the level of phosphorylate of ERK as a marker of RAS pathway activation. **d** Quantification of the ERK phosphorylation was measured in a total of three western blots for each variant (n = 3). One-way ANOVA. P value *** < 0.001; **** < 0.0001, ns = not significant. Data are presented as mean ± SD. EV = empty vector. **e** Western blot after expression of *RIT1* variants and with or without treatment using a MEK inhibitor or SHP2 inhibitor. The same parameters were assessed as in panel d. **f** Quantification of the ERK phosphorylation was measured in a total of three western blots for each variant (n = 3). One-way ANOVA. P value ** < 0.01; **** < 0.0001, ns = not significant. Data are presented as mean ± SD

was identified (c.229delinsTTGGATACAA p.A77delinsLDTT (referred to as *RIT1*^{P3}, hereafter) with a VAF of 13%.

RIT1 delins-induced ERK hyperphosphorylation can be reversed by pharmacological inhibition of MEK but not SHP2

All three delins variants are located close to the switch 2 domain of the RIT1 protein, a region that also harbors germline missense variants commonly associated with Noonan syndrome (Fig. 2A, B). To investigate the impact of these novel mutations on activation of the RAS pathway, we assessed ERK phosphorylation by Western blotting after the expression of *RIT1* in the HEK293T cells. We expressed *RIT1*^{P1}, *RIT1*^{P2}, *RIT1*^{P3}, *RIT1* wildtype (*RIT1*^{wt}), and two recurrent *RIT1* mutations found in Noonan syndrome (p.F82L and p.M90I). All three novel *RIT1* delins led to a significant increase in ERK phosphorylation, while overexpression of the two Noonan syndrome-associated *RIT1* mutations only induced a modest ERK hyperphosphorylation (Fig. 2C, D). Additionally, we examined the effects of the *RIT1* variants on PI3K/AKT signaling pathway activation by assessing the ratios of p-AKT (Thr308) as a substrate of PDK1 and p-AKT (Ser473) as the target of mTORC2 to the total levels of AKT. Interestingly, higher levels of phosphorylation at AKT-Threonine-308 were observed in the AVM associated delins, while the phosphorylation at Serine-473 remained unaffected (Online Resource 2).

Since RAS proteins act downstream of SHP2 and upstream of MEK and ERK in the RAS-MAPK signaling pathway, we hypothesized that RIT1-induced ERK hyperphosphorylation exhibits a differential response to treatment with SHP2 and MEK inhibition (Online Resource 3). Indeed, treatment of HEK293T cells with the SHP2 inhibitor SHP099 showed no effects on ERK phosphorylation. In contrast, MEK inhibition with PD0325901 reversed ERK phosphorylation close to baseline levels (Fig. 2E, F).

RIT1 delins variants lead to the formation of AVM-like lesions in zebrafish embryos

Having shown that the *RIT1* delins identified in AVM patients induced strong activation of the RAS-MAPK pathway, we next assessed whether their expression can lead to aberrant vascular development in the tail vasculature of zebrafish embryos. The zebrafish is an established model for the study of vascular development [16] that has also been applied to translational research [8, 17, 18]. To this end, we used plasmids, which contain the transcriptional upstream activating sequence (UAS) that controls the expression of wildtype or variant *RIT1* linked to GFP via the self-cleaving peptide P2A. Activation of the UAS element and thus expression of *RIT1* is dependent on the presence of the transcription factor Gal4. These plasmids were injected in the one-cell stage of *Tg(fli1a:Gal4; UAS:RFP)* embryos. While the plasmid integrated randomly into the DNA of cells of the zebrafish embryo, expression of RIT1-P2A-GFP was limited to endothelial cells that expressed Gal4 under the control of the endothelial fli1a promoter (Fig. 3A) [18]. Using this approach, we observed AVM-like lesions in the zebrafish embryo tail at 2 dpf. These lesions were characterized by aberrant connections between the dorsal aorta and the caudal vein. A common and severe phenotype exhibited a fusion of these arterial and venous vessels (Fig. 3B, Online Resource 4). In many embryos, the aorta and part of the caudal vein plexus directly downstream of the shunt at the proximal end of the AVM-like lesions were also fused, but a shunt could also be focal only (Online Resource 5 and 6). This fusion is in line with a recent study on *rasa1* mutant zebrafish with a similar phenotype of a distal fusion [19]. A significantly higher rate of AVM-like lesions at 48 h post fertilization (hpf) was observed in embryos expressing *RIT1*$^{P1-P3}$ delins compared to *RIT1*^{wt} (66–75% vs 24%, Fig. 3C). Next, we treated injected embryos with 100 nM trametinib during early development. This early treatment significantly reduced the formation of AVM-like lesions (31–39%, Fig. 4A, B), thereby supporting the assumption that AVM formation is critically dependent on hyperactivation of the RAS-MAPK pathway. To mimic a targeted treatment more closely in patients, we next treated zebrafish embryos with established AVM-like lesions after injection of *RIT1* delins with 100 nM trametinib from 48 hpf onwards and compared growth of the lesions in treated and untreated embryos over the following two days. DMSO-treated embryos in the control group showed a relative increase in the size of the lesion to 117.5%, while the size of the lesions in trametinib-treated embryos decreased to 83.4%; the difference between treated and untreated embryos was significant (Fig. 4C, D, Online Resource 7).

Trametinib induced reduction in AVM size and bleeding frequency in P1

As described above, P1 had a refractory disease with recurrent life-threatening bleeding episodes. Due to the aggressive course of the disease, treatment with thalidomide [20] was started but was only transiently effective before symptoms deteriorated again (Fig. 5A–C). The MRI showed a large AVM of the right side of the face that was progressive over time (Fig. 5D and Online Resource 8). Because of increasing disease severity, off-label treatment with trametinib (0.25 mg per day (1/2 capsules), 0.023 mg/kg/d) was started at the age of 2 years and 6 months. Dosage was increased to 0.5 mg per day (1 capsule), 0.045 mg/kg body weight after one month. Trametinib led to a significant clinical response with a decrease in frequency and severity of bleeding episodes, a

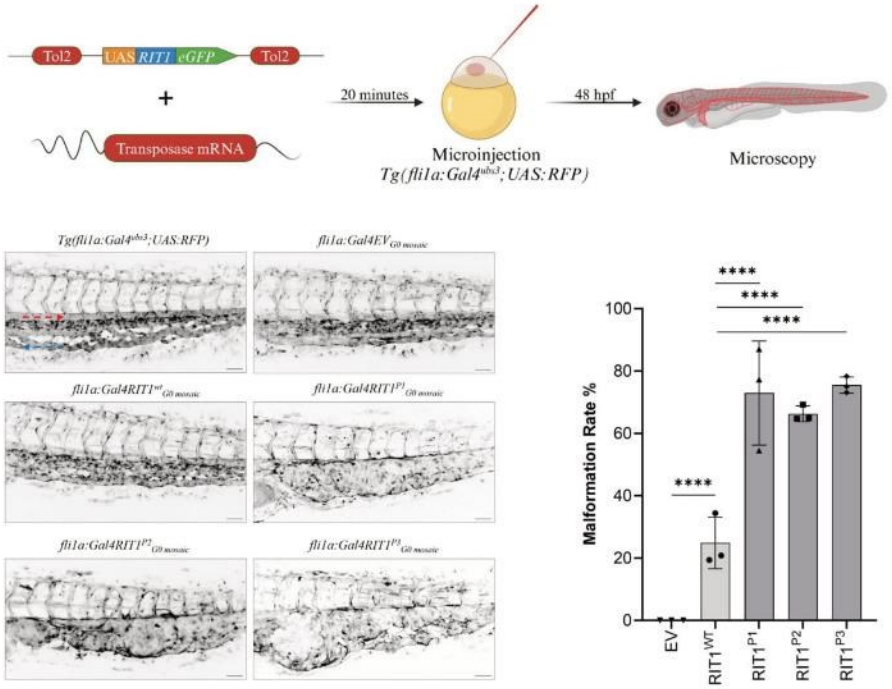

Fig. 3 Endothelial-specific mosaic expression of *RIT1* variants leads to the formation of AVM in zebrafish embryos. **a** Experimental layout: The plasmid containing human wildtype *RIT1* or *RIT1* variants, under the control of a UAS element and linked to GFP with a P2A sequence is mixed with transposase mRNA and injected into the one-cell stage of *Tg(fli1a:Gal4; UAS:RFP)* embryos. Thereafter, embryos are examined at 48 hpf. **b** Vascular network in the tail of an uninjected *Tg(fli1a:Gal4; UAS:RFP)*, EV and *RIT1* variants injected embryos. Arrows represent the direction of arterial and venous blood flow (red and blue arrow, respectively). Note the malformed vasculature with a fusion of the dorsal aorta and the caudal vein as well as dilation of the vessel. Scale bar 50 µm. **c** Quantification of the vascular anatomy at 48 hpf following the injection of plasmids containing the indicated *RIT1* variants, with and without treatment. n = 3. Number of total examined embryos: EV = 66, $RIT1^{WT}$ = 92, $RIT1^{P1}$ = 67, $RIT1^{P2}$ = 97, $RIT1^{P3}$ = 61. Fisher's exact test, two-tailed. P value **** < 0.0001. Data are presented as mean ± SD. *EV* empty vector

regression of the AVM as observed in the MRI (Fig. 5E), and a shrinking of the affected cheek (Fig. 5F). Due to improved disease control, the patient was able to attend preschool for the first time in her life. The patient tolerated trametinib treatment without significant adverse events and remained on this therapy for 9 months. At 2 years and 10 months of age, while on trametinib, the patient developed spontaneous rhinoliquorrhea and was diagnosed with a frontoethmoidal encephalocele, which, retrospectively, was already present in the first MRI at 6 months of age. She then underwent three neurosurgical operations; however, the cerebrospinal fluid (CSF) leak persisted and at the age of three years a ventriculoperitoneal (VP) shunt was implanted. After the placement of the VP shunt, the rhinoliquorrhea stopped. The VP shunt was replaced after 3 months due to a defect of the parietal skin overlying the shunt line. One month later, the patient developed a pneumococcal meningitis with cerebral edema and herniation leading to death at the age of 3 years and 3 months. We hypothesize that the frontoethmoidal encephalocele with difficult dural closure was a predisposing factor for this lethal infection but cannot rule out a contribution of trametinib treatment to this event. However, due to the absence of other adverse events (such as neutropenia or skin toxicity), and the safety profile of trametinib that does not include immunosuppressive effects, we consider this tragic fatal event after 9 months of trametinib treatment as unrelated to this medication.

Discussion

In this report, we describe three novel somatic activating *RIT1* delins variants in patients with peripheral fast-flow malformations. The exact prevalence of *RIT1* variants as the

cause for AVM cannot be determined precisely. However, with a total of three cases in the cohorts of vascular anomaly patients studied by this consortium, they are evidently much less common than variants of *MAP2K1* or *KRAS*. Considering the total number of AVMs sequenced and of AVMs harbouring a *RIT1* mutation, we roughly estimate the prevalence of *RIT1* mutations in AVMs at approximately 1 out of 30. Nevertheless, we strongly recommend that *RIT1* should be included in panels for genetic testing of patients with vascular malformations.

All three somatic mutations are located close to the switch 2 domain of *RIT1*, a domain that also harbors *RIT1* germline mutations commonly associated with Noonan syndrome. Interestingly, similar delins at the switch 2 domain of the RAS GTPases *KRAS* and *HRAS* have been described in vascular anomalies previously [21]. *RIT1* delins led to a strong ERK hyperphosphorylation that was much more pronounced than in Noonan-associated RIT1 missense changes. Considering the presumed role of RIT1 in the RAS-MAPK signaling pathway, treatment with a SHP2 inhibitor—as expected—did not influence ERK phosphorylation in cells transfected with the delins. In contrast, MEK inhibition completely rescued ERK hyperphosphorylation. These data suggest that *RIT1* delins act through overactivation of the canonical RAS-MAPK pathway.

Additionally, we observed overactivation of AKT in our biochemical assay, hinting at a known but so far underappreciated interconnection and crosstalk between the RAS and the AKT/mTOR signaling pathways in vascular anomalies. AKT activation has also been observed in patients with loss-of-function mutations in RASA1 (an inhibitor of the RAS pathway), where a consistent endothelial overactivation of mTORC1 could be found [22]. This is in line with data from brain AVMs due to KRAS mutations [23] as well as in other diseases, in which KRAS mutations activate the mTOR signaling pathway [24]. While there is little published data on the use of sirolimus in patients with AVM, it is currently not considered a viable option by experts in the field of vascular anomalies. A larger study on sirolimus for different kinds of vascular anomalies found only a very low rate of responders [25]. We hypothesize that *RIT1* delins close to the switch 2 region led to a distinct biochemical profile compared to missense mutations of Noonan syndrome, namely a stronger hyperphosphorylation of ERK, and—to a lesser extent—a phosphorylation of AKT at position T308. Exploring these functional differences of different mutations and the interaction of the RAS and the AKT/mTOR pathways might provide relevant insights into disease pathophysiology in the future.

To further assess the impact of the novel *RIT1* variants on vascular development, we used an approach that mimics the endothelial mosaicism that occurs in patients. In our previous work, we assessed various *TEK* mutations by endothelial-specific mosaic expression in zebrafish embryos and observed the development of venous malformations [18]. In the current work, we observed that *RIT1* mutations induced AVM-like lesions in zebrafish embryos, further confirming that overactivation of RAS-MAPK signaling caused by *RIT1* delins has a deleterious effect on vascular development. We refer to these lesions as AVM-like, as we observe a fast-flow shunt and a fusion of artery and vein but are still studying the biology of these shunts in greater detail in order to better understand the degree of similarity with AVMs in patients. Additionally, we show that MEK inhibition not only normalized ERK phosphorylation in vitro but also restored normal vascular development and decreased AVM-like lesion size in vivo during early and late treatment, respectively. These data further validate RAS-MAPK hyperactivation as the major driving mechanism for AVM formation and maintenance in the presence of the novel *RIT1* delins variants.

Trametinib is a mitogen-activated protein kinase (MAPK) kinase (MEK) inhibitor and as such an inhibitor of the RAS signaling pathway. By specifically binding to MEK1 and MEK2, trametinib inhibits the growth factor-mediated cell signaling and cellular proliferation in various cancers [26]. Due to the identification of the underlying mutations of the RAS signaling pathway in patients with AVMs [27–29] and certain complex lymphatic anomalies [30–32], trametinib has been used in patients with these diseases as an experimental drug with some success. Larger case series or even clinical trials studying the effect of trametinib on vascular anomalies driven by RAS activation have not been studied so far. To our knowledge, two clinical trials are currently registered at clinicaltrials.gov, which will study the effect of trametinib on AVMs prospectively (NCT04258046, NCT06098872), with additional trials using alternative MEK inhibitors such as cobimetinib (NCT05125471).

Our in vitro and in vivo findings and the available literature encouraged us to the off-label use of trametinib in our severely affected patient P1, who indeed responded very well with a significant reduction of AVM size and associated complaints, such as bleeding episodes. Unfortunately, the patient developed fatal meningitis, most likely due to an incidental encephalocele. While we consider this event as not related to trametinib treatment, it further highlights the need for controlled studies in the field of vascular anomalies, to assess treatment efficacy and tolerability and to advance care for patients with these diseases into an era of evidence-based personalized medicine.

In summary, our work introduces *RIT1* as a novel gene implicated in the pathogenesis of AVM. Functional testing in vitro and in vivo demonstrated the capacity of the novel *RIT1* variants to hyperactivate the RAS-MAPK pathway and induce the development of AVM. MEK inhibition led to biochemical normalization, prevention of AVM formation,

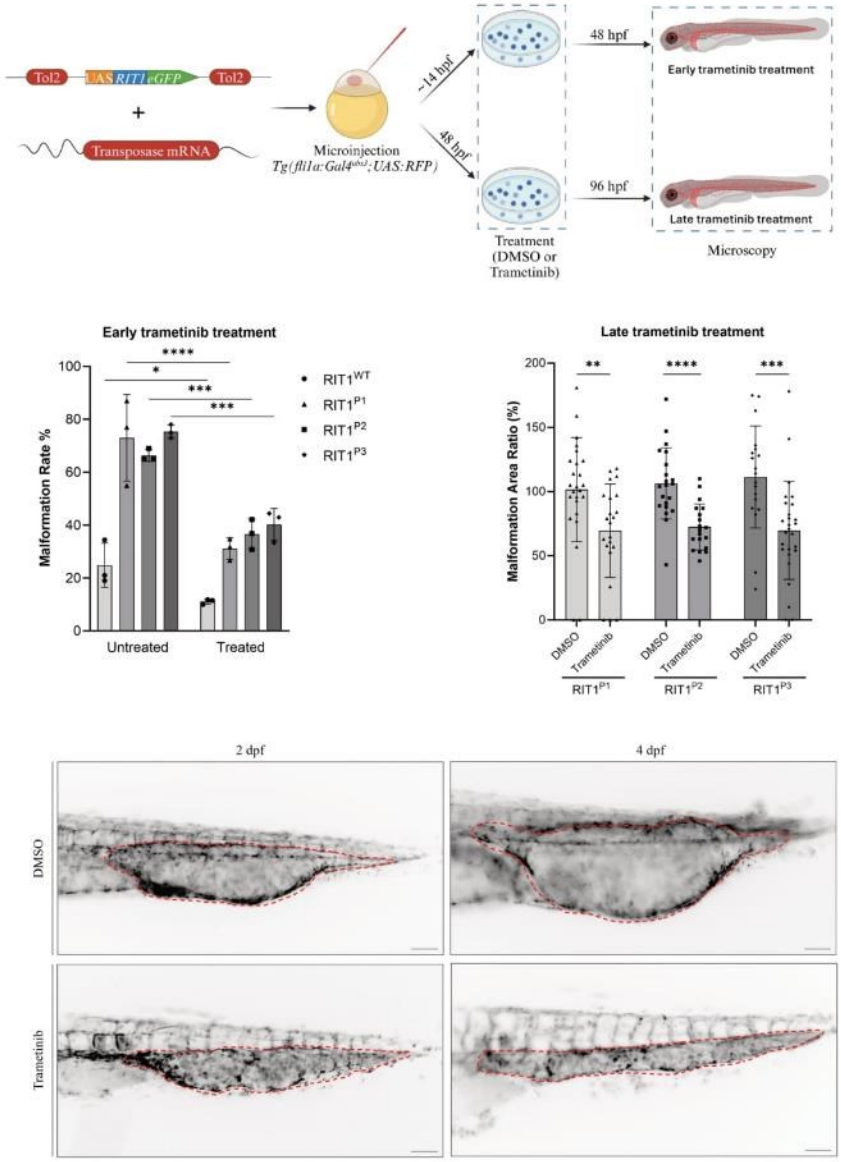

as well as a decreasing AVM size. We also present the first promising data on the use of trametinib in a patient with a somatic *RIT1* mutation, encouraging further investigation of MEK inhibition in patients with AVM in future clinical trials. However, our n = 1 approach in this study precludes definitive conclusions regarding treatment efficacy and safety. Larger-scale studies are needed to validate our findings, to delineate a more precise estimation of the

◂**Fig. 4** *RIT1* variants injected zebrafish embryos respond to early and late treatment with MEK inhibitor trametinib. **a** Experimental plan to assess the effect of trametinib on the *RIT1* injected zebrafish embryos after early and late treatments. Embryos are treated with trametinib either from 14hpf or 48 hpf on followed by an examination at 48 hpf (early treatment) or 96 hpf (late treatment) respectively. Presence of vascular malformation is calculated for early treatment embryos. Malformation area is calculated before and after trametinib treatment for each embryo in the late treatment group. **b** Quantification of the vascular anatomy at 48 hpf following the injection of plasmids containing the indicated *RIT1* variants and treatment at 14 hpf. Experiments were performed with three biological replicates. Number of total examined embryos post-treatment: $RIT1^{WT}=73$, $RIT1^{P1}=60$, $RIT1^{P2}=51$, $RIT1^{P3}=38$. Fisher's exact test, two-tailed. P value *< 0.05, ***< 0.001; ****< 0.0001. Data are presented as mean ± SD. **c** Quantification of the relative change in the size of the AVM-like lesions after 2 days of treatment. Experiments were performed with three biological replicates. Number of total examined embryos: $RIT1^{P1}=48$, $RIT1^{P2}=40$, $RIT1^{P3}=46$. Unpaired t-test, two-tailed. P value **< 0.01; ***< 0.001; ****< 0.0001. Data are presented as mean ± SD. **d** Example of image analysis to measure the relative change of lesion size during trametinib treatment from 2 to 4 dpf. Scale bar 50 µm

prevalence of *RIT1* mutations, to characterize their functional consequences on the RAS pathway and neighboring signaling pathways, and to assess the broader applicability of MEK inhibition in patients with RIT1-mutated vascular malformations.

Materials and methods

Patients/study approval

All subjects, and/or their legal guardians, gave written informed consent to genetic investigations, which were carried out with approval by the institutional review boards of the University Hospital Regensburg, Germany (17-854-101), University Hospital of Bern, Switzerland (2017-01960), and Boston Children's Hospital, Boston, MA, USA (IRB-P00025772).

Genetic testing

RIT1 was tested in a total of 691 samples by the partners' laboratories (235 in Magdeburg, 114 in Bern, 342 in Boston), including all types of vascular anomalies. Out of these samples, 118 were submitted for sequencing with the diagnosis of "AVM" (58 to Magdeburg, including by non-specialized centers, 35 to Bern, 25 to Boston). Brain AVMs were not included in the submitted samples. From these samples, one sample at each center harbored a *RIT1* mutation. Since sequencing results at Magdeburg also revealed mutations (e.g. in *TEK* or *GNAQ*) that according to current knowledge do not occur in AVMs, we conclude that phenotyping by non-specialized centers was in part incorrect and estimate that roughly 30–40 true AVM samples were sequenced in Marburg. This would be in line with a recently published cohort from Germany that included 29 patients with mutations in the RAS pathway [33]. We thus estimate the prevalence of *RIT1* mutations in AVMs at roughly 1 in 30 patients.

A tissue biopsy of the AVM of P1 was submitted to the Institute of Human Genetics, University Hospital Magdeburg, and the genomic DNA was extracted. Assuming a mosaic mutation as the cause of the disorder, ultradeep sequencing and enrichment using an Agilent SureSelect XT HS2 Custom Enrichment Panel with molecular barcoding (UMIs, 3 bp duplex) (Agilent Technologies) were performed. The library was sequenced on a NextSeq550 instrument (Illumina), 2 × 150 bp paired-end reads. The target regions had a mean coverage of > 3000× after demultiplexing. The varvis 1.20.0 analysis software (Limbus Medical Technologies GmbH) was used for analysis.

P2 has been included in the Bernese Congenital Vascular Malformation Registry, a prospective cohort of congenital extracranial/extraspinal vascular malformations that have been enrolling consecutive patients since 2008 [34]. As of October 2020, genetic testing is performed on tissue available from diagnostic biopsies of vascular malformations, using the TruSight Oncology 500 (TSO500; Illumina) Next Generation Sequencing (NGS) gene panel.

Resected tissue from P3 underwent targeted DNA NGS testing via the OncoPanel assay at the Center for Advanced Molecular Diagnostics (CAMD) at Brigham and Women's Hospital [35]. DNA was isolated using standard extraction methods (QIAGEN) and quantified with PicoGreen-based double-stranded DNA detection (Thermo Fisher Scientific). Indexed sequencing libraries were prepared from 50-ng sonically sheared DNA samples using Illumina TruSeq LT reagents (Illumina). Extracted DNA underwent targeted NGS using the KAPA HTP Library Preparation Kit (Roche), a custom RNA bait set (Agilent SureSelect) and sequenced with the Illumina HiSeq 2500 system.

Cell culture and western blot

Three million HEK293T cells were seeded in 10 cm cell culture plates supplemented with DMEM containing 10% fetal bovine serum (FBS) 12 h prior to transfection. At around 70% confluency levels cells were transfected using TurboFect transfection reagent (Thermo Fisher #R0532), with Flag-tagged *RIT1* variants in pCDNA constructs or empty vector (EV) as the negative control. The medium was refreshed at the 24 h' time point with MEK inhibitor (PD0325901, Selleckchem # S1036) and SHP2 inhibitor (SHP099, Selleckchem # S6388) being added to the transfected cells at 1 µM and 5 µM concentrations, respectively. At 48 h post-transfection, cells were washed in ice-cold

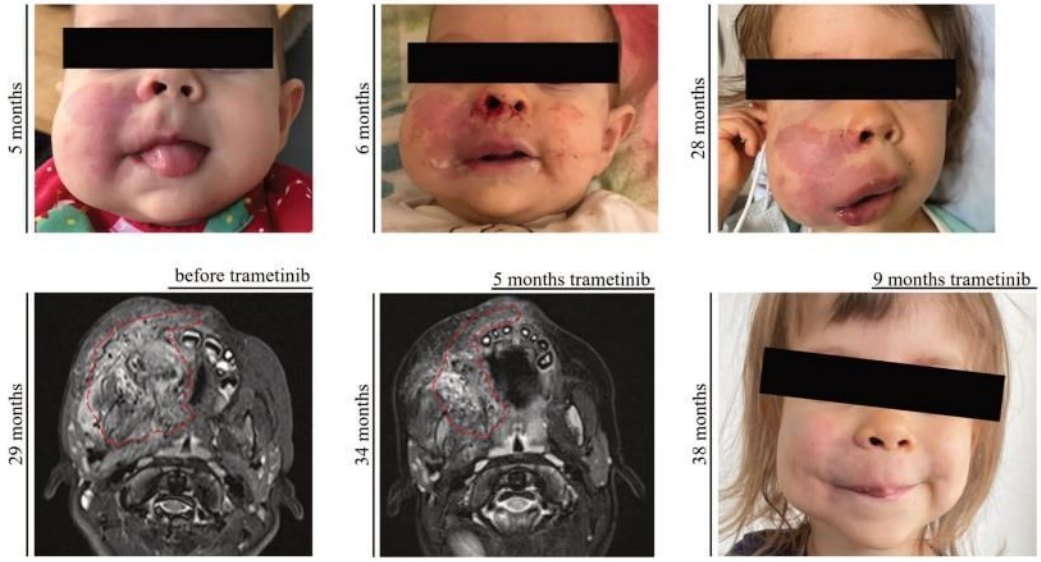

Fig. 5 Response to targeted therapy in P1. **a** Patient P1 at 5 months of age. **b** Patient P1 at 6 months of age (after a bleeding episode). **c** Patient P1 at 28 months of age, showing a significant and progressive enlargement of the right cheek due to the AVM. **d** MRI (transversal T2 STIR) of the Patient P1 before the start of trametinib treatment; red dashed line indicates the extent of the AVM. **e** MRI (transversal T2 TSE Dixon) of the Patient P1 after 5 months of treatment with trametinib; red dashed line indicates the now smaller extent of the AVM. **f** Patient P1 at 38 months of age, reduced volume of the right cheek and fading of the capillary malformation can be noted

phosphate-buffered saline (PBS) and lysed in ice-cold lysis buffer, containing 50 mM Tris/HCl pH 7.5, 5 mM MgCl2, 100 mM NaCl, 1% Igepal CA-630, 10% glycerol, 20 mM ß-glycerolphosphate, 1 mM Na-orthovanadate, EDTA-free inhibitor cocktail 1 tablet/50 ml. After the addition of Laemmli sample buffer, the samples were subjected to SDS-PAGE (12.5% polyacrylamide). Blots were detected by immunoblotting using a mouse anti-γ-Tubulin antibody (Sigma #T5326), a mouse anti-FLAG antibody (Sigma #F3165), a rabbit anti-ERK antibody (Cell signaling technology #9102), and a rabbit anti-p-ERK antibody (Cell signaling technology #4370), a rabbit anti-AKT (Cell signaling technology #9272), a rabbit anti-p-AKT-Thr308 (Cell signaling technol-ogy #2965), a rabbit anti-p-AKT-Ser473 (Cell signaling technology #4060). The immunoblots were detected using an Odyssey Fc Imaging System (LI-CORE Biosciences) and analyzed by Image Studio Lite Ver 5.2.

Zebrafish husbandry

Maintenance and breeding of zebrafish (*Danio rerio*) were performed in the fish facility of the Developmental Biology, Institute for Biology I, University of Freiburg under standard conditions. Only embryos up to 5 days post-fertilization were used. All experiments were carried out in accordance with German laws for animal care and the Regierungspräsidium Freiburg.

Plasmid preparation

Plasmids were designed using ApE—A plasmid editor version 3.0.8. *Homo sapiens RIT1* sequence was obtained from the online database Ensembl (Transcript ID: ENST00000368323.8), minimally codon optimized for *Danio rerio* and ordered as a plasmid including Tol2 sites, a UAS promoter, $RIT1^{P2}$, and P2A-GFP from Twist Bioscience (South San Francisco, CA, USA). Plasmids were purified using Wizard Plus SC Minipreps DNA Purification Systems (Promega, Walldorf, Germany, A1330) according to the manufacturer's instructions.

Mutagenesis

$RIT1^{wt}$, empty vector (EV), as well as all other *RIT1* mutations analyzed in this study were derived from the UAS:$RIT1^{P2}$-P2A-GFP construct using Q5 Site-Directed Mutagenesis (New England Biolabs, E0554S). Corresponding mutagenesis primers were designed

using NEBaseChanger version 1.3.3. All plasmids were sequenced by Eurofins genomics to confirm the expected sequence.

Tol2 transposase mRNA synthesis

8 µg of the plasmid that contains the transposase gene under control of the SP6 promoter were linearized using 4 µl of NotI-HF enzyme (New England Biolabs) for 1 h at 37 °C. The digested sample was purified using the QIAquick PCR Purification Kit according to the manufacturer's protocol. Capped Tol2 transposase mRNA was synthesized from purified DNA using the mMESSAGE mMACHINE™ SP6 Transcription Kit (ThermoFisher Scientific) according to the manufacturer's protocol. The resulting mRNA was separated into 5 µl aliquots and stored at − 20 °C to prevent freeze–thaw cycles.

Plasmid injection

The construct was then injected into *Tg(fli1a:Gal4FF^{ubs3}; UAS:RFP)* embryos at the one-cell stage together with Tol2 transposase mRNA [36], both at a concentration of 30 ng/µl. For better readability, *Tg(fli1a:Gal4FF^{ubs3}; UAS:RFP)* embryos injected with a gene of interest (e.g. UAS:RIT1^{P1}-P2A-GFP) are abbreviated as *fli1a:RIT1^{P1}$_{G0mosaic}$* instead of *Tg(fli1a:Gal4FF^{ubs3}; UAS:RFP)* and *Tg(UAS:RIT1^{P1}-P2A-GFP)$_{G0mosaic}$*.

Microscopy

Imaging plates for confocal microscopy were prepared in 35 mm glass bottom dish with 1.5% agarose in egg water, 1-phenyl 2-thiourea (PTU) and tricaine mix using previously designed and 3D printed molds (Online resource 9). Embryos anesthetized with 0.168 mg/ml tricaine in egg water at room temperature and gently positioned laterally inside the trenches. Confocal microscopy images were acquired as z-stacks with ZEISS Celldiscoverer 7 with LSM 900. Images were obtained with the 488 nm and 561 nm lasers, with a slice interval of 2–4 µm with a 20X (NA 0.7) objective or as brightfield images with 5x (NA 0.35) objective unless otherwise specified. For brightfield timelapse experiments, the interval was set to 1 s.

Fluorescence microscopy images for pre and post late treatment was acquired with ZEISS Axio Examiner D.1 fixed stage fluorescence microscope. During acquisition embryos were placed in 3 ml of E3 medium with tricaine (0.168 mg/ml) at room temperature and imaged with 10X (NA 0.15) objective. During imaging both, RFP and GFP channels acquired and only RFP channel is exported for representative images.

Lightsheet microscopy was performed with ZEISS Lightsheet 7 using water immersion W Plan-Apochromat 10x (NA 0.5) M27 75 mm objective. Images were obtained with the 488 nm and 561 nm lasers using single illumination, pivot scan on, with a slice interval of 2 µm. Timelapse interval is set to 1 s.

The color cyan was assigned for GFP channel. Colored versions of the images are included in the supplementary information. Images and videos were exported as.tif and. AVI (uncompressed) files, respectively using Fiji software.

Pharmacological treatments

For pharmacological treatments, injected zebrafish embryos were randomized into control and treatment groups. From the 10-somite stage or from 48 hpf on, embryos of the treatment group were transferred in E3 Medium (5 mM NaCl, 0.17 mM KCl, 0.33 mM $CaCl_2$, 0.33 mM Mg_2SO_4) containing 0.2 mM 1-phenyl 2-thiourea (PTU; Sigma, Taufkirchen, Germany, P7629) and MEK1/2 inhibitor Trametinib (MedChemExpress, GSK1120212; 10 mg) using 100× stock solutions dissolved in dimethyl sulfoxide (DMSO; Sigma, D2650). The treatment dose of trametinib was chosen at 100 nM, according to our previous publication [18], and by repeating of the toxicity assay in zebrafish embryos. Embryos of the control group were raised in E3 medium with 0.2 mM PTU and DMSO (equal amount to the treatment group). The response of the AVM-like lesion size to trametinib was calculated as follows: each embryo with an AVM-like lesion was imaged at the Axio Examiner, and the area of the lesion was divided by the area of the entire embryo to give a relative area of the malformation at 2 dpf. This was done to control for different embryo sizes and different embryo growth rates. This measurement was then repeated at 4 dpf (after treatment) and the relative area of the AVM-like lesion at 4 dpf was divided by the relative area 2 dpf, followed by multiplication with 100 to give a result in percent. A result greater than 100% showed an AVM-like lesion growing in size in relation to the embryo, a result less than 100% showed a regressing lesion.

Statistical analysis

The statistical analysis was performed using two-tailed Fisher's exact test of significance for malformation rate analysis and early pharmacological treatments and two-tailed unpaired t-test for late pharmacological treatment experiments and one-way ANOVA for in vitro experiments in GraphPad Prism version 10.2.2. The legends of the figures include information on sample sizes and significance. P value of < 0.05 was regarded as significant. Analyzed

data for zebrafish malformation rates and early pharmacological treatments was obtained from at least three independent experiments for each variant. The number of examined embryos is indicated in the figure legends for each variant. Data are presented as mean ± SD for all experiments. P value * < 0.05, ** < 0.01; *** < 0.001; **** < 0.0001. The structure of the RIT1 protein is predicted using AlphaFold database [37, 38].

Supplementary Information The online version contains supplementary material available at https://doi.org/10.1007/s10456-024-09934-8.

Acknowledgements The authors first and foremost acknowledge the patients and their families for providing their information and allowing us to conduct this work. We further acknowledge the Center for Vascular Anomalies at the Freiburg Center for Rare Diseases, the Hilda Biobank at the Department of Pediatrics and Adolescent Medicine, Freiburg, Germany, the Lighthouse Core Facility and Life Imaging Center (LIC) in Freiburg, Germany, and the zebrafish facility in the Institute of Biology I Zoology (Prof. Dr. Wolfgang Driever) at the University of Freiburg, Germany for their contribution. Four of the authors of this publication are members of the Vascular Anomalies Working Group (VASCA WG) of the European Reference Network for Rare Multisystemic Vascular Diseases (VASCERN)—Project ID: 769036. Five of the authors are members of the German Reference Network for Vascular Anomalies. FK was supported by the charity cycling tour "Tour der Hoffnung" and received funding from the GermanFederal Ministry of Education and Research (BMBF): EJPRD Joint Transnational Call 2023, NARRATIVE;FKZ 01GM2405). NM was part of the International Master Program in Biomedical Sciences (IMBS) and acknowledges the support received throughout the program. FB and MRA received funding from the German Research Foundation (Grant numbers: DFG AH 92/8-3 and IRTG 1902-p6) and the Foundation for Ageing Research of the HHU Düsseldorf. AH received the Walter Benjamin Fellowship from the German Research Foundation (Project number: 458322953). IB (Principle Investigator) and JR (Co-Investigator) were supported by the Swiss national Research Foundation, Synergia Grant CRSII5_193694 2021-2024.

Author contributions Friedrich G. Kapp: clinical care of patient, conceptualization of the study, writing—original draft preparation, writing—review and editing. Farhad Bazgir: in vitro analyses, formal analysis. Nagi Mahamammadzade: in vivo analyses, formal analysis. Mehrnaz Mehrabipour: in vitro analyses. Sarah M. Bernhard, Axel Karow, Caroline Seebauer, Walter A. Wohlgemuth: clinical care of patients, Annegret Holm, Whitney Eng: clinical care of patients, original draft preparation, writing—review and editing. Whitney Eng, Denny Schanze, and Martin Zenker: genetic analyses. Aviv Oppenheimer: in vivo analyses. Pia Kröning: writing—original draft preparation. Charlotte M. Niemeyer, Yvonne Döring, Mohammad R. Ahmadian, resources. Iris Baumgartner and Jochen Rössler: conceptualization, writing—original draft preparation, writing—review and editing, resources. All authors provided intellectual input, critical feedback, discussed results, and approved the final manuscript. Authors Friedrich G. Kapp, Farhad Bazgir, Nagi Mahammadzade, Iris Baumgartner and Jochen Rössler contributed equally to this work.

Funding Open Access funding enabled and organized by Projekt DEAL.

Data availability The data that support the findings of this study are available from the corresponding author upon reasonable request.

Declarations

Competing interests Friedrich G. Kapp has received consulting fees from Novartis. Jochen Rössler is currently an employee of Novartis Pharma. All other authors declare no conflicts of interest.

References

1. Mulliken JB, Glowacki J (1982) Hemangiomas and vascular malformations in infants and children: a classification based on endothelial characteristics. Plast Reconstr Surg 69(3):412
2. Wassef M, Blei F, Adams D, Alomari A, Baselga E, Berenstein A, on behalf of the ISSVA Board and Scientific Committee (2015) Vascular anomalies classification: recommendations from the International Society for the Study of Vascular Anomalies. Pediatrics 136(1):e203–e214. https://doi.org/10.1542/peds.2014-3673
3. Limaye N, Wouters V, Uebelhoer M, Tuominen M, Wirkkala R, Mulliken JB, Vikkula M (2009) Somatic mutations in angiopoietin receptor gene TEK cause solitary and multiple sporadic venous malformations. Nat Genet 41(1):118–124. https://doi.org/10.1038/ng.272
4. Limaye N, Kangas J, Mendola A, Godfraind C, Schlögel MJ, Helaers R, Vikkula M (2015) Somatic activating PIK3CA mutations cause venous malformation. Am J Hum Genet 97(6):914–921. https://doi.org/10.1016/j.ajhg.2015.11.011
5. Keppler-Noreuil KM, Rios JJ, Parker VER, Semple RK, Lindhurst MJ, Sapp JC, Biesecker LG (2015) PIK3CA-related overgrowth spectrum (PROS): diagnostic and testing eligibility criteria, differential diagnosis, and evaluation. Am J Med Genet A 167(2):287–295. https://doi.org/10.1002/ajmg.a.36836
6. Couto JA, Huang AY, Konczyk DJ, Goss JA, Fishman SJ, Mulliken JB, Greene AK (2017) Somatic MAP2K1 mutations are associated with extracranial arteriovenous malformation. Am J Hum Genet 100(3):546–554. https://doi.org/10.1016/j.ajhg.2017.01.018
7. Konczyk DJ, Goss JA, Smits PJ, Huang AY, Al-Ibraheemi A, Sudduth CL, Greene AK (2019) Arteriovenous malformation associated with a HRAS mutation. Hum Genet 138(11):1419–1421. https://doi.org/10.1007/s00439-019-02072-y
8. Al-Olabi L, Polubothu S, Dowsett K, Andrews KA, Stadnik P, Joseph AP, Kinsler VA (2018) Mosaic RAS/MAPK variants cause sporadic vascular malformations which respond to targeted therapy. J Clin Investig 128(4):1496–1508. https://doi.org/10.1172/JCI98589
9. Goss JA, Konczyk DJ, Smits PJ, Kozakewich HPW, Alomari AI, Al-Ibraheemi A, Greene AK (2019) Intramuscular fast-flow vascular anomaly contains somatic MAP2K1 and KRAS mutations. Angiogenesis 22(4):547–552. https://doi.org/10.1007/s10456-019-09678-w

10. Timbang MR, Richter GT (2020) Update on extracranial arteriovenous malformations: a staged multidisciplinary approach. Semin Pediatr Surg 29(5):150965. https://doi.org/10.1016/j.sempedsurg.2020.150965
11. El Sissy FN, Wassef M, Faucon B, Salvan D, Nadaud S, Coulet F, Eyries M (2022) Somatic mutational landscape of extracranial arteriovenous malformations and phenotypic correlations. J Eur Acad Dermatol Venereol 36(6):905–912. https://doi.org/10.1111/jdv.18046
12. Coulie J, Boon L, Vikkula M (2022) Molecular pathways and possible therapies for head and neck vascular anomalies. J Oral Pathol Med 51(10):878–887. https://doi.org/10.1111/jop.13318
13. Utami AM, Azahaf S, de Boer OJ, van der Horst CMAM, Meijer-Jorna LB, van der Wal AC (2021) A literature review of microvascular proliferation in arteriovenous malformations of skin and soft tissue. J Clin Transl Res 7(4):540–557
14. Liu AS, Mulliken JB, Zurakowski D, Fishman SJ, Greene AK (2010) Extracranial arteriovenous malformations: natural progression and recurrence after treatment. Plast Reconstr Surg 125(4):1185. https://doi.org/10.1097/PRS.0b013e3181d18070
15. McMorrow L, Shaikh M, Kessell G, Muir T (2017) Bleomycin electrosclerotherapy: new treatment to manage vascular malformations. Br J Oral Maxillofac Surg 55(9):977–979. https://doi.org/10.1016/j.bjoms.2017.10.002
16. Reischauer S, Stone OA, Villasenor A, Chi N, Jin S-W, Martin M, Stainier DYR (2016) Cloche is a bHLH-PAS transcription factor that drives haemato-vascular specification. Nature 535(7611):294–298. https://doi.org/10.1038/nature18614
17. Rödel CJ, Otten C, Donat S, Lourenço M, Fischer D, Kuropka B, Abdelilah-Seyfried S (2019) Blood flow suppresses vascular anomalies in a Zebrafish model of cerebral cavernous malformations. Circ Res 125(10):e43–e54. https://doi.org/10.1161/CIRCRESAHA.119.315076
18. Bell LM, Holm A, Matysiak U, Driever W, Rößler J, Schanze D, Kapp FG (2022) Functional assessment of two variants of unknown significance in TEK by endothelium-specific expression in zebrafish embryos. Hum Mol Genet 31(1):10–17. https://doi.org/10.1093/hmg/ddab196
19. Greysson-Wong J, Rode R, Ryu J-R, Chan JL, Davari P, Rinker KD, Childs SJ (2023) rasa1-related arteriovenous malformation is driven by aberrant venous signalling. Development 150(18):dev201820. https://doi.org/10.1242/dev.201820
20. Boon LM, Dekeuleneer V, Coulie J, Marot L, Bataille A-C, Hammer F, Vikkula M (2022) Case report study of thalidomide therapy in 18 patients with severe arteriovenous malformations. Nat Cardiovasc Res 1(6):562–567. https://doi.org/10.1038/s44161-022-00080-2
21. Eijkelenboom A, van Schaik FMA, van Es RM, Ten Broek RW, Rinne T, van der Vleuten C, Rehmann H (2019) Functional characterisation of a novel class of in-frame insertion variants of KRAS and HRAS. Sci Rep 9(1):8239. https://doi.org/10.1038/s41598-019-44584-7
22. Kawasaki J, Aegerter S, Fevurly RD, Mammoto A, Mammoto T, Sahin M, Chan J (2014) RASA1 functions in EPHB4 signaling pathway to suppress endothelial mTORC1 activity. J Clin Investig 124(6):2774–2784. https://doi.org/10.1172/JCI67084
23. Yan D, Hao Q, Chen Y, Li Z, Zhang H, Yuan K, Zhao Y (2022) mTOR-FABP4 signal is activated in brain arteriovenous malformations in humans. J Mol Med 100(9):1287–1297. https://doi.org/10.1007/s00109-022-02237-9
24. Pang M, Zhang G, Shang C, Zhang Y, Chen R, Li Z, Li Q (2023) Advances in the study of KRAS in brain arteriovenous malformation. Cerebrovasc Dis. https://doi.org/10.1159/000535139
25. Ji Y, Chen S, Yang K, Zhou J, Zhang X, Jiang X, Zhang Y (2021) A prospective multicenter study of sirolimus for complicated vascular anomalies. J Vasc Surg 74(5):1673-1681.e3. https://doi.org/10.1016/j.jvs.2021.04.071
26. Wright CJM, McCormack PL (2013) Trametinib: first global approval. Drugs 73(11):1245–1254. https://doi.org/10.1007/s40265-013-0096-1
27. Edwards EA, Phelps AS, Cooke D, Frieden IJ, Zapala MA, Fullerton HJ, Shimano KA (2020) Monitoring arteriovenous malformation response to genotype-targeted therapy. Pediatrics 146(3):e20193206. https://doi.org/10.1542/peds.2019-3206
28. Lekwuttikarn R, Lim YH, Admani S, Choate KA, Teng JMC (2019) Genotype-guided medical treatment of an arteriovenous malformation in a child. JAMA Dermatol 155(2):256–257. https://doi.org/10.1001/jamadermatol.2018.4653
29. Nicholson CL, Flanagan S, Murati M, Boull C, McGough E, Ameduri R, Maguiness S (2022) Successful management of an arteriovenous malformation with trametinib in a patient with capillary-malformation arteriovenous malformation syndrome and cardiac compromise. Pediatr Dermatol 39(2):316–319. https://doi.org/10.1111/pde.14912
30. Foster JB, Li D, March ME, Sheppard SE, Adams DM, Hakonarson H, Dori Y (2020) Kaposiform lymphangiomatosis effectively treated with MEK inhibition. EMBO Mol Med 12(10):e12324. https://doi.org/10.15252/emmm.202012324
31. Gordon K, Moore M, Van Zanten M, Pearce J, Itkin M, Madden B, Mansour S (2022) Case report: progressive central conducting lymphatic abnormalities in the RASopathies. Two case reports, including successful treatment by MEK inhibition. Front Genet 13:e1001105. https://doi.org/10.3389/fgene.2022.1001105
32. Li D, March ME, Gutierrez-Uzquiza A, Kao C, Seiler C, Pinto E, Hakonarson H (2019) ARAF recurrent mutation causes central conducting lymphatic anomaly treatable with a MEK inhibitor. Nat Med 25(7):1116–1122. https://doi.org/10.1038/s41591-019-0479-2
33. Schmidt VF, Kapp FG, Goldann C, Huthmann L, Cucuruz B, Brill R (2024) Extracranial vascular anomalies driven by RAS/MAPK variants: spectrum and genotype-phenotype correlations. J Am Heart Assoc 13(8):e033287. https://doi.org/10.1161/JAHA.123.033287
34. Bernhard SM, Tuleja A, Laine JE, Haupt F, Häberli D, Hügel U, Baumgartner I (2022) Clinical presentation of simple and combined or syndromic arteriovenous malformations. J Vasc Surg Venous Lymphat Disord 10(3):705–712. https://doi.org/10.1016/j.jvsv.2021.10.002
35. Garcia EP, Minkovsky A, Jia Y, Ducar MD, Shivdasani P, Gong X, Dong F (2017) Validation of OncoPanel: a targeted next-generation sequencing assay for the detection of somatic variants in cancer. Arch Pathol Lab Med 141(6):751–758. https://doi.org/10.5858/arpa.2016-0527-OA
36. Kwan KM, Fujimoto E, Grabher C, Mangum BD, Hardy ME, Campbell DS, Chien C-B (2007) The Tol2kit: a multisite gateway-based construction kit for Tol2 transposon transgenesis constructs. Dev Dyn 236(11):3088–3099. https://doi.org/10.1002/dvdy.21343
37. Jumper J, Evans R, Pritzel A, Green T, Figurnov M, Ronneberger O, Hassabis D (2021) Highly accurate protein structure prediction with AlphaFold. Nature 596(7873):583–589. https://doi.org/10.1038/s41586-021-03819-2
38. Varadi M, Anyango S, Deshpande M, Nair S, Natassia C, Yordanova G, Velankar S (2022) AlphaFold Protein Structure Database: massively expanding the structural coverage of protein-sequence space with high-accuracy models. Nucleic Acids Res 50(D1):D439–D444. https://doi.org/10.1093/nar/gkab1061

Authors and Affiliations

Friedrich G. Kapp[1] · Farhad Bazgir[2] · Nagi Mahammadzade[1] · Mehrnaz Mehrabipour[2] · Erik Vassella[3] · Sarah M. Bernhard[4,5] · Yvonne Döring[4,5,6] · Annegret Holm[1,7] · Axel Karow[8] · Caroline Seebauer[9] · Natascha Platz Batista da Silva[10] · Walter A. Wohlgemuth[11] · Aviv Oppenheimer[1] · Pia Kröning[12] · Charlotte M. Niemeyer[1] · Denny Schanze[13] · Martin Zenker[13] · Whitney Eng[14] · Mohammad R. Ahmadian[2] · Iris Baumgartner[4,5] · Jochen Rössler[1,15,16]

✉ Friedrich G. Kapp
friedrich.kapp@uniklinik-freiburg.de

✉ Jochen Rössler
jochen.roessler@insel.ch

1 Division of Pediatric Hematology and Oncology, Department of Pediatrics and Adolescent Medicine, Medical Center-University of Freiburg, Faculty of Medicine, University of Freiburg, VASCERN VASCA European Reference Centre, 79106 Freiburg, Germany

2 Institute of Biochemistry and Molecular Biology II, Medical Faculty and University Hospital, Heinrich-Heine University, Düsseldorf, Germany

3 Institute of Pathology and Tissue Medicine, University of Bern, Bern, Switzerland

4 Division of Angiology, Swiss Cardiovascular Center, Inselspital, Bern University Hospital, Bern, Switzerland

5 Department for BioMedical Research (DBMR), University of Bern, Bern, Switzerland

6 Institute for Cardiovascular Prevention (IPEK), Ludwig-Maximilians University Munich, Pettenkoferstr 9, 80336 Munich, Germany

7 Vascular Biology Program, Department of Surgery, Boston Children's Hospital, Harvard Medical School, Boston, MA, USA

8 Department of Pediatrics and Adolescent Medicine, Friedrich-Alexander-Universität Erlangen-Nürnberg (FAU), 91054 Erlangen, Germany

9 Department of Otorhinolaryngology, Regensburg University Medical Center, Franz-Josef-Strauß-Allee 11, 93053 Regensburg, Germany

10 Department of Radiology, Regensburg University Medical Center, Franz-Josef-Strauß-Allee 11, 93053 Regensburg, Germany

11 University Clinic and Policlinic of Radiology at the Martin-Luther-Universität Halle-Wittenberg, Halle, Germany

12 Department of General Pediatrics, Adolescent Medicine and Neonatology, Medical Center-University of Freiburg, Faculty of Medicine, University of Freiburg, 79106 Freiburg, Germany

13 Institute of Human Genetics, University Hospital Magdeburg, 39120 Magdeburg, Germany

14 Division of Hematology/Oncology, Boston Children's Hospital and Harvard Medical School, Boston, MA, USA

15 Department of Vascular Medicine, National Reference Center of Rare Lymphatic and Vascular Diseases, UA11 INSERM – UM IDESP, Campus Santé, Montpellier Cedex 5, France

16 Division of Paediatric Hematology and Oncology, Department of Paediatrics, Inselspital, Bern University Hospital, University of Bern, Bern, Switzerland

Supplementary Information

to

Somatic RIT1 delins in arteriovenous malformations hyperactivate RAS-MAPK signaling amenable to MEK inhibition

Journal name: Angiogenesis

Authors:

Friedrich G. Kapp[1 #*], Farhad Bazgir[2 *], Nagi Mahammadzade[1 *], Mehrnaz Mehrabipour[2], Erik Vassella[3], Yvonne Döring[4,5,6], Annegret Holm[1,7], Axel Karow[8], Caroline Seebauer[9], Natascha Platz Batista da Silva[10], Walter A. Wohlgemuth[11], Aviv Oppenheimer[1], Pia Kröning[12], Charlotte M. Niemeyer[1], Denny Schanze[13], Martin Zenker[13], Whitney Eng[14], Mohammad R. Ahmadian[2], Iris Baumgartner[4,5], Jochen Rössler[1,15,16 #]

[1]*Division of Pediatric Hematology and Oncology, Department of Pediatrics and Adolescent Medicine, Medical Center-University of Freiburg, Faculty of Medicine, University of Freiburg, 79106 Freiburg, Germany, VASCERN VASCA European Reference Centre*

[2]*Institute of Biochemistry and Molecular Biology II, Medical Faculty and University Hospital, Heinrich-Heine University, Düsseldorf, Germany*

[3]*Institute of Pathology and Tissue Medicine, University of Bern, Bern, Switzerland*

[4]*Division of Angiology, Swiss Cardiovascular Center, Inselspital, Bern University Hospital, Bern, Switzerland*

[5]*Department for BioMedical Research (DBMR), University of Bern, Switzerland*

[6]*Institute for Cardiovascular Prevention (IPEK), Ludwig-Maximilians University Munich, Pettenkoferstr 9, 80336, Munich, Germany*

[7]*Vascular Biology Program, Department of Surgery, Boston Children's Hospital, Harvard Medical School, Boston, MA, United States.*

[8]*Department of Pediatrics and Adolescent Medicine, Friedrich-Alexander-Universität Erlangen-Nürnberg (FAU), D-91054 Erlangen, Germany*

[9]*Department of Otorhinolaryngology, Regensburg University Medical Center, Franz-Josef-Strauß-Allee 11, 93053 Regensburg, Germany*

[10]*Department of Radiology, Regensburg University Medical Center, Franz-Josef-Strauß-Allee 11, 93053 Regensburg, Germany*

[11]*University Clinic and Policlinic of Radiology at the Martin-Luther-Universität Halle-Wittenberg, Halle, Germany*

[12]*Department of General Pediatrics, Adolescent Medicine and Neonatology, Medical Center-University of Freiburg, Faculty of Medicine, University of Freiburg, 79106 Freiburg, Germany*

[13]*Institute of Human Genetics, University Hospital Magdeburg, 39120 Magdeburg, Germany*

[14]*Division of Hematology/Oncology, Boston Children's Hospital and Harvard Medical School, Boston, MA, USA*

[15]*Department of Vascular Medicine, National Reference Center of Rare Lymphatic and Vascular Diseases, UA11 INSERM – UM IDESP, Campus Santé, Montpellier Cedex 5, France*

[16]*Division of Paediatric Hematology and Oncology, Department of Paediatrics, Inselspital, Bern University Hospital, University of Bern, Switzerland*

*Contributed equally to this work

[#]*Corresponding authors Email: friedrich.kapp@uniklinik-freiburg.de; jochen.roessler@insel.ch*

This file contains the following:

Additional Clinical and Laboratory Findings

Supplementary Figures S1 (Online Resource 1)

Supplementary Figures S2 (Online Resource 2)

Supplementary Figure S3 (Online Resource 3)

Supplementary Figure S4 (Online Resource 4)

Supplementary Video S1 (Online Resource 5)

Supplementary Video S2 (Online Resource 6)

Supplementary Figure S5 (Online Resource 7)

Supplementary Figure S6 (Online Resource 8)

Supplementary File S1 (Online Resource 9)

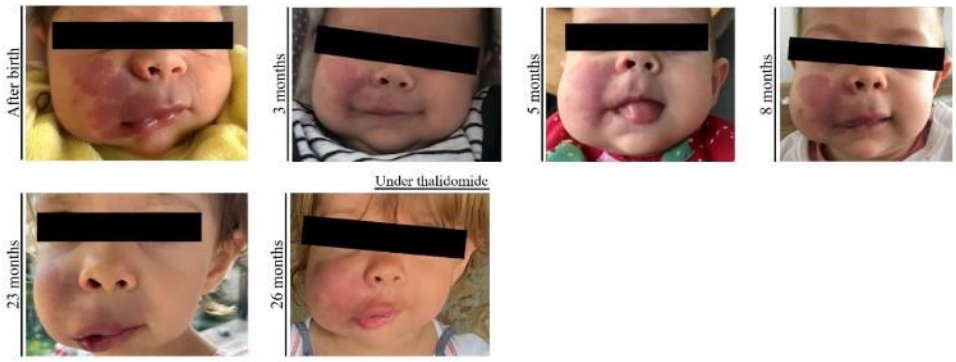

Supplemental Figure S1 (Online Resource 1). Patient P1 – Clinical evolution of disease.

Clinical photographs of Patient P1 show progressive growth of the lesion over time.

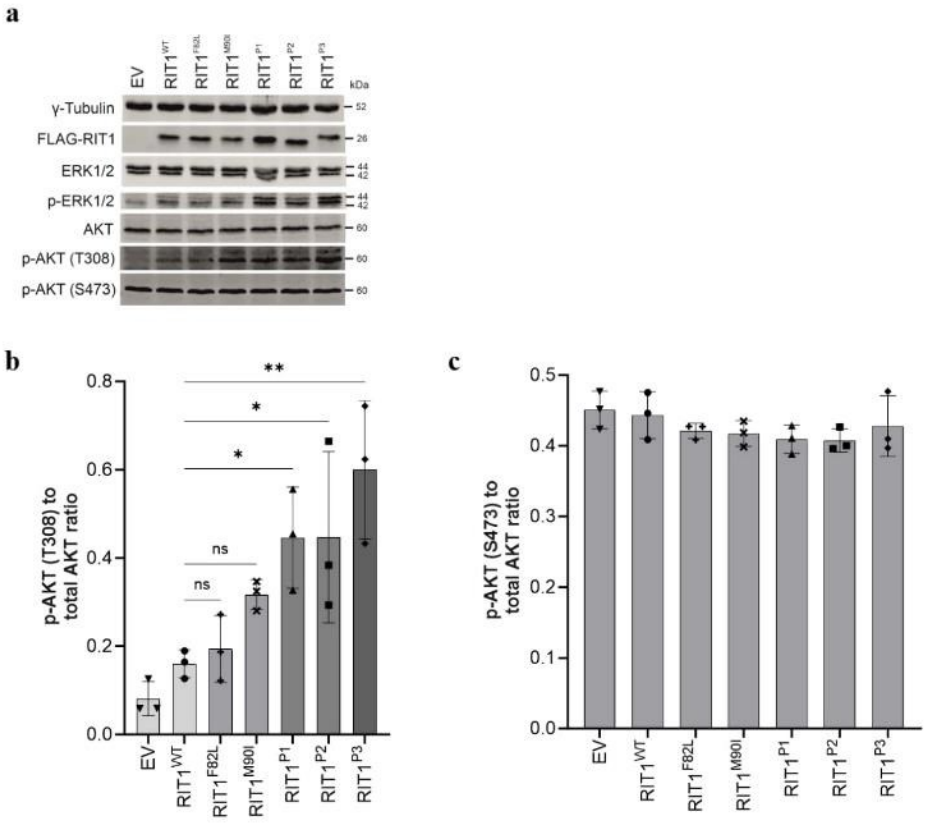

Supplemental Figure S2 (Online Resource 2). AKT phosphorylation after expression of *RIT1* variants *in vitro* in HEK293T cells.

a. Western blot after expression of *RIT1* variants to assess RAS-MAPK pathway and PI3K/AKT signaling pathway activation. Gamma tubulin served as loading control, FLAG-RIT1 confirms the expression of the construct, total ERK and AKT levels serve as a control to exclude the differential expression of ERK and AKT. p-ERK measures the level of phosphorylation of ERK as a marker of RAS pathway activation. p-AKT measures the level of phosphorylation of AKT as a marker of mTOR pathway activation.

b. Ratios of p-AKT (Thr308) as a substrate of PDK1 to total levels of AKT. Quantification of the AKT phosphorylation was measured in a total of three western blots (n=3). One-way ANOVA. P-value $*<0.05$, $**<0.01$. Data are presented as mean ± SD. EV = empty vector.

c. Ratios of p-AKT (Ser473) as the target of mTORC2 to total levels of AKT. Quantification of the AKT phosphorylation was measured in a total of three western blots (n=3). One-way ANOVA. The difference between groups is non-significant. Data are presented as mean ± SD. EV = empty vector.

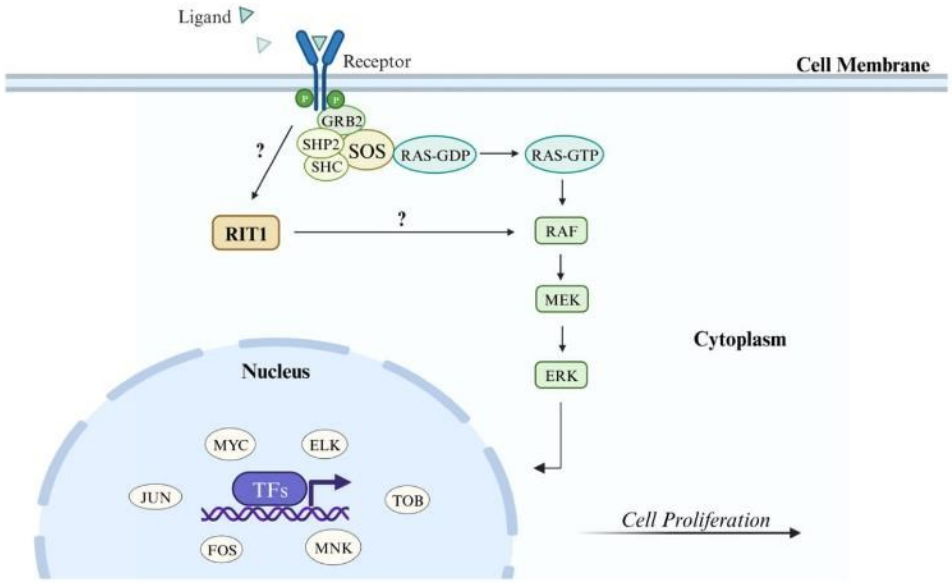

Supplemental Figure S3 (Online Resource 3). Schematic of the RAS signaling pathway.

SHP2 is upstream, MEK further downstream in the RAS-MAPK signaling pathway; created with BioRender.com.

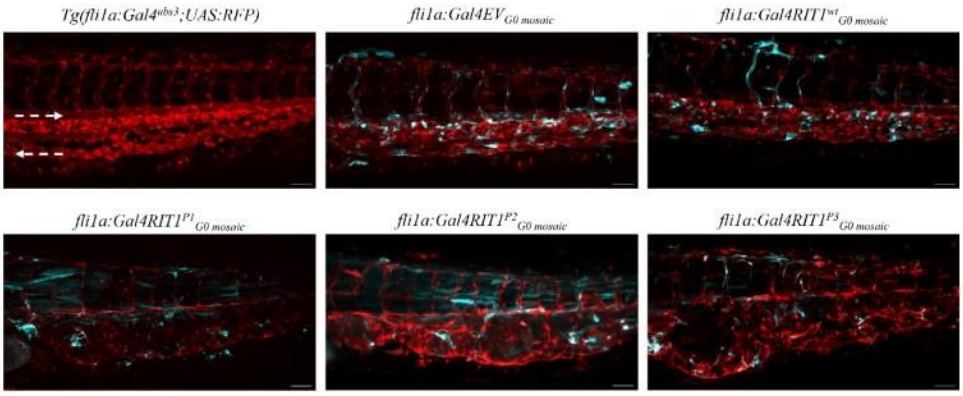

Supplemental Figure S4 (Online Resource 4). Figure 3b zebrafish AVM phenotype with assigned false colors.

Red color is assigned for RFP channel and cyan color is assigned for GFP channel. White arrows represent the direction of arterial (top) and venous blood flow (bottom) respectively. Scale bar 50 µm.

Supplemental Video S1 (Online Resource 5). Comparison of normal circulation and aberrant connection of aorta and caudal vein with fusion and dilation of vasculature in the tail distal to the AVM.

a. Notice that the blood in the dorsal aorta of the uninjected *Tg(fli1a:Gal4)* fish flows to the end of the tail and then returns in the caudal vein. Scale bar 50 µm.
b. Notice the aberrant flow in the dorsal aorta of the $RIT1^{P2}$ injected fish which moves into the caudal vein proximal in the tail, as well as a fusion of aorta and the upper part of the caudal vein plexus. Scale bar 50 µm.

Supplemental Video S2 (Online Resource 6). Positions of AV shunts in different zebrafish phenotypes.

a. Light-sheet time-lapse imaging of embryos with GFP tagged erythrocytes after $RIT1^{P3}$ injection. *Tg(fli:Gal4, UAS:RFP)* fish crossed with *Tg(LCR:GFP)* line and $RIT1^{P3}$ microinjections performed at the 1-cell stage. The shunt is only at the proximal end of the lesion but fusion of aorta and caudal vein plexus can also be observed distal to the shunt. Some erythrocytes sediment in the distal part of the lesion due to the proximal shunt and lack of blood flow in the distal part (and due to the upright position of the embryo during light-sheet microscopy). The size and pressure from the lesion are also prevents normal flow even in intersegmental vessels (ISVs). Scale bar 50 µm.
b. Example of an AV shunt (white arrow) after mosaic endothelial-specific expression of $MAP2K1^{K57N}$ in *Tg(fli1a:Gal4; UAS:RFP)* fish line. Blood flow and vascular architecture distal to the shunt is completely normal, indicating that a proximal shunt is not sufficient to lead to abnormal vascular development in the tail. Angiography is performed with Dextran, Fluorescein, 500,000 MW (#D7136) at 2dpf. Scale bar 50 µm.

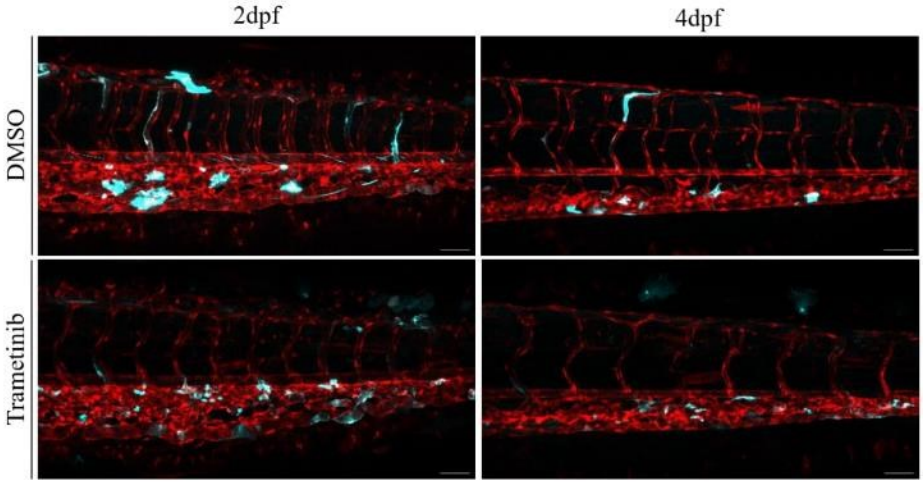

Supplemental Figure S5 (Online Resource 7). The effect of trametinib on empty vector injected embryos.

The effect of late trametinib treatment on empty vector injected embryos. Red color is assigned for RFP channel and cyan color is assigned for GFP channel. Scale bar 50 µm.

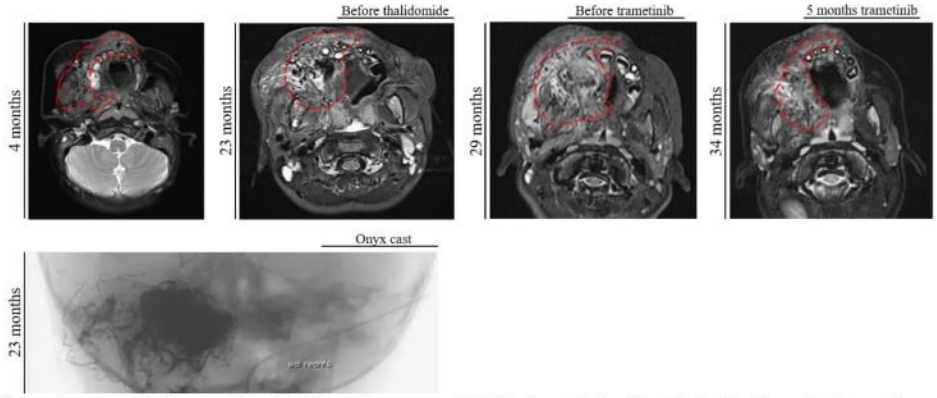

Supplemental Figure S6 (Online Resource 8). Patient P1 – Radiological evolution of disease.

(Upper panels) MRI images show the AVM's progression over time, non-response to thalidomide, and regression under trametinib treatment.

(Lower panel) Image of an angiography showing the extent of the Onyx cast on the right side of the face.

Supplemental File S1 (Online Resource 9). .STL file of the designed mould that is used to create imaging plates for Zeiss CD7 microscope.

Chapter VIII. Non-Invasive Mapping of Systemic Neutrophil Dynamics upon Cardiovascular Injury

Authors: Pascal Bouvain, Zhaoping Ding, Shiwa Kadir, Patricia Kleimann, Nils Kluge, Zeynep-Büsra Tiren, Bodo Steckel, Vera Flocke, Ria Zalfen, Patrick Petzsch,Thorsten Wachtmeister, Gordon John, Nirojah Subramaniam, Wolfgang Krämer, Tobias Strasdeit, **Mehrnaz Mehrabipour**, Jens M. Moll,Rolf Schubert, Mohammad Reza Ahmadian, Florian Bönner, Udo Boeken, Ralf Westenfeld, Daniel Robert Engel, Malte Kelm, Jürgen Schrader,Karl Köhrer, Maria Grandoch, Sebastian Temme and Ulrich Flögel

DOI: 10.1038/s44161-022-00210-w

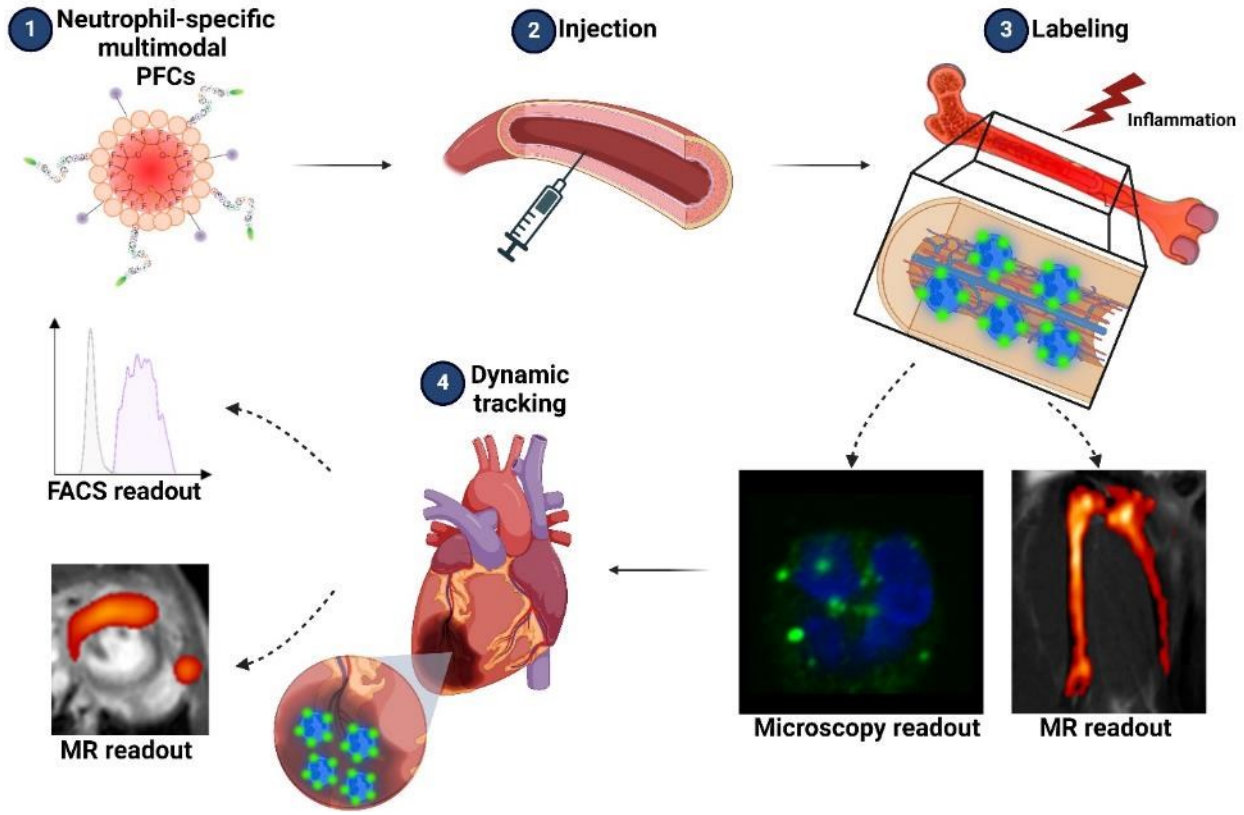

Status:	Published in February 2023
Journal:	Nature Cardiovascular Research
JIF:	9.4
Contribution:	5% Conducted SPR analysis to assess the binding characteristics of NP-specific peptides to human/murine neutrophils and monocytes, and generated the corresponding data and figures.

nature cardiovascular research

Article

https://doi.org/10.1038/s44161-022-00210-w

Non-invasive mapping of systemic neutrophil dynamics upon cardiovascular injury

Received: 7 September 2021

Accepted: 22 December 2022

Published online: 6 February 2023

Check for updates

Pascal Bouvain[1], Zhaoping Ding[1], Shiwa Kadir[1], Patricia Kleimann[1], Nils Kluge[1], Zeynep-Büsra Tiren[1], Bodo Steckel[1], Vera Flocke[1], Ria Zalfen[1], Patrick Petzsch[2], Thorsten Wachtmeister[2], Gordon John[3], Nirojah Subramaniam[4], Wolfgang Krämer[5], Tobias Strasdeit[6], Mehrnaz Mehrabipour[7], Jens M. Moll[7], Rolf Schubert[5], Mohammad Reza Ahmadian[7], Florian Bönner[8], Udo Boeken[9], Ralf Westenfeld[8], Daniel Robert Engel[4], Malte Kelm[8,10], Jürgen Schrader[1,10], Karl Köhrer[2], Maria Grandoch[11,13], Sebastian Temme[1,12,13] & Ulrich Flögel[1,8,10,13]

Neutrophils play a complex role during onset of tissue injury and subsequent resolution and healing. To assess neutrophil dynamics upon cardiovascular injury, here we develop a non-invasive, background-free approach for specific mapping of neutrophil dynamics by whole-body magnetic resonance imaging using targeted multimodal fluorine-loaded nanotracers engineered with binding peptides specifically directed against murine or human neutrophils. Intravenous tracer application before injury allowed non-invasive three-dimensional visualization of neutrophils within their different hematopoietic niches over the entire body and subsequent monitoring of their egress into affected tissues. Stimulated murine and human neutrophils exhibited enhanced labeling due to upregulation of their target receptors, which could be exploited as an in vivo readout for their activation state in both sterile and nonsterile cardiovascular inflammation. This non-invasive approach will allow us to identify hidden origins of bacterial or sterile inflammation in patients and also to unravel cardiovascular disease states on the verge of severe aggravation due to enhanced neutrophil infiltration or activation.

Neutrophils are an important part of the innate immune system[1] and play a crucial role in host defense against infections. They contribute not only to the development and progression of sterile inflammation in atherosclerosis but also to the healing process after ischemic insults such as stroke and myocardial infarction (MI)[2]. During inflammatory challenges, they are rapidly released from the bone marrow into the blood, which can lead to a tenfold increase in circulating neutrophils. Subsequently, neutrophils are recruited into inflamed areas where they internalize pathogens and cell debris, release reactive oxygen species (ROS) or generate nuclear extracellular traps[3]. Tracking of neutrophils by optical techniques has provided insight into new functions of neutrophils such as reverse transendothelial migration and tissue-specific recruitment mechanisms[4–6]. These methods are characterized by high sensitivity and spatial resolution, but systemic and non-invasive in vivo mapping with sufficient tissue penetration to monitor neutrophil trafficking from their origin in the bone marrow to the injured target organ was not feasible thus far.

Among the molecular imaging techniques capable of whole-body scanning, lately fluorine (^{19}F) MRI has emerged as a promising tool[7]. Fluorine-19 offers high sensitivity and is nearly absent from biological

A full list of affiliations appears at the end of the paper. e-mail: floegel@uni-duesseldorf.de

tissue. Thus, accumulation of ^{19}F gives rise to 'hot spots' without any natural background that can be merged with anatomical ^{1}H datasets to assess their location. To generate ^{19}F-based MRI probes, we made use of emulsified, biochemically inert perfluorocarbons (PFCs), which are characterized by a very high payload of ^{19}F. After intravenous injection, 'neat' PFCs are readily taken up by phagocytic immune cells, which has already been reported as a side effect during their clinical exploration as an artificial blood substitute[8]. Although neutrophils can also be labeled to a certain degree by conventional PFCs as bystander cells, highly specific visualization of this cell type requires active targeting[9,10] of ^{19}F tracers. Here, we raise this approach to a new level and introduce specific and multimodal PFC targeting for systemic and non-invasive 3D mapping of neutrophil dynamics by combined in vivo ^{1}H/^{19}F MRI with subsequent ex vivo validation by flow cytometry and fluorescence microscopy. In a first step, we proved the feasibility of tracking neutrophil recruitment in mice and expanded this thereafter to human neutrophils. With this approach, we were not only able to target neutrophils in the circulation but also within their hematopoietic niches and to follow their migration in vivo into injured tissue over time.

Results

Targeting murine neutrophils via murine neutrophil-specific peptide

For targeting murine neutrophils with PFCs, we used a small peptide (murine neutrophil-specific peptide, mNP) recently identified by phage display screening to specifically bind to the neutrophil-specific receptor CD177 (ref. [11]); a peptide with randomized sequence served as the control (Con). We modified these core peptides (Extended Data Fig. 1a) N terminally with carboxyfluorescein for fluorescence detection and C terminally with cysteine for coupling to maleimide PFCs (^{Mal}PFCs) to generate ^{mNP}PFCs and ^{Con}PFCs, respectively. Preformed ^{Mal}PFCs were equipped with a separate fluorescence label (rhodamine) for analysis of cellular uptake and to control for potential dissociation of the binding ligand and PFC (Extended Data Fig. 1b) by fluorescence-based methods. Importantly, all targeted PFCs were additionally PEGylated to block 'passive' uptake by phagocytic cells[12]. Subsequently, isolated murine immune cells were exposed ex vivo to the generated PFCs, and their targeting specificity was verified by flow cytometry. We observed a rapid and strong neutrophil-specific uptake of ^{mNP}PFCs, whereas only minor incorporation was observed for other immune cells, which is in line with the lack of CD177 expression in these other immune cell subtypes (Extended Data Fig. 2a,b). Similar results were obtained by ^{1}H/^{19}F MRI (Extended Data Fig. 2d; for superimposing the images of both nuclei, a 'hot iron' color look-up table was applied to ^{19}F images). Next, we verified the in vivo uptake of intravenously applied ^{mNP}PFCs by neutrophils within the bone marrow by flow cytometry. As soon as 2 h after intravenous (i.v.) injection, we found strong labeling of bone marrow neutrophils by ^{mNP}PFCs, while only negligible uptake was observed for ^{Con}PFCs (Extended Data Fig. 2c).

In parallel, we analyzed the biodistribution of ^{mNP}PFCs by ^{1}H/^{19}F MRI up to 24 h after i.v. injection. During this observation period, ^{mNP}PFCs were cleared from the blood pool and, as expected, concurrently accumulated also in the liver and spleen (Extended Data Fig. 3a). However, neither analysis of liver serum markers (GLDH, AST, ALP, ALT, bilirubin) nor histological examination of the liver and spleen revealed any evidence for adverse side effects of ^{mNP}PFCs (Extended Data Fig. 3b,c).

Systemic 3D mapping of neutrophil dynamics by ^{1}H/^{19}F MRI

To follow the trafficking of neutrophils from their hematopoietic niches into inflammatory foci, we used a model of cardiac ischemia and reperfusion injury (MI), well known to be associated with acute and massive neutrophil recruitment into the injured myocardium[13]. For monitoring the fate of neutrophils upon MI, mice received daily intravenous injections of ^{mNP}PFCs over 3 d before MI, and systemic labeling of neutrophils within the distinct bone marrow compartments was verified by in vivo ^{1}H/^{19}F MRI. Subsequently, mice were subjected to MI and, after 24 h, again scanned by MRI and/or analyzed by flow cytometry (timeline in Extended Data Fig. 4a,b).

Whole-body ^{1}H/^{19}F MRI before MI corroborated the finding that the labeling protocol with ^{mNP}PFCs resulted in strong ^{19}F uptake by bone marrow neutrophils, particularly in the femur, tibia, brachium, antebrachium and sternum, with the highest ^{19}F signals originating from the femur and tibia (Fig. 1a, left; for the sake of clarity, ^{19}F signals from the liver and spleen have been faded out (see Extended Data Fig. 4c for the enclosure of these organs)). Re-investigation 24 h after induction of MI revealed substantial reduction of ^{19}F signals in the bone marrow of the femur and tibia (Fig. 1a, right) with concomitant appearance of ^{19}F labeling in the infarcted heart. In line with these in vivo findings, flow cytometry identified the femur as the main neutrophil reservoir and also as the bone marrow compartment with the largest decrease in neutrophils 24 h after MI (Fig. 1b). Because this indicated the femur as the most important source for neutrophil release upon MI, we focused for the following on a more localized mapping approach with optimized spatial resolution and sensitivity for ^{1}H/^{19}F MRI of the hindlimb and heart. Of note, independent experiments with anti-Ly6G antibodies applied 48 and 24 h before ^{mNP}PFC application to deplete neutrophils resulted in strongly decreased ^{19}F signals in the bone marrow (Extended Data Fig. 5a), further corroborating the idea that these signals are predominantly caused by ^{mNP}PFC labeling of neutrophils.

Focal scanning of the thighs before and 24 h after MI confirmed the strong decrease of ^{19}F signals in the bone marrow of the femur after MI (Fig. 1c, top and bottom), which was most pronounced in the diaphysis (Extended Data Fig. 5b,c). In parallel, well-resolved images of the thorax unequivocally corroborated the simultaneous appearance of ^{19}F labeling in the heart (Fig. 1e, top). Cine MRI in combination with late gadolinium enhancement (LGE) demonstrated that the detected ^{19}F pattern perfectly matched the LGE-delineated myocardium (Fig. 1e, top). Quantification of ^{19}F data showed the emerging ^{19}F signal in the heart to be on the same order of magnitude as the decline in the bone marrow (Fig. 1d,f), strongly indicating that this is caused by ^{mNP}PFC-loaded neutrophils released from the femur and entering the infarcted myocardium. Importantly, animals that received ^{Con}PFCs exhibited significantly less labeling of the bone marrow before MI, which was unchanged after MI and led to only minor amounts of ^{19}F labeling in the infarcted region (Fig. 1d,f). Furthermore, application of neutralizing antibodies to inhibit the egress of ^{mNP}PFC-loaded neutrophils from the femur into the blood blunted MI-induced effects in the heart and femur (Fig. 1e,f and Extended Data Fig. 5d,e). Similarly, sham-operated animals treated with ^{mNP}PFCs showed only negligible ^{19}F signals (Fig. 1f): ischemic area (LGE) and functional impairment at this early point in time after MI were similar in all groups (Extended Data Fig. 5f). Remarkably, linear regression of the LGE-delineated myocardium and the ^{19}F integral resulted in a significant correlation of ischemic area and infiltrated neutrophils 24 h after MI (Fig. 2a, adjusted $R^2 = 0.961$). When extending the time window of our analysis to 1, 3, 6, 24, 48 and 72 h after MI, we observed a continuous increase in ^{19}F signal up to 24 h (Fig. 2b), which is in line with the infiltration kinetics of neutrophils after MI reported in the literature[14]. To further validate that ^{19}F patterns detected in vivo are localized within the infarcted myocardium, hearts were excised and analyzed by high-resolution ^{1}H/^{19}F MRI, which unequivocally pinpointed the ^{19}F signal within the infarct area (Fig. 2c). Additional histology confirmed the specific uptake of ^{mNP}PFCs by neutrophils in the infarcted heart, while signals from macrophages and monocytes were negligible (Fig. 3a–d). This was also corroborated by flow cytometry of immune cells isolated from the infarcted heart (Fig. 3e).

Conjugation is required for specific uptake of mNP

As described above, mNP-decorated PFCs specifically labeled murine neutrophils (Extended Data Fig. 2a,b and Fig. 4a, left), but when we additionally characterized the properties of the free mNP peptide itself,

https://doi.org/10.1038/s44161-022-00210-w

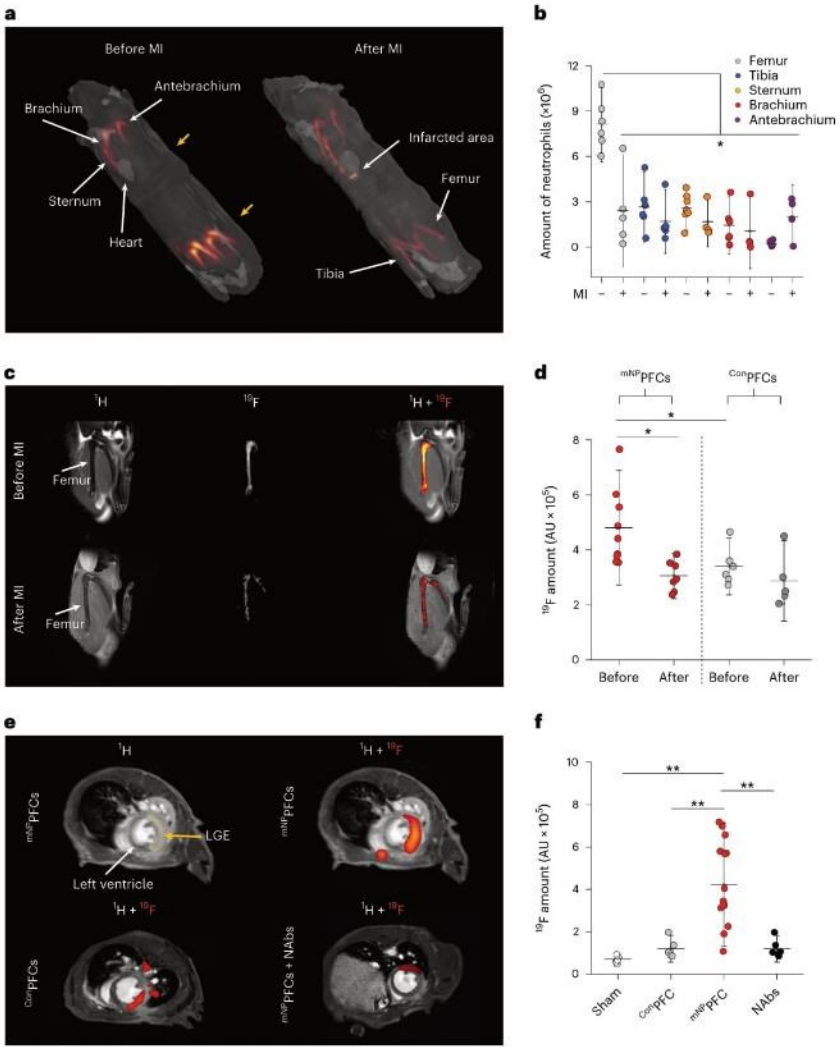

Fig. 1 | Mapping the trafficking of murine neutrophils after MI by ^{mNP}PFCs in vivo. a, Whole-body 3D ^{1}H/^{19}F MRI for systemic in vivo visualization of neutrophils before and after MI. Anatomical ^{1}H data were rendered transparent in grayscale with ^{19}F data overlaid in orange and red; for the sake of clarity, signals from the liver and spleen were faded out. Left, intravenous application of ^{mNP}PFCs before MI resulted in in situ labeling of neutrophils within their hematopoietic niches, showing the most prominent ^{19}F signal in the femur and tibia. The yellow arrows indicate the areas of the local scans from the femur and heart in **c**,**e**, respectively. Right, re-investigation 24 h after MI revealed a pronounced reduction of ^{19}F signals in the bone marrow of the femur and tibia with simultaneous appearance of ^{19}F labeling in the infarcted heart. **b**, Post-mortem flow cytometry of the different bone marrow compartments confirmed the in vivo findings in that the femur was not only the bone containing the highest number of neutrophils before MI but also the compartment with the strongest release of neutrophils as compared to all other bones. **c**, Focal ^{1}H/^{19}F MR images of the bone marrow after in vivo labeling with ^{mNP}PFCs and ^{Con}PFCs and subsequent MI. Left, the first column displays anatomical ^{1}H MR images of the femur, the second column shows corresponding background-free ^{19}F MR images, and the third column is an overlay of both datasets showing strong ^{19}F signals within the bone marrow after ^{mNP}PFC labeling (top) and a substantial signal drop 24 h after MI (bottom). **d**, Quantification demonstrated a significant reduction in ^{19}F femur signals after MI in the ^{mNP}PFC-treated group, whereas application of ^{Con}PFC resulted in low baseline labeling and almost no change after MI. AU, arbitrary units. **e**, Local ^{1}H/^{19}F MR images of the thorax revealed concomitant appearance of distinct ^{19}F signals in the infarcted region when bone marrow neutrophils were labeled with ^{mNP}PFCs. Top left, anatomical ^{1}H MR image with delineation of the infarcted myocardium by LGE (dotted line). Top right, overlay with the corresponding ^{19}F MR image confirms matching of the fluorine signal with detected LGE patterns. Bottom left and right, substantially lower ^{19}F deposition within the infarcted myocardium was observed after labeling with ^{Con}PFCs (left) or ^{mNP}PFCs when neutrophil egress was inhibited by neutralizing antibodies (NAbs, right). Neutralizing antibodies against CXCL1, CXCL2 and granulocyte colony-stimulating factor (G-CSF) as well as granulocyte–macrophage colony-stimulating factor (GM-CSF) were intraperitoneally injected 1 h before and 4 h after induction of MI (50 μg each at both time points). **f**, Quantification of the cardiac ^{19}F MR signal for all treatments. Data are mean ± s.d. of $n = 4–7$ (**b**), $n = 5–9$ (**d**) or $n = 6–15$ (**f**) independent experiments; $^{*}P < 0.05$, $^{**}P < 0.01$, verified by one-way ANOVA.

https://doi.org/10.1038/s44161-022-00210-w

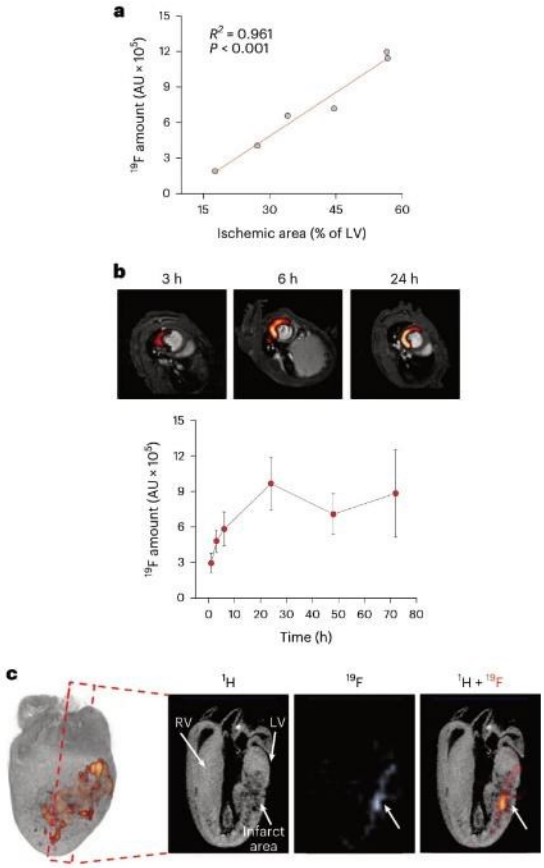

Fig. 2 | Correlation of the ^{19}F signal with ischemic area, its temporal development and ex vivo validation. a, Linear regression between ischemic area (LGE) and fluorine signal within the infarcted myocardium. **b**, Time course of neutrophil infiltration into the injured heart. The fluorine signal was determined 1, 3, 6, 24, 48 and 72 h after induction of MI (examples are given at the top). **c**, To further corroborate the location of the ^{19}F signal within the infarcted myocardium, hearts were excised, fixed with paraformaldehyde and analyzed by ex vivo high-resolution ^{1}H/^{19}F 3D MRI. In long-axis ^{1}H MR images, the infarcted area can be unequivocally identified as a dark structure within the bright intact myocardium. Importantly, the corresponding ^{19}F signal is restricted to the infarcted area, indicating infiltration of ^{mNP}PFC-labeled neutrophils only into the injured myocardium. Left, 3D volume rendering of the heart with superimposed ^{19}F signal. LV, left ventricle; RV, right ventricle. Data are mean ± s.d. of $n = 6$ (**a**) and $n = 5–6$ (**b**) independent experiments.

we surprisingly found that unbound mNP did not label neutrophils (Fig. 4a, right). To verify whether conjugation affects its binding, mNP was coupled to an eight-arm PEG_{2000}-maleimide molecule. Subsequent exposure of murine neutrophils to these conjugates indeed revealed much stronger uptake (Fig. 4b, left). This was not related to high avidity due to enhanced local density of mNP, because, even at very high concentrations, free mNP was not taken up by murine neutrophils (Fig. 4b, right). For additional information on the binding characteristics of mNP, we performed surface plasmon resonance spectroscopy (SPR, Extended Data Fig. 6a,b). To this end, mNP was conjugated to a sensor chip, and subsequently neutrophils (red) as well as monocytes (gray) were flushed over the sensor surface. As can be clearly recognized, SPR sensorgrams revealed rapid association of neutrophils with the immobilized mNP and a slow dissociation rate. By contrast, monocytes showed only a minor association with immobilized mNP (Extended Data Fig. 6a). Altogether, these data indicate that a certain degree of conjugation of mNP is required for binding and subsequent labeling of murine neutrophils, which clearly hampers broader translational application by coupling mNP to small molecular positron emission tomography (PET) or Gd tracers.

Targeting human neutrophils via hNP

Due to these restrictions of mNP binding, we altered the targeting strategy for human neutrophils and used a peptide that has been identified as specific for human neutrophils and does not require coupling to scaffolds for targeting (human neutrophil-specific peptide, hNP)[15]. We modified hNP as detailed above and verified its uptake by isolated human immune cells. As shown in Fig. 4c and Extended Data Fig. 6e, flow cytometry confirmed specificity of hNP for neutrophils again compared to a randomized control peptide and to other immune cell populations.

Because the binding target for hNP on human neutrophils was not yet identified, we next aimed to characterize its membrane receptor. For this, we cross-linked an hNP–TriCeps conjugate to the surface of isolated human neutrophils (Fig. 4d). After cell lysis, ligands were enriched, purified and identified by mass spectrometry[16]. In parallel, a transferrin–TriCeps conjugate was used for exclusion of nonspecific binding candidates. Subsequent data analysis revealed enrichment of 24 proteins for hNP compared to transferrin (Supplemental Table 1). Remarkably, volcano plots identified human CD177 as the most abundant protein (Fig. 4e), indicating that it is a binding partner for hNP, analogous to mNP binding to murine CD177. This was further corroborated by a second set of experiments with a modified spacer (Extended Data Fig. 6f). Subsequently, we transiently transfected Chinese hamster ovary (CHO) cells with plasmids encoding human CD177 and confirmed that transfected cells bound hNP but not the control peptide (Fig. 4f). Only the high-affinity anti-CD177 monoclonal antibody as a positive control displayed as strong an effect as hNP; untransfected CHO cells did not bind hNP or monoclonal antibodies against CD177, indicating absence of endogenous CD177 expression (Fig. 4f). Additionally, we stained neutrophils with hNP only or in combination with monoclonal antibodies against CD177, demonstrating that only CD177-positive neutrophils co-stain with hNP and anti-CD177 monoclonal antibody (Fig. 4g, top). Interestingly, a fraction of the human population does not express CD177 on neutrophils, and staining blood cells from CD177-negative volunteers did not show binding of anti-CD177 monoclonal antibody or hNP (Fig. 4g, bottom). Analogous to the murine neutrophil peptide, we finally performed SPR analyses of hNP: here, neutrophils exhibited an even stronger initial binding phase and slow dissociation, while monocytes displayed only negligible binding to the sensor chip (Extended Data Fig. 6c,d).

Of note, we observed no uptake of hNP by neutrophils from pigs, rats or mice (Extended Data Fig. 7a). Sequence analysis revealed only low-grade amino acid conservation of CD177 between those species, which may account for the specificity of hNP for human neutrophils (Extended Data Fig. 7b).

Visualization of human neutrophils by ^{19}F MRI using ^{hNP}PFCs

Next, hNP was coupled to PFCs, and the formed ^{hNP}PFCs were evaluated for labeling of immune cells from human blood. ^{hNP}PFCs avidly bound to neutrophils, whereas ^{Con}PFCs displayed only marginal binding (Fig. 5a). Importantly, we observed no binding to lymphocytes and only minor uptake by monocytes and their subtypes even under lipopolysaccharide (LPS) stimulation (Extended Data Fig. 8a). To confirm that the hNP-based targeting approach is also suitable for ^{19}F MRI, human neutrophils were incubated with ^{hNP}PFCs, separated from free ^{hNP}PFCs by density gradient centrifugation and subsequently subjected

to combined $^{1}H/^{19}F$ MRI. In T_2-weighted ^{1}H magnetic resonance (MR) images, cells can be identified as a small dark layer within the 'light' buffer band (arrow) superimposed on the dark Percoll layer below (Fig. 5b). As can be clearly recognized, cells exposed to ^{hNP}PFCs displayed significantly stronger ^{19}F signals than controls.

^{hNP}PFC uptake and impact on human neutrophil function

For longitudinal tracking, it would be highly desirable that ^{hNP}PFCs not only bind to but are also internalized by neutrophils to avoid shearing off of the targeting moieties from the cell surface. To explore uptake of the targeting peptide upon binding, we coupled the pH-sensitive dye pHrodo to hNP (^{rodo}hNP). Incubation of neutrophils with ^{rodo}hNP at 37 °C, but not at 4 °C, led to a massive increase in fluorescence intensity (Fig. 5c), strongly indicating energy-dependent internalization of the peptide and its deposition within the acidic endosomal–lysosomal compartments. Next, we monitored uptake of the coupled ^{hNP}PFCs by confocal immunofluorescence microscopy and observed unambiguous co-staining (yellow arrows) of rhodamine (→PFC) and carboxyfluorescein (→hNP) within cells, while ^{Con}PFCs resulted only in background signals (Fig. 5d).

In a competition approach, neutrophils were pretreated with hNP at high concentrations to block CD177-binding sites, which strongly inhibited subsequent ^{hNP}PFC uptake (Fig. 5e), further corroborating hNP specificity and excluding passive endocytosis. Moreover, differentiation between CD177$^-$ and CD177$^+$ neutrophils demonstrated that only the latter population could be labeled with ^{hNP}PFCs (Fig. 5f). Detailed physicochemical characterization of the emulsions excluded the idea that targeting of ^{hNP}PFCs may be related to any differences in size, size distribution, ζ potential, fluorescence intensity or ^{19}F content (Extended Data Fig. 8b). Furthermore, only tiny amounts of empty liposomes were observed as undesired side products of the PFC preparation (Extended Data Fig. 8c–e, red arrows).

To investigate whether the targeting agent impacts physiological neutrophil effector functions, we first performed bulk mRNA sequencing (~45,000 genes) of human neutrophils exposed to saline (control), ^{Con}PFCs or ^{hNP}PFCs. However, after Bonferroni correction of the datasets, we identified just six genes that exhibited only moderately different expression levels (*BTNL3*, *CLU*, *CXCL5*, *PF4*, *PPBP* and *RGPD5*; all upregulated) when comparing the targeting PFCs to saline and only one gene when comparing to ^{Con}PFCs (*RGPD5*, upregulated; Fig. 6a). As C–X–C chemokine ligand (CXCL)5 is known as a driver of neutrophil recruitment[17], we next verified their migration toward interleukin (IL)-8 in the presence of the targeting PFCs but found no evidence for any changes in their chemotactic properties (Fig. 6b). Furthermore, neither ^{hNP}PFCs nor the free peptide had any impact on human neutrophil ROS release (Fig. 6c). Additionally, we analyzed expression of the transmembrane proteins CD11b, CD63 and CD66b, reported as sensitive markers for human neutrophil activation[18–20]. Exposure of neutrophils to ^{hNP}PFCs did not affect expression of these proteins, while LPS as a positive control led to significantly increased levels of CD11b and CD66b (Fig. 6d). Of note, very similar results were obtained in corresponding experiments for ^{mNP}PFCs and murine neutrophils (Extended Data Fig. 9a–c). Bulk RNA sequencing of ~25,000 genes upon ^{mNP}PFC injection indicated only one gene with changed expression levels compared to saline (*Per1*, downregulated) and to ^{Con}PFCs (*Pagr1a*, upregulated), respectively (Extended Data Fig. 9a). Moreover, migration, ROS production and phagocytosis were also unaltered in the presence of the targeting PFCs (Extended Data Fig. 9c) as expression levels of murine activation markers CD11b, CD62L and CD63 (ref. [21]), while again LPS significantly increased CD11b and CD63 on the cell surface of murine neutrophils (Extended Data Fig. 9b).

Effect of inflammatory stimuli on ^{NP}PFC labeling

In a next step, we investigated whether ^{NP}PFC uptake by neutrophils is altered under pathological challenges. To mirror the conditions in murine trafficking experiments after MI (Fig. 1), we used isolated neutrophils from blood of patients with STEMI (that is, ST elevation MI) obtained within the first 24 h after MI and found substantially stronger cellular uptake of ^{hNP}PFCs than that of healthy volunteers (control) as demonstrated by both flow cytometry and ^{19}F MRI (Fig. 7a,b). Importantly, there was no ^{hNP}PFC incorporation by other blood cells from patients with STEMI (Extended Data Fig. 10a) and the elevated uptake was specific to hNP, because neither conventional PFCs nor dextran particles showed stronger internalization by neutrophils from patients with STEMI (Extended Data Fig. 10b,c).

To evaluate whether this observation is a cross-species phenomenon associated with various inflammatory stimuli, we employed a well-defined model of murine inflammation induced by subcutaneous implantation of a Matrigel plug doped with LPS[22]. Twenty-four hours after surgery, neutrophils were isolated from the blood, incubated ex vivo with ^{mNP}PFCs and subsequently analyzed by flow cytometry. In line with the findings above, we observed more rapid and potent uptake of ^{mNP}PFCs by murine neutrophils under LPS-stimulated conditions than under unstimulated conditions (control, Fig. 7c). Similar results were obtained in vivo: intravenous ^{mNP}PFC application resulted already after 1 h in much stronger ^{mNP}PFC incorporation into circulating neutrophils from LPS-challenged mice than that from healthy mice (Fig. 7d). Importantly, this effect was restricted to neutrophils, while lymphocytes and monocytes showed only minor and unaltered ^{mNP}PFC uptake under inflammatory conditions.

Next, we explored whether the enhanced incorporation of neutrophil-specific peptide PFCs (^{NP}PFCs) under inflammatory stimulus conditions is specifically related to altered surface expression levels of their target receptor CD177. First, we analyzed neutrophils isolated from blood and excised Matrigel–LPS plugs 24 h after implantation and found that surface expression of CD177 was indeed higher in blood neutrophils from stimulated mice than in those from unstimulated mice (control, Fig. 8a, left). However, neutrophils that were obtained

Fig. 3 | Identification of ^{mNP}PFC-labeled neutrophils in the infarcted heart. **a**, For identification of ^{mNP}PFC-labeled neutrophils in the infarcted heart, mice received injections of rhodamine-tagged ^{mNP}PFCs or ^{Con}PFCs 2 h before induction of MI and hearts were excised 2 h after induction of MI. The infarct area was visualized by 2,3,5-triphenyltetrazolium chloride (TTC) staining, which was found to colocalize with strong rhodamine signals derived from ^{mNP}PFC-labeled cells (bottom). By contrast, ^{Con}PFCs led to much weaker and spread-out signals only (top). Magnifications and histograms (fourth and fifth columns) demonstrated distinct signals for ^{mNP}PFCs but only diffuse patterns for ^{Con}PFCs. **b**, Left, examination of infarct (MI) and remote (RM) regions revealed strong rhodamine labeling colocalized with Ly6G staining in the injured tissue. Right, quantification confirmed the selective uptake of ^{mNP}PFCs versus ^{Con}PFCs. **c**, Analysis of ^{mNP}PFC uptake by cardiac neutrophils (left, Ly6G staining), macrophages (middle, major histocompatibility complex (MHC) II staining) and T cells (right, CD3 staining). Rhodamine signals were colocalized with neutrophils, while macrophages and T cells showed little or no signals. **d**, Quantification of mean fluorescence intensities (MFI) of individual cell types demonstrated significantly stronger labeling of neutrophils than of macrophages and T cells. **e**, To further corroborate the histological data, immune cells were isolated from the infarcted heart by Langendorff digestion and analyzed by flow cytometry. To identify the different immune cell clusters, cells were stained for CD45, CD11b, Ly6C and Ly6G. Neutrophils (CD45$^+$CD11b$^+$Ly6C$^-$Ly6G$^+$) were characterized by strong labeling after ^{mNP}PFC injection, while classical monocytes (CD45$^+$CD11b$^+$Ly6C$^+$Ly6G$^-$), macrophages (CD45$^+$CD11b$^+$Ly6C$^-$Ly6G$^-$) and lymphocytes (CD45$^+$CD11b$^-$Ly6C$^-$Ly6G$^-$) exhibited only low signal intensities in relation to animals injected with ^{Con}PFC. Data are mean ± s.d. of $n = 3$ (**a**), $n = 3$ (**b**), $n = 3$ (**c**), $n = 8–48$ (**d**) and $n = 6$ (**e**) independent experiments (**a**–**c**,**e**) or individual cell MFI measurements from three independent experiments (**d**). $^{**}P < 0.01$, $^{***}P < 0.001$, verified by two-sided Student's *t*-test (**b**) or one-way ANOVA.

https://doi.org/10.1038/s44161-022-00210-w

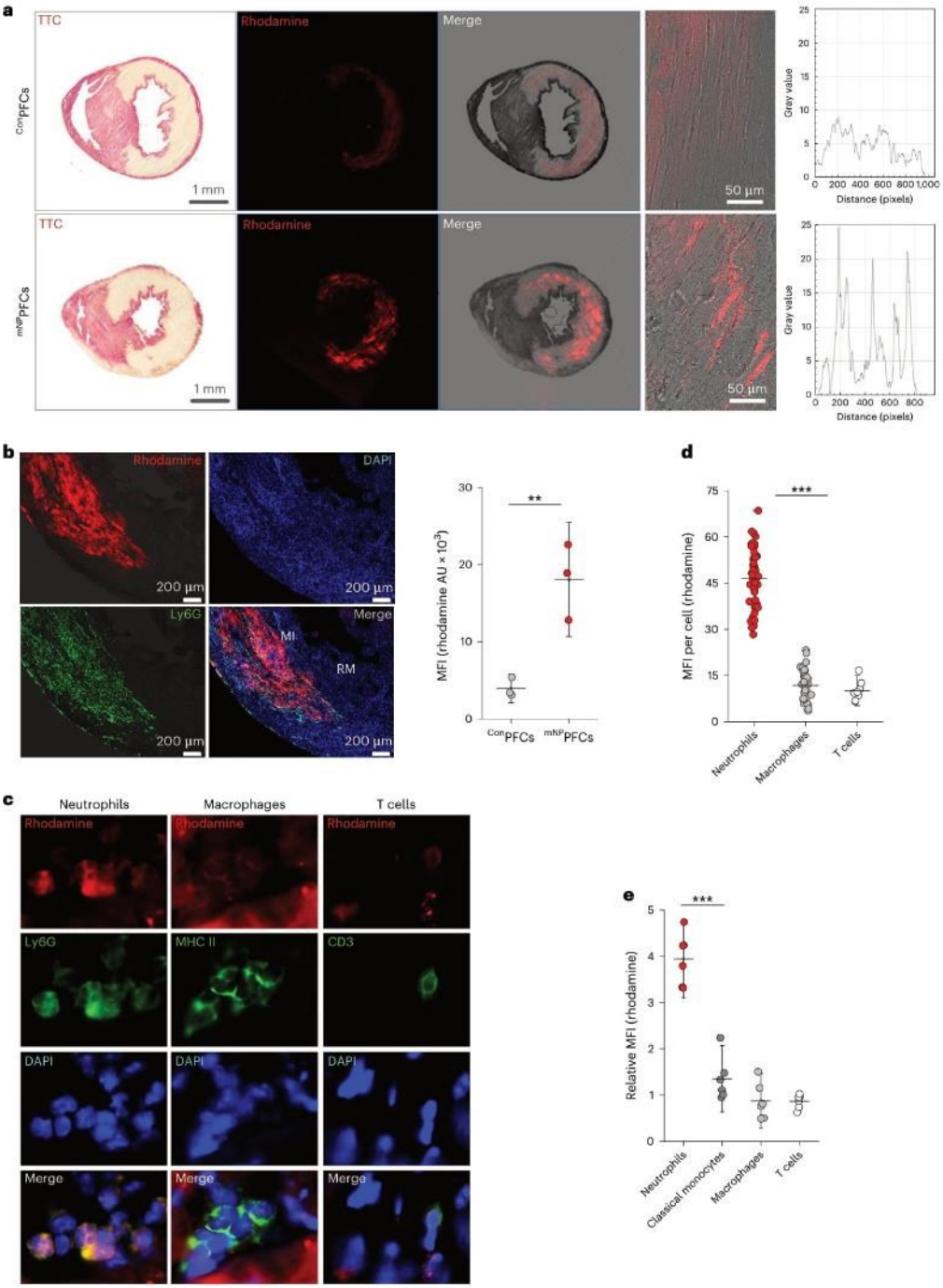

https://doi.org/10.1038/s44161-022-00210-w

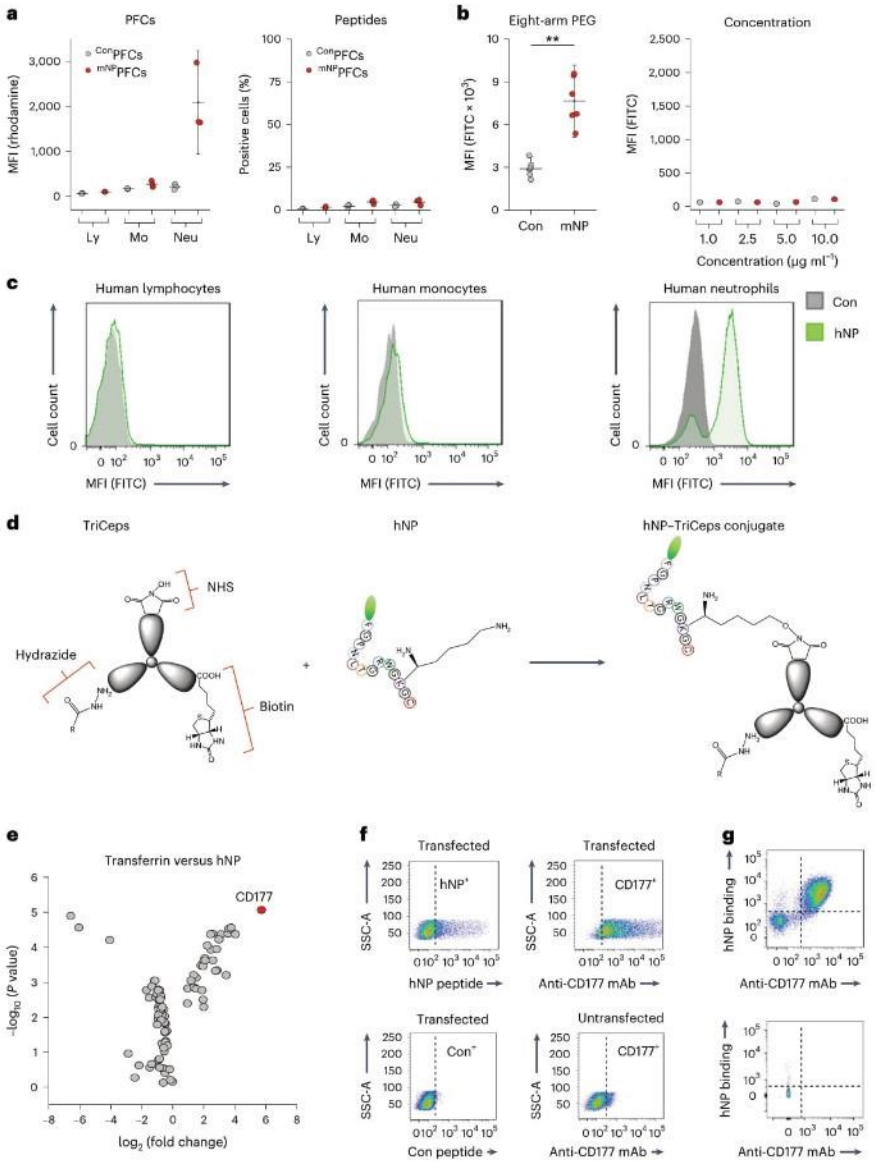

Fig. 4 | Limitations of mNP and identification of CD177 as a target for hNP on human neutrophils. a, Uptake of either ^{mNP}PFCs and ^{Con}PFCs (left) or the free peptides mNP and Con (right) by murine immune cells, quantified by flow cytometry. Note that ^{mNP}PFCs (red, left) were strongly taken up by neutrophils (Neu), whereas unconjugated free mNP (red, right) did not label neutrophils. Ly, lymphocytes; Mo; monocytes. **b**, Left, mNP (red) as well as the control peptide Con (gray) was conjugated to eight-arm PEG_{2000}-maleimide, and the uptake of these conjugates by neutrophils was analyzed by flow cytometry. Right, impact of increasing mNP and Con concentrations (1, 2.5, 5 and 10 μg ml^{-1}) on labeling of neutrophils. **c**, Representative flow cytometry histograms of human immune cells incubated with hNP (green) or its control peptide (Con, gray). **d**, Concept for identification of the binding target of hNP using TriCeps, which consists of an *n*-hydroxysuccinimide (NHS) group for conjugation to hNP, a hydrazide for binding to different sugar structures on the cell surface and biotin for purification. **e**, Isolated human neutrophils were incubated with the hNP–TriCeps conjugate, and, thereafter, cells were lysed and subjected to affinity purification. Volcano plot of mass spectrometric analysis identified CD177 as the most likely candidate target for hNP. **f**, To confirm CD177 as the binding partner for hNP, CHO cells were transiently transfected with plasmids encoding human CD177. The binding of hNP (top left) and Con (bottom left) as well as a CD177 monoclonal antibody (mAb) (top right) was determined by flow cytometry. Untransfected cells served as the control (bottom right). SSC, side scatter. **g**, Human neutrophils were co-stained with either hNP (top) or hNP and anti-CD177 monoclonal antibody (bottom), followed by flow cytometry: a CD177-positive donor (top) and a CD177-negative donor (bottom). Data are mean ± s.d. of $n = 5–6$ (**a**) or $n = 5–7$ (**b**) independent experiments; $^{***}P < 0.001$, verified by two-sided Student's *t*-test.

https://doi.org/10.1038/s44161-022-00210-w

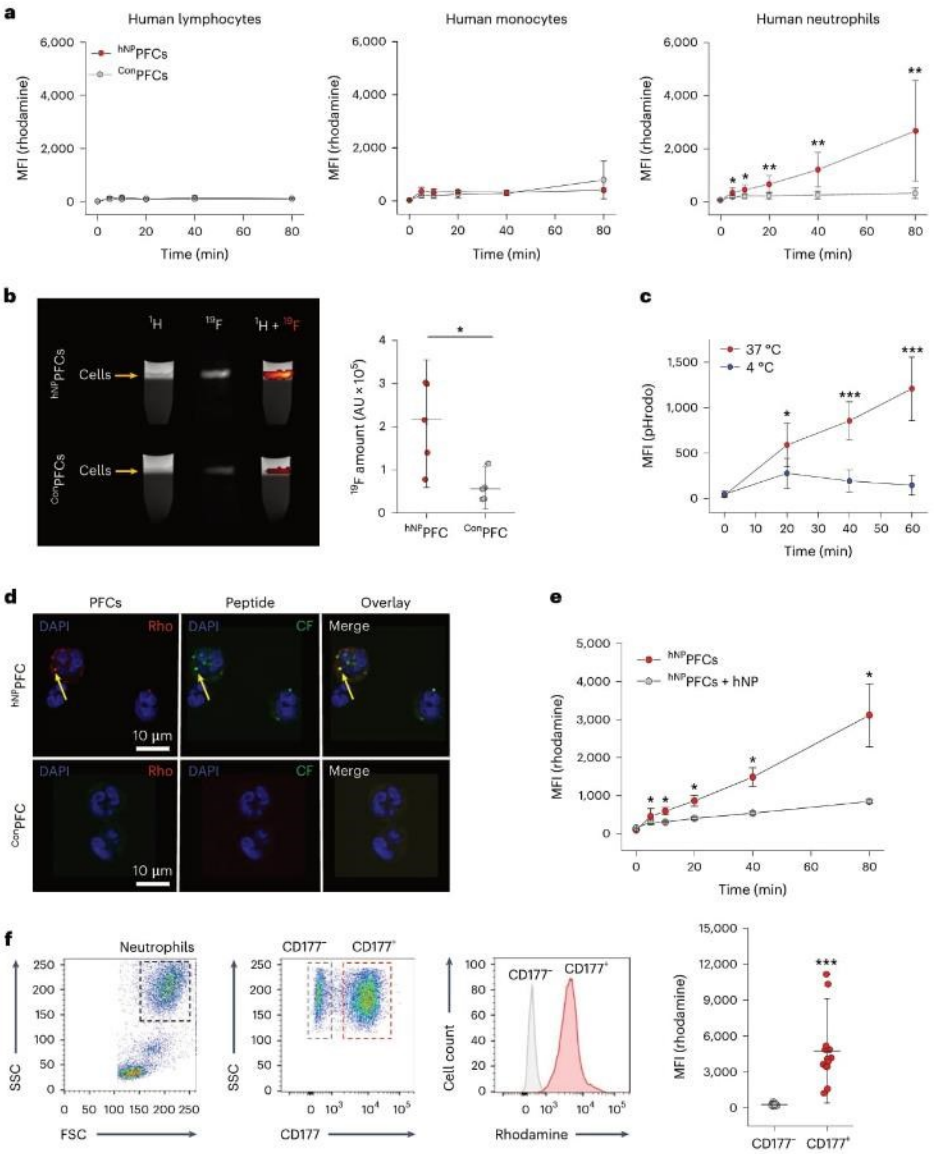

Fig. 5 | Specific targeting of human neutrophils by hNPPFCs. a, Uptake of hNPPFCs (red) or ConPFCs (gray) by human lymphocytes, monocytes or neutrophils over time as determined by flow cytometry. $^{**}P < 0.01$. **b**, For MRI analysis, human immune cells were incubated with hNPPFCs (top row) or ConPFCs (bottom row). After several washing steps, cells were purified by density gradient centrifugation and analyzed by MRI. First column, ^{1}H MR image of the centrifugation tube with the cell layer (arrow) on top of the dark Percoll layer; second column, ^{19}F MR image of the same area; third column, merge of both datasets. Quantification of the ^{19}F data is shown on the right. **c**, hNP was conjugated to the pH-sensitive dye pHrodo, incubated with neutrophils at 4 °C (blue) and 37 °C (red) and analyzed by flow cytometry. **d**, Confocal microscopy of neutrophils incubated with hNPPFCs (top) or ConPFCs (bottom). Fluorescence signals of PFCs (rhodamine; Rho) as well as ligands (carboxyfluorescein; CF) were recorded, and nuclei were counterstained with 4′,6-diamidino-2-phenylindole (DAPI) (blue). Accumulation of hNPPFCs within the endosomal–lysosomal system is highlighted by yellow arrows. **e**, Neutrophils were pretreated with hNP at 4 °C (gray) or left untreated (red), followed by incubation with hNPPFCs. At distinct time points, uptake of hNPPFCs was determined by flow cytometry. **f**, Human blood immune cells were incubated with hNPPFCs followed by staining for CD177 and flow cytometry. Neutrophils were gated with the appropriate FSC and SSC settings, and both subpopulations (CD177$^-$, CD177$^+$) were identified by CD177 staining. For the histogram plot and quantification, while CD177$^+$ neutrophils were positive for the rhodamine label of the hNPPFCs (red), CD177$^-$ neutrophils were rhodamine negative (gray). FSC, forward scatter. Data are mean ± s.d. of $n = 4$–6 (**a**), $n = 5$–6 (**b**), $n = 5$–6 (**c**), $n = 3$ (**d**), $n = 3$–4 (**e**) and $n = 13$ (**f**) independent experiments; $^{*}P < 0.05$, $^{***}P < 0.001$, verified by two-way ANOVA (**a**,**c**,**e**) or two-sided Student's *t*-test (**b**).

https://doi.org/10.1038/s44161-022-00210-w

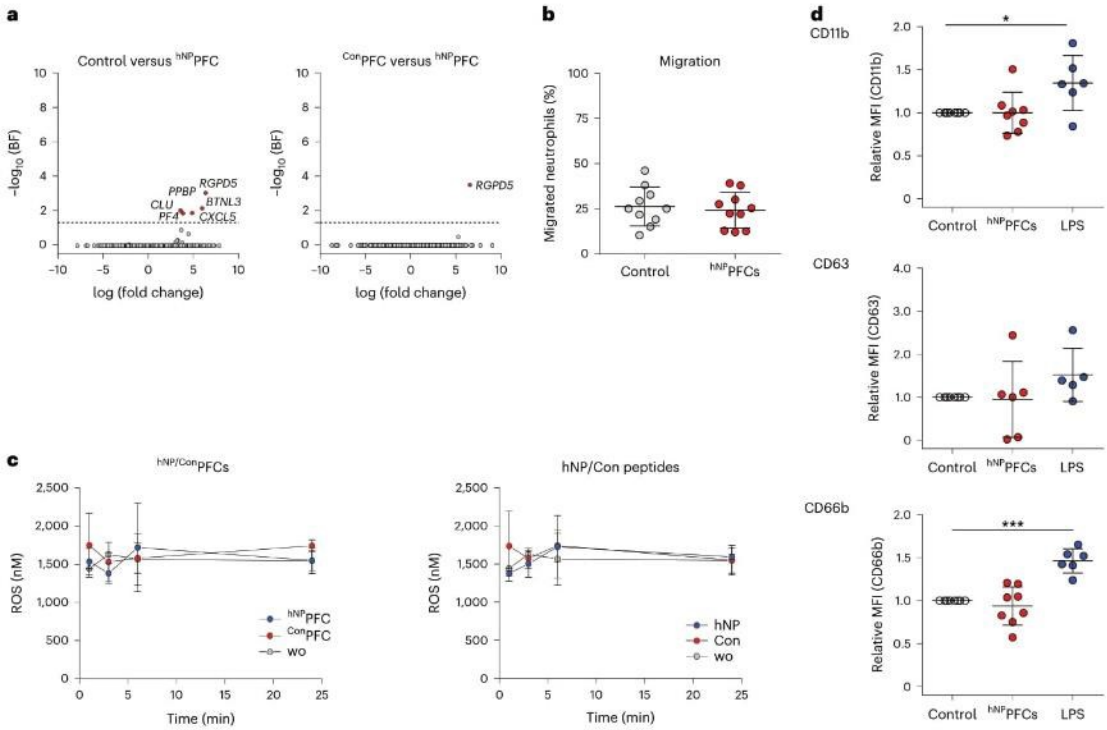

Fig. 6 | Targeting with hNPPFCs does not impact human neutrophil properties. a, Differentially expressed genes identified by bulk RNA sequencing of human blood neutrophils after incubation with hNPPFCs, ConPFCs or NaCl as the control. Volcano plots of differentially expressed genes for human neutrophils treated with saline compared to hNPPFCs (left) or ConPFCs compared to hNPPFCs (right). Genes marked in red are significantly upregulated with a $\log_2$ (fold change) greater than 1.5. BF, Bonferroni-corrected *P* values of the false discovery rate. In total, 45,413 RNA transcripts were analyzed. **b**, Migration of neutrophils treated with hNPPFCs (red) or left untreated (gray) toward IL-8. **c**, Neutrophils were incubated with hNPPFC or ConPFC or the hNP or Con peptides, and ROS generation was determined by enzyme-linked immunosorbent assay. wo, without any PFC. **d**, Cell surface expression of neutrophil activation markers: neutrophils were left untreated (gray, control), incubated with hNPPFCs (red) or stimulated with LPS (blue) as the positive control, followed by flow cytometry for CD11b (top), CD63 (middle) or CD66b (bottom). Mean fluorescence intensities were normalized to those of untreated cells. Data are mean ± s.d. of $n = 4$ (**a**), $n = 9–10$ (**b**), $n = 5–6$ (**c**) and $n = 5–8$ (**d**) independent experiments; $^*P < 0.05$, $^{***}P < 0.001$, verified by two-sided Bonferroni-corrected ANOVA (**a**) or two-way ANOVA (**d**).

directly from the inflammatory focus, that is, the Matrigel–LPS plug (tissue neutrophils) tended to exhibit even higher expression levels. Similar effects were observed after experimental MI (Fig. 8a, right): again, expression levels of CD177 were elevated in neutrophils isolated from blood of mice with MI (blood neutrophils) versus those of healthy control mice but highest in neutrophils from the infarcted heart (tissue neutrophils).

For human neutrophils, we detected comparable alterations of CD177 expression in neutrophils from patients with STEMI. As shown in Fig. 8b, we observed significantly higher CD177 levels in blood neutrophils from patients with STEMI than in healthy controls. To further investigate neutrophils from human inflammatory lesions, we used tissue samples derived from surgery of the oral cavity, specifically for pericoronitis, known for substantial neutrophil infiltration[23], and found once more the highest CD177 expression on those tissue neutrophils. Remarkably, neutrophils freshly isolated from explanted failing human hearts similarly showed strong CD177 expression and could be labeled with hNPPFCs as well (Extended Data Fig. 10d), highlighting the potential of our approach to track neutrophils also in cardiac inflammatory processes in patients.

In vivo determination of neutrophil state

In a final experimental series, we investigated whether the enhanced incorporation of mNPPFCs as a consequence of CD177 upregulation can be exploited to assess the inflammatory state of neutrophils in vivo. To this end, we monitored in situ ^{19}F incorporation into bone marrow neutrophils under stimulated conditions, employing again the Matrigel–LPS-based inflammation model. Twenty-four hours after plug implantation, mNPPFCs were applied, and, another 24 h later, mice were subjected to ^{1}H/^{19}F MRI. As shown in Fig. 8c,d, we observed a substantially stronger ^{19}F signal in the bone marrow upon LPS preactivation (bottom) than in PBS-treated controls (top). This effect became even more evident when relating the detected ^{19}F signal to the number of neutrophils present in the bone marrow as determined directly after MRI (Fig. 8e). This accounts for stimulated neutrophils already released from the bone marrow and revealed significantly stronger ^{19}F uptake in the LPS-treated group (Fig. 8e), in line with the enhanced surface expression of CD177 upon LPS challenge (Fig. 8a). Of note, the increase in mNPPFC incorporation into bone marrow neutrophils was on the same order of magnitude as the increase in circulating neutrophils observed under the same conditions (Fig. 7d), indicating

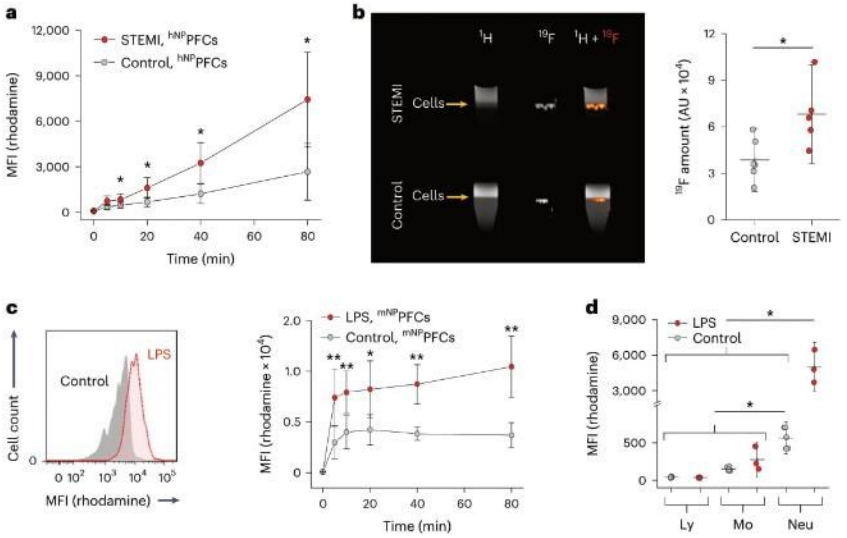

Fig. 7 | Inflammatory stimuli increase uptake of ^{NP}PFCs by neutrophils. **a**, Isolated neutrophils obtained from patients with STEMI 24 h after MI (red) and from healthy controls (gray) were exposed to ^{hNP}PFCs, and their uptake was determined over time by flow cytometry. **b**, Human neutrophils from patients with STEMI (top) or healthy controls (bottom) were incubated with ^{hNP}PFCs, purified by density gradient centrifugation and analyzed by ^{1}H/^{19}F MRI. Cells are visible in ^{1}H MR images as a small layer (arrow) in the bright aqueous phase on top of the black Percoll layer (left). Fluorine-19 MRI (middle) and subsequent fusion of both datasets (right) confirmed localization of the ^{19}F label within the cellular layer. Quantification of ^{19}F signals showed enhanced labeling of neutrophils from patients with STEMI (red) in comparison to controls (gray). **c**, Murine neutrophils isolated from mice with an inflammatory hot spot (Matrigel–LPS plug; red) or Matrigel–PBS as a control (gray) were incubated ex vivo with ^{mNP}PFCs and analyzed over time by flow cytometry. Histograms (left) display representative data after 40 min, and the time course of mean fluorescence values is illustrated on the right. **d**, ^{mNP}PFCs were intravenously injected in mice with a Matrigel–LPS or Matrigel–PBS (control) plug implanted 24 h before. One hour after injection, blood was withdrawn, and the in vivo uptake of ^{mNP}PFCs by lymphocytes (Ly), monocytes (Mo) and neutrophils (Neu) was analyzed by flow cytometry. Data are mean ± s.d. of $n = 5–8$ (**a**), $n = 5–6$ (**b**), $n = 4–5$ (**c**) and $n = 3–5$ (**d**) independent experiments; $^{*}P < 0.05$, $^{**}P < 0.01$, verified two-way ANOVA (**a**,**c**,**d**) or two-sided Student's *t*-test (**b**).

that our approach is suitable to mirror the state of neutrophils in both bone marrow and blood.

Discussion

Here, we report a new technique for global in vivo mapping of human and mouse neutrophils by equipping PFCs with peptides directed against human or murine CD177 for readout by ^{19}F MRI. This approach proved to be suitable for highly specific detection of neutrophils in vitro and in vivo. We were able to label neutrophils in situ, visualize them non-invasively within their different hematopoietic niches over the entire body and track their migration to the injured heart after MI in vivo. Locoregional analysis of the data revealed the femur as the largest neutrophil reservoir as well as the main source for neutrophil release upon MI, with the diaphysis as the most active compartment. We also demonstrated that both sterile (acute MI) and nonsterile (LPS) inflammation resulted in enhanced labeling of murine and human neutrophils, which can serve as an in vivo readout for their activation state.

Neutrophils have been visualized by a variety of different imaging modalities[5,24–27]. However, optical approaches are not yet ready for clinical routine imaging, while a whole-body imaging technique such as PET provides excellent sensitivity, for example, targeted imaging with ^{68}Ga-pentixafor proved useful for identification of chemokine (C–X–C motif) receptor 4 (CXCR4) expression patterns in the myocardium and systemic organs[28], which could already be exploited for imaging-based theranostics[29]. Nevertheless, in terms of specificity, this approach is somewhat limited as CXCR4 is not only strongly expressed by neutrophils but also by monocytes[30]. Furthermore, (targeted) PET probes are usually short-lived nuclide tracers, raising difficulties in tracking neutrophils over longer periods of time, as in the present study. The widely available MRI platform provides the inherent advantage of combining excellent anatomical resolution with the opportunity for overlaying additional tissue and cell information. For visualization by MRI, to our knowledge, only neutrophils incubated ex vivo with iron oxide nanoparticles have been used[26,31]. However, the susceptibility effects induced by the re-implanted cells are rather challenging to quantify and are often difficult to differentiate from other unspecific artifacts. By contrast, our approach does not interfere with the anatomical ^{1}H images, enabling precise anatomical localization of the ^{19}F hot spot and easy quantification, because the ^{19}F signal linearly correlates with the amount of the deposited PFCs. Decorating the PFC surface with binding peptides against human or mouse CD177 (hNP or mNP) ensured specific uptake of the targeted PFCs by neutrophils, while additional PEGylation masked the PFC droplets for passive internalization by other phagocytic immune cells[9,32,33].

Selecting CD177 as a neutrophil-specific target had the advantage that, even though it is linked to glycosyl-phosphatidylinositol (GPI), it exhibits no transmembrane domain that can transmit signals intracellularly; therefore, binding to CD177 is unlikely to have major effects on cell activation and functionality[34]. By contrast, binding to Ly6G, a common marker for murine neutrophils, is known, for example, to modulate their migration to inflammatory foci[35]. Similarly, approaches that target receptor components of the innate immune system via *N*-formylmethionine-leucyl-phenylalanine (fMLP)[36–38] or Fc-γ[39,40] on the neutrophil surface are prone to alter their activation state and furthermore are not highly specific for neutrophils. Transcriptome gene expression analysis of murine and human neutrophils exposed

https://doi.org/10.1038/s44161-022-00210-w

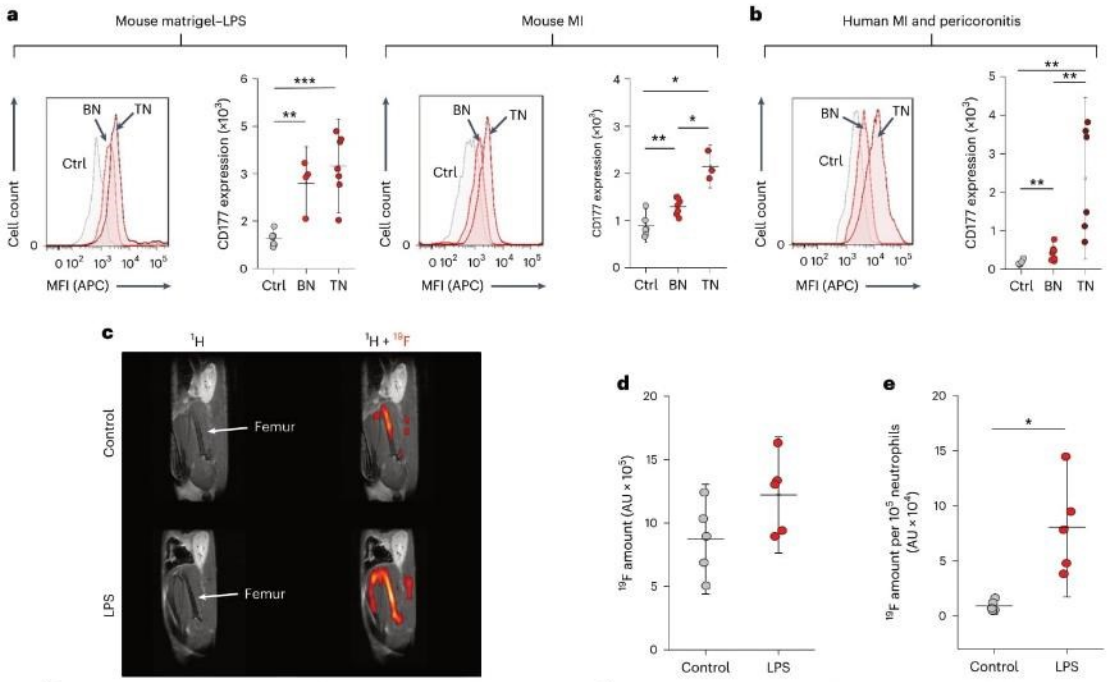

Fig. 8 | ^{NP}PFC loading as a readout for neutrophil-activation state. a, Cell surface expression of CD177 on murine neutrophils isolated from healthy controls (Ctrl, gray) after implantation of Matrigel–LPS (left) or after experimental MI (right) as determined by flow cytometry. Data were separated for circulating neutrophils isolated from the blood (BN, blood neutrophils, light red) and neutrophils obtained from the inflamed Matrigel plug or the infarcted heart (TN, tissue neutrophils, dark red). **b**, CD177 expression of human neutrophils isolated from blood of healthy controls (gray), patients with STEMI (blood neutrophils, light red) and neutrophils obtained from pericoronitis tissue specimens (tissue neutrophils). Similar to mice, CD177 expression was significantly increased in blood neutrophils compared to control values and again substantially higher in tissue neutrophils than in blood neutrophils. **c**, In vivo ^{mNP}PFC labeling of bone marrow neutrophils dependent on their activation state: ^{mNP}PFCs were intravenously injected into mice 24 h after implantation of Matrigel doped with LPS (bottom) or PBS as a control (top). Another 24 h later, the bone marrow was analyzed by ^{1}H/^{19}F MRI. **d**, Quantification of the total amount of ^{19}F in the bone marrow of LPS-stimulated mice compared to the control. **e**, Normalizing the ^{19}F signal to the number of neutrophils in the bone marrow demonstrated a significant increase in ^{mNP}PFC uptake per cell after LPS treatment as compared to the control. The number of neutrophils in the bone marrow was determined directly after MRI by flow cytometry. Data are mean ± s.d. of $n = 4–7$ for Matrigel experiments, $n = 3–7$ for MI (**a**), $n = 6–8$ (**b**), $n = 5$ (**d**) and $n = 5$ (**e**) independent experiments; $^{*}P < 0.05$, $^{**}P < 0.01$, $^{***}P < 0.001$, verified by one-way ANOVA (**a**,**b**) or two-sided Student's *t*-test (**e**).

to ^{NP}PFCs, ^{Con}PFCs or saline as well as additional functional analyses confirmed that our labeling approach has no critical effect on their phenotype. RNA-sequencing data of neutrophils incubated with the different compounds revealed only a few differentially expressed genes, when adjusting a threshold of 1.5-fold change in expression levels, and these alterations occurred over a very moderate range. The genes that were altered (*Per1* and *Pagr1*) in murine neutrophils are not directly linked to neutrophil function, and, among the six differentially expressed genes in human neutrophils, only *CXCL5* and *PF4* (encoding platelet factor 4) are related to neutrophil migration and function. However, we found no impact of our targeting agents on chemotaxis or ROS release of either human or murine neutrophils. In this context, it is important to note that stimulation of neutrophils with pro-inflammatory agents usually results in an order-of-magnitude higher upregulation or downregulation of several hundred genes[41–43]. In particular, genes encoding classical pro-inflammatory cytokines, chemokines and signaling pathways are upregulated such as IL-1β, tumor necrosis factor (TNF)-α, IL-6, IL-8, monocyte chemoattractant protein 1 (MCP-1) and the nuclear factor (NF)-κB pathway, but none of these were observed to be altered in RNA-sequencing data from neutrophils of both species after incubation with ^{NP}PFCs. Altogether, gene expression analysis as well as functional analysis data provided no evidence that our targeting approach with ^{NP}PFCs has any substantial impact on neutrophil functionality. These findings are further supported by previous observations that cross-linking of CD177 did not induce degranulation or oxidative burst[34].

Of note, the precise functional role of CD177 in vivo still remains elusive[44]. It has been reported that its expression is upregulated in inflammatory bowel and Kawasaki diseases[45,46]. Here, we extended this finding to sterile (acute MI) and bacterial (LPS) inflammation, indicating it as a general phenomenon that might be suitable for assessing the inflammatory state of neutrophils in vivo by enhanced ^{NP}PFC labeling. As CD177 is already expressed at the metamyeloid stage, our technology has the potential to provide insight into neutrophil dynamics from their formation and release from the bone marrow to migration into inflammatory foci. Although not feasible at the single-cell level, it allows us to monitor trafficking of the vast majority of neutrophils from their origin into the target tissue. Because this is also applicable to human neutrophils and PFCs have previously been evaluated in clinical trials, ^{hNP}PFCs clearly offer the option for transfer into the clinical setting. Interestingly, in contrast to mice, CD177 is not present on all neutrophils in humans. In our samples, approximately 50–60%

of all human neutrophils were labeled by ^{hNP}PFCs. Thus, in humans, this restricts our approach to the tracking of CD177-positive neutrophils, which, on the other hand, offers the opportunity to specifically understand the biology of this large subpopulation. However, given the increased labeling under inflammatory conditions, the sensitivity of this approach would be substantially amplified under most pathophysiological conditions.

In translation to the clinical setting, our approach will allow us to not only identify hidden origins of bacterial or sterile inflammation in patients but also to unravel disease states that are on the verge of severe aggravation due to enhanced neutrophil infiltration or activation. For example, neutrophils are well known to play a pivotal role after STEMI and are recruited in the first wave after the insult into the myocardium[47]. They contribute not only to the initial tissue response but are also key players in the so-called ischemia–reperfusion injury as well as microvascular obstruction, which is known as a major reason for adverse remodeling and re-hospitalization due to heart failure in patients after STEMI[48,49]. Importantly, there are recent reports that neutrophil infiltration after MI can be beneficially modulated by metoprolol[50,51]. Thus, our approach might help to identify high-risk patients with enhanced neutrophil activation and infiltration for tailored therapy to address their specific needs, which would be of substantial clinical value. Finally, as our approach is not limited to PFCs and MRI, the hNP ligand can easily be conjugated to tracers for other imaging modalities and may be further used as a theranostic tool[29].

Methods

Animal experiments were performed in accordance with national guidelines on animal care and were approved by the Landesamt für Natur, Umwelt, und Verbraucherschutz (Nordrhein-Westfalen, Germany, file references 81-02.04.2017.A468 (mice), 81-02.04.2020.A290 (mice), L84-02.04.2016.A322 (pigs) and 84-02.04.2014.A232 (rats)). All studies with human samples were conducted after informed consent according to the Declaration of Helsinki and local ethics board approval (Ethikkommission, Universitätsklinikum Düsseldorf, Germany; file references 2017114486 and 2021-1635). All study participants gave written informed consent.

Preparation of ^{NP}PFCs and ^{Con}PFCs

Peptides used in this study were previously identified by phage display screening approaches[11,15]. We modified the peptide sequences by adding a C-terminal cysteine for coupling reactions followed by three glycines as a spacer and an N-terminal carboxyfluorescein to enable fluorescence detection (Extended Data Fig. 1). Peptides were synthesized by Genaxxon BioScience with purity >95% (mNP, DFYKPMPNLRIT-GGG-C; related Con, SLAMFLTHSPEP-GGG-C; hNP, DLVTSKLQV-GGG-C; related Con, KQLSEMVTD-GGG-C). For TriCeps experiments, a modified hNP was used: DLVTSKLQV-GKG-C.

Maleimide PFCs. Nanoemulsions were composed of 20% (all wt/wt) PFCE (perfluoro-15-crown-5 ether; ABCR), 2.5% Lipoid S75 (Lipoid), 0.45% DSPE-PEG$_{2000}$ (1,2-distearoyl-*sn*-glycero-3-phosphoethanolamine-*N*-[amino(polyethylene glycol)-2000]; Lipoid), 0.05%, maleimide-PEG$_{2000}$-DSPE (Avanti Polar Lipids), 0.025% Lissamine-rhodamine-DHPE (Molecular Probes) and phosphate glycerol buffer up to 100%. Lipids were dissolved in chloroform and added to a round-bottom flask. Chloroform was removed in a rotary evaporator at 200 mbar and 40 °C. Thereafter, the evenly distributed lipids were resuspended in 10 mM phosphate buffer (pH 7.4), and PFCE was added dropwise. The crude emulsion was further processed on an LV1 Microfluidizer (Microfluidics) for five cycles at a process pressure of 1,000 bar.

For generation of ^{NP}PFCs or ^{Con}PFCs, peptides were coupled to ^{Mal}PFCs. The peptides were used in fivefold molar shortfall to maleimide and linked via the free sulfhydryl group of cysteine. After incubation for 24 h at 20 °C and 750 r.p.m., the nanoemulsions were stored at 4 °C.

Animal experiments

Animals used in this study were obtained from Janvier, housed at the central animal facility of Heinrich Heine University Düsseldorf on a 12-h light–dark cycle, fed with a standard chow diet and received tap water ad libitum. Male 10–12-week-old C57BL/6 mice (in total, $n = 180$) ranging from 20 to 30 g in body weight (BW) were used.

Immune cells from blood or bone marrow. Heparinized blood was withdrawn by venous puncture with a 23G cannula of the inferior vena cava. Erythrocytes were lysed by adding a fourfold volume of NH_4Cl buffer (pH 7.4). After 10 min of incubation, samples were centrifuged at 350*g* for 10 min at 20 °C. For isolation of neutrophils from the bone marrow, mice were killed by cervical dislocation, and bones were dissected. Afterward, cells were isolated from the bone marrow using established protocols[52].

Immune cells from Matrigel–LPS plugs. Mice were killed by cervical dislocation, and the Matrigel plug was carefully excised. The plug was incubated in DMEM containing 1 mg ml^{-1} collagenase II (Merck) for 10 min at 37 °C. Afterward, the sample was meshed through a cell strainer (40 µm), and isolated cells were resuspended in Miltenyi automated cell sorting (MACS) buffer.

Immune cells from infarcted hearts. Mice were killed, and the heart was excised and transferred into MACS buffer to flush out the blood. After mincing, samples were incubated with 1 mg ml^{-1} collagenase at 37 °C for 30 min under constant shaking and afterward meshed through a cell strainer (40 µm). To remove cardiomyocytes, samples were centrifuged at 55*g* for 5 min. The resulting supernatant containing the immune cells was used for further experiments.

In situ labeling of neutrophils for tracking after MI. For labeling of neutrophils before MI, mice were anesthetized (1.5% isoflurane) and 1 mmol per kg BW PFCs were injected intravenously via the tail vein on 3 consecutive days. Induction of MI was essentially carried out as previously described[53]. For inhibiting the egress of neutrophils from the bone marrow in a subset of experiments, a cocktail of neutralizing antibodies was injected i.p. 1 h before and 4 h after MI (CXCL1, CXCL2, G-CSF, GM-CSF, 50 µg each, Thermo Fisher). To generate neutropenic mice, 48 and 24 h before MI, 500 µg of the Ly6G-depletion antibody (BioXcell, clone 1A8) was injected i.p. in independent experiments.

Matrigel–LPS experiments. To induce defined inflammatory foci, we adopted a recently developed model of localized subcutaneous inflammation[22]. To this end, ice-cold Matrigel (Corning) was doped with LPS (1 µg µl^{-1}; *Salmonella typhimurium*, Sigma-Aldrich) and subcutaneously (s.c.) implanted into the neck of the mice. Twenty-four hours after implanting the plug, neutrophils were isolated from the blood and incubated ex vivo with ^{mNP}PFCs or ^{Con}PFCs. In separate experiments, 24 h after implantation, ^{mNP}PFCs or ^{Con}PFCs were injected intravenously, and immune cells were isolated from the blood. In further experiments, 1 d after plug injection, mice received 1 mmol per kg BW ^{mNP}PFCs, and, 24 h later, the bone marrow was analyzed by ^{1}H/^{19}F MRI. Thereafter, mice were killed, and neutrophils were isolated from the bone marrow for determination of cell numbers. In each case, immune cells were analyzed by flow cytometry.

^{mNP}PFC uptake by circulating immune cells and bone marrow neutrophils. Mice were kept in anesthesia (1.5% isoflurane) on a warming plate, and 1 mmol per kg BW ^{mNP}PFCs or ^{Con}PFCs were injected i.v. into the tail vein. One hour after injection, blood was collected from the vena cava, and immune cells were isolated. For in vivo uptake studies in the bone marrow, mice were treated as described above and killed 2 h later to isolate neutrophils from the bone marrow and analyzed by flow cytometry.

^{mNP}PFC uptake by immune cells isolated from the heart. ^{mNP}PFCs or ^{Con}PFCs (3 mM per kg BW) were injected intravenously 2 h before induction of MI. One hour after MI, murine immune cells were isolated from the heart using a Langendorff digestion protocol as described previously[54]. The resulting cell fractions were analyzed by flow cytometry. Cells were stained for CD45, CD11b, Ly6C and Ly6G for 20 min at 4 °C to identify lymphoid cells ($CD45^+CD11b^-$), classical monocytes ($CD45^+CD11b^+CD11C^+Ly6G^-$), macrophages ($CD45^+CD11b^+CD11C^-Ly6G^-$) and neutrophil granulocytes ($CD45^+CD11b^+CD11C^-Ly6G^+$). DAPI staining was performed to exclude dead cells from analysis.

Immune cell isolation from pig and rat blood. To obtain immune cells from pigs, heparinized blood was withdrawn from the ear vein of animals using a 22G vein catheter as previously described[55]. For rats, heparinized blood was withdrawn by cardiac puncture of the left ventricle using a 23G cannula. For both species, erythrocytes were lysed as described above. After 10 min of incubation, samples were centrifuged at 350*g* for 10 min at 20 °C.

Heart tissue histology and immunostaining

Neutrophils were prelabeled by i.v. injection of ^{mNP}PFCs or ^{Con}PFCs (3 mM per kg BW) 2 h before induction of MI, and heart samples were collected 2 or 24 h after surgery. The infarcted area was delineated by TTC staining (1%). Cryosections (40–60 µm) for MFI assessment and immunostaining were air dried and fixed with Zamboni fixative, and fluorescence images were immediately acquired. For subsequent immunostaining, tissue slices were permeabilized with Triton (1%, Sigma). Primary antibodies, including anti-Ly6G (neutrophils, 1:100), anti-MHC II (macrophages, 1:100) and anti-CD3 (T cells, 1:200), were incubated overnight at 4 °C. After three washing steps, FITC-labeled secondary antibodies were used to identify cell markers, and nuclei were counterstained with DAPI. MFI was quantified in the entire area of MI from at least six successive sections of each heart (500-µm interval). For cellular MFI, the rhodamine signal was quantified in areas where it was colocalized with the specific FITC-labeled cell markers. Micrographs were acquired with a fluorescence microscope (BX 61; Olympus) and analyzed with Fiji 1.52n[56].

Impact of ^{mNP}PFCs on gene expression and neutrophil function

Gene expression. One mM per kg BW ^{mNP}PFCs or saline were injected i.v. into mice, and, 2 h later, neutrophils were isolated from the bone marrow. Total RNA was isolated from purified neutrophils. For transcriptome analyses, DNase-digested total RNA samples were quantified (Qubit RNA HS Assay, Thermo Fisher), and quality control was performed by capillary electrophoresis using a fragment analyzer and the Total RNA Standard Sensitivity Assay (Agilent). All samples in this study showed high-quality RNA quality numbers (mean = 9.3). Library preparation was performed according to the manufacturer's protocol using the Illumina Stranded mRNA Prep, Ligation kit. Briefly, 25 ng total RNA was used for mRNA capturing, fragmentation, synthesis of cDNA, adaptor ligation and library amplification. Bead-purified libraries were normalized and finally sequenced on the NextSeq 1000 system (Illumina) with a single-read setup of 1 × 100 bp. The Illumina DRAGEN FASTQ Generation tool (version 3.8.4) was used to convert the BCL files to FASTQ files as well for adaptor trimming and demultiplexing. Data analyses of FASTQ files were conducted with CLC Genomics Workbench (version 22.0.1, Qiagen). The reads of all probes were adaptor (Illumina TruSeq) and quality trimmed (using default parameters: bases below Q13 were trimmed from the end of the reads; ambiguous nucleotides, maximum 2). Mapping was done against the *Mus musculus* (mm39, GRCm39.105, 12 January 2022) and the *Homo sapiens* (hg38, GRCh38.100, 5 June 2020) genome sequences.

Migration. One mM per kg BW ^{mNP}PFCs or saline were injected i.v., and, after 1 h, LPS-doped Matrigel was implanted s.c. into the neck of mice. After 2 h, the Matrigel plug was excised, and infiltrated neutrophils were isolated and stained with anti-CD11b and anti-Ly6G antibodies for flow cytometry.

Reactive oxygen species production. One mM per kg BW ^{mNP}PFCs or saline were injected i.v., and, 2 h later, neutrophils were isolated from the bone marrow, and extracellular ROS was measured in the cell supernatant by oxidation of dihydroethidium followed by UPLC analysis.

Phagocytosis. One mM per kg BW ^{mNP}PFCs or saline were injected i.v., followed by 100 µl FITC-labeled *Escherichia coli* particles (Thermo Fisher) 2 h later. Again, 2 h later, neutrophils were isolated from the blood and stained for Ly6G for 20 min at 4 °C. Thereafter, FITC labeling was determined by flow cytometry.

Cell surface activation markers. One mM per kg BW ^{mNP}PFCs or saline were injected i.v., and, 2 h later, neutrophils were isolated from the blood and stained for CD11b, CD62L and CD63. As a positive control, mice were implanted with LPS-doped Matrigel 24 h before blood withdrawal.

Liver serum markers and histology of liver and spleen after ^{mNP}PFC injection. ^{Con}PFCs, ^{mNP}PFCs (each at 1 mM per kg BW) or saline were injected i.v. over 3 consecutive days. Twenty-four hours after the last injection, mice were killed, and blood samples were withdrawn to determine GLDH, AST, ALP, ALT and bilirubin levels by standard clinical procedures. Furthermore, the liver and spleen were dissected, fixed in formalin and snap frozen. Subsequently, 4-µm cryosections were cut and stained with hematoxylin and eosin as described previously[57].

Biodistribution of ^{mNP}PFCs. To determine the biodistribution of ^{mNP}PFCs, 3 mM per kg BW ^{mNP}PFCs were injected intravenously, and ^{19}F signal intensities were determined in blood, liver and spleen at distinct time points after injection.

Experiments with human blood and tissue samples

In total, blood samples from 17 patients with STEMI were used (5 female, 12 male; aged 66.9 ± 13.6 years; troponin T, 3,398 ± 3,520 ng l^{-1}; creatine kinase, 933.4 ± 685.8 U l^{-1}; lactate dehydrogenase, 547.8 ± 259.9 U l^{-1}). Samples were analyzed 24 h after MI. Samples from the oral cavity of patients with pericoronitis (n = 6; 4 female, 2 male; 34.1 ± 21.7 years) and explanted human hearts (n = 3; 1 female, 2 male; 41.6 ± 18.2 years) were processed directly after surgery.

Immune cell isolation from human blood. Blood was collected from the vena brachialis, and erythrocytes were lysed as described above. After 10 min of incubation, samples were centrifuged at 350*g* for 10 min at 20 °C. For isolation of a purified neutrophil fraction, density gradient centrifugation was performed. Five milliliters of Ficoll 1.077 (Sigma-Aldrich) was layered on 5 ml Ficoll 1.119 (Sigma-Aldrich), and 20 ml of whole blood diluted 1:2 with PBS was carefully layered on the Ficoll 1.077. Samples were centrifuged at 350*g* for 20 min with low acceleration and brake. The neutrophil layer was isolated by careful aspiration and washed with PBS. Isolated cells were resuspended in MACS buffer.

Immune cell isolation from pericoronitis surgeries. Human pericoronitis samples were obtained through curettage of the alveolar socket, and the peridental tissue was stored in ice-cold saline. Afterward, samples were incubated in DMEM mixed with 1 mg ml^{-1} collagenase II (Merck) for 10 min at 37 °C. Samples were meshed through a cell strainer, and isolated cells were resuspended in MACS buffer.

Immune cell isolation from explanted human hearts. During orthotopic heart-transplant surgery in patients suffering from terminal heart failure, a tissue specimen of about ~5 g was excised from the

apex of the failing heart immediately after explantation. Tissues were immediately transferred to iced BIOPS buffer as described previously[58]. For subsequent isolation of immune cells, heart samples were cut into small pieces and digested with the Multi Tissue Dissociation Kit 2 (Miltenyi; 'adult rat heart' protocol) by incubating for 40 min at 37 °C with the specified enzyme mix using the 37C_Multi_G program by gentleMACS. Afterward, 7.5 ml DMEM with 20% FCS was added to stop enzymatic digestion. The sample was applied to a 70-µm cell filter and washed with 3 ml DMEM, followed by centrifugation for 5 min at 300*g*. The supernatant was discarded, and cells were resuspended in 1 ml DMEM and incubated with 10 µl ^{hNP}PFCs for 30 min at 37 °C on a vertical shaker. Afterward, cells were washed twice with MACS buffer and stained for CD45, CD11b and CD66b. DAPI staining was performed for exclusion of dead cells. The uptake of ^{hNP}PFCs into neutrophils ($CD45^+CD11b^+CD66b^+$) was determined by flow cytometry.

Cell culture experiments

Cell lines. CHO cells (ECACC 85050302) were cultivated in DMEM high-glucose medium (Gibco, Thermo Fisher Scientific) supplemented with 10% FBS (Gibco, Thermo Fisher Scientific), 60 mg l^{-1} penicillin and 100 mg l^{-1} streptomycin (Genaxxon BioScience) at 37 °C with 5% CO_2 in a water-saturated atmosphere.

Magnetic resonance imaging

General. All experiments were performed with a vertical 9.4 T Bruker AVANCE^{III} Wide Bore NMR spectrometer (Bruker) driven by ParaVision 5.1 and operating at frequencies of 400.21 MHz for ^{1}H measurements and 376.54 MHz for ^{19}F measurements using a Bruker microimaging unit, Micro2.5, with actively shielded gradient sets (1.5 T m^{-1}). Data were acquired using a 25-mm quadrature ^{19}F resonator with one channel tunable to both ^{1}H and ^{19}F. Mice were anesthetized with 1.5% isoflurane and kept at 37 °C. After acquisition of morphological ^{1}H images, the resonator was tuned to ^{19}F, and anatomically matching ^{19}F images were recorded essentially as described previously[59].

For whole-body images, mice were repositioned for coverage of thorax and brain, and abdomen and hindlimbs, respectively. Slice packages were placed in the axial direction, and datasets were subsequently merged using the 3D visualization software Amira (Mercury Computer Systems). Scan details are as follows: ^{1}H rapid acquisition with relaxation enhancement (RARE), repetition time (TR) = 3,500 ms, field of view (FOV) = 2.56 × 2.56 cm^2, matrix = 256 × 256, slice thickness (ST) = 1 mm, acquisition time (t_{Acq}) = 1.24 min; ^{19}F 3D RARE, TR = 2,500 ms, FOV = 2.56 × 2.56 cm^2, matrix = 64 × 64, ST = 45 mm, t_{Acq} = 1 h.

Bone marrow. Slice packages were placed in sagittal orientation to cover the complete bone marrow in the tibia and femur in both legs using the following scan details: ^{1}H RARE, TR = 2,000 ms, FOV = 4.00 × 2.56 cm^2, matrix = 256 × 256, ST = 1 mm, t_{Acq} = 1 min; ^{19}F RARE, TR = 2,500 ms, FOV = 4.00 × 2.56 cm^2, matrix = 64 × 64, ST = 3 mm, t_{Acq} = 10 min.

Cardiac. Images of mouse hearts were acquired in short-axis orientation using a retrospectively triggered fast low-angle shot cine sequence (IntragateFLASH, Bruker) as described previously[60]. Thereafter, hearts were excised, washed and fixed with PFA for 3D high-resolution post-mortem MRI: ^{1}H FISP, TR = 4 ms, FOV = 1.00 × 1.00 × 1.00 cm^3, matrix = 128 × 64 × 128, t_{Acq} 151 min; ^{19}F RARE, TR = 2,500 ms, FOV = 1.00 × 1.00 × 1.00 cm^3, matrix = 32 × 32 × 32, t_{Acq} = 10 h.

Analysis of biodistribution was carried out as described previously[61].

Isolated cells. After the incubation period, cells were subjected to density gradient centrifugation to separate PFC-loaded cells from free PFCs. Afterward, samples were analyzed by MRI to determine the ^{19}F signal within the cell layer as described previously[61].

Perfluorocarbons. For evaluation of ^{19}F content, 10 µl of the nanoemulsion was transferred into PCR tubes and measured with the following parameters: ^{1}H RARE, TR = 3,500 ms, RARE factor 16, FOV = 2.56 × 2.56 cm^2, matrix = 128 × 128, ST = 1 mm, t_{Acq} = 1 min; ^{19}F RARE, TR = 2,500 ms, RARE factor 32, FOV = 2.56 × 2.56 cm^2, matrix = 32 × 32, ST = 1 mm, t_{Acq} = 5 min.

Data analysis. MRI data were analyzed as described previously[62,63].

Flow cytometry

General. Flow cytometry was performed with a FACSCanto II (BD Biosciences) or LSRFortessa (BD Biosciences). Cells were gated with appropriate FSC–SSC settings and thresholds for excluding debris. To omit dead cells, samples were stained with 1 µg ml^{-1} DAPI (Merck). For analysis, cells were gated with FACSDiva 6 or FlowJo 7.1, and MFI and/or the number of positive cells was determined, depending on the experiment.

Human immune cells were discriminated by staining for CD45 (BioLegend, clone HI30), CD11b (BD Biosciences, clone ICRF44), CD14 (BioLegend, clone M5E2) and CD16 (BD Biosciences, clone 3G8) (lymphocytes, $CD45^+CD11b^-CD16^-$; classical monocytes, $CD45^+CD11b^+CD14^{++}CD16^-$; non-classical monocytes, $CD45^+CD11b^+CD14^+CD16^{++}$; neutrophils, $CD45^+CD11b^+CD16^+$). Murine immune cells were discriminated by staining for CD45 (BD Biosciences, clone 30-F11), CD11b (BioLegend, clone M1/70), Ly6G (BD Biosciences, clone 1A8), Ly6C (BioLegend, clone HK1.4) and F4/80 (BioLegend, clone BM8) (lymphocytes, $CD45^+CD11b^-Ly6G^-$; classical monocytes, $CD45^+CD11b^+Ly6G^-Ly6C^{hi}$; non-classical monocytes, $CD45^+CD11b^+Ly6G^-Ly6C^{lo}$; neutrophils, $CD45^+CD11b^+Ly6G^+$; eosinophils, $CD45^+CD11b^+Ly6G^+SSC^{hi}FSC^{lo}$). Both human and murine cells were stained for 20 min at 4 °C, followed by washing with 200 µl MACS buffer.

If not mentioned otherwise, neutrophil-specific peptide or Con (both at 1 µg ml^{-1}) were incubated for 20 min at 4 °C, while ^{NP}PFCs or ^{Con}PFCs were incubated at a concentration of 10 µl ml^{-1} for the indicated period of time, followed by two washing steps with 200 µl MACS buffer.

Immune cells from rat and pig were discriminated with appropriate forward and side scattering and rat immune cells additionally by CD11b (BD Biosciences, clone WT.5) staining.

Cell lines. CHO cells were gated with appropriate FSC–SSC settings. Approximately 1×10^5 cells were stained with anti-CD177 monoclonal antibody (BD Biosciences, clone Y127) and 1 µg ml^{-1} hNP or Con for 20 min at 4 °C. Afterward, samples were washed twice with MACS buffer and analyzed for CD177, hNP and Con binding.

Experiments with cells

Binding of hNP or mNP to immune cells. Cells were isolated from blood, resuspended in 100 µl and transferred to a 96-well plate, resulting in 1×10^5 cells in each well. Subsequently, cells were incubated with or without peptides. Their binding was analyzed by flow cytometry via detection of their fluorescence label.

Binding of free mNP to murine neutrophils. A total of 1×10^5 bone marrow neutrophils were incubated with increasing amounts of mNP. To investigate putative conjugation effects, we coupled mNP to eight-arm PEG_{2000}-maleimide (Sigma-Aldrich). mNP (or Con) was used at a twofold molar excess to maleimide for loading all binding sites with mNP or Con. Coupling was carried out at room temperature for 24 h with constant shaking. Afterward, 1×10^5 bone marrow neutrophils were incubated with 1 µg ml^{-1} of the constructs, and uptake was determined by flow cytometry.

For identification of the surface receptor for hNP on neutrophil granulocytes, coupling of the peptide to TriCeps and cell incubation were carried out according to manufacturer's instructions (Dualsystems)[16]. Samples were subsequently analyzed by Dualsystems.

For transient transfection of CHO cells, 2.5×10^5 cells were seeded in six-well plates. Twenty-four hours later, the medium was refreshed. One µg plasmid DNA[64] (human CD177) and 4 µl PEI MAX (Polysciences) were suspended in 100 µl saline, incubated for 15 min at room temperature and subsequently added to the wells. The medium was replaced after 24 h, and cells were cultivated further for 24 or 48 h. Thereafter, cells were detached with PBS with 2.5 mM EDTA, washed and resuspended in MACS buffer. Approximately 1×10^5 cells were stained with monoclonal antibodies against CD177 or hNP or Con and analyzed by flow cytometry.

Cell surface expression of CD177. Neutrophils were isolated from the blood of healthy mice as well as 24 h after Matrigel implantation or induction of MI and also directly from the inflammatory hot spot (Matrigel or infarct area). For human studies, neutrophils were isolated from the blood of healthy individuals and patients 24 h after STEMI as well as from tissue samples from oral surgeries (pericoronitis). Isolated immune cells were transferred into 96-well plates, stained and analyzed by flow cytometry.

Internalization of hNP into neutrophils. The pH-sensitive pHrodo maleimide dye (Thermo Fisher) was mixed with hNP at an equal molar ratio in PBS and incubated at room temperature for 1 h at 700 r.p.m. to enable the conjugation of hNP and pHrodo. Afterward, isolated neutrophils were incubated with 1 µg ml^{-1} of the pHrodo–hNP construct at 4 °C or 37 °C for 30 min. At distinct time points, cell samples were washed twice with MACS buffer, and uptake of the pHrodo–hNP construct was determined via its fluorescence signal by flow cytometry.

Binding and internalization of ^{NP}PFCs. A total of 1×10^6 cells were incubated with 10 µl of the emulsion over a period of 80 min at 37 °C. At distinct time points, 50 µl of the samples were transferred into 2 ml of ice-cold MACS buffer and analyzed for rhodamine fluorescence by flow cytometry.

To determine PFC uptake by human neutrophils by ^{19}F MRI, cells were isolated from 10 ml of whole blood by density centrifugation. Subsequently, neutrophils (5×10^6) were resuspended in 3 ml DMEM and incubated for up to 8 h at 37 °C under constant motion with 10 µl ^{hNP}PFCs. Afterward, cells were centrifuged at 350*g*, washed three times with PBS, resuspended in 1 ml MACS buffer, purified by Percoll gradient centrifugation and analyzed by ^{1}H/^{19}F MRI.

Fluorine-19 MRI of murine neutrophils. A total of 4×10^6 neutrophils isolated from bone marrow with the EasySep Mouse Neutrophil Enrichment Kit (Stemcell Technologies) were resuspended in 1 ml DMEM and incubated for 3 h with 50 µl ^{mNP}PFCs or ^{Con}PFCs at 37 °C. Afterward, cells were washed three times with PBS, fixed with PFA, pelleted by centrifugation and analyzed by ^{1}H/^{19}F MRI.

Fluorescence microscopy of human neutrophils. Neutrophils (1×10^6) were incubated with 50 µl ml^{-1} ^{hNP}PFCs or ^{Con}PFCs for 60 min at 37 °C, washed three times with MACS buffer, centrifuged onto a glass plate, fixed with 0.5% PFA and stained with 1 µg ml^{-1} DAPI to visualize nuclei. Finally, cells were embedded in MOWIOL and studied by confocal microscopy (Zeiss LSM 710 Meta, Zeiss). Images were analyzed using Fiji 1.52n[56].

hNP competition experiment. A total of 1×10^6 human neutrophils were incubated in 1 ml DMEM at 4 °C with or without 5 µg ml^{-1} hNP for 30 min. Subsequently, 10 µl ^{hNP}PFCs were added, and, at defined time points, 50 µl of the cell suspension was transferred into 2 ml ice-cold FACS buffer. Cells were analyzed by flow cytometry.

Analysis of reactive oxygen species. A total of 5×10^6 human neutrophils were incubated in 10 ml DMEM with or without 1 µg ml^{-1} peptide or 50 µl ml^{-1} emulsion. At distinct time points, cells were pelleted, and 1 ml of the supernatant was immediately frozen at −80 °C. Subsequently, the amount of ROS was determined by chemiluminescence analysis. Murine neutrophils were isolated from ^{mNP}PFC-treated or NaCl-treated animals, and 1×10^5 cells were incubated with dihydroethidium–HBSS buffer (20 µM) for 30 min at 37 °C. After centrifugation, 80 µl supernatant was used to determine ROS by UPLC measurement (Waters Acquity Bio H-Class with 2475 FLD Detector). To this end, gradients A and B (0.1% trifluoroacetic acid in 1 l water and acetonitrile, respectively) at a flow rate of 0.26 ml min^{-1} at 17 °C were used. Dihydroethidium was excited and detected at 480 nm and 580 nm, respectively.

Migration of neutrophils. A total of 1×10^6 isolated human neutrophils were incubated with or without 50 µl ^{hNP}PFCs for 1 h at 37 °C in 1 ml DMEM. After washing with DMEM, 1×10^5 of these cells were placed in a Boyden chamber containing 200 µl DMEM. The lower part of the chamber contained 100 ng ml^{-1} IL-8 in 1 ml DMEM. After 1 h in an incubator, the flow through was collected, and the number of neutrophils was counted by flow cytometry. Murine neutrophils were isolated from Matrigel–LPS plugs and stained for Ly6G. Afterward, cells were washed twice, and the number of neutrophils was determined by flow cytometry.

Analysis of cell surface activation markers. A total of 1×10^6 isolated human neutrophils were incubated with 50 µl ml^{-1} ^{hNP}PFCs, 1 µg ml^{-1} LPS or only DMEM for 1 h at 37 °C followed by intense washing with MACS buffer. Afterward, 1×10^5 cells were transferred into 96-well plates and stained for CD11b and CD63 (eBioscience, clone HSC6) or CD66b (eBioscience, clone G10F5) for 20 min at 4 °C. After two washing steps with MACS buffer, cells were analyzed by flow cytometry. A total of 1×10^5 isolated murine neutrophils were transferred into a 96-well plate and stained for CD11b, CD62L and CD63 for 20 min at 4 °C. After two washing steps with MACS buffer, cells were analyzed by flow cytometry.

Endocytic properties of neutrophils. Isolated human neutrophils were incubated for 30 min with 1 µg ml^{-1} 10 kDa FITC-labeled dextran particles (fluid-phase endocytosis) or for 80 min with 10 µl ml^{-1} PFCs. At distinct time points, samples were taken and transferred into 2 ml ice-cold PBS. Afterward, cells were centrifuged at 300*g* for 10 min, resuspended in MACS buffer and analyzed by flow cytometry. Murine neutrophils were isolated from ^{mNP}PFC-treated or NaCl-treated animals and stained for Ly6G for 20 min at 4 °C. After two washing steps, phagocytosis of FITC-conjugated *E. coli* particles was determined by flow cytometry.

Isolation of total RNA. Human blood samples were treated ex vivo with ^{hNP}PFCs or NaCl for 1 h, and afterward neutrophils and monocytes were isolated with the blood neutrophil-isolation kit (Miltenyi) or the monocyte-isolation kit (Stemcell) according to the manufacturer's protocol. Murine neutrophils and monocytes were isolated from ^{mNP}PFC- or NaCl-treated animals from the bone marrow with isolation kits (both from Stemcell) according to the manufacturer's protocol. Cell disruption was carried out with 100 µl RLT Plus buffer (Qiagen), and afterward RNA was isolated according to the manufacturer's protocol (Zymo Research, RNA Clean & Concentrator).

SPR analysis of the human and murine neutrophil-specific peptides. The interaction between human and murine neutrophils and monocytes with NPs was analyzed using a Biacore X100 system equipped with a CM5 sensor chip (Cytiva). Immobilization of NPs to the chip surface was performed by activation of carboxymethyl groups of the CM5 chip and introduction of reactive disulfide groups by reaction with EDC–NHS and PDEA (Cytiva), followed by covalent binding of the NPs via the C-terminal free sulfhydryl group (260 µg, 5 µl min^{-1}) and blockage of excess carboxyl groups. Afterward, human and murine

neutrophils and monocytes (analytes) were flowed over the immobilized ligand surface to record the binding response of the analytes to the ligand. After 60 s of analyte association, the chip surface was regenerated for a period of 300 s by dissociation of the analytes with running buffer. Additionally, increasing numbers of neutrophils were flushed over the immobilized peptide with a flow rate of 30 µl min^{-1}, and dissociation was measured for an identical period. The final report point, expressed in relative response units of the stability point, was calculated by subtracting the reference from the ligand response unit, indicating the level of interaction and comparative binding affinity. HBS-EP (10 mM HEPES, pH 7.4, 150 mM NaCl, 3.4 mM EDTA, 0.005% P20) and DPBS plus 0.005% P20 (Sigma-Aldrich) buffers at 25 °C were used in all experiments as binding and running buffers, respectively.

Characterization of ^{NP}PFCs and ^{Con}PFCs

Fluorescence. For fluorescence measurements, 10 µl PFCs were spotted on a glass plate and analyzed with an IVIS Lumina II system (PerkinElmer; GFP excitation and emission filters, 0.5-s excitation).

Dynamic light scattering and the ζ potential were measured as described previously[9,12] at 25 °C using a Nanotrac Wave II analyzer (Microtrac) driven by Microtrac FLEX Software 3.4.

Cryo-transmission electron microscopy. PFCs were diluted with sample buffer to minimize particle aggregation and therefore enable proper size measurements, which were carried out as previously described[12].

Statistics

No statistical methods were used to predetermine sample size. Experiments were not randomized, and the investigators were not blinded during experiments and outcome assessment. Unless otherwise indicated, all values are given as mean ± s.d. Statistical analysis was performed using OriginPro 2016 (OriginLab). Data were tested for Gaussian distribution using the D'Agostino and Pearson omnibus normality test. For comparison of parameters between the groups, a Student's *t*-test or one- or two-way ANOVA was used.

RNA-sequencing data. FASTQ files were analyzed with CLC Genomics Workbench (version 22.0.1, Qiagen). The reads of all probes were adaptor (Illumina TruSeq) and quality trimmed (using the default parameters: bases below Q13 were trimmed from the end of the reads; ambiguous nucleotides, maximum 2). Mapping was done against *M. musculus* (mm39, GRCm39.105, 12 January 2022) and *H. sapiens* (hg38, GRCh38.100, 5 June 2020) genome sequences, respectively. After grouping samples (for $n = 3$ biological replicates each) according to the individual experimental conditions, statistical differential expression was determined using the Differential Expression for RNA-Seq tool (version 2.6). The resulting *P* values were corrected for multiple testing by FDR and Bonferroni correction. *P* values ≤0.05 were considered significant.

Reporting summary

Further information on research design is available in the Nature Portfolio Reporting Summary linked to this article.

Data availability

All data supporting the findings of this study are available within the article and its Supplementary Information. RNA-sequencing data have been uploaded to the Gene Expression Omnibus (accession no. GSE217910). Raw MRI data are available from the corresponding author. Source data are provided with this paper.

References

1. Serhan, C. N. & Savill, J. Resolution of inflammation: the beginning programs the end. *Nat. Immunol.* **6**, 1191–1197 (2005).
2. Gaul, D. S., Stein, S. & Matter, C. M. Neutrophils in cardiovascular disease. *Eur. Heart J.* **38**, 1702–1704 (2017).
3. Segal, A. W. How neutrophils kill microbes. *Annu. Rev. Immunol.* **23**, 197–223 (2005).
4. Megens, R. T. A., Kemmerich, K., Pyta, J., Weber, C. & Soehnlein, O. Intravital imaging of phagocyte recruitment. *Thromb. Haemost.* **105**, 802–810 (2011).
5. Wang, J. et al. Visualizing the function and fate of neutrophils in sterile injury and repair. *Science* **358**, 111–116 (2017).
6. Stolik, S., Delgado, J. A., Pérez, A. & Anasagasti, L. Measurement of the penetration depths of red and near infrared light in human 'ex vivo' tissues. *J. Photochem. Photobiol. B* **57**, 90–93 (2000).
7. Bulte, J. W. M. Hot spot MRI emerges from the background. *Nat. Biotechnol.* **23**, 945–946 (2005).
8. Krafft, M. P. & Riess, J. G. Chemistry, physical chemistry, and uses of molecular fluorocarbon–hydrocarbon diblocks, triblocks, and related compounds—unique 'apolar' components for self-assembled colloid and interface engineering. *Chem. Rev.* **109**, 1714–1792 (2009).
9. Temme, S. et al. Noninvasive imaging of early venous thrombosis by ^{19}F magnetic resonance imaging with targeted perfluorocarbon nanoemulsions. *Circulation* **131**, 1405–1414 (2015).
10. Temme, S., Grapentin, C., Güden-Silber, T. & Flögel, U. Active targeting of perfluorocarbon nanoemulsions. In *Fluorine Magnetic Resonance Imaging* (eds Flögel, U. & Ahrens, E.) 103–139 (Pan Stanford Publishing, 2016).
11. Miettinen, H. M., Gripentrog, J. M., Lord, C. I. & Nagy, J. O. CD177-mediated nanoparticle targeting of human and mouse neutrophils. *PLoS ONE* **13**, e0200444 (2018).
12. Krämer, W. et al. Rational manufacturing of functionalized, long-term stable perfluorocarbon-nanoemulsions for site-specific ^{19}F magnetic resonance imaging. *Eur. J. Pharm. Biopharm.* **142**, 114–122 (2019).
13. Horckmans, M. et al. Neutrophils orchestrate post-myocardial infarction healing by polarizing macrophages towards a reparative phenotype. *Eur. Heart J.* **38**, 187–197 (2017).
14. Frangogiannis, N. G. Regulation of the inflammatory response in cardiac repair. *Circ. Res.* **110**, 159–173 (2012).
15. Mazzucchelli, L. et al. Cell-specific peptide binding by human neutrophils. *Blood* **93**, 1738–1748 (1999).
16. Frei, A. P. et al. Direct identification of ligand–receptor interactions on living cells and tissues. *Nat. Biotechnol.* **30**, 997–1001 (2012).
17. Santos, I. et al. CXCL5-mediated recruitment of neutrophils into the peritoneal cavity of Gdf15-deficient mice protects against abdominal sepsis. *Proc. Natl Acad. Sci. USA* **117**, 12281–12287 (2020).
18. Kuijpers, T. W. et al. Membrane surface antigen expression on neutrophils: a reappraisal of the use of surface markers for neutrophil activation. *Blood* **78**, 1105–1111 (1991).
19. Skubitz, K. M., Campbell, K. D., Iida, J. & Skubitz, A. P. CD63 associates with tyrosine kinase activity and CD11/CD18, and transmits an activation signal in neutrophils. *J. Immunol.* **157**, 3617–3626 (1996).
20. Skubitz, K. M., Campbell, K. D. & Skubitz, A. P. CD66a, CD66b, CD66c, and CD66d each independently stimulate neutrophils. *J. Leukoc. Biol.* **60**, 106–117 (1996).
21. Chadwick, J. W. et al. Tissue-specific murine neutrophil activation states in health and inflammation. *J. Leukoc. Biol.* **110**, 187–195 (2021).
22. Temme, S. et al. Technical advance: monitoring the trafficking of neutrophil granulocytes and monocytes during the course of tissue inflammation by noninvasive ^{19}F MRI. *J. Leukoc. Biol.* **95**, 689–697 (2014).

23. Sczepanik, F. S. C. et al. Periodontitis is an inflammatory disease of oxidative stress: we should treat it that way. *Periodontol. 2000* **84**, 45–68 (2020).
24. Gross, S. et al. Bioluminescence imaging of myeloperoxidase activity in vivo. *Nat. Med.* **15**, 455–461 (2009).
25. Xiao, L. et al. Synthesis of the Cyanine 7 labeled neutrophil-specific agents for noninvasive near infrared fluorescence imaging. *Bioorg. Med. Chem. Lett.* **20**, 3515–3517 (2010).
26. Wu, M. et al. MR imaging tracking of inflammation-activatable engineered neutrophils for targeted therapy of surgically treated glioma. *Nat. Commun.* **9**, 4777 (2018).
27. Rennen, H. J., Corstens, F. H., Oyen, W. J. & Boerman, O. C. New concepts in infection/inflammation imaging. *QJ Nucl. Med.* **45**, 167–173 (2001).
28. Thackeray, J. T. et al. Molecular imaging of the chemokine receptor CXCR4 after acute myocardial infarction. *JACC Cardiovasc. Imaging* **8**, 1417–1426 (2015).
29. Hess, A. et al. Molecular imaging-guided repair after acute myocardial infarction by targeting the chemokine receptor CXCR4. *Eur. Heart J.* **41**, 3564–3575 (2020).
30. Jung, K. et al. Targeting CXCR4-dependent immunosuppressive Ly6C^{low} monocytes improves antiangiogenic therapy in colorectal cancer. *Proc. Natl Acad. Sci. USA* **114**, 10455–10460 (2017).
31. Krieg, F. M., Andres, R. Y. & Winterhalter, K. H. Superparamagnetically labelled neutrophils as potential abscess-specific contrast agent for MRI. *Magn. Reson. Imaging* **13**, 393–400 (1995).
32. Grapentin, C. et al. Optimization of perfluorocarbon nanoemulsions for molecular imaging by ^{19}F MRI. In *Nanomedicine* (eds Seifalin, A., de Mel, A. & Kalaskar, D. M.) 268–286 (One Central Press, 2014).
33. Bouvain, P. et al. Dissociation of ^{19}F and fluorescence signal upon cellular uptake of dual-contrast perfluorocarbon nanoemulsions. *Magn. Reson. Mater. Phy.* **32**, 133–145 (2019).
34. Goldschmeding, R. et al. Further characterization of the NB 1 antigen as a variably expressed 56–62 kD GPI-linked glycoprotein of plasma membranes and specific granules of neutrophils. *Br. J. Haematol.* **81**, 336–345 (1992).
35. Wang, J.-X. et al. Ly6G ligation blocks recruitment of neutrophils via a β_2-integrin-dependent mechanism. *Blood* **120**, 1489–1498 (2012).
36. Locke, L. W. et al. A novel neutrophil-specific PET imaging agent: cFLFLFK–PEG–^{64}Cu. *J. Nucl. Med.* **50**, 790–797 (2009).
37. Zhang, Y. et al. Neutrophil targeting heterobivalent SPECT imaging probe: cFLFLF–PEG–TKPPR–^{99m}Tc. *Bioconjug. Chem.* **21**, 1788–1793 (2010).
38. Xiao, L. et al. A novel near-infrared fluorescence imaging probe for in vivo neutrophil tracking. *Mol. Imaging* **11**, 372–382 (2012).
39. Wang, Z., Li, J., Cho, J. & Malik, A. B. Prevention of vascular inflammation by nanoparticle targeting of adherent neutrophils. *Nat. Nanotechnol.* **9**, 204–210 (2014).
40. Nakatani, K. et al. Regulation of the expression of Fcγ receptor on circulating neutrophils and monocytes in Kawasaki disease. *Clin. Exp. Immunol.* **117**, 418–422 (1999).
41. Tsukahara, Y. et al. Gene expression in human neutrophils during activation and priming by bacterial lipopolysaccharide. *J. Cell. Biochem.* **89**, 848–861 (2003).
42. Subrahmanyam, Y. V. et al. RNA expression patterns change dramatically in human neutrophils exposed to bacteria. *Blood* **97**, 2457–2468 (2001).
43. Zhang, X. et al. Gene expression in mature neutrophils: early responses to inflammatory stimuli. *J. Leukoc. Biol.* **75**, 358–372 (2004).
44. Grieshaber-Bouyer, R. & Nigrovic, P. A. Neutrophil heterogeneity as therapeutic opportunity in immune-mediated disease. *Front. Immunol.* **10**, 346 (2019).
45. Zhou, G. et al. CD177$^+$ neutrophils as functionally activated neutrophils negatively regulate IBD. *Gut* **67**, 1052–1063 (2018).
46. Huang, Y.-H., Lo, M.-H., Cai, X.-Y., Liu, S.-F. & Kuo, H.-C. Increase expression of CD177 in Kawasaki disease. *Pediatr. Rheumatol. Online J.* **17**, 13 (2019).
47. Swirski, F. K. & Nahrendorf, M. Cardioimmunology: the immune system in cardiac homeostasis and disease. *Nat. Rev. Immunol.* **18**, 733–744 (2018).
48. de Waha, S. et al. Relationship between microvascular obstruction and adverse events following primary percutaneous coronary intervention for ST-segment elevation myocardial infarction: an individual patient data pooled analysis from seven randomized trials. *Eur. Heart J.* **38**, 3502–3510 (2017).
49. Heusch, G. Myocardial ischaemia–reperfusion injury and cardioprotection in perspective. *Nat. Rev. Cardiol.* **17**, 773–789 (2020).
50. García-Prieto, J. et al. Neutrophil stunning by metoprolol reduces infarct size. *Nat. Commun.* **8**, 14780 (2017).
51. Clemente-Moragón, A. et al. Metoprolol exerts a non-class effect against ischaemia–reperfusion injury by abrogating exacerbated inflammation. *Eur. Heart J.* **41**, 4425–4440 (2020).
52. Amend, S. R., Valkenburg, K. C. & Pienta, K. J. Murine hind limb long bone dissection and bone marrow isolation. *J. Vis. Exp.* https://doi.org/10.3791/53936 (2016).
53. Ding, Z. et al. Cardiac injection of USSC boosts remuscularization of the infarcted heart by shaping the T-cell response. *J. Mol. Cell. Cardiol.* **175**, 29–43 (2023).
54. Borg, N. et al. CD73 on T-cells orchestrates cardiac wound healing after myocardial infarction by purinergic metabolic reprogramming. *Circulation* **136**, 297–313 (2017).
55. Bönner, F. et al. Monocyte imaging after myocardial infarction with ^{19}F MRI at 3 T: a pilot study in explanted porcine hearts. *Eur. Heart J. Cardiovasc. Imaging* **16**, 612–620 (2015).
56. Schindelin, J. et al. Fiji: an open-source platform for biological-image analysis. *Nat. Methods* **9**, 676–682 (2012).
57. Homann, S. et al. Hyaluronan synthase 3 promotes plaque inflammation and atheroprogression. *Matrix Biol.* **66**, 67–80 (2018).
58. Scheiber, D. et al. Reduced myocardial mitochondrial ROS production in mechanically unloaded hearts. *J. Cardiovasc. Transl. Res.* **12**, 107–115 (2019).
59. Flögel, U. et al. Multi-targeted ^{1}H/^{19}F MRI unmasks specific danger patterns for emerging cardiovascular disorders. *Nat. Commun.* **12**, 5847 (2021).
60. Haberkorn, S. M. et al. Cardiovascular magnetic resonance relaxometry predicts regional functional outcome after experimental myocardial infarction. *Circ. Cardiovasc. Imaging* **10**, e006025 (2017).
61. Temme, S. et al. Synthetic cargo internalization receptor system for nanoparticle tracking of individual cell populations by fluorine magnetic resonance imaging. *ACS Nano* **12**, 11178–11192 (2018).
62. Flögel, U. et al. In vivo monitoring of inflammation after cardiac and cerebral ischemia by fluorine magnetic resonance imaging. *Circulation* **118**, 140–148 (2008).
63. Ebner, B. et al. Early assessment of pulmonary inflammation by ^{19}F MRI in vivo. *Circ. Cardiovasc. Imaging* **3**, 202–210 (2010).
64. Abdgawad, M. et al. Elevated neutrophil membrane expression of proteinase 3 is dependent upon CD177 expression. *Clin. Exp. Immunol.* **161**, 89–97 (2010).

Acknowledgements

We thank T. Straub (Experimental Cardiovascular Imaging), K. Freidel, A. Zimmermann and Y. Ostendorf (Translational Pharmacology) for

excellent technical assistance; M. Vucur and T. Lüdde (Department of Gastroenterology, Hepatology and Infectious Diseases) for analyzing liver serum markers; the Center for Advanced Imaging for help with confocal microscopy (up to here, all institutions are at the campus of Heinrich Heine University Düsseldorf, Germany) as well as T. Hellmark (Department of Nephrology, Lund University, Sweden) for providing the CD177 plasmid for transfection experiments. This work was supported by the German Research Foundation (CRC 1116 to M.K., J.S., M.G., U.F.; CRC 259 to F.B., M.K., M.G., U.F.; FL303/6-1/2 to U.F.; INST 208/764-1 FUGG to U.F.; RTG 2576 vivid to M.G.; TE1209/1-1/2 to S.T.; RU/FOR5427 SP4, EN984/15-1, EN984/16-1, CRC/TR296 P09, CRC/TR332 A3 and CRC/TR332 Z1 all to D.R.E.) and the European Network on Noonan Syndrome and Related Disorders (EJP-RD; NSEuroNet, grant number 01GM1921B, P2 to M.M. and M.R.A.).

Author contributions

Study conception and design: P.B., M.G., S.T., U.F.; execution of experiments and acquisition of data: P.B., Z.D., S.K., P.K., N.K., Z.-B.T., B.S., V.F., R.Z., N.S., W.K., T.S., M.M., J.M.M., S.T.; analysis and interpretation of data: P.B., S.K., P.P., T.W., R.S., M.R.A., D.R.E., J.S., K.K., M.G., S.T., U.F.; implementation of the clinical STEMI path, recruitment of patients and care of human blood and tissue samples: G.J., F.B., U.B., R.W., M.K.; drafting of the manuscript: P.B., S.T.; critical revision: F.B., D.R.E., M.K., J.S., M.G., U.F.; funding: M.R.A., D.R.E., M.K., J.S., M.G., S.T., U.F.

Competing interests

The authors declare no competing interests.

Additional information

Extended data is available for this paper at https://doi.org/10.1038/s44161-022-00210-w.

Supplementary information The online version contains supplementary material available at https://doi.org/10.1038/s44161-022-00210-w.

Correspondence and requests for materials should be addressed to Ulrich Flögel.

Peer review information *Nature Cardiovascular Research* thanks Kory Lavine, Paul Kubes and the other, anonymous, reviewer(s) for their contribution to the peer review of this work.

[1]Experimental Cardiovascular Imaging, Institute for Molecular Cardiology, Heinrich Heine University, Düsseldorf, Germany. [2]Biological and Medical Research Center (BMFZ), Medical Faculty, Heinrich Heine University, Düsseldorf, Germany. [3]Dental Office/Oral Surgery, Dr. G. John, Plauen, Germany. [4]Institute for Experimental Immunology and Imaging, Department of Immunodynamics, University Hospital Essen, University Duisburg-Essen, Essen, Germany. [5]Department of Pharmaceutical Technology and Biopharmacy, Albert Ludwig University, Freiburg im Breisgau, Germany. [6]Institute of Neuro- and Sensory Physiology, Heinrich Heine University, Düsseldorf, Germany. [7]Institute of Biochemistry and Molecular Biology II, Medical Faculty and University Hospital Düsseldorf, Heinrich Heine University, Düsseldorf, Germany. [8]Department of Cardiology, Pneumology and Angiology, University Hospital Düsseldorf, Düsseldorf, Germany. [9]Clinic for Cardiac Surgery, University Hospital Düsseldorf, Düsseldorf, Germany. [10]Cardiovascular Research Institute Düsseldorf (CARID), Heinrich Heine University, Düsseldorf, Germany. [11]Institute for Translational Pharmacology, Heinrich Heine University, Düsseldorf, Germany. [12]Department of Anesthesiology, University Hospital Düsseldorf, Düsseldorf, Germany. [13]These authors contributed equally: Maria Grandoch, Sebastian Temme, Ulrich Flögel. ✉e-mail: floegel@uni-duesseldorf.de

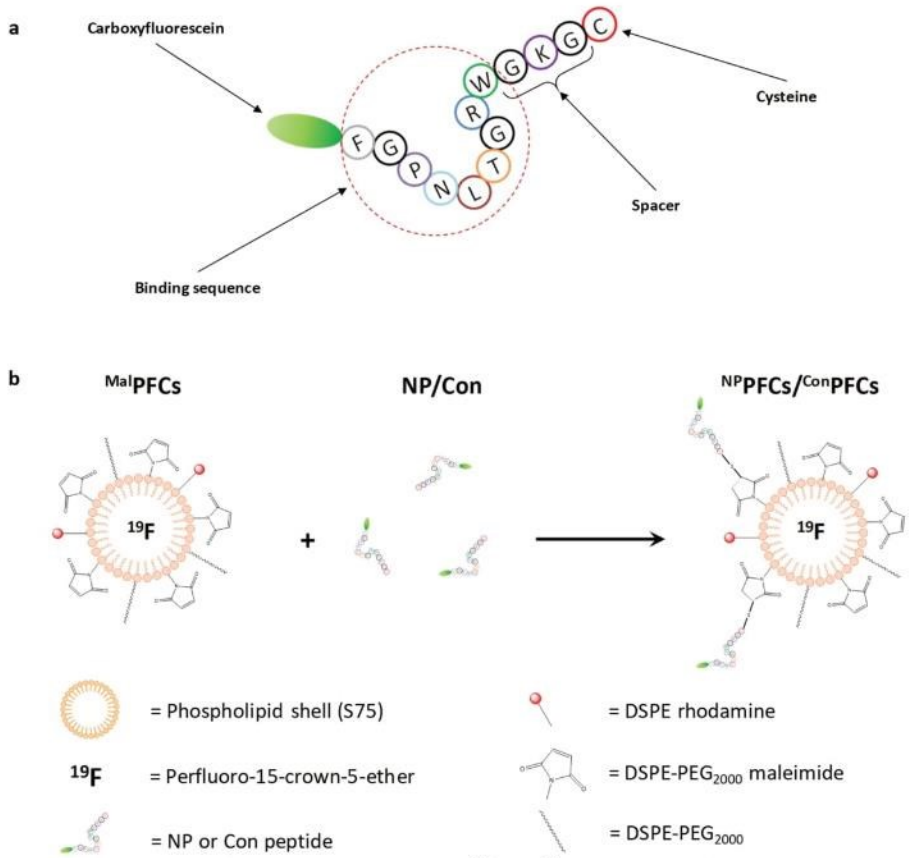

Extended Data Fig. 1 | Synthesis scheme for PFC-based nanotracers to target neutrophils. a, Basic structure of the used peptides for targeting neutrophils. The N-terminal carboxyfluorescein is incorporated for fluorescence-based analysis. For coupling the peptides to preformed ^{Mal}PFCs, a cysteine with a free sulfhydryl group is located at the C-terminus, next to the GGG spacer. The red dashed circle indicates the neutrophil binding sequence. **b**, For generating ^{NP}PFCs, preformed ^{Mal}PFCs were incubated with the peptides over night to form $^{NP/Con}$PFCs. ^{Mal}PFCs were equipped with a separate label (rhodamine) to control for a potential dissociation of binding peptide and PFC. To impair the passive uptake by monocytes/macrophages poly-ethylene-glycol (PEG) coupled lipids (DSPE-PEG_{2000} = 1,2-distearoyl-sn-glycero-3-phosphoethanolamine-N-[amino(poly-ethylene glycol)-2000]) were inserted in a 5 mol% ratio into the phospholipid shell of PFCs.

https://doi.org/10.1038/s44161-022-00210-w

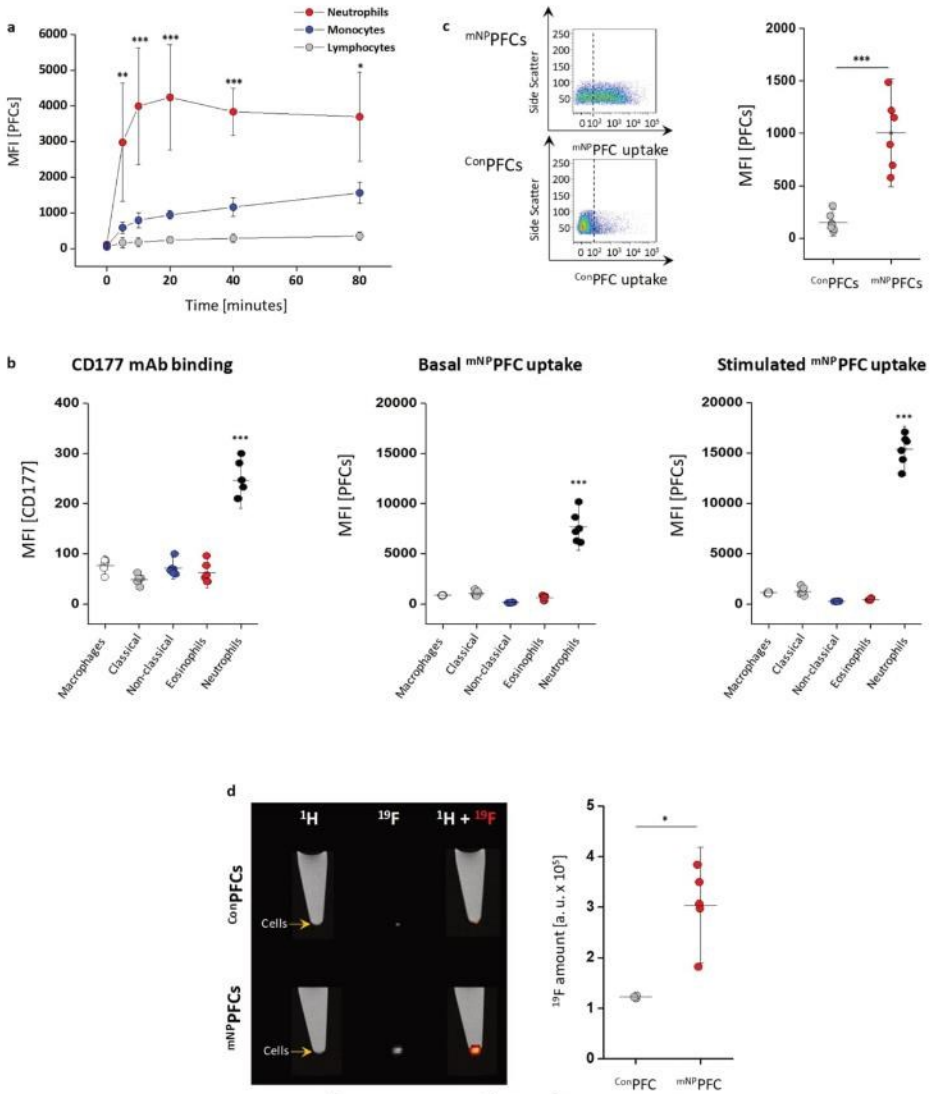

Extended Data Fig. 2 | Specific targeting of neutrophils by ^{mNP}PFCs. a, Flow cytometric analysis of murine blood leukocytes incubated with ^{mNP}PFCs over 80 min illustrating their predominant uptake by neutrophils (red) as compared to monocytes (blue) and lymphocytes (gray). **b**, To further validate specificity, binding of CD177 mAb as well as incorporation of ^{mNP}PFCs under basal and LPS-stimulated conditions were determined. Almost no binding/uptake into classical or non-classical monocytes as well as macrophages or eosinophils could be detected. In contrast to all other immune cell subsets, solely neutrophils showed a significant binding/uptake. **c**, Labelling of bone marrow neutrophils isolated 2 h upon intravenous injection of ^{mNP}PFCs or ^{Con}PFCs as determined via flow cytometry indicating a strong uptake of ^{mNP}PFCs and almost no incorporation of ^{Con}PFCs. **d**, To verify that cellular uptake of ^{mNP}PFCs can be visualized by ^{19}F MRI, we isolated murine neutrophils from the bone marrow, incubated the cells with ^{mNP}PFCs or ^{Con}PFCs for 3 h at 37 °C, washed intensively and pelleted the cells by centrifugation. Subsequently, cells were analyzed by ^{1}H/^{19}F MRI. Left: ^{1}H/^{19}F MRI of centrifugation tubes with neutrophils treated with ^{mNP}PFCs (lower panel) or ^{Con}PFCs (upper panel). The small neutrophil cell pellet is located at the bottom of the tube and can be identified by ^{1}H MRI (1st column) as slightly darker structure (arrows) compared to the bright phosphate buffer; corresponding ^{19}F MR images (2nd column) and superimposition of ^{1}H/^{19}F datasets (3rd column, with ^{19}F data color-coded in hot iron). Quantification of ^{19}F signals (4th column) clearly indicate substantial stronger ^{19}F uptake in ^{mNP}PFC-treated neutrophils (red) compared to cells incubated with ^{Con}PFCs (gray); a.u. = arbitrary units. Data are means ± SD of n = 4 (a), n = 6 (b), n = 6 (c) or n = 3-5 (d) independent experiments; * = $p > 0.05$, ** = $p < 0.01$, *** = $p < 0.001$, verified by two-way ANOVA (a), one-way ANOVA (b) or two-sided students t-test (c, d).

https://doi.org/10.1038/s44161-022-00210-w

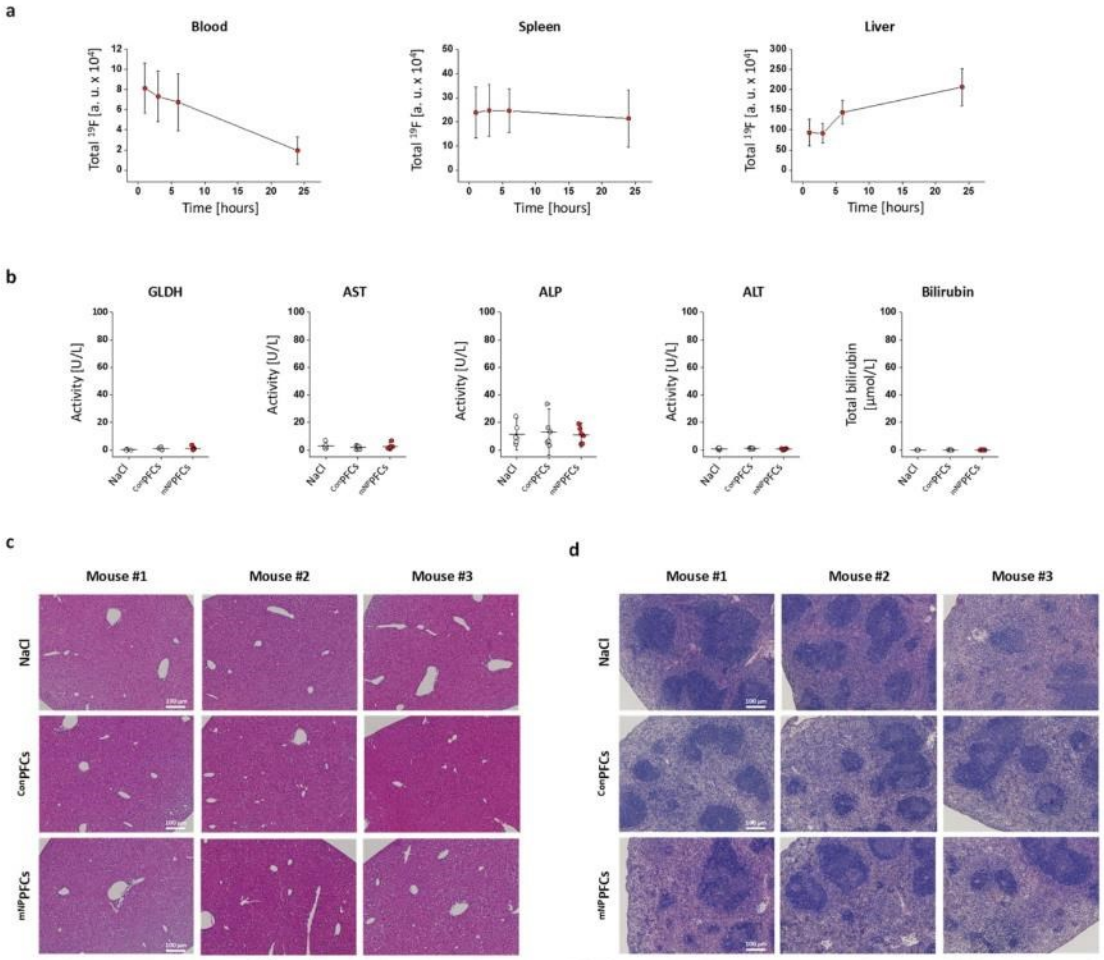

Extended Data Fig. 3 | Assessment of ^{mNP}PFC/^{Con}PFC biodistribution, liver serum markers and histology of liver and spleen. a, Biodistribution of intravenously injected ^{mNP}PFCs was determined *via* ^{19}F MRI measurements at distinct time points after injection (1, 3, 6 and 24 h after injection). Shown are quantification of fluorine signal intensities in the blood, liver and spleen indicating a fast wash-out from the blood accompanied by a strong influx into the liver while signal intensities in the spleen were constant over the entire observation period; a.u. = arbitrary units. **b**, Serum levels of GLDH (glutamate dehydrogenase), AST (aspartate aminotransferase), ALP (alkaline phosphatase), ALT (alanine aminotransferase) and bilirubin after intravenous application of NaCl as control, ^{Con}PFCs or ^{mNP}PFCs. **c** + **d**, 4 µm sections of liver (C) and spleen (D) stained with hematoxylin and eosin. Organs were excised and processed for histology 24 h post injection of NaCl (upper row), ^{Con}PFCs (middle), ^{mNP}PFCs (lower). Representative liver/spleen images of organs from three different animals are shown. Scale bars indicate 100 µm. Data are mean values ± SD of n = 6 (a), n = 4-6 (b) and n = 6 (c + d) independent experiments.

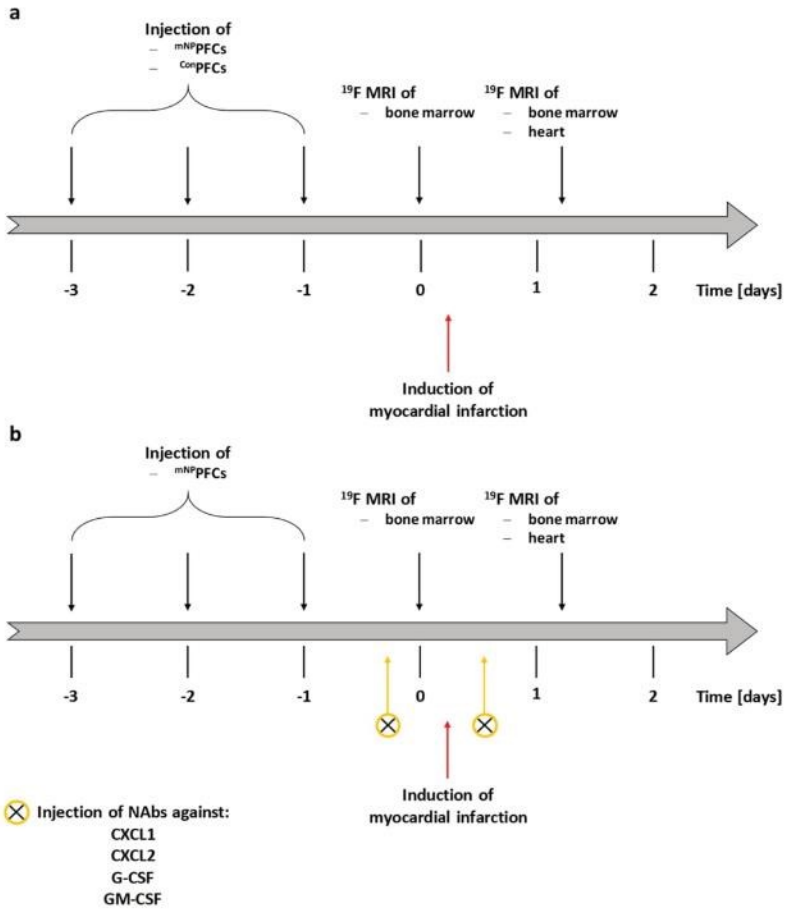

c

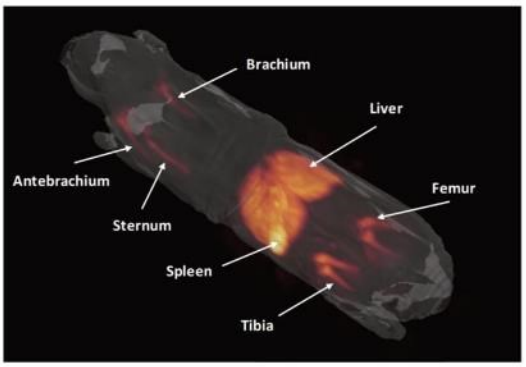

Extended Data Fig. 4 | See next page for caption.

https://doi.org/10.1038/s44161-022-00210-w

Extended Data Fig. 4 | Experimental timeline and whole body $^{1}H/^{19}F$ MRI of a ^{mNP}PFC-treated mouse. a, To label neutrophils within the bone marrow, ^{mNP}PFCs (or ^{Con}PFCs as control) were intravenously injected on three consecutive days (day −3, −2, −1) followed by $^{1}H/^{19}F$ MRI of the bone marrow on day 0. Subsequently, MI was induced and bone marrow and the infarcted heart were analyzed by combined $^{1}H/^{19}F$ MRI 24 h later. **b**, In separate experiments, neutralizing antibodies against CXCL1, CXCL2, G-CSF and GM-CSF were injected intraperitoneally (i. p.; 50 μg) 1 h before and 4 h post induction of MI to inhibit the MI-stimulated egress of neutrophils from the bone marrow and their infiltration into the heart. **c**, To determine the whole body biodistribution of ^{mNP}PFCs, ^{mNP}PFCs were intravenously injected daily over three consecutive days. Afterwards, whole body $^{1}H/^{19}F$ MRI measurements were performed to visualize the labelled neutrophils in the different bone marrow compartments. The bright ^{19}F spot in the middle represents the liver – an organ known to be as major site of (PFC) nanoparticle deposition.

https://doi.org/10.1038/s44161-022-00210-w

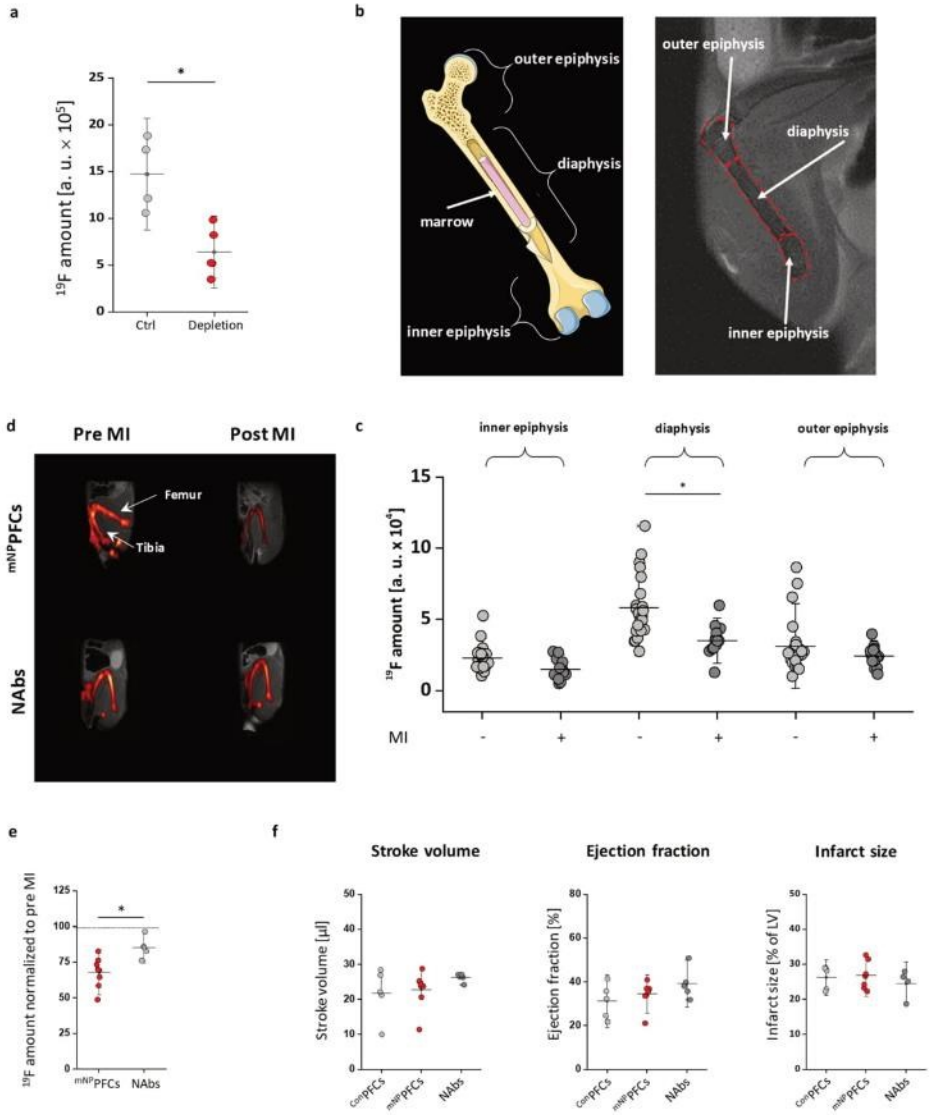

Extended Data Fig. 5 | mNPPFC incorporation into the bone marrow and cardiac function after MI. a, ***Impact of neutrophil depletion on mNPPFC incorporation into the bone marrow:*** For *in vivo* labeling of bone marrow neutrophils, mNPPFCs were injected intravenously and 24 h later the ^{19}F signal within the femur and tibia was determined (gray). Depletion of neutrophils by Ly6G Ab injection 48 and 24 h prior mNPPFC injection lead to significantly decreased ^{19}F bone marrow signals (red). **b** + **c**, ***Locoregional analysis of the femur ^{19}F signal before and after MI:*** **b**, Left: Schematic overview of the femur with the compartments inner/outer epiphysis and diaphysis. The marrow mainly belongs to the diaphysis whereas the growth of the bones takes place at the inner and outer epiphysis. At the right, an exemplarily compartmentalization of a murine ^{1}H MR scan of the femur with the inner and outer epiphysis as well as the diaphysis is shown. **c**, Quantification of the ^{19}F signal in the different femur compartments revealed highest mNPPFC uptake in the diaphysis before MI and a significant drop in this compartment after MI. The inner and outer epiphysis are characterized by lower fluorine intensities prior MI and smaller, non-significant decreases upon MI. **d** + **e**, ***Retention of bone marrow neutrophils by NAbs after MI:*** **d**, Antibodies against CXCL1, CXCL2, G-CSF and GM-CSF were injected intraperitoneally (i. p.) 1 h before and 4 h post induction of MI to inhibit the MI-stimulated egress of neutrophils from the bone marrow and their infiltration into the heart. Left: Combined ^{1}H/^{19}F MRI of the bone marrow (BM) before (left) and after MI (right). **e**, For quantification, the BM ^{19}F signal post MI was normalized to the ^{19}F signals detected before induction of MI. **f**, ***Ischemic area and functional cardiac parameters 1 day post MI:*** To exclude any effects on PFC distribution caused by differences in myocardial tissue impairment after MI between the individual experimental groups, we determined ischemic area, stroke volume and ejection fraction from ^{1}H MRI LGE cine measurements for each condition (LV = left ventricle). However, no significant differences between ConPFCs-, mNPPFCs- or mNPPFCs + NAbs-treated groups were found. Data are means ± SD of n = 4-5 (a), n = 7 – 11 (c), n = 5 – 8 (e) and n = 5 – 8 (f) independent experiments; * = $p < 0.05$, verified by two-sided students t-test (a, e) or one-way ANOVA (c).

https://doi.org/10.1038/s44161-022-00210-w

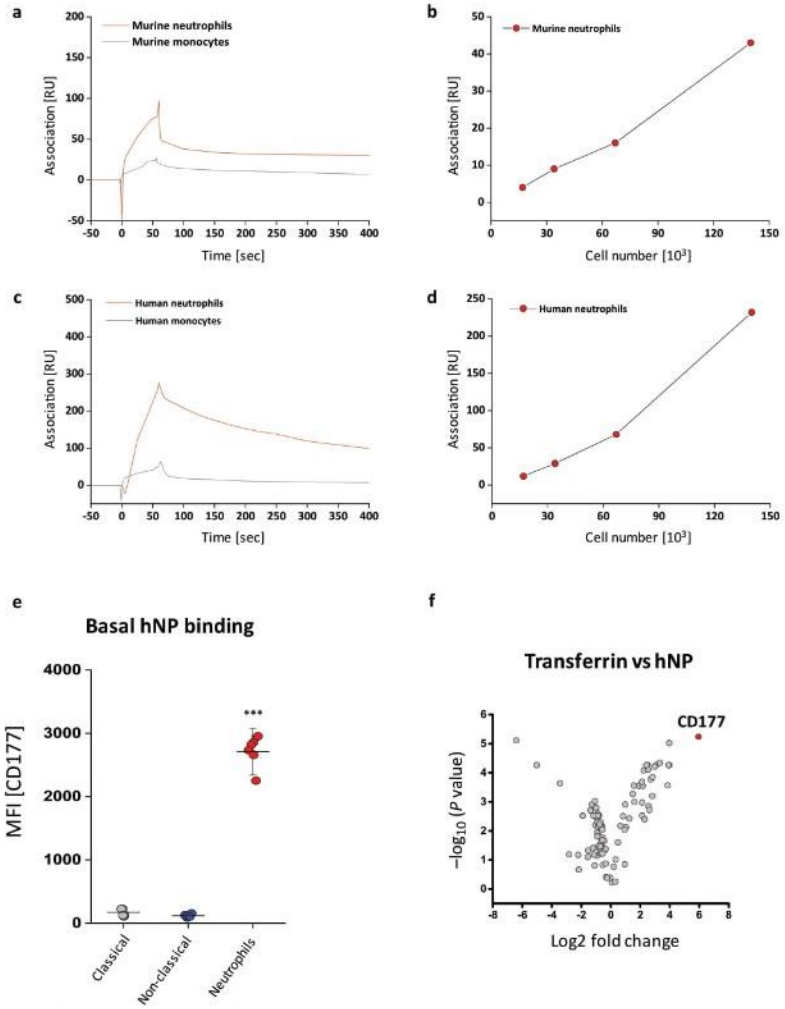

Extended Data Fig. 6 | Binding characterics of human and murine NP. a-d, ***Surface plasmon resonance spectroscopy (SPR) of NP binding to murine/human neutrophils and monocytes:*** Representative SPR sensograms of murine **a**, and human **c**, neutrophils (red) and monocytes (gray) binding to mNP and hNP, respectively. In each case 1.4×10^5 cells were flushed over the sensor chip. Binding curves of human and mouse neutrophils reveal a rapid association to the immobilized NP peptide and a slow dissociation rate (human K_d: 0.00449 s^{-1}, mouse K_d: 0.00901 s^{-1}). In contrast, human and mouse monocytes showed only a minor association with immobilized NP peptides. Furthermore, the SPR signal was determined for binding of the NP peptide with increasing cell numbers (1.7×10^4, 3.4×10^4, 6.7×10^4, and 1.4×10^5). Here, the observed SPR signal correlated almost linearly with the injected numbers of both murine **b**, and human **d**, neutrophils, and binding could be detected even for low cell numbers as 1.7×10^4 neutrophils. **e,** ***Binding of hNP to human monocyte subsets and neutrophils:*** Binding of the hNP peptide as determined by flow cytometry. We detected a strong binding by human neutrophils while classical as well as non-classical monocytes showed no binding at all. **f,** ***Validating identification of the hNP surface receptor with a modified spacer sequence:*** The modified spacer contained a lysine within the glycine spacer (-GKG- instead of –GGG-) which introduces a second conjugation site for the NHS group of the TriCeps™ to rule out any influence on the binding of the peptide. Subsequent mass spectroscopy revealed a similar protein profile and identified again CD177 as the most likely binding candidate. Data are means ± SD of n = 1 (a – d), n = 5-6 (e) and n = 1 (f) independent experiments; *** = $p < 0.001$, verified by one-way ANOVA.

https://doi.org/10.1038/s44161-022-00210-w

a

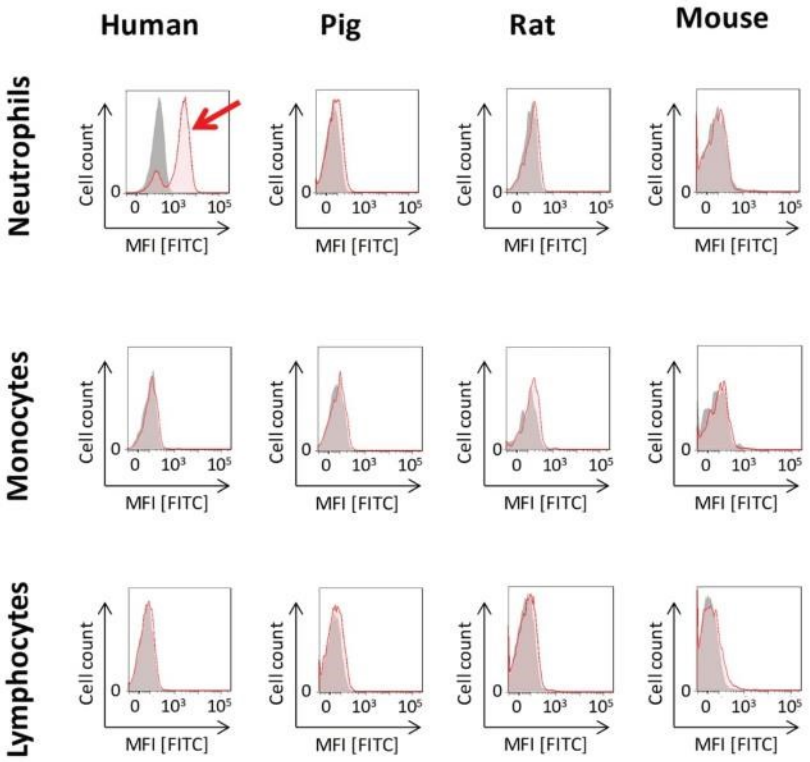

b

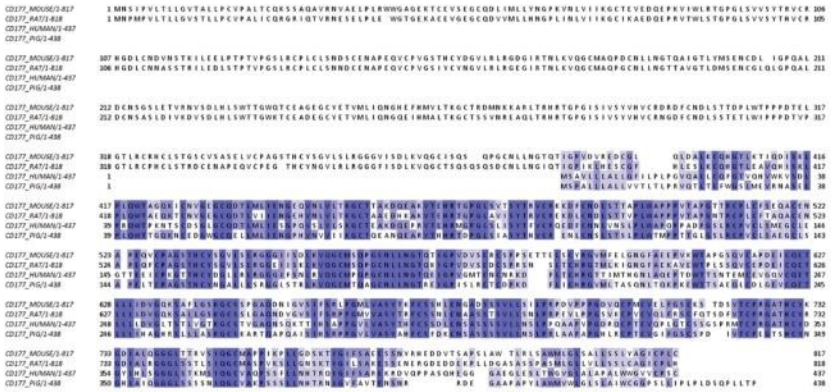

Extended Data Fig. 7 | Cross-species analysis of hNP binding and CD177 amino acid sequence. a, ***hNP does not bind to neutrophils from pigs, rats or mice:*** Determination of cross-species reactivity of hNP for pig, rat and mouse immune cells (neutrophils, lymphocytes, monocytes) analyzed by flow cytometry. The histogram overlays show binding studies with human immune cells (1st column) and leukocytes isolated from the blood of pigs (2nd column), rats (3rd column) or mice (4th column); gray = untreated cells, red = hNP treated cells. **b**, ***Cross-species analysis of CD177 amino acid sequence:*** Alignment of the protein sequence of CD177 from humans, mice, rats and pigs. Dark blue shows highly conserved sequence areas between all four species. Light blue indicates less conserved amino acids and white represents non-conserved areas.

https://doi.org/10.1038/s44161-022-00210-w

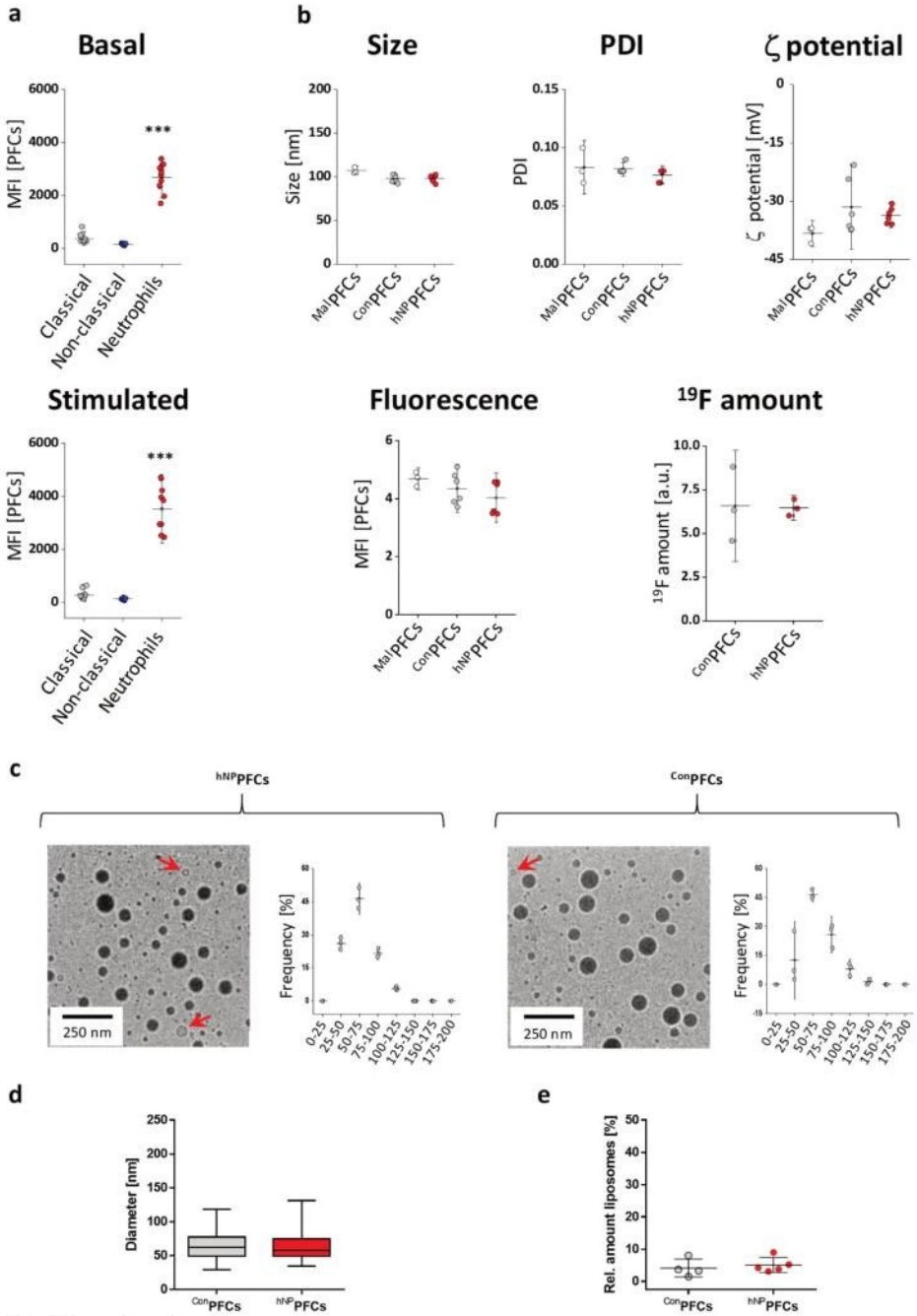

Extended Data Fig. 8 | See next page for caption.

https://doi.org/10.1038/s44161-022-00210-w

Extended Data Fig. 8 | Physicochemical properties and cellular uptake of ^{hNP}PFCs. a, ***Cellular uptake of ^{hNP}PFCs by human monocyte subsets and neutrophils:*** Human immune cells isolated from the blood of healthy volunteers were incubated with ^{hNP}PFCs. Subsequently, cells were stained with CD11b, CD14 and CD16 to differentiate between neutrophils (red), classical monocytes (gray) and non-classical monocytes (blue) and the cells were analyzed by flow cytometry. The cellular uptake of ^{hNP}PFCs was determined under unstimulated conditions (top) and after treatment with 1 µg/ml LPS (bottom). **b**, ***Physicochemical properties of the generated nanotracers:*** Characterization of size, size distribution and ζ potential of ^{Mal}PFCs and targeting PFCs (^{hNP}PFCs, ^{Con}PFCs) by dynamic light scattering (DLS). The rhodamine fluorescence signal of the PCS was determined by IVIS imaging and the ^{19}F content by ^{19}F MRI. **c-e**, ***Cryo transmission electron microscopy of the generated nanotracers:*** **c**, Cryo transmission electron microscopy (cryo-TEM) of ^{hNP}PFCs and ^{Con}PFCs. Graphs: The diameter of the PFCs was determined manually from three images categorized into 25 nm groups. The relative frequency of the number of PFCs in the range of 0-200 nm is displayed. Data are derived from three images for ^{hNP}PFCs and ^{Con}PFCs each. **d**, Box plot (box and whiskers; min to max) of the diameter of ^{Con}PFCs/^{hNP}PFCs calculated from cryo-TEM images. **e**, Relative amount of liposomes (%) in individual cryo-TEM images. The number of PFCs and liposomes was manually determined (n = 4/5 images). Red arrows in the cryo-TEM images indicate liposomes. Data are mean values ± SD of n = 5-6 (a), n = 3-6 (b), n = 3 (c), n = 3 (d) and n = 6 (e) independent experiments; *** = $p < 0.001$, verified by one-way ANOVA (a).

https://doi.org/10.1038/s44161-022-00210-w

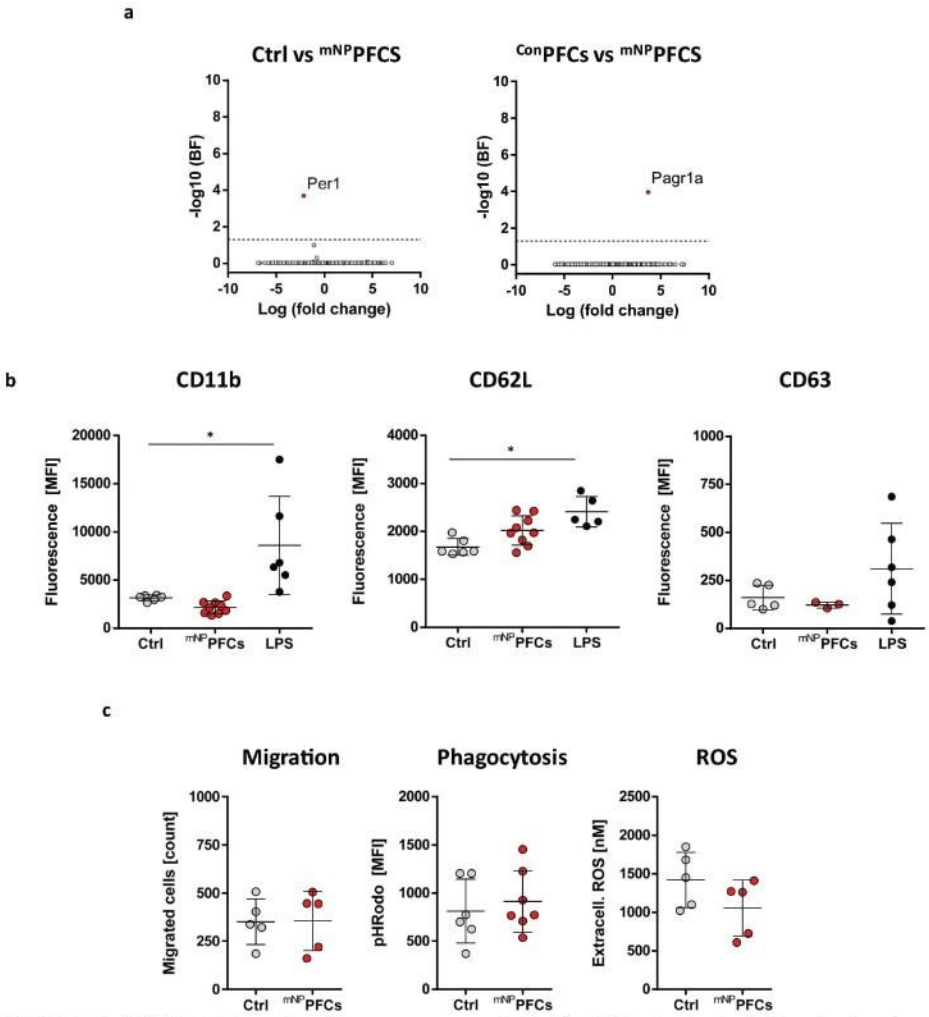

Extended Data Fig. 9 | Impact of ^{mNP}PFCs on murine neutrophils. **a**, Differentially expressed genes (DEGs) identified by bulk RNA sequencing of murine blood neutrophils after intravenous injection of ^{mNP}PFCs, ^{Con}PFCs or NaCl (Ctrl) as control. Volcano plots of DEGs for murine neutrophils of animals treated with saline compared to ^{mNP}PFCs (left), or ^{Con}PFCs compared to ^{mNP}PFC (right). Genes marked in red are significantly upregulated with a $\log_2$ (fold change) greater than 1.5. BF = Bonferroni corrected p-values of the false discovery rate. In total 25655 RNA transcripts were analyzed. **b**, Cell surface expression of CD11b, CD62L, CD63 on blood derived murine neutrophils after intravenous application of NaCl (Ctrl) or ^{mNP}PFCs. As a positive control, matrigel doped with 50 µg LPS was subcutaneously implanted into the neck of mice and after 24 h, neutrophils were isolated from the blood and analyzed by flow cytometry. **c**, Impact of ^{mNP}PFC incubation on neutrophil migration, phagocytosis and release of reactive oxygen species (ROS). Migration was determined in vivo by assessment of the infiltration of neutrophils into a matrigel/LPS plug; phagocytosis was determined by intravenous injection of FITC-labelled *E.coli* into mice and the subsequent removal and flow cytometric analysis of blood neutrophils; extracellular ROS were measured within the cell supernatant of blood neutrophils by oxidation of DHE (dihydroethidium) followed by UPLC analysis. Data are shown as means ± SD of n = 6 (a), n = 3-9 (b) and n = 5-7 (c) independent experiments. * = $p < 0.05$ verified by one-way ANOVA.

https://doi.org/10.1038/s44161-022-00210-w

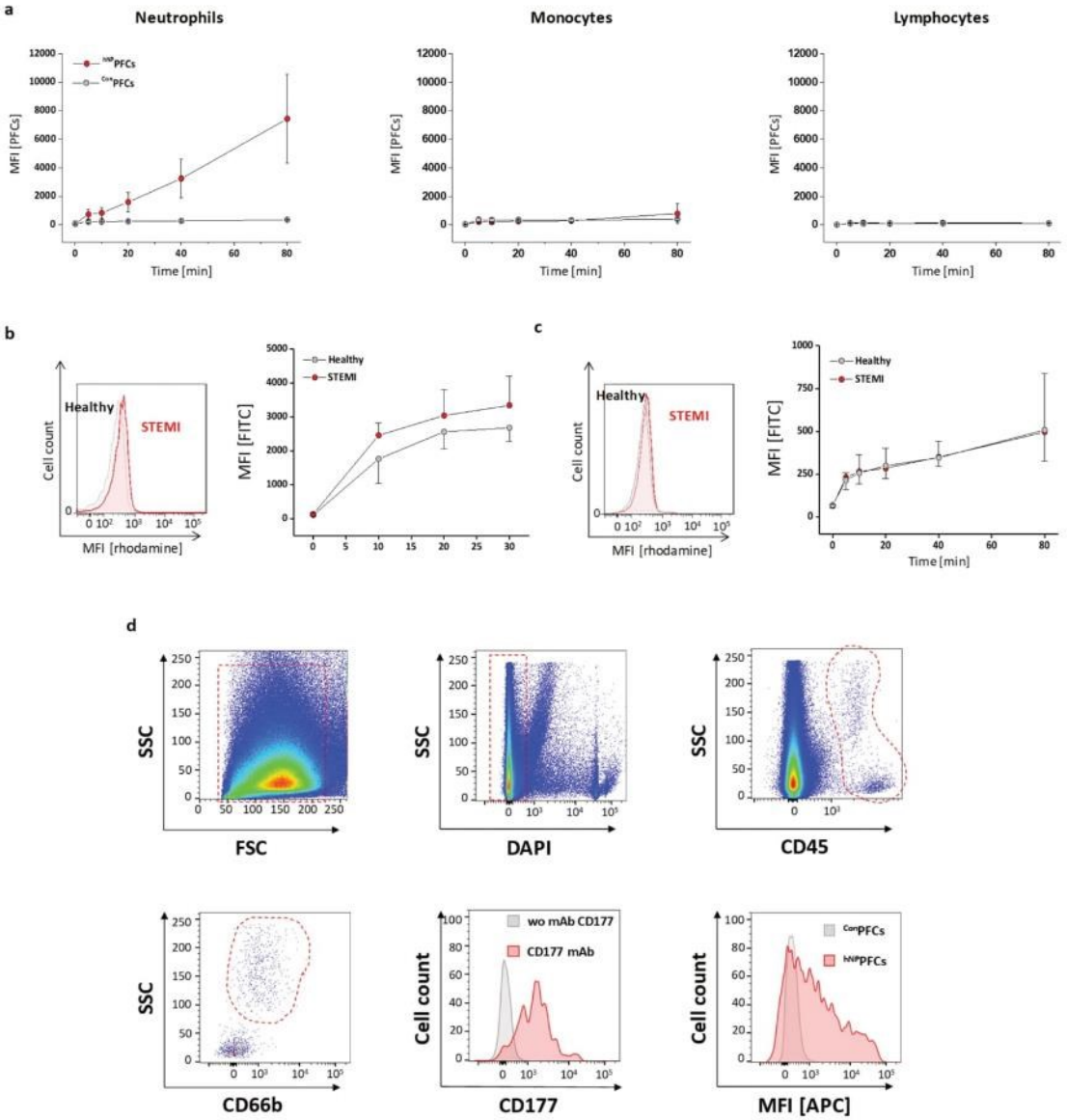

Extended Data Fig. 10 | Uptake of ^{hNP}PFCs by immune cells from patients. **a**, ***Uptake of ^{hNP}PFCs by immune cells from STEMI patients:*** Uptake of ^{hNP}PFCs (red) or ^{Con}PFCs (gray) by neutrophils, monocytes and lymphocytes from STEMI blood samples. While neutrophils show strong binding of ^{hNP}PFCs in comparison to ^{Con}PFCs, monocytes and lymphocytes show only negligible signals. **b** + **c**, ***Increased nanotracer uptake by STEMI patients is hNP-specific:*** **b**, Fluid-phase endocytosis by neutrophils from healthy controls as well as from STEMI patients was determined by incubation with FITC-labelled low molecular weight dextran-particles (10 kDa) over 30 min at 37 °C. At distinct time points the uptake was measured by flow cytometry indicating no significant differences between both groups. **c**, Phagocytosis was determined by incubation of neutrophils from healthy donors (gray) as well as from STEMI patients (red) with neat PFCs over 80 min at 37 °C. At distinct time points the uptake was measured via flow cytometry indicating no major differences between both groups. Left: Histogram overlays of healthy (gray) and STEMI (red) samples incubated with dextran particles (b) or PFCs (c). **d**, ***CD177 expression and ^{hNP}PFC uptake of neutrophils derived from tissue samples of explanted human hearts:*** Representative histograms of human heart samples. Dead cells were excluded from the analysis by DAPI staining. CD45 and CD11b stainings were carried out to identify neutrophils within the samples. These neutrophils exhibited both strong CD177 expression and uptake of ^{hNP}PFCs. Data are means ± SD of n = 4-6 (a), n = 4-5 (b + c) or n = 3 (d) independent experiments.

3 Discussion

Protein-protein and protein-lipid interactions play fundamental roles in mediating precise physiological interactions within cellular pathways. One key area of investigation was the fundamentals of PPIs, particularly how they occur selectively within numerous signaling pathways to recognize their binding partners. This doctoral thesis exemplifies this through an in-depth study of the SH3-PRM interaction, a classic example of signaling proteins communicating and executing cellular functions, which will be further discussed below (Chapters I and II). Additionally, this research highlighted the importance of protein-lipid interactions in various functions, including membrane dynamics, signal transduction, and inter- and intra-cellular communication. It also demonstrates how different membrane-binding modules in proteins, such as domains and motifs, facilitate membrane association and their involvement in disease progression (Chapter III).

Considering the roles of protein-protein and protein-lipid interactions in shaping signaling networks, a key focus was the MAPK pathway. This cascade regulates cellular processes, including proliferation, survival, growth, cell polarity and mobility [33]. In this context, the regulation of hub protein in MAPK, CRAF kinase, by PPI was investigated. Notably, SIRT4 was identified as a novel negative regulator of MAPK signaling through physical interaction with CRAF, adding a new layer of understanding to the regulatory mechanisms of this pathway (Chapter IV). This will be discussed in greater detail in the following parts. Additionally, the mechanisms regulating SIRT4 degradation under pseudohypoxic stress were investigated, focusing on how mitochondrial autophagy/mitophagy and proteasomal pathways impact SIRT4 stability (Chapter V).

Next, the role of mutagenesis in the MAPK signaling pathway components, RIT1 (Chapter VI) and SOS1 (Chapter VII), was examined in AVM disease. By analyzing the specific effects of these mutations on the RAS-MAPK and another important downstream cascade, the RAS-PI3K-AKT pathway, as well as the impact of drug inhibition, this work contributes to a deeper comprehension of the molecular mechanisms of AVM disease and highlights potential therapeutic targets, which will be discussed further in the subsequent sections.

Finally, the dissertation presents a novel non-invasive imaging technique that employs fluorine-loaded nanotracers to track neutrophil dynamics in cardiovascular injury, aiming to enhance the understanding of inflammation and refine diagnostic capabilities (Chapter VIII).

Overall, these projects collectively enhance our understanding of how protein-protein and protein-lipid interactions shape signaling pathways, elucidate the regulatory mechanisms within these pathways, and uncover the impacts of disease-associated mutations that lead to imbalanced signaling. They also offer potential therapeutic inhibitors and develop new diagnostic tools, with the goal of improving treatment strategies for various diseases.

3.1 Functional Analysis and Interaction Mapping of the Human SH3 Domains

Proteins contain modular domains capable of recognizing short peptide motifs, facilitating PPIs required for signal transduction [214]. SH3 domains are an example of modular domains found in 221 proteins (SH3-containing proteins; SH3CPs) that assist in signal transduction by predominantly recognizing specific peptide motifs (Proline-rich motifs; PRMs) [17], which are present in approximately 65.2% of the human proteome [215]. The SH3 superfamily is essential for many fundamental cellular processes, such as proliferation, cell survival, cell growth, actin reorganization, cell migration, endocytosis, apoptosis regulation, and proteasome degradation

[17]. The broad involvement of SH3 domains in cellular processes prompts important questions regarding the specificity of their interactions with PRMs. Understanding how SH3 domains recognize PRM motifs is key to deciphering their cellular functions.

Over the past decades, significant efforts have been made to elucidate how members of the SH3CP superfamily selectively recognize and bind to PRMs. For instance, a study by Carducci et al. (2012) provided an overview of the interaction landscape of the human SH3 protein family by integrating text mining of scientific literature and experimental data from high-density peptide arrays, storing the findings in the publicly accessible PepspotDB database [216]. More recently, a comprehensive analysis by Teyra et al. (2017) used high-throughput peptide-phage display and deep sequencing to map the specificity of human SH3 domains [217]. Moreover, hierarchical clustering allowed the researchers to organize SH3 domain specificity data into distinct profile classes, revealing that many SH3 domain families exhibit tightly clustered binding profiles. This is exemplified by a study by Verschueren et.al concluded that the specificity profiles of SH3 domains are largely conserved across four yeast species, *Saccharomyces cerevisiae, Ashbya gossypii, Candida albicans,* and *Schizosaccharomyces pombe*, indicating that high sequence identity within SH3 families predicts conserved binding specificity, while divergence often correlates with changes in binding specificity [218]. This finding suggests that specificity niches are conserved across large evolutionary distances, suggesting evolutionary stability and functional maintenance within these protein interaction networks. Nevertheless, it is important to remember that a protein's function is closely linked to its native tertiary structure. As the saying goes, “Structure is more highly conserved than sequence” [219]. Therefore, a comprehensive phylogenetic analysis that integrates sequence-structure relationships with biochemical annotations is essential for accurately identifying functional sites and understanding interactions from a sequence-structure-function perspective.

In this study, we systematically analyzed 298 SH3 domains from 221 SH3CPs. By combining evolutionary analysis with structural and biochemical data from the literature, we classified SH3 domains into ten families based on their PRM binding interfaces [220]. While most families converged on specific PRM patterns, some showed overlapping specificities, such as family one and family six for the RXXPXXP motif. These overlapping PRM sequences suggest that different SH3 domain families may exhibit distinct specificities yet recognize certain common motifs. This could be explained by potential functional redundancies, cooperative interactions, or shared regulatory pathways in cellular processes. Additionally, this classification was further validated by examining how different interface residues determine the affinity and specificity of SH3 domain interactions with PRMs. Besides the consideration of conserved residues of PRM-binding sites used for alignment and classification, our mutational analysis highlighted the significant role of non-conserved residues within each SH3 family in defining interaction specificity and affinity for PRMs. This underscores the dual role of both conserved and non-conserved SH3 domain residues in determining specificity and affinity. It is important to note that although *in silico* and *in vitro* studies offer valuable insights into the interaction specificity of modular domains, correlating these findings with *in vivo* PPIs is crucial for a more accurate understanding and assessment of signaling properties. A recent study by Dionne et al. (2021) detailed that while SH3 domains are known to mediate PPIs through their intrinsic binding specificities, their ability to define PPI specificity *in vivo* is heavily influenced by their host proteins. The study demonstrates that the identity of the host

protein and the positioning of SH3 domains within the host is crucial for determining PPI specificity [221].

Other than that, we specifically examined SOS1, a GEF involved in activating RAS proteins within the MAPK pathway, interaction with SH3 families, a PRM-containing protein showing co-occurrence of 13 out of 14 proline-rich consensus motifs. For that, we examined SOS1-derived PRPs (Proline-Rich Peptides) interaction with 25 representative SH3 domains selected from each family with low-throughput analyses, including pull-down assays, dot blotting, and fluorescence polarization. The results revealed, in most cases, weak micromolar affinity for SH3-PRP interactions. Reports suggest that the moderate affinities of SH3-domain-mediated interactions reflect a significant potential for dynamic remodeling, with rapid dissociation rates that depend on factors such as subcellular location and the availability of binding partners [222]. In addition, new models have been developed to account for these weak and transient PPIs. For instance, the SH3 domain-PRM interactions can be significantly increased by additional binding surfaces on the SH3 domain or its ligand. This enhancement can also result from having multiple SH3 domains or different domains within the same protein, or from the co-localization of interacting partners within a multi-protein complex [223, 224]. Additionally, our data revealed some high affinity newly discovered SH3 domain interactions of NCK1-2 and NCK1-3 (Non-Catalytic region of tyrosine Kinase adaptor protein1-SH3 domain 2 and 3), as well as ARHGAP12 (Rho GTPase Activating Protein 12) with WRCH1/RHOU (Wnt-1 Responsive CDC42 Homolog 1/RAS Homolog family member U)-derived RP2 and SOS1-derived P9 and P7, respectively. Further structural and biophysical characterization will be required to fully understand their function.

Furthermore, studies have highlighted the concept of proline-independent binding, where some SH3 domains interact with sequences that do not follow the traditional proline-rich motif. For instance, the RASA1 SH3 domain interacts with the GAP domain of DLC1 (Deleted In Liver Cancer 1 protein) [225] and kinase domains of Aurora [226], while the FYN-SH3 interacts with the SAP (Signaling lymphocyte Activation molecule-associated Protein)-SH2 domain [227]. These atypical interactions complicate the understanding of SH3 domain-mediated PPIs and suggest that SH3 domains possess a broader range of binding sequences. Generally, SH3 domains tend to maintain their binding specificities within species and across species, but there are exceptions where changes in binding specificity occur despite sequence similarities [218]. These exceptions might be due to the presence of proline-independent specificities. Moreover, this non-canonical proline-independent interaction might explain why 7 out of the 25 examined SH3 domains in this study showed no interaction with any of the 12 selected PRPs. Consequently, challenges persist in fully comprehending SH3-PRM interactions, especially in distinguishing between proline-dependent and proline-independent binding modes. Additionally, other than SH3s, numerous modular domain families, including WW (two highly conserved tryptophan amino acids), EVH1 (Ena/VASP Homology domain 1), GYF (Glycine-Tyrosine-Phenylalanine), Profilin, CAP-Gly (Cytoskeleton-Associated Protein-Glycine-rich), and UEV (Ubiquitin E2 Variant) have been reported as PRM-binding modules [228, 229]. Thus, exploring unique properties influencing interaction selectivity within each of these superfamilies is another issue to be addressed.

Moreover, disruption of SH3 domain interactions, deletion, or abnormal expression of SH3 domains is linked to the development of various human diseases, including cancer, leukemia, osteoporosis, Alzheimer's disease, and a range of infections [17]. Thus, continued investigation into SH3 domain interactions holds promise for advancing our understanding of cellular signaling

pathways and developing novel therapeutic strategies for diseases linked to abnormal SH3-mediated signaling.

3.2 SIRT4 as a New Interacting Partner and a Potential Inhibitor of CRAF Kinase in MAPK Signaling

In this study, we could identify a novel interaction between SIRT4, a tumor suppressor, and CRAF, a key kinase in the oncogenic MAPK signaling pathway [230]. Our findings show that CRAF selectively interacts with SIRT4 among the RAF kinases and sirtuins tested, with this interaction occurring between the N-terminal CRD of CRAF and the C-terminal region 3 (R3) of SIRT4. Mutational analysis of CRAF-CRD identifies gain-of-function mutations that enhance SIRT4 binding, highlighting the significance of these residues. Notably, SIRT4 specifically binds to CRAF in its inactive form (CRAF-pS259), and overexpression of functional SIRT4 leads to an accumulation of CRAF-pS259 and a reduction in MAPK signaling, as evidenced by decreased p-ERK1/2 levels. These results suggest that SIRT4 may have an extramitochondrial, anti-proliferative effect by sequestering CRAF, thereby interfering with CRAF-mediated activation of MEK1/2 and subsequent ERK1/2 phosphorylation.

In tumors with alterations in the MAPK pathway, an increasing number of oncogenic driver mutations have been identified in CRAF [231]. Moreover, the down-regulation or mutation of negative regulators is commonly observed during tumorigenesis. For example, PHLPP1/2, which acts as a negative regulator of CRAF by dephosphorylating it to diminish its signaling, often exhibits altered expression or functional impairment in cancer. In colorectal cancer patients, down-regulation of PHLPP genes and nonsense mutations (approximately 2-3% of cases) within the phosphatase domain of both isoforms are observed [156]. In another example, RKIP, an antimetastatic tumor suppressor that is down-regulated in various cancers [232], binds to the N-terminal region of CRAF and inhibits its phosphorylation and activation of MEK1/2 [152]. Similarly, the negative regulation of CRAF by SIRT4 aligns with previous studies showing SIRT4 down-regulation in various cancers and its inhibitory effects on cell proliferation [196, 200, 233-235]. Future studies should investigate the expression levels and mutational status of SIRT4 in different cancer types. The specific interaction between CRAF and SIRT4 presents an intriguing target for therapeutic intervention. Strategies to enhance this interaction or mimic the inhibitory effect of SIRT4 on CRAF could provide new approaches for treating cancers with hyperactive MAPK signaling.

The regulatory N-terminal region of CRAF plays a significant role in controlling its activation by interacting with several regulatory proteins. For example, the interaction between CRAF-RBD and arrestin-2, which organizes ERK2, MEK1, and CRAF into a scaffold, is believed to aid in releasing the kinase domain of CRAF, thereby enhancing the phosphorylation of MEK1 [139]. In addition, RKIP inhibits CRAF phosphorylation at residues S338 and Y340-Y341 and its ability to phosphorylate MEK by binding to the N-terminal region of CRAF and stabilization provided by high-affinity binding sites at the terminal ends of CRAF [151-154]. Similarly, RAP1 impedes CRAF activation by binding to the CRD domain of CRAF, diminishing oncogenic RAS clusters by competing with RAS for binding to CRAF within these nanoclusters [158]. In comparison, SIRT4 regulates CRAF activity through a similar mechanism by interacting with the N-terminal CRD domain, potentially sequestering inactive CRAF (pS259). However, the precise molecular mechanism by which SIRT4 promotes the accumulation of CRAF phosphorylation at S259

remains unclear. This could involve direct modulation of CRAF conformation, recruitment of kinases that phosphorylate S259, or inhibition of phosphatases that dephosphorylate S259.

In our study, we performed an extensive structural mutational analysis to explore the interaction between the CRD of CRAF and SIRT4. By selecting single and combined mutations based on sequence alignments of the CRD regions across CRAF, ARAF, and BRAF, we aimed to identify key interacting residues. Contrary to our expectations, these mutations did not result in a loss of function, but rather in a gain of function. To further investigate, we conducted molecular docking studies between the CRD of CRAF and full-length SIRT4, providing a 3D structural view of their interaction, revealing the binding interface involving key residues of the CRD and predominantly the R3 and, to a lesser extent, the R1 regions of SIRT4. Beyond the residues identified through mutational analysis of the CRAF-CRD domain, the docking and binding site analysis highlighted additional critical residues within the CRD and the R3 and R1 regions of SIRT4. Further mutational analysis is required to assess the functional significance of these newly identified residues. In addition, to gain a deeper and more detailed understanding of the molecular-level changes, it would be beneficial to investigate the effects of the CRAF-CRD mutants in a liquid environment and a dynamic system. Unfortunately, due to the lack of a complete structural model for CRAF, unlike BRAF, we were restricted to analyzing only the interactions between SIRT4 and the CRD domain. This limitation prevented us from exploring the autoinhibited closed conformations of the full CRAF protein in interaction with SIRT4.

Moreover, docking results revealed that the SIRT4-binding region of CRAF-CRD overlaps with residues critical for KRAS interaction and membrane association. Previous research identified seven essential basic residues within the CRD—R143, K144, K148, K157, R164, K171, and K179—that are vital for membrane binding, with particular emphasis on R143, K144, and K148 [236]. Our docking results show that in the inactive state of CRAF, residues R143, K157, and K179 are exposed and contribute to the SIRT4 interaction surface, while the remaining residues are shielded by 14-3-3 dimers. For KRAS binding, F141 and K179 are crucial for interaction with KRAS during CRAF activation [237]. Consistent with our docking analysis, both F141 and K179 are accessible in the inactive state of CRAF and are involved in SIRT4 binding. These observations indicate that the CRAF-CRD residues required for RAS and membrane interaction, which are necessary for CRAF activation, are occupied by SIRT4, which may help keep CRAF in its inactive state.

CRAF predominantly operates through the MAPK pathway but also targets a variety of proteins that influence multiple signaling pathways, resulting in diverse cellular responses. As demonstrated in the Figure 10A (Introduction section), these targets include cell cycle regulators (e.g., Rb [116], CDC25 [117], AuroraA-PLK1[118], CHK2 [119]), apoptosis modulators (e.g., BCL2 [120], ASK1 [121], MST2/STK3 [122], BAD [123], eEF1A1/2 [124]), and cytoskeletal components (e.g., ROK-α/ROCK-II [125], NF-κB [126], and DMPK [127]). While this study focuses on the MAPK pathway, it is important to consider how the CRAF-SIRT4 interaction might influence non-canonical CRAF-mediated pathways. In addition, given the known cytosolic roles of SIRT4 in cell cycle progression [193], regulating Wnt/β-catenin [211] and Hippo signaling pathways [212], and facilitating autophagosome-lysosome fusion through SNARE complex formation [213], it is important to explore how these functions intersect with its regulation of CRAF. In particular, the results from this study showed elevation of CRAF-pS259 levels following SIRT4 expression correlated with a reduction in the pYAP/YAP ratio, negatively modulating Hippo signaling

(unpublished data). Additionally, in this context, several questions remain unanswered: How is the CRAF-SIRT4 interaction regulated by different cellular stimuli? What are the physiological consequences of this interaction *in vivo*?

Given the diverse enzymatic activities of SIRT4, including deacetylase, deacylase, ADP-ribosyltransferase, and lipoamidase functions in mitochondria [238] and deacetylase in the cytosol [211-213] (Figure 12 and Figure 13), and considering that CRAF is a protein kinase, the precise nature of their functional interaction remains uncertain. Specifically, it is unclear whether CRAF is regulated through enzymatic reactions mediated by SIRT4 or if SIRT4 acts as a substrate for the enzymatic activity of CRAF. Notably, SIRT4 has three phosphorylation sites at S255, S261, and S262 [192, 239, 240], which were identified in mass spectrometry data but have not yet been experimentally validated. Further investigation is needed to determine whether these modifications are induced by CRAF kinase activity and to understand how they might influence SIRT4 function. Up to now, no acetylation has been reported for CRAF. Nevertheless, a recent study showed that SIRT1 regulates BRAF activity by deacetylating it at K601, which contrasts with the acetylation of BRAF by p300 acetyltransferase that enhances kinase activity and contributes to melanoma proliferation and resistance to BRAF-V600E inhibitors [241]. Therefore, further research is essential to understand the SIRT4-CRAF functional relationship and implications for cellular processes.

3.3 SOS1 Delins Characterization in Arteriovenous Malformations: Pathways to Targeted Therapy

Here, we report three novel SOS1 mutations associated with AVM. Our data present the first biochemical characterization of AVM-causing SOS1 mutations, suggesting that these mutations cause aberrant GEF activity of SOS1, as demonstrated by increased RAS-GTP levels in all three delins mutations. As a result, it causes subsequent hyperactivation of downstream signaling, as evidenced by elevated p-ERK levels. Notably, these SOS1 variants showed a decrease in AKT phosphorylation at T308, which is mediated by PDK1 and crucial for the initial activation of AKT, as well as a significant reduction in phosphorylation at S473, which is essential for the full activation of AKT. Additionally, our findings show that SHP2i (SHP099), KRAS:SOS1 (BI-3406), and MEKi (PD0325901) effectively reduced p-ERK levels, highlighting the potential for targeting different stages of the signaling pathway.

Previous studies observed the critical role of SOS-GEFs in endothelial cells and their involvement in angiogenesis [83, 84]. Studies also emphasize the importance of ERK phosphorylation, mediated by the MAPK cascade, in driving cell proliferation, a critical aspect of angiogenesis [242]. This aligns with our findings that SOS1 mutants lead to increased downstream ERK phosphorylation by enhancing GEF activity towards RAS, which in turn amplifies the RAS-MAPK pathway and promotes proliferative responses. Additionally, based on a previous study showing the SOS1, E3B1, and EPS8 complex have RAC-GEF activity *in* vitro [76], further investigation is needed to understand how AVM-associated mutations affect RAC activation.

Moreover, besides the MAPK pathway, others like PI3K are shown to contribute to angiogenesis [243]. Therefore, the effect of SOS1 delins was further investigated on the PI3K-AKT pathway by examining phosphorylation at T308, mediated by PDK1 and crucial for the initial activation of AKT, and phosphorylation at S473, essential for the full activation of AKT [49]. The results showed a decrease in AKT phosphorylation at T308 and S473. However, there is conflicting evidence

concerning the specific role of AKT. For example, studies demonstrated that inhibiting AKT disrupts vascular growth [244]. Nevertheless, expressing constantly active AKT1 mutants (T308A and S473A) inhibited proper capillary formation, suggesting that precise AKT activity regulation is crucial for normal angiogenesis and morphogenetic program [245]. Thereby, they observed a dynamic interplay between AKT and ERK during capillary-like network formation, where increased ERK activation correlated with reduced AKT phosphorylation and protein levels, necessary for proper network formation [245]. Further investigation is needed to observe how the correlation of ERK increase with the reduction in AKT observed in our experiment may contribute to AVM formation.

Our results indicate that SOS1-mutant variants are sensitive to the MEK inhibitor Mirdametinib, SHP2 inhibitor SHP099, and KRAS:SOS1 inhibitor BI-3406, which suggests potential treatment options for SOS1-mutant AVM in the future. The efficient results from MEK inhibition are consistent with studies showing that SOS1 mutants, such as the SOS1 N233Y mutation associated with lung tumors, are sensitive to other MEK inhibitors like Trametinib [246]. Furthermore, the selective KRAS:SOS1 inhibitor BI-3406, which binds to the catalytic site of SOS1 and disrupts its interaction with KRAS, thereby lowering GTP-loaded RAS levels and reducing cell proliferation [247], showed promising results in attenuating pERK levels in SOS1 delins. Notably, BI-3406 has been effective in inhibiting both pERK and proliferation in major KRAS mutants such as G12V, G12D, G12C, and G13D [248]. However, its efficacy against SOS1-driven mutants had not been demonstrated before. Furthermore, SHP2 inhibition upstream of SOS1 showed effective results in attenuating SOS1 delins but with less efficiency than MEKi and KRAS:SOS1 inhibitors. This might be due to research showing that SHP2 inhibition may not completely block signaling because activated SOS1 can bypass SHP2 to drive signaling even if SHP2 is inhibited [249-251].

The SOS1 gene harbors AVM-associated mutations within its N-terminal regulatory domain, particularly two in the PH domain and one in the linker region of the DH-PH unit. The N-terminal regions of SOS1 are crucial for maintaining its autoinhibition through interactions that stabilize an inactive conformation and restrain its catalytic activity. Upon activation, these domains also facilitate the recruitment of SOS1 to the plasma membrane and the subsequent release of autoinhibition [71, 72]. Interestingly, mutations affecting the N-terminal regulatory domain of SOS1 are prevalent in various cancers and RASopathies [70]. Notably, a detailed study on Noonan syndrome, a common RASopathy, analyzed the structural perturbations caused by specific amino acid substitutions. The study classified these mutations based on their effects on intermolecular interactions [78]. Particularly, PH domain lesions fall into classifications affecting the interaction between the HD, DH, and PH domains, thereby destabilizing the autoinhibited where the HD and DH domains block the distal RAS binding site [72, 78]. The effect of these AVM deletion mutations followed by long amino-acid insertions might change the interface of the HD and the DH-PH unit, which are conformationally coupled and need to be further analyzed. Another class of mutations affects the membrane-binding surface of the PH domain [78]. The predicted PIP2 binding residues of the PH domain are K456, R459, K472, and R489 [252], and the PA (Phosphatidic Acid) interacting region on the PH domain includes residues 472–483 [78, 253]. In patients 1 and 2, the location of the mutations does not overlap with membrane-binding sites, but in patient 3, the removal of R489 and the insertion of 14 amino acids might affect membrane binding, which needs further analysis. In general, based on the location of these mutations in this study, it can be postulated that AVM-associated mutations may affect SOS1 activity by interfering with the

autoinhibitory intradomain interactions mediated by the PH domain or by affecting PH domain membrane binding. Regardless of the exact mechanism through which SOS1 delins induce an oncogenic phenotype, our experiments demonstrate that this occurs through the activation of the RAS pathway. Further structural and membrane binding analysis is required to evaluate how the PH domain lesions lead to the constitutive activation of SOS1, resulting in enhanced and unregulated interaction with RAS and subsequent hyperactivation of the MAPK pathway.

3.4 RIT1 Delins in Arteriovenous Malformations: Implications for Targeted Therapy

This study identifies novel somatic RIT1 delins variants in patients with AVMs and demonstrates their role in hyperactivating the RAS-MAPK signaling pathway [254]. The functional significance of these variants was confirmed through *in vitro* and *in vivo* models, showing that the RIT1 variants lead to increased ERK phosphorylation and AVM formation in zebrafish embryos. Importantly, the study also highlights the potential therapeutic benefit of MEK inhibition, as demonstrated by the significant decrease in ERK phosphorylation and clinical improvement in a patient treated with Trametinib.

Previous studies have primarily associated AVMs with somatic mutations in other components of the RAS-MAPK pathway, such as HRAS [175], KRAS, BRAF [173], and MEK1 [174]. This study extends the spectrum of somatic alterations involved in AVM by implicating RIT1, a RAS-like protein, thereby providing new insights into the molecular mechanisms driving AVM development by modulating the RAS-MAPK pathway. In addition, based on the cross-talk between the RAS-MAPK and PI3K-AKT pathways, particularly RAS proteins regulating the PI3K pathway in oncogenesis [61], the impact of RIT1 variants on the PI3K-AKT signaling pathway was further explored. The results showed that AVM-associated RIT1 delins variants led to increased phosphorylation of AKT at T308, but not at S473, which are regulated by different kinases (PDK1 and mTORC2, respectively [49]). This suggests selective activation of the PI3K-AKT pathway, highlighting the potential involvement of the AKT pathway in sporadic AVM pathogenesis. This is despite the fact that the PI3K-AKT-mTOR pathway is typically predominant in slow-flow malformations, such as venous and lymphatic malformations [255, 256], whereas the RAS-MAPK pathway is usually associated with fast-flow malformations like AVM [174, 257, 258]. Nevertheless, involvement of increased PI3K-AKT in congenital AVM has also been observed, linked to the reduction of PTEN activity, which normally counteracts PI3K activity and limits AKT activation [176, 177]. Overall, the dual activation of both pathways by RIT1 variants suggests a more complex interplay between these signaling cascades in sporadic AVM pathogenesis.

A closer examination of the mutation locations reveals that the three novel RIT1 delins variants found in AVM patients are all situated near the switch II domain of the RIT1 protein. This finding is consistent with the observation that pathogenic mutations in the RIT1 gene tend to cluster in the G-domain, especially around the switch II region, which influences nucleotide and effector binding [92, 94]. Further structural analysis is needed to determine the precise effects of these mutations at the switch II region on GTPase activity and effector binding, and how they contribute to the hyperactivation of the downstream pathway.

In addition, our *in vitro* data shows mechanistic insight into effective MEK inhibitors, such as Mirdametinib, preventing ERK hyperphosphorylation. Combined with the reduction in AVM-like lesion size observed *in vivo*, this provides a strong rationale for further clinical trials. This is

particularly relevant given the limited efficacy and high relapse rates associated with current interventional and surgical treatments for AVMs [259]. This study also investigated the effects of SHP2 (SRC Homology-2 Protein tyrosine phosphatase) inhibition on RIT1-induced ERK hyperphosphorylation. SHP2 is a tyrosine phosphatase that acts upstream of RAS and is involved in the activation of the RAS-MAPK pathway. However, treatment with the SHP2 inhibitor, SHP099, did not affect ERK phosphorylation levels in HEK293T cells expressing RIT1 variants. This suggests that the hyperactivation of ERK in RIT1 variants may bypass SHP2, making SHP2 inhibitors less effective compared to MEK inhibitors. Recent research by Antonio, et al. (2023) shows that pathogenic RIT1 can recruit RAF kinases to the plasma membrane through weak binding, but this alone might not be enough to activate the MAPK pathway, which also requires classical RAS proteins. RIT1 increases RAF concentration and promotes its activation by RAS in response to RTK signaling. In the absence of RAS proteins, the ability of RIT1 to hyperactivate the MAPK pathway is limited. They also showed that pharmacological inhibition of MAPK, using inhibitors targeting SHP2 or SOS1, reduces downstream activation but does not affect RIT1-GTP levels [260]. The differences in SHP2 inhibitors effectiveness between the study by Antonio et al., which used 10 μM of RMC-4550, and our study, which used 5 μM of SHP099, suggest that higher concentrations or a different SHP2 inhibitor from an alternative source may be needed for effective inhibition. However, the conclusion remains that it is possible to bypass SHP2, and pathogenic RIT1 still depends on the canonical RAS-RAF-MAPK pathway. Furthermore, given the complexity of RIT1-AVM pathogenesis involving both MAPK and PI3K-AKT-mTORC1 pathways, a multi-target or combinatorial approach may be necessary to achieve optimal therapeutic outcomes.

References

1. Pérez, S. and I. Tvaroška, *Chapter 1 - Carbohydrate–Protein Interactions: Molecular Modeling Insights*, in *Advances in Carbohydrate Chemistry and Biochemistry*, D. Horton, Editor. 2014, Academic Press. p. 9-136.
2. Porras, P., et al., *Towards a unified open access dataset of molecular interactions.* Nat Commun, 2020. **11**(1): p. 6144.
3. Stein, A., et al., *Dynamic interactions of proteins in complex networks: a more structured view.* The FEBS journal, 2009. **276**(19): p. 5390-5405.
4. Rodina, A., et al., *Systems-level analyses of protein-protein interaction network dysfunctions via epichaperomics identify cancer-specific mechanisms of stress adaptation.* Nature Communications, 2023. **14**(1): p. 3742.
5. Perluigi, M. and E. Barone, *Aberrant protein networks in Alzheimer disease.* Nature Reviews Neurology, 2022. **18**(5): p. 255-256.
6. Ofran, Y. and B. Rost, *Analysing six types of protein-protein interfaces.* J Mol Biol, 2003. **325**(2): p. 377-87.
7. Braun, P. and A.-C. Gingras, *History of protein–protein interactions: From egg-white to complex networks.* PROTEOMICS, 2012. **12**(10): p. 1478-1498.
8. Rao, V.S., et al., *Protein-protein interaction detection: methods and analysis.* Int J Proteomics, 2014. **2014**: p. 147648.
9. Zhang, A., *Protein interaction networks: computational analysis*. 2009: Cambridge University Press.
10. Kim, P.M., et al., *Relating three-dimensional structures to protein networks provides evolutionary insights.* Science, 2006. **314**(5807): p. 1938-41.
11. Stollar, E.J. and D.P. Smith, *Uncovering protein structure.* Essays Biochem, 2020. **64**(4): p. 649-680.
12. Stahl, M.L., et al., *Sequence similarity of phospholipase C with the non-catalytic region of src.* Nature, 1988. **332**(6161): p. 269-72.
13. Hashimoto, S., et al., *Targeting AMAP1 and cortactin binding bearing an atypical src homology 3/proline interface for prevention of breast cancer invasion and metastasis.* Proc Natl Acad Sci U S A, 2006. **103**(18): p. 7036-41.
14. Rouka, E., et al., *Differential Recognition Preferences of the Three Src Homology 3 (SH3) Domains from the Adaptor CD2-associated Protein (CD2AP) and Direct Association with Ras and Rab Interactor 3 (RIN3).* J Biol Chem, 2015. **290**(42): p. 25275-92.
15. Lau, D.H., et al., *Critical residues involved in tau binding to fyn: implications for tau phosphorylation in Alzheimer's disease.* Acta Neuropathol Commun, 2016. **4**(1): p. 49.
16. Takeuchi, K., et al., *Structural and functional evidence that Nck interaction with CD3epsilon regulates T-cell receptor activity.* J Mol Biol, 2008. **380**(4): p. 704-16.
17. Mehrabipour, M., et al., *A Systematic Compilation of Human SH3 Domains: A Versatile Superfamily in Cellular Signaling.* Cells, 2023. **12**(16): p. 2054.
18. Cesareni, G. and D. Peluso, *SH3 and SH2: Prototypic Domains to Mediate Regulatory Mechanisms in the Cell*, in *Encyclopedia of Cell Biology*, R.A. Bradshaw and P.D. Stahl, Editors. 2016, Academic Press: Waltham. p. 112-121.
19. Symons, J.L., I. Levental, and K.R. Levental, *Lipidomic atlas of mammalian cell membranes reveals hierarchical variation induced by culture conditions, subcellular membranes, and cell lineages.* Biophysical Journal, 2021. **120**(3): p. 145a.
20. Han, X., *Lipidomics for studying metabolism.* Nature Reviews Endocrinology, 2016. **12**(11): p. 668-679.

21. Eiriksson, F.F., et al., *Lipidomic study of cell lines reveals differences between breast cancer subtypes.* PLoS One, 2020. **15**(4): p. e0231289.
22. Levental, K.R., et al., *Lipidomic and biophysical homeostasis of mammalian membranes counteracts dietary lipid perturbations to maintain cellular fitness.* Nature Communications, 2020. **11**(1): p. 1339.
23. Saliba, A.-E., I. Vonkova, and A.-C. Gavin, *The systematic analysis of protein–lipid interactions comes of age.* Nature Reviews Molecular Cell Biology, 2015. **16**(12): p. 753-761.
24. Butt, A.H., N. Rasool, and Y.D. Khan, *A Treatise to Computational Approaches Towards Prediction of Membrane Protein and Its Subtypes.* J Membr Biol, 2017. **250**(1): p. 55-76.
25. Levental, I. and E. Lyman, *Regulation of membrane protein structure and function by their lipid nano-environment.* Nature Reviews Molecular Cell Biology, 2023. **24**(2): p. 107-122.
26. Blobel, G., *Intracellular protein topogenesis.* Proc Natl Acad Sci U S A, 1980. **77**(3): p. 1496-500.
27. Allen, K.N., et al., *Monotopic Membrane Proteins Join the Fold.* Trends Biochem Sci, 2019. **44**(1): p. 7-20.
28. Bocharov, E.V., et al., *Helix-helix interactions in membrane domains of bitopic proteins: Specificity and role of lipid environment.* Biochimica et Biophysica Acta (BBA) - Biomembranes, 2017. **1859**(4): p. 561-576.
29. Neumann, J., et al., *Folding energetics and oligomerization of polytopic α-helical transmembrane proteins.* Archives of Biochemistry and Biophysics, 2014. **564**: p. 281-296.
30. Vinothkumar, K.R. and R. Henderson, *Structures of membrane proteins.* Quarterly Reviews of Biophysics, 2010. **43**(1): p. 65-158.
31. Renard, K. and B. Byrne, *Insights into the Role of Membrane Lipids in the Structure, Function and Regulation of Integral Membrane Proteins.* International Journal of Molecular Sciences, 2021. **22**(16): p. 9026.
32. Pelley, J.W., *5 - Membranes and Intracellular Signal Transduction*, in *Elsevier's Integrated Biochemistry*, J.W. Pelley, Editor. 2007, Mosby: Philadelphia. p. 37-46.
33. Roskoski, R., *ERK1/2 MAP kinases: Structure, function, and regulation.* Pharmacological Research, 2012. **66**(2): p. 105-143.
34. New, D.C. and Y.H. Wong, *Molecular mechanisms mediating the G protein-coupled receptor regulation of cell cycle progression.* Journal of molecular signaling, 2007. **2**(1): p. 2.
35. Kazemein Jasemi, N.S., et al., *The intramolecular allostery of GRB2 governing its interaction with SOS1 is modulated by phosphotyrosine ligands.* Biochem J, 2021. **478**(14): p. 2793-2809.
36. Huang, W.Y.C., et al., *A molecular assembly phase transition and kinetic proofreading modulate Ras activation by SOS.* Science, 2019. **363**(6431): p. 1098-1103.
37. Rezaei Adariani, S., et al., *Structural snapshots of RAF kinase interactions.* Biochemical Society Transactions, 2018. **46**(6): p. 1393-1406.
38. Braicu, C., et al., *A Comprehensive Review on MAPK: A Promising Therapeutic Target in Cancer.* Cancers, 2019. **11**(10): p. 1618.
39. Liu, F., et al., *Targeting ERK, an Achilles' Heel of the MAPK pathway, in cancer therapy.* Acta Pharm Sin B, 2018. **8**(4): p. 552-562.
40. Sugiura, R., R. Satoh, and T. Takasaki, *ERK: A Double-Edged Sword in Cancer. ERK-Dependent Apoptosis as a Potential Therapeutic Strategy for Cancer.* Cells, 2021. **10**(10).
41. Anjum, R. and J. Blenis, *The RSK family of kinases: emerging roles in cellular signalling.* Nature Reviews Molecular Cell Biology, 2008. **9**(10): p. 747-758.
42. Ke, X.-Y., et al., *MNK1 and MNK2 enforce expression of E2F1, FOXM1, and WEE1 to drive soft tissue sarcoma.* Oncogene, 2021. **40**(10): p. 1851-1867.
43. Roux, P.P. and J. Blenis, *ERK and p38 MAPK-activated protein kinases: a family of protein kinases with diverse biological functions.* Microbiology and molecular biology reviews, 2004. **68**(2): p. 320-344.

44. Evangelisti, C., et al., *Crosstalks of GSK3 signaling with the mTOR network and effects on targeted therapy of cancer.* Biochimica et Biophysica Acta (BBA) - Molecular Cell Research, 2020. **1867**(4): p. 118635.
45. Ding, Q., et al., *Erk Associates with and Primes GSK-3β for Its Inactivation Resulting in Upregulation of β-Catenin.* Molecular Cell, 2005. **19**(2): p. 159-170.
46. Wang, Z. *Regulation of Cell Cycle Progression by Growth Factor-Induced Cell Signaling*. Cells, 2021. **10**, 3327 DOI: 10.3390/cells10123327.
47. Balmanno, K. and S. Cook, *Tumour cell survival signalling by the ERK1/2 pathway.* Cell Death & Differentiation, 2009. **16**(3): p. 368-377.
48. Guo, Y.J., et al., *ERK/MAPK signalling pathway and tumorigenesis.* Exp Ther Med, 2020. **19**(3): p. 1997-2007.
49. Engelman, J.A., J. Luo, and L.C. Cantley, *The evolution of phosphatidylinositol 3-kinases as regulators of growth and metabolism.* Nature Reviews Genetics, 2006. **7**(8): p. 606-619.
50. Cohen, P. and S. Frame, *The renaissance of GSK3.* Nature Reviews Molecular Cell Biology, 2001. **2**(10): p. 769-776.
51. Potter, C.J., L.G. Pedraza, and T. Xu, *Akt regulates growth by directly phosphorylating Tsc2.* Nat Cell Biol, 2002. **4**(9): p. 658-65.
52. Burgering, B.M. and R.H. Medema, *Decisions on life and death: FOXO Forkhead transcription factors are in command when PKB/Akt is off duty.* J Leukoc Biol, 2003. **73**(6): p. 689-701.
53. Barthel, A., D. Schmoll, and T.G. Unterman, *FoxO proteins in insulin action and metabolism.* Trends in Endocrinology & Metabolism, 2005. **16**(4): p. 183-189.
54. Vivanco, I. and C.L. Sawyers, *The phosphatidylinositol 3-Kinase AKT pathway in human cancer.* Nat Rev Cancer, 2002. **2**(7): p. 489-501.
55. Fujita, N., et al., *Akt-dependent Phosphorylation of p27Kip1Promotes Binding to 14-3-3 and Cytoplasmic Localization*.* Journal of Biological Chemistry, 2002. **277**(32): p. 28706-28713.
56. Richardson, C.J., S.S. Schalm, and J. Blenis, *PI3-kinase and TOR: PIKTORing cell growth.* Seminars in Cell & Developmental Biology, 2004. **15**(2): p. 147-159.
57. Dan, H.C., et al., *Akt-dependent regulation of NF-{kappa}B is controlled by mTOR and Raptor in association with IKK.* Genes Dev, 2008. **22**(11): p. 1490-500.
58. Abdrabou, A., et al., *Rac1 S71 Mediates the Interaction between Rac1 and 14-3-3 Proteins.* Cells, 2019. **8**(9).
59. Soriano, O., et al., *The Crossroads between RAS and RHO Signaling Pathways in Cellular Transformation, Motility and Contraction.* Genes (Basel), 2021. **12**(6).
60. Higuchi, M., et al., *Akt mediates Rac/Cdc42-regulated cell motility in growth factor-stimulated cells and in invasive PTEN knockout cells.* Curr Biol, 2001. **11**(24): p. 1958-62.
61. Castellano, E. and J. Downward, *RAS Interaction with PI3K: More Than Just Another Effector Pathway.* Genes Cancer, 2011. **2**(3): p. 261-74.
62. Rommel, C., et al., *Differentiation stage-specific inhibition of the Raf-MEK-ERK pathway by Akt.* Science, 1999. **286**(5445): p. 1738-41.
63. Menges, C.W. and D.J. McCance, *Constitutive activation of the Raf-MAPK pathway causes negative feedback inhibition of Ras-PI3K-AKT and cellular arrest through the EphA2 receptor.* Oncogene, 2008. **27**(20): p. 2934-40.
64. Schulze, A., et al., *Analysis of the transcriptional program induced by Raf in epithelial cells.* Genes Dev, 2001. **15**(8): p. 981-94.
65. Winter, J.N., L.S. Jefferson, and S.R. Kimball, *ERK and Akt signaling pathways function through parallel mechanisms to promote mTORC1 signaling.* Am J Physiol Cell Physiol, 2011. **300**(5): p. C1172-80.
66. Carracedo, A., et al., *Inhibition of mTORC1 leads to MAPK pathway activation through a PI3K-dependent feedback loop in human cancer.* J Clin Invest, 2008. **118**(9): p. 3065-74.

67. Lehr, S., et al., *Identification of Major ERK-Related Phosphorylation Sites in Gab1.* Biochemistry, 2004. **43**(38): p. 12133-12140.
68. Zmajkovicova, K., et al., *MEK1 Is Required for PTEN Membrane Recruitment, AKT Regulation, and the Maintenance of Peripheral Tolerance.* Molecular Cell, 2013. **50**(1): p. 43-55.
69. Jun, J.E., I. Rubio, and J.P. Roose, *Regulation of ras exchange factors and cellular localization of ras activation by lipid messengers in T cells.* Frontiers in immunology, 2013. **4**: p. 239.
70. Baltanás, F.C., et al., *SOS GEFs in health and disease.* Biochimica et Biophysica Acta (BBA)-Reviews on Cancer, 2020. **1874**(2): p. 188445.
71. Sondermann, H., et al., *Structural Analysis of Autoinhibition in the Ras Activator Son of Sevenless.* Cell, 2004. **119**(3): p. 393-405.
72. Gureasko, J., et al., *Role of the histone domain in the autoinhibition and activation of the Ras activator Son of Sevenless.* Proceedings of the National Academy of Sciences, 2010. **107**(8): p. 3430-3435.
73. Lee, Y.K., et al., *Mechanism of SOS PR-domain autoinhibition revealed by single-molecule assays on native protein from lysate.* Nature Communications, 2017. **8**(1): p. 15061.
74. Chen, R.H., S. Corbalan-Garcia, and D. Bar-Sagi, *The role of the PH domain in the signal-dependent membrane targeting of Sos.* The EMBO journal, 1997.
75. Hoang, H.M., H.G. Umutesi, and J. Heo, *Allosteric autoactivation of SOS and its kinetic mechanism.* Small GTPases, 2021. **12**(1): p. 44-59.
76. Khanday , F.A., et al., *Sos-mediated activation of rac1 by p66shc.* Journal of Cell Biology, 2006. **172**(6): p. 817-822.
77. Tartaglia, M., G. Zampino, and B.D. Gelb, *Noonan Syndrome: Clinical Aspects and Molecular Pathogenesis.* Molecular Syndromology, 2010. **1**(1): p. 2-26.
78. Lepri, F., et al., *SOS1 mutations in Noonan syndrome: molecular spectrum, structural insights on pathogenic effects, and genotype–phenotype correlations.* Human mutation, 2011. **32**(7): p. 760-772.
79. Lissewski, C., et al., *Variants of SOS2 are a rare cause of Noonan syndrome with particular predisposition for lymphatic complications.* Eur J Hum Genet, 2021. **29**(1): p. 51-60.
80. Strzelec, K., et al., *Clinics and genetic background of hereditary gingival fibromatosis.* Orphanet J Rare Dis, 2021. **16**(1): p. 492.
81. Tumurkhuu, M., et al., *A novel SOS1 mutation in Costello/CFC syndrome affects signaling in both RAS and PI3K pathways.* J Recept Signal Transduct Res, 2013. **33**(2): p. 124-8.
82. Owens, M., et al., *SOS 1 frameshift mutations cause pure mucosal neuroma syndrome, a clinical phenotype distinct from multiple endocrine neoplasia type 2B.* Clinical endocrinology, 2016. **84**(5): p. 715-719.
83. Slevin, M., S. Kumar, and J. Gaffney, *Angiogenic Oligosaccharides of Hyaluronan Induce Multiple Signaling Pathways Affecting Vascular Endothelial Cell Mitogenic and Wound Healing Responses*.* Journal of Biological Chemistry, 2002. **277**(43): p. 41046-41059.
84. Wei, P., et al., *Differential endothelial cell gene expression by African Americans versus Caucasian Americans: a possible contribution to health disparity in vascular disease and cancer.* BMC Med, 2011. **9**: p. 2.
85. Trabalzini, L. and S.F. Retta, *Ras signaling: methods and protocols*. 2014: Springer.
86. Chenette, E.J. and C.J. Der, *5 - Lipid Modification of Ras Superfamily GTPases: Not Just Membrane Glue*, in *The Enzymes*, F. Tamanoi, C.A. Hrycyna, and M.O. Bergo, Editors. 2011, Academic Press. p. 59-95.
87. Zong, H., K. Kaibuchi, and L.A. Quilliam, *The insert region of RhoA is essential for Rho kinase activation and cellular transformation.* Mol Cell Biol, 2001. **21**(16): p. 5287-98.
88. Bos, J.L., H. Rehmann, and A. Wittinghofer, *GEFs and GAPs: Critical Elements in the Control of Small G Proteins.* Cell, 2007. **129**(5): p. 865-877.

89. Vigil, D., et al., *Ras superfamily GEFs and GAPs: validated and tractable targets for cancer therapy?* Nature Reviews Cancer, 2010. **10**(12): p. 842-857.
90. Mosaddeghzadeh, N., et al., *Electrostatic Forces Mediate the Specificity of RHO GTPase-GDI Interactions.* Int J Mol Sci, 2021. **22**(22).
91. Wes, P.D., M. Yu, and C. Montell, *RIC, a calmodulin-binding Ras-like GTPase.* Embo j, 1996. **15**(21): p. 5839-48.
92. Van, R., et al., *The molecular functions of RIT1 and its contribution to human disease.* Biochem J, 2020. **477**(15): p. 2755-2770.
93. Fang, Z., et al., *Biochemical Classification of Disease-associated Mutants of RAS-like Protein Expressed in Many Tissues (RIT1).* J Biol Chem, 2016. **291**(30): p. 15641-52.
94. Yaoita, M., et al., *Spectrum of mutations and genotype–phenotype analysis in Noonan syndrome patients with RIT1 mutations.* Human genetics, 2016. **135**: p. 209-222.
95. Migliori, A.D., L.A. Patel, and C. Neale, *The RIT1 C-terminus associates with lipid bilayers via charge complementarity.* Computational Biology and Chemistry, 2021. **91**: p. 107437.
96. Shi, G.X., W. Cai, and D.A. Andres, *Rit subfamily small GTPases: regulators in neuronal differentiation and survival.* Cell Signal, 2013. **25**(10): p. 2060-8.
97. Shi, G.X., L. Jin, and D.A. Andres, *Src-dependent TrkA transactivation is required for pituitary adenylate cyclase-activating polypeptide 38-mediated Rit activation and neuronal differentiation.* Mol Biol Cell, 2010. **21**(9): p. 1597-608.
98. Cai, W., G.X. Shi, and D.A. Andres, *Putting the Rit in cellular resistance: Rit, p38 MAPK and oxidative stress.* Commun Integr Biol, 2013. **6**(1): p. e22297.
99. Cai, W. and D.A. Andres, *mTORC2 is required for rit-mediated oxidative stress resistance.* PLoS One, 2014. **9**(12): p. e115602.
100. Shi, G.X. and D.A. Andres, *Rit contributes to nerve growth factor-induced neuronal differentiation via activation of B-Raf-extracellular signal-regulated kinase and p38 mitogen-activated protein kinase cascades.* Mol Cell Biol, 2005. **25**(2): p. 830-46.
101. Shao, H. and D.A. Andres, *A Novel RalGEF-like Protein, RGL3, as a Candidate Effector for Rit and Ras*.* Journal of Biological Chemistry, 2000. **275**(35): p. 26914-26924.
102. Hoshino, M., T. Yoshimori, and S. Nakamura, *Small GTPase proteins Rin and Rit Bind to PAR6 GTP-dependently and regulate cell transformation.* J Biol Chem, 2005. **280**(24): p. 22868-74.
103. Meyer Zum Büschenfelde, U., et al., *RIT1 controls actin dynamics via complex formation with RAC1/CDC42 and PAK1.* PLoS Genet, 2018. **14**(5): p. e1007370.
104. Castel, P., et al., *RIT1 oncoproteins escape LZTR1-mediated proteolysis.* Science, 2019. **363**(6432): p. 1226-1230.
105. Calcagni, G., et al., *Congenital heart defects in Noonan syndrome and RIT1 mutation.* Genet Med, 2016. **18**(12): p. 1320.
106. Yaoita, M., et al., *Spectrum of mutations and genotype-phenotype analysis in Noonan syndrome patients with RIT1 mutations.* Hum Genet, 2016. **135**(2): p. 209-22.
107. Gómez-Seguí, I., et al., *Novel recurrent mutations in the RAS-like GTP-binding gene RIT1 in myeloid malignancies.* Leukemia, 2013. **27**(9): p. 1943-6.
108. Rapp, U.R., et al., *Structure and biological activity of v-raf, a unique oncogene transduced by a retrovirus.* Proc Natl Acad Sci U S A, 1983. **80**(14): p. 4218-22.
109. Kozak, C., M.A. Gunnell, and U.R. Rapp, *A new oncogene, c-raf, is located on mouse chromosome 6.* J Virol, 1984. **49**(1): p. 297-9.
110. Huleihel, M., et al., *Characterization of murine A-raf, a new oncogene related to the v-raf oncogene.* Molecular and cellular biology, 1986. **6**(7): p. 2655-2662.
111. Ikawa, S., et al., *B-raf, a new member of the raf family, is activated by DNA rearrangement.* Molecular and cellular biology, 1988. **8**(6): p. 2651-2654.

112. Lavoie, H. and M. Therrien, *Regulation of RAF protein kinases in ERK signalling.* Nature reviews Molecular cell biology, 2015. **16**(5): p. 281-298.
113. Degirmenci, U., M. Wang, and J. Hu, *Targeting aberrant RAS/RAF/MEK/ERK signaling for cancer therapy.* Cells, 2020. **9**(1): p. 198.
114. Matallanas, D., et al., *Raf family kinases: old dogs have learned new tricks.* Genes & cancer, 2011. **2**(3): p. 232-260.
115. Baljuls, A., et al., *Positive Regulation of A-RAF by Phosphorylation of Isoform-specific Hinge Segment and Identification of Novel Phosphorylation Sites*.* Journal of Biological Chemistry, 2008. **283**(40): p. 27239-27254.
116. Davis, R.K. and S. Chellappan, *Disrupting the Rb-Raf-1 interaction: a potential therapeutic target for cancer.* Drug news & perspectives, 2008. **21**(6): p. 331.
117. Galaktionov, K., C. Jessus, and D. Beach, *Raf1 interaction with Cdc25 phosphatase ties mitogenic signal transduction to cell cycle activation.* Genes Dev, 1995. **9**(9): p. 1046-58.
118. Mielgo, A., et al., *A MEK-independent role for CRAF in mitosis and tumor progression.* Nat Med, 2011. **17**(12): p. 1641-5.
119. Advani, S.J., et al., *Kinase-independent role for CRAF-driving tumour radioresistance via CHK2.* Nat Commun, 2015. **6**: p. 8154.
120. Wang, H.G., et al., *Bcl-2 interacting protein, BAG-1, binds to and activates the kinase Raf-1.* Proc Natl Acad Sci U S A, 1996. **93**(14): p. 7063-8.
121. Alavi, A.S., et al., *Chemoresistance of endothelial cells induced by basic fibroblast growth factor depends on Raf-1-mediated inhibition of the proapoptotic kinase, ASK1.* Cancer Res, 2007. **67**(6): p. 2766-72.
122. O'Neill, E., et al., *Role of the kinase MST2 in suppression of apoptosis by the proto-oncogene product Raf-1.* Science, 2004. **306**(5705): p. 2267-70.
123. Kebache, S., et al., *Grb10 and active Raf-1 kinase promote Bad-dependent cell survival.* J Biol Chem, 2007. **282**(30): p. 21873-83.
124. Migliaccio, N., et al., *Raf kinases in signal transduction and interaction with translation machinery.* BioMolecular Concepts, 2013. **4**(4): p. 391-399.
125. Ehrenreiter, K., et al., *Raf-1 regulates Rho signaling and cell migration.* J Cell Biol, 2005. **168**(6): p. 955-64.
126. Baumann, B., et al., *Raf induces NF-κB by membrane shuttle kinase MEKK1, a signaling pathway critical for transformation.* Proceedings of the National Academy of Sciences, 2000. **97**(9): p. 4615-4620.
127. Shimizu, M., et al., *Rac-1 and Raf-1 kinases, components of distinct signaling pathways, activate myotonic dystrophy protein kinase.* FEBS Lett, 2000. **475**(3): p. 273-7.
128. Pandit, B., et al., *Gain-of-function RAF1 mutations cause Noonan and LEOPARD syndromes with hypertrophic cardiomyopathy.* Nature Genetics, 2007. **39**(8): p. 1007-1012.
129. Khazak, V., et al., *Selective Raf inhibition in cancer therapy.* Expert opinion on therapeutic targets, 2007. **11**(12): p. 1587-1609.
130. Wang, F., et al., *miR-195 is a key regulator of Raf1 in thyroid cancer.* Onco Targets Ther, 2015. **8**: p. 3021-8.
131. Qu, J., et al., *Hepatitis B virus regulation of Raf1 promoter activity through activation of transcription factor AP-2α.* Arch Virol, 2013. **158**(4): p. 887-94.
132. Wang, P., et al., *Targeting CRAF kinase in anti-cancer therapy: progress and opportunities.* Molecular Cancer, 2023. **22**(1): p. 208.
133. McTavish, C.J., et al., *Regulation of c-Raf Stability through the CTLH Complex.* Int J Mol Sci, 2019. **20**(4).
134. Andreu-Pérez, P., et al., *Protein arginine methyltransferase 5 regulates ERK1/2 signal transduction amplitude and cell fate through CRAF.* Sci Signal, 2011. **4**(190): p. ra58.

135. Chan, L.H., et al., *PRMT6 Regulates RAS/RAF Binding and MEK/ERK-Mediated Cancer Stemness Activities in Hepatocellular Carcinoma through CRAF Methylation.* Cell Rep, 2018. **25**(3): p. 690-701.e8.
136. Wang, X., et al., *Inhibition of ubiquitin-specific protease 13-mediated degradation of Raf1 kinase by Spautin-1 has opposing effects in naïve and primed pluripotent stem cells.* J Biol Chem, 2021. **297**(5): p. 101332.
137. Feng, D., et al., *O-GlcNAcylation of RAF1 increases its stabilization and induces the renal fibrosis.* Biochim Biophys Acta Mol Basis Dis, 2020. **1866**(3): p. 165556.
138. Verlande, A., et al., *Metabolic stress regulates ERK activity by controlling KSR-RAF heterodimerization.* EMBO reports, 2018. **19**(2): p. 320-336-336.
139. Qu, C., et al., *Scaffolding mechanism of arrestin-2 in the cRaf/MEK1/ERK signaling cascade.* Proceedings of the National Academy of Sciences, 2021. **118**(37): p. e2026491118.
140. Jang, E.R. and E. Galperin, *The function of Shoc2: A scaffold and beyond.* Communicative & integrative biology, 2016. **9**(4): p. e1188241.
141. Rajalingam, K. and T. Rudel, *"Prohibitin"g CRAF/MAPK Activation with Rocaglamides.* Chemistry & Biology, 2012. **19**(9): p. 1077-1078.
142. Ziogas, A., K. Moelling, and G. Radziwill, *CNK1 Is a Scaffold Protein That Regulates Src-mediated Raf-1 Activation*.* Journal of Biological Chemistry, 2005. **280**(25): p. 24205-24211.
143. Zang, M., C. Hayne, and Z. Luo, *Interaction between Active Pak1 and Raf-1 Is Necessary for Phosphorylation and Activation of Raf-1*.* Journal of Biological Chemistry, 2002. **277**(6): p. 4395-4405.
144. Wu, J., et al., *Polo-like kinase 1 induces epithelial-to-mesenchymal transition and promotes epithelial cell motility by activating CRAF/ERK signaling.* Elife, 2016. **5**.
145. Wang, X., et al., *PDCD6 cooperates with C-Raf to facilitate colorectal cancer progression via Raf/MEK/ERK activation.* J Exp Clin Cancer Res, 2020. **39**(1): p. 147.
146. Guo, H., et al., *RUVBL1, a novel C-RAF-binding protein, activates the RAF/MEK/ERK pathway to promote lung cancer tumorigenesis.* Biochem Biophys Res Commun, 2018. **498**(4): p. 932-939.
147. Hu, J., et al., *Allosteric activation of functionally asymmetric RAF kinase dimers.* Cell, 2013. **154**(5): p. 1036-1046.
148. Kolch, W., et al., *Protein kinase Cα activates RAF-1 by direct phosphorylation.* Nature, 1993. **364**(6434): p. 249-252.
149. Zimmermann, S. and K. Moelling, *Phosphorylation and Regulation of Raf by Akt (Protein Kinase B).* Science, 1999. **286**(5445): p. 1741-1744.
150. Dumaz, N. and R. Marais, *Protein kinase A blocks Raf-1 activity by stimulating 14-3-3 binding and blocking Raf-1 interaction with Ras.* J Biol Chem, 2003. **278**(32): p. 29819-23.
151. Wu, Z., et al., *Structural basis for RKIP binding with its substrate Raf1 kinase.* Biotechnology Letters, 2014. **36**(9): p. 1869-1874.
152. Rath, O., et al., *The RKIP (Raf-1 Kinase Inhibitor Protein) conserved pocket binds to the phosphorylated N-region of Raf-1 and inhibits the Raf-1-mediated activated phosphorylation of MEK.* Cellular Signalling, 2008. **20**(5): p. 935-941.
153. Parate, S., et al., *Exploring the binding interaction of Raf kinase inhibitory protein with the N-terminal of C-Raf through molecular docking and molecular dynamics simulation.* Frontiers in Molecular Biosciences, 2021. **8**: p. 655035.
154. Trakul, N., et al., *Raf Kinase Inhibitory Protein Regulates Raf-1 but Not B-Raf Kinase Activation*.* Journal of Biological Chemistry, 2005. **280**(26): p. 24931-24940.
155. Shukla, A., et al., *Sprouty 2: a novel attenuator of B-cell receptor and MAPK-Erk signaling in CLL.* Blood, 2016. **127**(19): p. 2310-21.
156. Li, X., et al., *PHLPP is a negative regulator of RAF1, which reduces colorectal cancer cell motility and prevents tumor progression in mice.* Gastroenterology, 2014. **146**(5): p. 1301-12.e1-10.

157. Feng, L., et al., *Spatial regulation of Raf kinase signaling by RKTG.* Proc Natl Acad Sci U S A, 2007. **104**(36): p. 14348-53.
158. Nussinov, R., et al., *The Mystery of Rap1 Suppression of Oncogenic Ras.* Trends Cancer, 2020. **6**(5): p. 369-379.
159. Yu, A., et al., *A novel phosphorylation site involved in dissociating RAF kinase from the scaffolding protein 14-3-3 and disrupting RAF dimerization.* Journal of Biological Chemistry, 2023. **299**(10).
160. Okamoto, K. and Y. Sako, *Two Closed Conformations of CRAF Require the 14-3-3 Binding Motifs and Cysteine-Rich Domain to be Intact in Live Cells.* J Mol Biol, 2023. **435**(6): p. 167989.
161. Mitra, S., et al., *Bipartite Role of Heat Shock Protein 90 (Hsp90) Keeps CRAF Kinase Poised for Activation.* J Biol Chem, 2016. **291**(47): p. 24579-24593.
162. Jaime-Garza, M., et al., *Hsp90 provides a platform for kinase dephosphorylation by PP5.* Nature Communications, 2023. **14**(1): p. 2197.
163. Adams, D.G., et al., *Positive Regulation of Raf1-MEK1/2-ERK1/2 Signaling by Protein Serine/Threonine Phosphatase 2A Holoenzymes*.* Journal of Biological Chemistry, 2005. **280**(52): p. 42644-42654.
164. Dougherty, M.K., et al., *Regulation of Raf-1 by direct feedback phosphorylation.* Molecular cell, 2005. **17**(2): p. 215-224.
165. Mehra, M., et al., *Evaluating the Quality, Readability, and Activity of Online Information on Brain Arteriovenous Malformations.* Cureus, 2023. **15**(9): p. e45984.
166. Fleetwood, I.G. and G.K. Steinberg, *Arteriovenous malformations.* The Lancet, 2002. **359**(9309): p. 863-873.
167. Berman, M.F., et al., *The epidemiology of brain arteriovenous malformations.* Neurosurgery, 2000. **47**(2): p. 389-397.
168. Goss, J.A., et al., *Somatic mutations in intracranial arteriovenous malformations.* PLoS One, 2019. **14**(12): p. e0226852.
169. Maddy, K., et al., *An updated review on the genetics of arteriovenous malformations.* Gene & protein in disease, 2023. **2**(2): p. 0312.
170. Wang, K., et al., *Perturbations of BMP/TGF-β and VEGF/VEGFR signalling pathways in non-syndromic sporadic brain arteriovenous malformations (BAVM).* Journal of medical genetics, 2018. **55**(10): p. 675-684.
171. Barbosa Do Prado, L., et al., *Recent Advances in Basic Research for Brain Arteriovenous Malformation.* International Journal of Molecular Sciences, 2019. **20**(21): p. 5324.
172. Shabani, Z., J. Schuerger, and H. Su, *Cellular loci involved in the development of brain arteriovenous malformations.* Frontiers in Human Neuroscience, 2022. **16**: p. 968369.
173. Hong, T., et al., *High prevalence of KRAS/BRAF somatic mutations in brain and spinal cord arteriovenous malformations.* Brain, 2019. **142**(1): p. 23-34.
174. Couto, J.A., et al., *Somatic MAP2K1 Mutations Are Associated with Extracranial Arteriovenous Malformation.* The American Journal of Human Genetics, 2017. **100**(3): p. 546-554.
175. Konczyk, D.J., et al., *Arteriovenous malformation associated with a HRAS mutation.* Hum Genet, 2019. **138**(11-12): p. 1419-1421.
176. Alsina-Sanchís, E., et al., *ALK1 Loss Results in Vascular Hyperplasia in Mice and Humans Through PI3K Activation.* Arterioscler Thromb Vasc Biol, 2018. **38**(5): p. 1216-1229.
177. Steiger, H.-J., *Recent progress understanding pathophysiology and genesis of brain AVM—a narrative review.* Neurosurgical Review, 2021. **44**(6): p. 3165-3175.
178. Eerola, I., et al., *Capillary malformation-arteriovenous malformation, a new clinical and genetic disorder caused by RASA1 mutations.* Am J Hum Genet, 2003. **73**(6): p. 1240-9.
179. Lubeck, B.A., et al., *Blood vascular abnormalities in Rasa1R780Q knockin mice: Implications for the pathogenesis of capillary malformation–arteriovenous malformation.* The American Journal of Pathology, 2014. **184**(12): p. 3163-3169.

180. Coccia, E., et al., *Prenatal Clinical Findings in RASA1-Related Capillary Malformation-Arteriovenous Malformation Syndrome.* Genes, 2023. **14**(3): p. 549.
181. Lapinski, P.E., et al., *Somatic second hit mutation of RASA1 in vascular endothelial cells in capillary malformation-arteriovenous malformation.* Eur J Med Genet, 2018. **61**(1): p. 11-16.
182. Sánchez-Espino, L.F., et al., *Single dominant lesion in capillary malformation-arteriovenous malformation (CM-AVM) syndrome.* Pediatric Dermatology. **n/a**(n/a).
183. Amyere, M., et al., *Germline Loss-of-Function Mutations in EPHB4 Cause a Second Form of Capillary Malformation-Arteriovenous Malformation (CM-AVM2) Deregulating RAS-MAPK Signaling.* Circulation, 2017. **136**(11): p. 1037-1048.
184. Kawasaki, J., et al., *RASA1 functions in EPHB4 signaling pathway to suppress endothelial mTORC1 activity.* J Clin Invest, 2014. **124**(6): p. 2774-84.
185. Hiepen, C., P.-L. Mendez, and P. Knaus, *It Takes Two to Tango: Endothelial TGFβ/BMP Signaling Crosstalk with Mechanobiology.* Cells, 2020. **9**(9): p. 1965.
186. Davis, R.B., et al., *Notch signaling pathway is a potential therapeutic target for extracranial vascular malformations.* Scientific Reports, 2018. **8**(1): p. 17987.
187. Wu, Q.-J., et al., *The sirtuin family in health and disease.* Signal Transduction and Targeted Therapy, 2022. **7**(1): p. 402.
188. North, B.J. and E. Verdin, *Sirtuins: Sir2-related NAD-dependent protein deacetylases.* Genome biology, 2004. **5**: p. 1-12.
189. Rajabi, N., et al., *Chapter Two - Targeting Sirtuins: Substrate Specificity and Inhibitor Design*, in *Progress in Molecular Biology and Translational Science*, W. Zheng, Editor. 2018, Academic Press. p. 25-69.
190. Teixeira, C.S., et al., *A molecular perspective on sirtuin activity.* International Journal of Molecular Sciences, 2020. **21**(22): p. 8609.
191. Zhang, X., et al., *Alternative Splicing Increases Sirtuin Gene Family Diversity and Modulates Their Subcellular Localization and Function.* Int J Mol Sci, 2021. **22**(2).
192. Quan, X., et al., *Implications of altered sirtuins in metabolic regulation and oral cancer.* PeerJ, 2023. **11**: p. e14752.
193. Bergmann, L., et al., *Subcellular Localization and Mitotic Interactome Analyses Identify SIRT4 as a Centrosomally Localized and Microtubule Associated Protein.* Cells, 2020. **9**(9).
194. Ahuja, N., et al., *Regulation of insulin secretion by SIRT4, a mitochondrial ADP-ribosyltransferase.* Journal of Biological Chemistry, 2007. **282**(46): p. 33583-33592.
195. Lang, A., et al., *SIRT4 interacts with OPA1 and regulates mitochondrial quality control and mitophagy.* Aging (Albany NY), 2017. **9**(10): p. 2163.
196. Fu, L., et al., *SIRT4 inhibits malignancy progression of NSCLCs, through mitochondrial dynamics mediated by the ERK-Drp1 pathway.* Oncogene, 2017. **36**(19): p. 2724-2736.
197. Haigis, M.C., et al., *SIRT4 inhibits glutamate dehydrogenase and opposes the effects of calorie restriction in pancreatic beta cells.* Cell, 2006. **126**(5): p. 941-54.
198. Han, Y., et al., *SIRT4 and Its Roles in Energy and Redox Metabolism in Health, Disease and During Exercise.* Front Physiol, 2019. **10**: p. 1006.
199. Mathias, R.A., et al., *Sirtuin 4 is a lipoamidase regulating pyruvate dehydrogenase complex activity.* Cell, 2014. **159**(7): p. 1615-25.
200. Bai, Y., et al., *Research Progress of Sirtuin4 in Cancer.* Front Oncol, 2020. **10**: p. 562950.
201. Min, Z., J. Gao, and Y. Yu, *The roles of mitochondrial SIRT4 in cellular metabolism.* Frontiers in Endocrinology, 2019. **9**: p. 783.
202. Nasrin, N., et al., *SIRT4 regulates fatty acid oxidation and mitochondrial gene expression in liver and muscle cells.* J Biol Chem, 2010. **285**(42): p. 31995-2002.
203. Laurent, G., et al., *SIRT4 represses peroxisome proliferator-activated receptor α activity to suppress hepatic fat oxidation.* Mol Cell Biol, 2013. **33**(22): p. 4552-61.

204. Luo, Y.X., et al., *SIRT4 accelerates Ang II-induced pathological cardiac hypertrophy by inhibiting manganese superoxide dismutase activity.* Eur Heart J, 2017. **38**(18): p. 1389-1398.
205. Tarantino, G., et al., *Circulating levels of sirtuin 4, a potential marker of oxidative metabolism, related to coronary artery disease in obese patients suffering from NAFLD, with normal or slightly increased liver enzymes.* Oxid Med Cell Longev, 2014. **2014**: p. 920676.
206. Lang, A. and R.P. Piekorz, *Novel role of the SIRT4-OPA1 axis in mitochondrial quality control.* Cell Stress, 2018. **2**(1): p. 1.
207. Shi, J.X., et al., *SIRT4 overexpression protects against diabetic nephropathy by inhibiting podocyte apoptosis.* Exp Ther Med, 2017. **13**(1): p. 342-348.
208. Ciccia, A. and S.J. Elledge, *The DNA damage response: making it safe to play with knives.* Mol Cell, 2010. **40**(2): p. 179-204.
209. Cosentino, C., D. Grieco, and V. Costanzo, *ATM activates the pentose phosphate pathway promoting anti-oxidant defence and DNA repair.* Embo j, 2011. **30**(3): p. 546-55.
210. Jeong, S.M., et al., *SIRT4 has tumor-suppressive activity and regulates the cellular metabolic response to DNA damage by inhibiting mitochondrial glutamine metabolism.* Cancer cell, 2013. **23**(4): p. 450-463.
211. Wang, Y., et al., *SIRT4-Catalyzed Deacetylation of Axin1 Modulates the Wnt/β-Catenin Signaling Pathway.* Front Oncol, 2022. **12**: p. 872444.
212. Yang, S., et al., *LATS1 K751 acetylation blocks activation of Hippo signalling and switches LATS1 from a tumor suppressor to an oncoprotein.* Sci China Life Sci, 2022. **65**(1): p. 129-141.
213. Huang, H., et al., *Acetylation of SCFD1 regulates SNARE complex formation and autophagosome-lysosome fusion.* Autophagy, 2023. **19**(1): p. 189-203.
214. Jadwin, J.A., M. Ogiue-Ikeda, and K. Machida, *The application of modular protein domains in proteomics.* FEBS Lett, 2012. **586**(17): p. 2586-96.
215. Ravi Chandra, B., et al., *Distribution of proline-rich (PxxP) motifs in distinct proteomes: functional and therapeutic implications for malaria and tuberculosis.* Protein Engineering, Design and Selection, 2004. **17**(2): p. 175-182.
216. Carducci, M., et al., *The protein interaction network mediated by human SH3 domains.* Biotechnology Advances, 2012. **30**(1): p. 4-15.
217. Teyra, J., et al., *Comprehensive analysis of the human SH3 domain family reveals a wide variety of non-canonical specificities.* Structure, 2017. **25**(10): p. 1598-1610. e3.
218. Verschueren, E., et al., *Evolution of the SH3 domain specificity Landscape in Yeasts.* PLoS One, 2015. **10**(6): p. e0129229.
219. Sadowski, M.I. and D.T. Jones, *The sequence–structure relationship and protein function prediction.* Current Opinion in Structural Biology, 2009. **19**(3): p. 357-362.
220. Kazemein Jasemi, N.S., et al., *Functional Classification and Interaction Selectivity Landscape of the Human SH3 Domain Superfamily.* Cells, 2024. **13**(2): p. 195.
221. Dionne, U., et al., *Protein context shapes the specificity of SH3 domain-mediated interactions in vivo.* Nature Communications, 2021. **12**(1): p. 1597.
222. Mayer, B.J. and K. Saksela, *SH3 domains.* Modular protein domains, 2004: p. 37-58.
223. Dionne, U., et al., *SRC homology 3 domains: multifaceted binding modules.* Trends in Biochemical Sciences, 2022. **47**(9): p. 772-784.
224. Hahn, S. and D. Kim, *Transient protein-protein interaction of the SH3-peptide complex via closely located multiple binding sites.* PLoS One, 2012. **7**(3): p. e32804.
225. Jaiswal, M., et al., *Functional cross-talk between ras and rho pathways: a Ras-specific GTPase-activating protein (p120RasGAP) competitively inhibits the RhoGAP activity of deleted in liver cancer (DLC) tumor suppressor by masking the catalytic arginine finger.* The Journal of biological chemistry, 2014. **289**(10): p. 6839-6849.

226. Gigoux, V., et al., *Identification of Aurora kinases as RasGAP Src homology 3 domain-binding proteins.* J Biol Chem, 2002. **277**(26): p. 23742-6.
227. Latour, S., et al., *Binding of SAP SH2 domain to FynT SH3 domain reveals a novel mechanism of receptor signalling in immune regulation.* Nat Cell Biol, 2003. **5**(2): p. 149-54.
228. Ball, L.J., et al., *Recognition of proline-rich motifs by protein–protein-interaction domains.* Angewandte Chemie International Edition, 2005. **44**(19): p. 2852-2869.
229. Li, Shawn S.-C., *Specificity and versatility of SH3 and other proline-recognition domains: structural basis and implications for cellular signal transduction.* Biochemical Journal, 2005. **390**(3): p. 641-653.
230. Mehrabipour, M., et al., *SIRT4 as a novel interactor and candidate suppressor of C-RAF kinase in MAPK signaling.* Life Sci Alliance, 2024. **7**(6).
231. Riaud, M., et al., *The role of CRAF in cancer progression: from molecular mechanisms to precision therapies.* Nature Reviews Cancer, 2024. **24**(2): p. 105-122.
232. Moghaddam, M., et al., *Cancer resistance via the downregulation of the tumor suppressors RKIP and PTEN expressions: therapeutic implications.* Explor Target Antitumor Ther, 2023. **4**(2): p. 170-207.
233. Tomaselli, D., et al., *Sirt4: A Multifaceted Enzyme at the Crossroads of Mitochondrial Metabolism and Cancer.* Front Oncol, 2020. **10**: p. 474.
234. Chen, Z., et al., *SIRT4 inhibits the proliferation, migration, and invasion abilities of thyroid cancer cells by inhibiting glutamine metabolism.* Onco Targets Ther, 2019. **12**: p. 2397-2408.
235. Hu, Y., et al., *Overexpression of SIRT4 inhibits the proliferation of gastric cancer cells through cell cycle arrest.* Oncol Lett, 2019. **17**(2): p. 2171-2176.
236. Li, S., et al., *Raf-1 Cysteine-Rich Domain Increases the Affinity of K-Ras/Raf at the Membrane, Promoting MAPK Signaling.* Structure, 2018. **26**(3): p. 513-525.e2.
237. Tran, T.H., et al., *KRAS interaction with RAF1 RAS-binding domain and cysteine-rich domain provides insights into RAS-mediated RAF activation.* Nat Commun, 2021. **12**(1): p. 1176.
238. Betsinger, C.N. and I.M. Cristea, *Mitochondrial Function, Metabolic Regulation, and Human Disease Viewed through the Prism of Sirtuin 4 (SIRT4) Functions.* J Proteome Res, 2019. **18**(5): p. 1929-1938.
239. Flick, F. and B. Lüscher, *Regulation of sirtuin function by posttranslational modifications.* Front Pharmacol, 2012. **3**: p. 29.
240. Yu, L.R., et al., *Improved titanium dioxide enrichment of phosphopeptides from HeLa cells and high confident phosphopeptide identification by cross-validation of MS/MS and MS/MS/MS spectra.* J Proteome Res, 2007. **6**(11): p. 4150-62.
241. Dai, X., et al., *Acetylation-dependent regulation of BRAF oncogenic function.* Cell reports, 2022. **38**(3).
242. Song, M. and S.D. Finley, *Mechanistic insight into activation of MAPK signaling by pro-angiogenic factors.* BMC Systems Biology, 2018. **12**(1): p. 145.
243. Nathan, J., R. Shameera, and G. Palanivel, *Studying molecular signaling in major angiogenic diseases.* Molecular and Cellular Biochemistry, 2022. **477**(10): p. 2433-2450.
244. Chen, J., et al., *Akt1 regulates pathological angiogenesis, vascular maturation and permeability in vivo.* Nat Med, 2005. **11**(11): p. 1188-96.
245. Hellesøy, M. and J.B. Lorens, *Cellular context-mediated Akt dynamics regulates MAP kinase signaling thresholds during angiogenesis.* Mol Biol Cell, 2015. **26**(14): p. 2698-711.
246. Cai, D., et al., *Identification and Characterization of Oncogenic SOS1 Mutations in Lung Adenocarcinoma.* Mol Cancer Res, 2019. **17**(4): p. 1002-1012.
247. Kessler, D., et al., *Targeting Son of Sevenless 1: The pacemaker of KRAS.* Current Opinion in Chemical Biology, 2021. **62**: p. 109-118.

248. Hofmann, M.H., et al., *BI-3406, a potent and selective SOS1–KRAS interaction inhibitor, is effective in KRAS-driven cancers through combined MEK inhibition.* Cancer Discovery, 2021. **11**(1): p. 142-157.
249. Nichols, R.J., et al., *RAS nucleotide cycling underlies the SHP2 phosphatase dependence of mutant BRAF-, NF1- and RAS-driven cancers.* Nat Cell Biol, 2018. **20**(9): p. 1064-1073.
250. Fedele, C., et al., *SHP2 Inhibition Prevents Adaptive Resistance to MEK Inhibitors in Multiple Cancer Models.* Cancer Discovery, 2018. **8**(10): p. 1237-1249.
251. Nichols, R.J., et al., *Efficacy of SHP2 phosphatase inhibition in cancers with nucleotide-cycling oncogenic RAS, RAS-GTP dependent oncogenic BRAF and NF1 loss.* bioRxiv, 2017: p. 188730.
252. Zheng, J., et al., *The solution structure of the pleckstrin homology domain of human SOS1. A possible structural role for the sequential association of diffuse B cell lymphoma and pleckstrin homology domains.* J Biol Chem, 1997. **272**(48): p. 30340-4.
253. Zhao, C., et al., *Phospholipase D2-generated phosphatidic acid couples EGFR stimulation to Ras activation by Sos.* Nat Cell Biol, 2007. **9**(6): p. 706-12.
254. Kapp, F.G., et al., *Somatic RIT1 delins in arteriovenous malformations hyperactivate RAS-MAPK signaling amenable to MEK inhibition.* Angiogenesis, 2024: p. 1-14.
255. Limaye, N., et al., *Somatic Activating PIK3CA Mutations Cause Venous Malformation.* Am J Hum Genet, 2015. **97**(6): p. 914-21.
256. Keppler-Noreuil, K.M., et al., *PIK3CA-related overgrowth spectrum (PROS): diagnostic and testing eligibility criteria, differential diagnosis, and evaluation.* Am J Med Genet A, 2015. **167a**(2): p. 287-95.
257. Al-Olabi, L., et al., *Mosaic RAS/MAPK variants cause sporadic vascular malformations which respond to targeted therapy.* J Clin Invest, 2018. **128**(4): p. 1496-1508.
258. Goss, J.A., et al., *Intramuscular fast-flow vascular anomaly contains somatic MAP2K1 and KRAS mutations.* Angiogenesis, 2019. **22**(4): p. 547-552.
259. Liu, A.S., et al., *Extracranial arteriovenous malformations: natural progression and recurrence after treatment.* Plast Reconstr Surg, 2010. **125**(4): p. 1185-1194.
260. Cuevas-Navarro, A., et al., *RAS-dependent RAF-MAPK hyperactivation by pathogenic RIT1 is a therapeutic target in Noonan syndrome-associated cardiac hypertrophy.* Sci Adv, 2023. **9**(28): p. eadf4766.

Acknowledgements

This thesis represents work carried out at the Department of Biochemistry and Molecular Biology II, Medical Faculty of the Heinrich Heine University, University Hospital Düsseldorf. I am deeply grateful for the financial support from the European Network on Noonan Syndrome and Related Disorders (NSEuroNet, grant number: 01GM1621B) and the German Research Foundation (DFG, grant number: AH 92/8-1).

I would like to express my sincere and deep gratitude to my supervisor, Professor Reza Ahmadian, for letting me join your lab and introducing me to the amazing world of cell signaling. You have always supported and encouraged me to think and work independently. At times, your expectations seemed beyond my capabilities, but they pushed me to grow. Knowing that you believe in me made difficult times feel less terrible.

I am particularly grateful to Dr Roland Piekorz. Despite your busy schedule, you always made time for me, offering invaluable advice and friendly support. I have learned so much from you, and I wouldn't be the researcher I am today without your guidance.

Special thanks to Professor Jürgen Scheller, head of department, for creating a supportive research environment and always backing our group, and to Dr. Doreen M. Floß for kindness and endless support.

I really appreciate the collaboration with my co-authors. Dr Radovan Dvorsky, Dr Saeideh Nakhaei-Rad, and Dr Jens M. Moll, your discussions and insights have been incredibly helpful.

I would like to thank all my former and present colleagues in the department for their kindness and continuous support. Niloufar, Silke, and Farhad, you shared your exceptional technical skills and taught me so much about lab work. My dear Niloufar, your friendship and support helped me through all those times I felt hopeless. Farhad, you were the best officemate. Silke, it was always inspiring to watch you in the lab; you were always kind and supportive.

Big thanks to all my dear friends and family who supported me and did not give up on me. Maman Mehri, I would never have come to this point if you had not taught me to work hard and to chase after my dreams. You made me strong; I love you! Mehrzad and Rasool, your unconditional support means the world to me. I have coped with many challenges during my PhD because of you.

Lastly, I would like to express my deepest gratitude to my husband, Amirhossein. You read me like a book, and that’s something wonderful. You were always there to support me and help clear my mind when I needed it most. You shared this entire amazing journey with me. Thank you for all your encouragement, support, and unconditional love.

Düsseldorf, August 2024

Eidesstattliche Erklärung

Ich versichere an Eides Statt, dass die Dissertation von mir selbständig und ohne unzulässige fremde Hilfe unter Beachtung der „Grundsätze zur Sicherung guter wissenschaftlicher Praxis an der Heinrich-Heine-Universität Düsseldorf“ erstellt worden ist. Diese Dissertation wurde in der vorgelegten oder einer ähnlichen Form noch bei keiner anderen Institution eingereicht und es wurden bisher keine erfolglosen Promotionsversuche von mir unternommen.

Düsseldorf, August 2024

Mehrnaz Mehrabipour